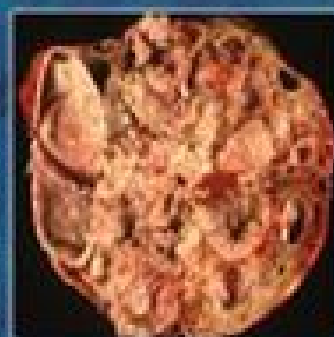
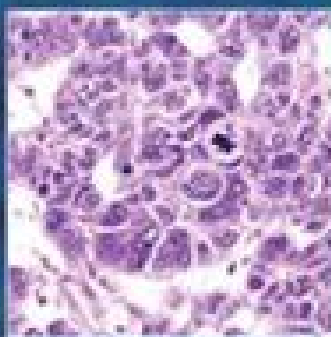
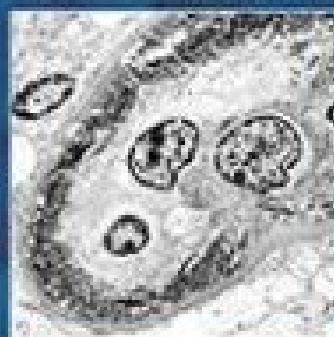
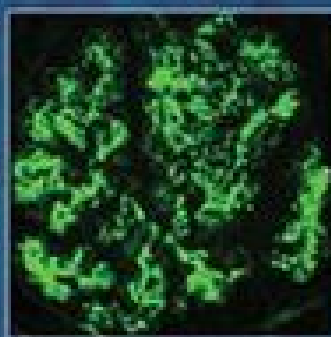
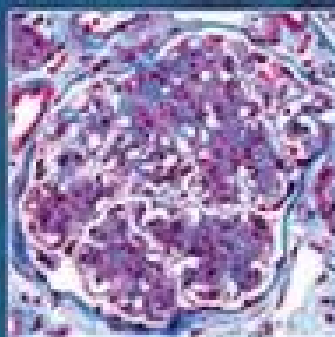


Includes interactive ebook with complete content

HEPTINSTALL'S PATHOLOGY OF THE KIDNEY

SEVENTH EDITION



VOLUME I

J. Charles Jennette • Jean L. Olson
Fred G. Silva • Vivette D. D'Agati

 Wolters Kluwer

Heptinstall's
Pathology
of the Kidney

SEVENTH EDITION

tahir99 - UnitedVRG

Heptinstall's Pathology of the Kidney

SEVENTH EDITION

EDITORS

J. Charles Jennette, MD

Kenneth M. Brinkhous Distinguished Professor
Chair of Pathology and Laboratory Medicine
Department of Pathology and Laboratory Medicine
Professor of Medicine, Division of Nephrology
and Hypertension
Executive Director, Division of Nephropathology
University of North Carolina at Chapel Hill
Chapel Hill, North Carolina

Jean L. Olson, MD

Professor
Director, Renal Pathology and Electron Microscopy
Department of Pathology
University of California San Francisco
San Francisco, California

Fred G. Silva, MD

Nephropathologist
Nephropath
Adjunct Professor of Pathology
Department of Pathology
University of Arkansas Medical School
Little Rock, Arkansas

Vivette D. D'Agati, MD

Professor of Pathology
Director, Division of Renal Pathology
Department of Pathology and Cell Biology
Columbia University College of Physicians and
Surgeons
New York, New York



Philadelphia • Baltimore • New York • London
Buenos Aires • Hong Kong • Sydney • Tokyo

Acquisitions Editor: Ryan Shaw
Product Manager: Kate Marshall
Production Product Manager: Priscilla Crater
Senior Manufacturing Coordinator: Beth Welsh
Marketing Manager: Dan Dressler
Designer: Stephen Druding
Production Service: SPi Global

Copyright © 2015 by Wolters Kluwer

Two Commerce Square
2001 Market Street
Philadelphia, PA 19103 USA
LWW.com

Sixth Edition © 2007, Lippincott Williams & Wilkins

Fifth Edition © 1998, Lippincott-Raven

Fourth Edition © 1992, Little, Brown and Co

Third Edition © 1982, Little, Brown and Co

Second Edition © 1974, Little, Brown and Co

First Edition © 1966, Little, Brown and Co

All rights reserved. This book is protected by copyright. No part of this book may be reproduced in any form by any means, including photocopying, or utilized by any information storage and retrieval system without written permission from the copyright owner, except for brief quotations embodied in critical articles and reviews. Materials appearing in this book prepared by individuals as part of their official duties as U.S. government employees are not covered by the above-mentioned copyright.

Printed in China

Library of Congress Cataloging-in-Publication Data

Heptinstall's pathology of the kidney. — Seventh edition / editors, J. Charles Jennette, Jean L. Olson, Fred G. Silva, Vivette D. D'Agati.

p. ; cm.

Pathology of the kidney

Includes bibliographical references and index.

ISBN 978-1-4511-4411-6 (set)

I. Jennette, J. Charles, editor of compilation. II. Olson, Jean L., editor of compilation. III. Silva, Fred G., editor of compilation. IV. D'Agati, Vivette D., editor of compilation. V. Title: Pathology of the kidney.

[DNLM: 1. Kidney Diseases—pathology. WJ 300]

RC903.9

616.6'2207—dc23

2013045099

Care has been taken to confirm the accuracy of the information presented and to describe generally accepted practices. However, the authors, editors, and publisher are not responsible for errors or omissions or for any consequences from application of the information in this book and make no warranty, expressed or implied, with respect to the currency, completeness, or accuracy of the contents of the publication. Application of the information in a particular situation remains the professional responsibility of the practitioner.

The authors, editors, and publisher have exerted every effort to ensure that drug selection and dosage set forth in this text are in accordance with current recommendations and practice at the time of publication. However, in view of ongoing research, changes in government regulations, and the constant flow of information relating to drug therapy and drug reactions, the reader is urged to check the package insert for each drug for any change in indications and dosage and for added warnings and precautions. This is particularly important when the recommended agent is a new or infrequently employed drug.

Some drugs and medical devices presented in the publication have Food and Drug Administration (FDA) clearance for limited use in restricted research settings. It is the responsibility of the health care provider to ascertain the FDA status of each drug or device planned for use in their clinical practice.

To purchase additional copies of this book, call our customer service department at (800) 638-3030 or fax orders to (301) 223-2320. International customers should call (301) 223-2300.

Visit Lippincott Williams & Wilkins on the Internet: at LWW.com. Lippincott Williams & Wilkins customer service representatives are available from 8:30 am to 6 pm, EST.

To my loving wife, Yvonne, my wonderful daughters, Jennifer and Caroline,
and my amazing granddaughters, Olivia and Augusta.

—*J. Charles Jennette*

In loving memory of my parents, Caroline and Arthur Olson.

—*Jean L. Olson*

To my lovely wife, Jean, and our wonderful daughter, Lindsay.

—*Fred G. Silva*

To my loving and supportive husband, Edward Imperatore, my sons,
Edward and Paul, and my grandson, Edward James.

—*Vivette D. D'Agati*

CONTRIBUTORS

Corinne Antignac, MD, PhD

Professeur
Génétique
Université Paris Descartes, Institut Imagine
INSERM U 1163 and Service de
Génétique
Hôpital Necker-Enfants Malades
Assistance Publique-Hôpitaux de Paris
Paris, France

Lois J. Arend, MD, PhD

Associate Professor
Department of Pathology
Johns Hopkins University School of Medicine
Baltimore, Maryland

Stephen M. Bonsib, MD

Nephropathologist
Nephropath
Little Rock, Arkansas

Sergey V. Brodsky, MD, PhD

Assistant Professor
Department of Pathology
The Ohio State University
Columbus, Ohio

Arthur H. Cohen, MD

Professor
Department of Pathology
Wake Forest University School of Medicine
Attending Physician
Department of Pathology
Wake Forest Baptist Medical Center
Medical Center Boulevard
Winston-Salem, North Carolina

Robert B. Colvin, MD

Pathologist-in-Chief, Emeritus
Department of Pathology
Massachusetts General Hospital
Benjamin Castleman Distinguished Professor
of Pathology
Harvard Medical School
Boston, Massachusetts

H. Terence Cook, FRCPath, FMedSci

Professor of Renal Pathology
Department of Medicine
Imperial College London
Professor of Renal Pathology
Department of Cellular Pathology
Hammersmith Hospital
London, United Kingdom

Vivette D. D'Agati, MD

Professor of Pathology
Director, Renal Pathology Laboratory
Columbia University College of Physicians and
Surgeons
New York, New York

John N. Eble, MD, MBA, FRCPA

Nordschow Professor and Chairman
Department of Pathology and Laboratory
Medicine
Indiana University
Chief Pathologist
Department of Pathology and Laboratory
Medicine
Indiana University Health
Indianapolis, Indianapolis

Andrew Z. Fenves, MD, FACP, FASN

Visiting Professor
Department of Medicine
Massachusetts General Hospital
Harvard Medical School
Boston, Massachusetts

Laura S. Finn, MD

Associate Professor
Department of Pathology
University of Washington Medical
Center
Division Chief of Anatomic Pathology
Director of Flow Cytometry
Department of Laboratories
Seattle Children's Hospital
Seattle, Washington

Agnes B. Fogo, MD

Professor
Department of Pathology, Microbiology and
Immunology
Vanderbilt University Medical Center
Nashville, Tennessee

Joseph P. Gaut, MD, PhD

Assistant Professor
Department of Pathology and Immunology
Division of Anatomic and Molecular
Pathology
Washington University School of Medicine
St. Louis, Missouri

David J. Grignon, MD

Centennial Professor and Vice Chair for
Clinical Programs
Department of Pathology and Laboratory
Medicine
Indiana University School of Medicine
Indianapolis, Indiana

Marie Claire Gubler, MD

Directeur de recherche
Director of Research Emeritus
Institut National de la Santé et de la Recherche
Médicale
Centre de Référence des Maladies Héritaires
de l'Enfant et de l'Adulte
Hôpital Necker-Enfants Malades
Paris, France

Mark Haas, MD, PhD

Professor
Department of Pathology and Laboratory
Medicine
Cedars-Sinai Medical Center Professional
Series
Attending Pathologist, Renal Pathology
Department of Pathology and Laboratory
Medicine
Cedars-Sinai Medical Center
Los Angeles, California

Laurence Heidet, MD, PhD

APHP
Service de Néphrologie Pédiatrique
Centre de référence pour les Maladies
Héréditaires de l'Enfant et de l'Adulte
(MARHEA)
Hôpital Necker-Enfants Malades
Paris, France

Guillermo A. Herrera, MD

Albert G. and Harriet G. Smith Professor
and Chair
Department of Pathology
Professor, Department Cellular Biology
and Anatomy
Louisiana State University Health Sciences
Center
Chief
Pathology Laboratory Services
Department of Pathology
University Health
Shreveport, Louisiana

Samy S. Iskandar, MB, BCh, PhD

Professor
Departments of Pathology and General
Surgery
Wake Forest School of Medicine and North
Carolina Baptist Hospital
Winston-Salem, North Carolina

Dagan Jenkins, BSc, PhD

Lecturer
Molecular Medicine Unit
UCL Institute of Child Health
London, United Kingdom

J. Charles Jennette, MD

Kenneth M. Brinkhous Distinguished
Professor
Chair of Pathology and Laboratory Medicine
Department of Pathology and Laboratory
Medicine
Professor of Medicine, Division of Nephrology
and Hypertension
Executive Director, Division of
Nephropathology
University of North Carolina at Chapel Hill
Chapel Hill, North Carolina

Neeraja Kambham, MD

Professor
Department of Pathology
Stanford University
Co-Director, Renal Pathology Lab
Department of Pathology
Stanford University Medical Center
Stanford, California

Michael Kashgarian, MD

Professor Emeritus of Pathology
Molecular Cellular and Developmental
Biology
Yale University
Attending Pathologist
Department of Anatomic Pathology
Yale New Haven Hospital
New Haven, Connecticut

Zoltan G. Laszik, MD, PhD

Professor of Pathology
University of California San Francisco
San Francisco, California

Helen Liapis, MD

Professor of Pathology and Immunology
Division of Anatomic and Molecular
Pathology
Washington University School of Medicine
St. Louis, Missouri

Glen S. Markowitz, MD

Professor of Pathology and Cell Biology
Columbia University, College of Physicians and
Surgeons
Columbia University Medical Center
New York, New York

Michael Mengel, MD

Associate Professor and Chair
Department of Laboratory Medicine and
Pathology
Section Head, Transplantation Pathology
Section Head, Immunohistochemistry
Division of Anatomic Pathology
University of Alberta
Edmonton, Alberta, Canada

Gilbert W. Moeckel, MD, PhD, FASN

Associate Professor
Renal Pathology and Electron Microscopy
Laboratory
Department of Pathology
Yale University School of Medicine
New Haven, Connecticut

Tibor Nadasdy, MD, PhD

Professor
Department of Pathology
The Ohio State University Wexner Medical
Center
Columbus, Ohio

Cynthia C. Nast, MD

Professor
Cedars-Sinai Medical Center
David Geffen School of Medicine at UCLA
Los Angeles, California

Volker Nickeleit, MD

Professor of Pathology
Director, Division of Nephropathology
Department of Pathology and Laboratory
Medicine
The University of North Carolina
at Chapel Hill
Chapel Hill, North Carolina

Jean L. Olson, MD

Professor
Director, Renal Pathology and Electron
Microscopy
Department of Pathology
University of California San Francisco
San Francisco, California

Maria M. Picken, MD, PhD

Professor of Pathology
Director of Surgical Pathology
Director of Solid Organ Transplant
Pathology
Director of Surgical Pathology Fellowship
Department of Pathology
Loyola University Medical Center
Maywood, Illinois

Matthew C. Pickering, MB, BS, PhD

Professor of Rheumatology
Wellcome Trust Senior Research Fellow in
Clinical Science
Centre for Complement & Inflammation
Research (CCIR)
Division of Immunology and Inflammation
Imperial College London
London, United Kingdom

Lorraine C. Racusen, MD

Professor
Department of Pathology
The Johns Hopkins University School of
Medicine
The Johns Hopkins Hospital
Baltimore, Maryland

Anjali A. Satoskar, MD

Associate Professor
Department of Pathology
Ohio State University
Wexner Medical Center
Columbus, Ohio

Ramesh Saxena, MD, PhD

Professor
Division of Nephrology
Department of Internal Medicine
UT Southwestern Medical Center
Dallas, Texas

Fred G. Silva, MD

Nephropathologist
Nephropath
Adjunct Professor of Pathology
Department of Pathology
University of Arkansas Medical School
Little Rock, Arkansas

Harsharan K. Singh, MD

Professor of Pathology and Laboratory Medicine
Director, Electron Microscopy Services,
University of North Carolina Hospitals
Associate Director, Division of Nephropathology
Department of Pathology and Laboratory
Medicine
The University of North Carolina at Chapel Hill
Chapel Hill, North Carolina

M. Barry Stokes, MB, BCH

Associate Professor
Department of Pathology and Cell Biology
Columbia University College of Physicians
and Surgeons
Attending Pathologist
Renal Pathology Laboratory
New York-Presbyterian Hospital
New York, New York

David B. Thomas, MD

Professor
Department of Pathology
University of Miami Miller School of Medicine
Miami, Florida

John E. Tomaszewski, MD

Professor and Chair
Department of Pathology and Anatomical
Sciences
State University of New York at Buffalo
School of Medicine and Biomedical Sciences
Buffalo, New York

Nosratola D. Vaziri, MD, MACP

Professor of Medicine, Physiology, and
Biophysics
Division of Nephrology and Hypertension
University of California, Irvine
Irvine, California

Paul J.D. Winyard, BM, BCh, PhD

Head, Nephro-Urology Unit
UCL Institute of Child Health
London, United Kingdom

Adrian S. Woolf, MD

Chair of Paediatric Science
Institute of Human Development
University of Manchester
Honorary Consultant in Paediatric Nephrology
Department of Paediatric Nephrology
Royal Manchester Children's Hospital
Manchester, United Kingdom

Xin J. (Joseph) Zhou, MD

Clinical Professor
Department of Pathology
Baylor University Medical Center at Dallas and
Texas A&M Health Science Center
Dallas, Texas
Director
Renal Path Diagnostics
Pathologists BioMedical Laboratories
Lewisville, Texas

This seventh edition of *Heptinstall's Pathology of the Kidney* has the greatest increase in new knowledge and new insights into kidney diseases of any prior new edition. This comprehensive text maintains the excellence established by Robert H. Heptinstall, who edited and to a considerable degree authored the first four editions of this classic text first published in 1966. Since the publication of the sixth edition in 2007, there have been extraordinary advances in the understanding of the cellular, molecular, and genetic basis for kidney diseases; in the knowledge of pathologic and clinical manifestations of kidney diseases; and in the utilization of pathologic findings for directing new and more precise treatment of kidney diseases. This seventh edition has been thoroughly updated to include in-depth reviews of these important new advances that have clarified our understanding of kidney diseases, redirected research on the mechanisms of kidney diseases, modified the pathologic diagnostic evaluation of kidney diseases, and improved the treatment and prevention of kidney diseases.

The authors who contributed to the seventh edition are among the most capable and accomplished renal pathologists in the world. All of these authors have extensive hands-on experience with diagnostic renal pathology, teaching renal pathology at major medical centers, and advancing the field through

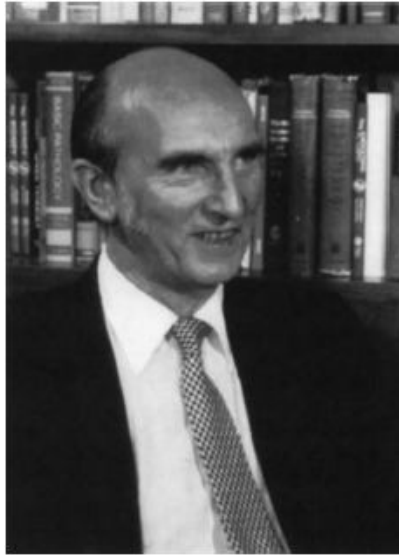
clinical and translational research. They have contributed thousands of articles to the literature on renal pathology. In fact, many of the major advances in our current understanding of renal pathology have been made by authors of chapters in this book. The editors thank all of the authors of the seventh edition for their truly outstanding contributions.

We are saddened by the recent passing of two extraordinary renal pathologists, Kendrick A. Porter and Gary S. Hill, who authored stellar chapters in earlier editions and were dear friends of Dr. Heptinstall. We are thankful for their many personal and professional contributions to our field of renal pathology.

All of the editors and authors are honored by the opportunity and challenge afforded us by Dr. Heptinstall to sustain his preeminent book on renal pathology. We and all others who are interested in the study of kidney diseases are forever indebted to him for establishing this classic text. We are convinced that the seventh edition of *Heptinstall's Pathology of the Kidney* is the most comprehensive, most authoritative, most thoroughly referenced, and best illustrated book on renal pathology ever produced.

J. Charles Jennette, MD
Jean L. Olson, MD
Fred G. Silva, MD
Vivette D. D'Agati, MD

Robert H. Heptinstall A Tribute



The first edition of *Pathology of the Kidney* by Robert H. Heptinstall marked the watershed between autopsy- and biopsy-based studies of renal disease in human beings. Before the *Pathology of the Kidney*, renal pathology textbooks related the clinical evolution of “renal syndromes” and the associated autopsy findings. The percutaneous renal biopsy initially described by Iversen and Brun only 15 years prior to the publication of *Pathology of the Kidney* allowed a more dynamic view of kidney disease, and the text drew heavily on renal biopsy studies and immunofluorescence and electron microscopic findings in renal tissue. This new information had to be integrated with the autopsy-based renal literature for, as “Heppy” wrote in the preface to the first edition, “we are almost completely ignorant of the sequence of events that takes place during the evolution of a given disease, and ... the nomenclature in use at the moment is most unsatisfactory. Most of our concepts and nomenclature of renal disease have been based on kidneys studied at autopsy, which except in rare instances represent the end stage of a process that has been going on for years. The renal biopsy has presented us with histological pictures that in the light of our present concepts are not only difficult to interpret but defy satisfactory labeling.” The enduring contribution of *Pathology of the Kidney* is that it brought order out of chaos and in doing so defined the central issues of modern renal pathology. Over the years, this classic textbook and its subsequent editions have provided guidance and insight not only to nephropathologists but also to nephrologists, renal physiologists, and the entire renal community.

The first edition of *Pathology of the Kidney* is also an outstanding example of medical authorship. The book was

written with wit and style, and it is scholarly, authoritative, and comprehensive. This monumental achievement is even more remarkable when one considers that the first four editions were essentially monographs.

How Heppy accomplished his goals of presenting biopsy-based pathology, relating it to the existing classifications, and identifying a pathogenetic sequence deserves exposition. Much of the text is written in the first person because it was based on his extensive experience with renal pathology in biopsy and autopsy material. When writing on disputed topics, however, he was careful to quote “widely the opinions of others.” A complete and critical reading of the literature allowed him to correlate biopsy studies of acute and evolving renal diseases with the end-stage findings and nomenclature from autopsy studies. In the few areas where he did not have personal experience, he was exact in quoting published material, and whenever possible he reviewed the pathology material obtained by others. The superb illustrations complemented the text by demonstrating the pathologic lesions in all their phases allowing a pathogenetic connection between acute and end-stage lesions. Finally, his experience as an experimental pathologist aided him in critically evaluating and identifying relevant experimental studies.

Late Ramzi S. Cotran, no mean scholar himself, acknowledged the comprehensive and scholarly nature of the *Pathology of the Kidney* by insisting that it was the place to begin not only the workup of a difficult case but also an experimental study. Thus, Heppy has provided a fair template for those who would write chapters in pathology textbooks. In so far as we succeed, the credit is his, and if we fail, the responsibility is ours.

PREFACE TO THE FIRST EDITION (1966)

The task of presenting a comprehensible account of the pathology of the kidney is surprisingly difficult, as I have found to my cost over the past 3 years. The main difficulties are twofold: first, we are almost completely ignorant of the sequence of events that takes place during the evolution of a given disease and, second, the nomenclature in use at the moment is most unsatisfactory. Most of our concepts and nomenclature of renal disease have been based on kidneys studied at autopsy, which except in rare instances represent the end stage of a process that has been going on for years. The renal biopsy has presented us with histologic pictures that in light of our present concepts are not only difficult to interpret but defy satisfactory labeling. Many of these pictures are doubtless early stages of a process whose end stage we already recognize, but others very likely represent processes with which we are quite unfamiliar. Only by conducting intelligently planned studies with repeat biopsies over a long period of time can we hope to resolve these problems, and a greater degree of cooperation between the various groups of investigators will be required than has been the case up to now.

Accepting the imperfect state of our knowledge, I have attempted to present an account of the more common diseases that affect the kidney. The book is mainly for the pathologist and the internist specializing in renal problems, but it is hoped that it will be of use to others, such as the urologist and the obstetrician.

The pathology of the various diseases has been presented in the light of both autopsy and biopsy experience, and although many of the views expressed are my own, this being an author's privilege, a balanced presentation has been attempted by quoting widely the opinions of others. The clinical sections are of necessity brief, for these aspects have been authoritatively dealt with on numerous occasions by people better qualified than I am. Experimental contributions have been quoted when appropriate, and in most chapters, the role of the newer techniques such as electron and fluorescence microscopy has been

described. The traditional chapter on renal physiology has been omitted, and for this, I offer no apology. This is a highly complex subject that can hardly be compressed into one chapter; it is also one that I am not competent to discuss. Renal tumors are not discussed because they are adequately considered in existing texts on surgical pathology.

I have been fortunate in persuading Dr. J.M. Kissane to write chapters on the development and congenital defects of the kidney and Dr. Kendrick A. Porter to write on renal transplantation. These two former colleagues of mine are experts in their fields, and their respective chapters amply reflect their competence.

I am very grateful to all those who supplied us with illustrations and material from which illustrations were made. Professor Paul Beeson was asked to read the two chapters on pyelonephritis and promptly replied with four single-spaced pages of comments and suggestions; I was chastened but grateful. Dr. Abou Pollack has been a constant source of pearls of wisdom and exotic material; I am much indebted to this fine pathologist. Most of the photomicrographs for my own chapters were prepared by Mr. Chester Reather, and these, as always, were of matchless quality. The wearisome job of checking the references was bravely carried out by Miss Virginia Shriver, and her efforts, and those of the staff of the William H. Welch Medical Library at Johns Hopkins, are much appreciated. The most difficult job of all was done by Miss Mary Lakin, my secretary, who, starting out with scraps of paper adorned by nearly undecipherable handwriting, restored order out of chaos and produced the final manuscript. It is impossible to thank her enough.

Lastly, it is a great pleasure to acknowledge the help and stimulus over the years of Dr. A.M. Joekes. The biopsies we saw together provided a nucleus for many of the thoughts that have been expressed in this book, and to him belongs much of the credit (or blame) for the finished product.

Robert H. Heptinstall

ACKNOWLEDGMENTS

Dr. Jennette thanks his wife, Yvonne, daughters, Jennifer and Caroline, and granddaughters, Olivia and Augusta, for forgiving the time spent away from them pursuing his passion for renal pathology. He thanks Dr. Fred Dalldorf for sparking his interest in renal pathology, Dr. Ron Falk for his decades of stimulating professional collaboration, and the many nephro-pathologists and nephrologists who have shared their insights on kidney disease with him. He especially thanks the nephro-pathology fellows and faculty who have been his associates at UNC over the years, including current faculty Volker Nickenleit, Sharan Singh, and Adil Gasim.

Dr. Olson thanks Drs. Manjeri Venkatachalam, Helmut Rennke, and Ramzi S. Cotran for their help during the formative part of her career. She also gives special thanks to Dr. Robert H. Heptinstall, her mentor and friend, for steering her toward renal pathology and for nurturing her early career.

Dr. Silva thanks all of the members of the Southwest Pediatric Nephrology Group (under the able direction of Dr. Ron Hogg) for the renal biopsy material used in the preparation of his chapters. He also thanks Dr. Conrad L. Pirani for all his years of mentoring.

Dr. D'Agati thanks above all her husband and children for the countless hours taken from them to pursue her career in renal pathology. She thanks Conrad L. Pirani for fellowship training, Jerry Appel and Jai Radhakrishnan for their valuable expertise and enthusiasm in clinical-pathologic studies, and the wonderful Columbia renal pathology team of Glen Markowitz, Barry Stokes, Leal Herlitz, Samih Nasr, and our many talented fellows for their support and stimulating collaborations. She respectfully acknowledges the thousands of patients with renal disease whose biopsies have provided a fascinating challenge and continuing education over the past three decades.

tahir99 - Uniteu

CONTENTS

Contributors vii
Preface ix
Tribute xi
Preface to the First Edition (1966) xiii
Acknowledgments xv

VOLUME 1

- 1** Renal Anatomy and Histology 1
Stephen M. Bonsib

- 2** Development of the Kidney 67
Adrian S. Woolf and Dagan Jenkins

- 3** Primer on the Pathologic Classification and Diagnosis of Kidney Disease 91
J. Charles Jennette, Fred G. Silva, Jean L. Olson, and Vivette D. D'Agati

- 4** Cystic Diseases and Developmental Kidney Defects 119
Helen Liapis and Paul J.D. Winyard

- 5** The Nephrotic Syndrome and Minimal Change Disease 173
Jean L. Olson

- 6** Focal Segmental Glomerulosclerosis 207
Vivette D. D'Agati and M. Barry Stokes

- 7** Membranous Glomerulonephritis 255
Glen S. Markowitz and Vivette D. D'Agati

- 8** Membranoproliferative Glomerulonephritis 301
Xin J. (Joseph) Zhou and Fred G. Silva

- 9** C3 Glomerulopathies, Including Dense Deposit Disease 341
H. Terence Cook and Matthew C. Pickering

- 10** Acute Postinfectious Glomerulonephritis and Glomerulonephritis Caused by Persistent Bacterial Infection 367
Anjali A. Satoskar, Tibor Nadasdy, and Fred G. Silva

- 11** Renal Injury Associated With Human Immunodeficiency Virus Infection and Therapy 437
Arthur H. Cohen and Cynthia C. Nast

- 12** IgA Nephropathy and IgA Vasculitis (Henoch-Schönlein Purpura) Nephritis 463
Mark Haas

- 13** Alport Syndrome, Familial Benign Hematuria, Nail-Patella Syndrome, Type III Collagen Glomerulopathy, and Pierson Syndrome 525
Marie Claire Gubler, Laurence Heidet, and Corinne Antignac

- 14** Renal Disease in Systemic Lupus Erythematosus, Mixed Connective Tissue Disease, Sjögren Syndrome, and Rheumatoid Arthritis 559
Vivette D. D'Agati and M. Barry Stokes

- 15** Anti-Glomerular Basement Membrane Glomerulonephritis and Goodpasture Syndrome 657
J. Charles Jennette and Volker Nickleit

- 16** Pauci-Immune and Antineutrophil Cytoplasmic Autoantibody-Mediated Crescentic Glomerulonephritis and Vasculitis 685
J. Charles Jennette and David B. Thomas

VOLUME 2

- 17** Renal Involvement in Polyarteritis Nodosa, Kawasaki Disease, Takayasu Arteritis, and Giant Cell Arteritis 715
J. Charles Jennette and Harsharan K. Singh

- 18** Thrombotic Microangiopathies 739
Zoltan G. Laszik, Neeraja Kambham, and Fred G. Silva

19 Renal Disease in Pregnancy 815

Agnes B. Fogo

20 Renal Disease Caused by Hypertension 849

Jean L. Olson

21 Diabetic Nephropathy 897

Jean L. Olson and Zoltan G. Laszik

22 Renal Diseases Associated With Plasma Cell Dyscrasias, Amyloidoses, and Waldenström Macroglobulinemia 951

Guillermo A. Herrera and Maria M. Picken

23 Glomerular Diseases With Organized Deposits 1015

Samy S. Iskandar and Guillermo A. Herrera

24 Pyelonephritis and Other Direct Renal Infections, Reflux Nephropathy, Hydronephrosis, Hypercalcemia, and Nephrolithiasis 1039

Helen Liapis, Joseph P. Gaut, John E. Tomaszewski, and Lois J. Arend

25 Acute and Chronic Tubulointerstitial Nephritis 1111

Sergey V. Brodsky and Tibor Nadasdy

26 Ischemic and Toxic Acute Tubular Injury and Other Ischemic Renal Injuries 1167

Gilbert W. Moeckel, Michael Kashgarian, and Lorraine C. Racusen

27 Renal Disease Caused by Inborn Errors of Metabolism, Storage Diseases, and Hemoglobinopathies 1223

Laura S. Finn

28 Renal Changes With Aging and End-Stage Renal Disease 1281

Xin J. (Joseph) Zhou, Andrew Z. Fenves, Nosratola D. Vaziri, and Ramesh Saxena

29 Renal Transplant Pathology 1321

Volker Nickleleit, Michael Mengel, and Robert B. Colvin

30 Renal Neoplasms 1461

John N. Eble and David J. Grignon

Index I-1

Renal Anatomy and Histology

Gross anatomy and macroscopic features of the kidneys and their environs 2

- Retroperitoneum 2
- Kidneys 2
- Renal vasculature 6
- Renal lymphatic system 10
- Renal innervation 11
- Calyces and renal pelvis 12

Architectural organization of the cortex and medulla 13

- Cortical labyrinth and medullary rays 13
- Cortical microvascularization 14
- Medulla 15

Nephrons 18

- Nephron number 19
- Types of nephrons 19

Renal corpuscle 21

- General structure and histology 21
- Cellular components of the glomerulus 24
- Glomerular matrix 37
- Blood vessels and the juxtaglomerular apparatus 42

Renal tubules 44

- Proximal tubule 46
- Thin limb of Henle 48
- Distal tubule 50
- Connecting tubule 51
- Collecting duct 52

Renal interstitium 58

- Interstitial cells and cytoarchitecture 58

The focus of this chapter is the gross anatomy, histology, and ultrastructure of the kidney, a remarkably complex organ that fosters exploration into its structural-functional intricacies with each technologic advance in molecular and cellular biology. Arsenals of sensitive and specific immunohistochemical reagents, molecular and genetic probes including tissue microarrays, are now available, and innovative techniques such as two-photon microscopy and *in vivo* imaging of the living kidney have emerged (1–5). These powerful tools enable investigators to explore new aspects of renal structure, renal function, and renal dysfunction and have led to the discovery of important genes and their products, whose role in normal renal physiology is a rapidly evolving field.

The content of this chapter draws on a compendium of contributions that began with Leonardo da Vinci and Andreas Versalius (Fig. 1.1), whose cadaver dissections provided the first detailed illustrations of the genital and urinary tract in the 16th century (6,7). One hundred years later, Marcello Malpighi, using the recent technologic innovation of Galileo Galilei, the light microscope, first described the renal corpuscles that bear his name (8,9). However, 200 years elapsed before major refinements in microscopes, and microscopic techniques such as thin histologic sections led to provocative discoveries of the fine structure of the kidney. William Bowman's intravascular dye studies (Fig. 1.2) published in 1842 revealed fundamental structural aspects of the nephron such as its vascular connections and unique peritubular capillary plexus (10,11). These early forays into renal microanatomy exposed complexities that begged for speculations regarding their functional correlates, leading to investigative journeys whose end is ever beyond the horizon.

In this chapter, the normal kidney is macroscopically displayed and then dissected at the cellular level, using both traditional microscopic and ultrastructural techniques, histochemistry and immunohistochemistry, and selected other modalities to illustrate features otherwise not demonstrable. Human material will be used when possible. Because perfusion-fixed animal tissue provides pristine ultrastructural detail of tubules unequaled by immersion-fixed human tissue, a number of illustrations used in past editions authored by Wilhelm Kriz

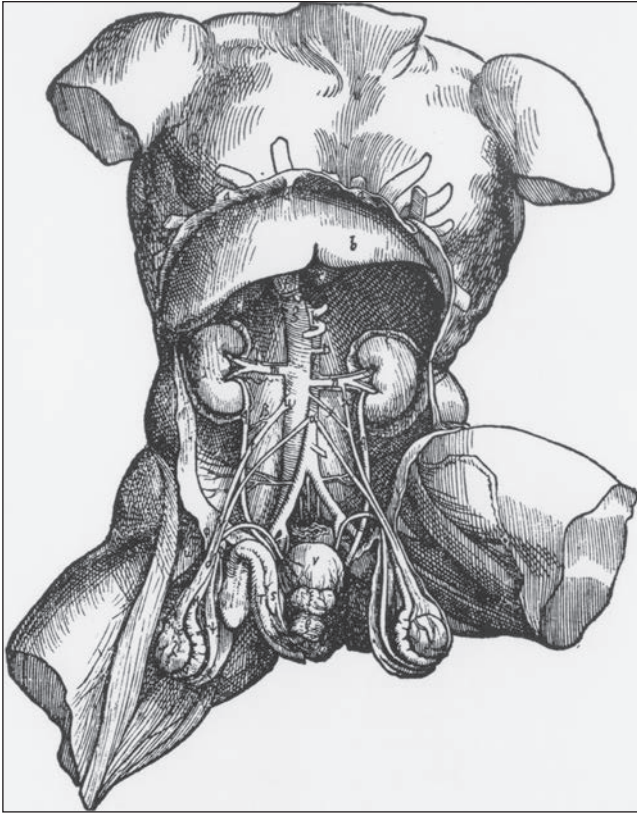


FIGURE 1.1 Andreas Versalius' 1543 illustration of the male genitourinary tract. Although most anatomic details are correct, the left kidney is incorrectly placed lower than the right kidney. (From Book 5 *De Humani Corporis Fabrica*.)

have been retained. The official nomenclature for structures of the kidney has been established by the Renal Commission of the International Union of Physiological Sciences (12). This terminology is used in this chapter (Table 1.1).

GROSS ANATOMY AND MACROSCOPIC FEATURES OF THE KIDNEYS AND THEIR ENVIRONS

Retroperitoneum

The retroperitoneum is a large compartment containing fat and several organs bounded anteriorly by the peritoneum and posteriorly by the transversalis fascia (Fig. 1.3). It is divided into three fascia-invested compartments or spaces: the anterior, posterior, and perirenal spaces (13–15). The anterior pararenal space contains the pancreas, duodenal loop, ascending and descending colon, and the hepatic, splenic, and proximal superior mesenteric arteries. The posterior pararenal space contains fat but no organs. The perirenal space is home to the kidneys and adrenal glands. Its anterior and posterior (Zuckerkindl) fascial investments are known as Gerota fascia, a loose connective tissue envelope that provides surgical dissection planes during radical nephrectomy. The perirenal space is bounded

medially by dense fat and the adventitial connective tissues of the aorta and vena cava that impede communication across the midline of perinephric processes such as urine leaks, hemorrhage, or infection (15).

Kidneys

The kidneys are paired retroperitoneal organs insulated by adipose tissue within Gerota fascia. They extend from the 12th thoracic vertebra to the 3rd lumbar vertebra. Their position is 2.5 cm lower in the erect position compared with their supine location, and they exhibit craniocaudal movement of 1.9 to 4.1 cm during respiration (14,16,17). The right kidney is slightly lower than the left kidney (in contrast to the drawing by Versalius, Fig. 1.1), and their upper poles are tilted slightly toward the midline. The kidneys are covered by a less than 1-mm-thick fibrous true capsule. It is adherent to the underlying renal cortical parenchyma but easily stripped off the normal kidney. This firm layer can be felt with introduction of the needle into the kidney during renal biopsy.

The newborn kidney is smaller than the adult kidney with the same reniform shape, but grossly, it is distinguished by prominent fetal lobations (Fig. 1.4). Renal weight in newborns ranges from 13 to 44 g; this increases by adulthood to 125 to 170 g in males and 115 to 155 g in females and has been shown to be proportional to body surface area (16,17). The number of glomeruli is constant in an individual between birth and adulthood; the increase in renal volume reflects expansion of tubular mass. The reduced tubular mass of the newborn kidney limits the capacity for salt and water regulation and explains neonates' susceptibility to dehydration. With age, there is a progressive decline in renal mass and weight, and therefore a decrease in renal reserve after the third decade, even in the absence of comorbid conditions (18–20). The loss of renal mass is primarily cortical and is proportional to the loss of (sclerosis of) functioning glomeruli. The average adult kidney is 11 to 12 cm long, 5 to 7 cm wide, and 2.5 to 3 cm thick. The left kidney is slightly larger than the right kidney. Renal volume can increase or decrease by 15% to 40% with major fluctuations in blood pressure, intravascular volume, or interstitial expansion by edema. The combined mass of the kidneys correlates with body surface area and is reduced in children of low birth weight (19,20).

The posterior surfaces of both kidneys are flatter than the anterior surface. The medial surface is concave with a 3-cm slit-like space called the *hilum*. The hilum is the vestibule through which pass the ureter, branches of the renal arteries and veins, nerves, and lymphatics as they enter and exit the renal sinus. The renal sinus is the fat-containing compartment housed within the confines of the kidney that also invests the calyceal and pelvic portions of the collecting system (Fig. 1.5).

The renal connective capsule extends a short distance into the renal sinus where it terminates. Portions of the renal cortex, the columns of Bertin, have no renal capsular investment (Fig. 1.6), resulting in direct continuity between the cortical interstitium and sinus tissues. This appears important in renal neoplasia, representing preferential routes for cancer dissemination (21). The subcapsular surface of the renal cortex may be smooth and featureless or may show grooves corresponding to the outlines of some or all of the individual renal lobes (Fig. 1.7). Persistence of distinct fetal lobations is common and

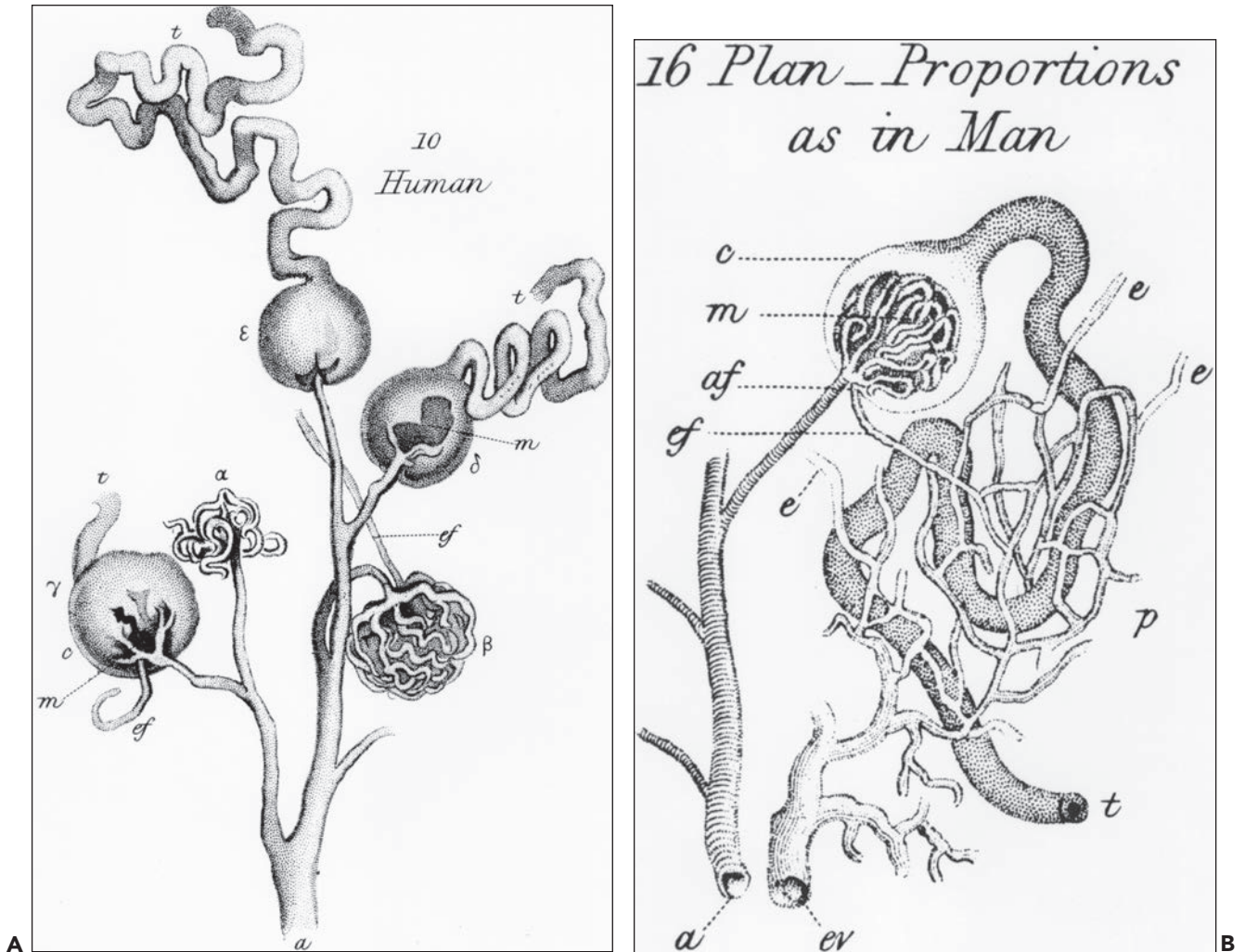


FIGURE 1.2 William Bowman's 1842 dye study. **A:** Illustration of the glomerular vascular supply. **B:** Illustration of the relationship between the efferent arteriole and peritubular capillary plexus and the proximal tubule. (From Bowman W. *Philos Trans R Soc Lond Biol* 1842;132:57.)

is a normal anatomic variant without functional consequences (22–24). In some of the kidneys, three subtle zones are created by two shallow superficial grooves that radiate from the hilum to the lateral border. The three regions correspond roughly to the upper pole, middle zone, and lower pole and usually reflect regions drained by the segmental veins.

The human kidney is a multipapillary type of mammalian kidney (Fig. 1.8). The cortex is continuous and undivided, and the medulla is discontinuous with individual pyramids that drain discrete regions of the associated cortex. Each lobe in a multipapillary kidney may be regarded as the counterpart of an entire unipapillary kidney, such as those in a rat or rabbit (22–24). Certain animals such as bears and whales have nonfused, multiple, unipapillary kidneys; each papilla is invested with the cortex that is autonomous in structure and function from its neighbors. The normal human kidney has a minimum of 11 to 14 lobes, each composed of a central conical medullary pyramid surrounded by a cap of cortex (22–31). Often, there are

six lobes in the upper pole and four lobes each in the middle zone and lower pole. By the 28th week of gestation, the number of renal lobes is established; however, with the subsequent increase in renal mass, a process of lobar fusion ensues. In the adult kidney, this reduces the number of renal pyramids and their corresponding calyces to 9 to 11. The pyramids, within their minor calyces, angle toward the major calyces and renal pelvis from a slightly anterior or posterior direction (Fig. 1.9) (26–28).

The lobar fusion affects pyramids in the polar region more than the midportion of the kidney, creating a mixed population of simple and compound pyramids that characterizes most human kidneys. Simple pyramids (Fig. 1.10) occur predominantly in the midpolar regions, drain a single lobe, and have a convex tip with slit-like openings of the ducts of Bellini, the area cribrosa. Compound pyramids are principally polar in location and drain two or more lobes (see Fig. 1.8). They have flattened to convex tips with rounded or gaping orifices of the

TABLE 1.1 Nomenclature of the kidney

Main divisions	Superficial nephron
Cortex	Midcortical nephron
Cortical labyrinth	Juxtamedullary nephron
Medullary ray	Short-looped nephron
Renal column (column of Bertin)	Long-looped nephron
Medulla	Nephron components
Outer medulla	Renal corpuscle
Outer stripe	Bowman capsule
Inner stripe	Glomerulus or glomerular tuft
Inner medulla	Parietal cell
Papilla	Peripolar cell
Renal pelvis	Podocyte
Pelvic cavity	Parietal podocyte
Major calyx	Endothelial cell
Minor calyx	Mesangial cell
Fornix	Mesangial matrix
Renal sinus	GBM
Renal hilum	Lamina rara interna
	Lamina densa
Vessels, nerves, and interstitium	Lamina rara externa
Renal vasculature	Urinary space (Bowman space)
Main renal artery and vein	Juxtaglomerular apparatus
Anterior and posterior arterial divisions	Granular cell
Segmental arteries: apical, upper, middle, lower, and posterior	Extraglomerular mesangium
Interlobar artery and vein	Extraglomerular mesangial cells (lakis cell, Goormaghtigh cell)
Arcuate artery and vein	Macula densa
Interlobular artery (cortical radiating) and vein	Tubular portion of the nephron
Perforating radial artery	Proximal tubule
Stellate vein	Proximal convoluted tubule
Afferent arteriole	Proximal convolutions (not synonymous with the PT)
Efferent arteriole	Straight part
Glomerular capillary	Loop of Henle
Peritubular capillary	Thin descending limb
Descending and ascending vasa recta	Thin ascending limb
Vascular bundle	Distal tubule
Interbundle capillary plexis	Thick ascending limb
Renal lymphatics	MD epithelium
Cortical	Distal convoluted tubule
Capsular	Distal convolutions (not synonymous with the DT)
Renal nerves	Connecting tubule
Renal interstitium	Collecting duct
Cortical	Cortical CD
Peritubular	Outer medullary CD
Periarterial	Inner medullary CD (duct of Bellini)
Medullary	
Nephron	
Nephron types	

ducts of Bellini, creating the potential for intrarenal reflux during urinary tract obstruction and infection (30,31).

The renal parenchyma consists of the granular brown cortex and the striated medulla (Fig. 1.10). The medullary pyramid is divided into an outer medulla, with an outer and inner stripe, and the inner medulla or papilla. In human beings, the relative volumes occupied by the cortex, outer medulla, and inner medulla are 70%, 37%, and 3%,

respectively (32). The renal cortex forms a 1.0-cm layer beneath the renal capsule and extends down between the renal pyramids forming the columns of Bertin. The midplane of a column of Bertin is the line of fusion of two renal lobes, with each half draining into adjacent pyramids. The bases of the pyramids have faint perpendicular cortical extensions, the medullary rays that contain the straight portion of the proximal tubules (PTs), thick ascending limbs (TALs), and

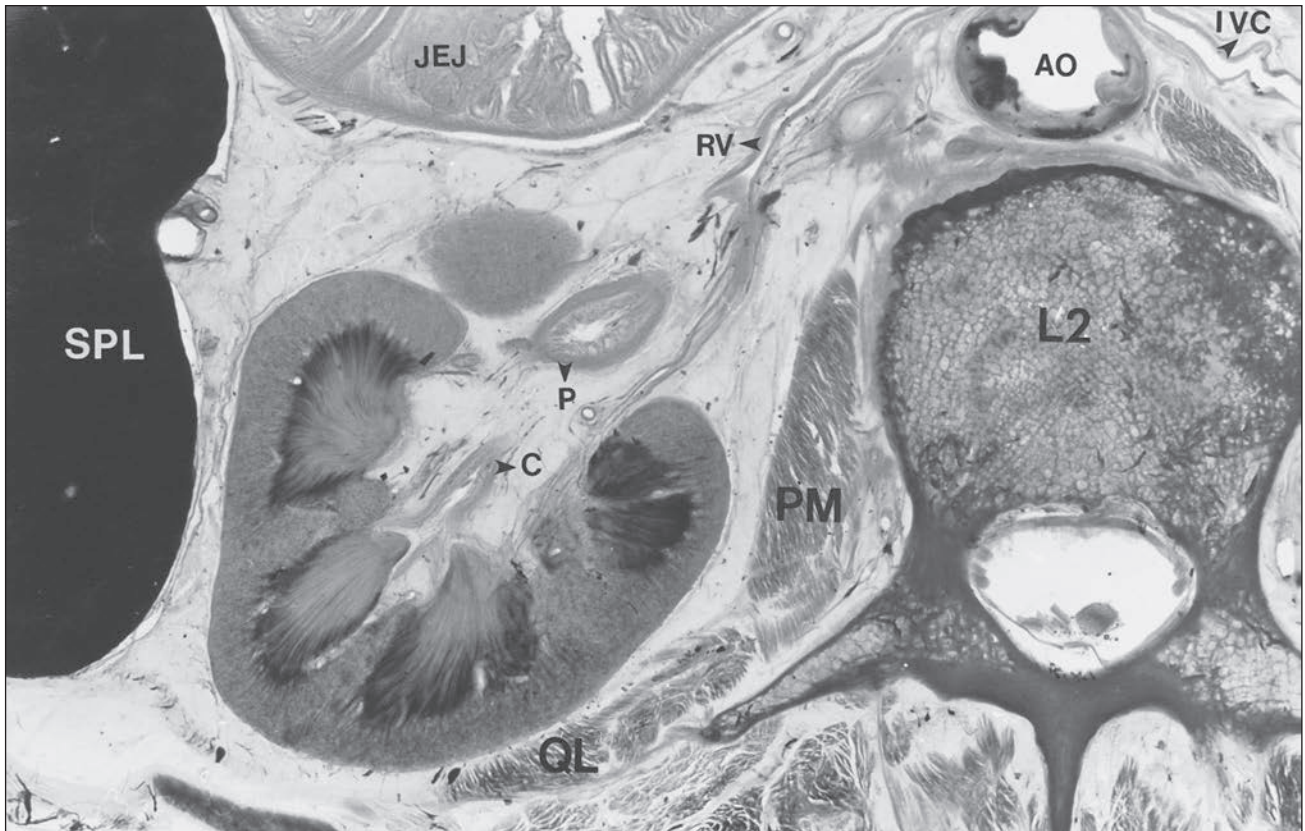


FIGURE 1.3 Cross section of a human cadaver at the level of the second lumbar vertebra viewed from above, demonstrating the relationships between the left kidney and adjacent organs. L2, second lumbar vertebra; AO, aorta; PM, psoas muscle; QL, quadratus lumborum muscle; SPL, spleen; JEJ, jejunum; C, calyx; P, pelvis; RV, renal vein; IVC, inferior vena cava.



FIGURE 1.4 Composite adult and newborn human kidneys. Notice the smooth subcapsular surface of the adult kidney and the prominent lobations of the newborn kidney.

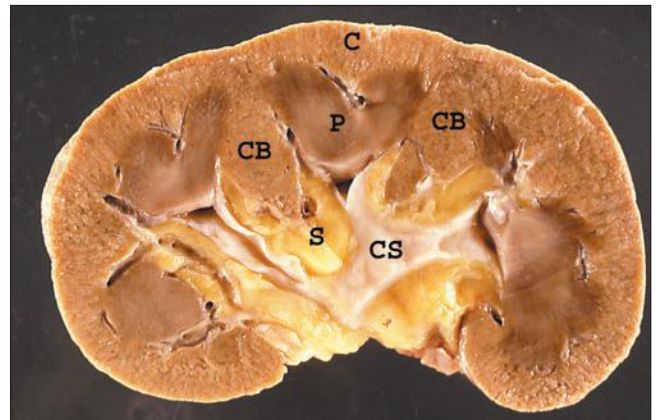


FIGURE 1.5 A hemisected human kidney shows the cortex (C) with columns of Bertin (CB) and renal pyramids (P). The renal papillae protrude into the minor calyces, which unite to form the major calyces. The collecting system (CS) is nestled within the fatty tissue of the renal sinus (S).

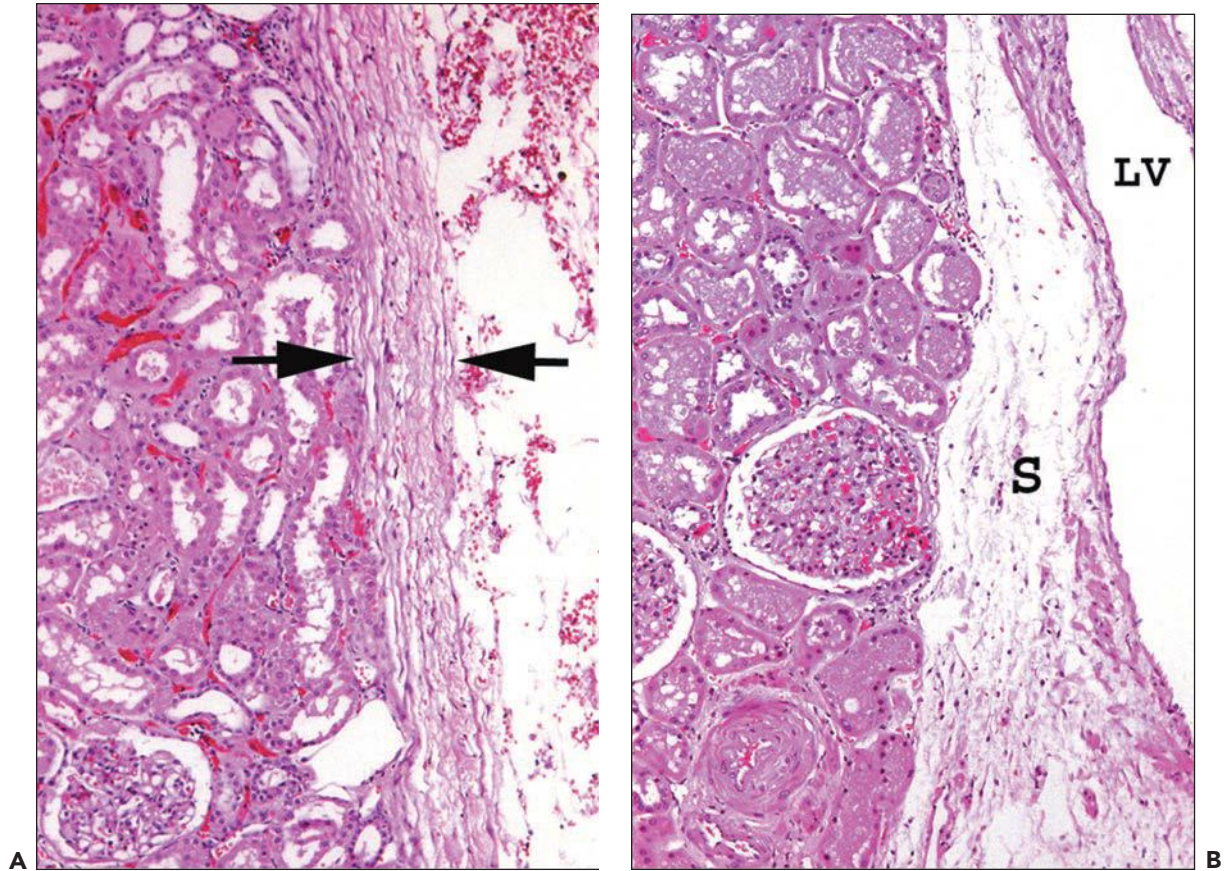


FIGURE 1.6 Human kidney. **A:** A dense connective tissue capsule (*between arrows*) separates the peripheral cortex from the perinephric fat ($\times 100$). **B:** The renal tubules and interstitium of the columns of Bertin have no connective tissue separation from the sinus (S) and its abundant lymphatics and vessels. ($\times 120$.) LV, lobar vein.

collecting ducts (CDs). The papilla protrudes into a minor calyx. Its tip, the area cribrosa (with cribriform appearance grossly), has from 20 to 70 openings of the papillary CDs (Bellini ducts); the large variation reflects simple versus compound pyramid arrangement (24,26,28).



FIGURE 1.7 Two normal adult human kidneys, one with retained lobations.

Renal Vasculature

The arterial supply to the kidneys follows a general blueprint. Knowledge of its details is useful in recognition of lesions resulting from an arterial abnormality (32–37). In 1901, Brödel first appreciated the distinctive renovascular segmentation of the kidney (33). The nomenclature currently in use was established by Graves (Fig. 1.11) in 1954 (34).

The main renal arteries arise from the aorta; the right artery is slightly longer and often arises slightly higher from the aorta than the left artery (33–35). Each main artery gives off a suprarenal artery to supply the adrenal glands and a ureteric artery to each ureter. The most common main renal arterial division pattern is to divide into anterior and posterior branches (Figs. 1.11 and 1.12) that give rise to five segmental renal arteries. Most commonly, the anterior branch gives rise to four segmental arteries: the apical, upper, middle, and lower segmental arteries. Two segmental arteries supply the middle anterior portions of the kidney, and two polar segmental branches supply both the anterior and posterior polar aspects of the kidney. The posterior branch continues as a fifth segmental branch, the posterior segmental artery, to supply the middle posterior portions of the kidney. However, deviation from this pattern is common. This may reflect variation in the origin of a segmental artery from

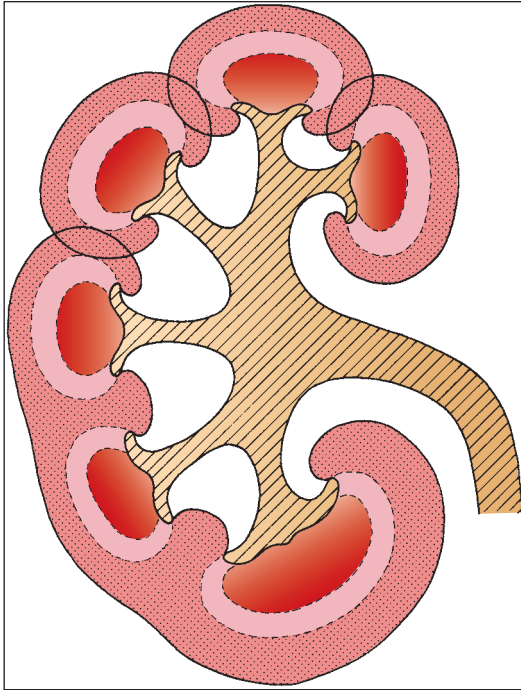


FIGURE 1.8 Diagram of the arrangement of the cortex and medulla in the human kidney and of its possible development.

Unipapillary kidney anlagen fuse to form a multipapillary kidney (upper part of the drawing). The interpyramidal cortical intrusions (septa of Bertin) reach down to the renal sinus. In addition to the fusion of the cortical tissue, pyramidal fusion occurs and is generally found in the polar regions (compound papilla, shown in the lower part of the drawing).

either anterior or posterior branches or arising separately from the aorta as an aberrant, accessory, or polar artery (Figs. 1.13 and 1.14), which occurs in 25% of the kidneys (32). Another variation is supply of the upper or lower pole by the posterior segmental artery or a branch from the posterior segmental artery.

From the five segmental arteries, the interlobar arteries, arcuate arteries, interlobular (cortical radiating) arteries, and arterioles are sequentially derived. All arteries are end arteries with no collateral blood flow. Thus, occlusion of a segmental artery or any of its subsequent branches results in infarction of the zone of parenchyma it supplies.

A segmental artery branches within the renal sinus, giving rise to several interlobar arteries. An interlobar artery pierces the parenchyma between the pyramid surface and a column of Bertin and forms a splay of six to eight arcuate arteries. The arcuate arteries curve along the corticomedul-lary junction and ascend up the lateral surface of the pyramid and over its basal surface to terminate at the midpoint of a renal lobe. Since the arcuate arteries do not anastomose, the central portion of the renal lobe is most susceptible to ischemic injury. At perpendicular or slightly oblique angles, the interlobular arteries (cortical radiating arteries) arise from an arcuate artery (Fig. 1.15) and may branch as they pass through the cortex toward the renal capsule. The interlobular arteries course between medullary rays and are encircled by tiers of five to six glomeruli, which they supply with an

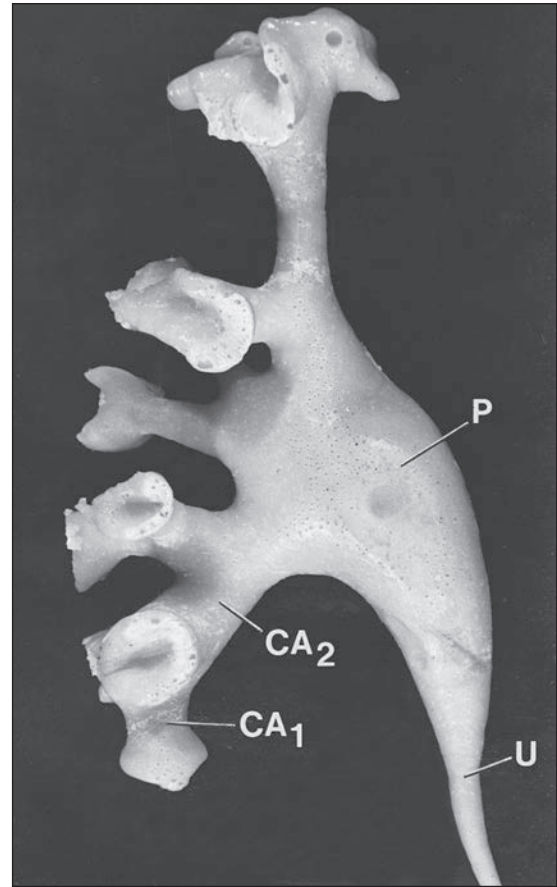


FIGURE 1.9 Minor calyces (CA_1) fuse to form major calyces (CA_2) that finally become the renal pelvis (P), which tapers to continue on as the ureter (U). Most calyces are angled toward the renal pelvis. Corrosion cast of a human renal pelvis. (From Sampaio FJB, Mandarim-De-Lacerda CA. 3-Dimensional and radiological pelvicaliceal anatomy for endourology. *J Urol* 1988;140:1352.)

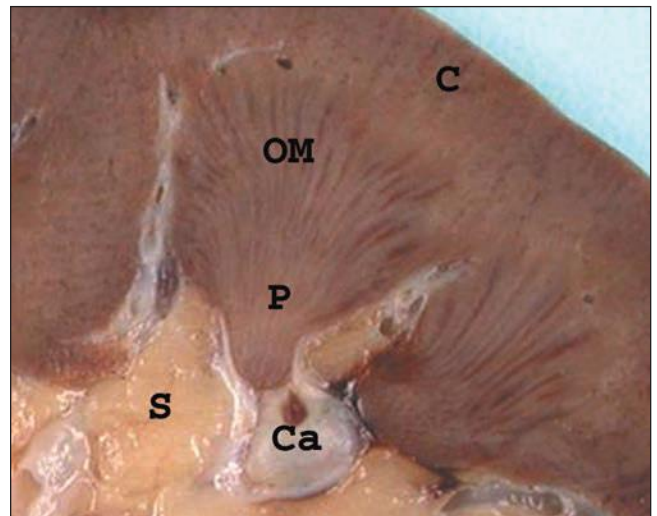


FIGURE 1.10 A simple human renal pyramid with a convex papilla (P) nestled within a minor calyx. S, sinus; OM, outer medulla; C, cortex; Ca, calyx.

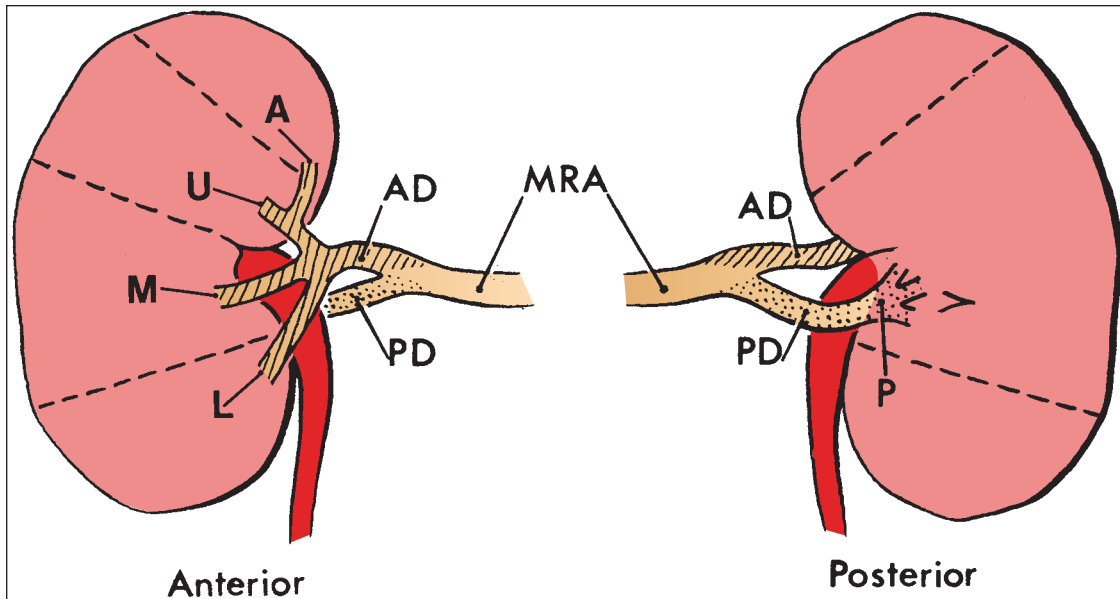


FIGURE 1.11 Diagram of the most common pattern of arterial supply to the kidneys demonstrating the main renal artery, anterior and posterior branches, and five segmental arteries. MRA, main renal artery; PD, posterior division; AD, anterior division. Segmental arteries are indicated by A (apical), U (upper), M (middle), L (lower), P (posterior). (Modified from Graves FT. The anatomy of the intrarenal arteries and its application to segmental resection of the kidney. *Br J Surg* 1954;42:132.)

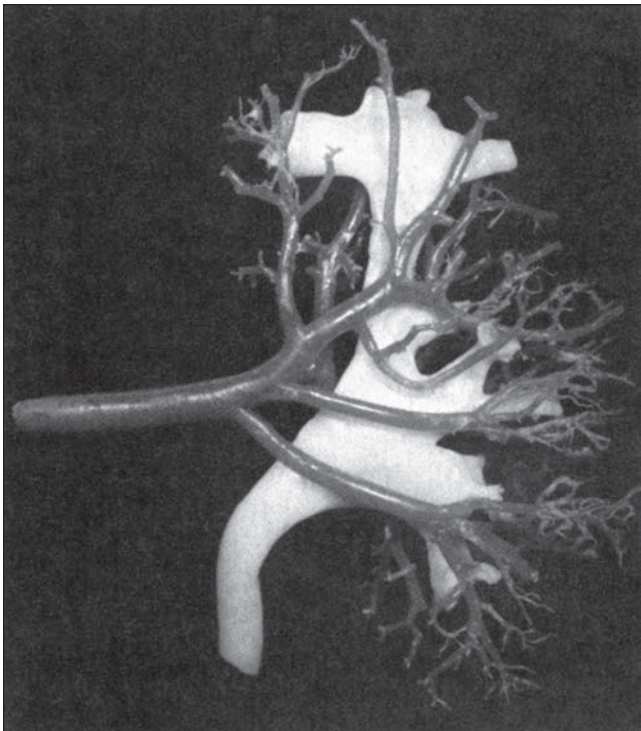


FIGURE 1.12 Cast of the arterial supply and collecting system of a human kidney. Notice the four anterior segmental arteries. (From Sampaio FJB, Aragao AHM. Anatomic relationship between the intrarenal arteries and the kidney collecting system. *J Urol* 1990;143:679.)

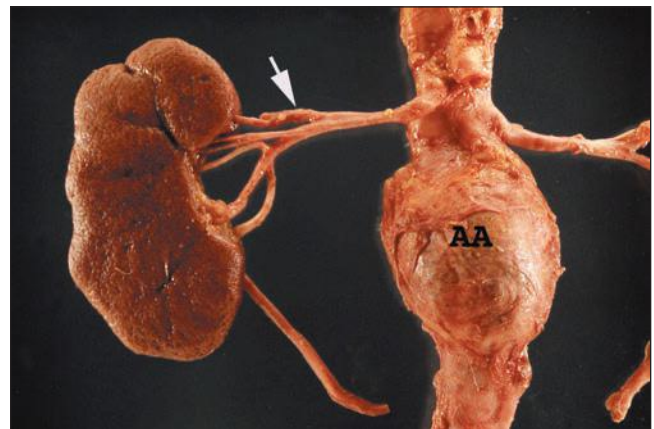


FIGURE 1.13 Human right kidney and aorta. The aorta has an aneurysm (AA). The main renal artery and its five segmental arteries are visible although not in the most common arrangement. The upper segmental artery branches first (arrow), and the posterior segmental artery appears to arise from the anterior group.

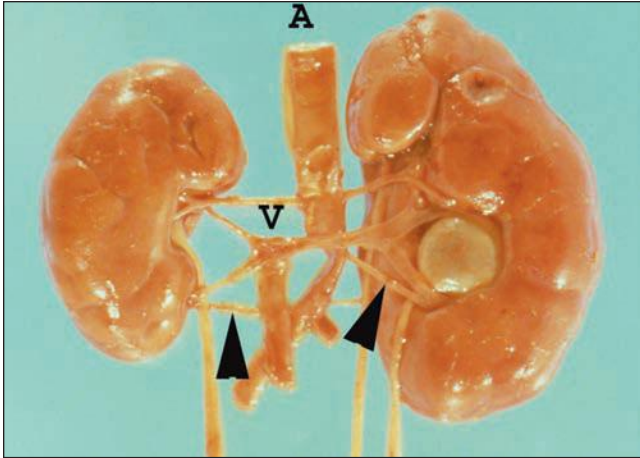


FIGURE 1.14 Newborn human kidneys. There are bilateral lower pole accessory (segmental) arteries (arrowheads). The crossing polar artery and segmental vein of the nonrotated duplex (two ureters) left kidney produced ureteropelvic junction obstruction. A, aorta; V, vena cava.

afferent arteriole (Figs. 1.15 and 1.16). The efferent arterioles, on exiting the glomeruli, form a portal system of capillaries that supplies the adjacent cortical tubules, or provides the main arteriolar flow to the renal medulla in the case of juxtamedullary glomeruli (Figs. 1.2B and 1.17; see Cortical Microvascularization section below). A few interlobular

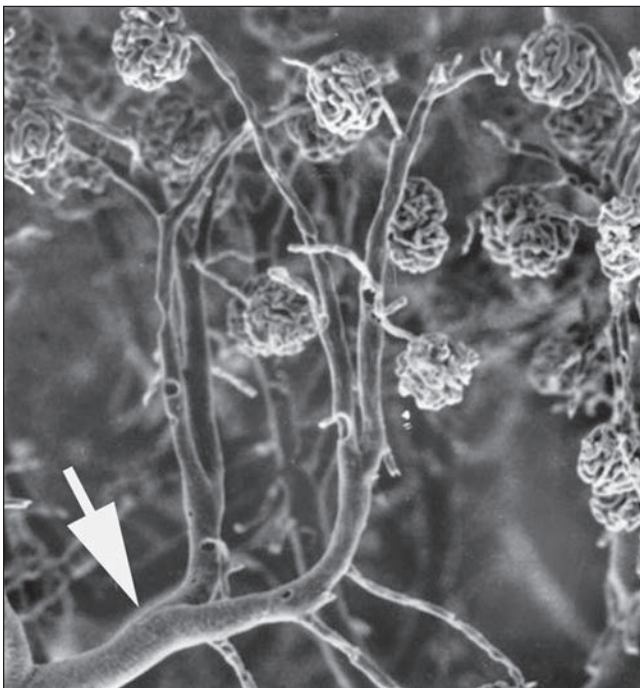


FIGURE 1.15 Arterial cast of the rat kidney. Two interlobular arteries give rise to arterioles that supply a single glomerulus. Arrow, arcuate artery. (From Gattone II VH, Evan AP, Willis LR, et al. Renal afferent arteriole in the spontaneously hypertensive rat. *Hypertension* 1983;5:8.)

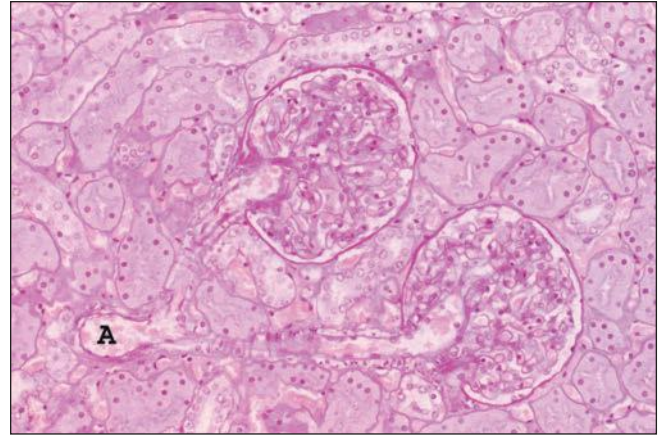


FIGURE 1.16 Normal human kidney. The interlobular artery (A) gives rise to two arterioles; each supplies one glomerulus. (PAS, $\times 200$.)

arteries reach the renal capsule and anastomose with branches of the suprarenal and gonadal arteries.

The renal medulla has a dual blood supply, originating in part from its corticomedullary base and in part from the lateral distal papilla (38). The principal blood supply arises

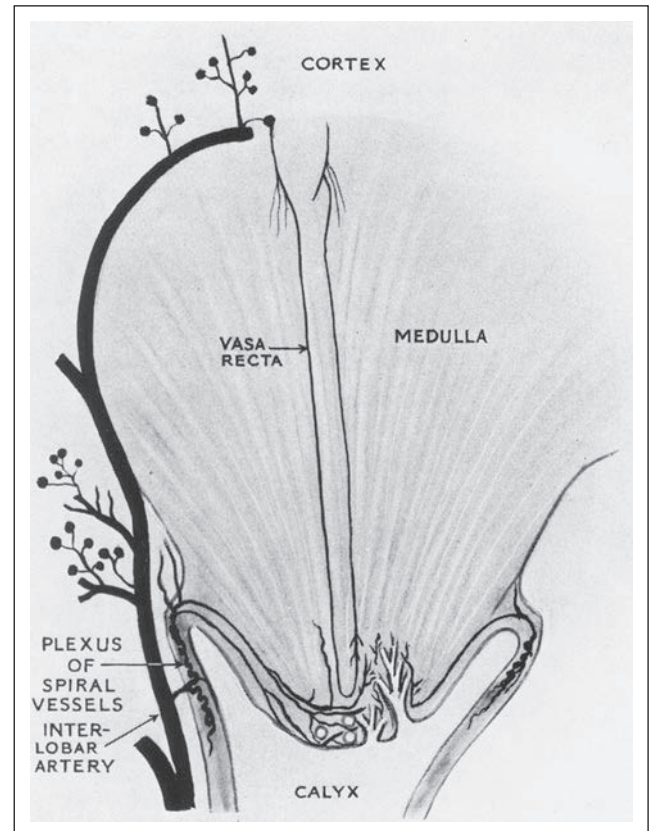


FIGURE 1.17 Diagram of the renal medulla showing its dual blood supply. (From Baker SB. The blood supply of the renal papilla. *Br J Urol* 1959;31:57. Reprinted from Wiley-Liss, Inc., Wiley Publishing Inc., a subsidiary of John Wiley & Sons, Inc., with permission.)

from juxtamedullary glomeruli. Their efferent arterioles course directly into the medulla, forming the descending vasa recta (Fig. 1.17). The second blood supply originates from an interlobar artery as it courses along a minor calyx. Several spiral artery branches enter the papilla at the calyceal fornices, sending arterioles to the papillary tip. These arterioles anastomose freely with arterioles from the opposite side, forming a plexus around the distal ducts of Bellini.

The major cortical venous return follows the arterial supply; the interlobular, arcuate, and interlobar veins run parallel to the arteries (Fig. 1.18) (39). A minority of veins originate as the stellate veins, draining the superficial cortex to join the arcuate veins. Unlike the arcuate and interlobar arteries, arcuate and interlobar veins are connected by abundant anastomoses and lateral tributaries that encircle the renal pyramids and calyces. Thus, the terms interlobar veins and intralobar veins are often used synonymously. The interlobar veins converge anterior to the pelvis and form two to three segmental veins that drain the three poles of the kidney and then unite to form the main renal vein. The convergence of the interlobar veins to form the main renal vein often occurs outside of the renal hilum. This is particularly common for the left main renal vein, which is substantially longer than the right main renal vein, because the vena cava lies to the right of the aorta (Fig. 1.19). No veins are located within the medulla.

Renal Lymphatic System

The kidneys have a dual lymphatic system (40,41). The major lymphatic drainage follows the vasculature. The lymphatics begin as small vessels in the adventitia of the peripheral interlobular (cortical radiating) arteries, enlarge, and become

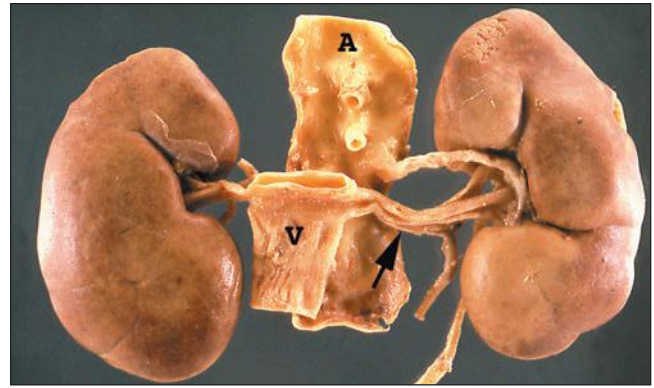


FIGURE 1.19 Human kidneys with aorta (A) and vena cava (V). The left main renal vein (arrow) is much longer than the right main renal vein.

more numerous as they descend to the corticomedullary junction and enter the renal sinus (Fig. 1.20). In humans, there are no lymphatic vessels amid the glomeruli and renal tubules, although some animals (e.g., dogs) appear to have periglomerular and periarteriolar lymphatics (40,41). During inflammatory processes, lymphatic neovascularization within the cortical labyrinth has been documented (42). With the recent identification of immunohistochemical markers specific for lymphatic endothelium, more will be learned about the dynamics of cortical lymphatics (43). Lymph eventually exits through the hilum and terminates in hilar and lateral paraaortic lymph nodes.

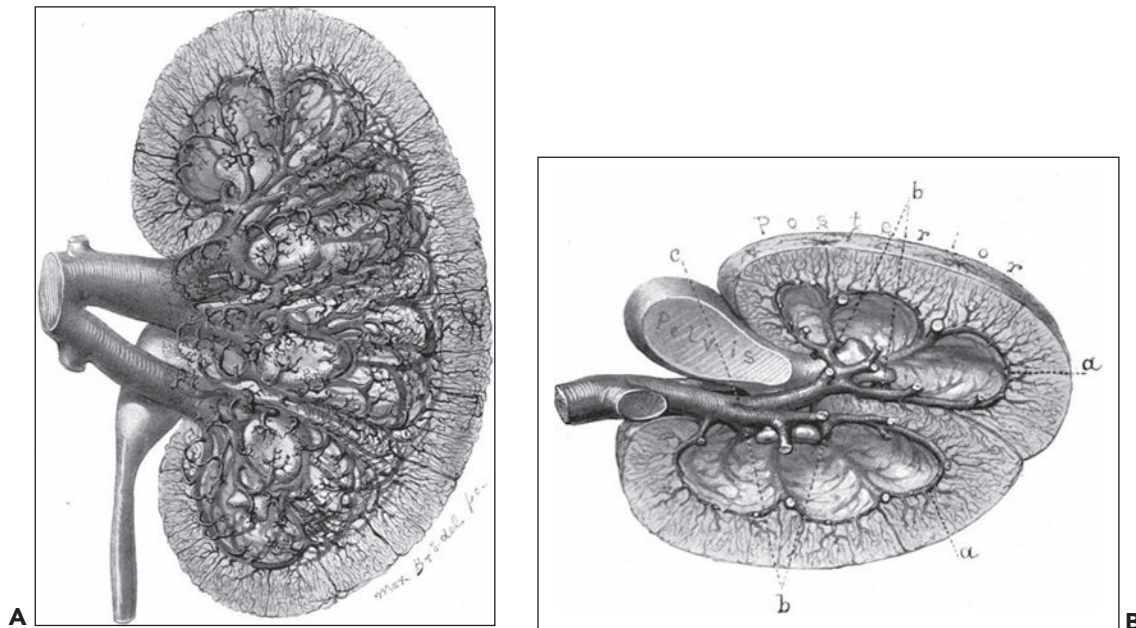


FIGURE 1.18 Brödel's 1903 artist's rendition of the human kidney following celloidin injection with tissue digestion, demonstrating details of the lush venous return. **A:** Anterior view of the left kidney. For the sake of clearness, the small veins of the cortex of the anterior portion have been omitted. **B:** The transverse section viewed from above. There is no collecting vein posterior to the renal pelvis; all of the veins of the posterior region cross over to the anterior portion between the necks of the minor calyces (b) to join the veins of the anterior region at a point indicated by c. (Brödel M. The intrinsic blood vessels of the kidney and their significance in nephrotomy. *Johns Hopkins Hosp Bull* 1901;118:10.)

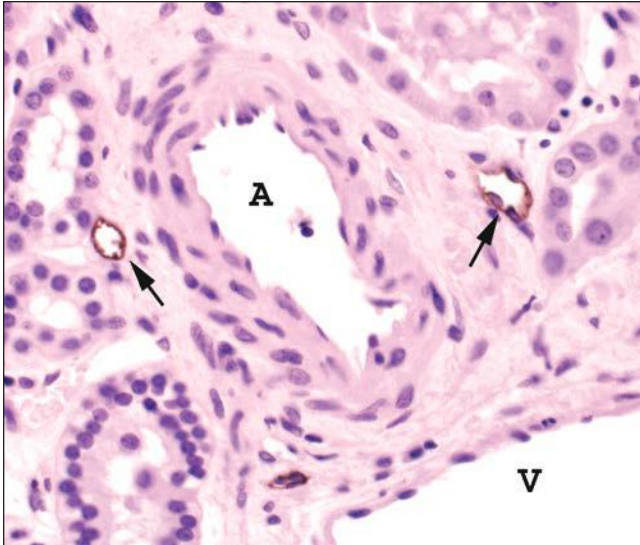


FIGURE 1.20 Human interlobular arteries and lymphatics. Adjacent to an interlobular artery (A) are several small lymphatics (arrows). These will converge and progressively enlarge as they drain toward the medulla. The lymphatic endothelium is stained for podoplanin, a lymphatic endothelial cell marker. V, vein (Immunoperoxidase stain for podoplanin, $\times 400$.)

The second separate lymphatic system exists within the renal capsule. It receives drainage from the most superficial cortex. Lymph courses along the capsule and around to the hilum to join the major lymphatic flow exiting the renal sinus. Valves present in the capsular system prevent retrograde flow back to the cortex. The capsular lymphatic system normally contributes little to lymph flow. However, under certain conditions such as urinary tract obstruction, it becomes the principal pathway for lymphatic flow (41).

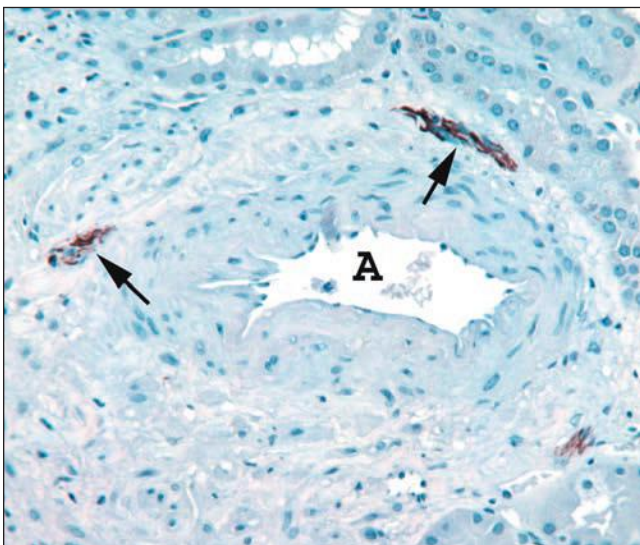


FIGURE 1.21 Human interlobular artery. The adventitia of this artery (A) contains three small nerves stained for neurofilament (arrows). (Immunoperoxidase stain for neurofilament.)

Renal Innervation

The celiac plexus sends sympathetic fibers via splanchnic nerves to synapse with ganglia in the renal plexus. Nerve fibers extend from the plexus to accompany the arterial system (Fig. 1.21) as it ramifies throughout the cortex (44–47). This system innervates the renal vasculature and extensively innervates the juxtaglomerular apparatus (JGA). Animal studies show that nerve fibers continue along with efferent arterioles and the descending vasa recta until they lose their smooth muscle layer. Nerve terminals also innervate cortical tubules, most concentrated in the pre-JGA thick ascending limb of Henle (Fig. 1.22). Sensory fibers from the kidney travel along the sympathetic pathways to T10–11, accounting for the flank location of renal-derived pain impulses.

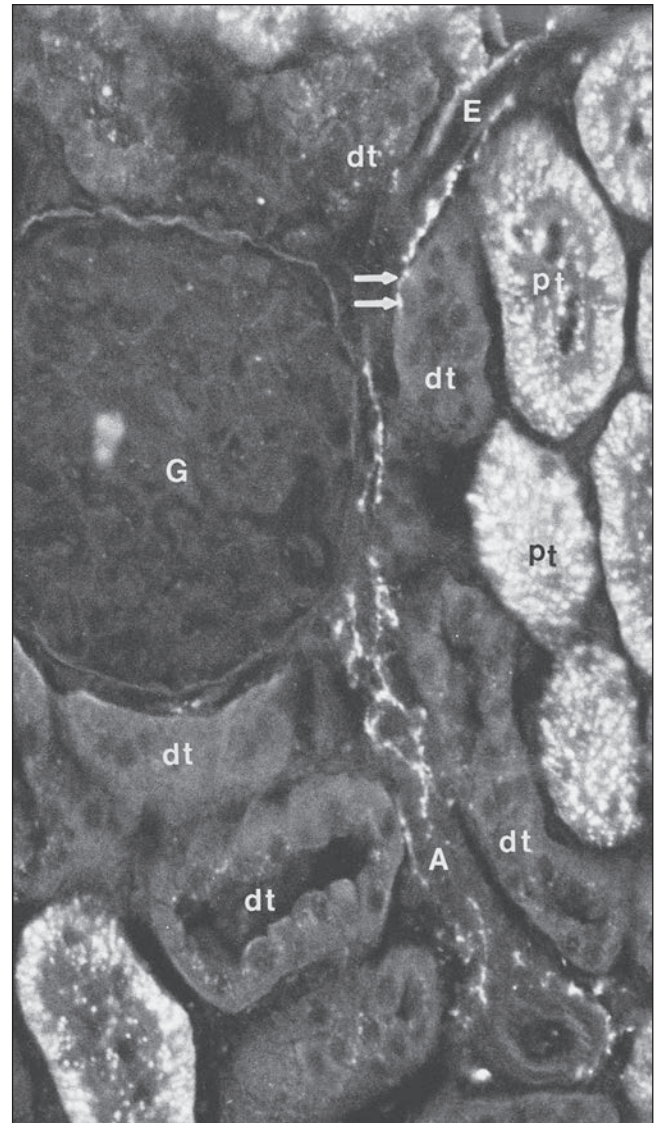


FIGURE 1.22 Nerve fibers viewed by catecholamine fluorescence histochemistry are seen along the afferent (A) and efferent (E) arterioles of the rat kidney. A spot of fluorescence (arrows) appears adjacent to a distal tubule (DT). G, glomerulus; PT, proximal tubule. ($\times 306$.) (From Barajas L. Innervation of the renal cortex. *Fed Proc* 1978;37:1192.)

Calyces and Renal Pelvis

The renal collecting system consists of the calyces, the sac-like renal pelvis, and the ureter (see Figs. 1.9 and 1.12) (48–51). The calyces and a portion of the renal pelvis are enveloped by the renal sinus fat. The most proximal portions of the collecting system are 9 to 11 funnel-shaped minor calyces that surround the individual papillary tips, both simple and compound (see Fig. 1.10). They have slender most proximal extensions termed *fornices*. The number of pyramids exceeds the number of calyces because of pyramid fusion. The major calyces represent the confluence of the minor calyces and unite to form the renal pelvis, which represents the expanded upper portion of the ureter. There is no distinct delineation between the pelvis and the ureter; rather, a gradual transition occurs.

The renal calyces and pelvis have a continuous muscular wall. Some smooth muscle fibers begin in the proximal fornices at the base of the papillae and extend along the calyces to the pelvis and ureter. In addition, there is a ring of smooth muscle that encircles the base of the pyramid. Pacemaker cells located in the most proximal fornix appear to initiate rhythmic peristaltic waves, 2 to 3 per minute, that aid urine movement toward the bladder (48–51). It has been proposed that

during the rhythmic contractions, the ring of muscle fibers compress the papillae creating positive and negative pressures (40,41). With contraction, the papilla is elongated, and its diameter decreases by 20%. Fluid is forced along the ducts of Bellini to the papillary tip, and the vasa recta capillaries collapse. Fluid is also forced into the collapsed CD cells. With relaxation, the negative pressure moves fluid from the CD cells into the interstitium and then into the descending and ascending vasa recta capillaries. Blood flow resumes first in the descending vasa recta capillaries and then in the ascending vasa recta capillaries, moving the water forward and thus contributing to the concentration mechanism of the renal papilla.

The collecting system is lined by a unique epithelium known as *transitional epithelium* or *urothelium*. This epithelium is specialized to adapt to pelvic distension with major changes in volume of the collecting system. Urothelium is also impermeable to withstand the chemical environment of the urine, which fluctuates tremendously in chemical composition. The urothelium is thinner in its initial portions in the minor calyces but usually has five or six cell layers in the non-distended pelvis and ureter. It is covered by a superficial layer of large rounded cells, the umbrella cells. The urothelium rests on

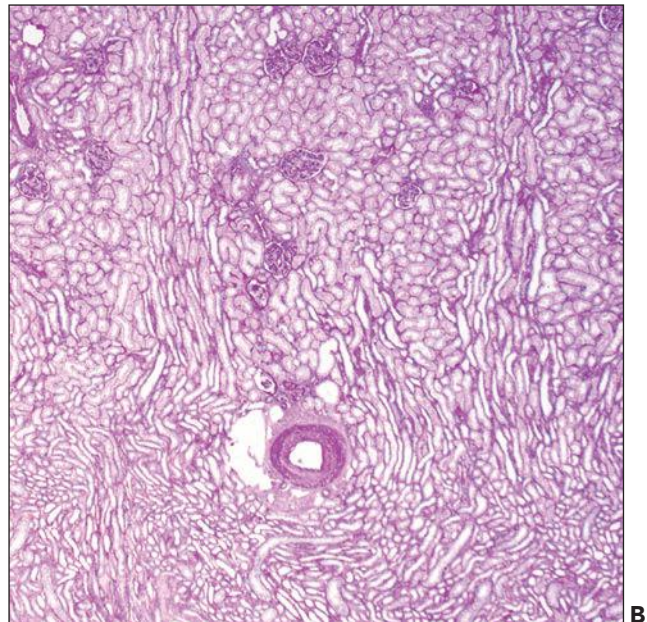
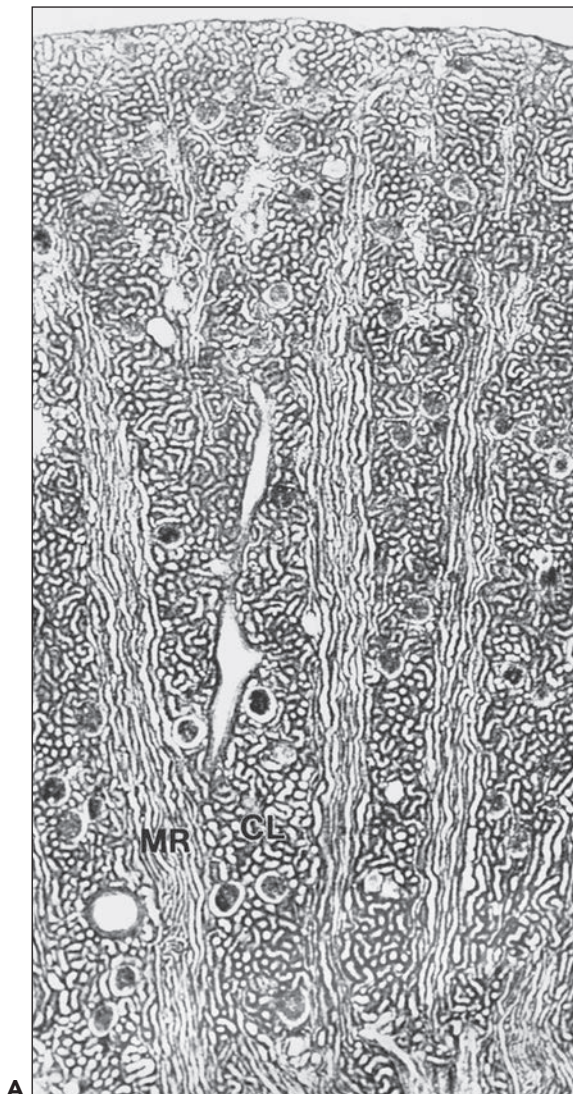


FIGURE 1.23 **A:** Longitudinal section through the cortex of a human kidney demonstrates the arrangement of the cortical labyrinth (CL) and the medullary rays (MRs). The cortical labyrinth contains the interlobular vessels and the glomeruli together with the convoluted tubules; the medullary rays contain the straight tubular portions and collecting ducts. (Paraffin section, $\times 75$.) **B:** This section from a human kidney shows two medullary rays with their longitudinally oriented tubules. An artery and glomeruli are centrally located within the cortical labyrinth between the two medullary rays. Notice that the tubules of the outer stripe of the outer medulla located beneath the artery appear similar to those in the medullary rays. (Periodic acid-Schiff, $\times 20$.)

a loose vascularized connective tissue layer, the lamina propria, with an underlying thin muscularis propria.

ARCHITECTURAL ORGANIZATION OF THE CORTEX AND MEDULLA

Cortical Labyrinth and Medullary Rays

The cortex of the human kidney is approximately 1 cm thick (excluding the column of Bertin) (see Figs. 1.5 and 1.10). It is organized into two architectural regions: the cortical labyrinth and the medullary rays (Figs. 1.23 and 1.24) (17,52–61). The cortical labyrinth contains the glomeruli, proximal, and distal convoluted tubules (DCTs), connecting tubules (CTs), and the initial portion of the CDs, as well as interlobular arteries and veins, arterioles, venules, capillaries,

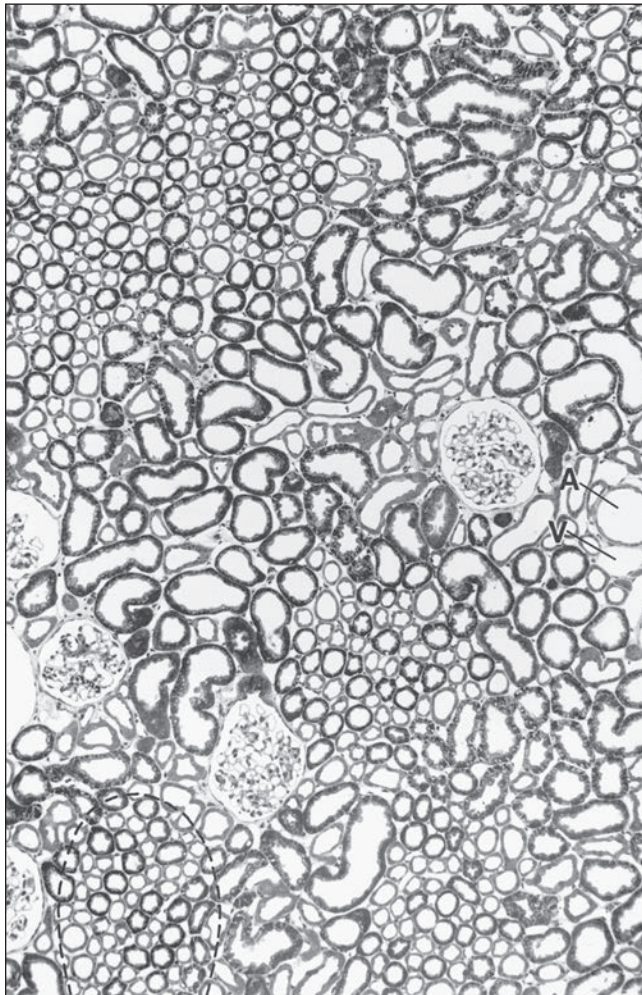


FIGURE 1.24 Cross-section (1- μm section of Epon-embedded tissue) through the cortex of the human kidney. In the cortex, the cortical labyrinth can clearly be delineated from the medullary rays (the cross section of one ray is marked by a *dashed line*). Within the labyrinth, the interlobular vessels (A, artery; V, vein), the glomeruli, and the convoluted tubular segments are found. The medullary rays contain the straight tubular segments and collecting ducts. ($\times 140$.)

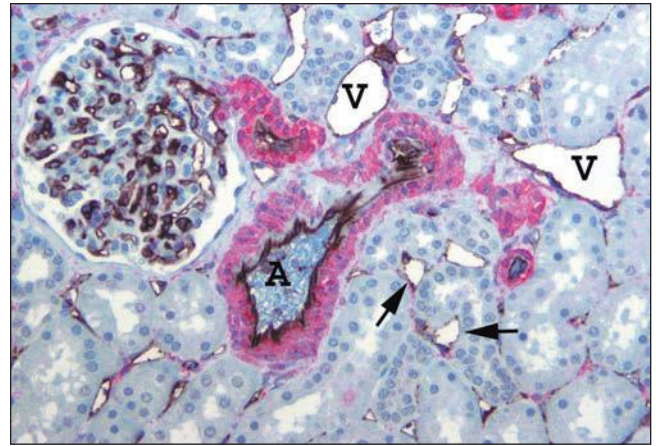


FIGURE 1.25 Human renal cortical labyrinth. The cortical labyrinth contains glomeruli, vessels, and tubules, mostly proximal tubules. The tubules have closely apposed basement membranes with little interstitial space, largely occupied by peritubular capillaries (*arrows*). The smooth muscle of the interlobular artery (A) and arterioles is stained red for smooth muscle actin. The veins (V) have very thin walls lacking smooth muscle. The endothelial cells of glomeruli, peritubular capillaries (*arrows*), and larger vessels are stained black for an endothelial marker, CD31. ($\times 150$.)

and lymphatics (Fig. 1.25). The principal components of the labyrinth, by volume, are the proximal convoluted tubules. In the normal cortex, the tubules are closely packed with their basement membranes (BMs) in close apposition. The interstitial space is scant and contains the peritubular capillary plexus and interstitial cells.

The medullary rays are elongated conical regions faintly visible in optimal planes of section of the renal cortex (see Fig. 1.10). Their name derives from the tubular segments they carry that are identical to those of the outer stripe of the outer medulla. They are, in effect, projections of medullary tissue into the cortex (see Fig. 1.23B). The medullary rays are aligned perpendicular to the corticomedullary junction. They form from the confluence of parallel arrays of CDs and the proximal and distal straight tubules of the superficial and midcortical nephrons as they course down into, and back up from, the medulla. The straight tubules of the superficial nephrons are in the central portion of a medullary ray; straight tubules from the deeper nephron form the outermost layers.

Renal Lobule

There are two anatomic versions of the renal lobule (17,52–56). In one version, the nephrons that empty into the CDs of a single medullary ray constitute a lobular unit. A general sense of the lobular organization is apparent in well-oriented histologic sections perpendicular to the medullary rays and parallel to the capsular surface (see Fig. 1.24). The other concept of a renal lobule is based on vascularization relationships. In this viewpoint, the interlobular artery is the center of the lobule, which then includes the nephrons it supplies (see Fig. 1.16). Its borders would be the CDs within the medullary rays. In both concepts of a renal lobule, the limits of the lobule are indistinct because there is no connective tissue separation from an adjacent lobular unit.

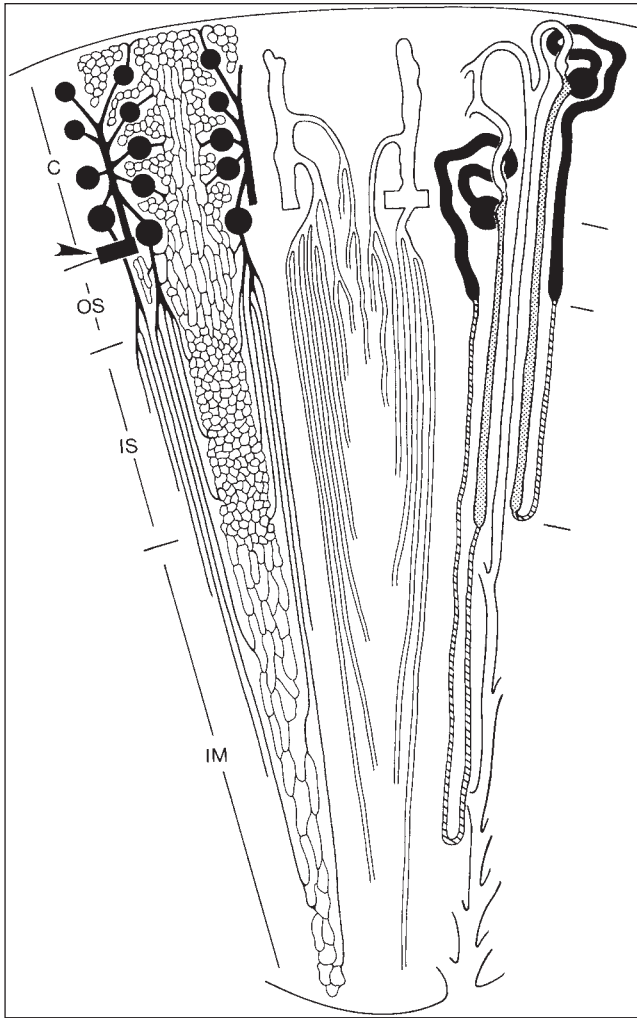


FIGURE 1.26 Schematic diagram of microvasculature and nephrons (not drawn to scale). C, cortex; OS, outer stripe; IS, inner stripe; IM, inner medulla. *Left:* Arterial vessels and capillaries. An arcuate artery (arrowhead) gives rise to an interlobular artery (cortical radial artery) from which afferent arterioles originate. Efferent arterioles from superficial and midcortical glomeruli split off into the cortical peritubular capillaries. Efferent arterioles of juxtamedullary glomeruli descend into the outer stripe and divide into the descending vasa recta, which supply the different capillary plexuses in the medulla. Middle: Venous vessels. Interlobular veins start in the superficial cortex. Stellate veins (characteristically found in the human kidneys), which begin on the renal surface, are not shown. The deep portions of interlobular veins and arcuate veins accept the ascending vasa recta, which drain the venous blood from the medulla. Ascending vasa recta and descending vasa recta together establish the vascular bundles. Note the dense pattern of ascending recta traversing the outer stripe as wide, tortuous channels. *Right:* A short- and a long-looped nephron together with a collecting duct. Glomeruli and proximal tubules are drawn black. Thin limbs are hatched; thick limbs are dotted. Distal convoluted tubules, connecting tubules (including an arcade), and collecting ducts are white. This drawing allows for the correlation of the location of tubules and vessels; the left, middle, and right views should be imagined as being superimposed on each other.

Cortical Microvascularization

The gross vasculature and general aspects of the initial portions of renal vascularization have been previously described. The microvascularization of the kidney (tubulovascular relationships) has been studied with various injection techniques, coupled with microscopic, ultrastructural, and radiographic techniques in many species. They show a similar pattern of organization (55–61).

The microvascularization of the cortex begins with the glomerular afferent arteriole (Figs. 1.26 and 1.27). The afferent arteriole enters the renal corpuscle at the hilum and immediately branches to form the capillary loops of the glomerular tuft; these loops ultimately converge to become the efferent arteriole. The efferent arterioles of the superficial and midcortical

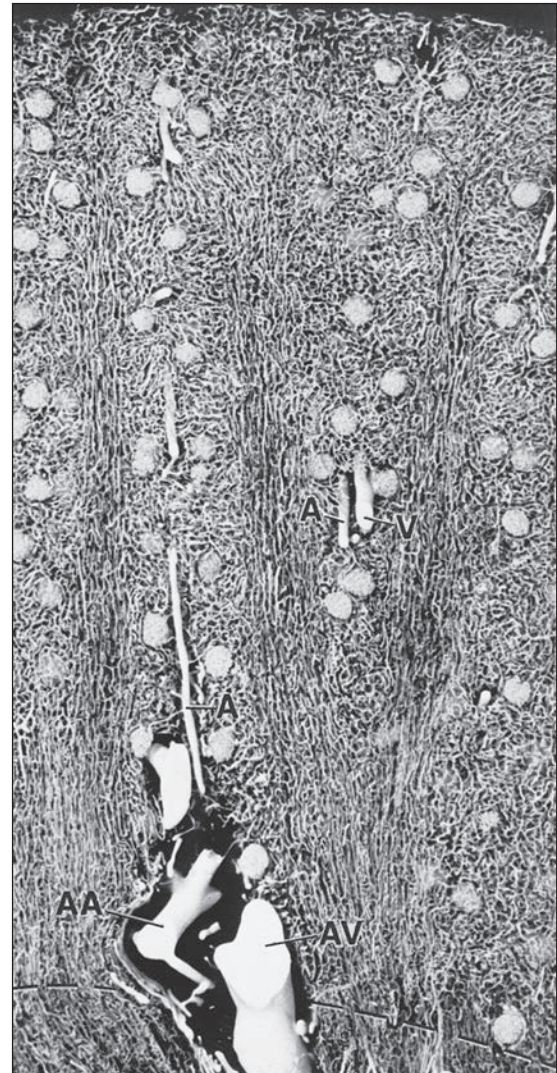


FIGURE 1.27 Longitudinal section through the cortex of a human kidney. The arteries have been injected with silicone rubber (Microfil). The different capillary patterns of the cortical labyrinth and of the medullary rays are visible. Within the cortical labyrinth, the interlobular (cortico-radial) arteries (A) and veins (V) as well as the glomeruli are found. Within the medullary rays, the capillary plexus consists of elongated meshes. ($\times 70$.) AA, arcuate artery; AV, arcuate vein.

nephrons are short and quickly transition into a peritubular capillary plexus that forms a uniformly distributed anastomosing vascular lattice amid the cortical tubules of the labyrinth. In the medullary rays the capillary plexus assumes a more longitudinal orientation, following the course of the straight tubules. The efferent arterioles of the deep or juxtamedullary glomeruli descend into the medulla as discussed below.

The tubules of the superficial glomeruli are perfused by capillaries derived from their efferent arterioles, whereas in the midcortical nephrons, efferent arterioles perfuse both tubules

of their originating nephron and tubules of adjacent nephrons. Since the efferent arterioles of the juxtamedullary nephrons enter the renal medulla, tubules of these nephrons are perfused by efferent arterioles of midcortical glomeruli. The peritubular capillary plexus of the cortex drains first from the medullary rays into the labyrinth and then enters small venules that converge and continue on as the major venous drainage previously discussed.

Medulla

The medulla is divided into an outer medulla, composed of an outer stripe and an inner stripe, and the inner medulla or papilla (Figs. 1.26 and 1.28). The anatomic limits of each region are defined by their differing tubular composition (Table 1.2). They also exhibit unique and physiologically important tubulovascular relationships (52–56,62–66).

Outer Medulla

OUTER STRIPE

The outer stripe is the thinnest portion of the renal medulla in humans but is thicker in other animals such as in the rat's unipapillary kidney (Fig. 1.29). The outer stripe contains the continuation of the straight portion of the PTs, CDs, and thick ascending limbs of Henle. The straight portion of the PTs and ascending thick limbs of the juxtamedullary nephrons are closest to the vascular bundles (Figs. 1.30 and 1.31). These are surrounded by the straight portion of the PTs and ascending thick limbs of the mid- and superficial nephrons. Farthest from the vascular bundles are the CDs, which reside in the interbundle zone.

INNER STRIPE

The beginning of the inner stripe is defined by transition of the straight portion of the PT into the thin descending limb of Henle (Figs. 1.28 and 1.32). The short-looped nephrons of the superficial and midcortex loop around to return to the cortex at various levels in the inner stripe. The vascular bundles beginning to aggregate in the outer stripe become well defined in the inner stripe (Fig. 1.33).

The tubulovascular organization of the inner stripe shows species variation that affects urine-concentrating ability. In humans and other species such as rabbits, pigs, and

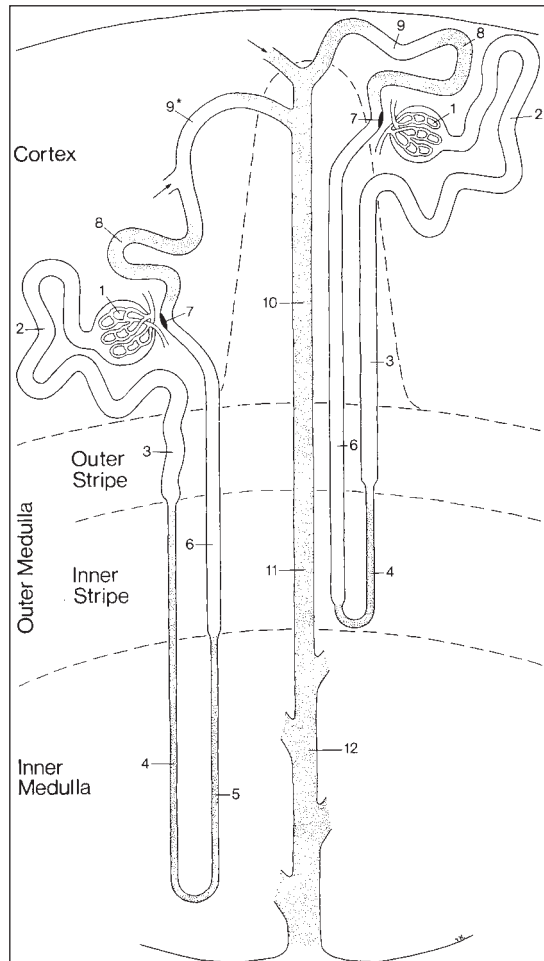


FIGURE 1.28 Schematic drawing of the nephron. This scheme depicts a short-looped and a long-looped nephron together with the collecting system. Not drawn to scale. Within the cortex, a medullary ray is delineated by a *dashed line*. 1: Renal corpuscle including Bowman capsule and the glomerulus (glomerular tuft). 2: Proximal convoluted tubule. 3: Proximal straight tubule. 4: Descending thin limb. 5: Ascending thin limb. 6: Distal straight tubule (thick ascending limb). 7: Macula densa located within the final portion of the thick ascending limb. 8: Distal convoluted tubule. 9: Connecting tubule. 9*: Connecting tubule of the juxtamedullary nephron that forms an arcade. 10: Cortical collecting duct. 11: Outer medullary collecting duct. 12: Inner medullary collecting duct. (From Kriz W, Bankir L, Bulger RE, et al. A standard nomenclature for structures of the kidney. The Renal Commission of the International Union of Physiological Sciences. *Kidney Int* 1988;33:1.)

TABLE 1.2

Tubular segments within each zone of the medulla

Outer stripe	Straight part of the proximal tubule (pars recta) Thick ascending limb of Henle Collecting ducts
Inner stripe	Thin descending limb Henle Thick ascending limb of Henle Collecting ducts
Inner medulla	Thin descending limb of Henle Thin ascending limbs of Henle Large collecting ducts (ducts of Bellini)

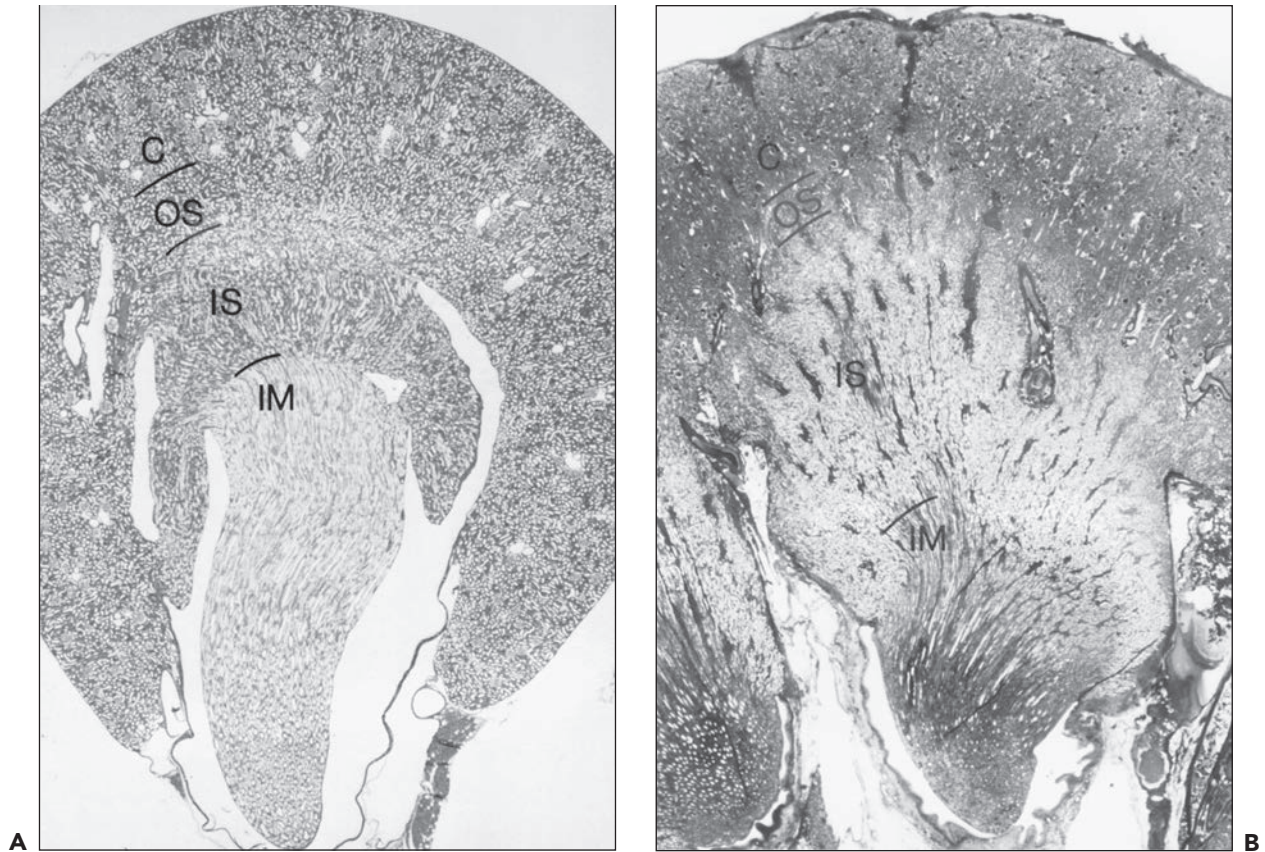


FIGURE 1.29 Longitudinal sections (with respect to the papilla) through a unipapillary kidney (rat) **(A)** and a single papilla of a multipapillary kidney (human) **(B)**. Note the different proportions of the individual zones. The outer stripe in the human kidney is very narrow, and the inner stripe is thick. (Paraffin sections, **A**: $\times 10$; **B**: $\times 3$.) C, cortex; OS, outer stripe; IS, inner stripe; IM, inner medulla.

monkeys, the vascular bundles are of the simple type, and the tubulovascular relationships of the outer stripe are maintained in the inner stripe. The descending thin limbs (DTLs) and ascending thick limbs of the long-looped juxtamedullary nephrons are situated close to the vascular bundle, whereas the DTLs and ascending thick limbs of the short-looped nephron and the CDs are more peripheral (Fig. 1.33). In other species, such as rat, mouse, and desert rodents, the vascular bundles are of the so-called complex type. In this type, DTLs of short-looped nephrons leave the interbundle region and curve toward the vascular bundles, intermingling with ascending vasa recta. The thick limbs of both short- and long-looped nephrons and the thin limbs of long-looped nephrons remain in the interbundle region with CDs. These histotopographic differences in tubulovascular relationships generally correlate with urinary concentration ability. However, exceptions do occur such as in the hamster with its simple vascular bundles and high concentration capacity.

Inner Medulla (Papilla)

The inner medulla is defined as the point at which the thin ascending limb of Henle of the long-looped nephrons transforms into the thick ascending limbs of Henle. The inner

medulla therefore contains the thin descending and thin ascending limbs of Henle derived from the long-looped nephrons of the deep cortex and the CDs (ducts of Bellini) (Figs. 1.28, 1.34, and 1.35). Since the short-looped and long-looped nephrons make their looping return back toward the cortex at various levels in the inner stripe of the outer medulla and the inner medulla, respectively, the absolute number of tubules decreases, which accounts for the tapering of the medulla toward the papillary tip. In parallel, the confluence of CDs with descent through the medulla results in a progressive increase in CD size from the outer medulla to the papillary tip. In animals with higher concentrating need, the inner medulla progressively increases in size relative to the rest of the kidney. At the papillary tip, the area cribrosa, the rest of Bellini epithelium transforms into the urothelium of the collecting system.

The vascular bundles become attenuated in the inner medulla as they lose their muscular investments and progressively decrease in number. The CDs remain peripheral to the vascular elements, and the thin descending and thin ascending limbs are interspersed within the vasculature. Near the papillary tip, the vasa recta disappear. The interstitial space increases distally, and interstitial cells become increasingly prominent (Fig. 1.35).

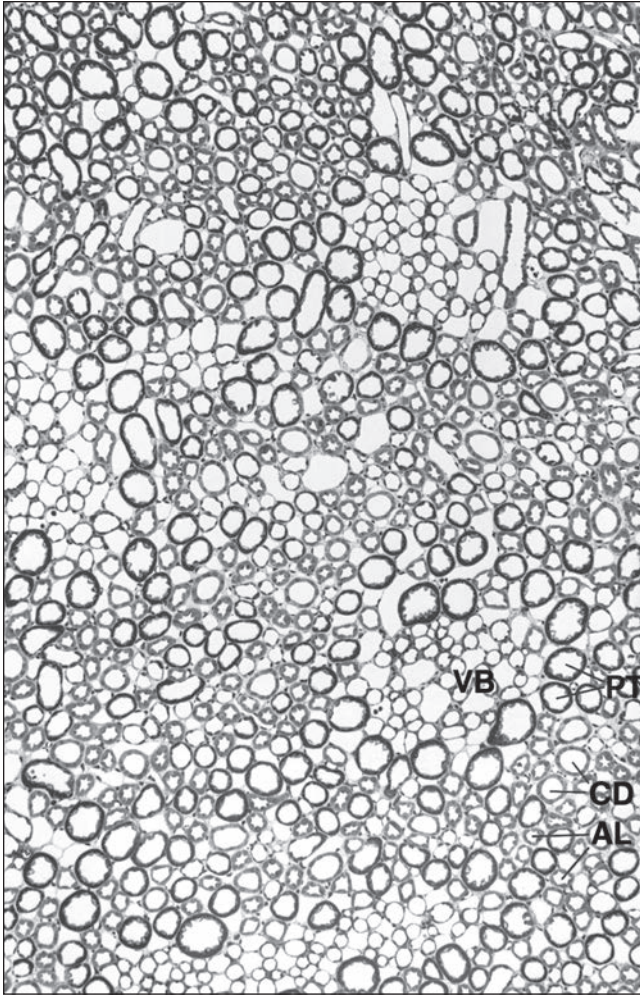


FIGURE 1.30 Cross section (1- μm section of Epon-embedded tissue) through the outer stripe in the outer medulla. The tubules are arranged around the vascular bundles (VB). In the vicinity of the bundles, the nearest segments are the straight proximal and distal tubules of the juxtamedullary nephrons. More peripherally located to them are the straight proximal and distal tubules of midcortical and superficial nephrons; the collecting ducts are lying distant from the bundles. ($\times 140$.) PT, proximal tubule; AL, ascending limb (straight parts of distal tubule); CD, collecting duct.

Medullary Microvascularization

The medullary blood supply has two sources as previously mentioned: the efferent arterioles of the juxtamedullary nephrons and arteriolar branches from the spiral arteries that are derived from the interlobar arteries and supply the papillary tip (see Figs. 1.17 and 1.26). There are no arteries, veins, or lymphatics within the renal medulla (62–66).

The principal blood supply to the medulla derives from efferent arterioles of the juxtamedullary glomeruli. The efferent arterioles begin as a splay of arterioles that descend toward the medulla, where they branch in the outer stripe. A few branches provide a capillary plexus to the tubules of the outer stripe, although most continue on into the inner stripe. They converge as the *descending arteriolar rectae*, forming organized

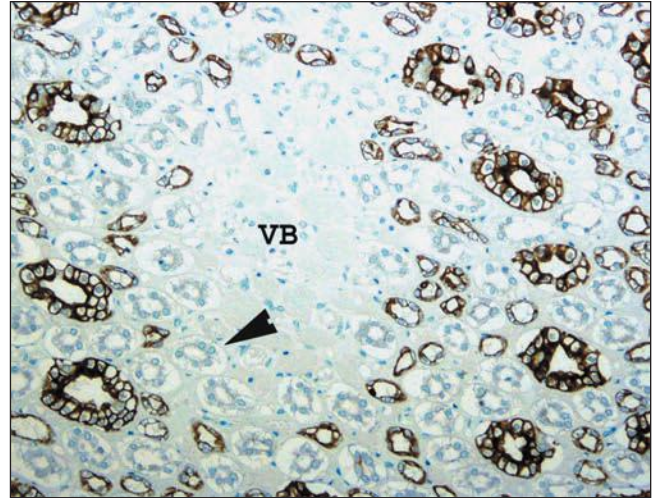


FIGURE 1.31 Human kidney, outer medulla. The central vascular bundles (VB) are surrounded by the descending straight tubules (arrowhead), which are unstained, and the smaller stained ascending thick limb tubules. The largest stained tubules are collecting ducts. (Immunoperoxidase stain for cytokeratin AE 1/3, $\times 250$.)

bundles in the inner stripe of the outer medulla (Figs. 1.33 and 1.36). At various points as they descend, additional branches supply the tubules within the interbundle regions of the inner stripe with a rich capillary plexus. The bundle size diminishes as it descends into the inner medulla.

The descending arteriolar rectae destined for the inner medulla supply no branches to the tubules of the inner stripe. Therefore, there is complete separation of the blood supply to the inner stripe from that of the inner medulla. The capillary plexus of the inner medulla is sparse but richer at the papillary tip than in the more superficial portions of the inner medulla where almost all the vessels are vasa recta arterioles. Arterioles from spiral arterial branches of the intralobar arteries contribute to the blood supply of the papillary tip (see Fig. 1.17). These compartmentalized vascular patterns provide a basis for the differing zones of medullary injury associated with the various causes of papillary necrosis.

As the arterioles enter the interbundle regions, they gradually lose their smooth muscle and pericytic coats to enter a fenestrated venous system that ascends back toward the cortex to form the *ascending venae rectae* (Figs. 1.26, 1.34, and 1.37). The inner medullary venous outflow occurs exclusively via vascular bundles. The inner medullary *ascending venae rectae* enter the vascular bundles at the junction of the inner and outer medulla and then leave the vascular bundles as they approach the outer stripe and course outward. The capillary plexus of the outer stripe also join the ascending venae rectae. These two venous outflows remain separate within the inner stripe, but both receive capillary venous outflow as they enter the outer stripe. This arrangement is important in urine concentration.

Within the outer stripe, the venous ascending venae rectae have a thin attenuated and fenestrated endothelium and represent a large fraction of the vascular plexus of the outer stripe,

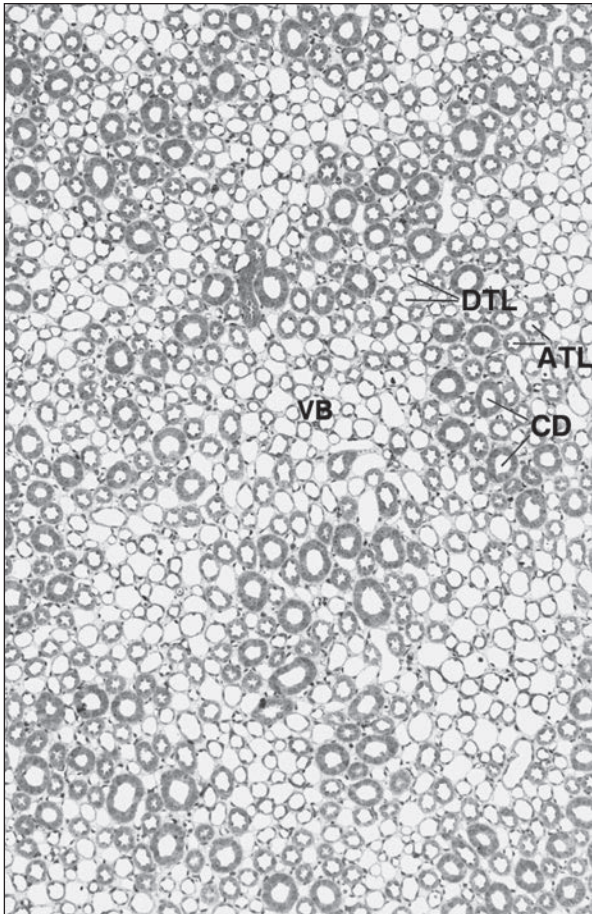


FIGURE 1.32 Cross-section (1- μ m section of Epon-embedded tissue) through the inner stripe of the outer medulla. The vascular bundles (VB) are well developed and surrounded by the limbs of short and long loops of Henle in an arrangement similar to that in the outer stripe. ($\times 140$.) DTL, descending thin limb; ATL, ascending thick limb; CD, collecting duct.

which is sparse in true capillaries. They also travel outward from the bundle as they enter the outer stripe. The ascending venules finally empty into interlobular or arcuate veins. The venae rectae and the arteriole rectae are arranged in close proximity throughout their course as they travel down to the papillary tip and back up. The intermingled venous and arterial limbs compose the countercurrent exchange system that maintains the medullary osmotic gradient.

NEPHRONS

The nephron consists of the metanephric-derived structures, the renal corpuscle, and a lengthy cylindrical epithelial-lined tubular component. The nephron does not, strictly speaking, include the CD, which is ureteric bud derived (28,32). However, it is not uncommon for the term *nephron* to be used in reference to both the true nephron components as well as the CD. The status of the CTs is unclear. Ultrastructural studies implicate ureteric bud origin, whereas microdissection studies support metanephric blastema derivation (28,32).

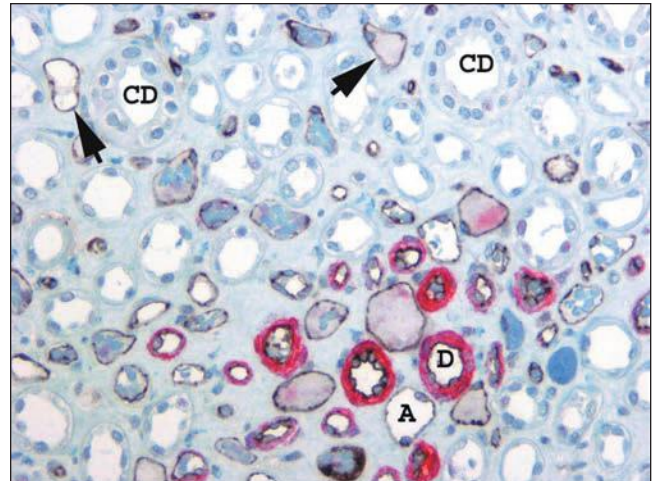


FIGURE 1.33 Human kidney, outer medulla. The descending arteriole rectae (D) in the vascular bundle have a prominent smooth muscle media (stained red for smooth muscle actin), whereas the thin ascending venae rectae (A) and the interbundle capillary plexus (arrows) have no smooth muscle but can be distinguished from the thin limbs of Henle because their endothelial cell lining is stained black with CD 31. ($\times 350$.) CD, collecting duct.

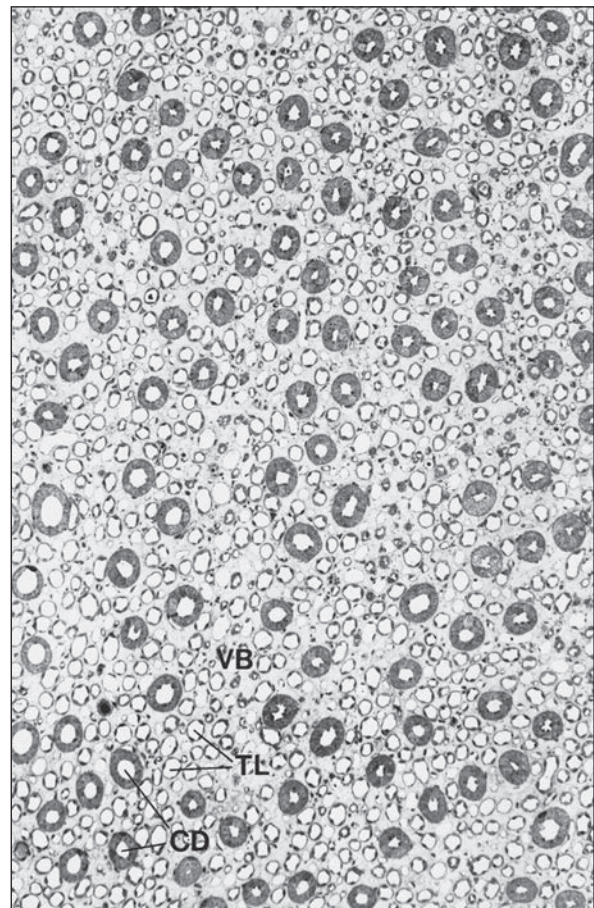


FIGURE 1.34 Cross-section (1- μ m section of Epon-embedded tissue) through the inner medulla. The vascular bundles (VB) are small and cannot clearly be separated from the surrounding thin limbs (TLs). ($\times 112$.) CD, collecting duct.

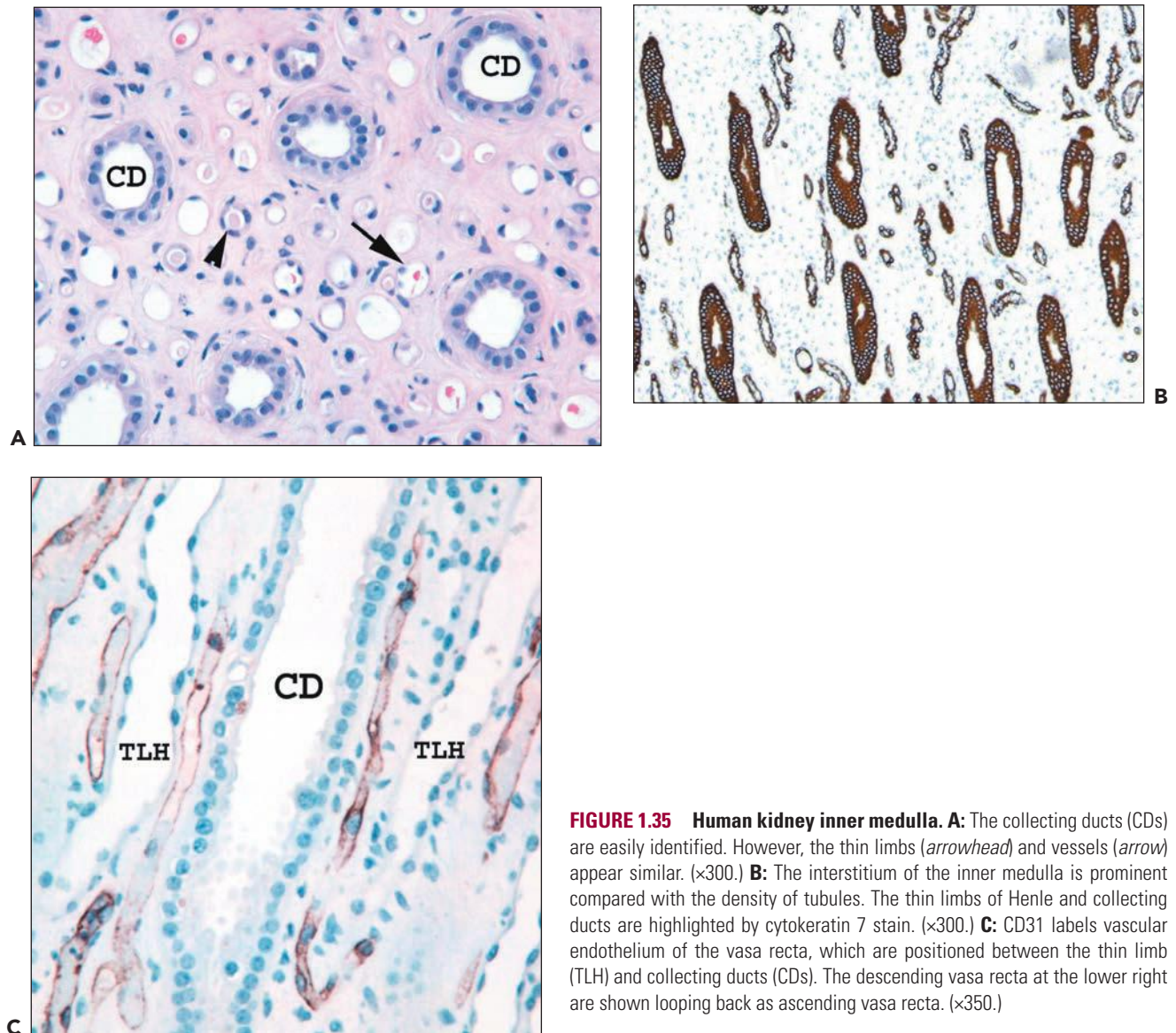


FIGURE 1.35 Human kidney inner medulla. A: The collecting ducts (CDs) are easily identified. However, the thin limbs (*arrowhead*) and vessels (*arrow*) appear similar. ($\times 300$.) **B:** The interstitium of the inner medulla is prominent compared with the density of tubules. The thin limbs of Henle and collecting ducts are highlighted by cyokeratin 7 stain. ($\times 300$.) **C:** CD31 labels vascular endothelium of the vasa recta, which are positioned between the thin limb (TLH) and collecting ducts (CDs). The descending vasa recta at the lower right are shown looping back as ascending vasa recta. ($\times 350$.)

The tubular portion of the nephron has complex spatial and topographic relationships with its microvasculature and demonstrates sequential variation in its cellular constitution tightly linked to function.

Nephron Number

The number of nephrons in the normal kidney is important because nephron number may play a role in the development of hypertension and progression of chronic renal disease (67–71). Nephron number is influenced by many factors that affect renal development. Low birth weight, preterm birth, reduced kidney mass and size, short stature, maternal hyperglycemia, maternal protein malnutrition, and gene polymorphism for *PAX2* and *RET* are associated with reduced nephron numbers (68). Low nephron numbers are associated with increased glomerular volume and an increased risk of hypertension. Older patients also have fewer nephrons because of age-related obsolescence (67–71). Recent studies have shown a broad range in nephron numbers, with some patients having

substantially fewer nephrons than others. Neugarten et al. (70) found that nephron numbers per kidney ranged from 400,000 to 800,000. Hughson et al. (71) found similar average numbers but an even broader range, between 227,000 and 1,825,000 nephrons per kidney, an eightfold range that varied with birth weight. In rats and rabbits, nephron numbers are much lower, estimated at 30,000 per kidney.

Types of Nephrons

Classification of nephrons is based on either topographic location in the cortex or on function (52–54). The three types of nephrons as classified according to their topographic location in the cortex are the superficial, midcortical, and juxtamedullary. As their name indicates, the superficial nephrons are located within the outer cortex. They send arterioles to the subcapsular regions. The juxtamedullary nephrons are deeply situated at the corticomedullary junction and send arterioles into the medulla, which converge to form the descending vascular bundles. The midcortical nephrons are situated between

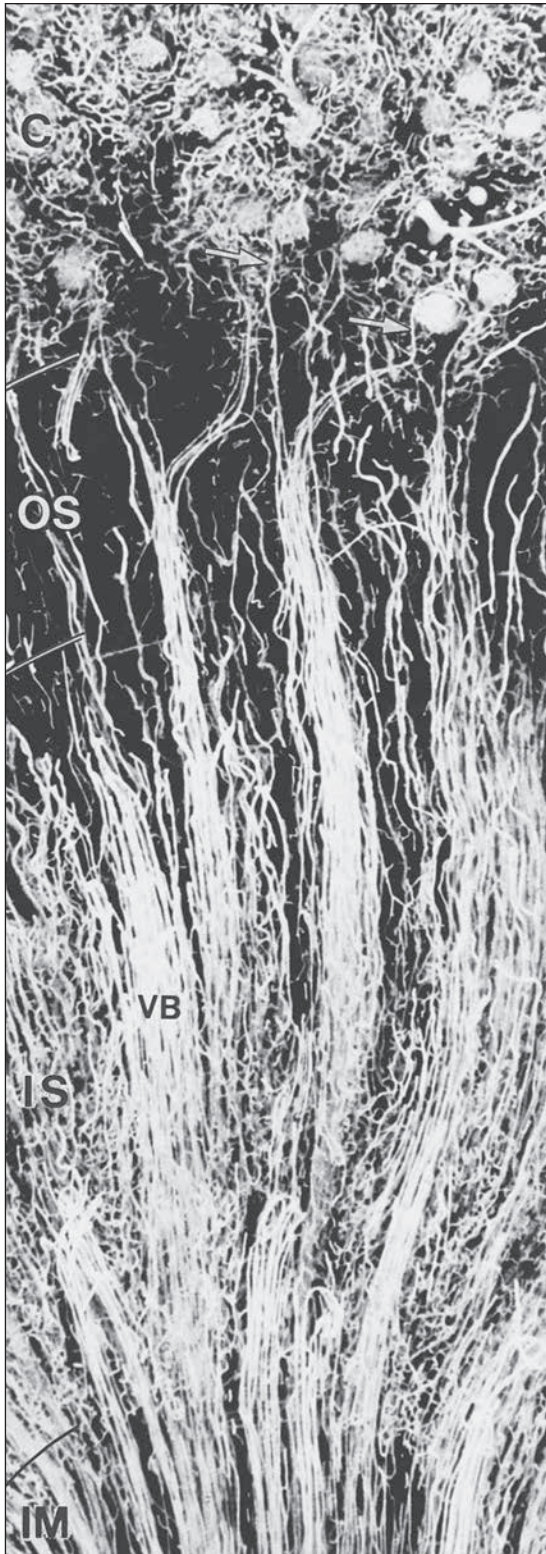


FIGURE 1.36 Arterial vessels of the medulla of a mouse injected with silicone rubber (Microfil). The juxtamedullary glomeruli give rise to efferent arterioles (*arrows*), which split into the descending vasa recta, establishing the arterial part of the vascular bundle (VB). The bundles are best developed in the inner stripe (IS) and decrease after transition into the inner medulla (IM). C, cortex; OS, outer stripe. ($\times 85$.)

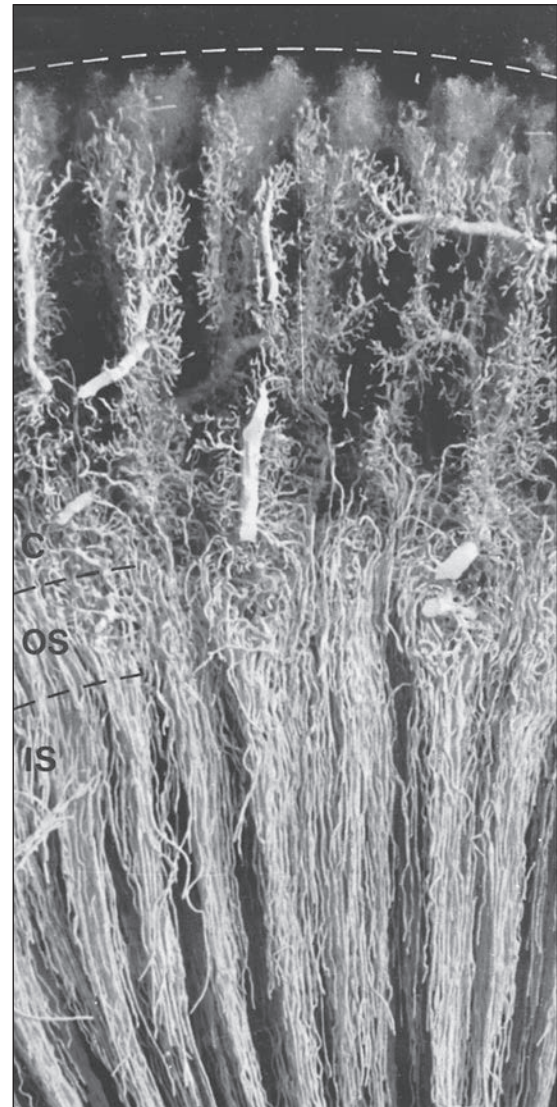


FIGURE 1.37 Venous vessels of rabbit kidney injected with silicone rubber (Microfil). The interlobular veins of the cortex accept the blood from the cortical plexuses and descend to the corticomedullary border. The venous vessels of the medulla are the ascending vasa recta, which ascend within and between the vascular bundles toward the corticomedullary border, where they empty into arcuate veins or the basal portions of the interlobular veins. C, cortex; OS, outer stripe; IS, inner stripe. ($\times 20$.)

the other two, but there is no distinct boundary between these three regions.

Nephrons are more commonly classified functionally by the length of their loop of Henle, which varies in the point at which it bends to return to the cortex (72). Short-looped nephrons arise in the superficial and midcortical regions. They send the loops of Henle into the outer medulla where they bend and return toward the cortex. Juxtamedullary and some deep midcortical nephrons are the long-looped nephrons. They send the loops of Henle into the inner medulla before bending at various levels to return to the cortex. The percentage of long-looped nephrons shows great species variation; to some degree,

this is related to the needs for urinary concentration and water conservation. However, urinary concentration correlates more with the complexity of medullary development rather than simply the number of long-looped nephrons (62–66). In the human kidney, approximately 15% of nephrons are long looped. In the rodent kidney, this is almost doubled to 28%, whereas in cats and dogs, all nephrons are long looped (72).

RENAL CORPUSCLE

General Structure and Histology

The renal corpuscle or glomerulus is a spherical to ellipsoid cluster of capillaries and matrix housed within a connective tissue structure, the Bowman capsule (BC). The BC is the dilated proximal-most extension of the PT (17,32,52,73–75). The glomerular tuft floats within a fluid-filled cavity, the Bowman space, and is tethered to the BC at its vascular pole. The glomerular tuft consists of the glomerular capillaries, and the glomerular

mesangium, which is contiguous with the extraglomerular mesangium that forms the central portion of the JGA. In rarely observed, optimally oriented sections, the glomerular vascular pole pedicle and the urinary pole outflow are usually positioned on opposite sides of the glomerulus (Fig. 1.38). The glomerulus has a mean diameter of approximately 200 μm in the adult human; juxtamedullary glomeruli and glomeruli in patients with a solitary kidney are larger (17,73).

The glomerular tuft consists of a central axial branching mesangium invested by a profusion of capillaries (17,32,52,73–77) (Figs. 1.38 to 1.41). The glomerular capillaries have a unique status within the vascular system; they are situated between two arteriolar systems. This arrangement is necessary to maintain, and to allow, modulation of the intravascular pressure required for glomerular filtration. The glomerular tuft is formed by an afferent arteriole that divides immediately on entering the BC to form lobules of glomerular capillaries. Two to five lobules are observed in reconstructions of rat glomeruli, although this lobular arrangement is difficult to appreciate in histologic sections.

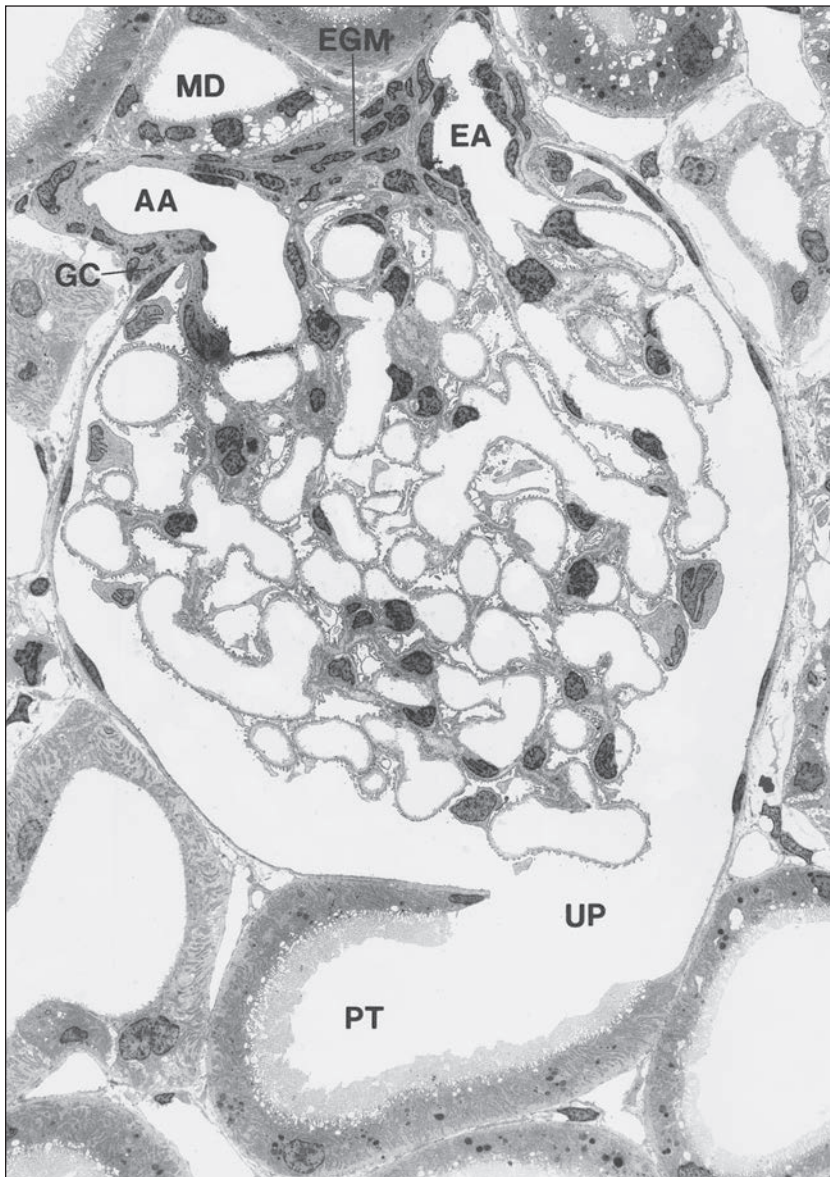


FIGURE 1.38 Glomerulus with juxtaglomerular apparatus of the rat kidney. The afferent arteriole (AA), the efferent (EA), and the extraglomerular mesangium (EGM) are in close contact with the macula densa (MD) of the thick ascending limb. UP, urinary pole; PT, proximal tubule; GC, granular cell. (Electron micrograph, $\times 900$.)

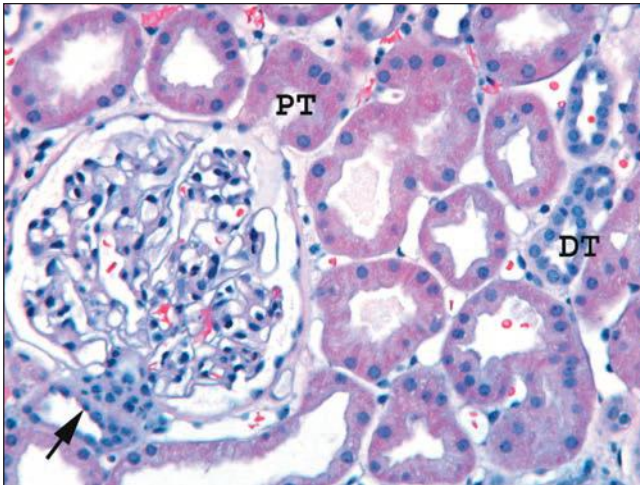


FIGURE 1.39 Human cortex. The macula densa (*arrow*) and the adjacent extraglomerular lacis cells are on the left; the ostium of the proximal tubule (PT) is on the right. The parietal epithelium lining Bowman capsule is flattened and abruptly transitions to the columnar proximal tubular epithelium at the urinary pole. Most tubules are proximal, but two distal tubules (DTs) are present. (H&E, $\times 200$.)

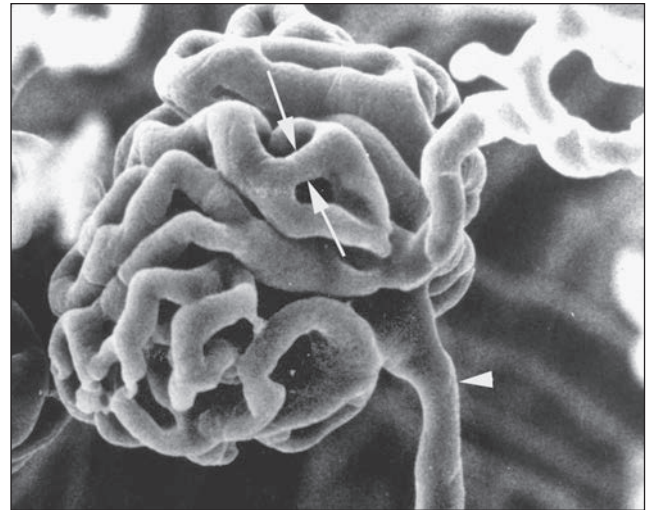


FIGURE 1.41 Scanning electron micrograph of a vascular cast of a rat glomerulus. The afferent arteriole (*arrowhead*) and efferent arteriole are shown. A capillary loop anastomosis is shown (*between arrows*). ($\times 450$.) (From Gattone VH II, Evan AP, Willis LR, et al. Renal afferent arterioles in the spontaneously hypertensive rat. *Hypertension* 1983;5:8.)

There are afferent, more peripherally arrayed glomerular capillary domains and efferent, more centrally located domains, with the former constituting most of the capillaries (73–77). There are multiple anastomoses between capillaries within a lobule, and between capillaries in separate lobules, creating a capillary network (Fig. 1.41).

The capillaries of the efferent domain converge on the vascular pole to become the efferent arteriole (77) (see Figs. 1.38 and 1.40). This convergence is established within the glomerular tuft and splits the two initial branches of the entering afferent arteriole as the efferent arteriole exits the glomerulus. The afferent arteriole has a larger diameter than the efferent arteriole due to a more substantial media and a larger lumen,

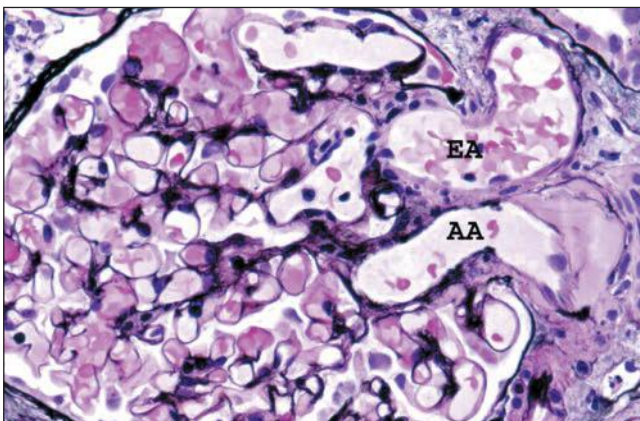


FIGURE 1.40 Human glomerulus with vascular pole. The thin delicate capillary loop basement membranes and slender profiles of mesangial matrix are stained black. The afferent arteriole is identified by the presence of hyalinosis. (Jones methenamine silver, $\times 400$.) AA, afferent arteriole; EA, efferent arteriole.

but these features are often difficult to appreciate since it is rare to capture both in an identical plane of section. The afferent arteriole in Figure 1.40 from a patient with hypertension is easy to recognize because of hyalinosis, which affects only the afferent arteriole in nondiabetics.

The glomerular tuft is supported by two forms of the extracellular matrix: the mesangial matrix and the glomerular capillary loop basal lamina (Fig. 1.42). A central scaffolding function is provided by the axial branching mesangial matrix. The encircling capillary loops are principally supported by their basal lamina, which forms an incomplete vascular cylinder since the mesangium constitutes a portion of the capillary loop wall. Although *basal lamina* is the correct anatomic term for the extracellular matrix layer demonstrable by electron microscopy that separates podocytes and endothelial cells, the basal lamina is commonly referred to as the *glomerular basement membrane* (GBM). The glomerular capillary loop component demonstrable by light microscopy (LM) includes both the cellular elements—podocytes and endothelial cells—and the central matrix component, the GBM.

The glomerulus consists of three cell types: mesangial cells, endothelial cells, and epithelial cells (17,52) (Fig. 1.42). Mesangial cells reside within the mesangial matrix. In the normal human glomerulus, mesangial cells should number no more than two per mesangial area. Endothelial cells completely line the inner surface of the glomerular capillaries with an attenuated layer of cytoplasm, and they have an oval nucleus that projects into the capillary lumen usually near the mesangial interface. There are two types of epithelial cells: podocytes, also known as the visceral epithelial cells, and parietal epithelial cells (PECs). Podocytes are arrayed along the exterior surface of the capillary loops and over the mesangial waist region (a region not covered by capillaries). They have prominent protruding nuclei and lightly stained cytoplasm. At the vascular pole, the podocytes transition into the PECs that line the BC. PECs are thin squamous-like epithelial cells that line the entire inner surface

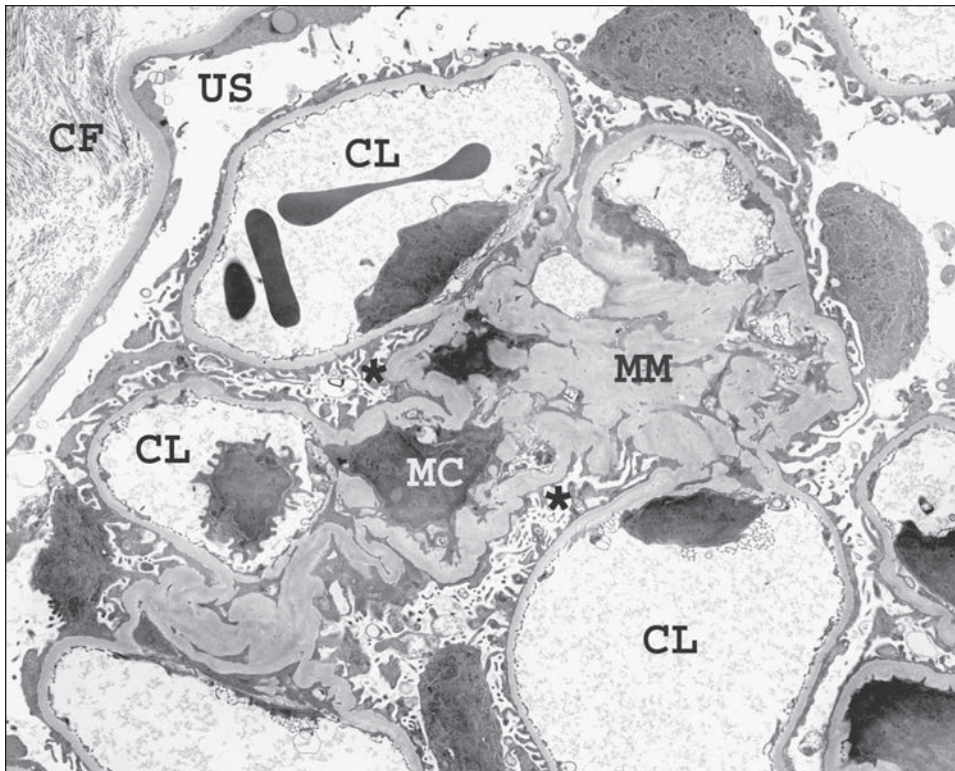


FIGURE 1.42 Transmission electron micrograph of a relatively normal human glomerulus. The mesangial matrix (MM) contains a mesangial cell (MC), and the capillary loops (CLs) are lined by thin fenestrated endothelium. The endothelial cell nuclei are located near the mesangial interface. Podocytes invest both the outer aspects of the capillary loops and the mesangial waist regions (*asterisk*). The urinary space (US) separates the glomerulus from the Bowman capsule, which is lined by flat parietal epithelial cells. Interstitial collagen fibrils (CF) are visible on the outer aspect of the basal lamina of the Bowman capsule. ($\times 2200$.)

of the BC. Parietal cells abruptly transition into columnar proximal tubular cells at the urinary pole (see Figs. 1.38 and 1.39).

In some glomeruli, two distinct cells may be interposed between the visceral and PECs, parietal podocytes, and periportal cells (78–80). The parietal podocyte is present in most glomeruli. It is a podocyte that sends cell processes to cover capillary loops as a typical podocyte but also sends cell processes to the parietal BM of the BC (79). Cell processes in both areas have foot processes (FPs) with slit diaphragms (SDs), suggesting some filtration function across the BC either into the JGA or the cortical interstitium.

Periportal cells are granulated glomerular epithelial cells that form around the vascular pole. Peripolar cells are present in only a minority of human glomeruli (3% to 28%), primarily in outer cortical glomeruli (79,80). These cells form junctional complexes with podocytes and PECs. Peripolar cells are closely associated with renin-containing cells in the afferent arteriolar wall. Periportal cells contain dense granules, morphologically similar to renin granules; but the granules do not appear to contain renin. Their function is not known.

The three glomerular cells—podocytes, endothelial cells, and mesangial cells—can often be recognized in hematoxylin and eosin (H&E)-stained sections, most readily identified in the peripheral portions of the glomerular tuft where structural relationships are best appreciated. The glomerular cells are difficult to identify separately in the central regions of the glomerulus and in the abnormal glomerulus. Histochemical stains that permit precise resolution of the relationship between cells and matrix components facilitate more confident cellular identification. Periodic acid-Schiff (PAS) stain and a silver-based stain, two commonly used stains in renal biopsy evaluation, are most suitable for this purpose. The mesangial matrix is well delineated by both stains. However, the silver stain reveals a more delicate detail of the GBM since it stains only the

lamina densa (Figs. 1.40 and 1.43). The PAS stain provides better cellular detail but stains all cytoplasmic and matrix components of the capillary loop. Appreciation of general structural features of the glomerulus and tubules is also possible by

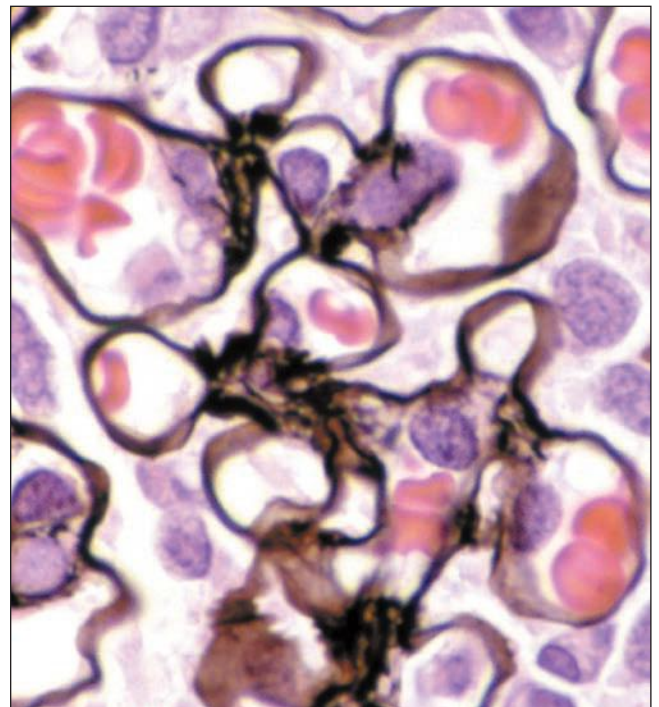


FIGURE 1.43 Normal human glomerulus. The thin delicate detail of the capillary loops and scant mesangium is nicely delineated by the Jones methenamine silver stain. ($\times 650$.)

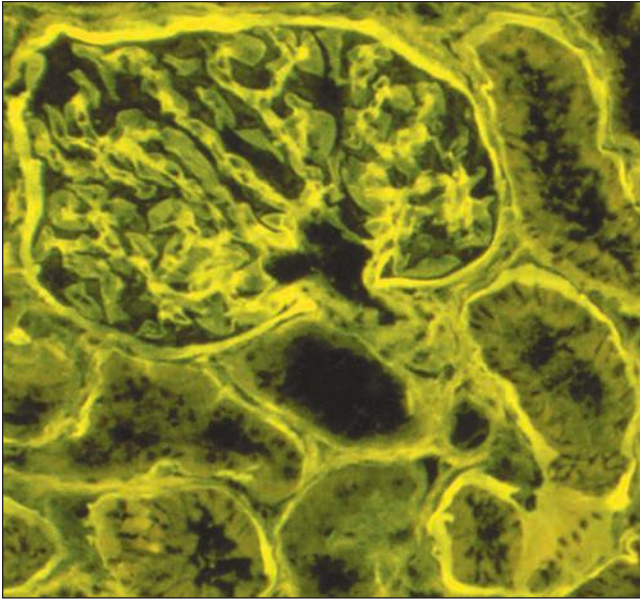


FIGURE 1.44 Normal human cortex. This H&E-stained section is viewed under fluorescent microscopy. The general architectural features of the glomerulus and tubules are easily recognized. (H&E, $\times 250$.)

viewing an H&E-stained section under fluorescence (Fig. 1.44). This is useful in kidney biopsies for correlation with immunofluorescence findings (81).

In addition to routine histochemical stains mentioned above that rely on relationships between cells and the matrix for cell identification, more precise analysis is possible. Many molecules can be targeted with modern immunohistochemical reagents and other techniques to identify specific matrix components, clarify cell lineage, assess cell cycling status, or identify other physiologically important molecules, such as adhesion molecules (integrins, selectins, cadherins), cytokines and their inhibitors, complement inhibitors, other protein inhibitors, antiinflammatory eicosanoids, antithrombotic molecules, antioxidants, heat shock proteins, and protein phosphatases.

Cellular Components of the Glomerulus

Podocyte

Podocytes are the largest cells in the glomerulus. They have a highly specialized three-dimensional structure and unique molecular profile closely linked to the critical functions they perform (82–94). Podocytes participate in GBM synthesis and repair, provide structural support for the capillary loop, and are the principal component governing the permselectivity of the capillary loop. Podocytes also participate in cross talk with endothelial cells and mesangial cells and may have contractile properties that affect capillary loop diameter (83,85,95–99).

The normal adult podocyte is a terminally differentiated cell that relinquishes mitotic capability during maturation once formation of FPs occurs (83,85,95–99). Nuclear division without cell division does on occasion occur, resulting in binucleated and multinucleated podocytes, a phenomenon that is most marked in nephropathic cystinosis (100). The state

of fixed quiescence appears necessary for proper podocyte cell function. Cell division requires reorganization of the cytoskeleton, which would disrupt the highly ordered arrangement of the FPs, affecting cell attachment to the GBM and the filtration selectivity of the SD. The quiescent state is maintained by a tightly regulated balance between several families of molecules that control cell cycle: cyclins, cyclin-dependent kinases, and the cyclin-dependent kinase inhibitors such as p21, p27, and p57. The mature podocyte expresses p27, p57, and cyclin D3 (95,101–104). Although podocytes were previously regarded as fixed in a terminally differentiated state, it is now clear that reentry into the cell cycle occurs in a few glomerular diseases, such as HIV nephropathy and other collapsing forms of focal segmental glomerulosclerosis, leading to the concept of the dysregulated podocyte. In these conditions, p21 is reexpressed, cyclin D1 increases, and p27, p57, and cyclin D3 decrease with resultant podocyte proliferation confirmed by PCNA and Ki-67 staining (95,101–104).

The molecular signature of podocytes is unique among epithelial cells of the kidney. Podocytes are the only cells in the adult kidney to express intranuclear WT-1 and are the only glomerular cells to express C3b receptor and at least in cell culture smooth muscle proteins smoothelin, calponin, and myocardin (Fig. 1.45) (94). Podocytes also have a paradoxical intermediate filament profile (105). Podocytes express vimentin, a ubiquitous intermediate filament expressed by mesenchymal cells but not usually by epithelial cells (Fig. 1.46A). Vimentin expression shows a restricted pattern, limited to the cell body and cell processes but absent in the FPs (Fig. 1.47). Cytokeratin, the intermediate filament of most epithelial cells, is not expressed in podocytes but is expressed in PECs and all other renal epithelial cells (Fig. 1.46B).

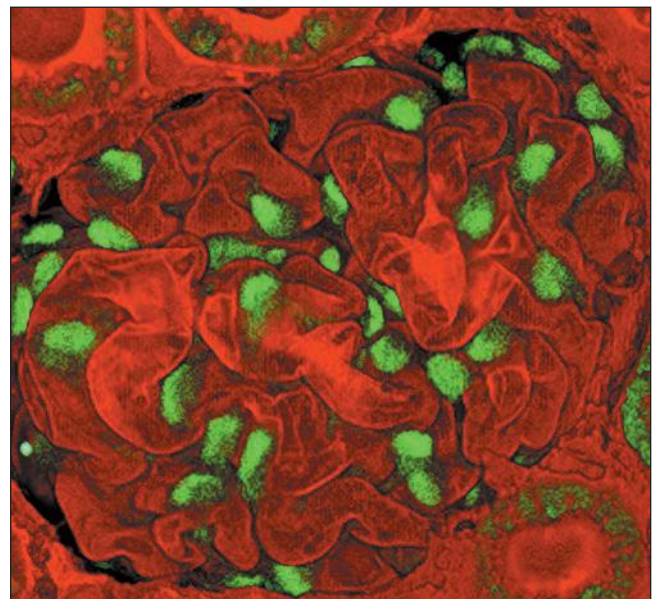


FIGURE 1.45 Two-photon microscopy of a rat glomerulus. Podocytes are the only renal cells of the mature kidney that express WT-1; note the intense nuclear stain. The GBM is stained with *Lens culinaris*. ($\times 550$.) (Photograph courtesy of Carrie Phillips, MD.)

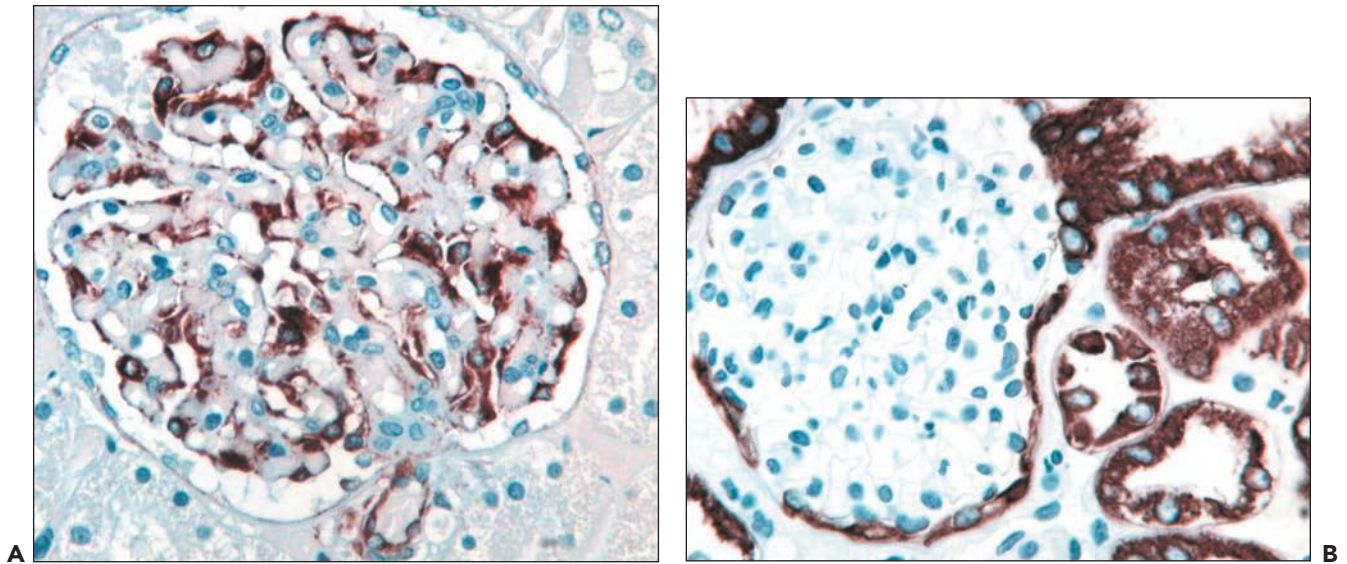


FIGURE 1.46 Human kidney. **A:** Podocytes express vimentin intermediate filaments while parietal epithelial cells are negative. (Immunoperoxidase stain for vimentin, $\times 350$.) **B:** Parietal epithelial cells and proximal and distal tubular cells express cytokeratin while podocytes are negative. (Immunoperoxidase stain for cytokeratin 8, $\times 300$.)

PODOCYTE ULTRASTRUCTURE

Podocytes are large octopus-like cells polarized relative to the GBM (86–88,92–94). Transmission electron microscopy and scanning electron microscopy (SEM) have unveiled their unique and complex structure (Figs. 1.48 and 1.49). Three major structural regions have been identified: the cell body, cell processes, and FPs. The cell body is usually located within a valley created by the reflection of adjacent capillary loops. The cell body contains the nucleus and other major organelles such as abundant rough endoplasmic reticulum (RER), an extensive Golgi

apparatus, mitochondria, and frequent lysosomes. Occasionally, rudimentary cilia are present projecting from the surface. The cell body does not rest directly on the GBM. It is separated from the GBM by the subpodocyte space and a layer of FPs (Fig. 1.49). Based on serial three-dimensional transmission electron microscope (TEM) reconstructions, the subpodocyte space covers approximately 60% of the GBM. It may be a dynamic compartment that can fluctuate in volume, restrict movement of the ultrafiltrate into the urinary space, provide a mechanism for podocyte participation in modulating capillary permeability, and chemically communicate with endothelial and mesangial cells possibly by reverse flux across the GBM (91).

Long, slender, arborizing cell processes extend from the cell bodies. These processes contain few organelles but are rich in microtubules and intermediate vimentin filaments that run parallel to the long axis (88–96). The cell processes participate in cell trafficking and maintain cell shape and rigidity. They may branch into secondary or even tertiary cell processes before investing multiple capillary loops (Figs. 1.48 and 1.49). The cell processes ultimately give rise to terminal structures called FPs or pedicels.

The name *foot processes* is derived from the original transmission electron microscopic studies of normal kidneys that revealed slender processes arranged perpendicular to the capillary loop BM (Fig. 1.50). The three-dimensional architecture of the podocyte and its FPs was first understood following the beautiful panoramic SEM studies published in the 1970s and 1980s (86–88) (see Fig. 1.49). These investigators demonstrated that the podocyte FPs are slender pectinate cytoplasmic finger-like extensions. The FPs have a smooth luminal surface and interdigitate with the FPs of adjacent podocytes. FPs are attached to the BM by integrins, the principal ones are $\alpha 3 \beta 1$ integrin and α and β dystroglycans (83,95–99).

The FPs contain numerous microfilaments, an actin-based cytoskeleton. These are oriented along the long axis of the FP and terminate in the basal cell membrane of the abluminal surface

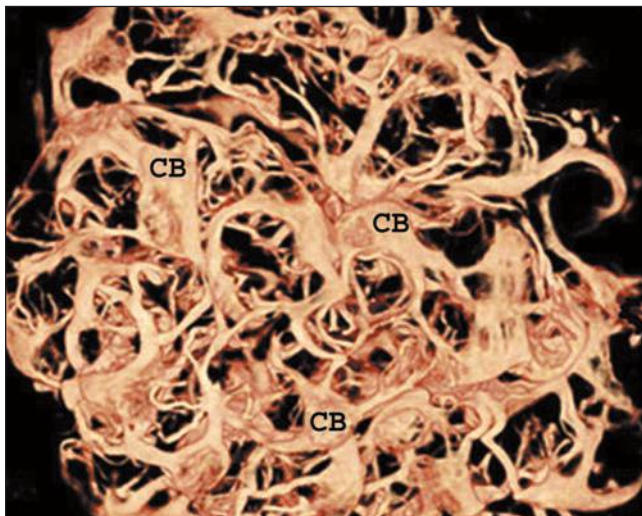


FIGURE 1.47 Two-photon image of a rat glomerulus. Vimentin intermediate filaments are restricted by the cell body (CB) and cell processes. The intervening foot processes are not visible since they lack vimentin. (Immunofluorescent stain for vimentin, $\times 600$.) (Photograph courtesy of Carrie Phillips, MD, and Indiana Center for Biological Microscopy.)

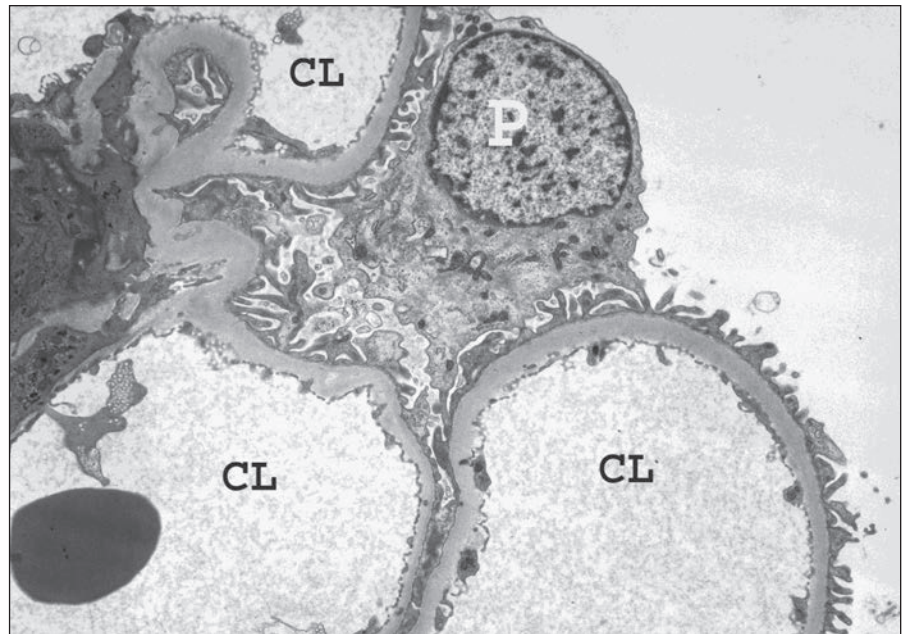


FIGURE 1.48 Transmission electron micrograph of a normal human glomerulus. The podocyte (P) cell body contains most of the organelles and resides within a trough formed by capillary loops. This podocyte extends cell processes to three capillary loops (CLs). ($\times 5000$.)



FIGURE 1.49 Scanning electron micrograph of a rat glomerulus. The slender podocyte cell processes, interdigitating foot processes (F), and filtration slits are elegantly displayed. The nucleus-containing cell body is located within a bend of the capillary loop. (From Andrews P. Morphological alterations of the glomerular (visceral) epithelium in response to pathological and experimental situations. *J Electron Micro Tech* 1988;9:115–144. Copyright © 1988. Reprinted from Wiley-Liss, Inc., Wiley Publishing Inc., a subsidiary of John Wiley & Sons, Inc., with permission.)

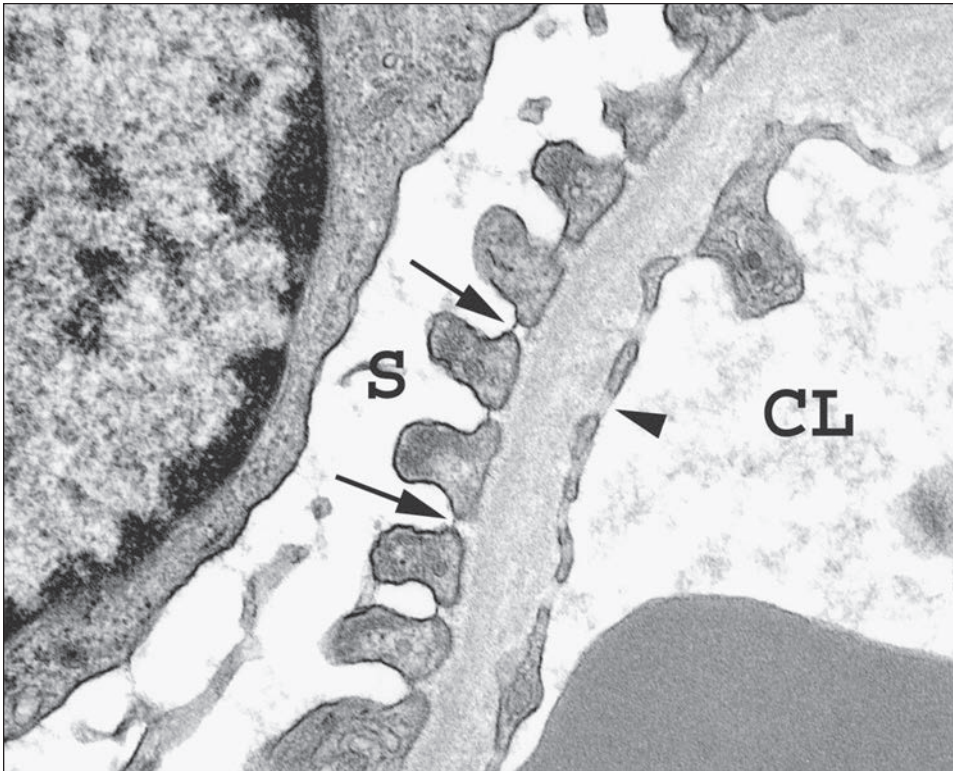


FIGURE 1.50 Transmission electron micrograph of a normal human glomerulus. The subpodocyte space (S) is shown with an underlying layer of podocyte foot processes that slightly indent the lamina rara externa. Slit diaphragms (arrows) connect adjacent foot processes. A fenestrated (arrow-head) endothelial cell lines the capillary loop (CL). (×11,200.)

(88–99). The folding structure of the capillary loops appears maintained by the numerous actin filament–stabilizing patches that form where each FP attaches to the GBM and also by terminal processes that bridge the narrow reflecting point of the GBM between adjacent capillaries at the mesangial waist region. The actin filament bundles may affect FP structure and influence capillary wall permeability. The FPs have a randomly skewed orientation relative to the long axis of an individual capillary loop. This arrangement is graphically demonstrated by the enzymatic digestion and NaOH maceration techniques that expose the abluminal or basal surface of the podocytes (94) (Fig. 1.51). The

skewed orientation of FPs may participate in hydraulic regulation by helping to resist expansion of the pressurized capillary loops.

Between adjacent FPs are slender slits bridged by a 30- to 50-nm-wide structure known as the SD, a key determinate of capillary loop permselectivity as discussed below. The SD is composed of proteins similar to those in an adherens junction (see Fig. 1.47). Rodewald and Karnovsky (106) first drew attention to the SD in 1974. They reported that the SD has a regularly arrayed zipper-like or ladder-like structure with a central bar and rectangular pores, particularly evident in tannic acid–treated tissue (Fig. 1.52). However, a recent study has

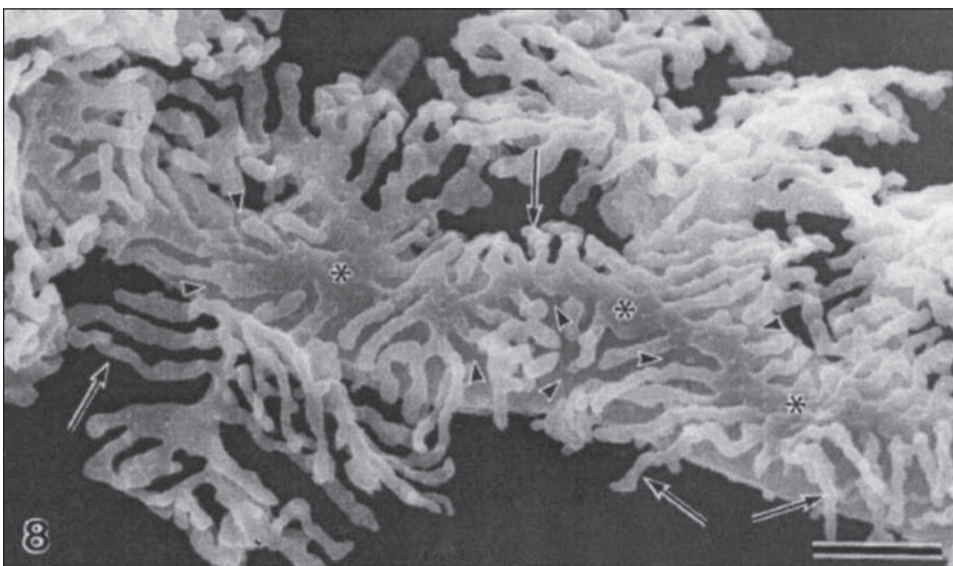


FIGURE 1.51 Scanning electron micrograph of a rat podocyte showing its basal aspect. Two major processes with terminal foot processes are displayed following digestion of glomerular matrix. Notice the irregular filigree pattern of cell processes and foot processes (arrow) that do not conform to the long axis (asterisks) of a capillary loop. (From Takahashi-Iwanaga H. Comparative anatomy of the podocyte: a scanning electron microscopic study. *Microsc Res Tech* 2002;57:196. Reprinted from Wiley-Liss, Inc., Wiley Publishing Inc., a subsidiary of John Wiley & Sons, Inc., with permission.)

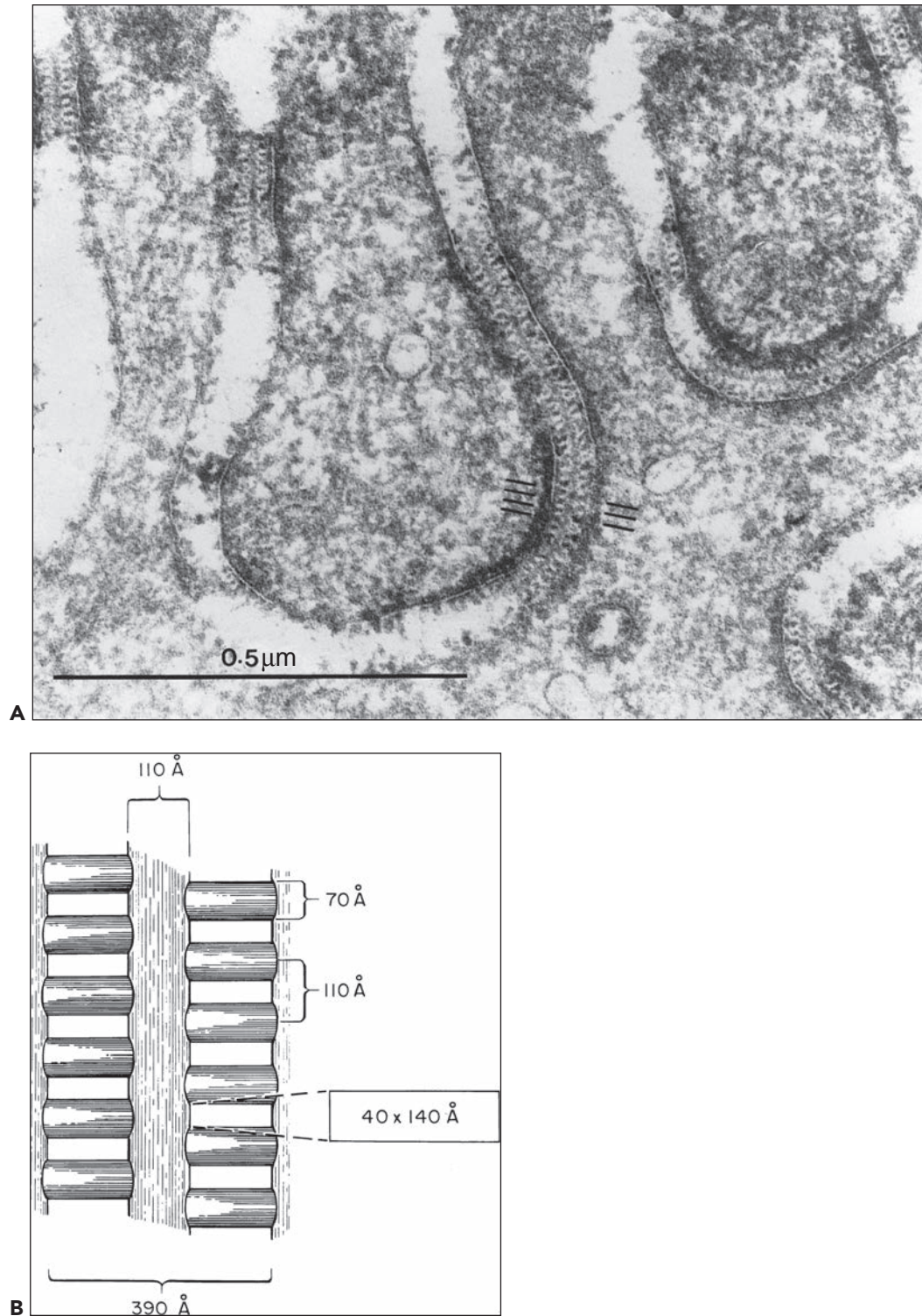


FIGURE 1.52 **A:** A slit diaphragm from a rat glomerulus. The central filament and cross-bridges are readily resolved in this micrograph. The marks indicate a region where cross-bridges appear to alternate on either side of the central filament. Also evident is the increased density of the cytoplasm opposite the points of attachment of the diaphragm to the epithelial cell membranes. Apparent discontinuities in the diaphragm represent regions where this structure has left the plane of section. ($\times 123,500$.) **B:** Schematic drawing of the epithelial slit diaphragm. The average cross-sectional dimensions of the pores between cross-bridges are indicated within the rectangle. (From Rodewald R, Karnovsky M. Porous substructure of the glomerular slit diaphragm in the rat and mouse. *J Cell Biol* 1974;60:423. Copyright ©1974 Rockefeller University Press.)

challenged this description. Employing SEM with a high-sensitivity detection system, Gagliardini et al. (107) demonstrated circular to ellipsoid openings in the SD with more variable size and shape and dimensions of 10 to 20 nm (Fig. 1.53).

PODOCYTES AND THE FILTRATION BARRIER

The filtration barrier of the glomerular capillary loop consists of the fenestrated endothelial cells, the GBM, and the SD (95–99,108–114). In the normally functioning capillary loop, the glomerular filtrate follows an extracellular route, passing through the endothelial fenestrations, traversing the GBM, and finally passing between FPs through the SD. Ultrafiltrate either

enters the urinary space directly or traverses the subpodocyte space prior to entering the urinary space (92). These layers of the capillary loop function in parallel, restricting the passage of cells and limiting filtration of macromolecules on the basis of charge, shape, and size. The endothelial cell and GBM impart charge selectivity; the GBM and especially the SD impart size and shape selectivity.

The most characteristic podocyte abnormality observed with disturbances in filtration function is FP effacement associated with alterations in the SD. This characteristic feature of proteinuric disorders was first demonstrated by Farquhar et al. (112) in 1957 with TEM in biopsies from patients with minimal change disease. Twenty years later, SEM studies demonstrated that FP effacement results from widening, shortening, and retraction of the FPs (84,86). This process requires engagement of contractile processes mediated by an actin-based cytoskeleton. Actin is soluble when monomeric but insoluble upon polymerization, forming filament networks, a highly regulated process involving over 100 known proteins, among which GTPases such as RhoA, Rac1, and Cdc42 are especially important (94). Understanding the mechanisms underlying maintenance of the normal FPs and SD structure, and their alteration in disease, has followed advances in understanding the molecular aspects of podocyte structure and function as discussed below (95–99,109–114).

PODOCYTE MOLECULAR DOMAINS AND FILTRATION FUNCTION

A number of molecules responsible for the maintenance of the complex three-dimensional structure of podocytes and important in its filtration function have been identified (Figs. 1.54 and 1.55). They reside in restricted molecular domains, somewhat distinct from, but functionally related to, the structural domains (83,95–99). These molecular domains include a luminal domain, an abluminal domain, and the SD domain. Although these domains are spatially separate, they are interconnected via the actin-based cytoskeleton, which couples molecular events in one domain to structural and functional alterations in other domains.

The apical (luminal) domain comprises the podocyte cell body, cell processes, and the FPs above the SD. This domain contains two important proteins, podocalyxin and GLEPP-1 (95–99,113,114). Podocalyxin is the major determinate of the podocyte negatively charged glycocalyx, easily demonstrated by colloidal iron or other cationic stains (Fig. 1.56). The glycocalyx may contribute to the maintenance of glomerular architecture and FP integrity since charge neutralization models and knockout mouse models induce FP effacement. Charge neutralization can affect FP architecture because podocalyxin is connected to the actin-based cytoskeleton (see Fig. 1.54). GLEPP-1 is another surface protein restricted to the apical FPs, identified as a receptor tyrosine phosphatase. It contains an extracellular domain with fibronectin type III repeats, a transmembranous domain, and a single ATPase domain. Its ligand and substrate are not known.

The basal (abluminal) domain consists of the basal aspect of the FPs. These are slightly embedded in the lamina rara externa of the GBM to a depth of 40 to 60 nm (see Fig. 1.54). The FPs are anchored by $\alpha\beta$ 1-integrin and α - and β -dystroglycans (95–99). $\alpha\beta$ 1-integrin binds to all major structural proteins of the GBM—collagen IV, laminin, entactin/nidogen, and

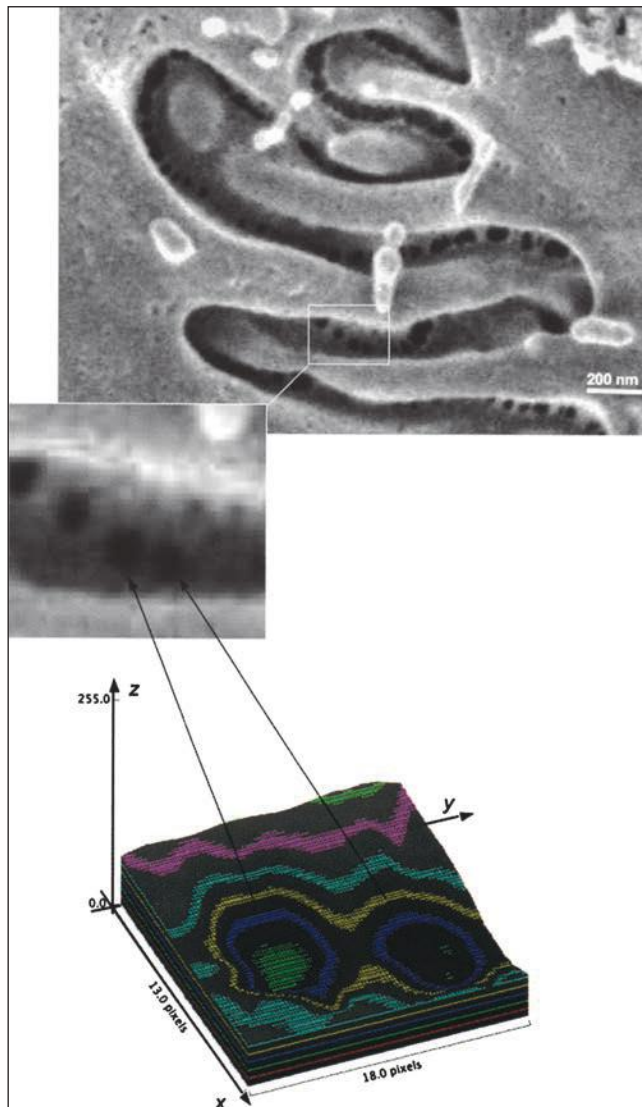


FIGURE 1.53 Schematic representation of the procedure used to evaluate pore dimension. **Top:** A representative image obtained at SEM (original magnification 200,000 \times) with an enlargement of the filtration slit pores. **Bottom:** Representation of the surface plot obtained using the software image J (v.1.43 NIH). (From Gagliardini E, Conti S, Begigni A, et al. Imaging the porous ultrastructure of the glomerular epithelial filtration slit. *J Am Soc Nephrol* 2010;21:2081.)

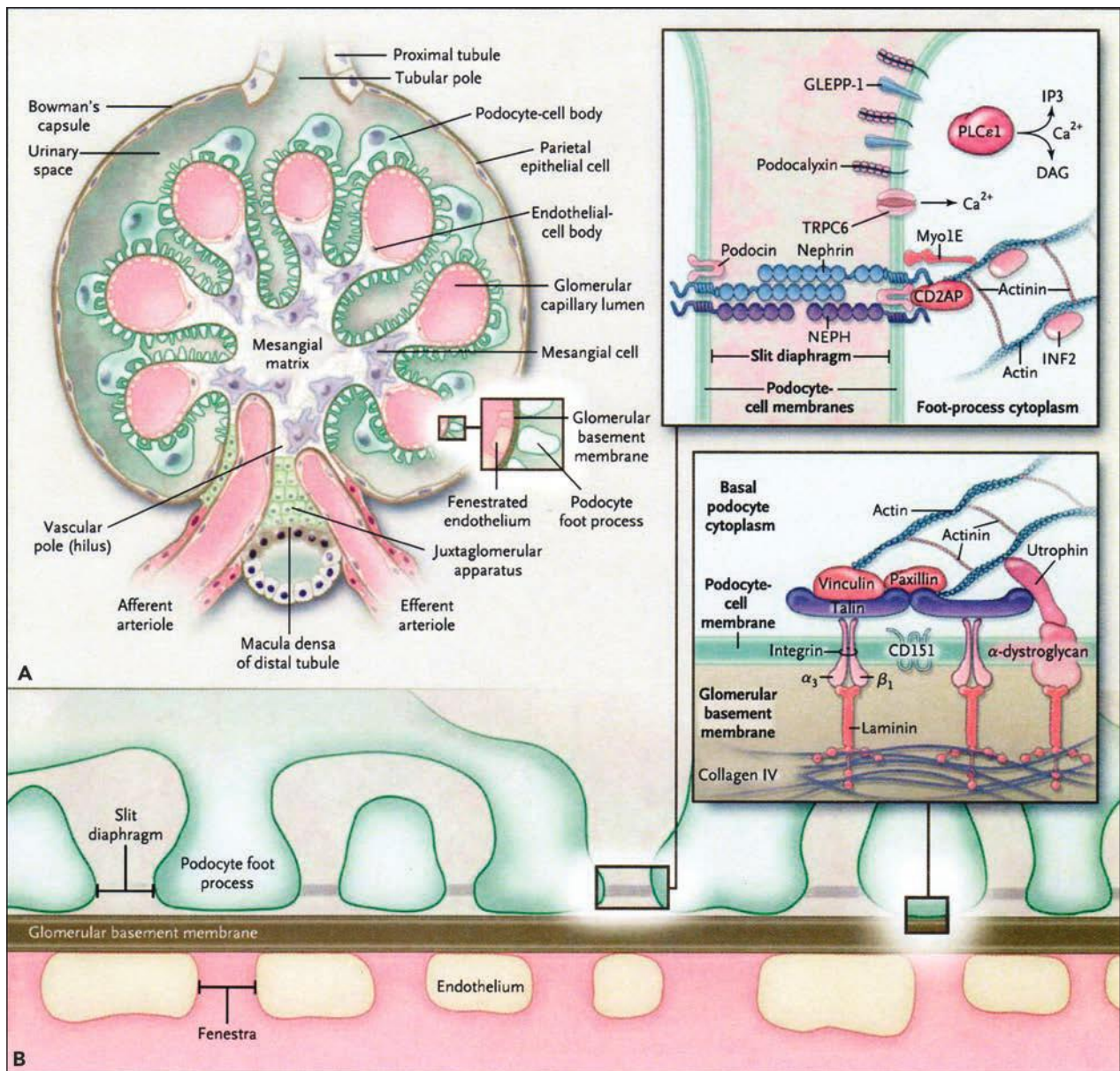


FIGURE 1.54 Normal glomerulus and glomerular filtration barrier. A: Each kidney contains approximately 1 million glomeruli, which comprise the filtering units of the kidney. The normal glomerulus is composed of a specialized bundle of capillaries that originates from branching of the afferent arteriole as it enters the hilus (or vascular pole). Between the afferent and efferent arterioles, bordered by the macula densa of the distal tubule, is the triangular juxtaglomerular apparatus, an endocrine organ involved in renin production and tubuloglomerular feedback. The glomerular capillaries are supported by the mesangial cells, which are invested in matrix and are continuous with the smooth-muscle cells of the hilar arterioles. The glomerular endothelial cell bodies are oriented toward the mesangium, whereas their fenestrated cytoplasm lines the inner aspect of the peripheral glomerular basement membrane. The glomerular basement membrane forms a scaffold for the glomerular capillaries and reflects over the mesangium. Along their outer aspect, the glomerular capillaries are supported by the podocytes, which reside in the urinary space and have interdigitating foot processes. The glomerular ultrafiltrate enters the urinary space and passes into the tubular pole (the origin of the proximal tubule), which lies opposite the vascular pole. **B:** The glomerular capillary wall and selected components of the filtration barrier are shown. On the urinary side, the interdigitating podocyte foot processes are aligned in regular arrays separated by filtration slit diaphragms located above the glomerular basement membrane. The fenestrated glomerular endothelium is present at the blood interface. The *inset* diagrams show some of the molecules that make up the slit diaphragm (**above**) and the basal surface of the podocyte (**below**). Nephrin is the major component of the slit diaphragm. Pairs of nephrin molecules extending out into the center of the slit from adjacent podocyte foot processes form homophilic interactions as well as heterophilic interactions with NEPH. The slit diaphragm complex includes podocin, which forms a hairpin turn within the podocyte membrane. Through interaction with CD2-associated protein (CD2AP), the slit diaphragm molecules are linked to the actin cytoskeleton, which is regulated by α -actinin-4, inverted formin 2 (INF2), and myosin 1E (Myo1E). Calcium generated by phospholipase C epsilon 1 (PLC ϵ 1) through diacylglycerol (DAG) and inositol triphosphate (IP3) and entering the cell through transient receptor potential cation channel 6 (TRPC6) regulates actin polymerization. At the basal surface, adhesion molecules $\alpha_3\beta_1$ integrin and α -dystroglycan are linked to laminin. Integrin is coupled to the actin cytoskeleton through a complex of talin, vinculin, and paxillin, whereas adhesion molecule α -dystroglycan links to actin through utrophin. Negatively charged molecules podocalyxin and glomerular epithelial protein 1 (GLEPP-1) are arrayed on the apical cell membrane. (From D'Agati VD, Kaskel FJ, Falk RJ. Focal segmental glomerulosclerosis. *N Engl J Med* 2011;365:2398).

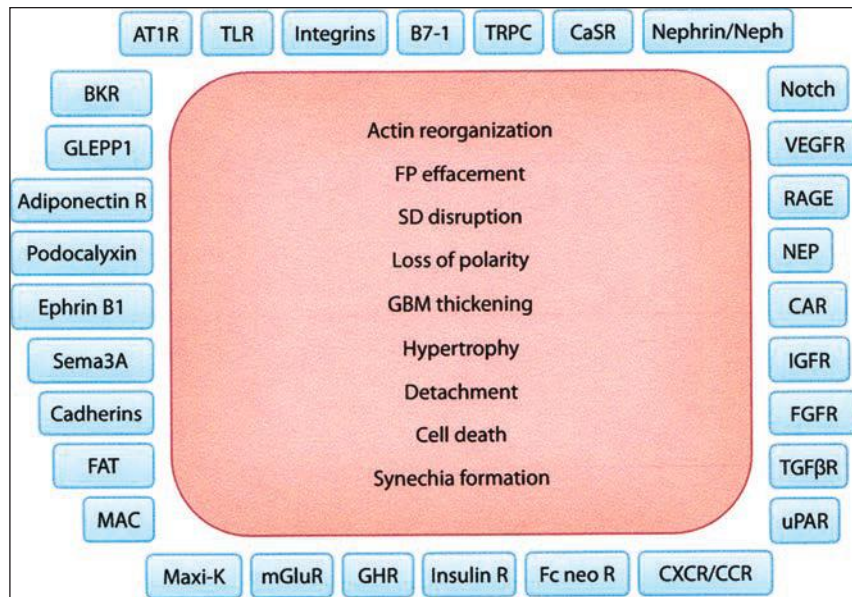


FIGURE 1.55 Podocyte plasma membrane proteins and a canonical pattern of injury. Shown is a (incomplete) list of membrane proteins that have been implicated in the regulation of podocyte function in health and disease. Injured podocytes respond with a finite repertoire of changes, as depicted here. Our ability to repair the pathways initiated by the molecules on the podocyte plasma membrane to the precise cellular phenotypes listed here will provide not only novel insight but enormous opportunities for successful therapeutic interventions. Abbreviations: adiponectin R, adiponectin receptor; AT1R, angiotensin type 1 receptor; BKR, bradykinin receptor; CAR, Coxsackie and adenovirus receptor; CaSR, calcium-sensing receptor; CXCR/CCR, C-X-C/C-C chemokine receptor; FAT, protocadherin FAT1; Fc neo R, neonatal Fc receptor; FGFR, fibroblast growth factor receptor; FP, foot process; GBM, glomerular basement membrane; GHR, growth hormone receptor; GLEPP1, glomerular epithelial (podocyte) protein 1; IGFR, insulin growth factor receptor; insulin R, insulin receptor; MAC, membrane attack complex; Maxi-K, large-conductance calcium-activated potassium channel (also known as BK channel); mGluR, metabotropic glutamate receptor; NEP, neutral endopeptidase; RAGE, receptor for advanced glycation end products; SD, slit diaphragm; Sema3A, semaphorin-3A; TGF β R, transforming growth factor β receptor; TLR, Toll-like receptor; TRPC, transient receptor potential canonical; uPAR, urokinase receptor; VEGFR, vascular endothelial growth factor receptor. (From Greka A, Mundel P. Cell biology and pathology of podocytes. *Annu Rev Physiol* 2012;74:299.)

fibronectin—and is linked to the actin-based cytoskeletal proteins actin, myosin, α -actinin, and synaptopodin by paxillin, talin, and vinculin.

Dystroglycan appears in the membrane of renal epithelial cells at the moment of mesenchymal-to-epithelial transformation. Dystroglycan is a dimer composed of α and β subunits, with transmembrane and extracellular components. α -Dystroglycan binds electrostatically to cationic domains of the GBM. β -Dystroglycan has an intracellular portion that is coupled to the actin cytoskeleton by urotrophin. $\alpha 3\beta 1$ -integrin and dystroglycan are both connected to the SD via the actin-based cytoskeleton. Thus, alterations in the SD structure can result in alterations in the FP attachment, a prerequisite for FP effacement to ensue.

The SD domain plays the pivotal role in capillary loop permselectivity (83,95–99,108–114). Appreciation of the role of the SD followed the identification of several genetic abnormalities in structural and signaling molecules critical for the functioning of the filtration barrier (see Figs. 1.54 and 1.55). The first molecule identified was nephrin (115). In 1998, Tryggvason et al. used mutational analysis by positional cloning to demonstrate that nephrin, encoded by the gene NPHS1, is mutated in Finnish-type congenital nephrotic syndrome. These patients have a variety of mutations often involving a single amino acid. When expressed, the mutant nephrin molecules may remain in the endoplasmic reticulum rather than being targeted to the cell surface to participate in the SD structure. Affected patients may lack SDs, and all develop severe proteinuria in utero.

This discovery was soon followed by identification of numerous other genes and their protein products that associate with nephrin in the FPs and SD (83,95–99,116–128). Mutation of many of these molecules is responsible for a

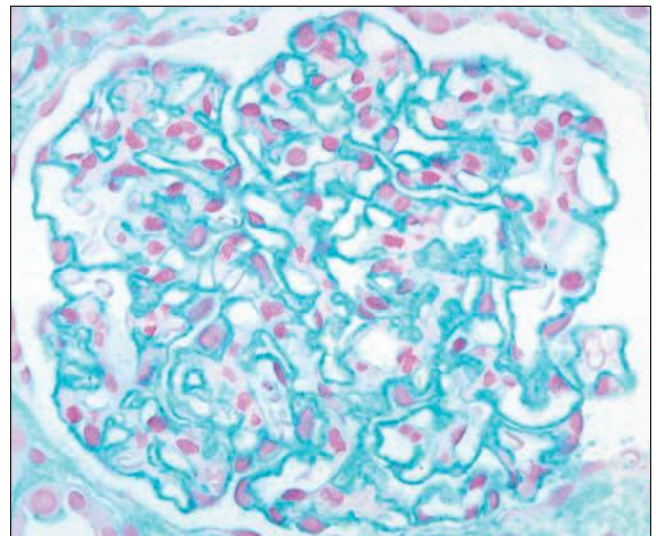


FIGURE 1.56 Human glomerulus. The podocyte glycocalyx is highlighted with a cationic colloidal iron stain. ($\times 400$.)

rapidly expanding list of hereditary and sporadic forms of steroid-resistant nephrotic syndrome in children and adults. These discoveries and the use of knockout mice have led to an explosion of new information about the molecular basis of normal capillary loop permeability and its modifications following injury or disease.

The SD shares certain molecular similarities with cell junctions. It contains ZO-1 protein-like tight junctions and FAT and P cadherin-like desmosomes and adherens junctions. The SD-modified adherens-type junction is tethered to the actin-based cytoskeleton. Interference with or abnormalities in one of the components of the SD results in its functional destabilization; FP effacement mediated via the actin-based cytoskeleton and proteinuria. A detailed schematic diagram of the FP and SD is shown in Figure 1.54, and a brief description of several key molecules appears below.

Nephrin, a member of the immunoglobulin superfamily, is expressed in several organs other than the kidney. Nephrin is a heavily glycosylated protein that consists of eight Ig-like domains, a fibronectin type III extracellular domain, a transmembrane domain, and a cytoplasmic domain. Nephrin is a major structural protein of the SD with important signaling properties. Oligomers of nephrin form through homophilic interactions within the SD. These associate within signaling microdomains of the FP cell membranes known as lipid rafts. *Lipid rafts* are microdomains rich in cholesterol and sphingolipids that facilitate protein-protein interactions in the signaling process. The cytoplasmic tails of nephrin (and neph1) contain tyrosine residues that may serve as targets for phosphorylation. Phosphorylation may influence the intracellular distribution of the nephrin cytoplasmic tails and their association with other molecules such as CD2AP and podocin to mediate and enhance the signaling process. CD2AP binds to the cytoplasmic tail of nephrin to function as a bridge between nephrin and the actin-based cytoskeleton.

Podocin is a member of the band 7 stomatin family. Podocin expression is limited to the kidney. The podocin molecule consists of a transmembrane domain and an intracellular membrane-associated hairpin-like structure. Podocin localizes to the point of attachment of the SD to the FP. Podocin contributes to the structural integrity of the SD and is involved in signaling. It forms dimers and oligomers in lipid rafts and interacts with nephrin, neph1, CD2AP, and transient receptor potential cation channel 6 (TRPC6) allowing the SD to act as a mechanosensor and modulate podocyte cytoskeleton and FPs in response to mechanical stimuli.

The transient receptor potential cation channel, TRPC6, is a Ca²⁺-permeable nonselective cation channel expressed in the podocyte and SD. It interacts with the GTPase RhoA. During TRPC-induced calcium influx, RhoA activity increases, which inhibits podocyte motility via effects on the actin cytoskeleton.

CD2AP is an intracellular adapter protein. It was originally discovered as the CD2 receptor in T cells and was found to orchestrate immunologic synapses between B and T cells. It is expressed in the kidney in podocytes, proximal and distal tubules (DTs), and the CD. CD2AP binds to the cytoplasmic tail of nephrin and links it directly to filamentous actin cytoskeleton. CD2AP also binds to actin-regulating proteins such as CAPZ, cortactin, and Rac1.

ZO-1 (zonula occludens-1) is a membrane protein and member of the membrane-associated guanylate kinase with

inverted orientation-1 protein family. It is expressed in podocytes, tubular cells, and endothelial cells. It is located at the point of attachment of the SD to the FP, as is podocin. It exists as two isoforms dependent on the presence or absence of an 80-amino-acid domain. It interacts with the cytoplasmic tail of neph1 and the actin-based cytoskeleton.

Neph1, Neph2, and Neph3 are transmembrane proteins restricted to the podocyte-SD complex. Like nephrin, they are members of the Ig superfamily. They have an extracellular domain within the SD that contains five immunoglobulin-like domains and an intracellular domain. Neph1 forms heterodimers and multimers with its intracellular and extracellular domains. The intracellular domains interact with podocin and ZO-1. The extracellular domains interact with nephrin and affect the actin cytoskeleton via Nck proteins.

α -Actinin-4, an actin-bundling molecule that cross-links actin filaments, is required for normal podocyte adhesion. It is regulated by extracellular signals that lead to decrease in affinity for actin following its phosphorylation.

Synaptopodin, a proline-rich actin-associated protein, binds to CD2AP and to α -actinin-4, regulating its actin-bundling function that affects the shape and motility of podocyte FPs.

Inverted formin 2 (INF2) is a member of the formin family of proteins, a highly conserved protein family that influences eukaryotic cell shape and motility. INF2 can polymerize and depolymerize actin and appears to coordinate podocyte actin and microtubule dynamics.

FAT1, a giant protocadherin located within the SD, has a long extracellular domain and a short cytoplasmic domain. The extracellular portion contains 34 cadherin repeats, 5 epidermal growth factors, and 2 laminin domains. Its cytoplasmic domains contain two potential β -catenin-binding regions. It may function (with P cadherin) in cell adhesion and as a spacer molecule to maintain the extracellular space.

The identification of molecules responsible for filtration function and maintenance of the complex three-dimensional structure of podocytes is a rapidly expanding field. The above list of molecules represents only a sample of those identified; many more remain to be discovered. These molecules provide a tantalizing glimpse into the complexity of podocyte biology. The linkage of spatially separate molecular domains through the actin-based cytoskeleton provides a mechanism that permits molecular events affecting one domain to elicit functional and structural consequences in other domains. However, much remains to be learned about the molecular orchestration and cooperation within the FP-SD unit, their relationship to matrix molecules, and the molecular consequences resulting from injury associated with circulating factors and immune complex deposits during glomerular diseases.

Parietal Epithelial Cell

The PEC is a flattened squamous-like cell that lines the inner surface of the BC (see Figs. 1.38 and 1.39) (129,130). They were first described by Sir William Bowman in 1842. At the vascular pole, PECs attach directly to podocytes, or there may be an intervening cell, either a parietal podocyte or a peripolar cell. At the urinary pole, parietal PECs abruptly transition into the columnar epithelium of the proximal convoluted tubule (see Figs. 1.38 and 1.39). The parietal cell surface contains scattered shallow projections and has one or two cilia, 10 μ m

long, that project near the nucleus (131). In contrast to the visceral epithelial cells, PECs contain cytokeratin intermediate filaments rather than vimentin (see Fig. 1.51B).

Although similar in appearance, the parietal cell layer is composed of a heterogeneous population of cells. Unlike podocytes, because they are not terminally differentiated, the parietal cells are capable of proliferation in response to diverse renal injuries (132–136). A subset of parietal cells express stem cell markers CD24 and CD133 and are capable of self-renewal and multidifferentiation. They exhibit a hierarchical organization around the BC (Fig. 1.57). PECs located near the tubular pole express CD24 and CD133 but lack podocyte markers such as podocalyxin (PDX); they may contribute to tubular cell regeneration following proximal tubular cell injury. PECs located between the tubular pole and the vascular pole express CD24, CD133, and PDX and contribute to the population cells of proliferating epithelial within cellular crescents and overlying segmental sclerosing lesions, most notably in focal segmental glomerulosclerosis and collapsing glomerulopathy. Parietal cells near the vascular pole lack CD24 and CD133 expression but express podocyte markers and may migrate onto the glomerular tuft, providing a renewable population of podocytes.

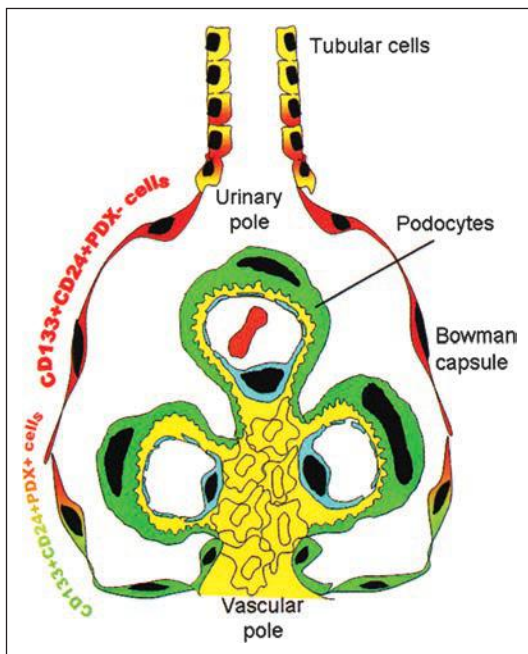


FIGURE 1.57 Schematic representation of the hierarchical distribution of CD133 + CD24 + PDX – and CD133 + CD24 + PDX + cells within human glomeruli. CD133 + CD24 + PDX – renal progenitors (red) are localized at the urinary pole in close continuity with tubular cells (yellow). A transitional cell population (CD133 + CD24 + PDX+, red/green) displays features of either renal progenitors (red) or podocytes (green) and localizes between the urinary pole and the vascular pole. At the vascular pole of the glomerulus, the transitional cells are localized in close continuity with the cells that lack CD133 and CD24 but exhibit the podocyte markers and phenotypic features of differentiated podocytes (green). (From Ronconi E, Sagrinati C, Angelotti ML, et al. Regeneration of glomerular podocytes by human renal progenitors. *J Am Soc Nephrol* 2009;20:322.)

Endothelial Cell

Renal endothelial cells are extremely diversified and must function in a broad range of environments coping with the extreme variations in osmolality and oxygenation that characterize the cortex and medulla. Glomerular capillary endothelial cells consist of a thin attenuated layer of cytoplasm with an oval nucleus usually adjacent to the mesangium (137–144) (see Figs. 1.42 and 1.50). Endothelial cells completely line the inner surface of the glomerular capillary loops. Endothelial cells have fenestrated regions and nonfenestrated regions. The fenestrations cover approximately 20% to 50% of the endothelial surface (96,137). They are round to oval and measure approximately 70 to 100 nm in diameter in humans (see Fig. 1.50). They are smaller in the rat. In contrast to most fenestrated endothelium, including those of the peritubular capillary plexus, the glomerular capillary endothelial cell fenestrations are open and lack a diaphragm (Fig. 1.58). The nonfenestrated regions contain most of the cytoplasmic organelles. The nonfenestrated regions are principally located over the mesangial interface and around the nucleus where ridges of cytoplasm radiate. The ridges contain microtubules and filaments to provide cytoskeletal support. Endothelial cells are connected to each other by gap junctions and shallow occluding junctions of the “leaky” type, and they form gap junctions with mesangial cells. Endothelial cell function is affected by podocytes with vascular endothelial growth factor (VEGF) playing an important role. Flow restriction attributable to the sub-podocyte space previously described may allow reverse flow across the GBM permitting cross talk between podocytes and endothelial cells.

Endothelial cells restrict cell passage across the capillary wall and provide an important charge barrier. They possess an endothelial surface layer (ESL) with two components, including a glycocalyx covalently bound to the endothelial cell membrane and a thicker layer, the cell coat, attached to the glycocalyx by charge-charge interactions (142–144). The ESL thickness has been difficult to determine with estimates of 50 to 300 nm. Because this exceeds the diameter of fenestrae, the ESL contributes significantly to the regulation of capillary loop permeability. Perturbation of the ESL and alteration of fenestrae, therefore, may contribute to the increased capillary loop permeability seen in disease states.

Endothelial cells are physiologically active cells that demonstrate phenotypic variability in the various vascular beds they populate (142–144). Endothelial cells share BM maintenance with podocytes, affect mesangial cell and podocyte function, and modulate vascular tone and glomerular filtration. Endothelial cells require signals such as VEGF and angiopoietins derived from podocytes and mesangial cells to maintain a stable phenotype. Glomerular endothelial cells express class 2 histocompatibility complexes, produce components of the coagulation system such as thrombomodulin, and also express interleukin 1, angiotensin II, adhesion molecules, endothelins, and nitric oxide. Endothelial cells can activate plasminogen to plasmin, can bind factors IXa and Xa, and are affected by numerous inflammatory cytokines, growth factors, and endotoxin.

Mesangial Cell

Mesangial cells reside within the central axial supporting the mesangial matrix and together with the matrix constitute the mesangium. Mesangial cells were first identified in 1929 by Zimmermann as “connective tissue” cells of the glomerulus (145).

Zimmermann recognized that mesangial cells have numerous cell processes. For decades, this feature was doubted by most other microscopists but ultimately confirmed in 1962 by Farquhar and Palade (146) using a recent technologic advance, the TEM.

The normal mesangial cell number is one or two cells per matrix area. Mesangial cells constitute 30% to 40% of the total number of glomerular cells (see Figs. 1.38 and 1.42). There are two types of mesangial cells. The predominant type has an irregular shape with multiple cytoplasmic processes that ramify throughout the matrix extending to the endothelium, mesangial waist GBM, and to other mesangial cells (91,93) (Figs. 1.59 and 1.60). The complexity and a remarkable uniformity of mesangial cell processes have been elegantly revealed by enzymatic extraction and maceration techniques (94,147) (Fig. 1.61). Somewhat similar to podocytes, mesangial cells have cell processes that give rise to a uniform array of short slender terminal processes that interdigitate with the mesangial matrix. Mesangial cells make direct contact with, and establish

gap junctions with, endothelial cells through fenestrations at the mesangium capillary loop interface (148) (Fig. 1.62).

Mesangial cells also send cell processes beneath the endothelium a short distance along the capillary loop (see Figs. 1.59 and 1.60). Mesangial cells establish gap junctions and form desmosomes with other mesangial cells and with the lacis cells of the JGA, resulting in ionic coupling of this entire system (94). Mesangial cells have similarities to smooth muscle or pericytic cells (149–155). They express vimentin intermediate filaments and contain an actin-based cytoskeleton with contractile proteins such as actin, myosin, α -actinin, and tropomyosin. Mesangial cells do not express actin by immunohistochemistry unless activated (150). Ultrastructural studies reveal microfilament bundles within the cytoplasmic processes. These terminate in the cell membrane as attachment plaques that tether mesangial cells to the mesangial matrix and the GBM at the mesangial waist (see Figs. 1.59 and 1.60). Mesangial cell membranes contain $\alpha 3\beta 1$ - and $\alpha 5\beta 1$ -integrins that establish contact between the intracellular

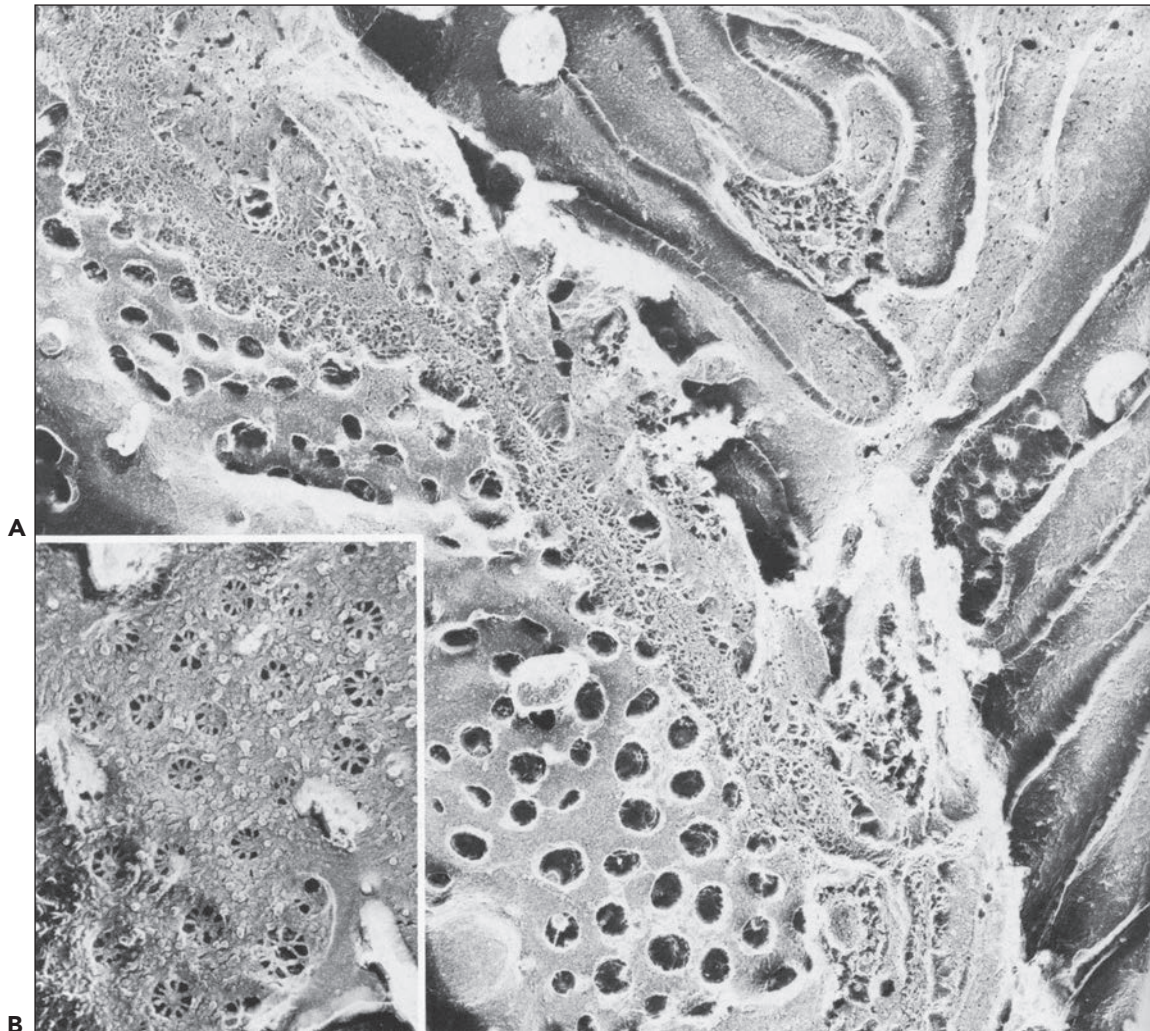


FIGURE 1.58 **A:** Deep etching of isolated rat glomeruli reveals interdigitating pedicels separated from the glomerular capillary by the thick, fibrous basement membrane. ($\times 75,000$.) **B:** The lack of diaphragms across the glomerular capillary fenestrae is in striking contrast to those gracing the peritubular capillary fenestrae. ($\times 83,000$.) (From Beare EL, Orci L. Epithelial fenestral diaphragms: a quick-freeze, deep-etch study. *J Cell Biol* 1985;100:418. Copyright ©1974 Rockefeller University Press.)

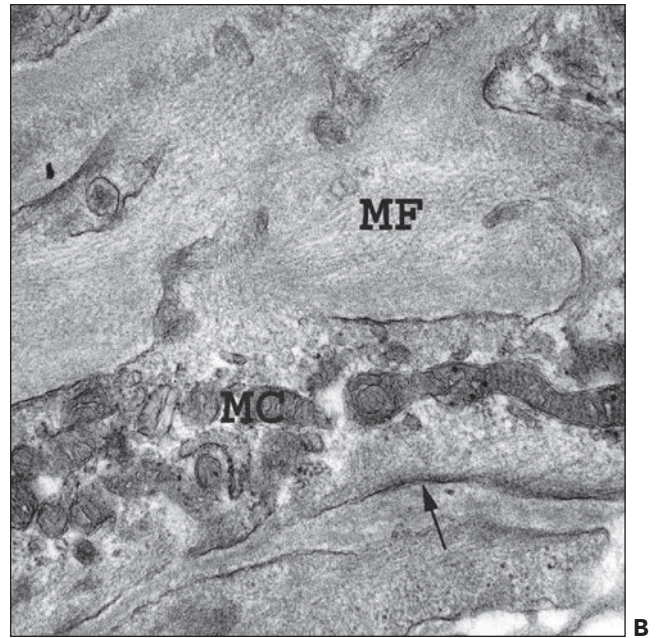
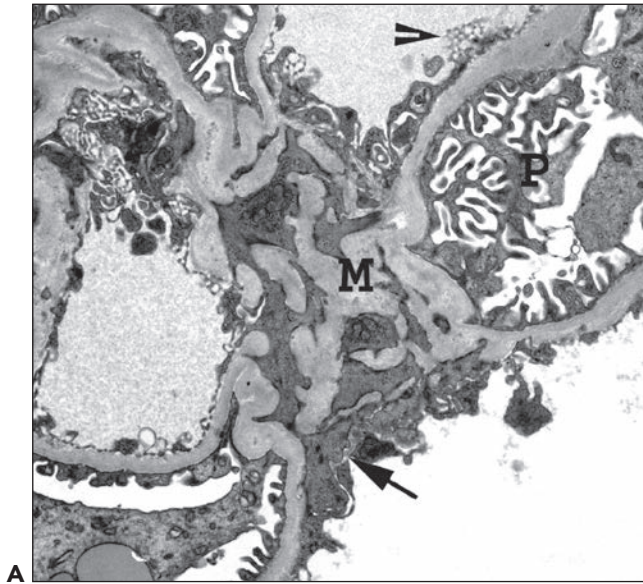


FIGURE 1.59 Human glomerulus. A: The mesangial cell sends long cell processes with short terminal processes throughout the mesangial matrix (M); some cell processes extend a short distance (*arrow*) beneath the endothelium of the capillary loop. Notice the dark mesangial cell anchoring attachment plaques and the sites of direct cell-to-cell contact with endothelial cells through mesangial matrix fenestrations. Short segments of endothelial cell fenestrations can be seen en face (*arrowhead*). P, podocyte. **B:** Notice the coarse microfibrillar (MF) quality of the mesangial matrix and the mesangial cell (MC) membrane attachment plaques (*arrow*). ($\times 17,500$.)

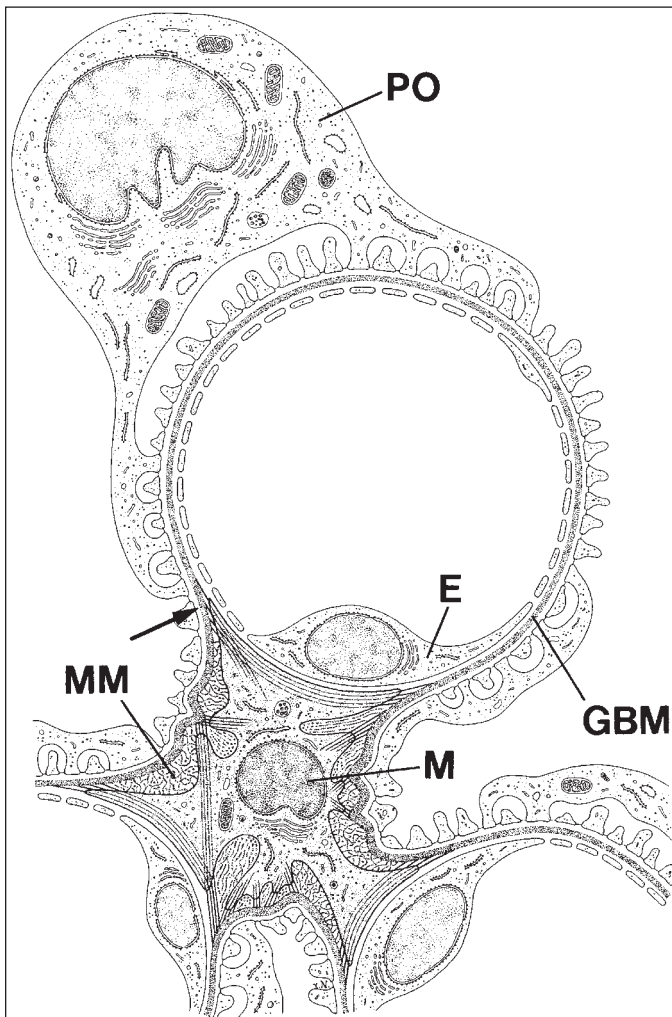


FIGURE 1.60 Schematic diagram shows the arrangement of structures in the glomerular tuft. Part of a glomerular lobule is shown, with three glomerular capillaries (two are incomplete) attached to a mesangial center. The glomerular capillary endothelium (E) is fenestrated. The peripheral part of the endothelial tube is surrounded by the glomerular basement membrane (GBM), which, at the mesangial angles (*arrow*), deviates from a pericapillary course and covers the mesangium. Interdigitating foot processes of the podocyte (PO) form the external layer of the filtration barrier. Podocyte foot processes are also found covering the paramesangial GBM. In the center, a mesangial cell (M) is shown. Its many processes contain microfilament bundles and run toward the GBM, to which the processes are connected. The mesangial matrix (MM) contains an interwoven network of microfilaments. (Modified from Kriz W. Die Harnableitenden Organe. In: Fleischhauer K, ed. *Benninghoff-Makroskopische und Mikroskopische Anatomie des Menschen*, Vol. 2: Kreislauf und Eingeweide. Munich: Urban & Schwarzenberg, 1985:413.)

FIGURE 1.61 Normal rat glomerulus scanning electron micrograph of the mesangial-endothelial cell interface following enzymatic digestion of matrix. The uniform and complex short cell process architecture of mesangial cells is revealed. Notice the nonfenestrated cell body (*arrows*) and fenestrated portion of an endothelial cell (E). ($\times 8000$.) (From Jones D. Enzymatic dissection of the glomerulus. *Lab Invest* 1985;52:453. Reprinted from *Laboratory Investigation*, 1985, Macmillan Publishers Ltd.)

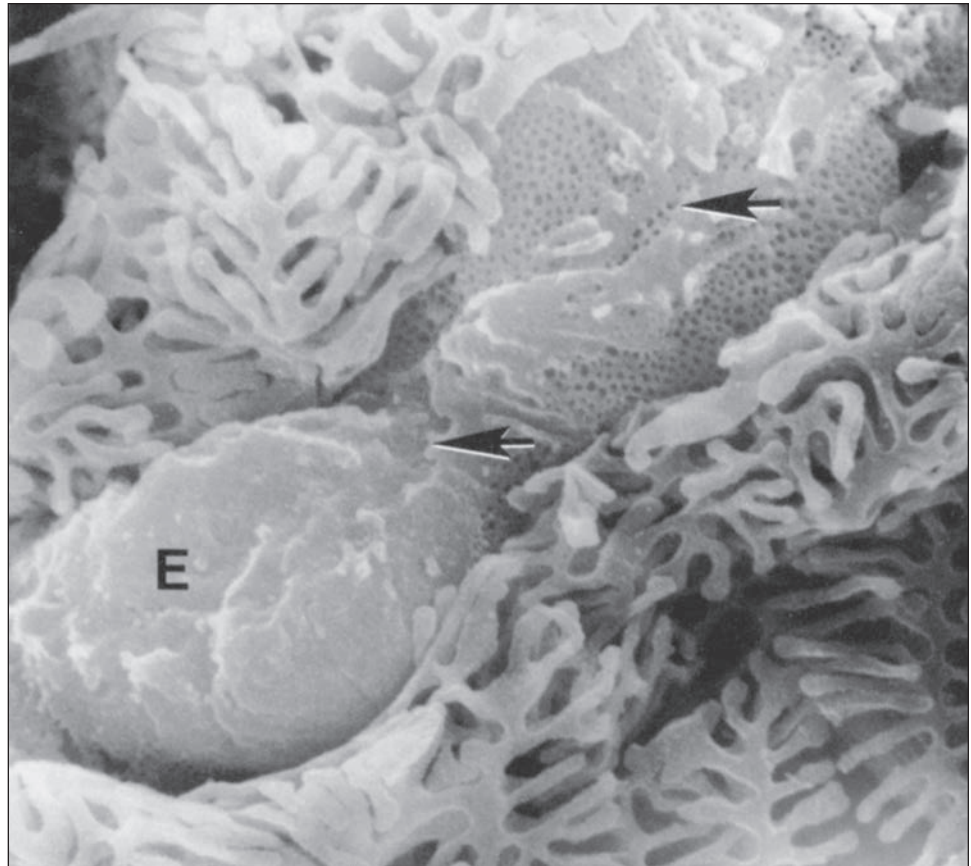
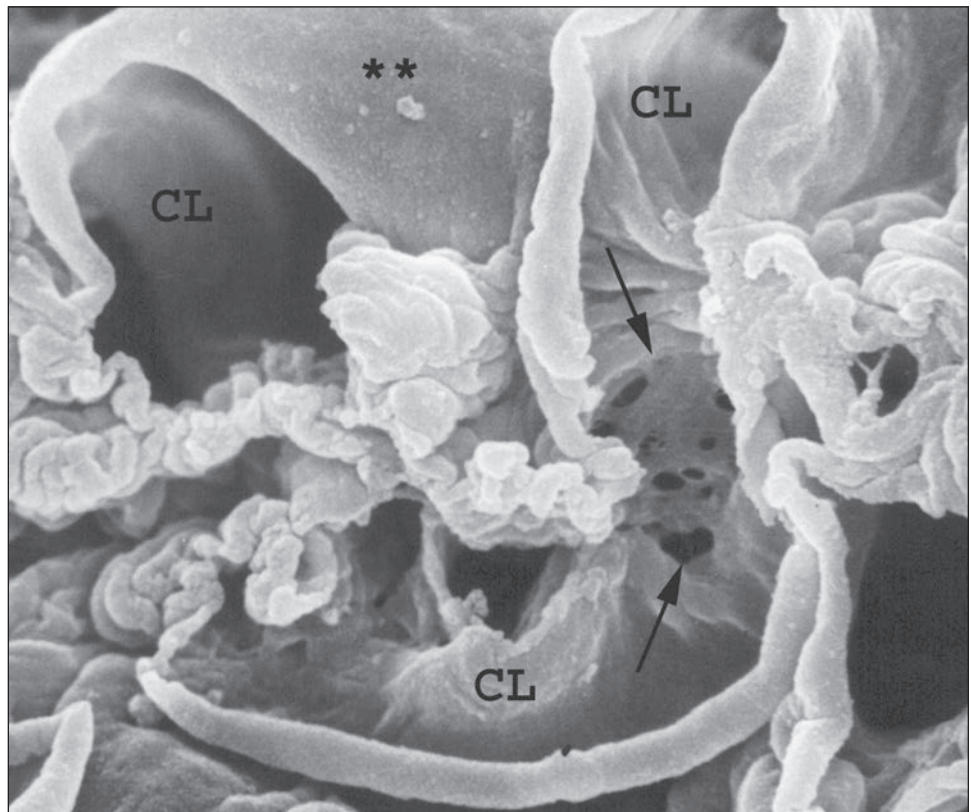


FIGURE 1.62 Scanning electron micrograph of a human glomerulus following detergent extraction of glomerular cells. Notice the smooth inside (CL) and outside (*double asterisk*) surfaces of the capillary loop basement membrane and the corrugated mesangial waist. The fenestrated mesangium (*arrows*) at the mesangial-endothelial interface, where direct cellular contact occurs, is displayed. ($\times 4200$.)



actin cytoskeleton at the attachment plaques to extracellular fibronectin that coats matrix microfibrils (148–156).

The smooth muscle properties of mesangial cells and their ultrastructural relationships with the matrix may suggest the capacity to generate mechanical forces. There is experimental evidence with use of vasoconstrictors *in vitro* and *in vivo* to suggest that mesangial cell contraction may have the potential to alter the capillary loop filtration dynamics by decreasing filtration surface area. Alternatively as postulated by Kriz (93,151), the role of a contractile apparatus may be static in nature, intended to counteract expansive intravascular forces and thereby stabilize the glomerular tuft. The drawing in Figure 1.60 illustrates this possibility. Mesangial cell processes that bind directly to the mesangial matrix and to the GBM are particularly prominent at the juxtacapillary region. Cell processes extend beneath the endothelium along the proximal portion of both mesangial-capillary loop junctions, and microfilament bundles connect the two opposing mesangial angles, extending to the opposite mesangial waist GBM. Mesangial cells

also generate various molecules in a paracrine and autocrine fashion and respond to these molecules during immune and nonimmune glomerular injuries with proliferation and matrix production or degradation (149,155,156). The second type of mesangial cell constitutes only 10% to 30% of the total number of glomerular cells in rodents. It has phagocytic properties and may be derived from the bone marrow. It may participate in turnover of immune complexes (156). It is not known if a comparable cell population exists in the human mesangium.

Glomerular Matrix

The extracellular matrix of the kidney plays diverse roles including filtration, cell adhesion, and providing important signals for cell function, migration, and differentiation; all of these functions are linked to specific molecular epitopes (157–171). The glomerulus has three distinct extracellular matrices: the GBM, mesangium, and BC. These matrices differ in function, which is reflected in differing molecular composition (Fig. 1.63). Within the tubular portion of the nephron, there

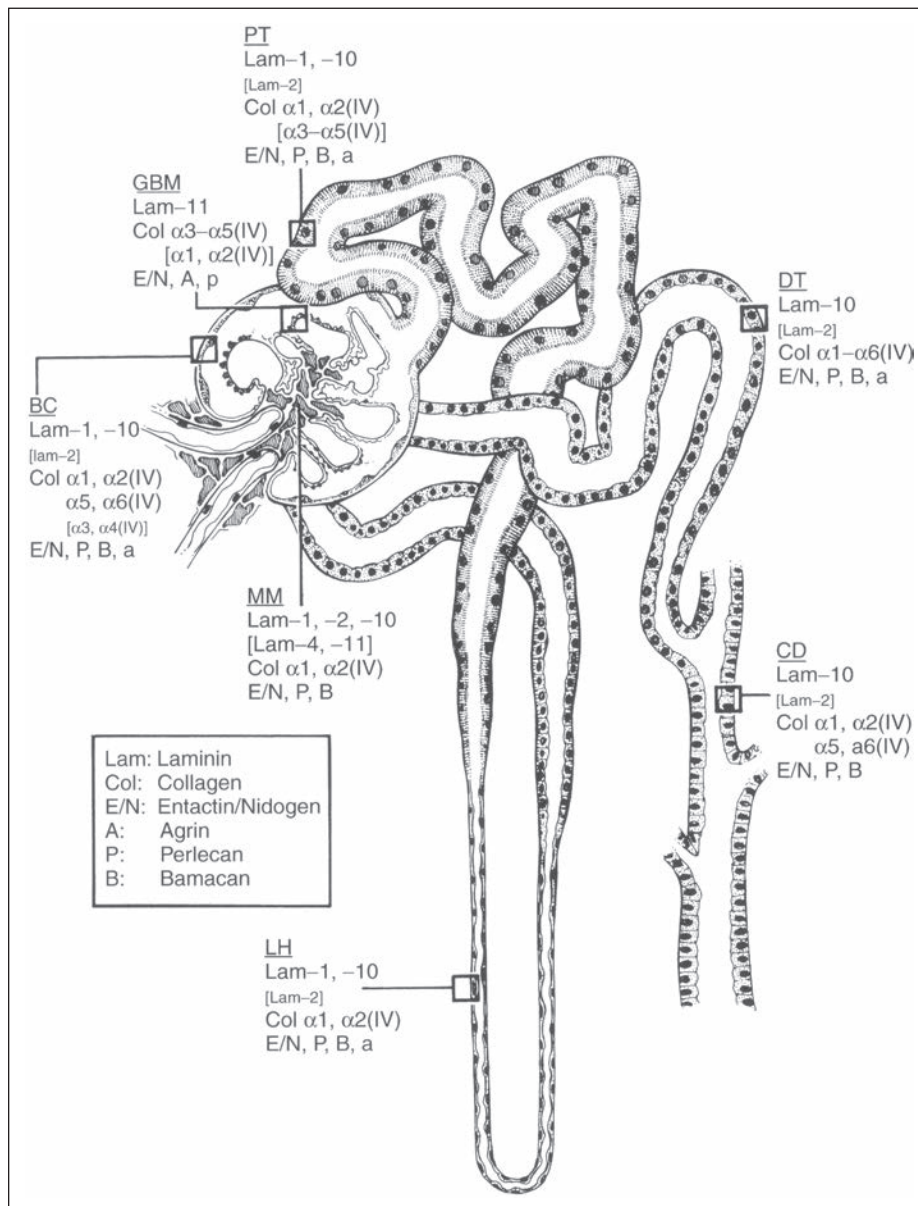


FIGURE 1.63 Schematic diagram of the nephron and an associated collecting duct with the components of the various basement membranes and of the mesangial matrix listed. Components in brackets were not observed in all species tested, and those in lower case or small font were observed only at low levels. As discussed in the text, laminin trimers are predicted based on immunohistochemical colocalization and thus could be incorrect. However, they still correctly describe which individual chains are present. GBM, glomerular basement membrane; MM, mesangial matrix; BC, Bowman capsule; PT, proximal tubule; LH, loop of Henle; DT, distal tubule; CD, collecting duct. (From Minor J. Renal basement membrane components. *Kidney Int* 1999;56:2016.)

is also segment-specific molecular heterogeneity of renal BM components, likely also linked to segment-specific functional differences. Some constituents of the BMs are developmentally regulated; most notable are the transitions in collagen type IV α -chains and laminin chains that coincide with morphologic transitions in the developing nephron (165–168).

Glomerular Capillary Loop Basement Membrane

Glomerular capillary loop basement membrane (GBM) consists of an intricately orchestrated meshwork positioned between podocytes and endothelial cells of the capillary loops. The GBM has sieve-like and ionic properties that contribute to capillary loop filtration, provides structural support, and contains ligands that serve as receptors that influence cell signaling and cell polarization (108,163–168). The GBM is twice the thickness of most capillary BMs in the body. In the adult human, it is 300 to 350 nm. The GBM is slightly thicker in men than in women and is thinner in children, who achieve adult thickness by age 10 to 12 years (169,170). The GBM thickness varies between species and is 110 to 160 nm in the rat.

The GBM consists of the fused basal lamina of its investing endothelial and visceral epithelial cells (157–164). It has a trilaminar appearance by electron microscopy, well demonstrated in rodents but less evident in humans. The three layers include an inner lamina rara interna, a thick central lamina densa, and an outer lamina rara externa. At the vascular pole and urinary pole, the GBM transitions into the BC BM and the tubular BM, respectively; these differ somewhat in composition. The major constituents of the GBM include type IV collagen, noncollagenous glycoproteins such as laminin and enactin/nidogen, and several sulfated proteoglycans, the major one being agrin (162–168). The central portion, the lamina densa, consists principally of type IV collagen and laminin, whereas other components are richer in the lamina rara interna and externa (Figs. 1.64 and 1.65). Enactin/nidogen cross-links

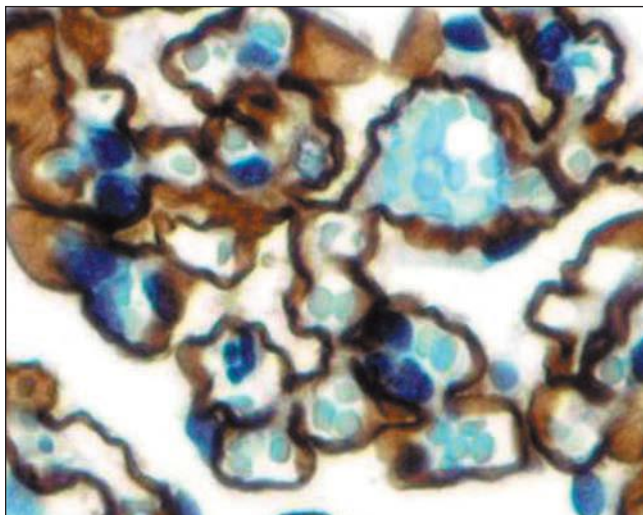


FIGURE 1.64 Human glomerulus type IV collagen α 5 chain stain. The glomerular capillary loop basement membrane is stained while the mesangial matrix is negative. (Immunoperoxidase stain for collagen type IV α 5-chain, $\times 650$.)

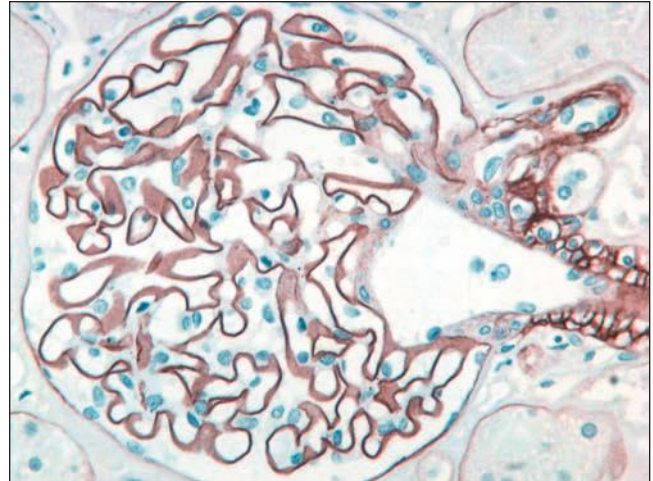


FIGURE 1.65 Human glomerulus LM-521 stain. The capillary loop basement membranes and basement membranes investing arteriolar smooth muscle are stained for this laminin isoform while the mesangial matrix is negative. (Immunoperoxidase stain for LM 521, $\times 400$.)

laminin and collagen type IV, whereas proteoglycans, such as agrin and perlecan, contribute to its negative charge and its hydration.

COLLAGEN TYPE IV

Understanding of type IV collagen began with Kefalides (172), who first discovered collagen type IV in the canine GBM in 1966. The triple helical protomeric substructure was identified by Timpl et al. and shown to self-assemble to form tetramers through N-terminal domains and dimers at their C-terminal domains (173,174). However, after years of intensive investigation of diseases of collagen type IV such as diabetes mellitus, Goodpasture syndrome, and Alport syndrome, Hudson et al. and other investigators unraveled the details of type IV α -chain molecular complexity and clarified the nature of their associations with other molecular constituents of the GBM (162–165,175–183). The α 1 and α 2 chains were first identified, followed by discovery of the α 3-chain; subsequently, the α 4, α 5, and α 6 chains were discovered, thus defining the six chains of the type IV collagen. X-ray crystallography elucidated its quaternary network structure (183).

Collagen is a family of molecules with 25 or more members. Collagen type IV is a 400-nm-long rod-shaped triple helix that consists of heterodimers of three α -chain combinations (α 1 to α 6) (Fig. 1.66). Each alpha chain has three domains: a short N-terminal 7S domain, a long central collagenous domain, and a C-terminal noncollagenous (NC1) domain. The collagen molecules are characterized by repeating glycine-X-Y sequences where X and Y can be any other amino acid. Unlike collagen types I, II, and III, collagen type IV contains interruptions of the typical glycine-X-Y repeats in the major collagenous domain that represent attachment sites for other BM molecules. All six α -chains have been sequenced and chromosomal locations identified (Table 1.3). The six α -chains assemble to form triple helical molecules called protomers. Only three sets of protomers have been discovered to form, so far, α 1. α 1. α 2(IV), α 3. α 4. α 5(IV), and α 5. α 5. α 6(IV).

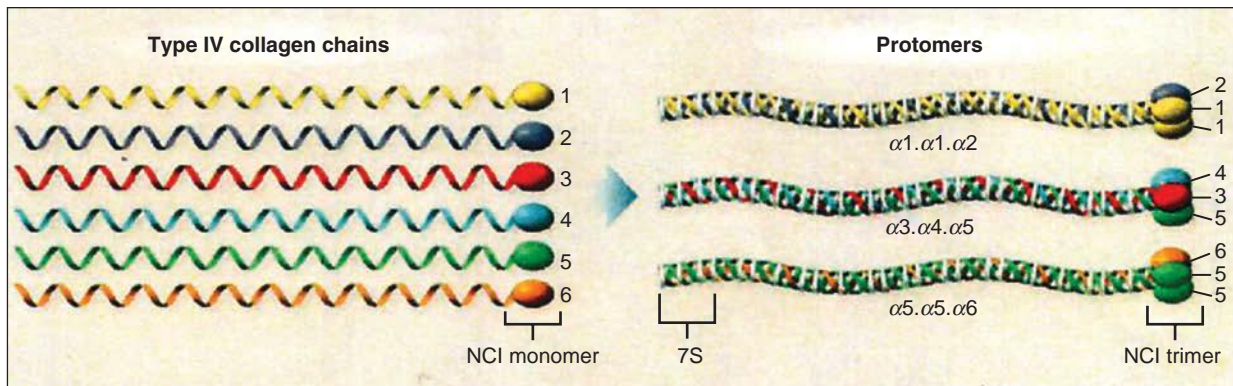


FIGURE 1.66 Triple-helical organization of the type IV collagen family. Six genetically distinct chains are arranged into three triple helical protomers that differ in their chain composition. Each protomer has a 7S triple-helical domain at the N terminal; a long triple-helical, collagenous domain in the middle of the molecule; and a noncollagenous domain (NCI) trimer at the C terminal. Interruptions on the Gly-Xaa-Yaa amino acid sequence at multiple sites along the collagenous domain confer flexibility, allowing for looping and supercoiling of protomers into networks. The selection of α -chains for association into trimeric protomers is governed by molecular recognition sequences encoded within the hypervariable regions of the NCI domains. (From Hudson BG, Tryggvason K, Sundaramoorthy M, et al. Alport's syndrome, Goodpasture's syndrome, and type IV collagen. *N Engl J Med* 2003;348:2543. Copyright © 2003 Massachusetts Medical Society. All rights reserved.)

The protomers combine to form networks by a combination of end-to-end C-terminal and side-to-side N-terminal associations, disulfide bonding, and supercoiling. The NCI domains of two α -chain protomers combine end to end to form protomeric hexamers. This is governed by molecular recognition sequences encoded within the NCI domains. At the opposite end of α -chain protomers, the 7S domains of four protomers unite side by side to form protomeric tetramers. Spontaneous supercoiling and looping of the triple helices are fixed with disulfide cross-links. The $\alpha 3 . \alpha 4 . \alpha 5 (IV) - \alpha 3 . \alpha 4 . \alpha 5 (IV)$ network is elegantly illustrated in the diagram of Hudson et al. in Figure 1.67, with an adjacent computer model of its crystal structure.

Only three sets of networks form: the $\alpha 1 . \alpha 1 . \alpha 2 (IV) - \alpha 1 . \alpha 1 . \alpha 2 (IV)$ network, the $\alpha 3 . \alpha 4 . \alpha 5 (IV) - \alpha 3 . \alpha 4 . \alpha 5 (IV)$ network, and the $\alpha 1 . \alpha 1 . \alpha 2 (IV) - \alpha 5 . \alpha 5 . \alpha 6 (IV)$ network; their distribution is heterogeneous. The $\alpha 1 . \alpha 1 . \alpha 2 (IV) - \alpha 1 . \alpha 1 . \alpha 2 (IV)$ network is essentially ubiquitous, forming a component of nearly all BMs of all animal phyla. However, the $\alpha 3 . \alpha 4 . \alpha 5 (IV) - \alpha 3 . \alpha 4 . \alpha 5 (IV)$ network and $\alpha 1 . \alpha 1 . \alpha 2 (IV) - \alpha 5 . \alpha 5 . \alpha 6 (IV)$ network are restricted to sites with more specialized functions. The mammalian kidney, eye, lung, testis, and

cochlea contain the $\alpha 3 . \alpha 4 . \alpha 5 (IV) - \alpha 3 . \alpha 4 . \alpha 5 (IV)$ network. The BC, skin, smooth muscle, and esophagus contain the $\alpha 1 . \alpha 1 . \alpha 2 (IV) - \alpha 5 . \alpha 5 . \alpha 6 (IV)$ network. The $\alpha 3 . \alpha 4 . \alpha 5 (IV)$ and the $\alpha 5 . \alpha 5 . \alpha 6 (IV)$ networks of the GBM and BC, respectively, are developmentally regulated. They are preceded by the $\alpha 1 . \alpha 1 . \alpha 2 (IV)$ network at the start of capillary loop formation and are gradually replaced by embryonic day 150. Mutation of particular alpha chains of the $\alpha 3 . \alpha 4 . \alpha 5 (IV) - \alpha 3 . \alpha 4 . \alpha 5 (IV)$ network can result in GBM defects ranging from thin BM nephropathy to Alport syndrome.

NONCOLLAGENOUS GLYCOPROTEINS AND PROTEOGLYCANs

Laminins are a family of molecules that represent the most abundant noncollagenous protein in nephron BMs (95–99,158–164,167,168). Laminins are large disulfide-bonded heterotrimers that, like collagen, consist of three chains: an α -, β -, and γ -chains. Two chains are glycosylated and cross-linked by disulfide bonds. There are at least five alpha chains ($\alpha 1$ to $\alpha 5$), four beta chains ($\beta 1$ to $\beta 4$), and three gamma chains ($\gamma 1$ to $\gamma 3$) that assemble to form at least 15 known heterotrimers.

Laminin trimers form intracellularly within the endoplasmic reticulum, are secreted, and then self-assemble, like collagen IV does. Laminins form a network with collagen IV and other glycoproteins such as entactin and proteoglycans. Laminin participates in epithelial cell and endothelial cell adhesion to the extracellular matrix and in cell signaling through interactions with numerous integrins and dystroglycan (162–168). Four laminin isoforms occur in the kidney: laminin 1 ($\alpha 1, \beta 1, \gamma 1$, now known as LM-111), laminin 2 ($\alpha 2, \beta 1, \gamma 1$, now known as LM-211), laminin 10 ($\alpha 5, \beta 1, \gamma 1$, now known as LM-511), and laminin 11 ($\alpha 5, \beta 2, \gamma 1$, now known as LM-521). These laminin isoforms have a restricted distribution in the kidney (see Fig. 1.63). Laminin 521 is the principal laminin in the GBM. Laminin 511 is developmentally expressed with transition from LM-511 to LM-521 in the mature GBM. Laminin LM-111, LM-211, and LM-511

TABLE 1.3 Collagen type IV

α -Chains	Chromosome	Glomerular localization
Collagen IV $\alpha 1$	13q34	GBM, mesangium, Bowman capsule
Collagen IV $\alpha 2$	13q34	GBM, mesangium, Bowman capsule
Collagen IV $\alpha 3$	2q35–q37	GBM
Collagen IV $\alpha 4$	2q35–q37	GBM
Collagen IV $\alpha 5$	Xq22	GBM, Bowman capsule
Collagen IV $\alpha 6$	Xq22	Bowman capsule

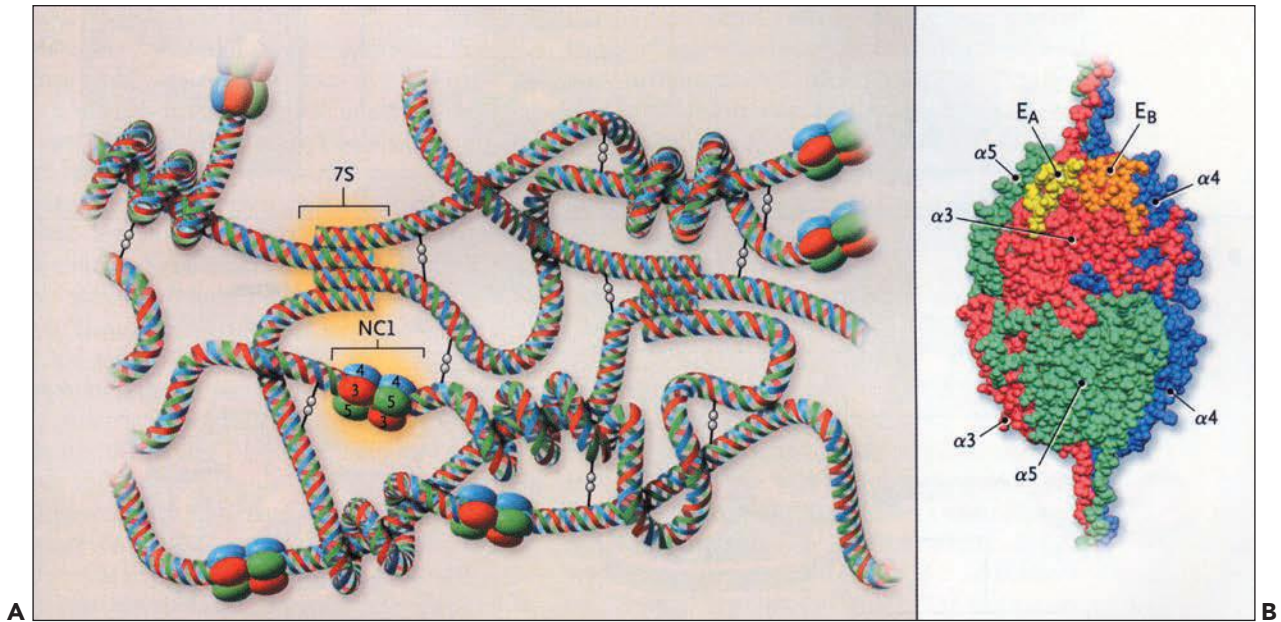


FIGURE 1.67 Assembly and network organization of collagen IV protomers. A: Protomers create basement membrane networks with other protomers by uniting two NC1 trimers to form an interface at the C terminal and by uniting four triple-helical 7S domains at the N terminal. A network composed of $\alpha3.\alpha4.\alpha5(\text{IV})$ protomers is illustrated, showing end-to-end connections of individual protomer units, supercoiling and looping of the triple helices, and disulfide cross-links between triple helical domains. The structure of the NC1 hexamer is determined by the particular α -chains that form a triple helical protomer and by the particular canonical protomers that can connect to adjoining protomers (NC1 box). Molecular recognition sequences encoded within the NC1 domains govern the selection of partner chains for both protomer and network assembly. The 7S domain also plays a key part in determining the specificity, affinity, and geometry of the tetramer formed through the connection of four protomers (7S box). Two other networks are composed of pairs of $\alpha1.\alpha1.\alpha2(\text{IV})$ hexamers or $\alpha1.\alpha1.\alpha3(\text{IV})\text{--}\alpha5.\alpha5.\alpha6(\text{IV})$ NC1 hexamers. The $\alpha3.\alpha4.\alpha5(\text{IV})\text{--}\alpha3.\alpha4.\alpha5(\text{IV})$ network differs from the others in that it has a greater number of disulfide cross-links between triple helical domains, which increases its resistance to proteolysis. **B:** The three-dimensional model of the $\alpha3.\alpha4.\alpha5(\text{IV})$ NC1 hexamer that is depicted in the NC1 box in (A). The three-dimensional structure and the location of epitopes were determined by computer modeling of the crystal structure of the $\alpha1.\alpha1.\alpha2(\text{IV})\text{--}\alpha1.\alpha1.\alpha2(\text{IV})$ hexamer and the apparent quaternary structure of the $\alpha3.\alpha4.\alpha5(\text{IV})$ hexamer. The hexamer is composed of two trimeric caps, each derived from adjacent protomers. Each trimer consists of an $\alpha3$ monomer (*red*), an $\alpha4$ monomer (*blue*), and an $\alpha5$ monomer (*green*). The monomers have a novel tertiary structure with two homologous subdomains, each of which is characterized by β -sheet motifs. The model depicts the location of the E_A (yellow) and the E_B (orange) regions that encompass two dominant epitopes for Goodpasture antibodies. The epitopes reside in the $\alpha3(\text{IV})$ NC1 domain, near the triple helical junction, and they are partially sequestered by interactions with the $\alpha5(\text{IV})$ and $\alpha4(\text{IV})$ domains, respectively. (From Hudson BG, Tryggvason K, Sundaramoorthy M, et al. Alport's syndrome, Goodpasture's syndrome, and type IV collagen. *N Engl J Med* 2003;348:2543–2556. Copyright © 2003 Massachusetts Medical Society. All rights reserved.)

are present in the mesangium, while the BC and the tubular BMs principally contain LM-111 and LM-511.

Entactin/nidogen (two names for the same molecule) has two isoforms. Nidogen-1 is present in the kidney. It is a 150-kDa single-chain glycoprotein (166–168). It has three globular domains (G1, G2, and G3) separated by two linear segments. It is a ubiquitous BM protein present in all renal BMs and peripheral mesangial regions. Nidogen-1 has a strong affinity for both the laminin α -chains (binds to G3 domain) and the triple helix of collagen IV (binds to G2 domain), serving as a link between these two molecules. It also binds perlecan and fibulin-1 and -2 (184). It is not known if entactin/nidogen has roles other than structural in BMs.

Proteoglycans are macromolecules that confer the negative charge to the GBM and keep the GBM network highly

hydrated by trapping water molecules in the interstices of the matrix (178,185,186). They are composed of glycosaminoglycan chains and contain either heparan sulfate or chondroitin sulfate. The three major proteoglycans are agrin, perlecan, and bamacan. Agrin has a highly negative charge due to sulfated glycosaminoglycan side chains (162–168). Agrin is the most abundant proteoglycan in the GBM, present in all three layers. Agrin is present at only low levels in TBMs. Agrin binds to laminin and dystroglycan and may therefore be involved in podocyte FP adhesion. Perlecan also contains heparan sulfate and contributes to the negative charge of the GBM. It is present in relatively small quantities in the subendothelial portion of the GBM. Bamacan is a chondroitin sulfate-containing proteoglycan. Bamacan exhibits a wide distribution in BMs. Bamacan is present in

the developing GBM but absent from the mature GBM, suggesting some role in development. Bamacan is present in all other renal BMs.

Mesangium

The mesangium, first described by Zimmerman in 1929 (145), consists of mesangial cells and mesangial matrix. The mesangium is a continuous tree-like branching matrix that provides the supporting infrastructure for the glomerulus (185,187). In three-dimensional reconstructions in the rat, the mesangium has three major trunks (Fig. 1.68). Short secondary branches arise from the major trunks. The mesangial base is contiguous with the extraglomerular mesangium at the glomerular vascular stalk and forms part of the JGA (see Fig. 1.38). Within the glomerulus, the capillary loops wrap around the mesangial matrix branches and may even form occasional mesangial loops whereby the matrix largely or completely encircles a capillary

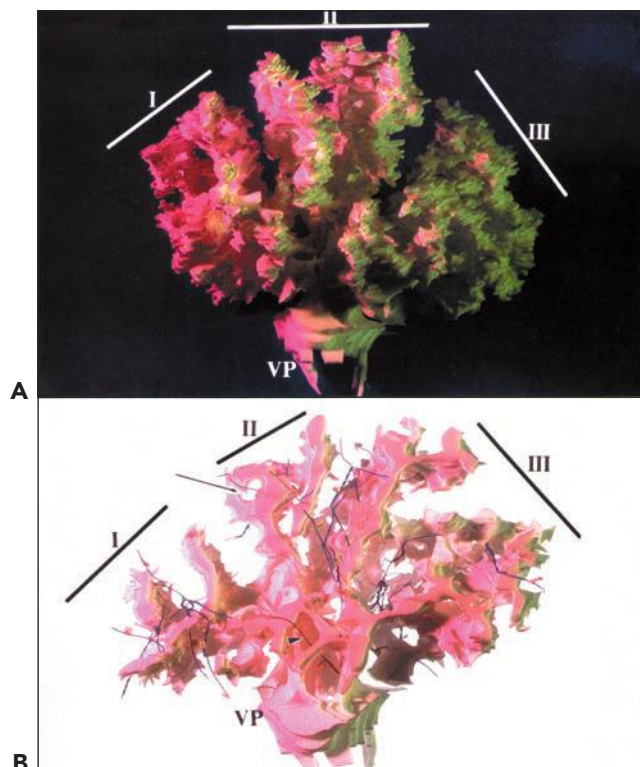


FIGURE 1.68 Photographs of a styrene model of the mesangium of a whole (rat) glomerulus illuminated by red and green light to enhance the three-dimensional structure. **A:** View from above. The whole mesangium is divided into three lobes (I, II, and III), and each extends to the periphery from the vascular pole (VP). **B:** View from the vascular pole. Wires show glomerular capillaries and the efferent arteriole at the vascular pole. The efferent arteriole possesses a substantial intraglomerular segment completely surrounded by the mesangium (arrowhead). In the periphery, a glomerular capillary is completely surrounded by mesangium (arrow). The authors termed the structure of the mesangium completely surrounding a capillary as the “mesangial loop.” (From Inkayo-Hayasaka K, Sakai T, Kobayashi N, et al. Three-dimensional analysis of the whole mesangium in the rat. *Kidney Int* 1996;50:672.)

loop. The mesangium interfaces with endothelial cells along the juxtacapillary region where matrix fenestrations allow direct contact between mesangial cells and endothelial cells and with the GBM in the paramesangial waist regions (see Figs. 1.42, 1.59, and 1.62).

The mesangial matrix differs from the GBM in filtration properties, ultrastructural appearance, and molecular composition (see Fig. 1.63). The mesangium is more porous than the GBM; macromolecules too large to pass through the GBM easily enter the mesangium (185,188–194). Its basic structure consists of an elastic scaffolding of unbranched noncollagenous microfibrils, best revealed by TEM with tannic acid staining. The microfibrils account for the coarsely fibrillar ultrastructural appearance of the mesangium (see Fig. 1.56B). The microfibrils resemble elastic fibers and contain similar proteins that are not present in the GBM (189–191). The major protein of the microfibril is fibrillin-1, which is particularly concentrated at the mesangial-endothelial interface and along the paramesangial-GBM interface. Additional proteins include emilin, microfibril-associated proteins (MAPs) 1 and 2, and latent transforming growth factor-binding protein-1 (LTBP-1). Elastin is not present within the mesangium but is present within the renal vasculature.

In addition to the microfibrillar scaffolding, the mesangial matrix contains type IV collagen (α -1 and α -2, but not α -3 to α -5 chains), type V collagen and laminin, LM-111, LM-211, LM-511, rather than LM-521 as for the GBM, and the proteoglycans perlecan and bamacan but lacks agrin, the dominant proteoglycan of the GBM (see Fig. 1.63). The most abundant matrix protein in the mesangium is fibronectin. Fibronectin coats the surface of the matrix microfibrils and, in concert with the other microfibril proteins, mediates attachment of microfibrils to mesangial cells via cell membrane α 3 β 1 and α 5 β 1 integrins. The microfibrils extend into the GBM lamina densa and attach to GBM structural proteins on opposing sides (see Fig. 1.60). This arrangement of microfibrils, which tethers mesangial cells to the GBM, may facilitate the transmission of mesangial contractile forces, and more important, it may counterbalance forces that could expand the mesangium (186,195,196).

Bowman Capsule

BC is a thick connective tissue barrier between the glomerular filtrate within the Bowman space and the interstitium (197). It is roughly spherical and lined along its inner surface by PECs. The BC is breached on opposing sides by the ostia of the PT and the entry and exit, respectively, of the afferent and efferent arterioles. The BC is continuous with the proximal tubular BM at the urinary pole and reflects onto the GBM at the vascular pole. Detailed ultrastructural studies of a rat BC reveal a multilayered structure consisting of 100-nm filament bundles composed of 5- to 15-nm filaments. The bundles are separated by lucent spaces and oriented in different directions between the BM layers. The major molecular constituents of BC are collagen type IV α -1,2 and α -5,6, laminins LM-111 and LM-511, entactin/nidogen, perlecan, and bamacan (185). The BC is invested on its outer aspect by interstitial connective tissue, 30-nm reticular fibers that contain type III collagen, and membrane-bound granular vesicles (also known as granular and vesicular structures and spherical microparticles). Interstitial fibroblasts attach to BC, providing the scaffold to

maintain the position of the glomerulus within the interstitial matrix.

Blood Vessels and the Juxtaglomerular Apparatus

Juxtaglomerular Apparatus

The JGA marks the end of the TAL and the beginning of the DCT. The JGA is a composite structure composed of specialized epithelial cells, the macula densa (MD), vascular components including portions of the afferent and efferent arterioles, and extraglomerular cells known as *lacis cells* (Figs. 1.38 and 1.69A) (184,198–206). This unit is richly innervated by sympathetic junctions of autonomic nerves that course along the arterioles and supply fine branches to smooth muscle cells, granular cells, and tubular cells (202) (see Fig. 1.22). The components of the JGA comprise a tightly integrated unit capable of regulating glomerular hemodynamics in response to hematogenous influences such as nitric oxide, hormones, blood pressure, and local influences, such as the composition of tubular fluid at the MD (204–216).

The epithelial component of the JGA is the MD epithelium. The MD consists of a plaque of specialized tubular cells, polarized to the glomerular side of the tubule and projecting into the lumen (Figs. 1.38, 1.69A, and 1.70). In contrast to its neighboring cells in the TAL, the MD cells are taller with an apical nucleus, small mitochondria, and a Golgi apparatus polarized toward the basal side of the cell. The MD cells have short surface microvilli but lack lateral interdigitation characteristic of other cells of the TAL. They do have variably sized lateral intercellular spaces that may expand or contract under

physiologic conditions. The MD cells lack Na⁺-K⁺-ATPase and surface Tamm-Horsfall protein (207,208). The absence of Tamm-Horsfall protein may impart a water permeability function critical to the electrolyte-monitoring function of the JGA.

The MD cells rest on a uniquely configured BM that is contiguous with the lacis cell matrix. On silver-stained sections, the MD BM appears thin and indistinct compared with the contralateral tubular BM (see Fig. 1.69A). By TEM and acellular SEM preparations, the MD BM has an irregular ridged contour with tunnel-like extensions into which basal processes of the MD cells extend (see Fig. 1.69B) (209). These may amplify the surface area for communication between lacis cells and MD cells and enhance cell attachment to the structural unit whose physical state is not static.

The central portion of the JGA is a wedge of extraglomerular mesangium known as the *lacis*, or the *polar cushion*. This cone-shaped structure has its base attached to the MD epithelium, while its apex blends with the mesangial stalk. The lacis is populated by the lacis cells (cells of Goormaghtigh). Ultrastructurally, these cells resemble mesangial cells. They are surrounded by a prominent extracellular matrix and have extensive cell processes that establish gap junctions with adjacent cells, excluding the MD cells. The lacis cells function as a physiologic liaison between MD cells and arteriolar smooth muscle cells and the arteriolar granular myoepithelioid cells.

The vascular components of the JGA include the terminal portion of the afferent arteriole and the proximal portion of the efferent arteriole. Some would also include the peripolar cells in the JGA, although the function of these cells remains

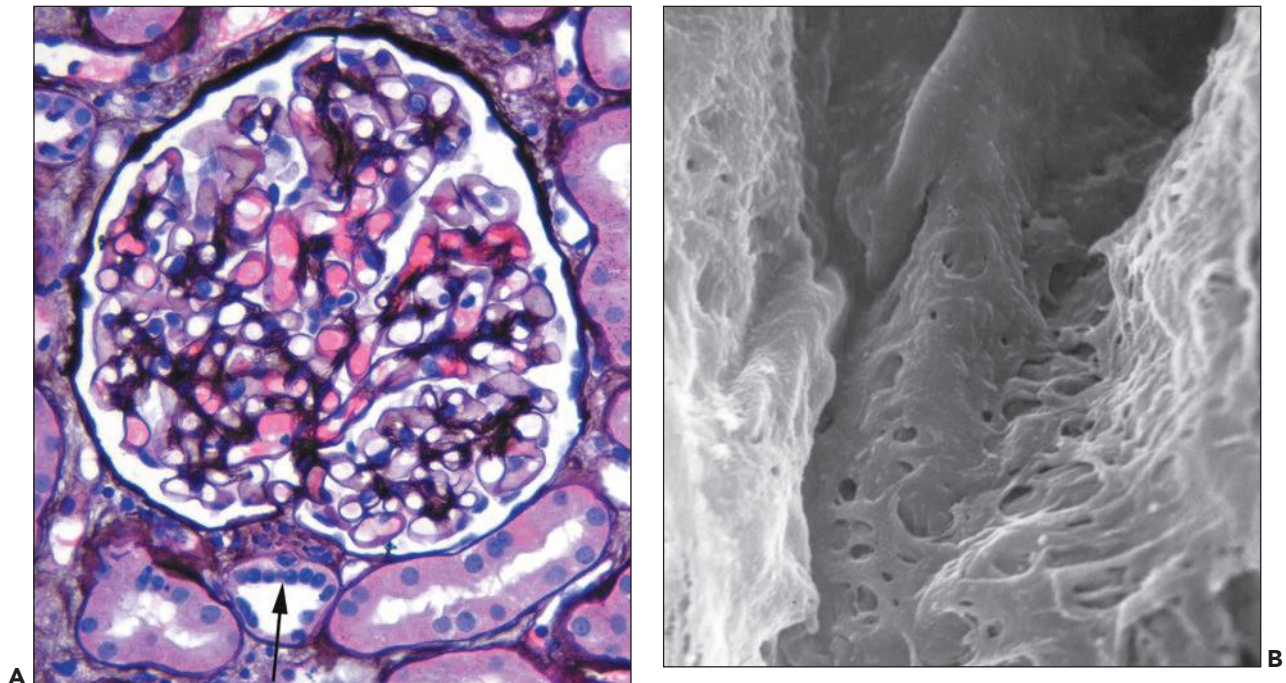


FIGURE 1.69 Human glomeruli. A: The macula densa has a less distinct (*arrow*) basement membrane on silver stain compared with the contralateral thick ascending limb basement membrane. (Jones methenamine silver stain, $\times 300$.) **B:** Scanning electron micrograph of the macula densa basement membrane luminal aspect following detergent removal of macula densa epithelium. Notice the ridged surface with numerous shallow invaginations into which macula densa epithelial cell processes extend. ($\times 17,500$.)

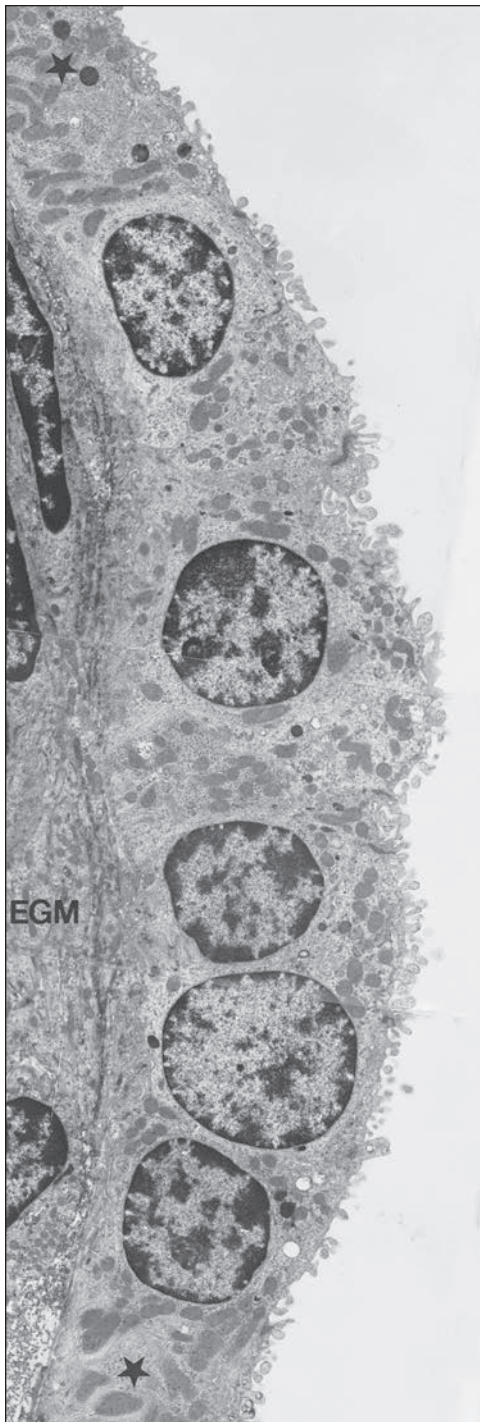


FIGURE 1.70 Macula densa of the rat. The macula densa is a plaque of some 20 polygonal cells, which are bordered peripherally by cells of the thick ascending limb (*stars*). The macula densa cells are characterized by large nuclei; the luminal cell membrane is densely covered by microvilli. The width of intercellular spaces between macula densa cells may change from narrow (as in this case) to dilated. The macula densa abuts the extraglomerular mesangium (EGM) separated by a tortuous basement membrane. ($\times 4500$.)

unknown. In the wall of the afferent arteriole, polarized toward the JGA, are small clusters of four or five modified smooth muscle cells known as *granular myoepithelioid cells* (210–212). These cells contain myofilaments and attachment plaques and have other features of smooth muscle cells but are also endowed with a prominent endoplasmic reticulum and a Golgi apparatus for synthesis and secretion of renin and angiotensin II (Fig. 1.71). These latter components are contained in variably sized and shaped dense granules. Similar granules can occasionally be seen in cells of the polar cushion. The smallest granules form at the exit point of the Golgi zone. They are rhomboidal with a paracrystalline substructure and known as *protogranules* (Fig. 1.71B). The protogranules coalesce to form large mature granules that exocytose following certain physiologic stimuli. The granular epithelioid cells have cell processes and establish gap junction contact with smooth muscle cells, other granular cells, lacis cells, and even endothelial cells. The number of granular cells varies greatly because filament-rich smooth muscle cells can undergo metaplasia to granular myoepithelioid cells and produce renin and angiotensin II.

Arteries and Veins

The structure of arteries and veins is similar to that of vessels elsewhere in the body (217–222). The arteries have a connective tissue adventitia, media consisting of smooth muscle cells and their investing basal lamina, and an endothelial cell-lined intima (Fig. 1.72). In the largest arteries, an internal elastic lamina and external elastic lamina divide the three regions. The smaller arteries have only an internal elastic lamina, which is lost with transition into arterioles. The periarterial adventitial connective tissue is a continuous sheath of collagen that invests the entire arterial and arteriolar system. It contains fibroblastic cells, scattered passenger cells such as dendritic cells, lymphocytes, and macrophages, intrarenal nerve fibers, and lymphatics (see Figs. 1.20 and 1.21).

The veins of the cortex have a thin to nonexistent smooth muscle media and are lined by endothelium (see Fig. 1.25). Veins are separate from the arterial adventitial sheath. As veins descend toward the medulla, they increase in caliber and acquire an interrupted smooth muscle media. The interlobar veins, segmental veins, and main renal vein progressively acquire a continuous and more substantial smooth muscle media.

Arterioles and Capillaries

Arterioles and capillaries of the cortex and medulla also resemble those structures in other organs (217–222). The afferent arterioles of the glomeruli are the terminal branches of the interlobular arteries (the cortical radiating arteries). Each arteriolar branch is from 170 to 280 μm long and usually supplies a single glomerulus. Arterioles are the main resistance vessels in the kidney, and they regulate renal blood flow by contraction or relaxation of medial smooth muscle cells. Arterioles are lined by nonfenestrated endothelial cells, have a smooth muscle media and thin connective tissue adventitia, but lack an elastic lamina (Fig. 1.73). The endothelial cells rest on a thin basal lamina, and the smooth muscle cells are invested by their own basal lamina. The afferent arterioles of the midcortical and superficial glomeruli have a larger caliber than their companion efferent arterioles and also have a thicker media with one to three layers of medial smooth muscle cells compared with the

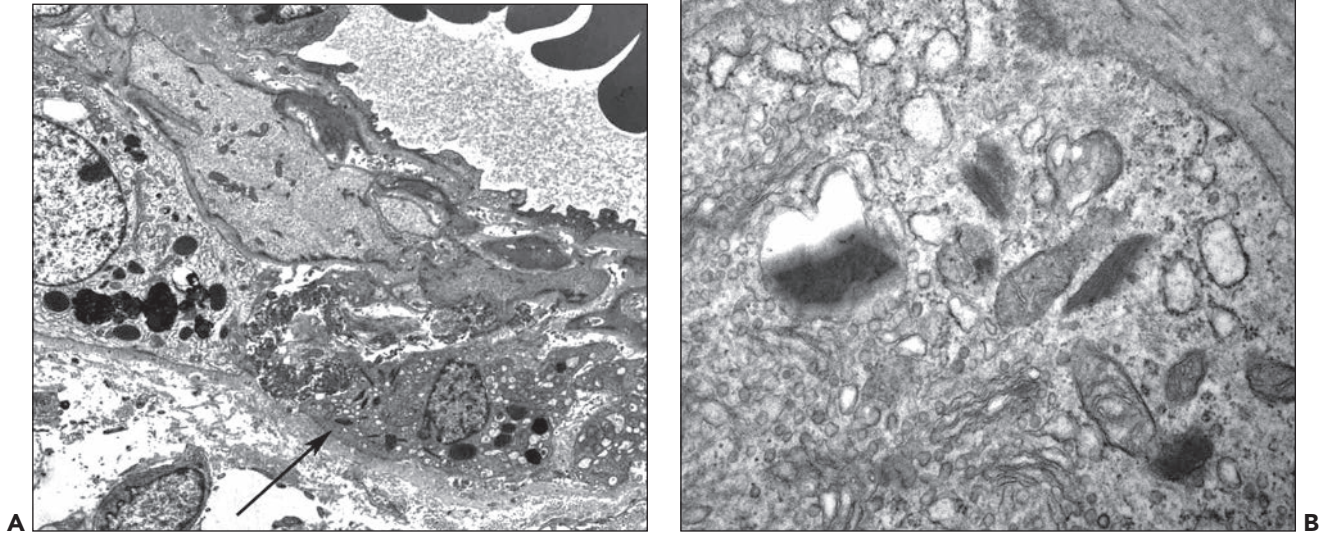


FIGURE 1.71 Human cortical afferent arteriole. **A:** It has an endothelial cell lining and two medial smooth muscle cells beneath. There are also two granular myoepithelioid cells at the bottom of the image. One cell contains rhomboid-shaped renin protogranules (*arrow*). To the right of its nucleus are several large round to oval electron dense granules representing coalesced renin protogranules. **B:** The renin producing smooth muscle cell of the afferent arteriole contains a large Golgi apparatus. Several electron dense rhomboid-shaped renin protogranules are present.

afferent arterioles, which usually have a single layer of smooth muscle.

The efferent arterioles of the superficial glomeruli are the longest and branch to generate capillary networks to supply the convoluted tubules of the cortical labyrinth. The midcortical efferent arterioles are shorter and supply the straight tubules of the medullary ray and adjacent cortical labyrinth tubules. The juxtamedullary efferent arterioles have a prominent

media, thicker than their companion afferent arterioles, with two to four layers of smooth muscle. They descend toward the medulla to form the vasa recta. As the vasa recta arterioles branch to enter the interbundle region, the smooth muscle cells are replaced by a pericyte layer that disappears at the origin of the medullary capillary plexus. The descending vasa recta arterioles show a progressive decrease in their smooth muscle layer as they descend, and this layer disappears in the inner medulla. The ascending vasa recta also lack a smooth muscle media. When the descending and ascending vasa recta are viewed in cross section in the outer medulla, they can be distinguished since the descending vasa recta have smooth muscle, whereas the ascending vasa recta have only an endothelial cell lining (see Fig. 1.33).

The capillaries of the cortex occupy the widened portions of the interstitium formed by confluence of the rounded contour of the tubules. These capillaries often have a portion of their wall closely apposed to tubular BMs. The peritubular capillaries are lined by a thin fenestrated endothelial cell layer and rest on a thin BM (Figs. 1.58 and 1.74). The endothelial fenestrations are closed by a thin diaphragm and often demonstrate a higher concentration in portions of the capillary apposed to the TBM, compared with the portion of endothelium facing the wider interstitium.

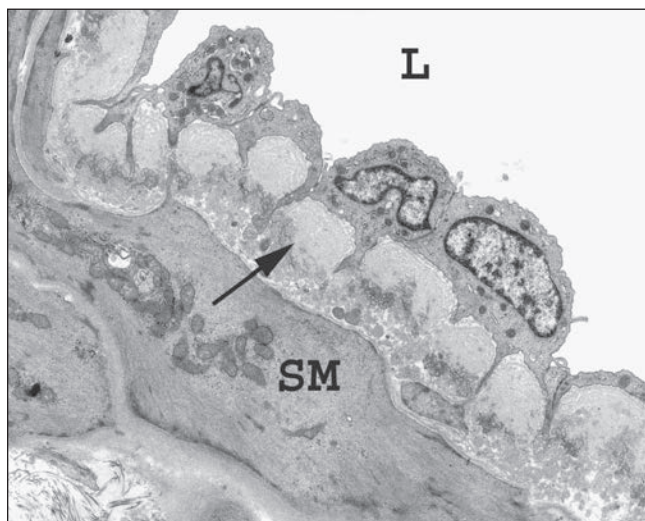


FIGURE 1.72 Human interlobular artery. The endothelium is separated from the contractile filament-rich smooth muscle (SM) cells by an internal elastic lamina and endothelial basement membrane (*arrow*). ($\times 2500$.) L, lumen.

RENAL TUBULES

The tubular portion of the nephron and CD consists of a lengthy epithelial-lined conduit of variable structure and function. The histology of renal tubules is optimized in perfusion-fixed kidney. As the quality of fixation decreases, delineation of a crisp cytologic detail decreases and tubules lose cytoplasmic

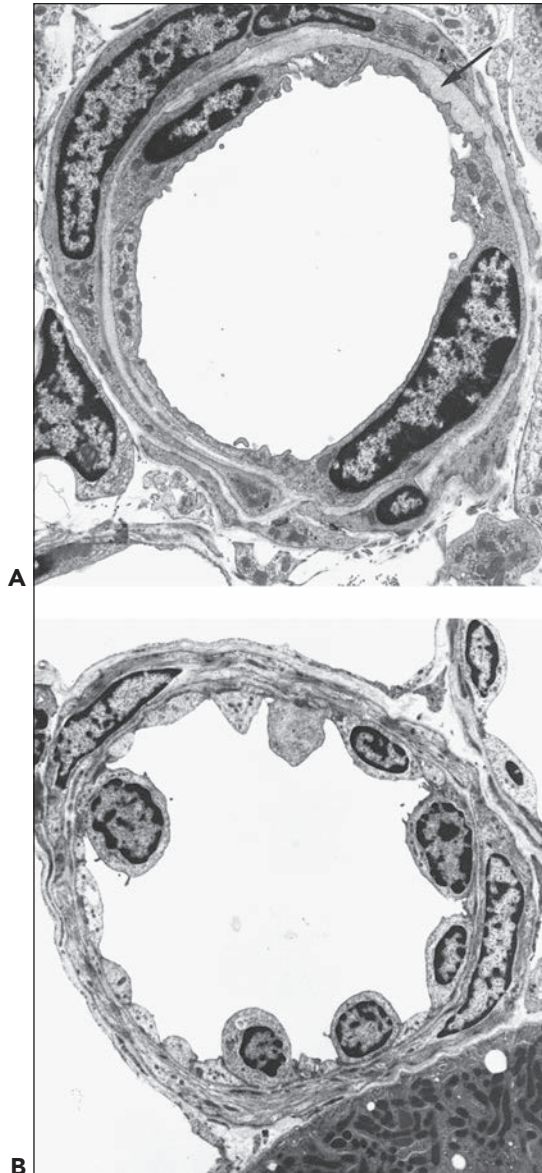


FIGURE 1.73 Glomerular efferent arterioles in the rat. **A:** Efferent arteriole of a midcortical glomerulus. The endothelial tube is encircled by a complete layer of smooth muscle cells. Conspicuous basement membrane-like material (*arrow*) lies beneath the endothelium, replacing a basement membrane proper. ($\times 4000$.) **B:** Juxtamedullary efferent arteriole. The endothelium is conspicuously composed of very many endothelial cell profiles. A complete muscle layer encircles the endothelial tube. ($\times 3000$.)

integrity and appear tattered. Tubular cytoplasm may fill the tubular lumen secondary to autolysis. Tubular segment identification by cytologic features, however, is still feasible in immersion-fixed tissue, especially when assisted by topography in large well-oriented sections. This becomes more difficult in randomly oriented human renal biopsy material, especially when affected by suboptimal fixation. There are immunohistochemical and histochemical probes that can provide tubular segment discrimination by capitalizing on differences in cytoskeletal proteins, adhesion molecules, cell receptors, and



FIGURE 1.74 Freeze-fracture replica of a peritubular capillary in the rat. The dense pattern of fenestrations in the capillary wall is visible. The thicker cytoplasmic strands of the endothelium contain pinocytotic vesicles (*arrows*). This type of endothelium is also found in cortical venules and veins and in ascending vasa recta. ($\times 12,800$.)

other segment-unique molecular products, permitting immunodissection to localize sites of a specific alteration. Most surgical pathology laboratories have a menu of staining options applicable to formalin-fixed tissue, allowing investigation of archival tissue (223–229). In the experimental laboratory, immunohistochemical reagents can be developed to capitalize on molecules with more restricted distribution, such as carbonic anhydrase in types A and B intercalated cell (IC), band 3 protein in type A ICs, or Tamm-Horsfall protein in the TAL.

Table 1.4 lists a sample of common, commercially available immunohistochemical reagents and lectins with their pattern of tubular staining in humans. Several reagents, such as cytokeratins 8 and 18, or certain lectins stain all tubules; other reagents have more restricted expression (223,224,230,231). Cytokeratins 7 and AE 1/3 localize to the DTs, loops of Henle, and CDs but spare PTs (Fig. 1.75). Cytokeratin 7 also spares the MD epithelium, while staining adjacent cells of the ascending thick limb and DCT. Other segment-restricted reagents include adhesion molecules such as E-cadherin, which is restricted to DTs and CDs but spares PTs, and CD-138

TABLE 1.4 Tubules: common antigens and lectins

Antigen	Proximal tubule			Distal tubule			
	Convoluted	Straight	Loop of Henle	Ascending thick limb	Macula densa	Convoluted	Collecting duct
Cytokeratin							
AE 1/3	Neg	Neg	Pos	Pos	Neg	Neg	Pos
CK 8	Pos	Pos	Pos	Pos	Pos	Pos	Pos
CK 18	Pos	Pos	Pos	Pos	Pos	Pos	Pos
CK 7	Neg	Neg	Pos	Pos	Neg	Pos	Pos-ind
34BE12	Neg	Neg	Neg	Neg	Neg	Neg	Pos
Other							
EMA	Neg	Neg	Pos	Pos	Pos	Pos	Pos-ind
CD 10	Pos	Pos	Neg	Neg	Neg	Neg	Neg
BB Ag	Pos	Pos	Neg	Neg	Neg	Neg	Neg
TH prot	Neg	Neg	Neg	Pos	Neg	Neg	Neg
E-cad	Neg	Neg	Pos	Pos	Pos	Pos	Pos
CD 138	Pos	Neg	Neg	Neg	Neg	Neg	Neg
B-3/CA	Neg	Neg	Neg	Neg	Neg	Neg	IC
Lectins							
WBA	Pos	Pos	Pos	Pos		Pos	Pos-ind
Con A	Pos	Pos	Pos	Pos		Pos	Pos
LTA	Pos	Pos	Pos	Neg		Neg	Med pos
DBA	Neg	Neg	Pos	Pos		Pos	Pos-ind
PNA	Neg	Neg	Pos	Pos		Pos	Pos-ind
SBA	Neg	Neg	Pos	Pos		Pos	Pos
UEA	Neg	Neg	Neg	Neg		Neg	Pos-ind

Pos, positive stain; Neg, negative stain; Pos-ind, positive stain in a selected population of cells that may represent differences in principal cell and intercalated cell staining; Med pos, medullary collecting ducts stain positive; IC, intercalated cell; A/E 1/3, cocktail containing CK 1-10, 13-6, and 19; 34BE12, cocktail containing CK 1, 5, 10, and 14; EMA, epithelial membrane antigen (human milk fat globule membrane); BB Ag, brush border antigen; TH-prot, Tamm-Horsfall protein; E-cad, E-cadherin; B-3, band 3 protein; CA, carbonic anhydrase; WGA, *Tritium vulgare* (wheat germ); Con A, *Concanavalin ensiformis* (jack bean); LTA, *Lotus tetragonolobus* (asparagus pea); PNA, *Arachis hypogaea* (peanut lectin); DBA, *Dolichos biflorus* (horse gram); SBA, glycine max (soybean); UEA, *Ulex europaeus* agglutinin I (gorse seed).

(syndecan), which stains PTs but not DTs and CDs. Lectins with restricted tubular segment distribution usually demonstrate either a PT profile or a DT and CD profile. Distinction between principal cells and ICs may be possible with several lectins, epithelial membrane antigen (EMA), and CK 7 (indicated by pos-ind in Table 1.4). The latter contention, however, is based on general cell cytology and distribution rather than on rigorous demonstration of cell specificity. EMA appears to stain the apical surface of CD principal cells, whereas ICs show diffuse cytoplasmic staining (Fig. 1.76A). Conversely, CK 7 appears to stain principal cells but not ICs, which stand out in negative relief (Fig. 1.76B). Caution should be exercised in the interpretation of these staining profiles, since the staining profile varies between species with some reagents and the immunophenotype of tubular cells may modulate during injury. The acquisition of vimentin intermediate filament expression and loss of some cytokeratin intermediate filament expression by human renal tubules undergoing atrophy or regeneration is an example.

Proximal Tubule

The human PT begins at the urinary pole of the glomerulus as an abrupt transition from flattened PECs to columnar PT cells (see Figs. 1.38 and 1.39) (232–236). Occasionally, PT cells extend into the BC, a process more prevalent in rodents than

in humans. The human PT is approximately 14 mm long and geographically divided into two regions: a cortical convoluted portion, the pars convoluta, and a straight portion within the medullary rays, the pars recta. The PT shows sequential heterogeneity in cell structure classified into S_1 , S_2 , and S_3 segments based on ultrastructural characteristics defined in the rat. These segments may not be strictly applicable to humans. The three segments have, in general, predictable topographic correlations. The S_1 segment corresponds to the initial 1/2 to 2/3 of the pars convoluta, and the S_2 segment comprises the remainder and extends in the initial pars recta. The S_3 portion comprises the remainder of the pars recta to its termination at the inner stripe of the outer medulla. The transition from S_1 to S_2 is gradual, but the transition to S_3 is more abrupt. There are no differences between nephron types, long or short, and segmentation within the PT.

Most of the tubules within the cortex, particularly in the cortical labyrinth, are PTs. PTs are easily distinguished from other tubular segments, even in immersion-fixed human tissue (Figs. 1.39 and 1.77). They are cuboidal to columnar cells with a round centrally located nucleus. They have densely eosinophilic cytoplasm, a staining property attributable to numerous mitochondria. PTs have basal vertical striations and indistinct cell borders, due to extensive basal cytoplasmic invaginations and lateral cell membrane interdigitations, respectively (see

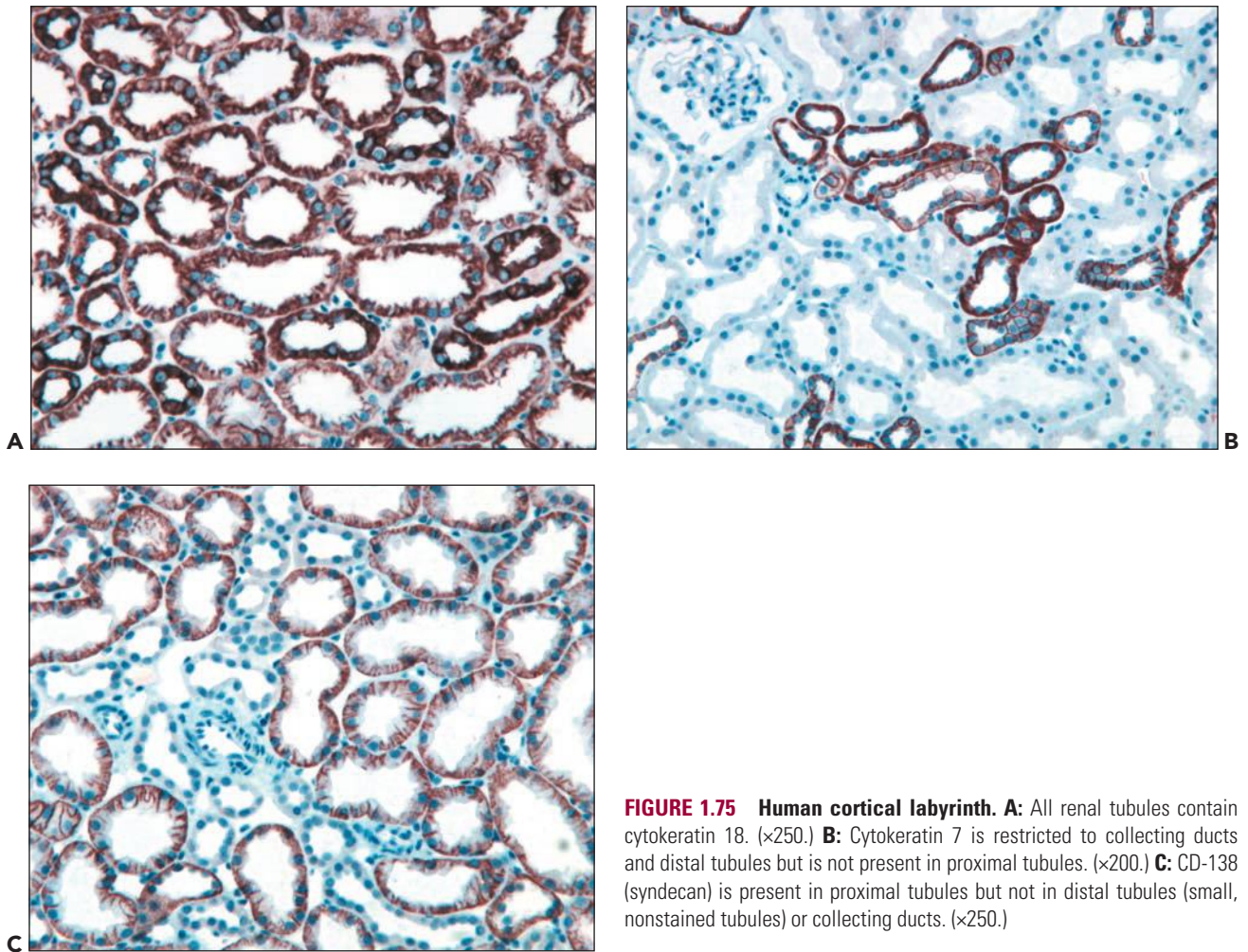


FIGURE 1.75 Human cortical labyrinth. **A:** All renal tubules contain cytokeratin 18. ($\times 250$.) **B:** Cytokeratin 7 is restricted to collecting ducts and distal tubules but is not present in proximal tubules. ($\times 200$.) **C:** CD-138 (syndecan) is present in proximal tubules but not in distal tubules (small, nonstained tubules) or collecting ducts. ($\times 250$.)

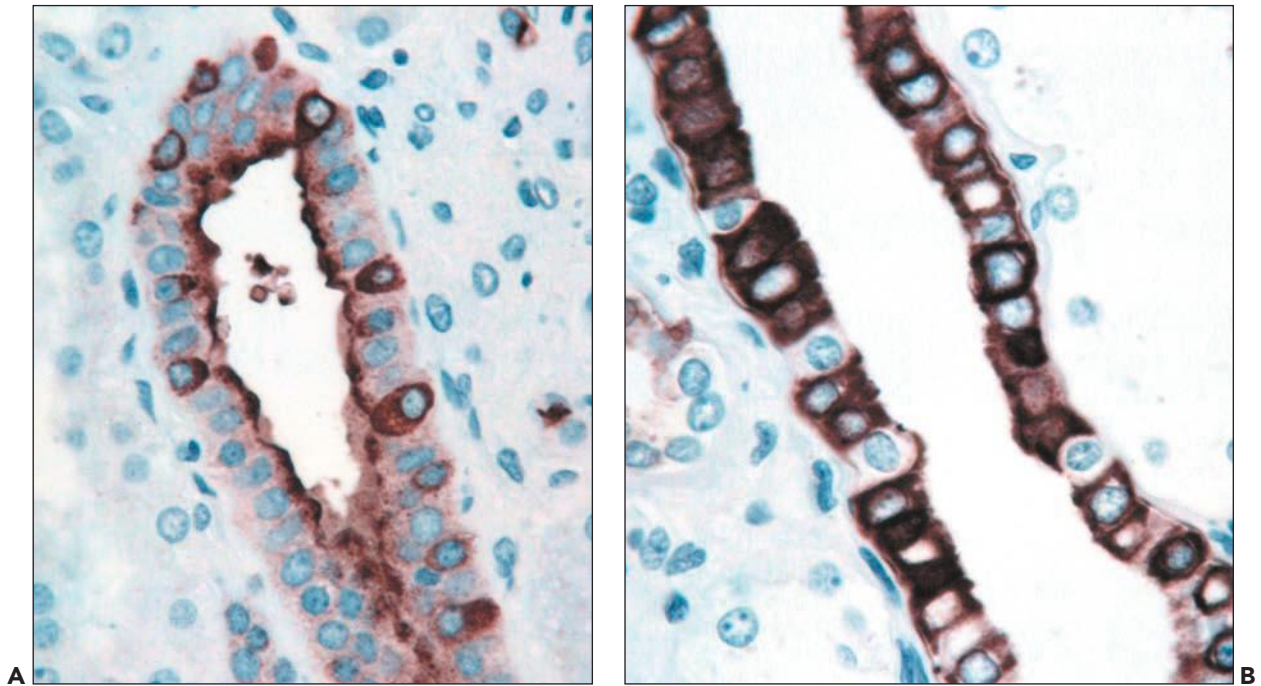


FIGURE 1.76 Human cortical collecting ducts. **A:** Collecting duct principal cells express epithelial membrane antigen at their luminal surface while probable intercalated cells exhibit diffuse cytoplasmic staining. ($\times 500$.) **B:** Collecting duct principal cells demonstrate diffuse cytoplasmic expression of cytokeratin 7, while probable intercalated cells are visible in negative relief. ($\times 500$.)

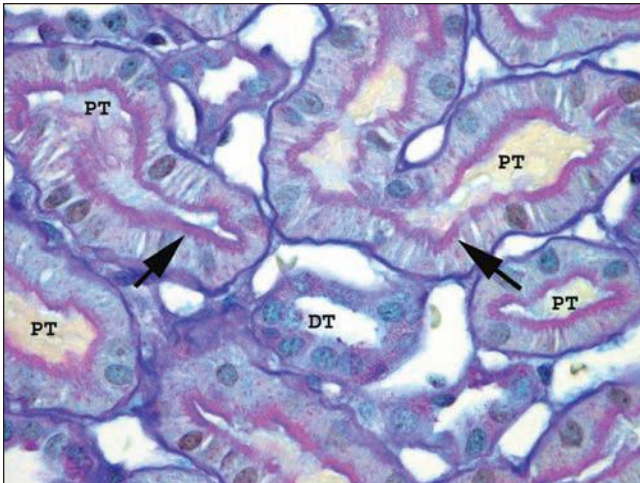


FIGURE 1.77 Human cortical labyrinth. Proximal convoluted tubule cells (PT) are taller than distal convoluted tubule cells (DT) and have a distinct brush border (arrows) that is stained red. (Lillie allochrome stain, $\times 500$.)

below). PTs (S_1 and S_2 segments) have a prominent microvillus or brush border, with a glycocalyx easily demonstrated by a PAS or equivalent stain (see Fig. 1.74). More specific targeting of this cytoplasmic domain can use immunohistochemical stains for villin within the microvilli (225). Additional immunohistochemical and histochemical reagents aid discrimination of PTs from DTs and CDs as mentioned above (Table 1.4).

Ultrastructure has been the defining modality to identify the three PT segments, S_1 , S_2 , and S_3 , using optimally fixed animal tissue, although there are species differences in the morphology of the three segments. The S_1 is the longest segment, and its cells are the largest. The most distinctive features of S_1 cells are extensive cell membrane specializations, apical microvilli, and basolateral infoldings (Figs. 1.78 and 1.79). The luminal surface has a lush carpet of long microvilli. The microvilli contain actin filaments that extend into the apical cytoplasm where they associate with a dense network of cytoplasmic microfilaments and microtubules. The lateral aspects of the cells have curtain-like interdigitations that extend from the apical surface to the base, with secondary and tertiary divisions developing toward the base (Fig. 1.80). These infoldings interdigitate with those of the adjacent cells and enclose numerous long mitochondria, arrayed perpendicular to the BM. The size and number of mitochondria diminish toward the cell surface. The basal portion of the cell has extensive cytoplasmic invaginations that also enclose mitochondria (237–239).

The surface amplification provided by the apical microvilli and the basolateral infoldings represents the anatomic basis for an enormous reabsorptive capacity (237–240). The PT is responsible for reabsorption of approximately 60% of the glomerular ultrafiltrate and also reclaims electrolytes, bicarbonate, and small molecules such as glucose and amino acids. The PT microvilli contain the water channel aquaporin 1, while high levels of $\text{Na}^+\text{-K}^+\text{-ATPase}$ activity reside in the basolateral cell membranes. Reabsorption is coupled with sodium transport. This requires abundant energy resources provided by the numerous mitochondria packed into the basolateral infolding (240–245).

The lateral apical surfaces of PT cells are attached by junctional complexes consisting of a continuous belt of tight junctions (zona occludens) and intermediate junctions (zona adherens), with occasional desmosomes (macula adherens) (246–248). The tight junctions appear “leaky” by freeze-fracture techniques since they possess a single junctional strand, which may permit paracellular ion transport. Gap junctions are also present in the lateral membranes, indicating the potential for electronic coupling between adjacent cells.

PTs have a prominent apical endocytic lysosomal apparatus (249–251). The cell membrane between the microvilli invaginates to form a system of pits and tubules. The cytoplasmic portions of these invaginations are “coated” with protein structures typical of clathrin cages and contain the gp330 Heymann nephritis antigen. Endocytic vesicles or endosomes are derived by pinching off membrane from the coated pits to form small vacuoles. These lack clathrin but are lined by glycocalyx that binds protein within the tubular lumen. Larger vacuoles are formed by fusion of the small vacuoles. The function of this complex system of coated pits, endosomes, and vacuoles is endocytosis of macromolecules such as protein. In human biopsies with severe proteinuria, the activity of this system is evident as prominent reabsorption droplets or so-called hyaline droplets that can fill the PT cytoplasm.

The PT cytoplasm also contains a prominent Golgi apparatus, abundant smooth endoplasmic reticulum (SER) and RER, numerous free ribosomes, and primary lysosomes, all located toward the luminal side of the nucleus (252,253). The endocytic vacuoles, described above, fuse with primary lysosomes derived from the Golgi apparatus, and its contents are degraded by acid hydrolases to form secondary lysosomes. Numerous peroxisomes or microbodies that contain catalase and oxidases are present amid the SER (253). The amount of SER exceeds the amount of RER and includes specialized cisternae situated close to the lateral cell membranes.

The S_1 segment gradually transitions into the S_2 segment, which comprises the terminal portions of the convoluted part of the PT and the proximal portions of the medullary ray straight tubule. The features so prominent in the S_1 segment cells such as the microvillus border, cytoplasmic complexities, numerous long mitochondria, and a prominent endocytic system remain, but are diminished in magnitude, in the S_2 segment (Fig. 1.80B). There are, however, more numerous peroxisomes, and the secondary lysosomes are larger in cells of the S_2 segment.

The S_3 segment begins within the medullary ray and terminates at the beginning of the inner stripe of the outer medulla. In general, the lush microvilli and extensive basolateral interdigitations and invaginations, prominent characteristics of the S_1 and S_2 segments, are absent in the S_3 segment (Fig. 1.80C). The S_3 segment is characterized by simple cuboidal cells with few cytoplasmic membrane complexities and fewer and smaller mitochondria. S_3 cells contain more peroxisomes and SER and may have larger and more numerous secondary lysosomes than the S_1 and S_2 segments.

Thin Limb of Henle

The limb of Henle (LH) has a DTL and an ascending thin limb (ATL) (254–264). The DTL begins at the border of the inner and outer stripe of the outer medulla, where the cuboidal

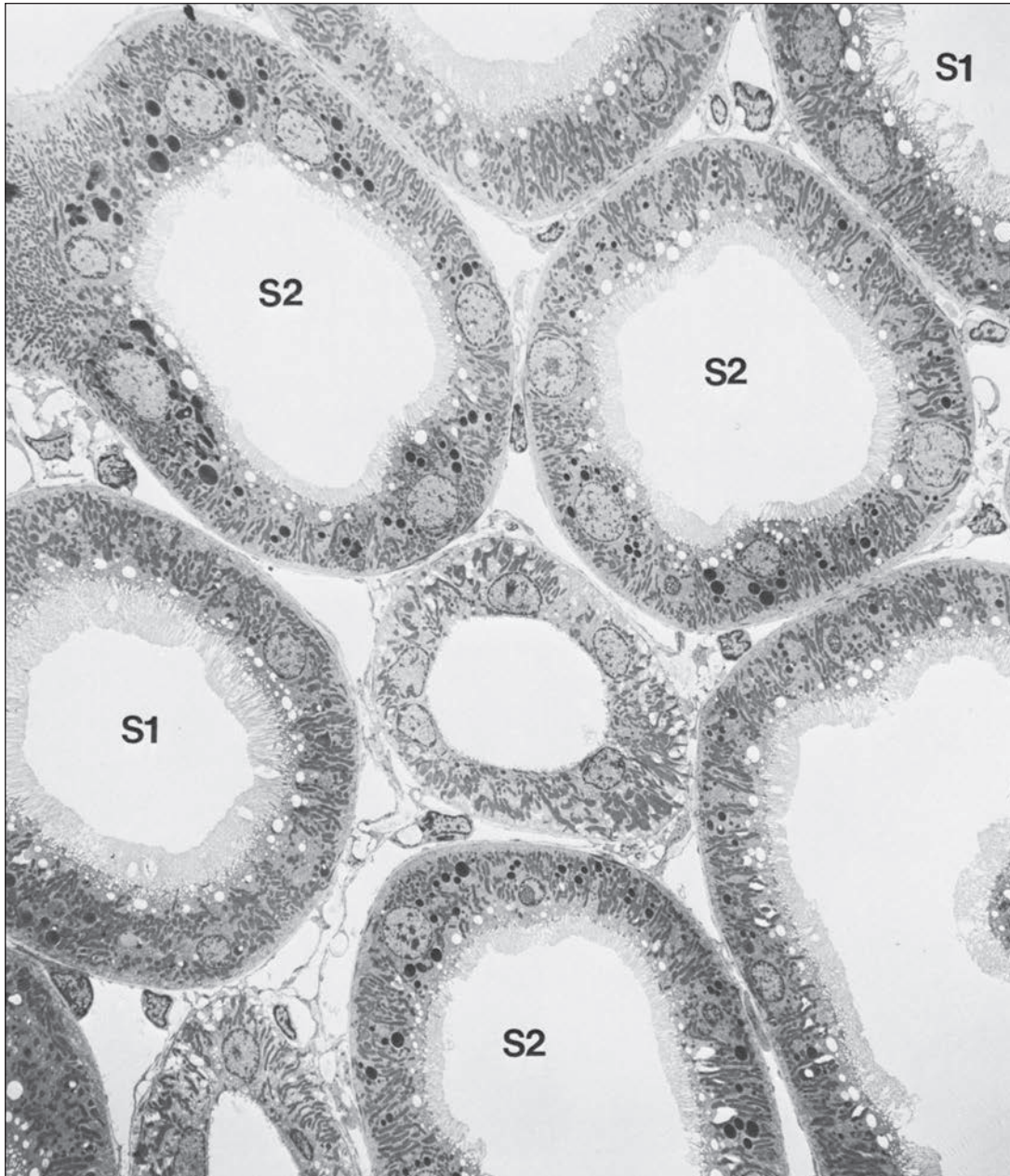


FIGURE 1.78 Electron micrograph of perfusion-fixed rat kidney shows the proximal convoluted tubules. Brush borders are clearly visible and are longer in the S_1 segment than in the S_2 segment. Mitochondria are visible as elongated structures. ($\times 1968$.) (From Maunsbach AB. The influence of different fixatives and fixation methods on the ultrastructure of rat kidney proximal tubule cells. I. Comparison of different perfusion fixation methods and of glutaraldehyde, formaldehyde, and osmium tetroxide fixatives. *J Ultrastruct Res* 1966;15:242.)

cells of the S_3 PT segment abruptly change to a flattened inconspicuous squamous-like epithelium (see Fig. 1.28). The DTL extends into the distal inner medulla. The ATL is confined to the inner medulla and transitions into the TAL of the DT as it enters the outer stripe. The epithelial cells of the DTL and ATL have attenuated cytoplasm devoid of a brush border and a nucleus that bulges into the lumen, creating a resemblance to the endothelial lining of a capillary. In well-oriented sections, the relationship between the vascular

bundles assists the identification of the LH since they reside near the vasa recta.

There are several types of thin limb epithelium defined by ultrastructure, with many interspecies variations that reflect functional differences in solute and water permeability intrinsic to the countercurrent concentration function. Differences in thin limb morphology between species involve mainly the initial portions of the DTL with variation in the degree of lateral interdigitation, number of microvilli, and structure

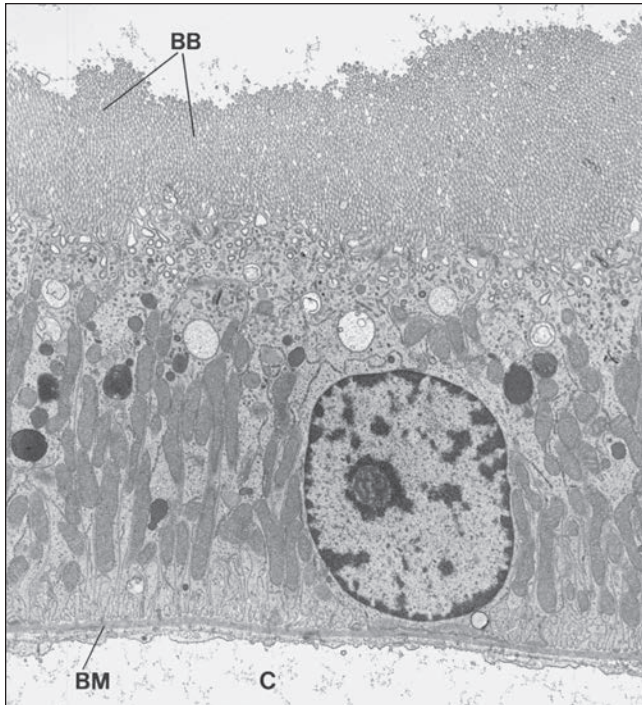


FIGURE 1.79 Proximal tubule epithelium (S_1) of a rat kidney viewed by transmission electron microscopy. The apical cytoplasmic zone contains a vacuolar apparatus with many small vesicles and larger lysosomal elements (either light- or dark-staining vacuoles); the latter are also found in deeper parts of the epithelium. Beneath the apical zone, the epithelium is made up of interdigitating cell processes that contain large mitochondria. ($\times 4550$). BB, brush border; BM, basement membrane; C, peritubular capillary.

of the tight junctions. In general, the DTL is permeable to water but has low permeability to sodium, whereas the ATL is largely impermeable to water but has a high permeability to sodium. Four cell types have been described in the LH in the rat. Whether their human counterpart exists is not known since detailed investigations of optimally fixed tissue are lacking (Fig. 1.81).

Type I DTL is present in the DTL of short-looped nephrons. It is lined by thin epithelial cells, which are the simplest of the four epithelia (Fig. 1.82). These cells have few organelles, no microvilli, and little cell membrane interdigitation. The cells are connected by deep tight junctions with multiple junctional strands and zones of membrane fusion. This results in poor permeability of solute that allows osmotic abstraction of water from the tubular lumen.

Type II DTL is present in the initial portions of the DTLs of long-looped nephrons in the outer medulla. It is thicker than type I DTL, in fact thicker than all other types (Fig. 1.83). It contains more organelles, has short surface microvilli, and has extensive lateral cell membrane interdigitation, the extent of which varies between species. The tight junctions between cells are shallow and leaky, with a single junctional strand and a limited zone of membrane fusion. The lateral interdigitations contain frequent mitochondria. The lateral cell membrane contains $\text{Na}^+\text{-K}^+\text{-ATPase}$ and carbonic anhydrase, and the surface

membrane contains aquaporin 1, indicative of active transport capability. As this epithelium advances into the inner medulla, it abruptly transitions into the third type of DTL.

Type III DTL cells are located in the inner medulla of the DTLs of long-looped nephrons. Its cells are the second thickest cells (Fig. 1.84). These cells contain more organelles than type I cells and have scattered short microvilli and some basolateral cell membrane complexity like type II DTL cells.

Type IV ATL cells line the bends of the long-looped nephrons and the entire ascending segment. These cells resemble the type I cells, having few organelles and no microvilli, but they do have lateral interdigitations. The tight junctions between cells are shallow with a single strand and a limited zone of membrane fusion, again creating a leaky epithelium relative to salt. It is relatively impermeable to water and lacks water channel proteins.

Distal Tubule

There are three distinct segments of the DT: the TAL, the DCT, and the MD, which represents the junction between the TAL and the DCT. The TAL begins at the border of the inner and outer medulla and terminates shortly beyond the MD (for details of the MD see Juxtaglomerular Apparatus above). The TAL has a medullary (MTAL) segment and a cortical (CTAL) segment that differs in appearance and function (265–270). There is a gradual transition from the ATL cells to the TAL cells of the MTAL.

The MTAL cells are small low cuboidal cells relative to proximal tubular cells, with eosinophilic cytoplasm and no brush border (Figs. 1.81B and 1.85). Their nucleus is apical and tends to produce a bulge into the tubular lumen. The MTAL cells have indistinct lateral borders and a striated basal aspect because of complex cytoplasmic invaginations that contain numerous elongated mitochondria. This is similar to PT S_1 and S_2 cells; however, the interdigitations extend only three quarters to the apical surface. The MTAL cells have numerous apical cytoplasmic vesicles and tubulovesicular profiles. The MTALs have tight junctions of intermediate depth and lack aquaporin water channel proteins since this segment is relatively impermeable to water. The MTALs actively reabsorb sodium; thus, the basolateral cell membranes contain $\text{Na}^+\text{-K}^+\text{-ATPase}$ activity that maintains medullary interstitial hypertonicity (271–274).

As the MTAL passes through the outer strip and enters the cortex, it transitions into the CTAL. The cells of the CTAL decrease in cell height but amplify their lateral surface area with basolateral interdigitations that extend to the apical surface. SEM of the luminal surfaces of both MTAL and CTAL cells shows no microvilli. The MTAL cells have a relatively smooth surface, whereas CTAL cells have shallow microprojections.

The DCT begins beyond the MD. The DCT cells are composed of single homogeneous cell type, similar to the CTAL cells but taller (Fig. 1.86). The transition from the CTAL to DCT is abrupt. At its termination, the DCT gradually ends in the CT with intermingling of DCT cells, CT cells, and ICs. The DCT cells are easily distinguished from PCT cells. They are smaller and have less eosinophilic cytoplasm, more closely spaced nuclei, and a different immunophenotype (see Fig. 1.39) (Table 1.4).

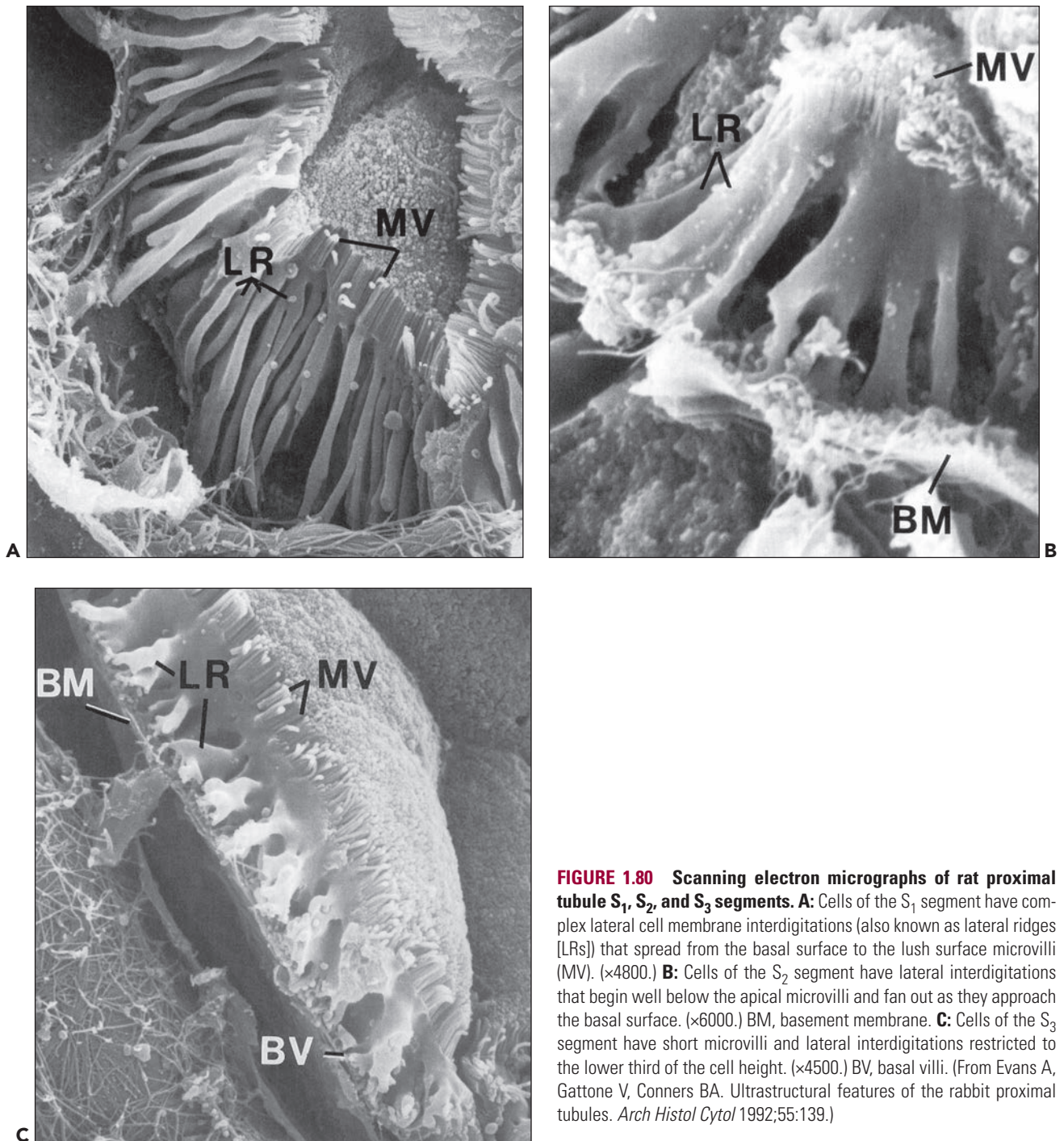


FIGURE 1.80 Scanning electron micrographs of rat proximal tubule S₁, S₂, and S₃ segments. **A:** Cells of the S₁ segment have complex lateral cell membrane interdigitations (also known as lateral ridges [LRs]) that spread from the basal surface to the lush surface microvilli (MV). (×4800.) **B:** Cells of the S₂ segment have lateral interdigitations that begin well below the apical microvilli and fan out as they approach the basal surface. (×6000.) BM, basement membrane. **C:** Cells of the S₃ segment have short microvilli and lateral interdigitations restricted to the lower third of the cell height. (×4500.) BV, basal villi. (From Evans A, Gattone V, Conners BA. Ultrastructural features of the rabbit proximal tubules. *Arch Histol Cytol* 1992;55:139.)

Distal convoluted epithelial cells have lateral and basal cell membrane amplification with short microvilli along the luminal surface. The lateral interdigitations begin at the base and extend along the lateral surface approximately two thirds of the epithelial cell height. The interdigitations contain elongated mitochondria. The DCT cells are connected by tight junctions of intermediate depth. Similar to the TAL cells, DCT cells are impermeable to water and their lateral cell membranes contain Na⁺-K⁺-ATPase activity that is higher than any other tubular segment. The nucleus is centrally located above the rows of

elongated basal mitochondria. The apical cytoplasm contains numerous small vesicles of unknown function.

Connecting Tubule

The CT connects the DCT to the CD (275). The CT contains CT cells and ICs. In humans, the CT cells have similarities to both DCT cells and CD cells. The cellular components of the CT include an intermingling of DCT cells at its beginning and CD principal cells at its termination.

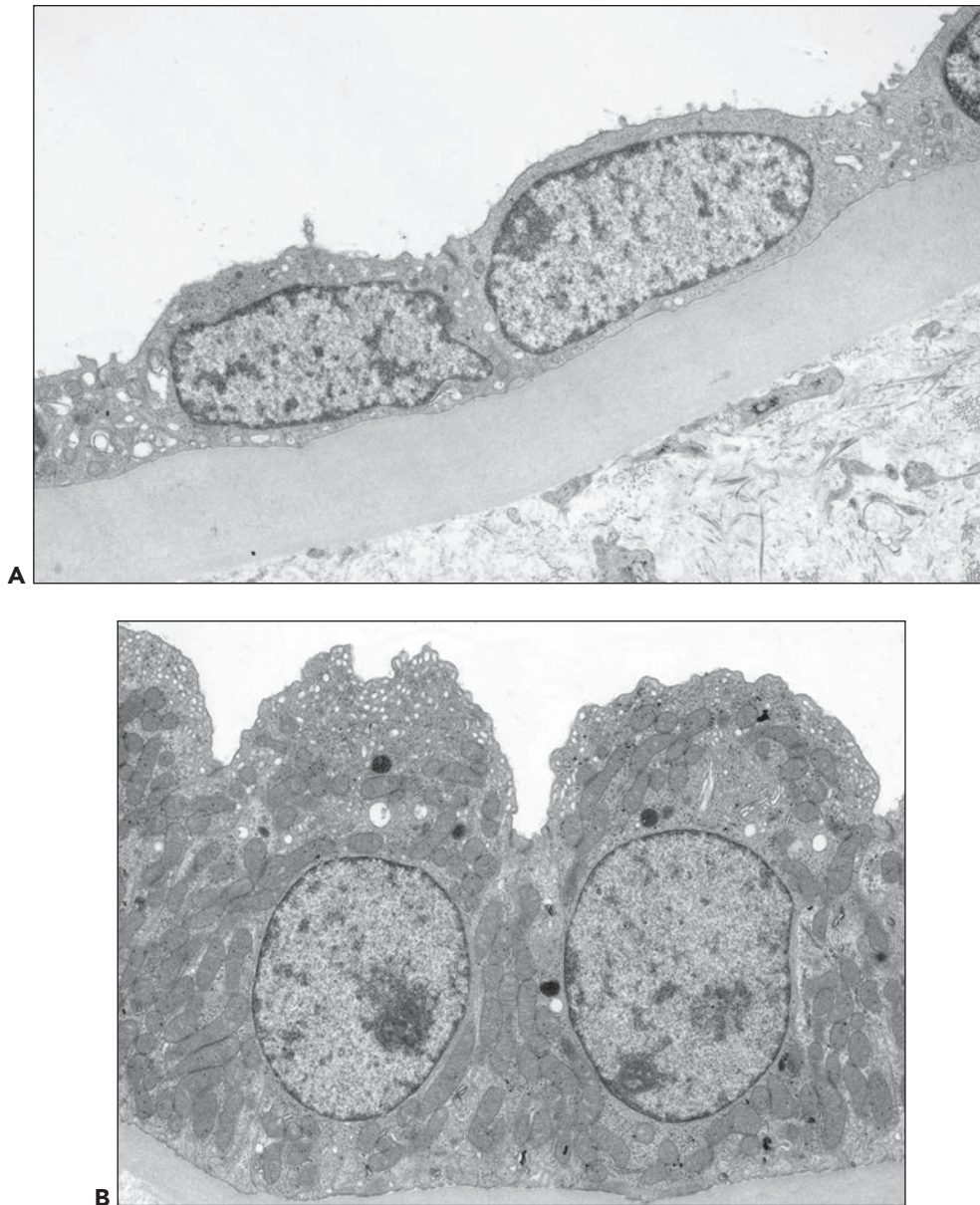


FIGURE 1.81 Electron micrograph of human outer medulla for comparison with animal counterparts. **A:** Thin descending limb. (x5000.) **B:** Thick ascending limb. (x4500.)

Collecting Duct

CDs begin in the cortex, descend through the cortex within the medullary rays, and terminate at the area cribrosa of the papillary tip. The CD has a cortical (CCD) portion that can be divided into an initial CT portion and two medullary ray portions, an outer medullary (OMCD) portion, and an inner medullary (IMCD) portion. These regions demonstrate significant cytologic heterogeneity. The cell size and tubular diameter of CD cells progressively increases from CCD to IMCD cells. CDs within the cortex and outer medulla receive no tributaries until they enter the inner medulla as the IMCD.

CDs contain two cell types, principal or CD cells and ICs (see Fig. 1.86). ICs are located predominately in the CCD

and OMCD. ICs are rare in the initial portions of the IMCD and then quickly disappear with no ICs in the mid and lower inner medulla. CD cells and ICs cannot be easily distinguished by LM but may be distinguished by immunohistochemistry (Table 1.4).

Collecting duct principal cells

The CCD cells are cuboidal with a centrally located nucleus, pale cytoplasm, and distinct lateral cell membranes (276,277). The cytoplasm is pale because the cells contain scant organelles (Figs. 1.87A and 1.88). The distinct cell borders reflect an absence of lateral cell membrane interdigitation. The luminal

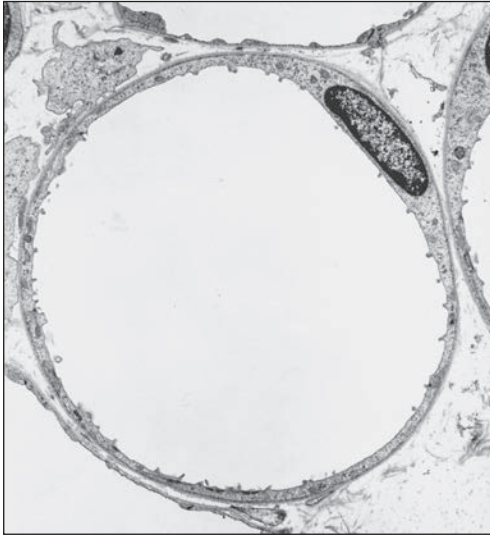
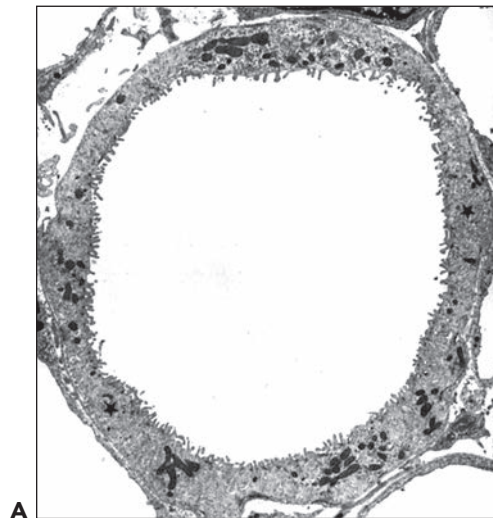
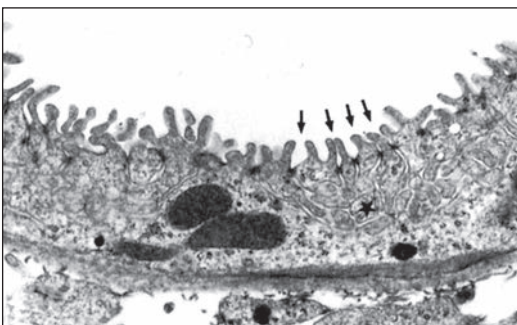


FIGURE 1.82 Cross-sectional profile of a thin descending limb of a shoot loop of Henle in the rat. The simplicity of the epithelium is evident. ($\times 4000$.)



A



B

FIGURE 1.83 Cross-sectional profile (**A**) and epithelium (**B**) of a descending thin limb of a long loop of Henle (upper portion) in the rat. The epithelium has a complex structure and extensive cellular interdigitation; some of the tight junctions are marked by *arrows* in (**B**). Note the labyrinth of extracellular spaces throughout the thickness of the epithelium (*asterisk*). (**A**: $\times 3750$; **B**: $\times 11,500$.)

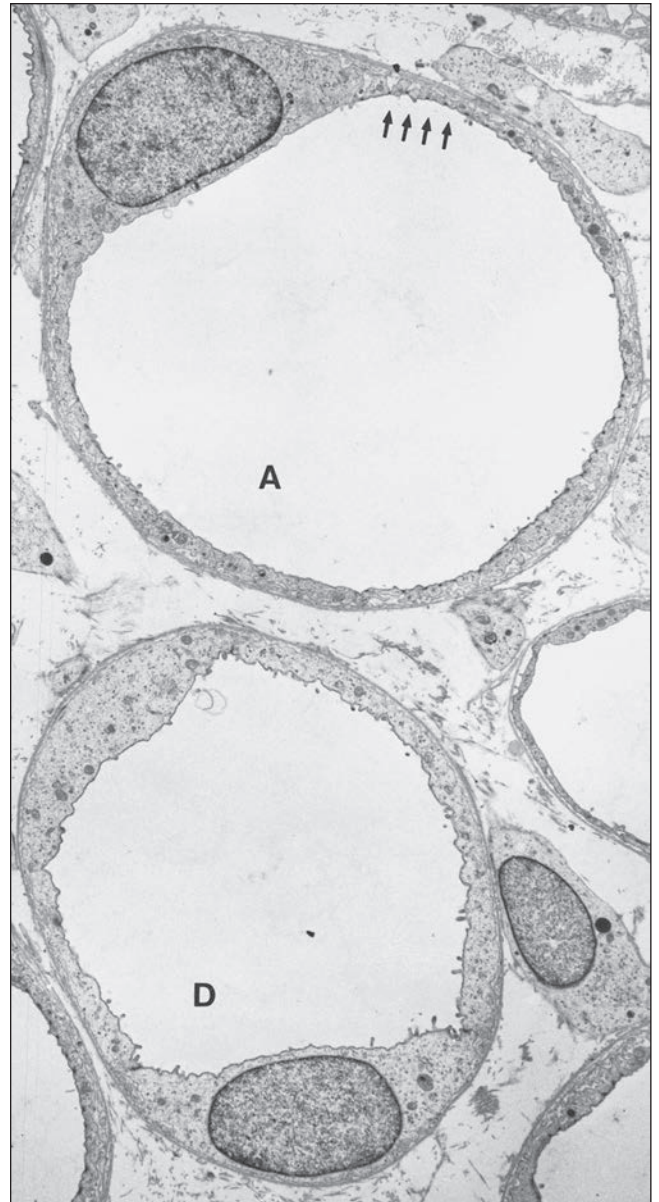


FIGURE 1.84 Cross-sectional profiles of a thin descending limb (**D**) and of a thin ascending limb (**A**) in the inner medulla of the rabbit. The epithelium of the lower portion of the descending limb is simply structured, whereas the epithelium of the ascending thin limb is made up of extensively interdigitating cells. Some of the shallow junctions between the cell profiles are marked by *arrows*. ($\times 3000$.)

surface is covered by shallow widely spaced microvilli and a single cilium. The cells are connected by apical deep tight junctions with several anastomosing strands and zones of membrane fusion (276–282). The lateral cell membranes of adjacent cells are connected by numerous desmosomes and narrow folds of interlocking cell membrane. There are regular, tightly spaced, basal infoldings and are shallow compared with those of the DCT cells. The basal infoldings lack mitochondria and other organelles. The few mitochondria and other organelles present

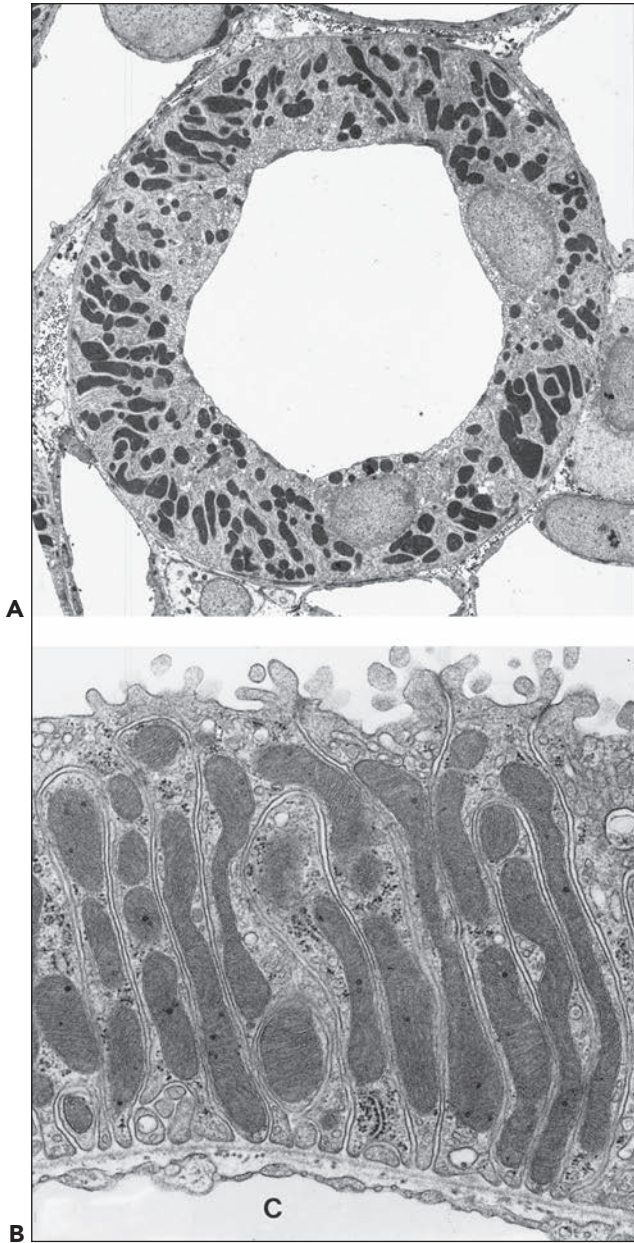


FIGURE 1.85 Thick ascending limb (distal straight tubule) of the rat. Cross-sectional profile (A) and longitudinal section (B) through the epithelium of the medullary part. The epithelium is made up of cells that interdigitate with their neighbors (very similar to the interdigitation in the proximal tubule). The cell processes are filled with large mitochondria. Beneath the luminal cell membrane, there are membrane-bound vacuoles. The luminal cell membrane bears some short, stubby microvilli. C, capillary. (A: $\times 2324$; B: $\times 13,280$.)

are arrayed above the infoldings. Within the apical cytoplasm are numerous tubulovesicular profiles (279–281).

Principal cells have abundant vasopressin V_2 receptors and participate in bulk water transport under the influence of vasopressin. By freeze-fracture techniques, the luminal membrane and the apical cytoplasmic vesicles contain patches of

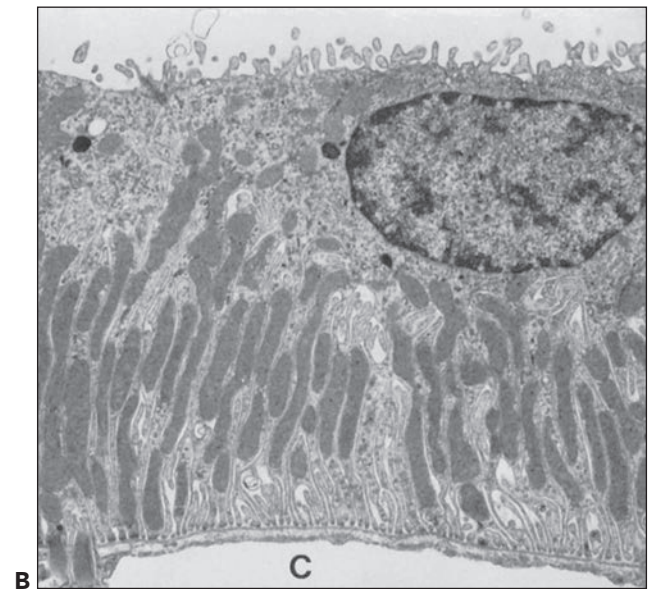
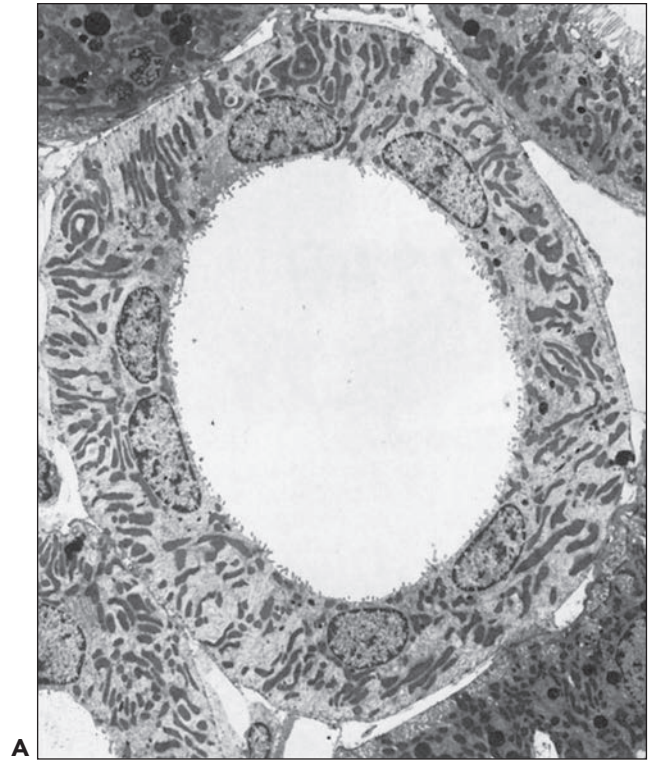


FIGURE 1.86 Distal convoluted tubule of the rat in cross-sectional profile (A) and longitudinal section through the epithelium (B). The epithelium is structured similarly to that of the distal straight tubule in the medulla. The nuclei are typically located in the apical region of the epithelium. In (B), the heavily interdigitating cell processes filled with mitochondria are visible. C, capillary. (A: $\times 22,500$; B: $\times 8000$.)



FIGURE 1.87 Collecting duct cell of the cortical collecting duct (principal cell) in the rabbit. Note the characteristic basal labyrinth, which is established by short basal infoldings. The cellular folds at this site generally do not contain mitochondria. ($\times 5760$.)

intramembranous particles believed to represent water channels of aquaporin 2 class (Fig. 1.89). The basolateral membranes contain vasopressin-insensitive aquaporins 3 and 4 (282–297). Under the influence of vasopressin, water permeability of the luminal membrane is increased, associated with bulk flow of water across the basolateral membrane. This results in opening up of the lateral cell membrane infoldings to create lateral intercellular spaces. Rapid control of water permeability is mediated by recycling of water channels between the intracellular vesicles and the apical cell membrane (291–296). The basolateral cell membranes also contain abundant $\text{Na}^+\text{-K}^+\text{-ATPase}$ because of the role of CDs in salt balance.

There is an increase in cell height and simplification of the basal membrane infoldings with progression from

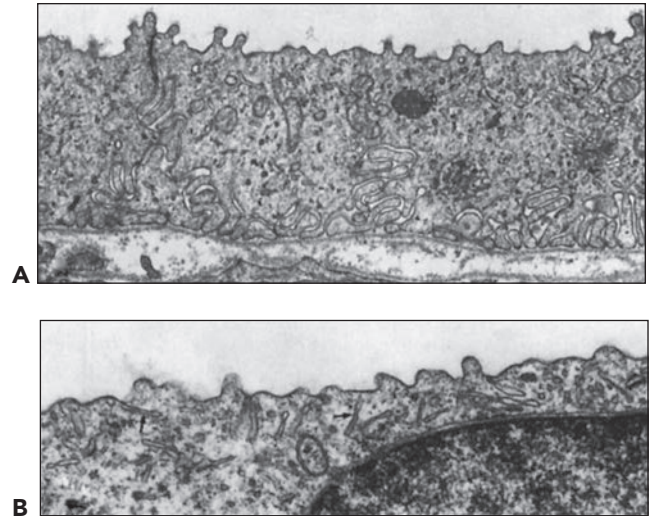


FIGURE 1.89 Epithelium of the inner medullary collecting duct (middle portion) in the rat. **A:** Within the epithelium, three zones may be described: a basal zone with basal infoldings; a middle zone containing profiles of Golgi apparatus, mitochondria, and lysosomal elements; and a thin apical zone with tubular and vesicular profiles. ($\times 9520$.) **B:** The apical zone with many elongated tubular profiles (arrows) is shown. The membranes of these tubulovesicular profiles carry the water channels. Note the deep tight junction in (A). ($\times 19,380$.)

the CCD to the OMCD (see Fig. 1.86B). Concurrently, the number of cell organelles decreases, while the depth of the tight junctions increases. The IMCD cells are columnar rather than cuboidal. The depth of their tight junctions is decreased relative to OMCD cells. In the distal papilla, there is an abrupt transition to the columnar cell of the ducts of Bellini (Figs. 1.88 and 1.90). The IMCD has been further

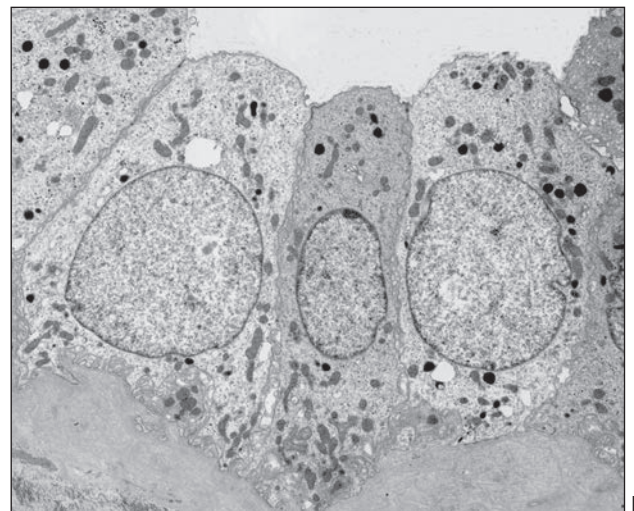
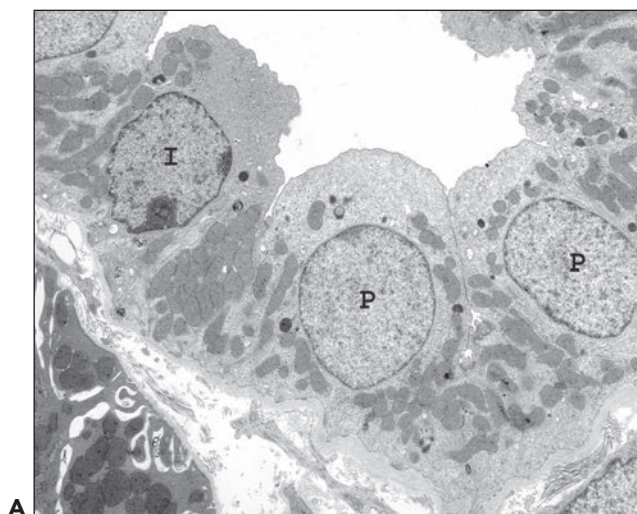


FIGURE 1.88 Electron micrographs of human collecting ducts. **A:** Cortical collecting duct with two principal cells (P) and a type B intercalated cell (I). ($\times 3500$.) **B:** Outer medullary collecting duct showing principal cells that are larger (taller) than their cortical counterpart in (A). ($\times 3500$.)

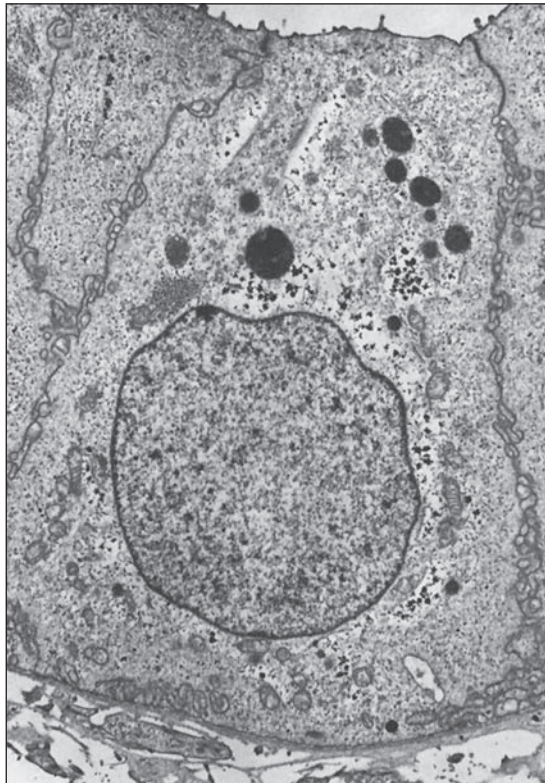
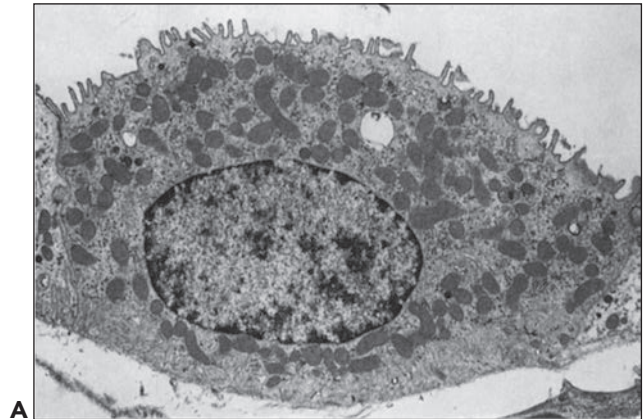


FIGURE 1.90 A papillary collecting duct cell of a human kidney. The papillary collecting ducts are composed of a homogeneous population of tall collecting duct cells. ($\times 4500$.)

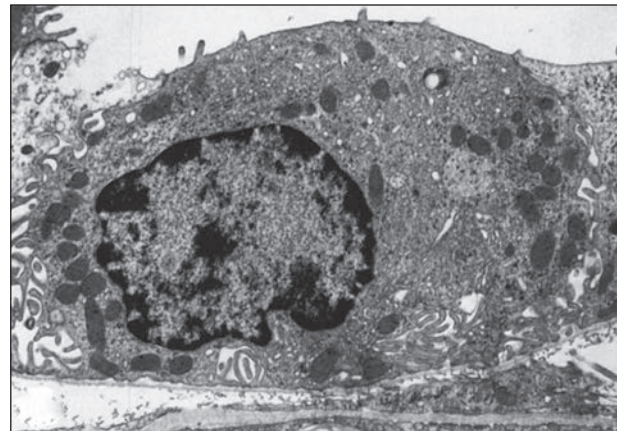
functionally divided into three segments, IMCD1, IMCD2, and IMCD3, or more recently into two segments, the initial IMCD and the terminal IMCD. The initial IMCD corresponds to IMCD1, and the terminal IMCD corresponds to IMCD2 and IMCD3.

Intercalated Cells

ICs are most numerous in the CCD. The ratio of ICs to CD cells varies between species, occurring in a ratio of approximately 2 ICs:3 CD cells in the rat and rabbit cortex. ICs decrease in number in the OMCD and finally disappear in the IMCD. ICs are polygonal to rounded cells, difficult to distinguish from CD cells, although they have differing immunohistochemical profiles as previously discussed (Table 1.4). When identified, ICs often appear flask shaped with a broad base and a narrow surface encroached on by adjacent CD cells. ICs have been referred to as the *dark cells* because on toluidine-stained $1\ \mu$ sections, they have darkly stained cytoplasm compared with the CD cells. This property reflects their content of mitochondria, which are more numerous than in CD cells (Figs. 1.91 and 1.92). ICs have sparse shallow lateral infoldings and prominent basal interdigitations. In addition to the usual organelles, ICs have apical vesicles, tubulovesicular profiles, and flat cisternae that are studded by rod-shaped structures on their cytoplasmic aspect (Fig. 1.93). These studded structures are believed to correspond to dense arrays of rod-shaped particle visible by freeze fracture.



A



B

FIGURE 1.91 Cortical intercalated cells in the rat. Two types are distinguished. **A:** The A type contains luminal microfolds and a dense assembly of mitochondria predominantly in the apical cytoplasm. ($\times 5700$.) **B:** The B type has a smooth luminal surface with few microvilli. The cytoplasm is densely filled with small vesicles reaching down to the basal aspect of the cell. Mitochondria are predominantly found in the lateral and basal parts of the cell. ($\times 6840$.)

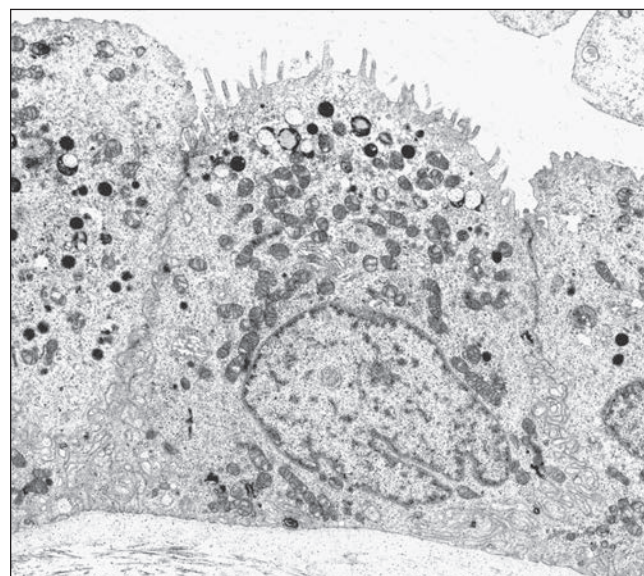


FIGURE 1.92 Human cortical collecting duct intercalated cell type A for comparison with Figure 1.89A. ($\times 6500$.)

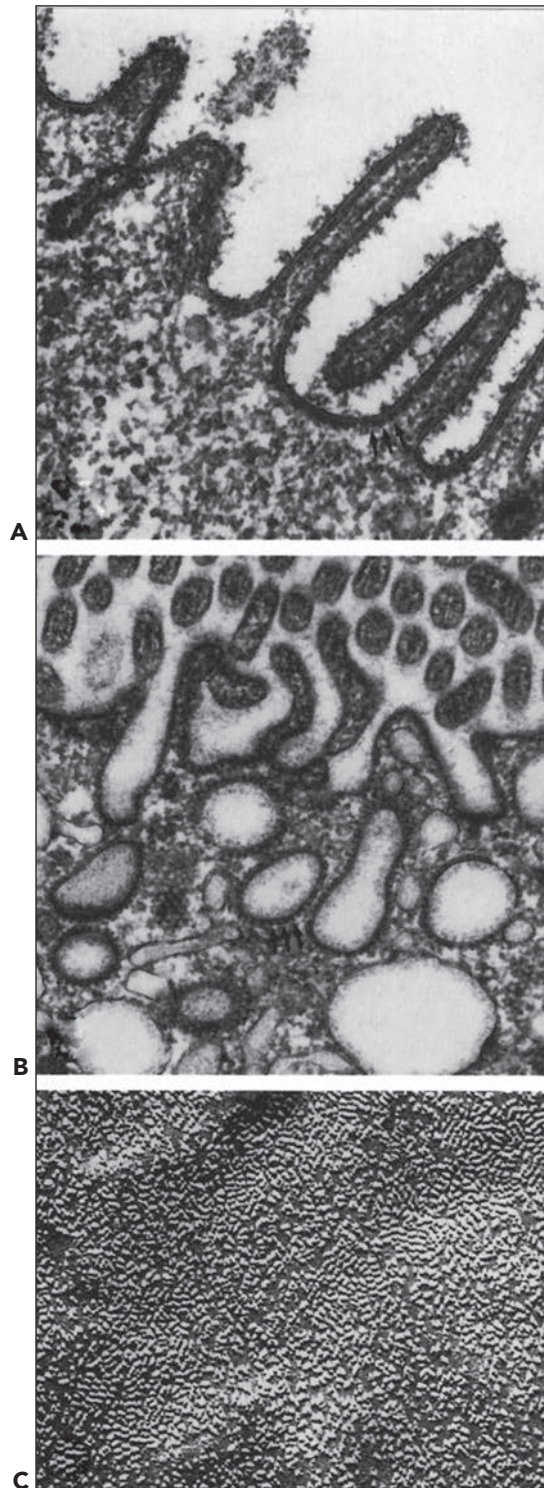


FIGURE 1.93 Intercalated cell, type A, in the rat. **A:** The luminal cell membrane is shown to be characteristically covered on its cytoplasmic side by “studs” (arrows). ($\times 58,000$.) **B:** Studs are also found on tubulovesicular profiles located in the apical cytoplasm. ($\times 41,000$.) **C:** In freeze-fracure replicas of the luminal membrane, characteristic rod-shaped particles are encountered, which are generally believed to correspond to the studs seen in transmission electron microscopy. ($\times 54,000$.)

There are two types of ICs, type A and type B, which differ in ultrastructure and can be distinguished by enzyme histochemistry. Type A ICs have more numerous mitochondria and more prominent microfolds or microprojections on their apical surface membrane (Figs. 1.91A, 1.92, and 1.93). These are not microvilli but are ridges or microplicae when viewed by SEM (Fig. 1.94). Type B ICs have fewer mitochondria, larger basolateral infolding, more abundant apical vesicles, tubulovesicular profiles, and flat cisternae, and a more simplified luminal surface with fewer microplicae than type A ICs (see Figs. 1.87A and 1.91B). The latter feature makes separation of type B ICs from CD cells by SEM difficult compared with type A cells.

Type A and B ICs are distinguished by the presence of luminal or basolateral H^+ ATPase (297). The type A IC contains a luminal H^+ ATPase, responsible for proton secretion, and a basolateral HCO_3^-/Cl^- exchanger related to red blood cell band 3 protein. Type B ICs contain basolateral H^+ ATPase and is responsible for bicarbonate secretion with a HCO_3^-/Cl^- exchanger distinct from band 3 protein. Type A ICs also contain larger amounts of carbonic anhydrase II enzyme compared with type B ICs.



FIGURE 1.94 Scanning electron microscopy of cortical collecting duct (rat) shows the luminal aspect of collecting duct cells and intercalated cells (stars), characteristically adorned by microfolds. The microfolds represent an amplification of the membrane. ($\times 6000$.) C, cilium on a collecting duct cell.

This appearance of IC is further complicated because both types may be in an active or in an inactive state. When active, the proton pumps are in the luminal or basolateral cell membranes. When inactive, the proton pumps are present within the tubulovesicular system. Shuttling back and forth occurs with shifts in cellular activity. It is conceivable that a single cell type exists, with shifts in activity and reverses in cell polarity dependent on metabolic demands.

RENAL INTERSTITIUM

The cortical and medullary interstitium is the extravascular peritubular compartment (17,52). The interstitium consists of a matrix of 15- to 30-nm microfibrils; type I, III, and VI collagen; sulfated and nonsulfated glycosaminoglycans; glycoproteins such as fibronectin; and fluid that houses interstitial cells, fibroblasts and dendritic cells, and the peritubular capillary plexus (17,52,298–308). The interstitium is normally inconspicuous, especially in the cortex. The innocuous appearance is deceptive. All intrarenal solute and fluid exchange processes traverse the interstitium between tubules and peritubular capillaries. Interstitial cells and matrix play important roles in the developing kidney and participate in determining the outcome of the injured kidney. Under the influence of cytokines, growth factors, or other molecules, interstitial cells can proliferate or transform into myofibroblast-like cells, acquiring enhanced capacity for matrix synthesis contributing to interstitial fibrosis (305–308).

The estimated cortical interstitial volume in humans ranges from 5% to 20% and is estimated at 5% in the rat but is capable of rapid expansion in acute tubulointerstitial diseases (17,52). The cortical interstitium is divided into the peritubular interstitium and the periarterial connective tissue sheath. The peritubular interstitium is represented by slender zones of separation between adjacent closely apposed tubules and wider portions created by the round contours of the tubules. The peritubular interstitium has scant cellularity, and its wider portions contain the peritubular capillaries, which are often closely apposed to the TBM (Figs. 1.25 and 1.95). The periarterial connective tissue sheath is a fluid-rich loose connective collar that surrounds all arteries. Proximally, it is contiguous with the connective tissue of the pelvic wall, and it terminates at the afferent arteriole. It contains fibroblasts, macrophages, small nerve fibers, and lymphatics (see Figs. 1.2 and 1.21). The interstitium is more prominent in the medulla compared with the cortex where the three zones, the outer stripe and inner stripe of the outer medulla and the inner medulla, have increasing amounts of interstitial space, 3% to 5%, 10%, and 30% to 40%, respectively (21).

Interstitial Cells and Cytoarchitecture

The cells of the peritubular interstitium include resident fibroblasts and small numbers of migrating cells of the immune system such as dendritic cells, macrophages, and lymphocytes (66,298–308). Fibroblasts, the most numerous and important cells, provide structural support to the kidney, function in matrix production and turnover, and participate in immune processes. Several proteins have been utilized to identify interstitial fibroblasts in the normal state and in diseased kidneys. There include fibroblast-specific protein 1, S100A4, cadherin

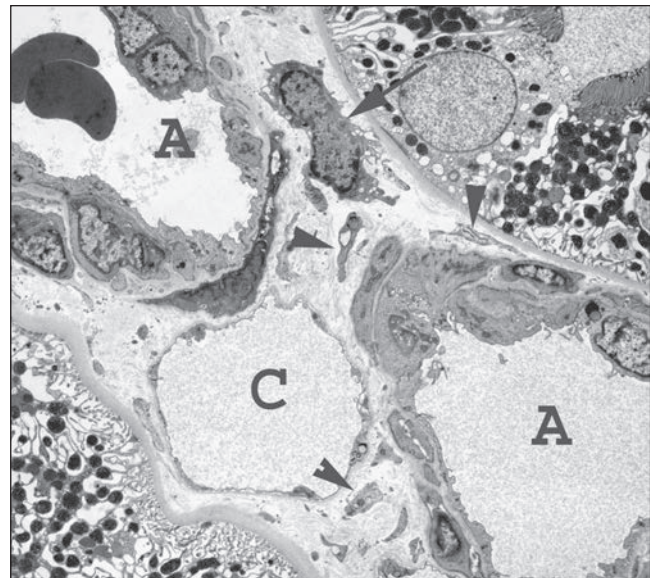


FIGURE 1.95 Human cortical interstitium. The cell body and nucleus (arrow) of an interstitial fibroblast is positioned between tubules and arteriolar cross sections (A). Notice the numerous thin profiles of fibroblast cell processes (arrowheads) that ramify throughout the interstitium. ($\times 1800$.) C, peritubular capillary.

9, and soluble guanylyl cyclase and membrane-bound ecto-5'-nuclease (305,306). A subpopulation of cortical fibroblasts may synthesize erythropoietin, whereas modified fibroblasts in the medulla have an antihypertensive action (309–322). There are several morphologic types of interstitial fibroblasts: the periarterial sheath fibroblast, cortical and medullary interstitial fibroblasts, and a lipid-laden fibroblast known as the *renal medullary interstitial cell* (318,321,322).

Renal fibroblasts of all types contain protein-synthesizing organelles such as anastomosing profiles of the RER, free ribosomes, and a Golgi apparatus but scant other organelles. Fibroblasts have a stellate nucleus and contain a cytoskeleton of actin-based microfilaments that stain for F-actin and form cytoplasmic attachment plaques (302). The attachment plaques resemble intermediate junctions and connect adjacent fibroblasts to each other and anchor cells to the BMs of tubules, glomeruli, and vessels. The periarterial sheath fibroblast contains more numerous organelles and a more extensive actin-based cytoskeleton compared with the cortical interstitial fibroblast. The cortical interstitial fibroblasts have complex cytoplasmic profiles and long slender branching cell processes that show a regular pattern of secondary and tertiary branching (Figs. 1.95 and 1.96). The branching cell processes establish intercellular and matrix connections to form an elaborate three-dimensional network (303) (Fig. 1.97). In cooperation with the interstitial matrix, this fibroblast network provides a scaffold for the glomeruli, tubules, and vessels of the kidney.

During inflammatory processes, myofibroblasts appear in the interstitium. Although by ultrastructural features there is a continuum between conventional or quiescent fibroblasts and the activated myofibroblast, there is evidence that myofibroblasts may be derived from a fibroblast pool associated with the vascular tree, the perivascular fibroblasts (305). A myofibroblast

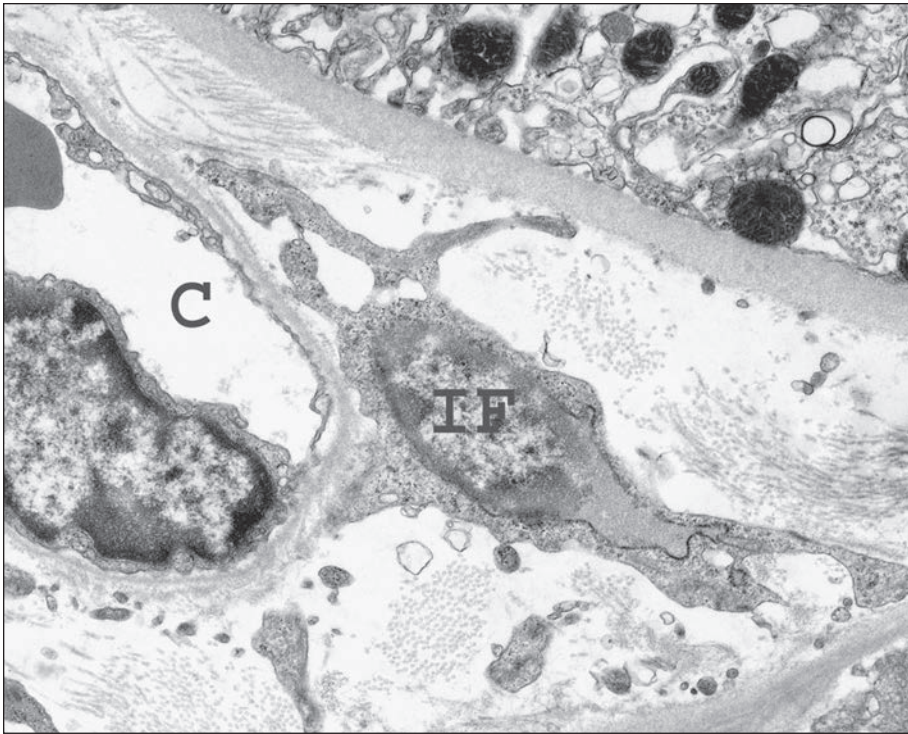


FIGURE 1.96 Human cortical interstitium. This cortical interstitial fibroblast (IF) sends cell processes to support two tubules and a peritubular capillary (C). ($\times 4500$.)

stains for alpha smooth muscle actin has increased quantities of microfilaments with dense bodies and dilated RER, features consistent with enhanced contractile properties and matrix synthetic capabilities.

The renal medulla contains conventional interstitial fibroblasts and lipid-laden fibroblasts, the renal medullary interstitial cells mentioned previously (301,304,314–322). The phenotype of the medullary interstitial fibroblast shows progressive variation from the outer stripe toward the inner medulla. Fibroblasts in the outer stripe are identical to those in the peritubular cortex. Fibroblasts within the inner stripe have more prominent cytoskeleton, thicker cell processes,

and dilated perinuclear cisterns and RER cisterns (Fig. 1.98). Smooth muscle actin can regularly be demonstrated in these cells, but it is demonstrable in cortical interstitial fibroblasts only following activation. Fibroblasts within the inner medulla show progressive enlargement of cell processes and cell cytoskeleton compared with those of the inner stripe and demonstrate a distinctive spatial orientation. They are oriented in a strictly perpendicular axis relative to the long axis of the tubules, resembling rungs of a ladder (Figs. 1.99 and 1.100). Inner medullary fibroblasts have opposing cytoplasmic extensions that establish horizontal contacts between the BMs of the loop of Henle and vasa recta, maintaining their parallel

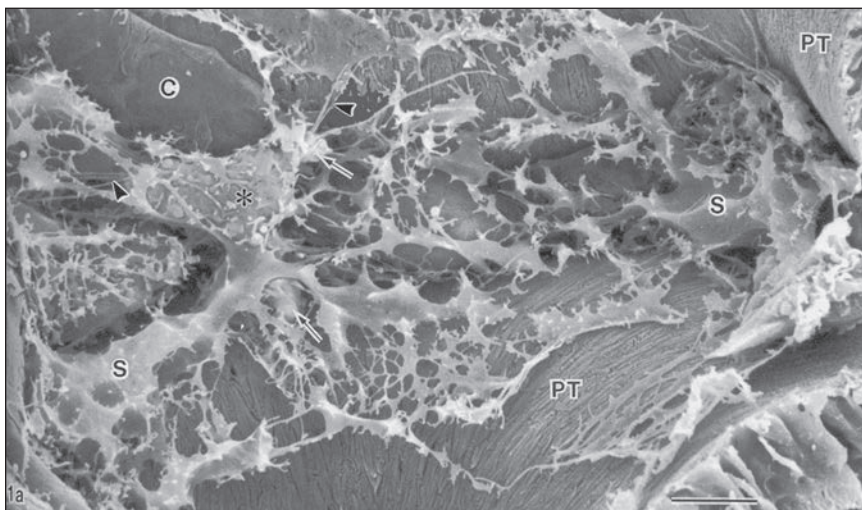


FIGURE 1.97 Cortical interstitium of a rat following NaOH extraction of matrix. The complex filigree pattern of the fibroblast cell process scaffold is apparent. C, capillary; PT, proximal tubule; S, fibroblast or "sustentacular cell." (From Takahashi-Iwanaga H. The three-dimensional cytoarchitecture of the interstitial tissue in the rat kidney. *Cell Tissue Res* 1991;264:269.)



FIGURE 1.98 Human outer medulla. A lipid-containing renal medullary interstitial cell (*arrow*) with dilated endoplasmic reticulum cisternae sends four thick cell processes to bridge the space between a thin limb of Henle and an interstitial capillary. ($\times 4500$.) TDL, thin descending limb.

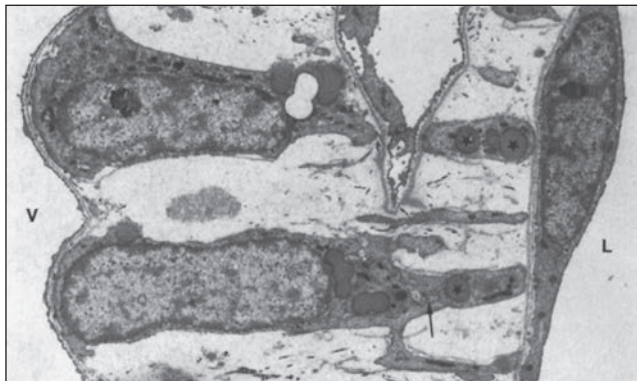


FIGURE 1.99 Lipid-laden interstitial cells. A longitudinal section through the papilla of the rat, by electron microscopy. Two lipid-laden interstitial cells are shown, spanning the distance between an ascending vasa rectum (V) and a limb (L) of a loop of Henle. The lipid droplets (*stars*) as well as the characteristically dilated cisternae of the endoplasmic reticulum (*arrow*) are seen. Note the density of the interstitial matrix between the cells. ($\times 19,380$.)

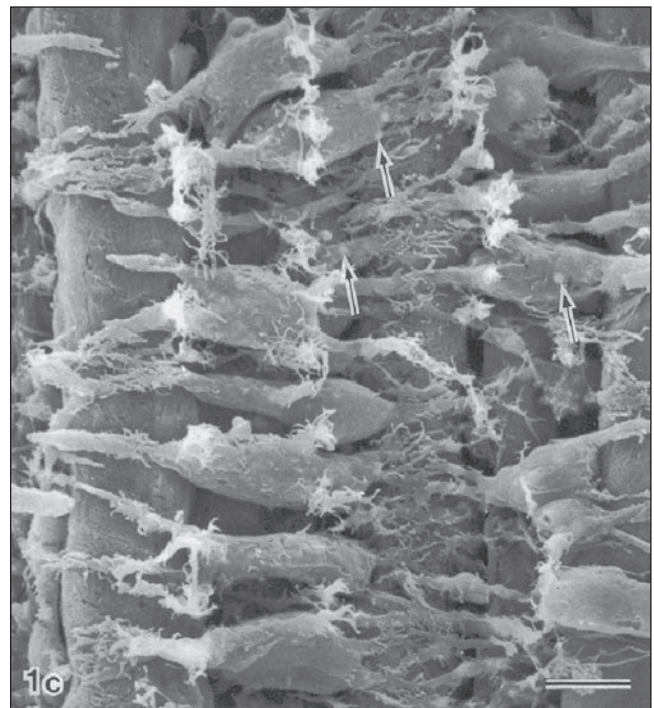


FIGURE 1.100 Inner medulla of a rat following NaOH matrix digestion. The interstitial fibroblasts are arranged in a ladder-like fashion. The cell processes wrap around the thin loops of Henle and the interstitial capillaries. *Arrows*, lipid droplets. (From Takahashi-Iwanaga H. The three-dimensional cytoarchitecture of the interstitial tissue in the rat kidney. *Cell Tissue Res* 1991;264:269.)

orientation. Since the fibroblast processes completely wrap around the limbs of Henle and vasa recta, they may also function to maintain luminal patency.

The lipid-containing renal medullary interstitial cells are most abundant in the inner medulla. Although renal medullary interstitial cells contain attachment plaques, participate in matrix production, and provide a scaffold function to support of tubules and vessels like other interstitial fibroblasts, they also contain prostaglandin precursors: arachidonic acid, phospholipids, and cholesterol. These products are believed to contribute to an antihypertensive function or influence medullary blood flow.

Dendritic cells of bone marrow origin are the second most numerous interstitial cells (323–325). They occupy peritubular spaces in the cortex and medulla and are most concentrated in the inner stripe of the outer medulla. Dendritic cells resemble fibroblasts since they have a similar stellate morphology and contain abundant RER and free ribosomes. In contrast to interstitial fibroblasts, dendritic cells have more rounded nuclei and a more prominent Golgi apparatus, and they lack an actin cytoskeleton and cell membrane attachment plaques. Dendritic cells contain fewer lysosomes than macrophages and contain Birbeck granules, a special invagination of the cell membrane that serves as an antigen reservoir during dendritic cell maturation.

Dendritic cells are defined by their specialized antigen presentation and immune effector cell regulation functions. They belong to the mononuclear phagocytic system. They are antigen-expressing cells participating in innate and adaptive immunity, self-tolerance, and overall tissue hemostasis. They take up and process antigen for presentation to T cells in the context of surface major histocompatibility class (MHC) II molecules. Dendritic cells have a rapid turnover, exiting through the lymphatics to lymphatic organs for antigen presentation.

Macrophages are resident tissue phagocytic cells. They are predominately located in the periarterial connective tissue sheath (323–325). They have a large cell body and short cell processes. They contain a prominent lysosomal system with primary and secondary granules, vacuoles, and small endocytic vesicles. Lymphocytes are rare in the normal kidney; neutrophils and plasma cells are virtually absent.

REFERENCES

- Betsholtz C, He L, Takemoto M, et al. The glomerular transcriptome and proteome. *Nephron Exp Nephrol* 2007;106:e32–e36.
- Stojnev S, Pejcic M, Dolicanin Z, et al. Challenges of genomics and proteomics in nephrology. *Ren Fail* 2009;31:765–772.
- Molitoris B, Sandoval RM. Techniques to study nephron function: Microscopy and imaging. *Pflugers Arch* 2009;458:203–209.
- Perkins D, Verma M, Park KJ. Advances of genomic science and systems biology in renal transplantation: A review. *Semin Immunopathol* 2011;33:211–218.
- Je JC, Chuang PY, Ma'ayan A, et al. Systems biology of kidney diseases. *Kidney Int* 2012;81:22–39.
- Clark W. *The Drawings of Leonardo da Vinci in the Collection of Her Majesty the Queen at Windsor Castle, Edinburgh, England*. London: R & R Clark Ltd, 1966.
- DeBroe ME, Sacre D, Snelders ED, et al. The Flemish anatomist Andreas Vesalius (1514–1564) and the kidney. *Am J Nephrol* 1997;17:252.
- Hayman JM Jr. Malpighi's concerning the structure of the kidneys. A translation and introduction. *Ann Med Hist* 1925;7:242.
- Mezzogiorno A, Mezzogiorno V, Esposito V. History of the nephron. *Am J Nephrol* 2002;22:213.
- Bowman W. On the structure and use of the malpighian bodies of the kidney, with observations on the circulation through that gland. *Philos Trans R Soc Lond Biol* 1842;132:57.
- Fine LG. William Bowman's description of the glomerulus. *Am J Nephrol* 1985;5:437.
- Kriz W, Bankir L. A standard nomenclature for structure of the kidney. The Renal Commission of the International Union of Physiological Sciences (IUPS). *Anat Embryol (Berl)* 1988;178:N1.
- Davidson AL. *Radiology of the Kidney*. Philadelphia: WB Saunders, 1985.
- Kaye KW, Goldberg ME. Applied anatomy of the kidney and ureter. *Urol Clin North Am* 1982;9:3.
- Lee SL, Young MK, Rha SE. Comprehensive reviews of the interfascial plane of the retroperitoneum: normal anatomy and pathologic entities. *Emerg Radiol* 2010;17:3.
- Suramo I, Paivansalo M, Myllyla V. Cranio-caudal movements of the liver, pancreas and kidneys in respiration. *Acta Radiol Diagn (Stockh)* 1984;25:129.
- Clapp WL. Adult kidney. In: Sternberg SS, ed. *Histology for the Pathologist*. New York: Raven Press, 1992:677.
- Epstein M. Aging and the kidney. *J Am Soc Nephrol* 1996;7:1106.
- Hodson CJ. Physiological changes in size of the kidneys. *Clin Radiol* 1961;12:91.
- Kasike BL, Umen AJ. The influence of age, sex, race, and body habitus on kidney weight in humans. *Arch Pathol Lab Med* 1986;110:55.
- Bonsib SM. The renal sinus is the principal invasive pathway: A prospective study of 100 renal cell carcinomas. *Am J Surg Pathol* 2004;28:15.
- Fine H. The development of the lobes of the metanephros and fetal kidney. *Acta Anat (Basel)* 1982;113:93.
- Hodson J. The lobar structure of the kidney. *Br J Urol* 1972;44:246.
- Sykes D. The morphology of renal lobulations and calices, and their relationship to partial nephrectomy. *Br J Surg* 1964;51:294.
- Sampaio FJB. Anatomic classification of the kidney collecting system for endourologic procedure. *J Endourol* 1988;2:247.
- Osathanondh V, Potter EL. Development of human kidney as shown by microdissection, II: Renal pelvis, calyces, and papillae. *Arch Pathol* 1963;76:277.
- Ransley PG, Risdon RA. Renal papillary morphology in infants and young children. *Urol Res* 1975;3:111.
- Potter EL. *Normal and Abnormal Development of the Kidney*. Chicago: Year Book Medical Publishers, 1972.
- Sampaio FJ, Mandarim-De-Lacerda CA. 3-dimensional and radiological pelviccaliceal anatomy for endourology. *J Urol* 1988;140:1352.
- Dillon MJ, Goonasekera CD. Reflux nephropathy. *J Am Soc Nephrol* 1998;9:2377.
- Hodson CJ. Neuhauser lecture. Reflux nephropathy: A personal historical review. *AJR Am J Roentgenol* 1981;137:451.
- Oliver J. *Nephrons and Kidneys: A Quantitative Study of Development and Evolutionary Renal Architectonics*. New York: Harper & Row, 1968.
- Brödel M. The intrinsic blood vessels of the kidney and their significance in nephrotomy. *Bull Johns Hopkins Hosp* 1901;12:10.
- Graves FT. The anatomy of the intrarenal arteries and its application to segmental resection of the kidney. *Br J Surg* 1954;42:132.
- Sampaio FJ, Aragao AH. Anatomical relationship between the intrarenal arteries and the kidney collecting system. *J Urol* 1990;143:679.
- Sampaio FJ. Vascular anatomy at the ureteropelvic junction. *Urol Clin North Am* 1998;25:251.
- Sykes D. The arterial supply of the human kidney with special reference to accessory renal arteries. *Br J Surg* 1963;50:368.
- Baker SB. The blood supply of the renal papilla. *Br J Urol* 1959;31:53.
- Satyapal KS. Classification of the drainage patterns of the renal veins. *J Anat* 1995;186(Pt 2):329.
- Cuttino JT, Clark RL, Jennette JC. Microangiographic demonstration of human intrarenal microlymphatic pathways. *Urol Radiol* 1989;11:83.
- Holmes MJ, O'Morchoe PJ, O'Morchoe CC. Morphology of the intrarenal lymphatic system. Capsular and hilar communications. *Am J Anat* 1977;149:333.
- Sakamoto I, Ito Y, Mizuno M, et al. Lymphatic vessels develop during tubulointerstitial fibrosis. *Kidney Int* 2008;5:828.
- Bonsib SM. Renal lymphatics, and lymphatic involvement in sinus invasive (pT3b) clear cell renal cell carcinomas: a study of 40 cases. *Mod Pathol* 2006;19:746,753.

44. McLachlan EM, Luff SE. Sympathetic innervation of renal and extrarenal arterial vessels. *Kidney Int Suppl* 1992;37:S56.
45. Barajas L, Powers K, Wang P. Innervation of the renal cortical tubules: a quantitative study. *Am J Physiol* 1984;247:F50.
46. Barajas L, Liu L, Powers K. Anatomy of the renal innervation: intrarenal aspects and ganglia of origin. *J Physiol Pharmacol* 1992;70:735.
47. Reddy S, Kumar P, Prasad K. Histomorphometric and sympathetic innervation of the human renal artery: a cadaveric study. *Urol Ann* 2011;3:141-146.
48. Dixon JS, Gosling JA. The musculature of the human renal calices, pelvis and upper ureter. *J Anat* 1982;135:129.
49. Schmidt-Nielsen B. The renal pelvis. *Kidney Int* 1987;31:621.
50. Dwyer TM, Schmidt-Mielson B. The renal pelvis: machinery that concentrates urine in the papilla. *Neuro Physiol Sci* 2003;18:1.
51. Schmidt-Mielson B, Schmidt-Nielsen B. On the function of the mammalian renal papilla and the peristalsis of the surrounding pelvis. *Acta Physiol* 2011;202:379.
52. Rouiller C. General anatomy and histology of the kidney. In: Rouiller C, Muller AF, eds. *The Kidney: Morphology, Biochemistry and Physiology*. New York: Lippincott, 1989:67.
53. Knepper M, Burg M. Organization of nephron function. *Am J Physiol* 1983;244:F579.
54. Kriz W, Kaissling B. Structural organization of the mammalian kidney. In: Seldin DW, Giebisch GH, eds. *The Kidney: Physiology and Pathophysiology*. New York: Raven Press, 1992:707.
55. Beeuwkes R III. The vascular organization of the kidney. *Annu Rev Physiol* 1980;42:531.
56. Beeuwkes R. Vascular tubular relationships in the human kidney. In: Leaf A, Giebisch G, Bolis L, et al., eds. *Renal Pathophysiology*. New York: Raven Press, 1980:155.
57. Casellas D, Mimran A. Shunting in renal microvasculature of the rat: a scanning electron microscopic study of corrosion casts. *Anat Rec* 1981;201:237.
58. Ljungqvist A, Lagergren C. Normal intrarenal arterial pattern in adult and ageing human kidney. A microangiographical and histological study. *J Anat* 1962;96:285.
59. Barger AC, Herd JA. The renal circulation. *N Engl J Med* 1971;284:482.
60. Moffat DB, Fourman J. The vascular pattern of the rat kidney. *J Anat* 1963;97:543.
61. Koushanpour E, Kriz W. *Renal Physiology: Principles, Structure and Function*. 2nd ed. New York: Springer-Verlag, 1986:82.
62. Kriz W. Structural organization of the renal medulla: comparative and functional aspects. *Am J Physiol* 1981;241:R3.
63. Kriz W. Structural organization of renal medullary circulation. *Nephron* 1982;31:290.
64. Kriz W. Structural organization of the renal medullary counterflow system. *Fed Proc* 1983;42:2379.
65. Lemley KV, Kriz W. Cycles and separations: the histotopography of the urinary concentrating process. *Kidney Int* 1987;31:538.
66. Lemley KV, Kriz W. Anatomy of the renal interstitium. *Kidney Int* 1991;39:370.
67. Bertam JF, Douglas-Denton RN, Diouf B, et al. Human nephron number: implications for health and disease. *Pediatr Nephrol* 2011;26:1529.
68. Luyckx VA, Brenner BM. The clinical importance of nephron mass. *J Am Soc Nephrol* 2010;21:898.
69. Hoy WE, Bertram JF, Denton RD. Nephron number, glomerular volume, renal disease and hypertension. *Curr Opin Nephrol Hyperten* 2008;17:258.
70. Neugarten J, Kasiske B, Silbiger SR, et al. Effects of sex on renal structure. *Nephron* 2002;90:139.
71. Hughson M, Farris AB III, Douglas-Denton R, et al. Glomerular number and size in autopsy kidneys: the relationship to birth weight. *Kidney Int* 2003;63:2113.
72. Jamison RL. Short and long loop nephrons. *Kidney Int* 1987;31:597.
73. Murakami T. Vascular arrangement of the rat renal glomerulus. A scanning electron microscope study of corrosion casts. *Arch Histol Jpn* 1972;34:87.
74. Winkler D, Elger M, Sakai T, et al. Branching and confluence pattern of glomerular arterioles in the rat. *Kidney Int Suppl* 1991;32:S2.
75. Shea SM. Glomerular hemodynamics and vascular structure. The pattern and dimensions of a single rat glomerular capillary network reconstructed from Ultrathin sections. *Microvasc Res* 1979;18:129.
76. Gattone VH II, Evan AP, Willis LR, et al. Renal afferent arteriole in the spontaneously hypertensive rat. *Hypertension* 1983;5:8.
77. Elger M, Sakai T, Kriz W. The vascular pole of the renal glomerulus of rat. *Adv Anat Embryol Cell Biol* 1998;139:1.
78. Alcorn D, Ryan GB. The glomerular peripolar cell. *Kidney Int* 1993;44;(Suppl 42):S-35.
79. Gardiner DS, Lindop GB. The granular peripolar cell of the human glomerulus: a new component of the juxtaglomerular apparatus? *Histopathology* 1985;9:675.
80. Gibson IW, Downie I, Downie TT, et al. The parietal podocyte: a study of the vascular pole of the human glomerulus. *Kidney Int* 1992;41:211.
81. Bonsib SM, Reznicek MJ. Renal biopsy frozen section: a fluorescent study of hematoxylin and eosin-stained sections. *Mod Pathol* 1990;3:204.
82. Jefferson JA, Alpers CE, Shankland SJ. Podocyte biology for the bedside. *Am J Kidney Dis* 2011;58:835.
83. Andrews P. Morphological alterations of the glomerular (visceral) epithelium in response to pathological and experimental situations. *J Electron Microscop Tech* 1988;9:115.
84. Pavenstadt H, Kriz W, Kretzler M. Cell biology of the glomerular podocyte. *Physiol Rev* 2003;83:253.
85. Andrews PM, Porter KR. A scanning electron microscopic study of the nephron. *Am J Anat* 1974;140:81.
86. Yu Y, Leng C-C, Terada N, et al. Scanning electron microscopic study of the renal glomerulus by an in vivo cryotechnique combined with freeze substitution. *J Anat* 1998;192:595.
87. Takahashi-Iwanaga H. Comparative anatomy of the podocyte: a scanning electron microscopic study. *Microsc Res Tech* 2002;57:196.
88. Vasmant D, Maurice M, Feldmann G. Cytoskeleton ultrastructure of podocytes and glomerular endothelial cells in man and in the rat. *Anat Rec* 1984;210:17.
89. Drenckhahn D, Franke RP. Ultrastructural organization of contractile and cytoskeletal proteins in glomerular podocytes of chicken, rat, and man. *Lab Invest* 1988;59:673.
90. Kriz W, Mundel P, Elger M. The contractile apparatus of podocytes is arranged to counteract GBM expansion. *Contrib Nephrol* 1994;107:1.
91. Neal CR, Crook H, Bell E, et al. Three-dimensional reconstruction of glomeruli by electron microscopy reveals a distinct restrictive urinary subpodocyte space. *J Am Soc Nephrol* 2005;16:1223.
92. Kriz W, Kretzler M, Provoost AP, et al. Stability and leakiness: opposing challenges to the glomerulus. *Kidney Int* 1996;49:1570.
93. Welsh GI, Saleem MA. The podocyte cytoskeleton-key to a functioning glomerulus in health and disease. *Nat Rev Nephrol* 2012;8:14.
94. Jones DB. Enzymatic dissection of the glomerulus. *Lab Invest* 1985;52:453.
95. Greka A, Mundel P. Cell biology and pathology of podocytes. *Annu Rev Physiol* 2012;74:299.
96. Garg P, Rabelink T. Glomerular proteinuria: a complex interplay between unique players. *Adv Chronic Kidney Dis* 2011;18:233.
97. Patrakka J, Tryggvason K. Molecular make-up of the glomerular filtrations barrier. *Biochem Biophys Res Commun* 2010;396:164.
98. Cheng H, Harris RC. The glomerulus-a view from the outside-the podocyte. *Int J Biochem Cell Biol* 2010;42:1380-1387.
99. Patrakka J, Tryggvason K. New insights into the role of podocytes in proteinuria. *Nat Rev Nephrol* 2009;5:463.
100. Bonsib SM, Horvath F Jr. Multinucleated podocytes in a child with nephrotic syndrome. *Am J Kid Dis* 1999;34:966.
101. Nagata M, Shu Y, Tomari S. Role of cell cycle molecules in the pathophysiology of glomerular epithelial cells. *Microsc Res Tech* 2002;57:203.
102. Nagata M, Tomari S, Kanemoto K, et al. Podocytes, parietal cells, and glomerular pathology: the role of cell cycle proteins. *Pediatr Nephrol* 2003;18:3.
103. Griffin SV, Petermann AT, Durvasula RV, et al. Podocyte proliferation and differentiation in glomerular disease: role of cell-cycle regulatory proteins. *Nephrol Dial Transplant* 2003;18(Suppl 6):vi8.
104. Kreidberg JA. Podocyte differentiation and glomerulogenesis. *J Am Soc Nephrol* 2003;14:806.

105. Stamenkovic I, Skalli O, Gabbiani G. Distribution of intermediate filament proteins in normal and diseased human glomeruli. *Am J Pathol* 1986;125:465.
106. Rodewald R, Karnovsky MJ. Porous substructure of the glomerular slit diaphragm in the rat and mouse. *J Cell Biol* 1974;60:423.
107. Gagliardini E, Conti S, Begigni A, et al. Imaging the porous ultrastructure of the glomerular epithelial filtration slit. *J Am Soc Nephrol* 2010;21:2081.
108. Miner JH. Glomerular basement membrane composition and the filtration barrier. *Pediatr Nephrol* 2011;26:1413.
109. Barisoni L, Mundel P. Podocyte biology and the emerging understanding of podocyte diseases. *Am J Nephrol* 2003;23:353.
110. Tryggvason K, Wartiovaara J. Molecular basis of glomerular permselectivity. *Curr Opin Nephrol Hypertens* 2001;10:543.
111. Akhtar M, Al Mana H. Molecular basis of proteinuria. *Adv Anat Pathol* 2004;11:304.
112. Farquhar MG, Vernier RL, Good RA. An electron microscope study of the glomerulus in nephrosis, glomerulonephritis, and lupus erythematosus. *J Exp Med* 1957;106:649.
113. Sawada H, Stukenbrok H, Kerjaschki D, et al. Epithelial polyanion (podocalyxin) is found on the sides but not the soles of the foot processes of the glomerular epithelium. *Am J Pathol* 1986;125:309.
114. Orlando RA, Takeda T, Zak B, et al. The glomerular epithelial cell anti-adhesion podocalyxin associates with the actin cytoskeleton through interactions with ezrin. *J Am Soc Nephrol* 2001;12:1589.
115. Tryggvason K. Unraveling the mechanisms of glomerular ultrafiltration: nephrin, a key component of the slit diaphragm. *J Am Soc Nephrol* 1999;10:2440.
116. Benzing T. Signaling at the slit diaphragm. *J Am Soc Nephrol* 2004;15:1382.
117. Barisoni L, Kopp JB. Update in podocyte biology: putting one's best foot forward. *Curr Opin Nephrol Hypertens* 2003;12:251.
118. Chugh SS, Kaw B, Kanwar YS. Molecular structure-function relationship in the slit diaphragm. *Semin Nephrol* 2003;23:544.
119. Mundel P, Shankland SJ. Podocyte biology and response to injury. *J Am Soc Nephrol* 2002;13:3005.
120. Yuan H, Takeuchi E, Salant DJ. Podocyte slit-diaphragm protein nephrin is linked to the actin cytoskeleton. *Am J Physiol Renal Physiol* 2002;282:F585.
121. Saleem MA, Ni L, Witherden I, et al. Co-localization of nephrin, podocin, and the actin cytoskeleton: evidence for a role in podocyte foot process formation. *Am J Pathol* 2002;161:1459.
122. Roselli S, Gribouval O, Boute N, et al. Podocin localizes in the kidney to the slit diaphragm area. *Am J Pathol* 2002;160:131.
123. Asanuma K, Yanagida-Asanuma E, Faul C, et al. Synaptopodin orchestrates actin organization and cell motility via regulation of RhoA signaling. *Nat Cell Biol* 2006;8:485.
124. Schnabel E, Anderson JM, Farquhar MG. The tight junction protein ZO-1 is concentrated along slit diaphragms of the glomerular epithelium. *J Cell Biol* 1990;111:1255.
125. Lehtonen S, Zhao F, Lehtonen E. CD2-associated protein directly interacts with the actin cytoskeleton. *Am J Physiol Renal Physiol* 2002;283:F734.
126. Sellin L, Huber TB, Gerke P, et al. NEPH1 defines a novel family of podocin interacting proteins. *FASEB J* 2003;17:115.
127. Liu G, Kaw B, Kurfis J, et al. NepH1 and nephrin interaction in the slit diaphragm is an important determinant of glomerular permeability. *J Clin Invest* 2003;112:209.
128. Inoue T, Yaoita E, Kurihara H, et al. FAT is a component of glomerular slit diaphragms. *Kidney Int* 2001;59:1003.
129. Romagnani P. Parietal epithelial cells: their role in health and disease. *Contrib Nephrol* 2011;169:23.
130. Ohse T, Pippin JW, Chang AM, et al. The enigmatic parietal epithelial cell is finally getting noticed: a review. *Kidney Int* 2009;76:1225.
131. Webber WA, Lee J. The ciliary pattern of the parietal layer of Bowman's capsule. *Anat Rec* 1974;180:449.
132. Becker JU, Hoerning A, Schmid KW, et al. Immigrating progenitor cells contribute to human podocyte turnover. *Kidney Int* 2007;72:1468.
133. Lazzeri E, Mazzinghi B, Romagnani P. Regeneration and the kidney. *Curr Opin Nephrol Hypertens* 2010;19:248.
134. Singh SKS, Jeansson M, Quaggin SE. New insights into the pathogenesis of cellular crescents. *Curr Opin Nephrol Hypertens* 2011;20:258.
135. Appel D, Kershaw DB, Smeets B, et al. Recruitment of podocytes from glomerular parietal epithelial cells. *J Am Soc Nephrol* 2009;20:333.
136. Smeets B, Kuppe C, Sicking E-M, et al. Parietal epithelial cells participate in the formation of sclerotic lesions in focal segmental glomerulosclerosis. *J Am Soc Nephrol* 2011;22:1262.
137. Doby DC, Eknoyan G, Magill LS, et al. A quantitative evaluation of the glomerular capillary endothelium in rat and human kidneys: utilization of vascular perfusion, freeze-cracking of tissue, and scanning electron microscopy. *J Electron Microscop Tech* 1984;1:185.
138. Bearer EL, Orci L. Endothelial fenestral diaphragms: a quick-freeze, deep-etch study. *J Cell Biol* 1985;100:418.
139. Hjalmarsson C, Johanasson BR, Haraldsson B. Electron microscopic evaluation of the endothelial surface of glomerular capillaries. *Microvasc Res* 2004;67:9.
140. Abrahamson DR. Development of kidney glomerular endothelial cells and their role in basement membrane assembly. *Organogenesis* 2009;5:275.
141. Ballermann BJ. Glomerular endothelial cell differentiation. *Kidney Int* 2005;67:1668.
142. Ichimura K, Stan RV, Kurihara H, Sakai T. Glomerular endothelial cells form diaphragms during development and pathologic condition. *J Am Soc Nephrol* 2008;19:1463.
143. Molitoris BA, Sandoval RM. Kidney endothelial dysfunction: ischemia, localized infections and sepsis. In: Kellum JA, Ronco C, Vincent J-L, eds. *Controversies in Acute Kidney Injury*. Basel: Karger, 2011:108.
144. Fogo AB, Kon V. The glomerulus—a view from the inside—the endothelial cell. *Int J Biochem Cell Biol* 2010;42:1388.
145. Zimmermann KW. Über den Bau des Glomerulus der menschlichen. *Z Mikrosk Anat Forsch* 1929;18:520.
146. Farquhar MG, Palade GE. Functional evidence for the existence of a third cell type in the renal glomerulus. Phagocytosis of filtration residues by a distinctive "third" cell. *J Cell Biol* 1962;13:55.
147. Takahashi-Iwanaga H. SEM observation of mesangial cells in the rat kidney by NaOH maceration combined with freeze cracking. *Acta Med Biol* 1991;39:37.
148. Pricam C, Humbert F, Perrelet A, et al. Gap junctions in mesangial and lacin cells. *J Cell Biol* 1974;63:349.
149. Schlöndorff D, Banas B. The mesangial cell revisited: no cell is an island. *J Am Soc Nephrol* 2009;20:1179.
150. Cortes P, Mendez M, Riser BL, et al. F-actin fiber distribution in glomerular cells: structural and functional implications. *Kidney Int* 2000;58:2452.
151. Kriz W, Elger M, Mundel P, et al. Structure-stabilizing forces in the glomerular tuft. *J Am Soc Nephrol* 1995;5:1731.
152. Kikkawa Y, Virtanen I, Miner JH. Mesangial cells organize the glomerular capillaries by adhering to the G domain of laminin alpha 5 in the glomerular basement membrane. *J Cell Biol* 2003;161:187.
153. Mene P, Simonson MS, Dunn MJ. Physiology of the mesangial cell. *Physiol Rev* 1989;69:1347.
154. Schlöndorff D. The glomerular mesangial cell: an expanding role for a specialized pericyte. *FASEB J* 1987;1:272.
155. Abboud HA. Mesangial cell biology. *Exp Cell Res* 2012;318:979.
156. Herrera GA, Turbat-Herrera EA, Teng J. Mesangial homeostasis and pathobiology: their role in health and disease. *Contrib Nephrol* 2011;169:6.
157. Schock F, Perrimon N. Molecular mechanisms of epithelial morphogenesis. *Annu Rev Cell Dev Biol* 2002;18:463.
158. Aumailley M, Gayraud B. Structure and biological activity of the extracellular matrix. *J Mol Med* 1998;76:253.
159. Woolf AS, Loughna S. Origin of glomerular capillaries: is the verdict in? *Exp Nephrol* 1998;6:17.
160. Sariola H, Timpl R, von der Mark K, et al. Dual origin of glomerular basement membrane. *Dev Biol* 1984;101:86.
161. Timpl R, Dziadek M. Structure, development, and molecular pathology of basement membranes. *Int Rev Exp Pathol* 1986;29:1.
162. Minor JH. Building the glomerulus: a matricentric view. *J Am Soc Nephrol* 2005;16:857.
163. Haraldsson B, Nystrom J, Deen WM. Properties of the glomerular barrier and mechanisms of proteinuria. *Physiol Rev* 2008;88:451.
164. Miner JH. Organogenesis of the kidney glomerulus. *Organogenesis* 2011;7:75.

165. Abrahamson DR, Hudson BG, Stroganova L, et al. Cellular origins of type IV collagen networks in developing glomeruli. *J Am Soc Nephrol* 2009;20:1471.
166. Kanwar YS, Danesh SS, Chugh SS. Contribution of proteoglycans toward the integrated function of renal glomerular capillaries. *Am J Pathol* 2007;171:9.
167. Aumailley M, Bruckner-Tuderman L, Carter WG, et al. A simplified laminin nomenclature. *Matrix Biol* 2005;24:326.
168. Minor JH, Patton BL, Lentz DJ, et al. The laminin alpha chains: expression, developmental transitions, and chromosomal locations of alpha 1-5, identification of heterotrimeric laminins 8-11 and cloning of a novel alpha3 isoform. *J Cell Biol* 1997;137:685.
169. Jorgensen F, Bentzon MW. The ultrastructure of the normal human glomerulus. Thickness of glomerular basement membrane. *Lab Invest* 1968;18:42.
170. Steffes MW, Barbosa J, Basgen JM, et al. Quantitative glomerular morphology of the normal human kidney. *Lab Invest* 1983;49:82.
171. Martinez-Hernandez A, Chung AE. The ultrastructural localization of two basement membrane components: entactin and laminin in rat tissues. *J Histochem Cytochem* 1984;32:289.
172. Kefalides NA. A collagen of unusual composition and a glycoprotein isolated from canine glomerular basement membrane. *Biochem Biophys Res Commun* 1966;22:26.
173. Timpl R, Brown JC. Supramolecular assembly of basement membranes. *Bioessays* 1996;18:123.
174. Yurchenco PD, Furthmayr H. Self-assembly of basement membrane collagen. *Biochemistry* 1984;23:1839.
175. Hudson BG, Reeders ST, Tryggvason K. Type IV collagen: structure, gene organization, and role in human diseases. Molecular basis of Goodpasture and Alport syndromes and diffuse leiomyomatosis. *J Biol Chem* 1993;268:26033.
176. Kalluri R, Wilson CB, Weber M, et al. Identification of the alpha 3 chain of type IV collagen as the common autoantigen in antibodies against basement membrane disease and Goodpasture syndrome. *J Am Soc Nephrol* 1995;6:1178.
177. Hudson BG, Tryggvason K, Sundaramoorthy M, et al. Alport's syndrome, Goodpasture's syndrome, and type IV collagen. *N Engl J Med* 2003;348:2543.
178. Tryggvason K. Molecular properties and diseases of collagens. *Kidney Int Suppl* 1995;49:S24.
179. Harvey SJ, Zheng K, Sado Y, et al. Role of distinct type IV collagen networks in glomerular development and function. *Kidney Int* 1998;54:1857.
180. Netzer KO, Suzuki K, Itoh Y, et al. Comparative analysis of the noncollagenous NC1 domain of type IV collagen: identification of structural features important for assembly, function, and pathogenesis. *Protein Sci* 1998;7:1340.
181. Boutaud A, Borza DB, Bondar O, et al. Type IV collagen of the glomerular basement membrane. Evidence that the chain specificity of network assembly is encoded by the noncollagenous NC1 domains. *J Biol Chem* 2000;275:30716.
182. Borza DB, Bondar O, Ninomiya Y, et al. The NC1 domain of collagen IV encodes a novel network composed of the alpha 1, alpha 2, alpha 5, and alpha 6 chains in smooth muscle basement membranes. *J Biol Chem* 2001;276:28532.
183. Sundaramoorthy M, Meiyappan M, Todd P, et al. Crystal structure of NC1 domains. Structural basis for type IV collagen assembly in basement membranes. *J Biol Chem* 2002;277:31142.
184. Eknoyan G, Rubens R, Lameire N. The juxtaglomerular apparatus of Norbert Goormaghtigh—a critical appraisal. *Nephrol Dial Transplant* 2009;24:3876.
185. Michael AF. The glomerular mesangium. *Contrib Nephrol* 1984;40:7.
186. Lemley KV, Elger M, Koeppen-Hagemann I, et al. The glomerular mesangium: capillary support function and its failure under experimental conditions. *Clin Invest* 1992;70:843.
187. Inkyo-Hayasaka K, Sakai T, Kobayashi N, et al. Three-dimensional analysis of the whole mesangium in the rat. *Kidney Int* 1996;50:672.
188. Makino H, Hironaka K, Shikata K, et al. Mesangial matrices act as mesangial channels to the juxtaglomerular zone. Tracer and high-resolution scanning electron-microscopic study. *Nephron* 1994;66:181.
189. Sterzel RB, Hartner A, Schlotzer-Schrehardt U, et al. Elastic fiber proteins in the glomerular mesangium in vivo and in cell culture. *Kidney Int* 2000;58:1588.
190. Mundel P, Elger M, Sakai T, et al. Microfibrils are a major component of the mesangial matrix in the glomerulus of the rat kidney. *Cell Tissue Res* 1988;254:183.
191. Couchman JR, Beavan LA, McCarthy KJ. Glomerular matrix: synthesis, turnover and role in mesangial expansion. *Kidney Int* 1994;45:328.
192. Kanwar YS, Rosenzweig LJ, Jakubowski ML. Distribution of de novo synthesized sulfated glycosaminoglycans in the glomerular basement membrane and mesangial matrix. *Lab Invest* 1983;49:216.
193. Iglesias-De La Cruz MC, Ruiz-Torres MP, De Lucio-Cazana FJ, et al. Phenotypic modifications of human mesangial cells by extracellular matrix: the importance of matrix in the contractile response to reactive oxygen species. *Exp Nephrol* 2000;8:97.
194. Houser MT, Scheinman JI, Basgen J, et al. Preservation of mesangium and immunohistochemically defined antigens in glomerular basement membrane isolated by detergent extraction. *J Clin Invest* 1982;69:1169.
195. Sakai T, Kriz W. The structural relationship between mesangial cells and basement membrane of the renal glomerulus. *Anat Embryol (Berl)* 1987;176:373.
196. Kriz W, Elger M, Lemley KV, et al. Mesangial cell-glomerular basement membrane connections counteract glomerular capillary and mesangium expansion. *Am J Nephrol* 1990;10(Suppl 1):4.
197. Mbassa G, Elger M, Kriz W. The ultrastructural organization of the basement membrane of Bowman's capsule in the rat renal corpuscle. *Cell Tissue Res* 1988;253:151.
198. Barajas L. The ultrastructure of the juxtaglomerular apparatus as disclosed by three-dimensional reconstructions from serial sections. The anatomical relationship between the tubular and vascular components. *J Ultrastruct Res* 1970;33:116.
199. Barajas L. Anatomy of the juxtaglomerular apparatus. *Am J Physiol* 1979;237:F333.
200. Isler H, Krstic R. Scanning electron microscopy of the juxtaglomerular apparatus in the freeze-fractured rat kidney. *Arch Histol Jpn* 1981;44:15.
201. Kaissling B, Kriz W. Variability of intercellular spaces between macula densa cells: a transmission electron microscopic study in rabbits and rats. *Kidney Int Suppl* 1982;12:S9.
202. Barajas L, Wang P. Simultaneous ultrastructural visualization of acetylcholinesterase activity and tritiated norepinephrine uptake in renal nerves. *Anat Rec* 1983;205:185.
203. Taugner R, Schiller A, Kaissling B, et al. Gap junctional coupling between the JGA and the glomerular tuft. *Cell Tissue Res* 1978;186:279.
204. Schnermann J, Homer W. Smith Award lecture. The juxtaglomerular apparatus: from anatomical peculiarity to physiological relevance. *J Am Soc Nephrol* 2003;14:1681.
205. Crowley SD, Coffman TM. Recent advances involving the rennin-angiotensin system. *Exp Cell Res* 2012;318:1049.
206. Peti-Peterdi J, Harris RC. Macula densa signaling mechanisms of renin release. *J Am Soc Nephrol* 2010;21:1093.
207. Komlosi P, Fintha, Bell PD. Unraveling the relationship between macula densa cell volume and luminal solute concentration/osmolality. *Kidney Int* 2006;70:865.
208. Serafini-Cessi F, Malagolini N, Cavallone D. Tamm-Horsfall glycoprotein: biology and clinical relevance. *Am J Kidney Dis* 2003;42:658.
209. Bonsib SM, Plattner SB. Acellular scanning electron microscopy of spicular renal amyloidosis. *Ultrastruct Pathol* 1986;10:497.
210. Taugner R, Buhle CP, Hackenthal E, et al. Morphology of the juxtaglomerular apparatus and secretory mechanisms. *Contrib Nephrol* 1984;43:76.
211. Cantin M, Araujo-Nascimento MD, Benchimol S, et al. Metaplasia of smooth muscle cells into juxtaglomerular cells in the juxtaglomerular apparatus, arteries, and arterioles of the ischemic (endocrine) kidney. An ultrastructural-cytochemical and autoradiographic study. *Am J Pathol* 1977;87:581.
212. Ryan GB, Alcorn D, Coghlan JP, et al. Ultrastructural morphology of granule release from juxtaglomerular myoepithelioid and peripolar cells. *Kidney Int Suppl* 1982;12:S3.
213. Kirk KL, Bell PD, Barfuss DW, et al. Direct visualization of the isolated and perfused macula densa. *Am J Physiol* 1985;248:F890.
214. Cantin M, Gutkowska J, Lacasse J, et al. Ultrastructural immunocytochemical localization of renin and angiotensin II in the juxtaglomerular cells of the ischemic kidney in experimental renal hypertension. *Am J Pathol* 1984;115:212.

215. Inagami T, Kawamura M, Naruse K, et al. Localization of components of the renin-angiotensin system within the kidney. *Fed Proc* 1986;45:1414.
216. Kriz W. A periarterial pathway for intrarenal distribution of renin. *Kidney Int Suppl* 1987;20:S51.
217. Moffat DB. The fine structure of the blood vessels of the renal medulla with particular reference to the control of the medullary circulation. *J Ultrastruct Res* 1967;19:532.
218. Rosivall L, Peti-Peterdi. Heterogeneity of the afferent arteriole—correlations between morphology and function. *Nephrol Dial Transplant* 2006;21:2703.
219. Jones WR, O'Morchoe CC. Ultrastructural evidence for a reabsorptive role by intrarenal veins. *Anat Rec* 1983;207:253.
220. Gattone VH II, Luft FC, Evan AP. Renal afferent and efferent arterioles of the rabbit. *Am J Physiol* 1984;247:F219.
221. Kriz W, Bachmann S. Pre- and postglomerular arterioles of the kidney. *J Cardiovasc Pharmacol* 1985;(7 Suppl 3):S24.
222. Edwards JG. Efferent arterioles of glomeruli in the juxtamedullary zone of the human kidney. *Anat Rec* 1956;125:521.
223. Silva FG, Nadasdy T, Laszik Z. Immunohistochemical and lectin dissection of the human nephron in health and disease. *Arch Pathol Lab Med* 1993;117:1233.
224. Truong LD, Phung VT, Yoshikawa Y, et al. Glycoconjugates in normal human kidney. A histochemical study using 13 biotinylated lectins. *Histochemistry* 1988;90:51.
225. Grone HJ, Weber K, Helmchen U, et al. Villin—a marker of brush border differentiation and cellular origin in human renal cell carcinoma. *Am J Pathol* 1986;124:294.
226. Le Hir M, Dubach UC. The cellular specificity of lectin binding in the kidney. II. A light microscopical study in the rabbit. *Histochemistry* 1982;74:531.
227. Sikri KL, Foster CL, MacHugh N, et al. Localization of Tamm-Horsfall glycoprotein in the human kidney using immuno-fluorescence and immuno-electron microscopical techniques. *J Anat* 1981;132:597.
228. Brown D, Roth J, Kumpulainen T, et al. Ultrastructural immunocytochemical localization of carbonic anhydrase. Presence in intercalated cells of the rat collecting tubule. *Histochemistry* 1982;75:209.
229. Dobyan DC, Magill LS, Friedman PA, et al. Carbonic anhydrase histochemistry in rabbit and mouse kidneys. *Anat Rec* 1982;204:185.
230. Hennigar RA, Sens DA, Othersen HB, et al. Distribution of fucose substance in kidney and related neoplasms. Absence of lectin-reactive alpha-fucose from the vasculature of bilateral Wilm's tumors. *Arch Pathol Lab Med* 1988;112:908.
231. Hennigar RA, Schulte BA, Spicer SS. Heterogeneous distribution of glycoconjugates in human kidney tubules. *Anat Rec* 1985;211:376.
232. Maunsbach AB, Christensen EI. Functional ultrastructure of the proximal tubule. In: Windhager E, ed. *Handbook of Physiology*. New York: Oxford University Press, 1992:41.
233. Bulger RE, Cronin RE, Dobyan DC. Survey of the morphology of the dog kidney. *Anat Rec* 1979;194:41.
234. Tisher CC, Bulger RE, Trump BF. Human renal ultrastructure. I. Proximal tubule of healthy individuals. *Lab Invest* 1966;15:1357.
235. Ericsson JL, Trump BF. Electron microscopic studies of the epithelium of the proximal tubule of the rat kidney. III. Microbodies, multivesicular bodies, and the Golgi apparatus. *Lab Invest* 1966;15:1610.
236. Evan AP, Gattone VH II, Connors BA. Ultrastructural features of the rabbit proximal tubules. *Arch Histol Cytol* 1992;55(Suppl):139.
237. Rostgaard J, Thuneberg L. Electron microscopical observations on the brush border of proximal tubule cells of mammalian kidney. *Z Zellforsch Mikrosk Anat* 1972;132:473.
238. Welling LW, Welling DJ. Shape of epithelial cells and intercellular channels in the rabbit proximal nephron. *Kidney Int* 1976;9:385.
239. Bulger RE, Siegel FL, Pendergrass R. Scanning and transmission electron microscopy of the rat kidney. *Am J Anat* 1974;139:483.
240. Welling LW, Welling DJ. Surface areas of brush border and lateral cell walls in the rabbit proximal nephron. *Kidney Int* 1975;8:343.
241. Berry CA, Ives HE, Rector FC Jr. Renal transport of glucose, amino acids, sodium, chloride, and water. In: Brenner B, ed. *The Kidney*. Philadelphia: WB Saunders, 1996:334.
242. Brown D, Katsura T, Kawashima M, et al. Cellular distribution of the aquaporins: a family of water channel proteins. *Histochem Cell Biol* 1995;104:1.
243. Knepper MA, Wade JB, Terris J, et al. Renal aquaporins. *Kidney Int* 1996;49:1712.
244. Ernst SA. Transport ATPase cytochemistry: ultrastructural localization of potassium-dependent and potassium-independent phosphatase activities in rat kidney cortex. *J Cell Biol* 1975;66:586.
245. Kinne R, Schmitz JE, Kinne-Saffran E. The localization of the Na⁺-K⁺-ATPase in the cells of rat kidney cortex: a study on isolated plasma membranes. *Pflugers Arch* 1971;329:191.
246. Kuhn K, Reale E. Junctional complexes of the tubular cells in the human kidney as revealed with freeze-fracture. *Cell Tissue Res* 1975;160:193.
247. Roesinger B, Schiller A, Taugner R. A freeze-fracture study of tight junctions in the pars convoluta and pars recta of the renal proximal tubule. *Cell Tissue Res* 1978;186:121.
248. Silverblatt FJ, Bulger RE. Gap junctions occur in vertebrate renal proximal tubule cells. *J Cell Biol* 1970;47:513.
249. Rodman JS, Kerjaschki D, Merisko E, et al. Presence of an extensive clathrin coat on the apical plasmalemma of the rat kidney proximal tubule cell. *J Cell Biol* 1984;98:1630.
250. Rodman JS, Seidman L, Farquhar MG. The membrane composition of coated pits, microvilli, endosomes, and lysosomes is distinctive in the rat kidney proximal tubule cell. *J Cell Biol* 1986;102:77.
251. van Deurs B, Christensen EI. Endocytosis in kidney proximal tubule cells and cultured fibroblasts: a review of the structural aspects of membrane recycling between the plasma membrane and endocytic vacuoles. *Eur J Cell Biol* 1984;33:163.
252. Priestley GC, Malt RA. Membrane-bound ribosomes in kidney: methods of estimation and effect of compensatory renal growth. *J Cell Biol* 1969;41:886.
253. Kalmbach P, Fahimi HD. Peroxisomes: identification in freeze-etch preparations of rat kidney. *Cell Biol Int Rep* 1978;2:389.
254. Kaissling B, Kriz W. Morphology of the loop of Henle, distal tubule, and collecting duct. In: Windhager E, ed. *Handbook of Physiology*. New York: Oxford University Press, 1992:109.
255. Knepper MA, Danielson RA, Saidel GM, et al. Quantitative analysis of renal medullary anatomy in rats and rabbits. *Kidney Int* 1977;12:313.
256. Schwartz MM, Karnovsky MJ, Vehkatalalam MA. Ultrastructural differences between rat inner medullary descending and ascending vasa recta. *Lab Invest* 1976;35:161.
257. Schwartz MM, Venkatachalam MA. Structural differences in thin limbs of Henle: physiological implications. *Kidney Int* 1974;6:193.
258. Bulger RE, Tisher CC, Myers CH, et al. Human renal ultrastructure. II. The thin limb of Henle's loop and the interstitium in healthy individuals. *Lab Invest* 1967;16:124.
259. Schiller A, Taugner R, Kriz W. The thin limbs of Henle's loop in the rabbit. A freeze fracture study. *Cell Tissue Res* 1980;207:249.
260. Allen F, Tisher CC. Morphology of the ascending thick limb of Henle. *Kidney Int* 1976;9:8.
261. Schwartz MM, Karnovsky MJ, Venkatachalam MA. Regional membrane specialization in the thin limbs of Henle's loops as seen by freeze-fracture electron microscopy. *Kidney Int* 1979;16:577.
262. Bankir L, Bouby N, Trinh Trang Tan MM, et al. Anatomy and function, role in urine concentrating mechanisms. In: Gruenfeld JB, ed. *Advances in Nephrology. Thick Ascending Limb of Henle's Loop*. Chicago: Year Book Medical Publishers, 1987:69.
263. Knepper MA, Rector RC Jr. Urine concentration and dilution. In: Brenner BM, ed. *The Kidney*. Philadelphia: WB Saunders, 1996:532.
264. Madsen KM, Tisher CC. Structural-functional relationships along the distal nephron. *Am J Physiol* 1986;250:F1.
265. Crayen ML, Thoenes W. Architecture and cell structures in the distal nephron of the rat kidney. *Cytophysiologie* 1978;17:197.
266. Kone BC, Madsen KM, Tisher CC. Ultrastructure of the thick ascending limb of Henle in the rat kidney. *Am J Anat* 1984;171:217.
267. Kaissling B, Peter S, Kriz W. The transition of the thick ascending limb of Henle's loop into the distal convoluted tubule in the nephron of the rat kidney. *Cell Tissue Res* 1977;182:111.
268. Tisher CC, Bulger RE, Trump BF. Human renal ultrastructure, 3: the distal tubule in healthy individuals. *Lab Invest* 1968;18:655.
269. Welling LW, Welling DJ, Hill JJ. Shape of cells and intercellular channels in rabbit thick ascending limb of Henle. *Kidney Int* 1978;13:144.

270. Garg LC, Knepper MA, Burg MB. Mineralocorticoid effects on Na-K-ATPase in individual nephron segments. *Am J Physiol* 1981;240:F536.
271. Greger R. Ion transport mechanisms in thick ascending limb of Henle's loop of mammalian nephron. *Physiol Rev* 1985;65:760.
272. Myers CE, Bulger RE, Tisher CC, et al. Human ultrastructure. IV: collecting duct of healthy individuals. *Lab Invest* 1966;15:1921.
273. Stanton BA, Biemesderfer D, Wade JB, et al. Structural and functional study of the rat distal nephron: effects of potassium adaptation and depletion. *Kidney Int* 1981;19:36.
274. Kaissling B. Ultrastructural characterization of the connecting tubule and the different segments of the collecting duct system in the rabbit kidney. *Curr Probl Clin Biochem* 1977;8:435.
275. LeFurgey A, Tisher CC. Morphology of rabbit collecting duct. *Am J Anat* 1979;155:111.
276. Welling LW, Evan AP, Welling DJ. Shape of cells and extracellular channels in rabbit cortical collecting ducts. *Kidney Int* 1981;20:211.
277. Hagege J, Gabe M, Richet G. Scanning of the apical pole of distal tubular cells under differing acid-base conditions. *Kidney Int* 1974;5:137.
278. Brown D, Shields GI, Valtin H, et al. Lack of intramembranous particle clusters in collecting ducts of mice with nephrogenic diabetes insipidus. *Am J Physiol* 1985;249:F582.
279. Pricam C, Humbert F, Perrelet A, et al. A freeze-etch study of the tight junctions of the rat kidney tubules. *Lab Invest* 1974;30:286.
280. Schiller A, Forssmann WG, Taugner R. The tight junctions of renal tubules in the cortex and outer medulla. A quantitative study of the kidneys of six species. *Cell Tissue Res* 1980;212:395.
281. Verkman AS, Lencer WI, Brown D, et al. Endosomes from kidney collecting tubule cells contain the vasopressin-sensitive water channel. *Nature* 1988;333:268.
282. Kaissling B, Le Hir M. Distal tubular segments of the rabbit kidney after adaptation to altered Na- and K- intake. I. Structural changes. *Cell Tissue Res* 1982;224:469.
283. Le Hir M, Kaissling B, Dubach UC. Distal tubular segments of the rabbit kidney after adaptation to altered Na- and K-intake. II. Changes in Na-K-ATPase activity. *Cell Tissue Res* 1982;224:493.
284. Brown D, Gluck S, Hartwig J. Structure of the novel membrane-coating material in proton-secreting epithelial cells and identification as an H⁺ATPase. *J Cell Biol* 1987;105:1637.
285. Brown D, Hirsch S, Gluck S. An H⁺-ATPase in opposite plasma membrane domains in kidney epithelial cell subpopulations. *Nature* 1988;331:622.
286. Brown D, Hirsch S, Gluck S. Localization of a proton-pumping ATPase in rat kidney. *J Clin Invest* 1988;82:2114.
287. Ridderstrale Y, Kashgarian M, Koeppen B, et al. Morphological heterogeneity of the rabbit collecting duct. *Kidney Int* 1988;34:655.
288. Schwartz GJ, Barasch J, Al-Awqati Q. Plasticity of functional epithelial polarity. *Nature* 1985;318:368.
289. Verlander JW, Madsen KM, Tisher CC. Effect of acute respiratory acidosis on two populations of intercalated cells in rat cortical collecting duct. *Am J Physiol* 1987;253:F1142.
290. Kishore BK, Mandon B, Oza NB, et al. Rat renal arcade segment expresses vasopressin-regulated water channel and vasopressin V2 receptor. *J Clin Invest* 1996;97:2763.
291. Ganote CE, Grantham JJ, Moses HL, et al. Ultrastructural studies of vasopressin effect on isolated perfused renal collecting tubules of the rabbit. *J Cell Biol* 1968;36:355.
292. Woodhall PB, Tisher CC. Response of the distal tubule and cortical collecting duct to vasopressin in the rat. *J Clin Invest* 1973;52:3095.
293. Knepper MA. Molecular physiology of urinary concentrating mechanism: regulation of aquaporin water channels by vasopressin. *Am J Physiol* 1997;272:F3.
294. Brown D. Membrane recycling and epithelial cell function. *Am J Physiol* 1989;256:F1.
295. Verkman AS. Mechanisms and regulation of water permeability in renal epithelia. *Am J Physiol* 1989;257:C837.
296. Ernst SA, Schreiber JH. Ultrastructural localization of Na⁺,K⁺-ATPase in rat and rabbit kidney medulla. *J Cell Biol* 1981;91:803.
297. Aukland K, Bogusky RT, Renkin EM. Renal cortical interstitium and fluid absorption by peritubular capillaries. *Am J Physiol* 1994;266:F175.
298. Alcorn D, Maric C, McCausland J. Development of the renal interstitium. *Pediatr Nephrol* 1999;13:347.
299. Sundelin B, Bohman SO. Postnatal development of the interstitial tissue of the rat kidney. *Anat Embryol (Berl)* 1990;182:307.
300. Bohman SO. The ultrastructure of the renal interstitium. In: Brenner BM, Stein OH, eds. *Contemporary Issues in Nephrology*. New York: Churchill Livingstone, 1983:1.
301. Kaissling B, Le Hir M. The renal cortical interstitium: morphological and functional aspects. *Histochem Cell Biol* 2008;130:247.
302. Takahashi-Iwanaga H. The three-dimensional cytoarchitecture of the interstitial tissue in the rat kidney. *Cell Tissue Res* 1991;264:269.
303. Bulger RE, Nagle RB. Ultrastructure of the interstitium in the rabbit kidney. *Am J Anat* 1973;136:183.
304. Grgic I, Duffield JS, Humpherys BD. The origin of interstitial myofibroblasts in chronic kidney disease. *Pediatr Nephrol* 2012;27:183.
305. Desmouliere A, Gabbiani G. Myofibroblast differentiation during fibrosis. *Exp Nephrol* 1995;3:134.
306. Pillebout E, Burtin M, Yuan HT, et al. Proliferation and remodeling of the peritubular microcirculation after nephron reduction: association with the progression of renal lesions. *Am J Pathol* 2001;159:547.
307. Ru Y, Eyden B. The ultrastructure of human tubulo-interstitial fibrosis. *J Submicrosc Cytol Pathol* 2003;35:147.
308. Le Hir M, Eckardt KU, Kaissling B, et al. Structure-function correlations in erythropoietin formation and oxygen sensing in the kidney. *Klin Wochenschr* 1991;69:567.
309. Bachmann S, Le Hir M, Eckardt KU. Co-localization of erythropoietin mRNA and ecto-5'-nucleotidase immunoreactivity in peritubular cells of rat renal cortex indicates that fibroblasts produce erythropoietin. *J Histochem Cytochem* 1993;41:335.
310. Maxwell PH, Osmond MK, Pugh CW, et al. Identification of the renal erythropoietin-producing cells using transgenic mice. *Kidney Int* 1993;44:1149.
311. Kaissling B, Hegyi I, Loffing J, et al. Morphology of interstitial cells in the healthy kidney. *Anat Embryol (Berl)* 1996;193:303.
312. Schiller A, Taugner R. Junctions between interstitial cells of the renal medulla: a freeze-fracture study. *Cell Tissue Res* 1979;203:231.
313. Muirhead EE. The medullipin system of blood pressure control. *Am J Hypertens* 1991;4:556S-568S.
314. Vernace MA, Mento PF, Maita ME, et al. Osmolar regulation of endothelin signaling in rat renal medullary interstitial cells. *J Clin Invest* 1995;96:183.
315. Hughes AK, Barry WH, Kohan DE. Identification of a contractile function for renal medullary interstitial cells. *J Clin Invest* 1995;96:411.
316. Dawson TP, Gandhi R, Le Hir M, et al. Ecto-5'-nucleotidase: localization in rat kidney by light microscopic histochemical and immunohistochemical methods. *J Histochem Cytochem* 1989;37:39.
317. Bohman SO. The ultrastructure of the renal medulla and the interstitial cells. In: Mandal AK, Bohman SO, eds. *The Renal Papilla and Hypertension*. New York: Plenum Medical Book Company, 1980:7.
318. Nagano M, Ishimura K, Fujita H. Fine structural study on the development of the renal medullary interstitial cells (known to secrete antihypertensive factors) of Wistar Kyoto as well as spontaneously hypertensive rats. *J Electron Microsc* 1988;21:223.
319. Gandhi R, Le Hir M, Kaissling B. Immunolocalization of ecto-5'-nucleotidase in the kidney by a monoclonal antibody. *Histochemistry* 1990;95:165.
320. Le Hir M, Kaissling B. Distribution of 5'-nucleotidase in the renal interstitium of the rat. *Cell Tissue Res* 1989;258:177.
321. Bulger RE, Trump BF. Fine structure of the rat renal papilla. *Am J Anat* 1966;118:685.
322. Nelson PJ, Rees AJ, Griffin MD, et al. The renal mononuclear phagocytic system. *J Am Soc Nephrol* 2012;23:194.
323. Wang Y, Harris DCH. Macrophages in renal disease. *J Am Soc Nephrol* 2011;22:21.
324. Duffield JS. Macrophages and immunologic inflammation of the kidney. *Semin Nephrol* 2010;30:234.
325. Rees AJ. Monocyte and macrophage biology: an overview. *Semin Nephrol* 2010;30:216.

Development of the Kidney

Cellular events in kidney development 68

- Cell proliferation 68
- Cell death 68
- Morphogenesis 69
- Migration 69
- Differentiation 69

Anatomy of development of the human kidney 69

- The pronephros 69
- The mesonephros 69
- The metanephros 70
- Formation of the human renal pelvis and calyces 70
- Formation of the human collecting duct system and nephrons 72
- The lower renal tract: urinary bladder and ureter 74

Studying kidney development 74

- Descriptive studies: anatomy and gene expression patterns 74
- Transcription factors 75
- Growth factors 77
- Adhesion molecules 78
- Diverse other molecules 78
- Functional studies in vitro 78
- Functional studies in vivo 78
- Relationships between human malformations and mouse mutants 79

Mechanisms of development of metanephric mesenchyme 79

- Molecular control of survival and induction of the metanephric mesenchyme 79
- Cell lineages arising from metanephric mesenchyme 80

- Nephron tubule formation from metanephric mesenchyme 80

Mechanisms of ureteric bud-collecting duct development 82

- Branching morphogenesis of the ureteric bud 82
- Renal pelvis and ureter 82

Blood vessels in the developing kidney 83

- Developmental anatomy of the renal vasculature 83
- Mechanisms of formation of renal blood vessels 84
- Stroma, renal capsule, and innervation of the developing kidney 84

Developmental kidney disorders account for a wide spectrum of disease in fetuses, children, and adults (1–6). As assessed by registries from developed countries, such disorders typically account for about half of all children who require dialysis and kidney transplantation for end-stage renal disease. Renal agenesis (absent kidneys) and dysplasia (poorly differentiated and metaplastic tissues) represent profound defects of morphogenesis; renal hypoplasia (too few nephrons) is a term used to describe kidneys that have differentiated but contain significantly fewer nephron units than normal. *Congenital anomalies of the kidney and urinary tract* (CAKUT) is a useful phrase coined by Ichikawa et al. (7) that emphasizes that kidney malformations often coexist with lower renal tract anomalies. CAKUT encompasses the following: agenesis, dysplasia, hypoplasia, ectopia, and duplication of the kidney; ureter anomalies such as megaureter, ureteropelvic junction obstruction, ureterovesical junction obstruction, vesicoureteric reflux, duplication, ureterocoele, and ectopic termini; bladder anomalies such as exstrophy and persistent cloaca; and urethral malformations such as atresia and posterior urethral valves. On the other hand, the use of the CAKUT diagnostic label, while

convenient, should not obviate the need to document the exact renal tract dysmorphology found in a particular patient, nor should it be assumed that there will be one underlying pathogenesis for CAKUT. Thus, the use of the term is analogous to using a disease group designation such as “glomerulonephritis” or “tubulopathy.” As medical and surgical therapies are refined, a new cohort of young babies with severe kidney malformations and renal failure, who might otherwise have perished, are surviving childhood (8,9); as yet, it is too early to know how they will fare through adulthood.

It has been suggested that essential hypertension, which manifests later in life, is initiated before birth by a little understood phenomenon called *fetal programming*, hence suggesting a novel but unexplained link between development and adult disease (10). Environmental influences somehow transmitted from the mother to the fetus during gestation may alter the growth trajectory of the developing kidney. Indeed, rats born to mothers fed low-protein diets have fewer nephrons, and such diets can alter cell turnover and gene expression in the forming kidneys (11,12). Furthermore, adults with essential hypertension have fewer glomeruli per kidney versus individuals with normal blood pressure, and it is now appreciated that the numbers of glomeruli per kidney show a wide variation even within populations of “normal, normotensive individuals” (13,14).

It is therefore important to understand how such a range of kidney malformations might arise, and, to do this, one must not only address the nature of the malformations themselves but also understand normal kidney development. The morphology and histology of the key types of human renal malformations were first comprehensively defined by Edith Potter in her landmark book *Normal and Abnormal Development of the Kidney* (1), and this area is reviewed in detail in Chapter 4 in this book (15).

In this chapter, we summarize the anatomy of normal human kidney development; in addition, we present mechanistic and functional insights derived from both animal experiments and human genetic diseases that are accompanied by renal malformations. The main focus is on the *metanephric kidney*, which forms the adult mammalian organ; the section on anatomy features human data, although rodent genetic models and organ culture will also be used when they inform the mechanisms of renal tract development. Although the term *nephrogenesis* is often used as a substitute for all aspects of kidney development, we here use the term in its more exact meaning to refer to the generation of the nephron lineage. We also briefly allude to the development of the lower renal tract (i.e., the renal pelvis, ureter, and bladder). Because of space limitations, we are unable to review the expanding literature on renal tract differentiation in animals other than mammals, and here, the reader should seek recent reviews in relation to the fly, fish, and amphibians (16–18).

In the future, an understanding of the normal anatomy and mechanisms of kidney development will offer insight into human renal disease. For example, the Wilms tumor-1 (*WT1*) gene is not only involved in normal kidney development but has also been found to be mutated in certain types of renal malignancy and glomerular disease (19). In addition, in the polycystic kidney diseases (PKDs), renal epithelial biology appears to revert to a less differentiated state (15,20,21). Detailed discussion of disorders is beyond the limits of this chapter, but they are addressed in detail elsewhere in this book (15,22).

CELLULAR EVENTS IN KIDNEY DEVELOPMENT

A number of key biologic events occur during kidney development. They can be broadly classified as the birth, death, migration, and specialization of individual cells, as well as the acquisition of complex shapes by groups of cells. In real life, several of these processes may be occurring at the same time, but it is useful to consider them separately here.

Cell Proliferation

Cell proliferation is required for growth of the developing kidney. Proliferation is prominent in the *nephrogenic zone*, which is located in the outer cortex of the metanephros (23). Although there are no published measurements of the numbers of cells in human metanephroi, it is of note that total cell numbers in the rat metanephros increase from approximately 2×10^4 on the day of formation of the embryonic organ to 2×10^6 only 2 days later (11); the morphologic changes during this period correspond to the period of growth of the human metanephros between about 5 and 7 weeks' gestation. By contrast, proliferation is rare in the postnatal normal human kidney, although it is readily detected in cysts of dysplastic kidneys resected surgically in childhood (23). It is considered that *stem cells* are located in the outer cortex of the metanephros and are capable of division to generate a copy of themselves and also a different type of cell that will subsequently mature (24,25); both the stem cells and their early progeny are called *precursor cells*. Although stem cells were previously considered to be absent from the mature mammalian kidney, evidence suggests that they may exist as rare subpopulations in adult organs and that they may be mobilized to replenish the organ following renal injury (26,27).

Cell Death

Not all cells formed in the developing kidney are destined to survive the fetal period. In rodents, a considerable amount of *programmed cell death* occurs during normal kidney development, and these cells generally die by *apoptosis* (11,28). This term describes a form of death that is accompanied by nuclear condensation and fragmentation and that is associated with activation of caspase enzymes. Apoptosis probably plays a role in determining the final number of nephrons and also the cell content of individual nephron tubules; it may also have a role in the remodeling that occurs during formation of the collecting ducts, renal pelvis, and lower tract. Early kidney growth thus involves a fine balance between cell proliferation and cell death.

An excess of proliferation is associated with renal neoplasms (e.g., Wilms tumor) and epithelial cyst growth during cyst formation (23). Conversely, excessive apoptosis would inhibit overall kidney growth and has been reported in the human dysplastic kidneys (29), which generally undergo spontaneous regression either before birth or in the 1st year of postnatal life (30). Excess renal apoptosis has also been reported to occur in experimental kidney malformations induced by teratogens (e.g., retinoic acid [RA]) (31), maternal low-protein diets (11), obstruction of fetal urinary flow (32), and mutations of genes expressed in the first stages of metanephric development (33–35).

Morphogenesis

Morphogenesis describes the process by which groups of cells acquire specialized three-dimensional shapes during development. Two examples during kidney development include the formation of nephron tubules from renal mesenchymal cells, a mesenchymal to epithelial phenotypic conversion, and the serial branching of the ureteric bud to form the collecting duct system. These normal processes are described in detail below; both are profoundly disrupted in human dysplastic kidney malformations (1,3). Another example of morphogenesis is the restructuring of just-formed nephrons into longer, thinner tubules. In the embryonic fly kidneys, it is well established that “convergent extension” occurs, in which already existing cells undergo rearrangements to form a thinner, longer tubule (16). Perhaps a similar phenomenon occurs, for example, as loops of Henle grow from the deep cortex into the forming medulla/papilla of the metanephric kidney. In mammals, however, rapid tubule extension appears at least in part driven by proliferation, with mitotic spindles orientated along the length of the growing tubule; notably, immature tubules become cystic when the orientation of spindles is randomized (36). In the adult mammalian kidney, *de novo* formation of nephrons does not take place; however, the damaged adult kidney is capable of regenerating epithelia within already existing tubules, and, in other types of animals, such as certain fish, new nephrons and tubules continue to be generated throughout normal life (37,38).

Migration

Cell migration, driven by rearrangements within the cytoskeleton, is a widespread event in mammalian development (39). Within the developing kidney itself, migration of cells occurs as endothelial (40) and mesangial (41) cell precursors invade nascent glomeruli, attracted by growth factors secreted by immature podocytes.

Differentiation

As renal precursor cells become phenotypically specialized, they are said to undergo *differentiation*. The term *lineage* describes the series of phenotypes that are displayed by the progeny of a precursor cell during the formation of specialized renal epithelial, interstitial fibroblast, mesangial, smooth muscle, and endothelial cells. It is generally considered that cells derived from the ureteric bud are confined to epithelia of the collecting ducts and urothelium of the renal pelvis, ureter, and bladder trigone. By contrast, metanephric mesenchymal cells can, as assessed by various experimental strategies in animals, give rise to a wide range of cell types including nephron epithelia (from glomerulus to distal tubule), endothelia, and mesangial and vascular wall cells (25,42,43).

ANATOMY OF DEVELOPMENT OF THE HUMAN KIDNEY

The summary of anatomic events presented here is based, to a large extent, on previous accounts (1,2,44–51); other specific references will be cited, as appropriate. Unless otherwise stated, the specific timings refer to human kidney development.

The intermediate layer of the mammalian embryo that forms during gastrulation is called the *mesoderm*. The kidneys

develop from the nephrogenic cords, masses of intermediate mesoderm located between the dorsal somites and the lateral plate mesoderm behind the embryonic coelom. Three successive excretory systems are formed: the *pronephros* from the most cranial (cervicodorsal) segments of the nephrogenic cord, the *mesonephros* from the intermediate (dorsolumbar) segments, and the *metanephros* from the most caudal (initially sacral) segments. The pronephros and the mesonephros are transient organs, although both are essential to the formation of the definitive kidney from the metanephros. Other mesonephric derivatives form structures in the fully developed organism. Although the pronephros, mesonephros, and metanephros form sequentially in the developing embryo, there is some overlap so that the mesonephros begins to develop before the pronephros has disappeared, and likewise, the metanephros forms before the mesonephros has entirely regressed. Some authorities (52) have regarded a strict delineation of the three sets of the embryonic kidneys as artificial, viewing the whole system as a single unit, the *holonephros*. However, in mammals, including man, the mesonephros and metanephros at least can be clearly recognized as separate organs.

The Pronephros

The most cranial portion of the nephrogenic cord between the 7th and 14th somites develops as the pronephros from the end of the 3rd week after conception. The pronephros consists only of a few rudimentary tubules opening proximally to the coelomic cavity by nephrostomes and coalescing distally to form the pronephric duct, which grows caudally to the cloaca. The pronephros rapidly involutes and cannot be identified by day 25 of gestation; however, the pronephric duct survives as the mesonephric duct.

The Mesonephros

Just before the pronephros disappears, the mesonephros begins to develop from day 24 of gestation from the dorsolumbar segments of the nephrogenic cord below the pronephros, growing to form a prominent (urogenital) ridge that bulges into the coelomic cavity (Fig. 2.1A). A series of vesicles form, each of which develops into a nephron consisting of a glomerulus and a tubule with thicker-walled proximal and thinner distal segments (Fig. 2.1B). Capillaries forming each mesonephric segment establish connections with the primitive aorta by an afferent arteriole and with the posterior cardinal vein by an efferent arteriole. The tubules morphologically resemble proximal and distal tubules found in the metanephros, although there is no equivalent of the loop of Henle. Each mesonephric tubule joins an excretory duct (originally the *pronephric duct*, but now called the *mesonephric* or *wolffian duct*) that gradually extends caudally to communicate with the cloaca at the 26th to 28th somite stage (about 4 weeks postconception). Although it is possible that some excretory function is performed by the mesonephros in the human embryo, it is only transitory. By the end of the first trimester, all the mesonephric glomeruli involute, but some mesonephric structures do persist. In the male, remnants of a number of caudal mesonephric tubules develop as the efferent ducts of the epididymis. The mesonephric duct forms the duct of the epididymis, the seminal vesicle, and the ejaculatory

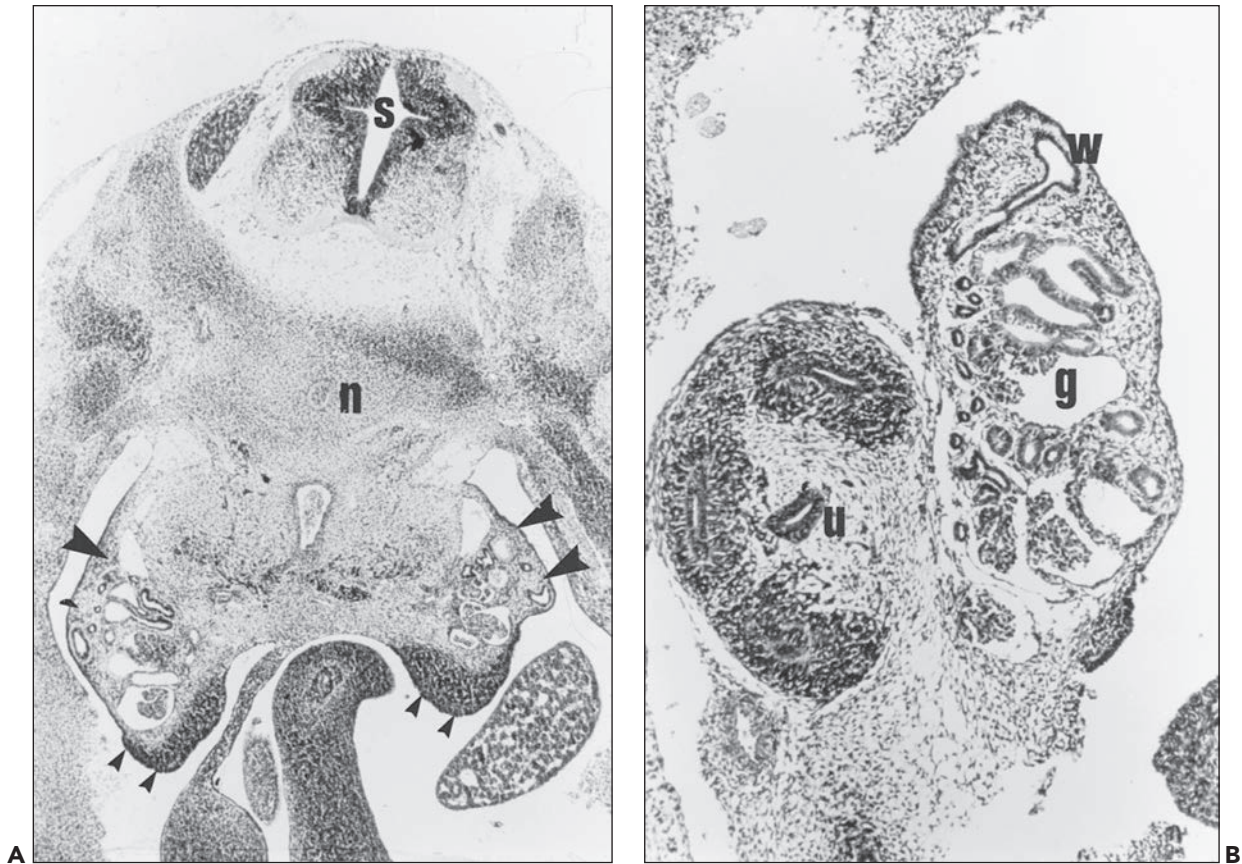


FIGURE 2.1 Early human metanephros and the mesonephros. **A:** Transverse section of a 5- to 6-week gestation human embryo showing mesonephros (*large arrowheads*) and relatively undifferentiated gonadal ridge (*small arrowheads*). Also shown is the spinal cord (s) with the notochord (n) degenerating in a mass of cartilage that will form the vertebral body. (H&E, $\times 12.5$.) **B:** Six-week human embryo showing the metanephros (*left*) and the mesonephros (*right*). The ureteric bud (u) in the center of the metanephros has branched twice, and the mesenchyme is condensing around the branch tips. In contrast, the mesonephros is much more differentiated and contains glomeruli (g) connected to tubules that drain into the wolffian duct (w). (H&E, $\times 50$.) (Courtesy of Dr. P. J. D. Winyard, Institute of Child Health, London, UK.)

duct. In the female, apart from a few vestigial and inconstant structures, such as the epoophoron, the paroophoron, and Gartner duct, the whole mesonephros degenerates during the 3rd month of gestation.

The Metanephros

The metanephros forms the definitive kidney and is developed in two parts: the renal parenchyma from the caudal end of the nephrogenic cord, called the *metanephric mesenchyme*, and the collecting ducts, calyces, renal pelvis, and ureter from the *ureteric bud*. This is a hollow posteromedial offshoot arising during the 5th week (5-mm stage) from the caudal end of the mesonephric duct opposite the 28th somite, where it curves medially to join the cloaca. The proximal end of the ureteric bud grows dorsally and cranially toward the metanephric mesenchyme, while its distal end extends caudally as the embryo elongates. The ureteric bud develops a slightly swollen cranial tip, the ampulla, to be distinguished from the remaining tubular interstitial portion. When the ureteric bud impinges on the renal mesenchyme (Fig. 2.2), the latter is pushed upward to lie dorsal to the caudal end of the degenerating mesonephros.

Here, it is situated behind the peritoneum but ventral to the corresponding umbilical artery. As the ampulla of the ureteric bud contacts the metanephric blastema, which now forms a cap of densely packed cells, it undergoes a process of rapid dichotomous branching, each branch forming a new ampulla; each ampulla has the capacity for further dichotomous branching and ultimately to induce nephron formation from the metanephric mesenchyme (compare Fig. 2.2, the metanephros at 5 weeks' gestation, with Fig. 2.1B, the metanephros at 6 weeks' gestation).

Formation of the Human Renal Pelvis and Calyces

This process, together with the development of nephrons and collecting ducts, has been studied by Osathanondh and Potter (44,45) by microdissection of the fetal kidneys (Figs. 2.3 and 2.4). These authors showed that the renal pelvis and major calyces formed from the first three to six generations of ureteric bud branches (branching occurs more rapidly at the poles than in the midzone) and the minor calyces formed from the subsequent generation of branches. Because

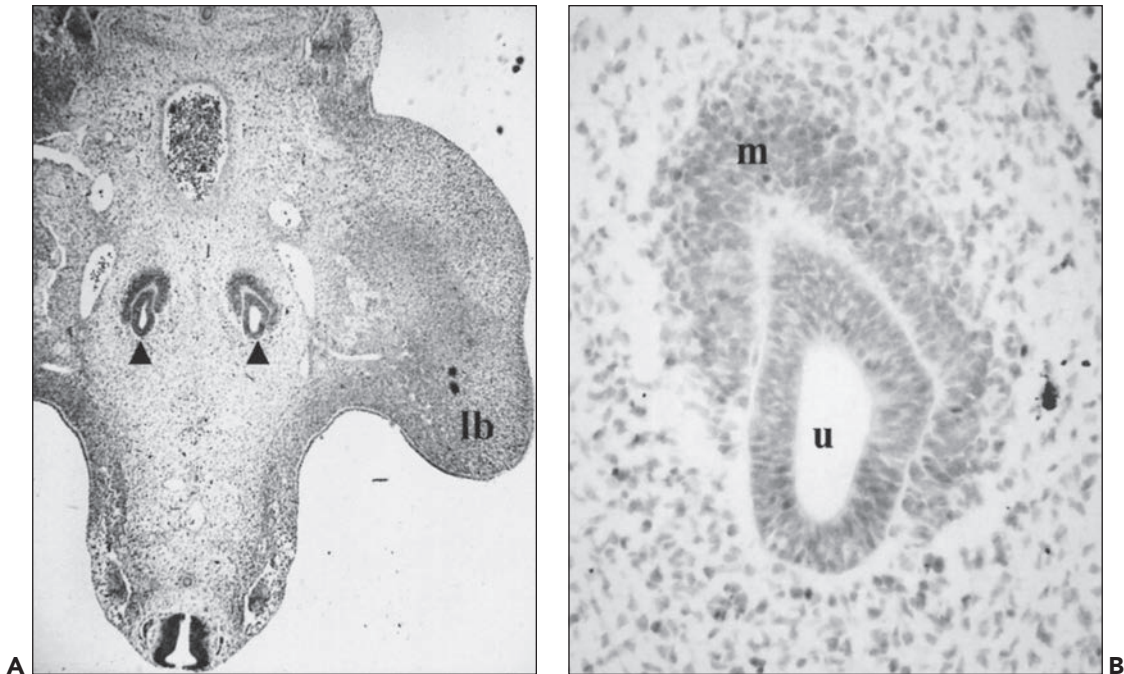


FIGURE 2.2 Human metanephros at the ureteric bud stage. **A:** Transverse section of a human embryo, approximately 5 weeks' gestation, showing paired metanephric kidneys (*arrowheads*), one on each side of the midline. A lower limb bud (*lb*) is seen on the right (hematoxylin, $\times 12.5$). **B:** High power of (**A**) shows one of the ureteric buds (*u*) capped by the metanephric mesenchyme (*m*), which is demarcating from the surrounding loosely packed, intermediate mesoderm.

branching is so rapid at this stage, the interstitial portions of the branches are very short, and indeed, sometimes a number of branches appear to arise from a single stem. Distension of the whole system, which is ascribed to the onset of urine production as nephrons start to function, results in the coalescence of the first generations of branches to give the more familiar appearance of the pelvicaliceal system seen postnatally. This is completed by about the 10th to 12th week of gestation. When the minor calyces are formed, some 20 or so ampullae are related to each minor calyx, and it is from these that the papillary collecting ducts originate. Further branching

of these ampullae is associated with nephron formation, and these branchings proceed more slowly with longer intervening periods of interstitial growth. From about the 11th week, the spherical expansion of the calyces is limited by the development of nephrons associated with their own and surrounding collecting duct systems that form the developing renal papillae. The minor calyces are indented by the papillae and change from spherical to a wineglass shape, with the cup-shaped portion around the developing papilla and a narrower stem-like infundibular portion connecting to the major calyx. This process is achieved by about the 14th week of gestation

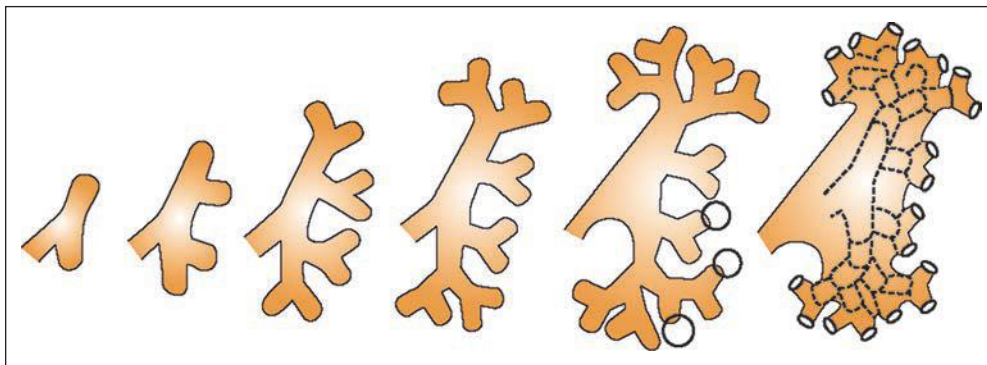


FIGURE 2.3 Development of the renal pelvis. Diagram represents coalescence of the third through fifth generations of branches (*circled*) of the ureteric bud to form the renal pelvis. (Modified from Osathanondh V, Potter EI. Development of the kidneys as shown by microdissection. II. Renal pelvis, calyces and papillae. *Arch Pathol* 1963;76:277–289.)

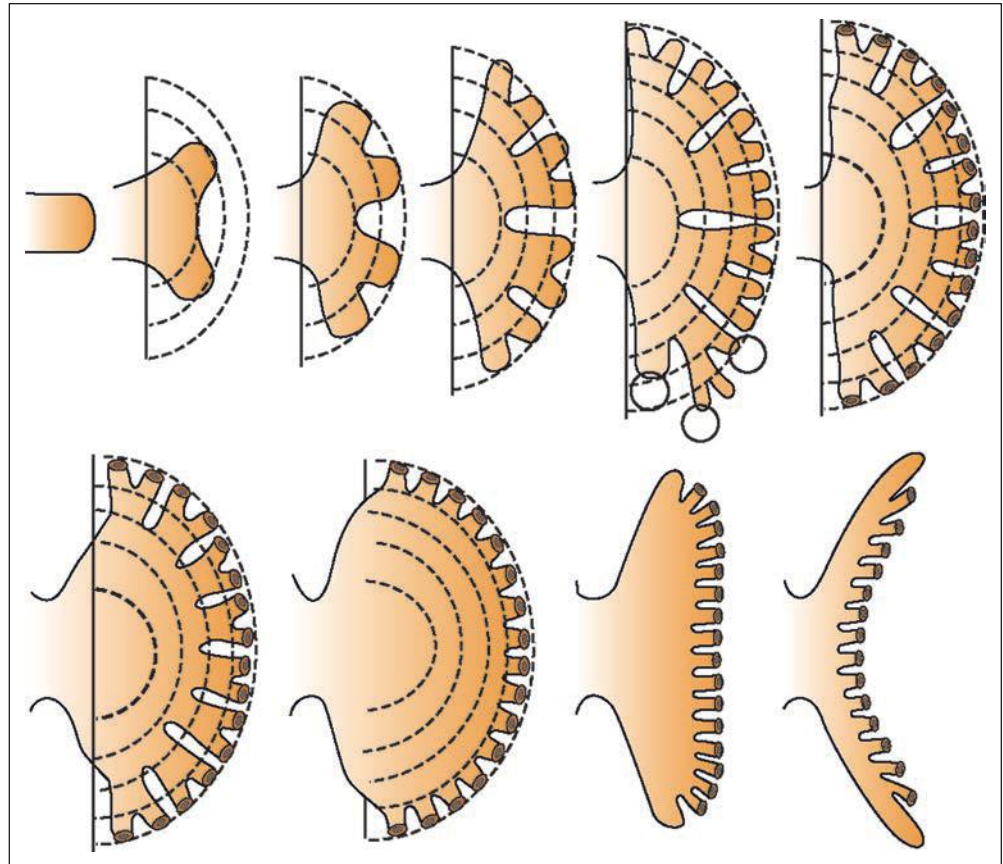


FIGURE 2.4 Development of renal calyces and papillae.

Diagrams depict coalescence of the third to fifth generations of branches (circled) of the primordial calyx and inward prolapse of the renal papilla. (Modified from Osathanondh V, Potter EI. Development of the kidneys as shown by microdissection. II. Renal pelvis, calyces and papillae. *Arch Pathol* 1963;76:277–289.)

and can be appreciated in histologic sections of the fetal kidneys at this gestational age.

Formation of the Human Collecting Duct System and Nephrons

From the end of the 7th week (18- to 20-mm stage), the development of the collecting duct system and nephrons proceeds in parallel. The nephrons develop from oval condensations of metanephric mesenchymal cells that become related to the ampullary tip of each branch of the ureteric bud (Fig. 2.5). Some cells in each condensation form a hollow (nephrogenic) vesicle, while others form a separate solid cap for the next subdivision of the ampulla. Each hollow vesicle elongates and folds back on itself to become S-shaped (Fig. 2.6). The proximal end of the upper limb joins and becomes continuous with the lumen of the related ureteric bud ampulla. The upper and middle limbs of the nephrogenic vesicle elongate farther and differentiate to form the proximal and distal convoluted tubules and the loop of Henle. Adjacent to the lower limb of the vesicle, a tuft of capillaries develops, and this forms the glomerular tuft. This invaginates the lower limb, which becomes concave. The outer layer cells become flattened to form the parietal layer of the Bowman capsule, while the inner layer cells remain columnar and stretch over the developing tuft capillaries to form the visceral epithelial cells of the glomerulus. Since nephrons are attached to the growing tips of the ureteric bud branches at this stage, they advance progressively with the ampullae away from

the future hilus of the kidney, the interstitial portions of the collecting ducts forming the future medullary collecting ducts.

After the 14th week of gestation, the first period of nephron induction ends and the second period commences. The second period of nephrogenesis, which lasts until about the 22nd week of gestation, is characterized by the formation of nephron

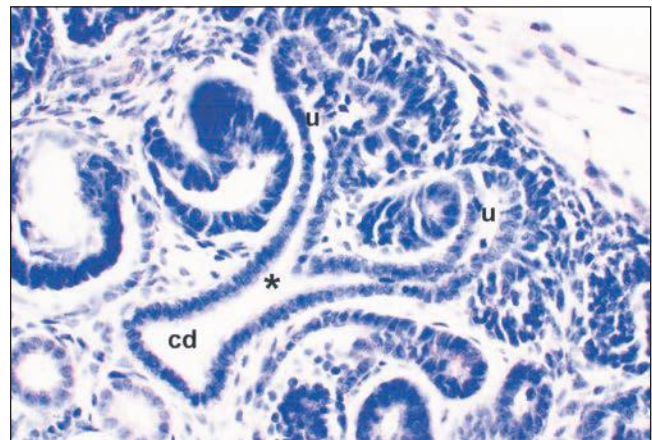


FIGURE 2.5 Metanephros from a 7-week human fetus. A branch point (asterisk) of the ureteric bud/collecting duct (cd) lineage leading to two ureteric bud ampullae (u). (hematoxylin, $\times 100$.)

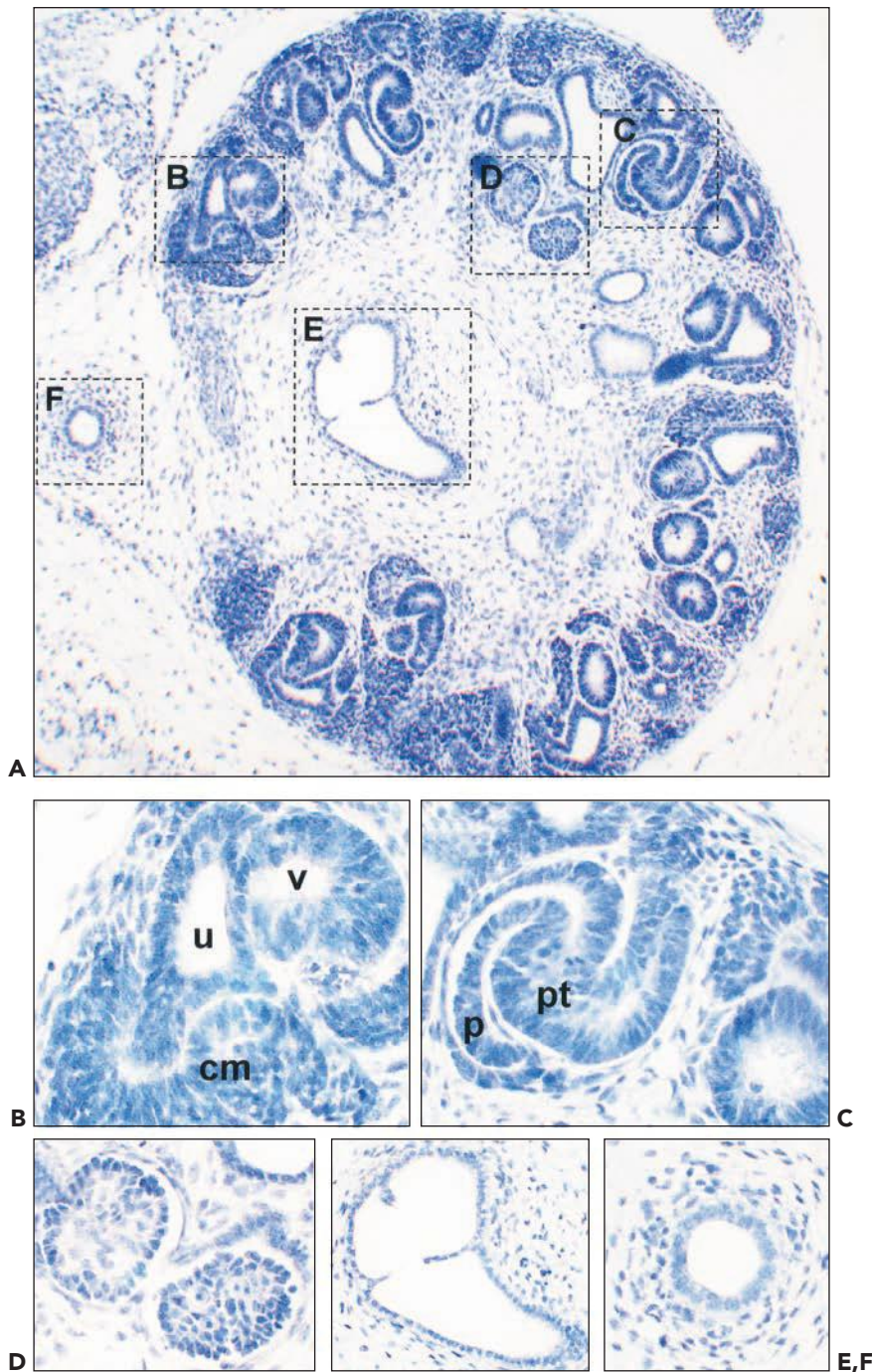


FIGURE 2.6 Metanephros from a 7-week human fetus. **A:** Low-power view of whole metanephros. Boxed areas are shown in higher powers in subsequent frames. (Hematoxylin, $\times 12.5$.) **B:** Nephrogenic zone showing the ampulla of a ureteric bud (u) branch, condensed metanephric mesenchyme (cm), and a primitive nephron vesicle (v) that has just undergone the mesenchymal-to-epithelial transition. **C:** An S-shaped body: the primitive nephron is segmenting into the glomerulus, with cuboidal podocytes (p) with the adjacent proximal tubule (pt). **D:** The first layer of glomeruli is noted in the deep cortex. **E:** The renal pelvis lined by a monolayer of the urothelium. **F:** The ureter consists of a 1–2 cell thick layer of the urothelium surrounded by mesenchyme differentiating into smooth muscle.

arcades. Each ampulla ceases to divide and becomes capable of inducing the formation of a further three to six nephrons. With the induction of further nephrons, the connecting tubule of the older nephron shifts the position of its point of attachment away from the ampulla to the connecting tubule of the next-formed nephron, so they are joined together in a string or arcade of between four and seven nephrons. The innermost and first-formed member of each nephron arcade is a nephron formed during the first period of nephrogenesis and becomes a juxtamedullary nephron in the fully developed organ. The loops of Henle are longest in these nephrons, extending almost to the papillary tip.

In the third period of nephrogenesis, from the 22nd to the 36th week of gestation, the ampullae advance to the peripheral cortex beyond the region of nephron arcades. A further four to seven nephrons form and are attached separately just behind the ampullary tips (Fig. 2.7). No further divisions of the ampullae occur, and as each new nephron is added, the ampullae advance farther toward the surface. Cell proliferation, as assessed by immunolocalization of proliferating cell nuclear antigen (PCNA), is depicted in the cortex and medulla of a late second trimester human fetal kidney in Figure 2.8. At about 36 weeks, the ampullae cease to function and disappear. No new nephrons are then formed, the last to develop

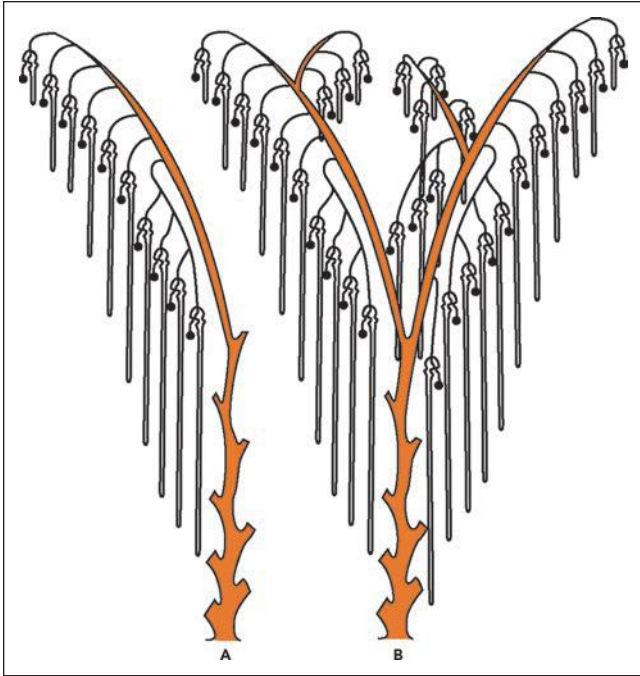


FIGURE 2.7 Arrangement of nephrons at birth as revealed by microdissection. **A:** Usual pattern with, sequentially, an arcade of four nephrons that drain into a tributary of the collecting duct and six nephrons that drain individually into the collecting duct. **B:** Possible variations. (Modified from Osathanondh V, Potter EI. Development of the kidneys as shown by microdissection. II. Renal pelvis, calyces and papillae. *Arch Pathol* 1963;76:277–289.)

producing the subcapsular so-called nephrogenic zone that can be seen in the fetal kidneys up to 36 weeks and is useful in dating gestational age.

In the fourth period of kidney development, from 36 weeks to term, no new nephrons are formed, and this period is one of purely interstitial growth. Loops of Henle continue to lengthen, and the proximal and distal tubules become longer and more tortuous. In mature infants at birth, some 20% of the loops of Henle are still within the renal cortex (53). In recent years, dissector methodology has been used to quantify the number of glomeruli in the human kidneys (13,14,54). Depending on the laboratory making these measurements, mean numbers per kidney in “normal” individuals can vary, for example, between about 0.7 and 1.5×10^6 , and all studies have emphasized the wide range of nephron numbers measured within populations. There are indications that numbers may be reduced in some populations with essential hypertension and that glomerular volume tends to be inversely proportional to numbers per kidney. A potential criticism, however, of studies that have assessed adult kidneys would be that the results underestimate numbers present at birth if some glomeruli might be “lost” as the kidney ages. There are likely to be several causes for variations in numbers of glomeruli generated per kidney within normal populations. An environmental modulator may be poor nutrition during gestation, as well demonstrated in experimental animals (11,12), while genetic

modifiers may include common variants, or “polymorphisms,” of genes that drive nephrogenesis (55).

The Lower Renal Tract: Urinary Bladder and Ureter

As the initial steps of metanephric development occur, the lower renal tract is beginning to form. By 28 days of gestation, the mesonephric duct drains into the urogenital sinus, which is forming as the cloaca is divided into the sinus and rectum by the caudal extension of the urorectal septum. The epithelia of the sinus and mesonephric duct fuse, and the ureteric bud arises as described above. By 33 days of gestation, the mesonephric duct below the ureteric bud fuses with the urogenital sinus and will contribute to the trigone. As part of these morphogenetic steps, the ureteric bud origin enters the bladder directly by day 37 to become the ureteric orifice. Between 28 and 35 days of gestation, the ureter appears to be patent, but from 37 to 47 days’ gestation, a membrane temporarily blocks the ureterovesical junction (56) and the ureter becomes occluded. This is followed by recanalization of the elongating ureter, which is complete by 8 weeks (57). By the end of the first trimester, the epithelium of the ureter differentiates into the pseudostratified urothelium, and the ureter has a submucosal course on entering the bladder. Myogenesis begins in the upper part of the ureter at 12 weeks (58). The first layer of vascularized glomeruli is present by 8 to 9 weeks and would be expected to filter blood to produce urine, which would enter the lower renal tract. The urogenital membrane ruptures on day 48 of gestation, thus providing a connection between the nascent bladder and outside of the body. At 7 weeks of gestation, the urinary bladder appears as a cylinder of epithelium surrounded by mesenchymal tissue (59). Within this urogenital sinus, mesenchyme differentiates into the smooth muscle layers of the detrusor, a process that commences in the ventral part of the bladder dome (59). The allantois, a second outflow tract on the anterior of the developing bladder, appears at 21 days of gestation; it regresses by the end of the first trimester by 12 weeks of gestation, and its remnant is marked by the median umbilical ligament.

STUDYING KIDNEY DEVELOPMENT

Descriptive Studies: Anatomy and Gene Expression Patterns

In *descriptive* studies, the anatomy of the kidney is documented through the embryonic and fetal periods. Patterns of cell division, programmed cell death, differentiation, and morphogenesis can be related to changing regional patterns of gene expression in terms of mRNA and protein using the respective techniques of *in situ* hybridization and immunohistochemistry. Such observations provide the essential foundations for the generation of hypotheses regarding the molecular mechanisms of kidney development. Most of the data on gene expression are derived from studies with experimental animals, and it is generally assumed that overall patterns will be the same in humans. The GenitoUrinary Development Molecular Anatomy Project (GUDMAP) provides an accessible and searchable database

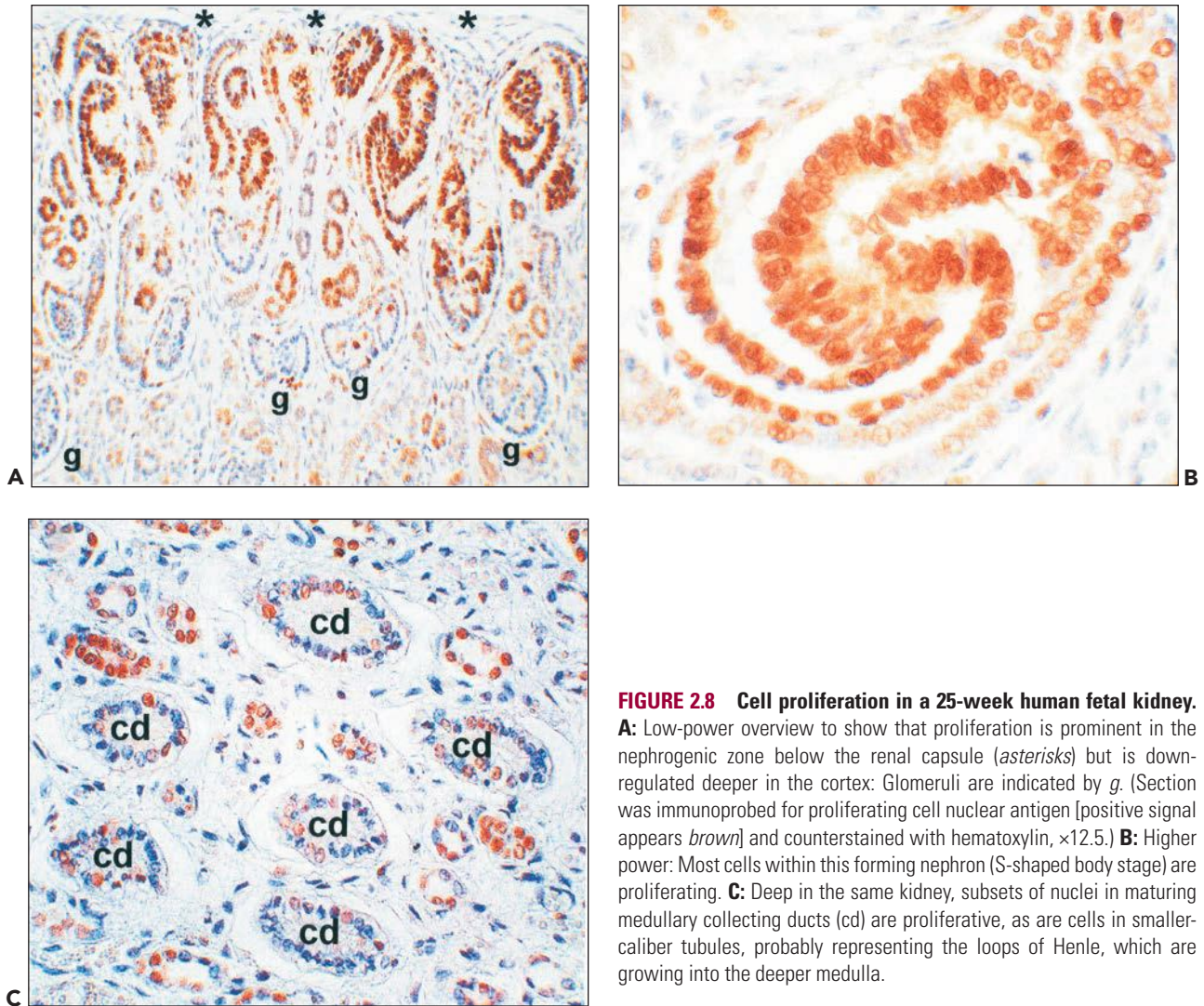


FIGURE 2.8 Cell proliferation in a 25-week human fetal kidney. **A:** Low-power overview to show that proliferation is prominent in the nephrogenic zone below the renal capsule (*asterisks*) but is down-regulated deeper in the cortex: Glomeruli are indicated by *g*. (Section was immunoprobed for proliferating cell nuclear antigen [positive signal appears *brown*] and counterstained with hematoxylin, $\times 12.5$.) **B:** Higher power: Most cells within this forming nephron (S-shaped body stage) are proliferating. **C:** Deep in the same kidney, subsets of nuclei in maturing medullary collecting ducts (*cd*) are proliferative, as are cells in smaller-caliber tubules, probably representing the loops of Henle, which are growing into the deeper medulla.

that documents the expression patterns of many thousands of gene transcripts through mouse renal tract development (60). Such databases can then be used to construct interconnecting networks of genes and their products, to help understand complex biologic pathways involved in renal tract development (61). Research collections of normal human fetal tissues have been made following ethical approval (62), and these are proving informative for gene expression studies in the developing renal tract (63–66).

Three main classes of molecules are expressed during kidney development (Table 2.1). These are the *transcription factors*, *growth factors*, and *cell adhesion/extracellular matrix proteins*. It should be noted that italics are used when referring to the gene that codes for these molecules, whereas regular type-script is used when referring to the gene product (e.g., mRNA or protein). Strictly, capital letters are often used to abbreviate the human gene or gene product (e.g., *WT1* gene and WT1 protein), whereas lower case is used for animal genes (e.g., *wt1* gene and wt1 protein). In this chapter, for simplicity, we have generally used the human system when discussing the genes and their products.

Transcription Factors

These proteins have domains that bind DNA and that regulate the expression of other genes; in other words, they can enhance or switch off the transcription into mRNA. Because of these regulatory roles, the transcription factors have been likened to conductors of an orchestra, and the normal program of development can be perceived as being defined and directed by the sequential expression of these factors. These molecules can be classified into families that share similar DNA-binding protein motifs and domains. One of these motifs is called the *zinc finger*, which describes an elongated projection of the molecule that intercalates with DNA. An example of a transcription factor with multiple zinc fingers is the Wilms tumor 1 (WT1) protein, which is expressed in mesenchyme at the inception of the metanephros and also in mature podocytes (33,67,68). If the mouse gene is ablated by a *null mutation*, no kidneys are formed, while other types of mutation cause glomerular diseases (Denys-Drash and Fraser syndromes) and Wilms tumor (19). Some other examples of transcription factors expressed during renal tract development include the HOX family, which contain DNA-binding *homeodomains*

TABLE 2.1 Genetic bases of mouse kidney defects based on mutants

Mouse gene	Full name	Disease description ^a	Reference
Genes coding for transcription factors and related molecules			
<i>Bf2</i>	Brain factor 2/homologue of <i>Drosophila</i> forkhead	Renal hypoplasia	151
<i>Brn1(Foxd1)</i>	Retarded loop of Henle development		152
<i>Emx2</i>	Empty spiracles 2	Renal agenesis	135
<i>Foxc1</i>	Forkhead box c1	Duplex kidney	153
<i>Foxc2</i>	Forkhead box c2	Renal hypoplasia	153
<i>Foxd1</i>	Forkhead box c2	Fused kidneys	154
<i>Hnf1b</i>	Hepatocyte nuclear factor 1 β	Renal cysts	36,76
<i>Hoxa11/Hoxd11^b</i>	Homeobox a11 and d11	Renal agenesis or hypoplasia	69
<i>Lim1 (Lhx1)</i>	Lim homeobox 1	Absent kidneys	155
<i>Lmx1b</i>	Lim homeobox transcription factor 1 β	Glomerular podocyte immaturity	156
<i>N-Myc</i>	Avian myelocytomatosis viral oncogene homologue	Hypoplastic mesonephros	157
<i>Pax2</i>	Paired box 2	Renal agenesis in null mutant; renal hypoplasia in heterozygous mice	71
<i>Pod1</i>	Podocyte 1	Failure of renal epithelial differentiation	158
<i>Rara/Rarb^{2b}</i>	Retinoic acid receptor α and β 2	Kidney and ureter malformations	159–161
<i>Sall1</i>	sal-like 1/homologue of <i>Drosophila</i> spalt	Renal agenesis	162
<i>Six1 and Six2</i>	Homologues of <i>Drosophila</i> sine oculis	Renal agenesis	24,163
<i>Wt1</i>	Wilms tumor 1	Renal agenesis in null mutants; proteinuria in heterozygous mice	33,67
Genes coding for growth factors and molecules implicated in their signaling pathways			
<i>Agt</i>	Angiotensinogen	Hypoplastic papilla and hypotension	91
<i>Agtr1a/Agtr1^b</i>	Angiotensin receptor type 1a and 1b	Hypoplastic papilla and hypotension	91,92
<i>Agtr2</i>	Angiotensin receptor type 2	Diverse renal tract malformations in males (gene on the X chromosome)	93
<i>Angpt2</i>	Angiopoietin 2	Disorganized peritubular capillaries	80
<i>Bmp4</i>	Bone morphogenetic protein 4	Wide range of kidney and ureter malformations in heterozygous effect/null mutants die before nephrogenesis ^b	94
<i>Bmp7</i>	Bone morphogenetic protein 7	Renal dysplasia	95
<i>Fgf7</i>	Fibroblast growth factor 7	Renal hypoplasia	164
<i>Fgf10</i>	Fibroblast growth factor 10	Renal agenesis (can substitute for Gdnf in ureteric bud growth)	81
<i>Gdnf</i>	Glial cell line-derived neurotrophic factor	Renal agenesis	77,78
<i>Gremlin</i>	Bmp antagonist	Renal agenesis	96,165
<i>Notch2</i>	Receptor for delta	Glomerular capillary defects in hypomorphs (not a complete null mutant)	166
<i>Pdgfrb</i>	Platelet-derived growth factor receptor B	Absent mesangial cells	41
<i>Ret</i>	Rearranged during transfection/Gdnf receptor	Renal agenesis or dysplasia	77
<i>Robo2</i>	Roundabout 2; receptor for slit 2	Duplex kidneys	167
<i>Shh</i>	Sonic hedgehog	Renal hypoplasia and ureter malformations	98
<i>Slit2</i>	Homologue of <i>Drosophila</i> slit	Duplex kidneys	167
<i>Spry1</i>	Homologue of <i>Drosophila</i> sprouty; modulates growth factor signaling	Duplex kidneys	168
<i>Wnt4</i>	Wingless-type MMTV integration site family member 4	Renal hypoplasia	103
<i>Wnt11</i>	Wingless-type MMTV integration site family member 11	Renal hypoplasia	104
<i>Vegf</i>	Vascular endothelial growth factor	Congenital glomerular disease	88,169
Genes coding for cell adhesion/extracellular matrix proteins			
<i>Fras1</i>	Fraser syndrome 1	Renal agenesis	34,119
<i>Frem2</i>	Fras1-related extracellular matrix 1	Diverse renal malformations	170
<i>Itga8</i>	Integrin α 8	Dysplastic kidneys	116
<i>Lamab2</i>	s-Laminin/laminin β 2	Nephrotic syndrome	113
<i>Nephrin</i>	Congenital nephrotic syndrome 1; NPHS1	Congenital nephrotic syndrome	108

TABLE 2.1 Genetic bases of mouse kidney defects based on mutants (*Continued*)

Mouse gene	Full name	Disease description ^a	Reference
Genes coding for diverse other classes of proteins			
<i>Bcl2</i>	B-cell CLL/lymphoma 2; cell survival molecule	Renal hypoplasia and apoptosis	121
<i>Cox2</i>	Cyclooxygenase 2; enzyme	Renal hypoplasia	122
<i>Eya1</i>	Eyes absent 1	Renal agenesis	123,124
<i>Hs2st</i>	Heparan sulfate 2-sulfotransferase	Renal agenesis	125
<i>Mpv17</i>	Peroxisomal membrane protein disrupted by viral insertion	Glomerulosclerosis	171
<i>Pkd1</i>	Polycystin 1	Metanephric cysts in null mutants; postnatal PKD in heterozygous mice	126
<i>Pkd2</i>	Polycystin 2	Metanephric cysts in null mutants; postnatal PKD in heterozygous mice	127
<i>Upll</i>	Uroplakin II	Hydronephrosis and vesicoureteric reflux	129
<i>Uplll</i>	Uroplakin III	Hydronephrosis and ureteric obstruction	130

^aThe disease is described in clinical terms rather than giving the mechanisms, many of which are outlined in the main text.

^bPhenotype is present when two similar genes are knocked out.

Unless otherwise stated, the malformations occur in null mutants in which there is no gene activity; in other cases, the disease occurs in mice with one copy of the gene ablated (i.e., heterozygous mice).

(69), and the PAX family, which contain DNA-binding *paired domains* (70–72) (Fig. 2.9). The specific gene targets of certain of these transcription factors are being investigated. For example, WT1 down-regulates *PAX2* (73); up-regulates amphiregulin, a growth factor that stimulates tubule formation in the metanephros (74); and modulates the expression of WNT4, a growth factor implicated in early nephron differentiation (67). Another transcription factor called hepatocyte nuclear factor 1 β (HNF1 β) promotes the expression of a battery of genes that maintain the differentiated state of renal epithelia; when *HNF1 β* is mutated, renal tubules become cystic (36,65,75,76).

Growth Factors

Many growth factors are produced by, and act within, the metanephros (Table 2.1). When secreted by one cell and acting on a neighbor, they are called *paracrine factors*. When acting on

the producing cell, they are called *autocrine factors*. Recently, another mode of interaction, called *juxtacrine*, has been described: here, the growth factor is inserted into the plasma membrane of the cell that synthesized it and interacts with receptors on adjoining cells. Growth factors bind to cell surface receptors, the *receptor tyrosine kinases* being a large group. On ligand binding, these receptors dimerize and become phosphorylated, thereafter transducing signals into the cell. Growth factors not only can cause cell division but can also stimulate cell survival, apoptosis, differentiation, or morphogenesis. One of the most important in kidney development, at least based on animal studies, is glial cell line–derived neurotrophic factor (GDNF), which is secreted by the renal mesenchyme and activates a receptor called RET, which is expressed by the adjacent ureteric bud (77–79). Other factors expressed in the developing kidney that signal through receptor tyrosine kinases include the angiopoietins (ANGPTs) (80), fibroblast growth

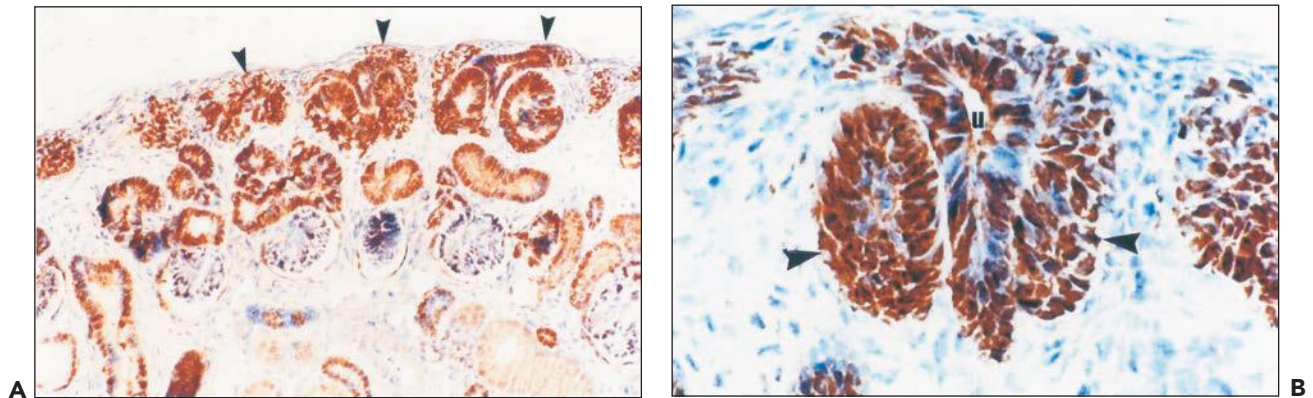


FIGURE 2.9 Immunohistochemistry for the PAX2 transcription factor. **A:** A 10-week human fetal kidney shows intense expression in the nephrogenic zone (*arrowheads*). (Counterstained with hematoxylin; positive PAX2 immunostaining in brown, $\times 40$.) **B:** Higher power of the nephrogenic zone showing PAX2 protein in nuclei of the ureteric bud ampulla (u) and mesenchymal condensates (*arrowheads*).

factors (FGFs) (81), hepatocyte growth factor (HGF) (82), insulin-like growth factors (IGFs) (83,84), neurotrophins (85), platelet-derived growth factors (PDGFs) (41,86), transforming growth factor- α (TGF α), and related molecules (74,87) and vascular endothelial growth factor (VEGF) (40,42,88,89). Other growth factors implicated in renal tract development bind to receptors that are not tyrosine kinases; they include angiotensin II (90–93), bone morphogenetic proteins (BMPs) (94–96), leukemia inhibitory factor (LIF) (97), sonic hedgehog family (SHH) (98) and related pathways (99), transforming growth factor- β (TGF β) (100,101), tumor necrosis factor- α (TNF α) (102), and wingless-type MMTV integration site family members (WNT) (67,103,104).

Adhesion Molecules

Adhesion molecules are of two main types: those that mediate the attachment of cells to one another (the *cell-cell* adhesion molecules) and those that mediate the attachment of cells to the surrounding matrix (the *cell-matrix* adhesion molecules). Examples of the former group include the neural cell adhesion molecule (NCAM) (105), whose adhesive properties are independent of calcium, and E-cadherin (also known as *uvomorulin*), whose adhesive properties depend on calcium (106). Nephrin is a molecule that bridges the gap between foot processes of podocytes (107,108). Molecules within the second group include fibronectin (109), galectin-3 (110,111), laminins (112–114), collagens (115), and other proteins that not only bind to plasma membranes via integrin receptors (116) but also interact with each other. Anosmin-1 is an adhesion molecule with homologies to NCAM and fibronectin. The *KALI* gene, which encodes the protein, is mutated in X-linked Kallmann syndrome: individuals with this syndrome have renal agenesis (64). *KALI* mRNA is expressed in the metanephros, and the protein coats the surface of mesonephric duct/ureteric bud derivatives where it may mediate the effects of growth factors as well as having direct effects on cell adhesion (117,118). Other extracellular matrix/cell membrane-associated molecules can also modulate growth factor signaling, either by sequestering growth factors or by modulating binding between growth factors and their signaling receptors. Examples include glypican-3 (GPC3), a heparan sulfate proteoglycan anchored to the cell surface, and *FRAS1*, a cell membrane protein that has a large extracellular portion; mutations of *GPC3* and *FRAS1* genes cause renal malformations not only in mutant mice but also in humans where the renal anomalies manifest as a component of the Simpson-Golabi-Behmel and Fraser syndromes, respectively (119,120).

Diverse Other Molecules

Other types of molecule are expressed in the developing renal tract and affect differentiation and morphogenesis (Table 2.1). These include the following: B-cell lymphoma 2; cell survival molecule (BCL2), a protein that prevents apoptosis (121); cyclooxygenase 2 (COX2), an enzyme involved in synthesis of prostaglandins (122); EYA1, a molecule with protein phosphatase activity that activates mesenchymal transcription factors (123,124); heparan sulfate 2-sulfotransferase, an enzyme that modifies proteoglycan polymers and most likely affects their ability to modulate actions of growth factors (125); polycystin 1 and 2, proteins inserted into the plasma

membrane, which together act as a calcium channel and which are mutated in autosomal dominant PKDs (20,21,126,127); renin, the enzyme that cleaves angiotensinogen (43,128); and uroplakins (UPs), which coat the apical surface of the urothelium, making it watertight, and which may also control the differentiation of the lower renal tract (59,129,130). Finally, an increasing number of proteins expressed in renal differentiation have been found to be localized to the centrosome, an organelle involved in cell division, and in the primary cilium, a structure derived from the centrosome, which is thought to transduce epithelial differentiation signals triggered by urine flow (20,21,131).

Functional Studies In Vitro

Classic experiments using organ culture of metanephric rudiments clearly demonstrated that interactions between different types of cells are necessary for normal development (132–134). By recombining either the ureteric bud or the renal mesenchyme derived from mutant mice (see below) with its wild-type partner, it has been possible to implicate specific genes made by each component in the induction processes (104,135). The growth of the metanephros in organ culture can be modulated by administration of antibodies (82,111,112,136) (Fig. 2.10) or antisense oligonucleotides/small interfering RNA (137–140), which prevent the generation of proteins expressed during early development of the metanephros. Other techniques include the study of cell lineage using the transfer of reporter genes into nephrogenic precursors (42,141–143) and the generation of nephrogenic cell lines to allow the study of developmental determinants at the level of the isolated single cell; such lines have been generated from normal rodent cells (25,82,144) as well as from the normal embryonic (145) and even dysplastic human kidneys (100).

Functional Studies In Vivo

Experiments that aim to perturb the kidney development in situ include physical interruption of the mesonephric duct to cause the failure of metanephric development (146), anatomic obstruction to inhibit fetal urinary flow and record effects on kidney and bladder development (32,147,148), and the administration of teratogens during critical phases of nephrogenesis (31,149,150). The most informative experiments have been those that have prevented the expression of genes expressed during nephrogenesis by homozygous recombination. In this technique, mouse embryonic stem cells can be genetically engineered in vitro and then be integrated into early embryos to create chimeric mice. If the altered cells contribute to the germ line, then animals with homozygous and heterozygous gene deletions can be generated by further breeding. The renal phenotypes of these *null mutant* or *knockout* mice, which include the absence of metanephric development, have so far suggested that tens of genes are essential for normal kidney development in vivo; a selection of these genes is listed in Table 2.1 (33,34,41,76–78,80, 92–95,98,103,104,108,113,116,121–130,135,151–170). In all probability, many more key genes remain to be implicated. Many of these mouse models also have defects in other diverse nonrenal systems because the same genes are expressed in those organs during development.

A useful variation on this theme of genetic manipulation is the ability to ablate gene activity in particular populations of

cells within the developing renal tract, rather than in the whole animal, using the *Cre-lox* system in which tissue-specific promoters drive the expression of the Cre recombinase enzyme, which deletes genes flanked by *lox* sites. In this manner, genes can be selectively deleted, for instance, in the ureteric duct/collecting duct lineage or in podocytes (76,98,169,171), and their possible actions can be further defined. In addition, in some strains of mice, mutations have arisen spontaneously or have been induced by mutagenesis; these have also proven informative when specific genes have been implicated in animals with renal tract malformations (34).

In many of these models, a renal malformation manifests only when both alleles are mutated, whereas in others, a dose effect is apparent. For example, when one allele is lost, renal hypoplasia occurs, whereas renal agenesis is found when both alleles are mutated (172). When a specific gene is ablated in mice, the severity of renal malformation is often found to vary depending on the background strain, suggesting the existence of genetic modifiers of disease severity. When two structurally similar molecules are expressed at identical locations in the metanephros, it may be necessary to knock out both of them to produce a renal tract malformation (159–161).

Although many molecules have been functionally implicated in kidney development based on their expression patterns and using organ culture studies, mice with null mutations of these genes have sometimes been found to have apparently normal kidney development *in vivo*, even when the mutation is studied in several strains. This suggests that some molecules expressed in the metanephros either are of little functional significance or are redundant in the whole animal (82,173). It is probable that, in organ culture, differentiation is suboptimal and hence rather easy to perturb; by contrast, in the whole animal, the system of growth is far more robust.

Relationships Between Human Malformations and Mouse Mutants

These genetic experiments in mice complement our increasing knowledge that certain human renal malformations are caused by inherited mutations of genes expressed during nephrogenesis. In several cases, mutations of homologous genes cause malformations in both species, and some examples are listed in Table 2.2 (34,70–72,75,76,123,124,129,162,170,174–176).

MECHANISMS OF DEVELOPMENT OF METANEPHRIC MESENCHYME

Molecular Control of Survival and Induction of the Metanephric Mesenchyme

A key observation regarding cell interactions in mammalian kidney development was made by Clifford Grobstein more than 50 years ago (132). When he isolated the just-formed murine metanephric rudiment and cultured mesenchyme and ureteric bud in isolation, the former failed to survive and the bud did not branch. In contrast, on recombining both tissues, the mesenchymal cells underwent an epithelial transition to form nephrons, whereas the ureteric bud branched serially to form

TABLE 2.2

Selected genes expressed in the developing renal tract that, when mutated, cause human and mouse kidney malformations

Branchiootorenal syndrome

Human disease: Dominant *EYA1* mutation with renal agenesis, dysplasia, and calyceal anomalies. Also features branchial fistulae and deafness (174). Mouse mutant model (123,124)

Fraser syndrome

Human disease: Recessive *FRAS1* and *FREM2* mutations (34,170). Renal agenesis and cystic dysplasia. Also features fused digits and cryptophthalmos. Mouse mutant model (34,170)

Renal-coloboma syndrome

Human disease: Dominant *PAX2* mutation with vesicoureteric reflux and renal hypoplasia; also features optic nerve colobomas (70). Mouse mutant models (71,72)

Renal adysplasia

Human: Dominant *UPIII* mutations with vesicoureteric reflux and renal dysplasia (175)
Mouse mutant model (129)

Renal cysts and diabetes syndrome

Human disease: Dominant *HNF1β* mutation with solitary functioning kidney, cystic dysplasia, and glomerular cysts; also features diabetes mellitus and uterus malformations (65,75)
Mouse mutant model (76).

Townes-Brocks syndrome

Human disease: Dominant *SALL1* mutation with spectrum of renal tract malformations including renal agenesis and hypoplasia, horseshoe kidney, and posterior urethral valves; also features imperforate anus and digit malformations (176)
Mouse mutant model (162)

collecting ducts. In addition, Grobstein found that the embryonic spinal cord could efficiently stimulate the development of the isolated metanephric mesenchyme, a result reminiscent of Greunwald's earlier observation that neural tissue placed next to intermediate mesoderm could stimulate the production of nephron tubules *in situ* (177). Grobstein reported that no other embryonic mesenchymal cells could be stimulated to produce nephron tubules by either the ureteric bud or heterologous inducers. It could therefore be concluded that, in the course of normal development, the metanephric mesenchyme had been programmed to form nephrons but that it required additional inductive signals from the ureteric bud to permit its survival and differentiation. Similarly, a message must be sent from the metanephric mesenchyme to the ureteric bud to facilitate its own morphogenesis. In general, when one tissue affects the behavior of another, the cross-talk must involve either direct cell-cell or cell-matrix interactions or be mediated by soluble molecules such as growth factors. It is only recently that we have begun to interpret Grobstein's classic observations in terms of cell biology and molecular mechanisms.

The isolated metanephric mesenchyme dies by apoptosis. *TNFα* colocalizes with apoptotic cells during involution of the avian mesonephros (178), and addition of this molecule to

mouse metanephric organ culture increases apoptosis (102). A candidate for a ureteric bud–derived mesenchymal survival factor is FGF2 (179); this molecule can prevent excess apoptosis of metanephric mesenchyme, although it is not sufficient, on its own, to induce further differentiation of the nephron lineage. Explanted mesenchymes can also be saved from accelerated programmed cell death by the proximity of the embryonic spinal cord (132). Although one report showed that WNT1, a secreted molecule expressed in the embryonic spinal cord, can prevent death of metanephric mesenchyme and induce it to differentiate, WNT1 is not expressed by the ureteric bud itself (180). Although other members of the WNT family are expressed in the metanephros, they do not seem to have a primary inducing role. As examples, although WNT11 is expressed by the ureteric bud ampullae and appears to enhance GDNF signaling, null mutant mice have small, rather than absent, kidneys (104), and in mice lacking WNT4, the renal mesenchyme begins to differentiate but then fails to form tubules (103). Mesenchymal expression of the transcription SIX2 appears critical to maintain a progenitor-like state within a subpopulation destined to form nephrons (24).

Homozygous null mutations of the *WT1* gene are informative regarding survival of the metanephric mesenchyme (33). WT1 is expressed at low levels in the just-formed metanephric mesenchyme and is up-regulated during differentiation into nephron precursors. In null mutant mice, the absence of WT1 protein causes accelerated death in the intermediate mesoderm, which would normally form the metanephric mesenchyme, hence producing a renal agenesis phenotype. Of note, teratogenic doses of RA reduce WT1 expression in the metanephric mesenchyme, and this is associated with increased apoptosis in this tissue (31). Although the *WT1* gene has been much studied, it is still unclear exactly how its normal expression rescues the metanephric mesenchyme from an untimely death.

A similar renal agenesis phenotype can be generated in mice that are homozygous null mutants for the following:

- The transcription factor *LIMI*, which is necessary for differentiation of the intermediate mesoderm that is destined to form the metanephros, in part through up-regulating *PAX2* (155,181)
- The transcription factor *PAX2* (71), which acts as a survival signal in the ureteric bud/collecting duct lineage (182)
- The transcription factor *SALL1*, which, like WT1, is expressed in the metanephric mesenchyme and is somehow necessary for stimulation of the ureteric bud invasion (162)
- *EYA1*, which codes for a molecule with protein phosphatase activity, which is expressed in both uninduced and induced metanephric mesenchyme, and which is needed to activate *SIX1* and up-regulate GDNF expression (123,124)
- *SIX1*, a transcription factor expressed in the metanephric mesenchyme, which acts in a transcription factor network downstream of *EYA1* and upstream of *PAX2* and *SALL1* (163)
- The growth factor *GDNF* or its receptor tyrosine kinase, *RET*, which establishes a paracrine signaling system between the mesenchyme and the ureteric bud (77,78)
- Gremlin, a growth factor expressed by the metanephric mesenchyme, which antagonizes the antibranching molecules BMP4 (165)

In these cases, the primary defect is a lack of outgrowth of the ureteric bud from the mesonephric duct: the failure of survival and therefore differentiation of the metanephric mesenchyme are likely to be secondary to the lack of proximity of its normal inducer tissue. Disappearance of the metanephric mesenchyme, most likely associated with apoptosis, is also a feature of mice that lack *FRAS1*, a cell surface molecule that is expressed by, and coats the surface of, the ureteric bud and that somehow mediates inductive events between the bud and mesenchyme: it is mutated in the human Fraser syndrome, which features absent or dysplastic kidneys (34,119). Mice lacking *EMX2*, a transcription factor expressed in both the ureteric bud and the metanephric mesenchyme, have a similar disappearing metanephros phenotype (135).

Cell Lineages Arising From Metanephric Mesenchyme

Stem cells are probably present in the mesenchyme of the human nephrogenic cortex, and there are likely to be (as yet undefined) growth factors that maintain these cells in an undifferentiated, proliferating state (145). Such an activity is probably separate from the prevention of apoptosis of the metanephric mesenchyme, discussed above. The isolated metanephric mesenchyme can be induced to differentiate into glomerular epithelia, proximal and distal tubules, as well as stromal cells (or interstitial fibroblasts) (133,134,183). Therefore, it has been postulated that there might exist a common progenitor cell that could give rise to epithelial and stromal/interstitial cells. Direct proof for this hypothesis would require the identification, tagging, and subsequent lineage analysis of a single metanephric mesenchymal cell: this has yet to be achieved. At present, it is equally possible that there exist individual precursors within the mesenchyme with potential to become interstitial or nephron cells. Metanephric mesenchyme also harbors endothelial precursor cells: several studies, discussed below, demonstrated, first, that some mesenchymal cells express a set of endothelial-specific genes even before anatomically overt capillaries can be detected and, second, that the just-formed metanephros can form capillaries after transplantation to other sites or culture in a hypoxic atmosphere (42,184,185). Sequeira Lopez et al. (43) found that a subset of metanephric mesenchymal cells express renin, and these seem to have the ability to differentiate into multiple cell types, including vascular and tubule cells. Classically, the whole of the collecting duct system has been envisaged to derive from the ureteric bud (134). However, when isolated metanephric mesenchyme was retrovirally tagged and subsequently recombined with native ureteric bud, although most labeled cells appeared in glomeruli and proximal and distal tubules, other labeled cells appeared in the collecting duct system (142). Collectively, these experiments suggest that lineages arising from metanephric mesenchymal cells may be more diverse than previously considered.

Nephron Tubule Formation From Metanephric Mesenchyme

Metanephric precursor cells that differentiate into nephrons are said to undergo a *phenotypic conversion* from mesenchymal to epithelial cells. The former are loosely packed and nonpolarized, whereas the latter cells form sheets of tightly packed monolayers with specialized apical (luminal), basal, and lateral plasma membrane domains. The first morphologic step in this

TABLE 2.3 Patterns of gene expression in normal human embryonic kidneys

	PAX2	Cell proliferation	WT1	BCL2
Undifferentiated mesenchyme	–	Rare +	+	–
Mesenchymal condensate	++	++	+	++
Comma- and S-shaped bodies	++	++	+	+
Glomerular podocytes	–	Rare +	++	–
Tips of ureteric bud (ampullae)	++	++	–	–
Immature collecting ducts	+	+	–	–
Mature collecting ducts	Rare +	Rare +	–	–

–, no staining; + to ++, increasing intensity of staining present in most cells in the designated population; rare +, <10% of cells of these populations showed positive immunostaining.

process is the aggregation of mesenchymal cells to form a condensate. The application of either FGF2 (142), a growth factor made by the metanephros, or lithium (186), an exogenous chemical, to metanephric mesenchyme stimulates differentiation up to, but not beyond, the stage of condensation. During normal human nephrogenesis, the aggregated cells increase the expression of WT1 and also BCL2 and PAX2 (23) (Table 2.3 and Fig. 2.9). Thus, while WT1 appears to be necessary for the survival and induction of renal mesenchyme, BCL2 and PAX2 protect nephron precursors from death in their earliest stage of morphogenesis. Inhibition of PAX2 in metanephric organ culture prevents nephron formation (137), and mice null mutant for *BCL2* have hypoplastic kidneys (121). It is also of interest that in the human cystic dysplastic kidneys, there is little BCL2 or PAX2 expression in the poorly differentiated tissues surrounding dysplastic tubules (23), a location where high levels of apoptosis have been reported (29): the enhanced death may explain the tendency for these organs to involute prenatally or postnatally (30,187).

Next, the mesenchymal condensate forms a lumen and differentiates into increasingly mature nephron precursors: the vesicle and comma- and S-shaped bodies, described above. This process is associated with major changes of expression of adhesion molecules. The mesenchymal cell-cell adhesion molecule, NCAM, is down-regulated (105), and E-cadherin appears at sites of cell-cell contact in the primitive nephron. Cell biology studies have implicated the latter molecule as playing a key part in the genesis of the epithelial phenotype; for example, experimentally induced expression of E-cadherin in fibroblasts redistributes Na⁺-K⁺-ATPase to sites of cell-cell contact, as is found in epithelia (188), and blockade of E-cadherin in epithelial cells interferes with integrity of cell-cell junctions called zonula adherens and zonula occludens (189).

Collagen I and fibronectin are prominent matrix components expressed by the renal mesenchyme, but these molecules are switched off during the transition to nephron epithelia; instead, the primitive tubular epithelia begin to synthesize a basement membrane of collagen IV, laminin, heparan sulfate, and nidogen. Metanephric organ culture data support the idea that the interaction of laminin-1, a cruciform trimeric molecule, with a cell surface receptor, $\alpha 6$ integrin, is essential for lumen formation during early nephrogenesis (112,190). Other interactions of laminin-1 with the α -dystroglycan complex (191), located on the cell surface of nascent epithelia, and with nidogen, a mesenchymal-derived matrix protein, are also

implicated in nephron tubulogenesis. Interestingly, the interaction between laminin-1 and $\alpha 6$ integrin is also implicated in the migration of the amphibian pronephric duct (192). Induced metanephric mesenchyme begins to express another integrin, $\alpha 8$, and this interacts with a ligand, nephronectin, on the adjacent ureteric bud branches; mice with null mutation for *$\alpha 8$ integrin* fail to undergo the mesenchymal to epithelial transition (116,193). Later in nephrogenesis, as glomerular epithelial podocytes mature, their basement membranes become both depleted of laminin $\beta 1$ and rich in laminin $\beta 2$ (113). Mice in which the latter gene is deleted suffer from an infantile nephrotic syndrome, despite the appearance of grossly structurally normal glomeruli at birth, and humans with LAMB2 mutations have proteinuria from an early age (114).

As nephron tubules form from condensates, not only do interactions occur between the extracellular matrix and the cell surface but there is also an accompanying profound reorganization of the cytoskeleton (194,195). For example, in undifferentiated mesenchyme, microtubules form an array radiating from the centrosome, a small organelle located near the nucleus. Epithelial cells are said to be *polarized* and have distinct apical, lateral, and basal sides, and this is reflected by microtubules that run from the top to the bottom of the cell. The centrosome contains two core structures made of α and β tubulin called centrioles: in the mesenchymal to epithelial transition, one of the centrioles, called the mother, gives rise to a tubulin axoneme, which protrudes into the tubule lumen from the apical cell surface. The extension that is sheathed by the plasma membrane is called the primary cilium and is thought to act as a sensor of urine flow, which somehow transduces differentiation signals into the epithelial cell (196). Several of the proteins that are mutated in human cystic kidney disorders (e.g., autosomal dominant and recessive PKD, nephronophthisis, and the Bardet-Biedl and oral-facial-digital syndromes) are normally located in the centrosome and/or the primary cilium (21,64,131,197).

Growth factors have also been functionally implicated in maturation of early nephrons. LIF is secreted by the ureteric bud and, in rodent organ culture and in combination with other factors such as TGF α and FGF2, is a potent stimulator of nephron formation from the metanephric mesenchyme (97). WNT4 is a secreted molecule produced by metanephric mesenchymal cells shortly before they aggregate: in homozygous null mutant mice, the metanephric mesenchyme appears to be induced and it begins to condense, but mature nephrons fail to form (103,198). BMP7 may also have functions in nephron formation. Null

mutant mice have a range of defects such as reduced numbers of nephrons (95,199), and in cell culture studies, the addition of the factor can drive the conversion of dedifferentiated renal epithelia into a more mature phenotype (200).

Less is known about the molecular controls of differentiation of primitive nephrons into different segments such as glomerular epithelia, proximal tubule, and loop of Henle. A molecule called NOTCH1 becomes activated in just-formed nephrons and appears to be needed for formation of glomerular and proximal tubule epithelia (201). A transcription factor called BRN1 is expressed in the thick ascending limb of the loop of Henle, and in mice that are null mutant for this gene, morphogenesis of the loop of Henle is defective and there is reduced expression of regionally expressed genes such as uromodulin and the Na⁺-K⁺-2Cl⁻ cotransporter (152). More is known about genes that maintain the differentiated state of the glomeruli. Here, WT1 has a role: it is expressed in maturing podocytes, and heterozygous mutations in mice have glomerular sclerosis (68). Similarly, human *WT1* mutations cause glomerular disease in the Denys-Drash and Fraser syndromes (19). *Nephrin* (*NPHS1*) is mutated in the congenital nephrotic syndrome of the Finnish type, and the protein it encodes forms part of the slit diaphragm situated between podocyte foot processes (107); mice that are null mutant for this gene lack slit diaphragms and develop proteinuria and edema as neonates (108). *Podocin* (*NPHS2*), a gene mutated in an autosomal recessive form of human steroid-resistant nephrotic syndrome, codes for an integral membrane protein located at the insertion site of the slit diaphragm: it associates with nephrin and also with CD2AP (T-lymphocyte surface CD2 antigen-associated protein), which links extracellular stimuli with the cytoskeleton (202). *LMXB1* is a podocyte transcription factor that appears to be essential for their normal differentiation from nephron precursors; the gene is mutated in the nail-patella syndrome, which features proteinuria (203).

MECHANISMS OF URETERIC BUD-COLLECTING DUCT DEVELOPMENT

Branching Morphogenesis of the Ureteric Bud

In vitro ureteric bud growth is dependent on the presence of the metanephric mesenchyme (132,134,204). Importantly, the epithelia of the ureteric bud express various receptor tyrosine kinases that transduce differentiation signals on binding to growth factors produced by the adjacent metanephric mesenchyme. RET is expressed in the branching tips of the ureteric bud and is down-regulated as collecting ducts mature (77,78); RET expression itself is enhanced by signals from adjacent stroma initiated by activation of RA receptors (160). GDNF, the main ligand for RET, is expressed in the metanephric mesenchyme adjacent to the ureteric bud ampullae (77,78,119). Mice with homozygous null mutations of either the ligand or the receptor have absent kidneys because of defective outgrowth of the bud from the mesonephric duct (77,78). Within the metanephric mesenchyme, the expression of this growth factor is controlled by a network of transcription factors and related molecules including EYA1, HOXD11, and PAX2 (71,119). Recently, other studies have suggested that the normal point of initiation of the ureteric

bud on the mesonephric duct is defined by the expression of yet other genes: these include *FOXC1*, *BMP4*, *SPROUTY1*, and *ROBO2* (see Table 2.1). Mouse mutations of any one of these genes result in ectopic budding and duplicated renal tracts (94,153,167,168). Their gene products limit the extent of GDNF expression within the intermediate mesoderm to the field destined to become metanephric mesenchyme and also modulate the response of the RET-expressing duct to the paracrine growth factor.

Epithelial branching morphogenesis also occurs during the development of the lung, pancreas, thymus, liver, prostate, salivary glands, and mammary glands and requires the presence of mesenchymal cells or mesenchymal-derived factors. This observation suggests that there exist common molecules derived from mesenchyme that regulate epithelial growth. One such may be HGF which, within the metanephros, is secreted by mesenchymal cells. MET, its receptor tyrosine kinase, is expressed by the adjacent ureteric bud, and antisera that block the bioactivity of HGF also prevent the branching of the ureteric bud in organ culture (Fig. 2.10) (82). Other growth factors appear to inhibit renal branching morphogenesis: these include BMP4 (94) and TGFβ (101). Of note, TGFβ is prominently expressed in the human dysplastic kidneys, where it may be implicated in defective collecting duct branching (1) and the metaplastic transition of epithelia to a smooth muscle-like phenotype (100).

In fact, there are a series of positive and negative influences on ureteric bud formation that ensure that just one ureteric bud (and hence ureter) is formed from each mesonephric duct at its near distal end (205). When balance is disturbed, either the bud does not form (resulting in renal tract agenesis) or too many buds are generated (resulting in duplicated renal tracts). Certainly, molecules of the extracellular matrix also play their parts as well as growth factors. For example, collagen I is permissive for branching, whereas components in the mature basement membrane appear inhibitory (206). Extracellular matrix molecules situated at the interface of the bud and mesenchyme interact with integrin cell surface receptors (207,208). This not only provides physical links between different types of cells but may also, via “outside-in signaling,” modulate expression of genes coding for effector molecules such as GDNF (119,208).

As the bud branches, the stems of the system mature into the collecting ducts containing potassium-secreting principal cells and the proton handling intercalated cells. Within the latter category, α intercalated cells move protons into the tubule lumen, and β intercalated cells secrete bicarbonate. In cell culture, it appears that there is some plasticity regarding the lineage of the three types of cell (209). There is evidence that corticosteroids can enhance the differentiation of collecting ducts (210). Galectin-3 is a cell surface molecule that is expressed by the maturing collecting duct and that acts as a brake on branching morphogenesis (110,111); remarkably, it also appears to be critical for the terminal differentiation of intercalated cells by polymerizing an extracellular matrix protein called hensin (211), and experimental genetic deletion of this molecule causes distal renal tubular acidosis (212).

Renal Pelvis and Ureter

A detailed review of mechanisms that control growth of the lower urinary tract (renal pelvis, ureter, and bladder) is beyond the scope of this chapter, and readers are referred to recent

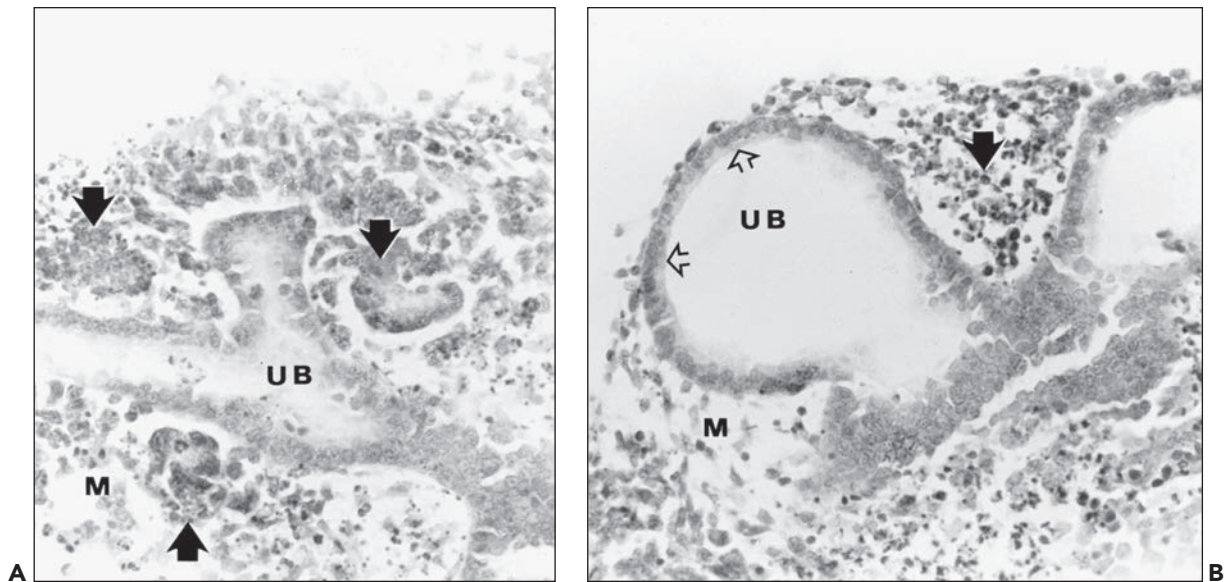


FIGURE 2.10 Blockade of hepatocyte growth factor in metanephric organ culture. **A:** Histology of embryonic day-11 mouse metanephric rudiments after 3 days' growth in organ culture. Primitive nephrons (*closed arrows*) have formed from undifferentiated mesenchyme (M) close to the branching tips of the ureteric bud (UB). **B:** In the presence of a blocking antibody to hepatocyte growth factor, the ureteric bud (UB) has branched poorly and is dilated (*open arrowheads*). It is surrounded by undifferentiated mesenchyme with pyknotic nuclei (*closed arrow*). These data suggest that this metanephric growth factor is necessary for the differentiation of nephrons and the ureteric bud. (Modified from Woolf AS, Kolatsi-Joannou M, Hardman P, et al. Roles of hepatocyte growth factor/scatter factor and the met receptor in early development of the metanephros. *J Cell Biol* 1995;128:171.)

reviews (205,213,214). RA receptors, and hence vitamin A, are implicated in the remodeling that takes place as the caudal end of the mesonephric duct, and the ureteric bud become incorporated into the nascent bladder to form the trigone and lower part of the ureter (161). AT2, an angiotensin II receptor that mediates apoptosis, is involved in the sculpting of the lower urinary tract (93), and BMP4 is implicated in the early linear growth of the ureter (94). As the ureter matures, it acquires a muscle coat, and the differentiation of smooth myocyte progenitors is in part controlled by SHH, which is secreted by the developing urothelium (98) and which stimulates a signaling cascade in adjacent myocyte precursors involving BMP4 and transcription factors and related molecules such as teashirt-3, myocardin, and serum response factor. Ureteric peristalsis initiates before birth and, in rodent models, is under the control of the KIT receptor tyrosine kinase and angiotensin: most likely, the failure of myocyte differentiation and function can lead to a state of functional obstruction of fetal urine flow, with subsequent secondary aberration of kidney growth. With regard to the urothelium itself, FGF7 enhances proliferation and differentiation of the pseudostratified epithelium. The most lumenally located urothelial cells are called *umbrella cells*, and their apical surface is almost totally covered by an asymmetric unit membrane composed of plaque proteins of the UP family. The UPs here contribute to the watertight properties of the epithelium and may also have roles in differentiation/morphogenesis of the lower renal tract because null mutant mice suffer from bladder and ureteric malformations (129,130). Of note, *UPIIIA* mutations have been reported in a subset of children born with primary vesicoureteric reflux

and severe renal malformations (175). The fetal human ureter undergoes a period when it is not patent, but the factor(s) that determine(s) normal recanalization is/are not known (56,57): ureters attached to the human multicystic dysplastic kidneys characteristically have an obstructed lumen (1) and hence may represent a failure of recanalization. Of note, mice that are null mutant for *UPII* have hydronephrosis accompanied by ureteric obstruction with the lumens filled with urothelial cells (130). In order for the bladder to become functionally mature, autonomic neurons must innervate the detrusor and internal sphincter muscle. Aberrations of these processes underlie human congenital bladder malfunction in the prune belly syndrome (66), when the detrusor is underactive, and the urofacial syndrome (215,216), in which both the detrusor and internal sphincter are overactive.

BLOOD VESSELS IN THE DEVELOPING KIDNEY

Developmental Anatomy of the Renal Vasculature

When first formed, the human metanephros is at the level of the upper sacral segments and receives its blood supply from the lateral sacral branches of the aorta. Largely, as a result of differential growth of the caudal end of the embryo, the kidneys are found at a progressively higher level. This ascent of the kidney from its originally sacral to its ultimate lumbar position, which it reaches between the 5th and 8th week of gestation, is associated with its blood supply being derived from stem branches of the aorta at a progressively higher level, until

the definitive renal arteries, arising from the aorta at about the level of the second lumbar vertebra, are reached. In contrast to adult renal vessels (apart from the juxtaglomerular cells), the walls of the early renal vasculature synthesize renin, especially at arterial branch points (217).

The most mature nephrons, located toward the center of the metanephros, acquire capillary loops within glomeruli and a patent Bowman space. Electron microscopy shows that the initially multilayered visceral glomerular epithelium forms a monolayer of podocytes that touch the endothelium by foot processes; the tripartite glomerular basement membrane, consisting of two outer electron-lucent regions (laminae rarae) and a central dense region (lamina densa), can be seen between the podocytes and endothelial cells. Experimental data from rodents show that the glomerular basement membrane is synthesized by both the endothelium and epithelium (218). After fusion of the two membranes, there are sequential changes in the isoforms of collagen IV chains that are expressed and that can be correlated with the progressive restriction of filtration of macromolecules (115,219). Apart from glomerular capillaries, there exist other capillary beds. Peritubular capillaries are fenestrated and surround cortical tubules and medullary collecting ducts; they provide oxygen and nutrients to tubules and transport reclaimed solutes and water. Vasa recta arise from efferent arterioles of deep glomeruli, descending into the medulla as pericyte-coated vessels and ascending as fenestrated capillaries; they are intimately associated with the descending and ascending limbs of the loops of Henle as well as collecting ducts and are thus involved in urinary concentration. Murine vasa recta reach structural maturity about 1 month postnatally.

Mechanisms of Formation of Renal Blood Vessels

New endothelia can be formed in two ways during development (220). During *vasculogenesis*, precursor cells differentiate in situ into mature endothelia. In contrast, during the process called *angiogenesis*, preexisting capillaries sprout and migrate to form new vessels in other locations. The first embryonic endothelia, including those in the yolk sac and heart primordia, form by vasculogenesis, but there is some controversy regarding the origin of kidney vessels. The mechanisms of formation of renal blood vessels have recently been reviewed (221). One line of experimental evidence suggests that the first renal endothelia arise by angiogenesis or the ingrowth of preexisting vessels. At the inception of nephrogenesis, there are no patent capillaries in the renal blastema (42,221), and although the explanted rodent metanephros will undergo considerable epithelial differentiation in organ culture, the glomeruli that are formed in this milieu lack capillaries (133). Second, when the mouse metanephros is transplanted onto the avian chorioallantoic membrane, the glomeruli that develop are invaded by host endothelial cells (222). It could, however, be argued that neither of these experiments provides a correct setting for renal vasculogenesis.

On the other hand, other reports provide evidence that renal vasculogenesis is important. Genetic studies, bioassays, and patterns of gene expression have shown that vascular VEGF and the angiopoietin families have central roles in embryonic blood vessel formation (220). Undifferentiated metanephric cells express receptor tyrosine kinases for both VEGF and the angiopoietins; the early metanephros also expresses these growth factors, hence providing circumstantial

evidence for the presence of endothelial precursors in the metanephros (42,223,224). When the rodent metanephric kidneys are grown in organ culture in hypoxic conditions or in the presence of exogenous VEGF, endothelia grow in situ between forming tubules (40,42,184), again suggesting vasculogenesis. More impressively, when the rodent metanephroi are transplanted into the anterior chamber of the eye (185) or into the nephrogenic zone of the developing kidneys (42), grafts form glomeruli with plentiful capillary loops, and these endothelial cells express donor-specific markers. Furthermore, renal hypoxia can be demonstrated in vivo, at least during the later stages of rodent metanephric development (225), and other genetic evidence suggests that renin-expressing metanephric mesenchymal cells give rise to vascular structures (43). Collectively, the data are consistent with the idea that at least part of the renal vasculature arises in situ, and its differentiation is controlled by growth factors that may be, in part, up-regulated by hypoxia.

The podocyte is an in vivo source of VEGF (226), essential to maintain integrity of maturing glomerular endothelia, as demonstrated in mice with VEGF genetically and specifically down-regulated in glomeruli; these mice still appear to have peritubular capillaries (169). Of interest, podocytes themselves may be targets of VEGF, where the VEGFR2 receptor growth may modulate glomerular barrier function via interaction with nephrin (227). Questions remain regarding sources and nature of molecules controlling differentiation of nonglomerular capillaries within the kidney. Tubules in the kidney certainly express VEGF (228), and in the future, perhaps tubule segment-specific null mutations of VEGF may be informative regarding whether this molecule also enhances differentiation of cortical peritubular capillaries and vasa recta. Mice null mutant for angiopoietin 2 form abnormal cortical peritubular capillaries that appear to become surrounded by pericyte-like cells: this may result from aberrant signaling between nascent endothelia and surrounding mesenchymal precursors (80).

Stroma, Renal Capsule, and Innervation of the Developing Kidney

Compared with the formation of nephrons, little is known about the mechanisms that control the maturation of renal blastema into the stromal cells or interstitial fibroblasts. There is evidence that the metanephric stroma expresses specific molecules that modulate nephron formation (183). For example, the GD3 ganglioside is expressed by stromal cells surrounding the stalk of the ureteric bud (136); antibodies to the latter molecule prevent bud morphogenesis. Metanephric stroma expresses several characteristic transcription factors: mice null mutant for *BF2* (brain factor 2/homologue of *Drosophila* forkhead; also called *FOXD1*) have small, fused kidneys with reduced numbers of nephrons (151); vitamin A initiates a signal via stromal RA receptors that maintain the expression of RET in the adjacent ureteric bud (161); mice null mutant for *PODI* have defective ureteric bud branching (158). Along the same lines, evidence now shows that cells in the renal capsule express specific genes and that they too direct nephrogenesis: capsule cells express the *FOXD1* transcription factor, and mutant mice have fused pelvic kidneys and disorganized parenchyma (154).

Grobstein (132) found that when the embryonic spinal cord was placed on the opposite side of a filter to that of the isolated metanephric blastema, nephrons were induced

to differentiate. Further investigations showed that neurons appeared to have penetrated the mesenchyme through the microscopic pores of the filter; if the neural tissue of the spinal cord was destroyed, leaving its supporting tissue intact, the induction did not occur (229). As assessed by antibodies against neurofilaments and neural cell surface gangliosides, neuronal cell bodies are observed around the rodent ureteric bud in vivo and their terminals end around mesenchymal condensates (230). This observation supports the hypothesis that the earliest stages of kidney development may be partly dependent on the innervation of the organ. Neurotrophin-3 is important for the survival and differentiation of these nerves, but the factor itself did not trigger nephron formation in isolated metanephric blastema (85). Subsets of metanephric stromal cells have some neuronal characteristics; for example, they contain neurofilaments and express receptors for neurotrophic factors (85,231). In this respect, it is interesting that the adult rodent kidney is thought to contain a small population of stem cells that can be isolated and induced in culture to generate cells with neuronal characteristics (26).

ACKNOWLEDGMENT

We thank Professor R. Anthony Risdon for input into a previous version of this chapter; Dr. Paul J.D. Winyard for preparation of some of the figures; and the Medical Research Council and Wellcome Trust–funded Human Embryo Bank for providing tissues collected under ethical approval.

REFERENCES

- Potter EL. *Normal and Abnormal Development of the Kidney*. Chicago: Year Book Medical Publishers, 1972.
- Wiesel A, Queisser-Luft A, Clementi M, et al. Prenatal detection of congenital renal malformations by fetal ultrasonographic examination: an analysis of 709,030 births in 12 European countries. *Eur J Med Genet* 2005;48:131–144.
- Woolf AS, Price K, Scambler PJ, et al. Evolving concepts in human renal dysplasia. *J Am Soc Nephrol* 2004;15:998.
- Kerecuk L, Schreuder MF, Woolf AS. Human renal tract malformations: perspectives for nephrologists. *Nat Clin Pract Nephrol* 2008;4:312–325.
- Farrugia MK, Woolf AS. Congenital urinary bladder outlet obstruction. *Fetal Matern Med Rev* 2010;21:155–173.
- Lewis MA, Shaw J, Sinha MD, et al. UK Renal Registry 12th Annual Report (December 2009): Demography of the UK paediatric renal replacement therapy population in 2008. *Nephron Clin Pract* 2010;115(Suppl 1):c279–c288.
- Ichikawa I, Kuwayama F, Pope JC IV, et al. Paradigm shift from classic anatomic theories to contemporary cell biological views of CAKUT. *Kidney Int* 2002;61:889.
- Smith JM, Stablein DM, Munoz R, et al. Contributions of the Transplant Registry: The 2006 Annual Report of the North American Pediatric Renal Trials and Collaborative Studies (NAPRTCS). *Pediatr Transplant* 2007;11:366–373.
- Wedekin M, Ehrlich JH, Offner G, et al. Renal replacement therapy in infants with chronic renal failure in the first year of life. *Clin J Am Soc Nephrol* 2010;5:18–23.
- Dötsch J, Plank C, Amann K, et al. The implications of fetal programming of glomerular number and renal function. *J Mol Med (Berl)* 2009;87:841–848.
- Welham SJM, Wade A, Woolf AS. Protein restriction in pregnancy is associated with increased apoptosis of mesenchymal cells at the start of rat metanephrogenesis. *Kidney Int* 2002;61:1231.
- Welham SJM, Riley PR, Wade A, et al. Maternal diet programs embryonic kidney gene expression. *Physiol Genomics* 2005;22:48.
- Hughson M, Farris AB III, Douglas-Denton R, et al. Glomerular number and size in autopsy kidneys: the relationship to birth weight. *Kidney Int* 2003;63:2113.
- Keller G, Zimmer G, Mall G, et al. Nephron number in patients with primary hypertension. *N Engl J Med* 2003;348:101.
- Liapis H, Winyard PJD. Renal developmental defects and cystic diseases. In: Jennette JC, Olson JL, Silva FG, D'Agati W, eds. *Heptinstall's Pathology of the Kidney*, 7th ed. Philadelphia: Lippincott Williams & Wilkins, 2014.
- Denholm B, Skaer H. Bringing together components of the fly renal system. *Curr Opin Genet Dev* 2009;19:526–532.
- Ebarasi L, Oddsson A, Hultenby K, et al. Zebrafish: a model system for the study of vertebrate renal development, function and pathophysiology. *Curr Opin Nephrol Hypertens* 2011;20:416–424.
- Jones EA. *Xenopus*: a prince among models for pronephric kidney development. *J Am Soc Nephrol* 2005;16:313.
- Scholz H, Kirschner KM. A role for the Wilms' tumor protein WT1 in organ development. *Physiology (Bethesda)* 2005;20:54.
- Harris PC. 2008 Homer W. Smith Award: insights into the pathogenesis of polycystic kidney disease from gene discovery. *J Am Soc Nephrol* 2009;20:1188–1198.
- Gascue C, Katsanis N, Badano JL. Cystic diseases of the kidney: ciliary dysfunction and cystogenic mechanisms. *Pediatr Nephrol* 2011;26:1181–1195.
- Grignon DJ, Eble JN. Renal neoplasms. In: Jennette JC, Olson JL, Silva FG, D'Agati W, eds. *Heptinstall's Pathology of the Kidney*, 7th ed. Philadelphia: Lippincott Williams & Wilkins, 2014.
- Winyard PJD, Sams V, Risdon RA, et al. The PAX2 transcription factor is expressed in cystic and hyperproliferative dysplastic epithelia in human kidney malformations. *J Clin Invest* 1996;98:451.
- Kobayashi A, Valerius MT, Mugford JW, et al. Six2 defines and regulates a multipotent self-renewing nephron progenitor population throughout mammalian kidney development. *Cell Stem Cell* 2008;3:169–181.
- Fuente Mora C, Ranghini E, Bruno S, et al. Differentiation of podocyte and proximal tubule-like cells from a mouse kidney-derived stem cell line. *Stem Cells Dev* 2012;21:296–307.
- Oliver JA, Maarouf O, Cheema FH, et al. SDF-1 activates papillary label-retaining cells during kidney repair from injury. *Am J Physiol Renal Physiol* 2012;302:F1362–F1373.
- Ronconi E, Sagrinati C, Angelotti ML, et al. Regeneration of glomerular podocytes by human renal progenitors. *J Am Soc Nephrol* 2009;20:322–332.
- Araki T, Saruta T, Okano H, et al. Caspase activity is required for nephrogenesis in the developing mouse metanephros. *Exp Cell Res* 1999;248:423–429.
- Winyard PJD, Nauta J, Lirenman DS, et al. Deregulation of cell survival in cystic and dysplastic renal development. *Kidney Int* 1996;49:135.
- John U, Rudnik-Schoneborn S, Zerres K, et al. Kidney growth and renal function in unilateral multicystic dysplastic kidney disease. *Pediatr Nephrol* 1998;12:567.
- Tse HK, Leung MB, Woolf AS, et al. Implication of Wt1 in the pathogenesis of nephrogenic failure in a mouse model of retinoic acid-induced caudal regression syndrome. *Am J Pathol* 1995;166:1295.
- Attar R, Quinn F, Winyard PJD, et al. Short-term urinary flow impairment deregulates PAX2 and PCNA expression and cell survival in fetal sheep kidneys. *Am J Pathol* 1998;152:1225.
- Kreidberg JA, Sariola H, Loring JM, et al. WT-1 is required for early kidney development. *Cell* 1991;74:679.
- McGregor L, Makela V, Darling SM, et al. Fraser syndrome and mouse blebbed phenotype caused by mutations in *FRAS1/Fras1* encoding a putative extracellular matrix protein. *Nat Genet* 2003;34:203.
- Clark P, Dziarmaga A, Eccles M, et al. Rescue of defective branching nephrogenesis in renal-coloboma syndrome by the caspase inhibitor, Z-VAD-fmk. *J Am Soc Nephrol* 2004;15:299–305.
- Fischer E, Legue E, Doyen A, et al. Defective planar cell polarity in polycystic kidney disease. *Nat Genet* 2006;38:21–23.
- Elger M, Hentschel H, Litteral J, et al. Nephrogenesis is induced by partial nephrectomy in the elasmobranch *Leucoraja erinacea*. *J Am Soc Nephrol* 2003;14:1506.

38. Diep CQ, Ma D, Deo RC, et al. Identification of adult nephron progenitors capable of kidney regeneration in zebrafish. *Nature* 2011;470:95–100.
39. Salbreux G, Charras G, Paluch E. Actin cortex mechanics and cellular morphogenesis. *Trends Cell Biol* 2012;22(10):536–545.
40. Tufro A, Norwood VF, Carey RM, et al. Vascular endothelial growth factor induces nephrogenesis and vasculogenesis. *J Am Soc Nephrol* 1999;10:2125.
41. Soriano P. Abnormal kidney development and hematological disorders in platelet derived growth factor β -receptor mutant mice. *Genes Dev* 1994;8:1888.
42. Loughna S, Hardman P, Landels E, et al. A molecular and genetic analysis of renal glomerular capillary development. *Angiogenesis* 1997;1:84.
43. Sequeira Lopez ML, Pentz ES, Nomasa T, et al. Renin cells are precursors for multiple cell types that switch to the renin phenotype when homeostasis is threatened. *Dev Cell* 2004;6:719.
44. Osathanondh V, Potter EL. Development of kidneys as shown by microdissection. I. Preparation of tissues with reasons for possible misinterpretation of observations. *Arch Pathol* 1963;76:271.
45. Osathanondh V, Potter EL. Development of kidneys as shown by microdissection. II. Renal pelvis, calyces and papillae. *Arch Pathol* 1963;76:277.
46. Osathanondh V, Potter EL. Development of kidneys as shown by microdissection. III. Formation and interrelationship of collecting ducts and nephrons. *Arch Pathol* 1963;76:290.
47. Osathanondh V, Potter EL. Development of the human kidney as shown by microdissection. IV. Development of tubular portions of nephrons. *Arch Pathol* 1966;82:391.
48. Osathanondh V, Potter EL. Development of the human kidney as shown by microdissection. V. Development of vascular pattern of glomerulus. *Arch Pathol* 1966;82:403.
49. Larsen WJ. *Human Embryology*, Vol. 1. New York: Churchill Livingstone, 2001.
50. Moore KL, Persaud TVN. *The Developing Human: Clinically Oriented Embryology*, Vol. 1. Philadelphia: WB Saunders, 2003.
51. Risdon RA, Woolf AS. Development of the kidney. In: Jennette JC, Olson JL, Schwartz MM, et al., eds. *Heptinstall's Pathology of the Kidney*, 5th ed. Philadelphia: Lippincott-Raven, 1998:67.
52. Torrey TW. The early development of the human nephros. *Contrib Embryol Carnegie Inst* 1954;35:175.
53. Fetterman GH, Shuplock NA, Philipp FJ, et al. The growth and maturation of human glomeruli and proximal convolutions from term to adulthood. *Pediatrics* 1965;35:609.
54. Zimanyi MA, Hoy WE, Douglas-Denton RN, et al. Nephron number and individual glomerular volumes in male Caucasian and African American subjects. *Nephrol Dial Transplant* 2009;24:2428–2433.
55. Zhang Z, Quinlan J, Hoy W, et al. A common RET variant is associated with reduced newborn kidney size and function. *J Am Soc Nephrol* 2008;19:2027–2034.
56. Alcaraz A, Vinaixa F, Tejedo-Mateu A, et al. Obstruction and recanalization of the ureter during embryonic development. *J Urol* 1991;145:410.
57. Ruano-Gil D, Coca-Payeras A, Tejedo-Mateu A. Obstruction and normal recanalization of the ureter in the human embryo. Its relation to congenital ureteric obstruction. *Eur Urol* 1975;1:287.
58. Matsuno T, Tokunaka S, Koyanagi T. Muscular development in the urinary tract. *J Urol* 1984;132:148.
59. Jenkins D, Winyard PJ, Woolf AS. Immunohistochemical analysis of sonic hedgehog signalling in normal human urinary tract development. *J Anat* 2007;211:620–629.
60. Harding SD, Armit C, Armstrong J, et al. The GUDMAP database—an online resource for genitourinary research. *Development* 2011;138:2845–2853.
61. Yu J, Valerius MT, Duah M, et al. Identification of molecular compartments and genetic circuitry in the developing mammalian kidney. *Development* 2012;139:1863–1873.
62. Lindsay S, Copp AJ. MRC-Wellcome Trust Human Developmental Biology Resource: enabling studies of human developmental gene expression. *Trends Genet* 2005;21:586–590.
63. Ostrer H, Wilson DI, Hanley NA. Human embryo and early fetus research. *Clin Genet* 2006;70:98–107.
64. Duke V, Winyard PJD, Thorogood PV, et al. *KAL*, a gene mutated in Kallmann's syndrome, is expressed in the first trimester of human development. *Mol Cell Endocrinol* 1995;110:73.
65. Kolatsi-Joannou M, Bingham C, Ellard S, et al. Hepatocyte nuclear factor 1 β : a new kindred with renal cysts and diabetes, and gene expression in normal human development. *J Am Soc Nephrol* 2001;12:2175.
66. Weber S, Thiele H, Mir S, et al. Muscarinic acetylcholine receptor M3 mutation causes urinary bladder disease and a prune-belly-like syndrome. *Am J Hum Genet* 2011;89:668–674.
67. Essafi A, Webb A, Berry RL, et al. A wt1-controlled chromatin switching mechanism underpins tissue-specific wnt4 activation and repression. *Dev Cell* 2011;21:559–574.
68. Natoli TA, Liu J, Eremina V, et al. A mutant form of the Wilms' tumor suppressor gene WT1 observed in Denys-Drash syndrome interferes with glomerular capillary development. *J Am Soc Nephrol* 2002;13:2058–2067.
69. Schwab K, Hartman HA, Liang HC, et al. Comprehensive microarray analysis of Hoxa11/Hoxd11 mutant kidney development. *Dev Biol* 2006;293:540–554.
70. Sanyanusin P, Schimmentil LA, McNoe LA, et al. Mutation of the PAX2 gene in a family with optic nerve colobomas, renal anomalies and vesico-ureteral reflux. *Nat Genet* 1995;9:358.
71. Gong KQ, Yallowitz AR, Sun H, et al. A Hox-Eya-Pax complex regulates early kidney developmental gene expression. *Mol Cell Biol* 2007;27:7661–7668.
72. Keller SA, Jones JM, Boyle A, et al. Kidney and retinal defects (*Krd*), a transgene-induced mutation with a deletion of mouse chromosome 19 that includes the *Pax2* locus. *Genomics* 1994;23:309.
73. Ryan G, Steele-Perkins V, Morris JF, et al. Repression of Pax-2 by WT1 during normal kidney development. *Development* 1995;121:867.
74. Lee SB, Huang K, Palmer R, et al. The Wilms tumor suppressor WT1 encodes a transcriptional activator or amphiregulin. *Cell* 1999;98:663.
75. Adalat S, Woolf AS, Johnstone KA, et al. HNF1B mutations associate with hypomagnesemia and renal magnesium wasting. *J Am Soc Nephrol* 2009;20:1123–1131.
76. Gresh L, Fischer E, Reimann A, et al. A transcriptional network in polycystic kidney disease. *EMBO J* 2004;23:1657.
77. Costantini F. GDNF/Ret signaling and renal branching morphogenesis: from mesenchymal signals to epithelial cell behaviors. *Organogenesis* 2010;6:252–262.
78. Chi X, Michos O, Shakya R, et al. Ret-dependent cell rearrangements in the Wolffian duct epithelium initiate ureteric bud morphogenesis. *Dev Cell* 2009;17:199–209.
79. Skinner MA, Safford SD, Reeves JG, et al. Renal aplasia in humans is associated with RET mutations. *Am J Hum Genet* 2008;82:344–351.
80. Pitera JE, Woolf AS, Gale NW, et al. Dymorphogenesis of kidney cortical peritubular capillaries in angiotensin-2 deficient mice. *Am J Pathol* 2004;165:1895.
81. Michos O, Cebrian C, Hyink D, et al. Kidney development in the absence of Gdnf and Spry1 requires Fgf10. *PLoS Genet* 2010;6:e1000809.
82. Woolf AS, Kolatsi-Joannou M, Hardman P, et al. Roles of hepatocyte growth factor/scatter factor and met in early development of the metanephros. *J Cell Biol* 1995;128:171.
83. Matsell DG, Bennett T, Armstrong RA, et al. Insulin-like growth factor (IGF) and IGF binding protein gene expression in multicystic renal dysplasia. *J Am Soc Nephrol* 1997;8:85.
84. Rogers SA, Ryan G, Hammerman MR. Insulin-like growth factors I and II are produced in the metanephros and are required for growth and development in vitro. *J Cell Biol* 1991;113:1447.
85. Karavanov A, Sainio K, Palgi J, et al. Neurotrophin-3 rescues neuronal precursors from apoptosis and promotes neuronal differentiation in the embryonic metanephric kidney. *Proc Natl Acad Sci U S A* 1995;92:11279.
86. Alpers CE, Hudkins KL, Ferguson M, et al. Platelet-derived growth factor A-chain expression in developing and mature human kidneys and in Wilms' tumor. *Kidney Int* 1995;48:146.
87. Rogers SA, Ryan G, Hammerman MR. Metanephric transforming growth factor- α is required for renal organogenesis in vitro. *Am J Physiol* 1992;262:F533.

88. Eremina V, Baelde HJ, Quaggin SE. Role of the VEGF—a signaling pathway in the glomerulus: evidence for crosstalk between components of the glomerular filtration barrier. *Nephron Physiol* 2007;106:32–37.
89. Tufro A. VEGF spatially directs angiogenesis during metanephric development in vitro. *Dev Biol* 2000;227:558.
90. Yosypiv IV, Schroeder M, El-Dahr SS. Angiotensin II type 1 receptor-EGF receptor cross-talk regulates ureteric bud branching morphogenesis. *J Am Soc Nephrol* 2006;17:1005–1014.
91. Fogo A, Yoshida Y, Yared A, et al. Importance of angiogenic action of angiotensin II in the glomerular growth of maturing kidneys. *Kidney Int* 1990;38:1068.
92. Tsuchida S, Matsusaka T, Chen X, et al. Murine double nullizygotes of the angiotensin type 1A and 1B receptor genes duplicate severe abnormal phenotypes of angiotensin nullizygote. *J Clin Invest* 1998;15:755.
93. Nishimura H, Yerkes E, Hohefellner K, et al. Role of the angiotensin type 2 receptor gene in congenital anomalies of the kidney and urinary tract, CAKUT, of mice and men. *Mol Cell* 1999;3:1.
94. Miyazaki Y, Oshima K, Fogo A, et al. Bone morphogenetic protein 4 regulates the budding site and elongation of the mouse ureter. *J Clin Invest* 2000;105:863.
95. Dudley AT, Lyons KM, Robertson EJ. A requirement for bone morphogenetic protein-7 during development of the mammalian eye and kidney. *Genes Dev* 1995;9:2795.
96. Michos O, Gonçalves A, Lopez-Rios J, et al. Reduction of BMP4 activity by gremlin 1 enables ureteric bud outgrowth and GDNF/WNT11 feedback signalling during kidney branching morphogenesis. *Development* 2007;134:2397–2405.
97. Barasch J, Yang J, Ware CB, et al. Mesenchymal to epithelial conversion in rat metanephros is induced by LIF. *Cell* 1999;99:377.
98. Yu J, Carroll TJ, McMahon AP. Sonic hedgehog regulates proliferation and differentiation of mesenchymal stem cells in the mouse metanephric kidney. *Development* 2002;129:5301.
99. Cain JE, Islam E, Haxho F, et al. GLI3 repressor controls functional development of the mouse ureter. *J Clin Invest* 2011;121:1199–1206.
100. Yang SP, Woolf AS, Yuan HT, et al. Potential biological role of transforming growth factor β 1 in human congenital kidney malformations. *Am J Pathol* 2000;157:1633.
101. Bridgewater D, Di Giovanni V, Cain JE, et al. β -catenin causes renal dysplasia via upregulation of Tgf β 2 and Dkk1. *J Am Soc Nephrol* 2011;22:718–731.
102. Cale CM, Klein NJ, Morgan G, et al. Tumour necrosis factor- α inhibits epithelial differentiation and morphogenesis in the mouse metanephric kidney in vitro. *Int J Dev Biol* 1998;42:663.
103. Stark K, Vainio S, Vassileva G, et al. Epithelial transformation of metanephric mesenchyme in the developing kidney regulated by *Wnt-4*. *Nature* 1994;372:679.
104. Majumdar A, Vainio S, Kispert A, et al. Wnt11 and Ret/Gdnf pathways cooperate in regulating ureteric bud branching during metanephric kidney development. *Development* 2003;130:3175.
105. Pode-Shakked N, Metsuyanim S, Rom-Gross E, et al. Developmental tumorigenesis: NCAM as a putative marker for the malignant renal stem/progenitor cell population. *J Cell Mol Med* 2009;13:1792–1808.
106. Esteban MA, Tran MG, Harten SK, et al. Regulation of E-cadherin expression by VHL and hypoxia-inducible factor. *Cancer Res* 2006;66:3567–3575.
107. Ruotsalainen V, Ljungberg P, Wartiovaara J, et al. Nephric is specifically located at the slit diaphragm of glomerular podocytes. *Proc Natl Acad Sci U S A* 1999;96:7962.
108. Putaala H, Soininen R, Kilpelainen P, et al. The murine nephrin gene is specifically expressed in kidney, brain and pancreas: inactivation of the gene leads to massive proteinuria and neonatal death. *Hum Mol Genet* 2001;10:1.
109. Sakai T, Larsen M, Yamada KM. Fibronectin requirement in branching morphogenesis. *Nature* 2003;423:876.
110. Winyard PJD, Bao Q, Hughes RC, et al. Epithelial galectin-3 during human nephrogenesis and childhood cystic diseases. *J Am Soc Nephrol* 1997;8:1647.
111. Bullock SL, Johnson TM, Bao Q, et al. Galectin-3 modulates ureteric bud branching in organ culture of the developing mouse kidney. *J Am Soc Nephrol* 2001;12:515.
112. Klein G, Langeder M, Timpl R, et al. Role of laminin A chain in the development of epithelial cell polarity. *Cell* 1988;55:331.
113. Noakes PG, Miner JH, Gautam M, et al. The renal glomerulus of mice lacking s-laminin/laminin β 2: nephrosis despite molecular compensation by laminin β 1. *Nat Genet* 1995;10:400.
114. Zenker M, Aigner T, Wendler O, et al. Human laminin beta2 deficiency causes congenital nephrosis with mesangial sclerosis and distinct eye abnormalities. *Hum Mol Genet* 2004;13:2625–2632.
115. Miner JH. Organogenesis of the kidney glomerulus: focus on the glomerular basement membrane. *Organogenesis* 2011;7:75–82.
116. Muller U, Wang D, Denda S, et al. Integrin α 8 β 1 is critically important for epithelial-mesenchymal interactions during kidney morphogenesis. *Cell* 1997;88:603.
117. Hardelin JP, Juilliard AK, Moniot B, et al. Anosmin-1 is a regionally restricted component of basement membranes and interstitial matrices during organogenesis: Implication for the developmental anomalies of X chromosome-linked Kallmann syndrome. *Dev Dyn* 1999;215:26.
118. Gonzalez-Martinez D, Kim SH, Hu Y, et al. Anosmin-1 modulates fibroblast growth factor receptor 1 signalling in human gonadotropin-releasing hormone olfactory neuroblasts through a heparan sulphate-dependent mechanism. *J Neurosci* 2004;24:10384.
119. Pitera JE, Scambler PJ, Woolf AS. Fras1, a basement membrane-associated protein mutated in Fraser syndrome, mediates both the initiation of the mammalian kidney and the integrity of renal glomeruli. *Hum Mol Genet* 2008;17:3953–3964.
120. Cano-Gauci DF, Song HH, Yang H, et al. Glycican-3-deficient mice exhibit developmental overgrowth and some of the abnormalities typical of Simpson-Golabi-Behmel syndrome. *J Cell Biol* 1999;146:255.
121. Sorenson CM, Rogers SA, Korsmeyer SJ, et al. Fulminant metanephric apoptosis and abnormal kidney development in bcl-2-deficient mice. *Am J Physiol* 1995;268:F73.
122. Morham SG, Lanhenbach R, Loftin CD, et al. Prostaglandin synthase 2 gene disruption causes severe renal pathology in the mouse. *Cell* 1995;83:473.
123. Xu PX, Adams J, Peters H, et al. Eya1-deficient mice lack ears and kidneys and show abnormal apoptosis of organ primordia. *Nat Genet* 1999;23:113.
124. Li X, Oghi KA, Zhang J, et al. Eya protein phosphatase activity regulates Six1-Dach-Eya transcriptional effects in mammalian organogenesis. *Nature* 2003;426:247.
125. Bullock SL, Fletcher JM, Beddington RS, et al. Renal agenesis in mice homozygous for a gene trap mutation in the gene encoding heparan sulphate 2-sulphotransferase. *Genes Dev* 1998;12:1894.
126. Boulter C, Mulroy S, Webb S, et al. Cardiovascular, skeletal, and renal defects in mice with a targeted disruption of the Pkd1 gene. *Proc Natl Acad Sci U S A* 2001;98:12174.
127. Wu G, Markowitz GS, Li L, et al. Cardiac defects and renal failure in mice with targeted mutation of Pkd2. *Nat Genet* 2000;24:75.
128. Yosypiv IV. Renin-angiotensin system in ureteric bud branching morphogenesis: insights into the mechanisms. *Pediatr Nephrol* 2011;26:1499–1512.
129. Hu P, Deng FM, Liang FX, et al. Ablation of uroplakin III gene results in small urothelial plaques, urothelial leakage, and vesicoureteral reflux. *J Cell Biol* 2000;151:961.
130. Kong XT, Deng FM, Hu P, et al. Roles of uroplakins in plaque formation, umbrella cell enlargement, and urinary tract diseases. *J Cell Biol* 2004;167:1195.
131. Bettencourt-Dias M, Hildebrandt F, et al. Centrosomes and cilia in human disease. *Trends Genet* 2011;27:307–315.
132. Grobstein C. Morphogenetic interaction between embryonic mouse tissues separated by a membrane filter. *Nature (London)* 1953;172:869.
133. Bernstein J, Cheng F, Roszka J. Glomerular differentiation in metanephric culture. *Lab Invest* 1981;45:183.
134. Saxen L. *Organogenesis of the Kidney*. Cambridge: Cambridge University Press, 1987:1.
135. Miyamoto N, Yoshida M, Kuratani S, et al. Defects of urogenital development in mice lacking Emx2. *Development* 1997;124:1653.
136. Sariola H, Aufderheide E, Bernhard H, et al. Antibodies to cell surface ganglioside GD3 perturb inductive epithelial-mesenchymal interactions. *Cell* 1988;54:235.

137. Rothenpieler UW, Dressler GR. *Pax-2* is required for mesenchymeto-epithelium conversion during kidney development. *Development* 1993;119:711.
138. Davies JA, Ladomery M, Hohenstein P, et al. Development of an siRNA-based method for repressing specific genes in renal organ culture and its use to show that the *Wt1* tumour suppressor is required for nephron differentiation. *Hum Mol Genet* 2004;13:235.
139. Tufro A. Morpholino-mediated gene knockdown in mammalian organ culture. *Methods Mol Biol* 2012;886:305–309.
140. Davies JA, Unbekandt M. siRNA-mediated RNA interference in embryonic kidney organ culture. *Methods Mol Biol* 2012;886:295–303.
141. Woolf AS, Bosch RJ, Fine LG. Gene transfer into the mammalian kidney: microtransplantation of retrovirus-transduced metanephric tissue. *Exp Nephrol* 1993;1:41.
142. Qiao J, Cohen D, Herzlinger D. The metanephric blastema differentiates into collecting system and nephron epithelia in vitro. *Development* 1995;121:3207.
143. Steenhard BM, Ison KS, Cazcarro P, et al. Integration of embryonic stem cells in metanephric kidney organ culture. *J Am Soc Nephrol* 2005;16:1623.
144. Karp SL, Ortiz-Arduan A, Li S, et al. Epithelial differentiation of metanephric mesenchymal cells after stimulation with hepatocyte growth factor or embryonic spinal cord. *Proc Natl Acad Sci U S A* 1994;91:5286.
145. Burrow C, Wilson PD. A putative Wilms tumor-secreted growth factor activity required for primary culture of human nephro-blasts. *Proc Natl Acad Sci U S A* 1993;90:6066.
146. Boyden EA. Experimental obstruction of the mesonephric ducts. *Proc Soc Exp Biol Med* 1927;24:572.
147. Beck AD. The effect of intrauterine urinary obstruction upon the development of the fetal kidney. *J Urol* 1971;105:784.
148. Thiruchelvan N, Nyirady P, Peebles DM, et al. Urinary outflow obstruction increases apoptosis and deregulates Bcl-2 and Bax expression in the fetal ovine bladder. *Am J Pathol* 2003;162:1271.
149. Gage JC, Sulik KK. Pathogenesis of ethanol-induced hydronephrosis and hydroureter as demonstrated following in vivo exposure of mouse embryos. *Teratology* 1991;44:299.
150. Fujinaka H, Miyazaki Y, Matsusaka T, et al. Salutary role for angiotensin in partial urinary tract obstruction. *Kidney Int* 2000;58:2018.
151. Hatini V, Huh SO, Herzlinger D, et al. Essential role of stromal mesenchyme in kidney morphogenesis revealed by targeted disruption of Winged Helix transcription factor *BF-2*. *Genes Dev* 1996;10:1467.
152. Nakai S, Sugitani Y, Sato H, et al. Crucial roles of *Brn1* in distal tubule formation and function in mouse kidney. *Development* 2003;130:4751.
153. Kume T, Deng K, Hogan BL. Murine forkhead/winged helix genes *Foxc1* (*Mf1*) and *Foxc2* (*Mfh1*) are required for the early organogenesis of the kidney and urinary tract. *Development* 2000;127:1387.
154. Levinson RS, Batourina E, Choi C, et al. *Foxd1*-dependent signals control cellularity in the renal capsule, a structure required for normal renal development. *Development* 2005;132:529.
155. Kobayashi A, Kwan KM, Carroll TJ, et al. Distinct and sequential tissue-specific activities of the LIM-class homeobox gene *Lim1* for tubular morphogenesis during kidney development. *Development* 2005;132:2809–2823.
156. Miner JH, Morello R, Andrews KL, et al. Transcriptional induction of slit diaphragm genes by *Lmx1b* is required in podocyte differentiation. *J Clin Invest* 2002;109:1065.
157. Stanton BR, Perkins AS, Tessarollo L, et al. Loss of *N-myc* function results in embryonic lethality and failure of the epithelial component of the embryo to develop. *Genes Dev* 1992;6:2235.
158. Quaggin SE, Schwartz L, Cui S, et al. The basic-helix-loop-helix protein *pod1* is critically important for kidney and lung organogenesis. *Development* 1999;126:5771.
159. Mendelsohn C, Lohnes D, Decimo D, et al. Function of the retinoic acid receptors (RAR) during development. *Development* 1994;120:2749.
160. Batourina E, Gim S, Bello N, et al. Vitamin A controls epithelial/mesenchymal interactions through Ret expression. *Nat Genet* 2001;27:74.
161. Batourina E, Choi C, Paragas N, et al. Distal ureter morphogenesis depends on epithelial cell remodeling mediated by vitamin A and Ret. *Nat Genet* 2002;32:109.
162. Nishinakamura R, Matsumoto Y, Nakao K, et al. Murine homologue of *SALL1* is essential for ureteric bud invasion in kidney development. *Development* 2001;128:3105.
163. Xu PX, Zheng W, Huang L, et al. *Six1* is required for the early organogenesis of the mammalian kidney. *Development* 2003;130:3085.
164. Qiao J, Uzzo R, Obara-Ishihara T, et al. *FGF-7* modulates ureteric bud growth and nephron number in the developing kidney. *Development* 1999;126:547.
165. Michos O, Panman L, Vintersten K, et al. Gremlin-mediated BMP antagonism induces the epithelial-mesenchymal feedback signaling controlling metanephric kidney and limb organogenesis. *Development* 2004;131:3401.
166. McCright B, Gao X, Shen L, et al. Defects in development of the kidney, heart and eye vasculature in mice homozygous for a hypomorphic *Notch2* mutation. *Development* 2001;128:491.
167. Grieshammer U, Ma L, Plump AS, et al. *SLIT2*-mediated *ROBO2* signaling restricts kidney induction to a single site. *Dev Cell* 2004;6:709.
168. Basson MA, Akbulut S, Watson-Johnson J, et al. *Sprouty1* is a critical regulator of GDNF/RET-mediated kidney induction. *Dev Cell* 2005;8:229.
169. Eremina V, Sood M, Haigh J, et al. Glomerular-specific alterations of VEGF-A expression lead to distinct congenital and acquired renal diseases. *J Clin Invest* 2003;111:707.
170. Jadeja S, Smyth I, Pitera JE, et al. Identification of a new gene mutated in Fraser syndrome and mouse myelencephalic blebs. *Nat Genet* 2005;37:520.
171. Pitera JE, Turmaine M, Woolf AS, et al. Generation of mice with a conditional null Fraser syndrome 1 (*Fras1*) allele. *Genesis* 2012;50(12):892–898. doi: 10.1002/dvg.22045.
172. Cullen-McEwan LA, Kett MM, Dowling J, et al. Nephron number, renal function, and arterial pressure in aged GDNF heterozygous mice. *Hypertension* 2003;41:335.
173. Schmidt C, Bladt F, Goedecke S, et al. Scatter factor/hepatocyte growth factor is essential for liver development. *Nature* 1995;373:699.
174. Abdelhak S, Kalatzis V, Heilig R, et al. A human homologue of the *Drosophila* eyes absent gene underlies branchio-oto-renal syndrome and identifies a novel gene family. *Nat Genet* 1997;15:157.
175. Jenkins D, Bitner-Glindzicz M, Malcolm S, et al. De novo Uroplakin IIIa heterozygous mutations cause human renal adysplasia leading to severe kidney failure. *J Am Soc Nephrol* 2005;16:2141.
176. Faguer S, Pillet A, Chassaing N, et al. Nephropathy in Townes-Brocks syndrome (*SALL1* mutation): imaging and pathological findings in adulthood. *Nephrol Dial Transplant* 2009;24:1341–1345.
177. Gruenwald P. Stimulation of nephrogenic tissues by normal and abnormal inductors. *Anat Rec* 1943;86:321.
178. Wride MA, Lapchak PH, Sanders EJ. Distribution of TNF-like protein correlates with some regions of programmed cell death in the chick embryo. *Int J Dev Biol* 1994;38:673.
179. Perantoni AO, Dove LF, Karavanova I. Basic fibroblast growth factor can mediate the early inductive events in renal development. *Proc Natl Acad Sci U S A* 1995;92:4696.
180. Herzlinger D, Qiao J, Cohen D, et al. Induction of kidney epithelial morphogenesis by cells expressing *Wnt-1*. *Dev Biol* 1994;166:815.
181. Tsang TE, Shawlot W, Kinder SJ, et al. *Lim1* activity is required for intermediate mesoderm differentiation in the mouse embryo. *Dev Biol* 2000;223:77.
182. Clark P, Dziarmaga A, Eccles M, et al. Rescue of defective branching nephrogenesis in renal-coloboma syndrome by the caspase inhibitor, *Z-VAD-fmk*. *J Am Soc Nephrol* 2004;15:299.
183. Cullen-McEwan LA, Caruana G, et al. The where, what and why of the developing renal stroma. *Nephron Exp Nephrol* 2005;99:e1–e8.
184. Loughna S, Yuan HT, Woolf AS. Effects of oxygen on vascular patterning in *Tie1/LacZ* metanephric kidneys in vitro. *Biochem Biophys Res Commun* 1998;247:361.
185. Hyink DP, Tucker DC, St John PL, et al. Endogenous origin of glomerular endothelial and mesangial cells in graft of embryonic kidneys. *Am J Physiol* 1996;270:F886.
186. Davies JA, Garrod DR. Induction of early stages of kidney tubule differentiation by lithium ions. *Dev Biol* 1995;167:50.
187. Kuwertz-Broeking E, Brinkmann OA, Von Lengerke HJ, et al. Unilateral multicystic dysplastic kidney: experience in children. *BJU Int* 2004;93:388.

188. McNeill H, Ozawa M, Kemler R, et al. Novel function of the cell adhesion molecule uvomorulin as an inducer of cell surface polarity. *Cell* 1990;62:309.
189. Gumbiner B, Stevenson B, Grimaldi A. The role of the cell adhesion molecule uvomorulin in the formation and maintenance of the epithelial junctional complex. *J Cell Biol* 1988;107:1575.
190. Sorokin L, Sonnenberg A, Aumailley M, et al. Recognition of the laminin E8 cell-binding site by an integrin possessing the $\alpha 6$ subunit is essential for epithelial polarization in developing kidney tubules. *J Cell Biol* 1990;111:1265.
191. Durbeej M, Larsson E, Ibraghimov-Beskrovnaya O, et al. Non-muscle α -dystroglycan is involved in epithelial development. *J Cell Biol* 1995;130:79.
192. Morris AR, Drawbridge J, Steinberg MS. Axolotl pronephric duct migration requires an epidermally derived, laminin 1-containing extracellular matrix and the integrin receptor $\alpha 6 \beta 1$. *Development* 2003;130:5601.
193. Brandenberger R, Schmidt A, Linton J, et al. Identification and characterization of a novel extracellular matrix protein nephronectin that is associated with integrin $\alpha 8 \beta 1$ in the embryonic kidney. *J Cell Biol* 2001;154:447.
194. Baccalao R. The role of the cytoskeleton in renal development. *Semin Nephrol* 1995;15:285.
195. Musch A. Microtubule organisation and function in epithelial cells. *Traffic* 2004;5:1.
196. Nauli SM, Alenghat FJ, Luo Y, et al. Polycystins 1 and 2 mediate mechanosensation in the primary cilium of kidney cells. *Nat Genet* 2003;33:129.
197. Eley L, Yates LM, Goodship JA. Cilia and disease. *Curr Opin Genet Dev* 2005;15:308.
198. Kispert A, Vainio S, McMahon AP. Wnt-4 is a mesenchymal signal for epithelial transformation of metanephric mesenchyme in the developing kidney. *Development* 1998;125:4225.
199. Jena N, Martin-Seisdedos C, McCue P, et al. BMP7 null mutation in mice: Developmental defects in skeleton, kidney and eye. *Exp Cell Res* 1997;230:28.
200. Zeisberg M, Hanai J, Sugimoto H, et al. BMP-7 counteracts TGF- β 1-induced epithelial-to-mesenchymal transition and reverses chronic renal injury. *Nat Med* 2003;9:964.
201. Cheng HT, Miner JH, Lin M, et al. γ -secretase activity is dispensable for mesenchyme-to-epithelial transition but required for podocyte and proximal tubule formation in developing mouse kidney. *Development* 2003;130:5031.
202. Schwarz K, Simons M, Reiser J, et al. Podocin, a raft-associated component of the glomerular slit diaphragm, interacts with CD2AP and nephrin. *J Clin Invest* 2001;108:1583.
203. Witzgall R. How are podocytes affected in nail-patella syndrome? *Pediatr Nephrol* 2008;23:1017–1020.
204. Maizels M, Simpson SB. Primitive ducts of renal dysplasia induced by culturing ureteral buds denuded of condensed renal mesenchyme. *Science* 1983;219:509.
205. Woolf AS, Davies JA. Cell biology of ureter development. *J Am Soc Nephrol* 2013;24(1):19–25.
206. Santos OFP, Nigam SK. HGF-induced tubulogenesis and branching of epithelial cells is modulated by extracellular matrix and TGF- β . *Dev Biol* 1993;160:293.
207. Zent R, Bush KT, Pohl ML, et al. Involvement of laminin binding integrins and laminin-5 in branching morphogenesis of the ureteric bud during kidney development. *Dev Biol* 2001;238:289.
208. Kiyozumi D, Takeichi M, Nakano I, et al. Basement membrane assembly of the integrin $\alpha 8 \beta 1$ ligand nephronectin requires Fraser syndrome-associated proteins. *J Cell Biol* 2012;197:677–689.
209. Fejes-Toth G, Naray-Fejes-Toth A. Differentiation of renal β -intercalated cells to α -intercalated and principal cells in culture. *Proc Natl Acad Sci U S A* 1992;89:5487.
210. Slotkin TA, Seidler FJ, Kavlock RJ, et al. Fetal dexamethasone exposure accelerates development of renal function: relationship to dose, cell differentiation and growth inhibition. *J Dev Physiol* 1992;17:55.
211. Hikita C, Vijayakumar S, Takito J, et al. Induction of terminal differentiation in epithelial cells requires polymerization of hensin by galectin-3. *J Cell Biol* 2000;151:1235.
212. Gao X, Eladari D, Levieil F, et al. Deletion of hensin/DMBT1 blocks conversion of b- to a-intercalated cells and induces distal renal tubular acidosis. *Proc Natl Acad Sci U S A* 2010;107:21872–21877.
213. Mendelsohn C. Using mouse models to understand normal and abnormal urogenital tract development. *Organogenesis* 2009;5:306–314.
214. Lye CM, Fasano L, Woolf AS. Ureter myogenesis: putting Teashirt into context. *J Am Soc Nephrol* 2010;21:24–30.
215. Ochoa B. Can a congenital dysfunctional bladder be diagnosed from a smile? The Ochoa syndrome updated. *Pediatr Nephrol* 2004;19:6–12.
216. Daly SB, Urquhart JE, Hilton E, et al. Mutations in HPSE2 cause urofacial syndrome. *Am J Hum Genet* 2010;86:963–969.
217. Reddi V, Zaglul A, Pentz ES, et al. Renin-expressing cells are associated with branching of the developing kidney vasculature. *J Am Soc Nephrol* 1998;9:63.
218. Sariola H, Timpl R, von der Mark K, et al. Dual origin of glomerular basement membrane. *Dev Biol* 1984;101:86.
219. Abrahamson DR, Hudson BG, Stroganova L, et al. Cellular origins of type IV collagen networks in developing glomeruli. *J Am Soc Nephrol* 2009;20:1471–1479.
220. Eichmann A, Yuan L, Moyon D, et al. Vascular development: from precursor cells to branched arterial and venous networks. *Int J Dev Biol* 2005;49:259.
221. Woolf AS, Yuan HT. The development of kidney blood vessels. In: Vize PD, Woolf AS, Bard JBL. *The Kidney: From Normal Development to Congenital Disease*. San Diego: Academic Press, 2003:251.
222. Sariola H, Ekblom P, Lehtonen E, et al. Differentiation and vascularisation of the metanephric kidney grafted on the chorioallantoic membrane. *Dev Biol* 1983;96:427.
223. Gao X, Chen X, Taglienti M, et al. Angioblast-mesenchyme induction of early kidney development is mediated by Wt1 and Vegfa. *Development* 2005;132:5437–5449.
224. Kolatsi-Joannou M, Li X, Suda T, et al. Expression and potential role of angiopoietins and Tie-2 in early development of the mouse metanephros. *Dev Dyn* 2001;222:120.
225. Freeburg PB, Robert B, St John PL, et al. Podocyte expression of hypoxia-inducible factor (HIF)-1 and HIF-2 during glomerular development. *J Am Soc Nephrol* 2003;14:927.
226. Simon M, Grone HJ, Jöhren O, et al. Expression of vascular endothelial growth factor and its receptors in human renal ontogenesis and in adult kidney. *Am J Physiol* 1995;268:F240.
227. Bertuccio C, Veron D, Aggarwal PK, et al. Vascular endothelial growth factor receptor 2 direct interaction with nephrin links VEGF-A signals to actin in kidney podocytes. *J Biol Chem* 2011;286:39933–39944.
228. Villegas G, Lange-Sperandio B, Tufto A. Autocrine and paracrine functions of vascular endothelial growth factor (VEGF) in renal tubular epithelial cells. *Kidney Int* 2005;67:449–457.
229. Sariola H, Ekblom P, Henke-Fahle S. Embryonic neurons as in vitro inducers of differentiation of nephrogenic mesenchyme. *Dev Biol* 1989;132:271.
230. Sariola H, Holm K, Henke-Fahle S. Early innervation of the metanephric kidney. *Development* 1988;104:589.
231. Sainio K, Nonclerq D, Saarma M, et al. Neuronal characteristics in embryonic renal stroma. *Int J Dev Biol* 1994;38:77.

Primer on the Pathologic Classification and Diagnosis of Kidney Disease

Renal pathology history 91

The role of the renal biopsy 92

Technical considerations 93

- Risks 93
- Pathologic evaluation 93
- Specimen adequacy 94
- Semiquantitation of pathologic findings 94

Approach to renal diagnosis 94

- Renal syndromes 95
- Identification of the primary site of injury 95

The pathologic diagnosis of glomerular disease 95

- Light microscopic evaluation of glomeruli 97
- Immunohistologic evaluation of glomeruli 98
- Electron microscopic evaluation of glomeruli 99

The pathologic diagnosis of tubular disease 101

- Acute tubular injury 104
- Hyaline droplet change 105
- Vacuolar change 105
- Hemosiderin, other pigments in renal tubular epithelium, and signs of heavy metal poisoning 105
- Viral intranuclear inclusions 106
- Tubulitis 108
- Tubular casts 108
- Tubular atrophy 109
- Mitochondrial abnormalities 109
- Tubular basement membrane changes 109

The pathologic diagnosis of interstitial disease 110

- Primary and secondary interstitial disease 111
- Acute and chronic tubulointerstitial nephritis 111
- Pathologic processes involving the renal interstitium 112

- Edema 112
- Leukocytic infiltrates 112
- Granulomas 112
- Infectious agents 114
- Immune aggregates 114
- Fibrosis 114
- Other causes of interstitial expansion 114

The pathologic diagnosis of renal vascular disease 114

This chapter begins with a very brief history of renal pathology, discusses the role of the renal biopsy in the care of patients with kidney disease, and presents basic concepts of pathologic evaluation of kidney diseases. The emphasis in this chapter is on the pathologic evaluation of native kidney lesions in renal biopsy specimens, and thus is most relevant to the medical renal diseases covered in Chapters 5 through 28. Renal developmental defects and cystic diseases are covered in Chapter 4, renal transplant pathology in Chapter 29, and renal neoplasms in Chapter 30.

RENAL PATHOLOGY HISTORY

Noteworthy elucidation of the clinical and gross pathologic manifestations of kidney disease began during the 19th century with the studies of Bright, Rayer, Rokitansky, von Frerichs, and others (1). Beginning in the second half of the 19th century and extending into the 20th century, Ellis, Fahr, and Klebs made major advances in the pathologic classification of kidney disease using light microscopy on post-mortem specimens. Pioneered by Alwall, Brun, Iverson, and Kark in the 1950s, the renal biopsy allowed access to the early stages of kidney diseases and provided an opportunity to make a pathologic diagnosis that could inform clinical care. By the 1960s, the first modern renal pathologists, including Bergstrand, Churg, Germuth, Habib, McCluskey, and Spargo

were utilizing the newly available techniques of electron microscopy and immunofluorescence microscopy (IFM) to rapidly advance the understanding of kidney diseases and to refine classification and diagnosis. These advances and those that have followed are chronicled in the seven editions to date of the textbook on pathology of the kidney first published by Robert Heptinstall in 1966 (2) and culminating, at least for now, with this seventh edition.

THE ROLE OF THE RENAL BIOPSY

The traditional approach to renal biopsy analysis is to identify the pathology by systematically examining the different histologic compartments (glomeruli, tubules, interstitium, and blood vessels). Once the site and nature of the lesions are determined, the pathologist makes a final diagnosis by integrating the histopathology with IFM and electron microscopy findings, and with clinical information including relevant laboratory data. This chapter serves as a guide to renal biopsy evaluation by focusing on each renal compartment and its pathology in turn, and it refers the reader to detailed discussions of the specific diseases in other chapters of the book.

Several factors make evaluation of renal pathology challenging, especially in renal biopsy specimens. There are a limited number of stereotypic renal responses to injury. In other words, diverse pathogenetic mechanisms may produce a similar morphologic response. As a corollary, only a few findings are pathognomonic in renal pathology such as the reaction of the Congo red stain for amyloid (see Chapter 22), the linear staining for monoclonal immunoglobulin in glomerular and tubular basement membranes (TBMs) in monoclonal immunoglobulin deposition disease (see Chapter 22), and the unique intramembranous dense deposits seen by electron microscopy in dense-deposit disease (DDD) (see Chapter 9). Even the venerable Kimmelstiel-Wilson lesion of diabetic glomerulosclerosis (see Chapter 21) and the fibrils of amyloid seen by electron microscopy (see Chapters 22 and 23) are now subject to differential diagnoses.

The second major problem is the small size of the biopsy, although the amount of tissue that is sufficient for a specific diagnosis is influenced by the disease that is present. For example, one glomerulus with amyloid identified by light or IFM is adequate for a diagnosis of amyloidosis and one glomerulus with the pathognomonic features of DDD by electron microscopy is sufficient for diagnosis. On the other hand, failure to detect glomerular lesions in a small sample with only a few glomeruli does not allow ruling out diseases with focal glomerular lesions, such as focal segmental glomerulosclerosis (FSGS) and pauci-immune focal necrotizing glomerulonephritis. Small sample size also impairs the assessment of the overall severity, activity, and chronicity of the disease, which can be as important in prognostication and therapeutic decisions as is the specific disease diagnosis.

Another problem is that it is not always easy to identify the primary lesion because more than one compartment may be involved by the primary process, secondary processes may intervene, and major findings may be subtle. Finally, progression of many forms of renal injury toward end-stage disease results in nonspecific chronic changes that obscure the nature

of the original pathologic process. As Simeon Burt Wolbach, former Chairman of Pathology at Harvard, noted, "It is often difficult to ascertain the nature of the edifice that has burnt down from a study of the ashes" [quoted in Ref. (3)]. In spite of these problems, the pathologic interpretation of a renal biopsy specimen remains an important guide for the clinician in the diagnosis, prognosis, and therapy of renal disease.

The renal biopsy has been used to identify pathogenetic mechanisms and to establish clinicopathologic correlations between pathologic findings and clinical symptoms. The renal biopsy is frequently necessary to distinguish among diseases with similar clinical presentations. For example, the many diseases that cause the nephrotic syndrome, nephritic syndrome, and acute renal failure (ARF) have vastly different prognostic and therapeutic implications, exemplifying the importance of the renal biopsy in differential diagnosis. Table 3.1 lists clinical manifestations of renal disease that may prompt pathologic evaluation. Traditionally, nonneoplastic renal diseases that are managed primarily by nephrologists (i.e., medical renal diseases) are diagnosed by examination of renal biopsies by renal pathologists (nephropathologists), whereas neoplastic renal diseases and diseases of the urinary tract that are managed primarily by urologists and may lead to partial or complete nephrectomy without prior biopsy are evaluated by urologic pathologists. Table 3.2 lists most of the diseases that should be considered when evaluating native renal biopsy specimens and specifies the chapters in this book that review each category of disease.

The primary role of the renal biopsy is to provide a diagnosis and information about disease activity and chronicity that allow the clinician to make an informed prognosis and choose the optimal therapy. In some instances, a specific cause of the renal injury may be identified by pathologic examination or suggested by the pathologic findings and subsequently confirmed clinically. This may lead to elimination of the cause and resolution of the disease. Determination of the relative amount

TABLE 3.1 Clinical manifestations of renal disease

Microalbuminuria
Subnephrotic proteinuria
Nephrotic-range proteinuria
Nephrotic syndrome
Asymptomatic hematuria
Microhematuria
Macrohematuria (gross hematuria)
Acute nephritis
Rapidly progressive glomerulonephritis
Hypertension
Thrombotic microangiopathy
Acute kidney injury
Chronic renal failure
Urinary tract infection
Urinary tract obstruction
Nephrolithiasis
Renal malformation/cysts
Renal tumor
Renal transplant dysfunction

TABLE 3.2 Native kidney diseases encountered in renal biopsy specimens from patients with medical renal native kidney disease

Disease	Chapter
Glomerular and vascular diseases	
Minimal change disease	5
Focal segmental glomerulosclerosis	6
IgM nephropathy	6
C1q nephropathy	6
Diffuse mesangial sclerosis	5
Finnish-type congenital nephrotic syndrome	5
Membranous glomerulonephritis	7
Membranoproliferative glomerulonephritis	8
Dense-deposit disease	9
C3 glomerulonephritis (GN)	9
Cryoglobulinemic GN	22
IgA nephropathy	12
IgA vasculitis (Henoch-Schönlein purpura)	12
Acute postinfectious GN	10
IgA-dominant postinfectious GN	10
Infectious GN	10
Lupus nephritis	14
Anti-GBM disease	15
ANCA disease	16
Polyarteritis nodosa or other arteritis	17
Diabetic glomerulosclerosis	21
Idiopathic nodular glomerulosclerosis	21
Smoking-related nodular glomerulosclerosis	21
Monoclonal immunoglobulin deposition disease	22
Amyloidosis	22
Fibrillary GN	23
Immunotactoid glomerulopathy	23
Fibronectin glomerulopathy	23
Collagenofibrotic glomerulopathy	13
Alport syndrome/hereditary nephritis	13
Thin basement membrane lesion/nephropathy	13
Preeclampsia/eclampsia	19
Thrombotic microangiopathy (TTP and HUS)	18
Arterionephrosclerosis (hypertensive nephrosclerosis)	20
Renal artery stenosis atrophy (endocrinzation)	20
Atheroembolization (cholesterol embolization)	20
Calcineurin inhibitor toxicity	29
Fabry disease	27
LCAT deficiency	27
Lipoprotein glomerulopathy	27
Sickle cell glomerulopathy	27
Tubulointerstitial diseases	
Acute tubular injury	26
Acute tubular necrosis	26
Cortical necrosis/infarct (focal or diffuse)	26
Light chain (myeloma) cast nephropathy	22
Light chain tubulopathy (light chain Fanconi syndrome)	22
Myoglobin/hemoglobin cast nephropathy	26
Nephrocalcinosis/nephrolithiasis	24
Phosphate nephropathy	24
Oxalosis	27
Acute TIN	25

TABLE 3.2 Native kidney diseases encountered in renal biopsy specimens from patients with medical renal native kidney disease (*Continued*)

Disease	Chapter
Acute pyelonephritis	24
Chronic pyelonephritis/reflux nephropathy	24
Xanthogranulomatous or malacoplakia TIN	24
Granulomatous tubulointerstitial nephritis	24
IgG4 related disease	24
Chronic tubulointerstitial nephritis NOS	24
Nephronophthisis/medullary cystic disease	4
End-stage kidney	28

GN, glomerulonephritis; GBM, glomerular basement membrane; ANCA, antineutrophil cytoplasmic autoantibody; TTP, thrombotic thrombocytopenic purpura; HUS, hemolytic uremic syndrome; LCAT, lecithin cholesterol acyltransferase.

of acute, potentially reversible injury versus irreversible scarring, which may not be apparent from the clinical findings, is equally important. In cases with advanced chronic injury, the decision not to treat lesions that are deemed to be too advanced to respond to therapy may be based on the renal biopsy findings. Furthermore, renal biopsy is the only way to recognize and describe some new renal diseases, for example, the adverse effects of new drugs. Finally, renal biopsy is required in clinical trials to ensure that the disease process and the disease severity are comparable among the study groups and to serve as a baseline for evaluating therapeutic efficacy.

TECHNICAL CONSIDERATIONS

Risks

The clinician must balance the information to be gained and its impact on patient care against the risks associated with a renal biopsy; however, renal biopsy using the spring-loaded biopsy gun with ultrasound guidance is a very safe procedure (4). Following a biopsy procedure, microscopic hematuria occurs in about 35% of patients, but gross hematuria is seen in less than 0.5%. A perirenal hematoma is identified in approximately 65% of patients, depending upon the diligence of the search. Transfusion is required as a consequence of less than 1% of biopsies and nephrectomy in less than 0.1%. Mortality is extremely rare. To obtain optimal tissue for pathologic evaluation without increased morbidity, 14- or 16-gauge needles are recommended for renal biopsies in adults and 16- or 18-gauge needles in children younger than 8 years old (4).

Pathologic Evaluation

Light microscopic morphology is assessed on 2- to 3- μ m histologic sections stained routinely with hematoxylin and eosin, methenamine silver–periodic acid (Jones stain), Masson trichrome, and periodic acid–Schiff (PAS) (5). Congo red and thioflavin T for amyloid may be used routinely or only when amyloidosis is suspected based on clinical or pathologic findings. An immunohistology technique (either immunofluorescence

or immunoperoxidase) to demonstrate deposits of immunoglobulins (IgG, IgM, IgA, kappa, and lambda light chains) and complement components (C3 and C1q) is required for adequate pathologic evaluation (5). Electron microscopy is a valuable adjunct that is required for the diagnosis of some diseases, such as fibrillary glomerulonephritis and thin basement membrane nephropathy, and may reveal a diagnosis that was unsuspected after light and IFM examination, such as Fabry disease or hereditary nephritis. In addition, several special techniques are recommended, such as special immunohistochemistry for infectious pathogens (e.g., BK virus) and cell types (e.g., B lymphocytes versus T lymphocytes), and ultrastructural morphometric techniques to measure basement membrane thickness and the diameter of abnormal fibrils or microtubules. Renal biopsies should be processed only in laboratories that are proficient in the performance and interpretation of these tests (5).

Specimen Adequacy

How much renal tissue is necessary for a pathologic diagnosis is a complex question, and the answer depends on the indication for biopsy. If the differential diagnosis includes diseases defined by immunohistology or ultrastructure, tissue must be processed for these studies as well as for light microscopy. A single glomerulus may be sufficient for the diagnosis of diffusely distributed glomerular diseases with specific pathologic features, such as amyloidosis or membranous glomerulonephritis. However, in many cases, specimen adequacy is a statistical consideration of the number of glomeruli required to answer either of two questions. First, how many glomeruli are required to exclude focal pathology? Second, what proportion of the glomeruli is involved? A discussion of these questions follows.

Diagnosis of diseases involving only a proportion of the total number of glomeruli (focal) requires the demonstration of only one abnormal glomerulus, and the relevant question is how many normal glomeruli are needed to confidently exclude focal pathology. Assuming that the disease is randomly distributed among the glomeruli, the glomeruli are independently affected, and the glomerular sample is random, the probability of finding any number of abnormal glomeruli in the renal biopsy can be represented by the binomial equation (6). The number of abnormal glomeruli in the biopsy is a function of the sample size and the proportion of abnormal glomeruli in the kidney (6). In a kidney with 10% glomerular involvement, a biopsy containing 10 glomeruli will have a 35% chance of having no abnormal glomeruli, but when glomerular involvement is 35%, the chance of finding no abnormal glomeruli in a biopsy with 10 glomeruli is less than 5%. Thus, a biopsy with few glomeruli cannot exclude focal disease with a low proportion of glomerular involvement, and the minimal sample needed to exclude focal disease present in fewer than 10% of the glomeruli with greater than 90% confidence is at least 20 glomeruli. Complicating the issue of adequate sampling is the possibility of segmental involvement of an individual glomerulus, defined as involvement of only a portion of the glomerular tuft area. This is particularly important in such diseases as FSGS, lupus nephritis, and pauci-immune focal crescentic glomerulonephritis, where careful serial sectioning of the biopsy increases the diagnostic yield. Most renal pathologists section each biopsy with 20 or more serial sections to maximize the likelihood of identifying such focal renal lesions.

Assignment of patients to groups (stratification) based on the proportion of abnormal glomeruli in the biopsy is a more complex problem. For example, the distribution of abnormal glomeruli found in biopsies from patients with systemic lupus erythematosus (SLE) with mild focal (less than 20%), moderate focal (20% to 50%), and diffuse (50% or more) glomerular involvement can be calculated from the binomial equation (6). Small differences between groups (e.g., 10%) require more than 100 glomeruli to achieve statistical significance, and a minimum of 20 to 25 glomeruli is necessary to detect relatively large differences (25% to 40%).

In study design, the limitations of morphologic stratification must be appreciated or incorrectly classified patients will dilute the study outcomes. The inclusion of patients from a good prognosis group in a bad prognosis group will improve the outcome in both groups without changing the overall incidence of bad outcomes. Attention to the statistical rules will lead to results that are internally consistent within groups and reliably different between groups. A final caveat is that observations made on the even more limited samples studied by electron microscopy should be extrapolated to the whole kidney cautiously. Because of the need for integration of information gleaned from all three modalities of biopsy workup, it is important for the same pathologist to evaluate the findings by light microscopy, immunofluorescence, and electron microscopy.

Semiquantitation of Pathologic Findings

Pirani et al. (7) pioneered the use of semiquantitative renal pathologic changes “to force the pathologist to look at all elements of renal histology” in a systematic fashion. This approach was used in the context of lupus glomerulonephritis to develop indices of disease activity and chronicity based on semiquantitative observations (8). Additional examples of systematic approaches to semiquantitative evaluation in renal pathology are exemplified in the Banff classification for renal allograft pathology (9,10) and the Oxford classification for IgA nephropathy (11,12).

Certain quantitative and semiquantitative features should be included in every biopsy report, including the number of glomeruli; the number of glomeruli with specific lesions; the amount of mesangial matrix and an assessment of glomerular cellularity (in the mesangial, endocapillary and extracapillary zones of the glomerular corpuscle); the proportion of the biopsy occupied by interstitial inflammatory infiltrates, interstitial fibrosis, and tubular atrophy; and the distribution and intensity of immune deposits.

APPROACH TO RENAL DIAGNOSIS

The complex microscopic anatomy of the kidney necessitates an examination of all the histologic elements (glomeruli, tubules, interstitium, and blood vessels) in multiple serial sections to avoid missing pathologic lesions. Anatomic complexity results from organization of the glomeruli and their tubules into functional units, the nephrons. Their organized distribution in the kidney underlies the characteristic histologic appearance of the cortex, the medulla, and the tubules in the cortical labyrinth and the medullary rays. Glomerular, tubular, and vascular relationships are important. The afferent arteriole perfuses the glomerulus directly, and the cortical tubules are supplied

by postglomerular efferent arterioles that are distributed to several adjacent nephrons (see Chapter 1). Following complete glomerular sclerosis, blood flow and glomerular filtration cease, and the dependent tubules undergo both ischemic and functional atrophy with adjacent interstitial fibrosis. Such secondary tubulointerstitial changes should not be mistaken for primary tubulointerstitial disease. Likewise, primary vascular disease can cause secondary changes in glomeruli and tubules. Because of the anatomic interdependence of the tissue compartments of the kidney, determining which compartment—glomeruli, tubules, interstitium, or vessels—was the initial target of injury is often difficult, if not impossible, in specimens with advanced chronic changes affecting all compartments. An approach that weighs the severity of injury in each compartment is often helpful; disproportionately severe injury is usually found in the compartment that bore the original pathologic insult.

When evaluating renal pathology associated with chronic nephron loss, one must be cognizant of renal adaptive mechanisms. Reduction in renal mass causes compensatory hypertrophy as single-nephron glomerular filtration rate increases in remnant nephrons to maintain homeostasis. This leads to a mixture of hypertrophied functioning glomeruli and tubules, and atrophic nonfunctioning nephrons in chronic renal disease. The kidney can compensate for irreversible damage by hypertrophy and hyperfunction of surviving nephrons, but these adaptive changes may result in secondary, maladaptive injury, such as the development of FSGS.

Renal Syndromes

Clinical syndromes, laboratory abnormalities, or imaging abnormalities are convenient starting points for the identification and evaluation of diseases of the kidney and urinary tract (see Table 3.1). They narrow the differential diagnosis and facilitate the deductive reasoning that leads to a specific diagnosis. The syndromes related to injury to glomerular capillaries (acute nephritis, nephrotic syndrome, asymptomatic hematuria, asymptomatic proteinuria, and rapidly progressive glomerulonephritis) are quite specific for glomerular disease, and they are helpful in the differential diagnosis. In contrast, the clinical presentations of diseases targeting the tubules, interstitium, and blood vessels seen in renal biopsies tend to be less specific. Because they often have a nonspecific presentation of acute or chronic renal insufficiency, the renal biopsy may be the only means to diagnose these conditions. Finally, some diseases, such as SLE, may have more than one presentation with different syndromes or a mixture of syndromes. In addition, a particular clinical presentation may not reflect the severity of the underlying pathology. For example, a patient with lupus nephritis may have mild hematuria, low-level proteinuria, and normal serum creatinine although the renal biopsy reveals a severe active lupus glomerulonephritis that requires immediate institution of immunosuppressive therapy.

Identification of the Primary Site of Injury

In renal disease diagnosis, identifying which renal compartment is the primary site of injury is the most basic decision and is the first step in determining the pathologic diagnosis and classification of renal disease. Because of the complicating factors discussed previously, including the complexity of renal microscopic anatomy, involvement of more than one compartment in some diseases, and superimposed chronic and

compensatory changes, this decision is often difficult and benefits from extensive experience.

Primary involvement of each histologic compartment has characteristic histopathology with or without distinctive immunohistologic or ultrastructural features. For example, disease affecting the glomeruli exhibits histologic signs of inflammation including hypercellularity, infiltrating leukocytes, fibrinoid necrosis, segmental sclerosis, glomerular basement membrane (GBM) remodeling, immune deposits by immunohistology, or diagnostic findings by electron microscopy such as immune complex-type deposits, fibrillary deposits, microtubular deposits or GBM abnormalities. Likewise, interstitial inflammation, tubular epithelial simplification or necrosis, and vascular sclerosis, hyalinosis, inflammation, necrosis, or thrombosis are characteristic of interstitial, tubular, and vascular diseases, respectively. Primary injury in each compartment may be associated with secondary changes in the others, and the assignment of primary injury assumes a hierarchic relationship among the compartments. Thus, when glomerular injury is associated with changes in the tubules, interstitium, and blood vessels, the glomerular lesion is usually primary because of known relationships between the glomerular efferent blood supply, tubular perfusion, glomerular injury, and hypertensive vascular disease. In contrast, because the tubules and interstitium are vulnerable to secondary changes, the presence of glomerular and vascular injury raises the possibility that the tubular and interstitial disease is secondary rather than primary. After evaluating the renal biopsy and integrating the pathologic findings with the clinical presentation and laboratory data, the nephropathologist usually is able to identify the primary site of disease.

THE PATHOLOGIC DIAGNOSIS OF GLOMERULAR DISEASE

Glomerular diseases are the pathologic processes most often identified in renal biopsy specimens from native kidneys (Table 3.3) (13). The complexity and variety of glomerular diseases pose a considerable challenge for the pathologist. Glomerular diseases have a broad variety of clinical presentations including asymptomatic hematuria, asymptomatic proteinuria, nephrotic syndrome, acute nephritis, rapidly progressive nephritis, ARF, and chronic renal failure. Pathologic evaluation of a glomerular disease by light microscopy rarely allows a definitive diagnosis. More often than not, immunohistology or electron microscopy or both are required to reach the most definitive and clinically useful diagnosis. Glomerular lesions often evolve over time, for example, as active inflammatory lesions transform into chronic sclerotic lesions. Knowledge of these dynamic transitions is important not only for diagnosis but also for prognostication, which involves assessment of the activity and chronicity of disease at the time of biopsy. Further complicating the pathologic diagnosis of glomerular diseases is the frequent concurrence of secondary pathologic changes in the tubules, interstitium, and extraglomerular vessels that may be even more conspicuous than are the primary glomerular changes.

Renal biopsy reports should use widely accepted descriptive terminology in describing glomerular pathology (Table 3.4) as well as widely accepted diagnostic terminology (see Tables 3.2

TABLE 3.3 **Relative frequency of various diagnoses among 7257 native kidney biopsy specimens evaluated in the University of North Carolina Nephropathology Laboratory**

Diseases that typically cause the nephrotic syndrome (40% of all renal biopsy specimens, $n = 2922$)

- Focal segmental glomerulosclerosis (all variants) ($n = 920$)
- Idiopathic membranous glomerulonephritis ($n = 847$)
- Minimal change glomerulopathy ($n = 398$)
- Diabetic glomerulosclerosis ($n = 246$)
- Type I membranoproliferative glomerulonephritis ($n = 190$)
- Amyloidosis ($n = 108$)
- C1q nephropathy ($n = 99$)
- Fibrillary glomerulonephritis ($n = 59$)
- Monoclonal immunoglobulin deposition disease ($n = 26$)
- Dense-deposit disease and C3 glomerulonephritis ($n = 14$)
- Preeclampsia/eclampsia ($n = 6$)
- Immunotactoid glomerulopathy ($n = 6$)
- Collagenofibrotic glomerulopathy ($n = 3$)

Diseases that typically cause hematuria and nephritis (29% of biopsies, $n = 2109$)

- Lupus nephritis (all classes) ($n = 636$)
- IgA nephropathy ($n = 538$)
- Idiopathic immune complex proliferative glomerulonephritis ($n = 375$)
- Pauci-immune/antineutrophil cytoplasmic autoantibody (ANCA) glomerulonephritis ($n = 301$)
- Postinfectious acute diffuse proliferative glomerulonephritis ($n = 86$)
- Thin basement membrane lesion or nephropathy ($n = 82$)
- Antiglomerular basement membrane antibody (anti-GBM) disease ($n = 56$)
- Alport syndrome/hereditary nephritis ($n = 35$)

Diseases other than glomerulonephritis that typically cause ARF (5% of biopsies, $n = 371$)

- Thrombotic microangiopathy (all types) ($n = 126$)
- Acute TIN ($n = 101$)
- Acute tubular epithelial injury ($n = 69$)
- Atheroembolization ($n = 34$)
- Light chain cast nephropathy ($n = 31$)
- Cortical necrosis ($n = 10$)

Diseases other than those already listed that typically manifest as chronic renal failure (8%, $n = 583$)

- Arterionephrosclerosis ($n = 229$)
- Chronic sclerosing glomerulonephritis ($n = 166$)
- End-stage kidney not otherwise specified ($n = 114$)
- Chronic TIN ($n = 74$)
- Miscellaneous other diseases ($n = 344$)

Adequate tissue with nonspecific abnormalities (5%, $n = 370$)

- No pathologic lesion identified (2%, $n = 141$)
- Inadequate tissue for definitive diagnosis (6%, $n = 417$)

These were the frequencies of these diseases in patients who were selected for renal biopsy and thus are different from the frequencies of these diseases among all patients with a particular clinical presentation.

Modified from Jennette JC, Falk RJ. Glomerular clinicopathologic syndromes. In: Greenberg A, Cheung AK, Coffman TM, et al., eds. *National Kidney Foundation Nephrology Primer*, 5th ed. San Diego: Academic Press, 2009:148.

TABLE 3.4 **Glossary of terms used to describe histologic lesions in glomeruli**

Term	Definition
Focal	Involving <50% of glomeruli
Diffuse	Involving $\geq 50\%$ of glomeruli
Segmental	Involving part of a glomerular tuft
Global	Involving all of a glomerular tuft
Mesangial hypercellularity	Four or more nuclei in the contiguous matrix of a peripheral mesangial segment
Endocapillary hypercellularity	Increased cellularity internal to the GBM composed of leukocytes, endothelial cells, and mesangial cells
Lobular	Consolidated expansion of glomerular segments representing major anatomic subunits (lobules) of the glomerular tuft formed by dichotomous branchings of the afferent arteriole. (hypersegmentation)
Extracapillary hypercellularity	Increased cellularity in Bowman space or more than one layer of parietal or visceral epithelial cells
Crescent	Extracapillary hypercellularity other than the epithelial hyperplasia of the collapsing variant of FSGS, often accompanied by fibrin extravasation into Bowman space.
Fibrinoid necrosis	Lytic destruction of cells and matrix with deposition of acidophilic fibrin-rich material and often accompanied by GBM rupture and apoptosis of infiltrating leukocytes
Mesangiolytic	Detachment of the paramesangial GBM from the mesangial matrix resulting in a capillary aneurysm, or lytic dissolution of the mesangial matrix
Sclerosis	Increased collagenous extracellular matrix that is expanding the mesangium, obliterating capillary lumens, or forming adhesions to Bowman capsule
Hyaline	Glassy acidophilic extracellular material

and 3.3). To complicate matters further, the pattern of injury observed in a renal biopsy specimen is a snapshot of a dynamic process of glomerular injury in a patient who may have different patterns of glomerular injury over time (Fig. 3.1) (14). For example, a patient with IgA nephropathy or a patient with lupus nephritis may have a mild mesangial proliferative glomerulonephritis early in the course of disease that evolves into a focal proliferative glomerulonephritis with more destructive segmental lesions, and still later progresses to a diffuse proliferative glomerulonephritis that ultimately results in chronic sclerosing glomerulonephritis.

Because each light microscopic pattern of glomerulonephritis can have many different causes with very different prognoses, recognition of the specific cause of the injury in a given specimen is as important as, if not more important than, categorizing the light microscopic phenotype. For example, consider focal glomerulonephritis caused by IgA nephropathy versus lupus nephritis versus antineutrophil cytoplasmic

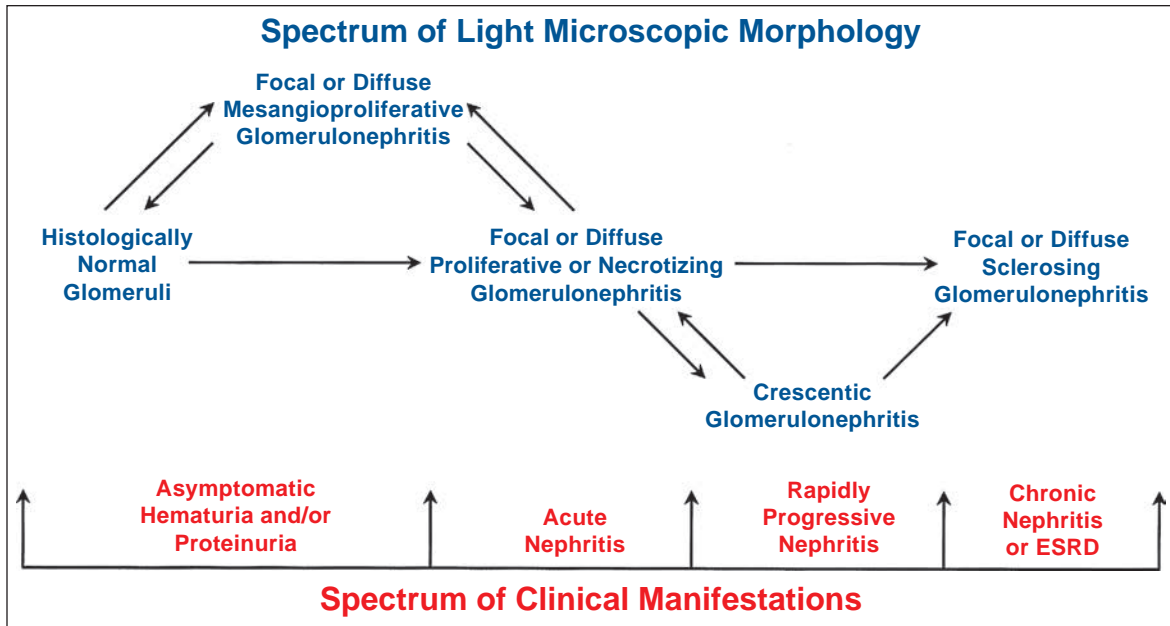


FIGURE 3.1 Diagram showing the correlation of various histopathologic patterns of glomerular response to injury correlated with the usual clinical manifestations of renal injury caused by the injury. Also depicted with arrows are possible transformations in the light microscopic expressions of glomerular inflammation over time. Many different specific categories of glomerulonephritis can cause these histologic expressions of inflammatory injury (e.g., IgA nephropathy and lupus nephritis). (Modified from Jennette JC, Falk RJ. Diagnosis and management of glomerular diseases. *Med Clin North Am* 1997;81:653.)

antibodies (ANCA) glomerulonephritis; each has a very different prognosis and very different lesion-specific treatment. Likewise, recognition of crescentic glomerulonephritis by light microscopy does little more than confirm the clinical impression of rapidly progressive glomerulonephritis. The more important determination is detection of the cause of the crescentic glomerulonephritis by integration of data from light microscopy, IFM electron microscopy, serology, and other laboratory and clinical observations. The algorithm in Figure 3.2 demonstrates some of the observations by immunofluorescence and electron microscopy that are useful in resolving the differential diagnosis in a patient who has light microscopic evidence for glomerulonephritis. Bear in mind that an optimal approach to pathologic diagnosis of a glomerular disease is based not only on identifying the presence of features that are indicative of a specific disease but also on noting the absence of features that are indicative of alternative diseases.

Glomerular diseases occur not only as diseases that primarily target the kidneys but also as components of systemic diseases. For example, glomerular disease can be secondary to SLE, diabetes mellitus, amyloidosis, monoclonal immunoglobulin deposition disease, hypertension, and systemic vasculitis such as ANCA vasculitis, IgA vasculitis (Henoch-Schönlein purpura) or cryoglobulinemic vasculitis. Thus, once a distinct pattern of glomerular injury is identified, the possibility of a secondary rather than a primary process must be considered. For example, is IgA-dominant immune complex disease IgA nephropathy (a primary process) or secondary to IgA vasculitis or to staphylococcal infection? Likewise, is type I membranoproliferative glomerulonephritis (MPGN) an idiopathic (primary) process or secondary to an identifiable cause, such

as cryoglobulinemia, hepatitis B infection, subacute bacterial endocarditis, monoclonal IgG, C3 glomerulopathy, and so forth? The distinction between primary and secondary disease often requires knowledgeable integration of information not only from the light, immunofluorescence, and electron microscopy observations but also from clinical and laboratory data. As much as any other anatomic pathology subspecialty, and more than most, optimal diagnosis of pathologic findings in kidney specimens requires careful correlation with clinical data. To complicate matters further, some glomerular diseases coexist, producing dual glomerulopathies. This situation is particularly applicable to common conditions. For example, membranous glomerulonephritis or pauci-immune focal crescentic glomerulonephritis may occur superimposed on diabetic nephropathy. Thus, the pathologist should always remain open-minded to the possibility of superimposed diseases, especially when confronted with disparate pathologic changes that cannot be explained by a single disease process.

Light Microscopic Evaluation of Glomeruli

Refer to Chapter 1 for a more detailed description of glomerular structure than in the following summary. A glomerulus is composed of a tuft of capillaries supported by a mesangial core. Podocytes (visceral epithelial cells) cover the urinary surface of the capillaries and mesangium. Podocytes are continuous at the glomerular hilum with the parietal epithelium that covers Bowman capsule, which transition at the tubular pole into the epithelium of the proximal tubule. Each glomerulus has an endocapillary compartment and an extracapillary compartment separated by the GBM. The endocapillary compartment includes the endothelial cells, mesangial cells, and any leukocytes in the capillary lumens or mesangium. Normally,

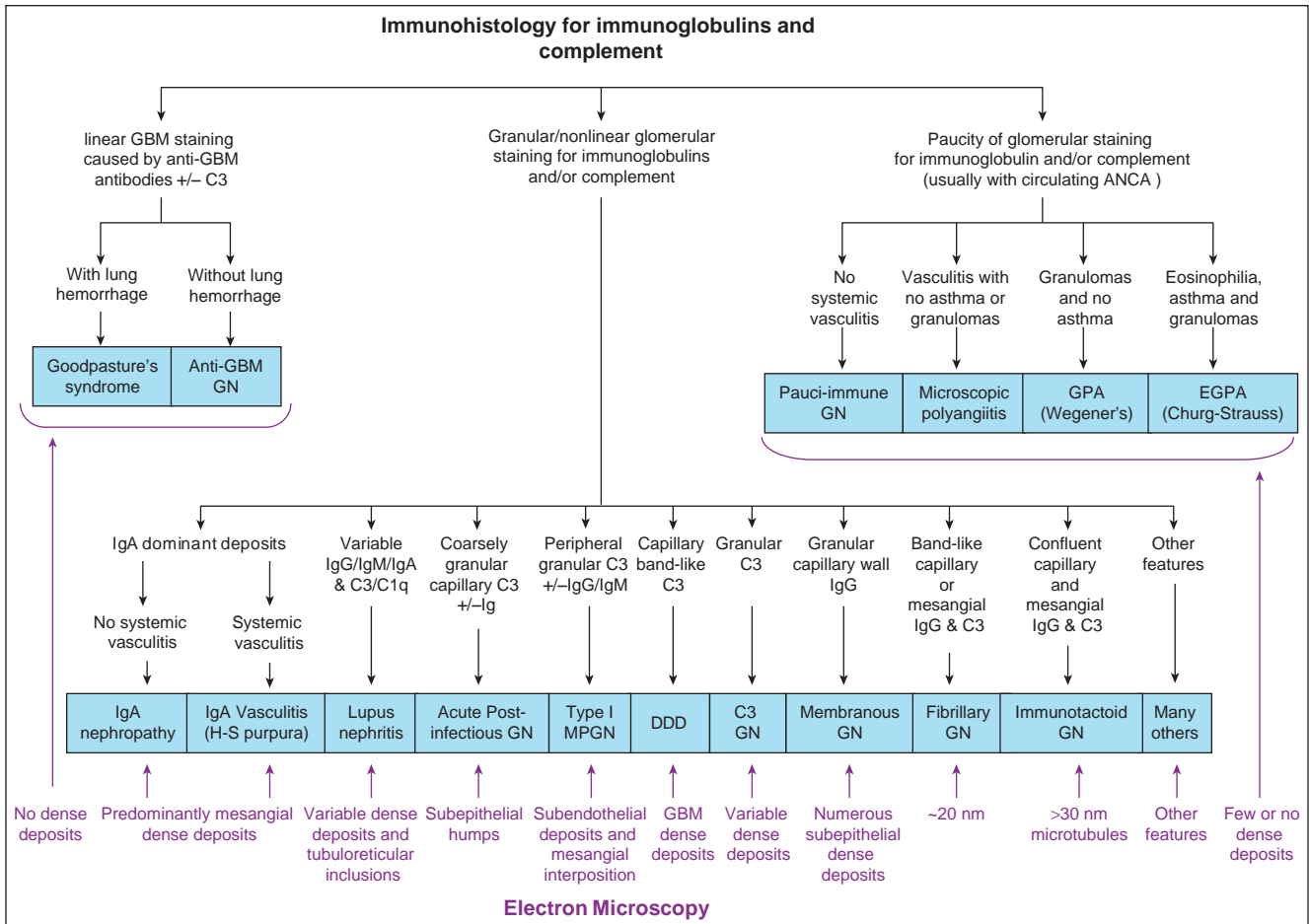


FIGURE 3.2 Algorithm for diagnosing immune-mediated glomerular diseases based on integration of IFM electron microscopy, serology, and other laboratory and clinical data. (Modified from Jennette JC, Falk RJ. Diagnosis and management of glomerular diseases. *Med Clin North Am* 1997;81:653.) GBM: glomerular basement membrane, GN: glomerulonephritis, ANCA: anti-neutrophil cytoplasmic autoantibodies, GPA: granulomatosis with polyangiitis, EGPA: eosinophilic granulomatosis with polyangiitis, H-S: Henoch-Schonlein, MPGN: membranoproliferative GN, DDD: dense deposit disease

in a 2- to 3- μm histologic section, there are no more than one (or rarely two) endothelial nuclei per capillary lumen and no more than three nuclei in a peripheral segment of contiguous mesangial matrix. The mesangium coalesces at the vascular pole of the glomerulus, and there may be more nuclei in the contiguous matrix at this location. The extracapillary compartment includes the visceral and parietal epithelial cells and any cells within Bowman space. Normally, there is a single layer of podocytes and parietal epithelial cells, and no cells in Bowman space. The normal glomerulus contains distinct extracellular matrix domains that comprise the GBM, the mesangial matrix, and the basement membrane of Bowman capsule.

Light microscopic evaluation of the glomerulus requires careful examination of each glomerulus for any abnormalities in overall architecture with special attention to increased or decreased cellularity and increased, disrupted, or altered extracellular matrix. Table 3.4 provides a glossary of conventional descriptive terms for glomerular histologic abnormalities, and some of the most common patterns of injury are illustrated in Figure 3.3. Light microscopic descriptions of glomerular lesions should include an indication of the type of injury (e.g.,

endocapillary hypercellularity), the distribution within glomeruli (e.g., segmental versus global), and the involvement among glomeruli (focal versus diffuse). Table 3.5 lists several major histologic expressions of glomerular pathology and the diseases that can produce these patterns of injury. Note that each pattern of injury can be caused by multiple glomerular diseases and that most glomerular diseases can manifest as more than one pattern of injury. In most instances, immunohistology and/or electron microscopy are required to make specific pathologic diagnoses (see Fig. 3.2).

Immunohistologic Evaluation of Glomeruli

In the evaluation of glomerular diseases, immunohistology usually is directed at the identification of pathogenic immunoglobulin and complement molecules. Either immunofluorescence or immunoenzyme microscopy can be used to determine the distribution, pattern, and composition of glomerular immune deposits (Fig. 3.4). Antibodies that are used routinely in the evaluation of glomerular diseases include antibodies specific for IgG, IgA, IgM, kappa light chains, lambda light chains, C3, C1q, and fibrin/fibrinogen. Many pathologists also use antibody to albumin, which is useful to highlight the tissue

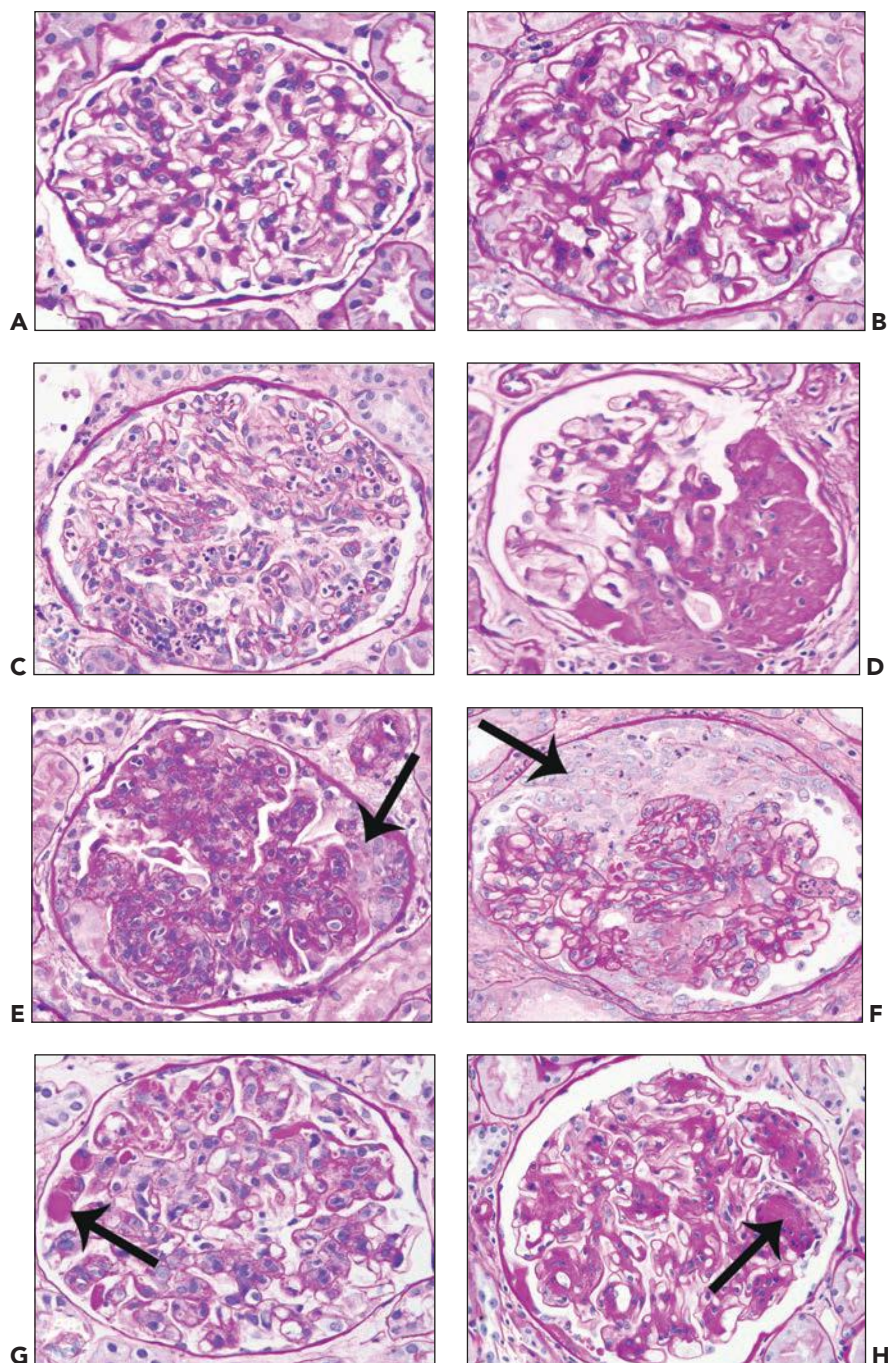


FIGURE 3.3 Patterns of glomerular injury observed by light microscopy in PAS-stained sections. **A:** Normal glomerulus with thin GBMs, scanty mesangial matrix, and normal cellularity. **B:** Membranous glomerulonephritis with thickened GBMs compared with the normal glomerulus and normal cellularity. **C:** Postinfectious acute diffuse proliferative glomerulonephritis with global endocapillary hypercellularity including numerous neutrophils in capillary lumens. **D:** FSGS with perihilar segmental sclerosis. **E:** Diffuse proliferative glomerulonephritis with global endocapillary hypercellularity and slight extracapillary hypercellularity (crescent formation) (*arrow*). **F:** ANCA-associated pauci-immune necrotizing and crescentic glomerulonephritis with a cellular crescent (*arrow*). **G:** Cryoglobulinemic glomerulonephritis with endocapillary hypercellularity and several hyaline thrombi (*arrow*). **H:** Diabetic glomerulosclerosis with global mesangial matrix expansion and segmental nodules (*arrow*).

architecture because of its low-level staining of renal basement membranes and staining of protein resorption droplets in tubules and podocytes in proteinuric conditions. The glomerular and extraglomerular location, intensity, and pattern of staining are observed, recorded, and reported. Glomerular staining is categorized as mesangial or capillary wall or both. As with light microscopic lesions, the distribution is described as focal or diffuse, and segmental or global. Capillary wall staining is described as granular, linear, or bandlike. The location of the capillary wall staining in the GBM (intramembranous), between the GBM and the podocytes (subepithelial), or between the GBM and endothelial cells (subendothelial) sometimes can be discerned. Some diseases, such as IgA

nephropathy and anti-GBM disease, can only be diagnosed by immunohistology, whereas the diagnosis of other diseases is confirmed or refined by immunohistology. The top half of the algorithm in Figure 3.2 shows how different observations by IFM can guide the resolution of the differential diagnosis in a patient with glomerular diseases.

Electron Microscopic Evaluation of Glomeruli

Nephropathology is the only anatomic pathology subspecialty that uses transmission electron microscopy for routine evaluation of specimens. Electron microscopy allows detailed evaluation of the cellular and extracellular contents of each glomerular compartment and assessment of the thickness, contour, and integrity

TABLE 3.5 Patterns of glomerular injury observed by light microscopy and some but not all of the diseases that can cause each pattern of injury

No abnormality by light microscopy

No glomerular disease
Glomerular disease with no light microscopic changes (e.g., minimal change disease, thin basement membrane nephropathy)
Mild or early glomerular disease (e.g., lupus nephritis, IgA nephropathy, C1q nephropathy, membranous glomerulonephritis, amyloidosis, Alport syndrome, etc.)

Thick capillary walls without hypercellularity or mesangial expansion

Membranous glomerulonephritis (primary or secondary) with thick GBM
Thrombotic microangiopathy with expanded subendothelial zone
Preeclampsia/eclampsia with endothelial swelling
Fibrillary glomerulonephritis with predominance of capillary wall deposits

Thick walls with mesangial expansion but little or no hypercellularity

Diabetic glomerulosclerosis with diffuse rather than nodular sclerosis
Secondary membranous glomerulonephritis with mesangial immune deposits
Amyloidosis
Monoclonal immunoglobulin deposition disease
Fibrillary glomerulonephritis
Dense-deposit disease
C3 glomerulonephritis

Focal segmental glomerular sclerosis without hypercellularity

Focal segmental glomerulosclerosis
Chronic sclerotic phase of focal glomerulonephritis
Hereditary nephritis (Alport syndrome)

Mesangial or endocapillary hypercellularity

Focal or diffuse mesangioproliferative glomerulonephritis^a
Focal or diffuse (endocapillary) proliferative glomerulonephritis^a
Acute diffuse proliferative postinfectious glomerulonephritis
Membranoproliferative glomerulonephritis
Dense-deposit disease

Extracapillary hypercellularity

ANCA crescentic glomerulonephritis (paucity of immunoglobulin by IFM)
Anti-GBM crescentic glomerulonephritis (linear immunoglobulin by IFM)
Immune complex and C3 glomerulopathy crescentic glomerulonephritis (granular immunoglobulin and/or complement by IFM)
Collapsing variant of FSGS (including HIV nephropathy)

Membranoproliferative, lobular, or nodular pattern

Membranoproliferative glomerulonephritis
Dense-deposit disease
C3 glomerulonephritis
Diabetic glomerulosclerosis with nodular mesangial expansion (KW nodules)

TABLE 3.5 Patterns of glomerular injury observed by light microscopy and some but not all of the diseases that can cause each pattern of injury (*Continued*)

Monoclonal immunoglobulin deposition disease with nodular sclerosis
Thrombotic microangiopathy
Fibrillary glomerulonephritis
Immunotactoid glomerulopathy

Advanced diffuse global glomerular sclerosis

End-stage glomerular disease
End-stage vascular disease
End-stage tubulointerstitial disease

A specific disease (e.g., lupus nephritis or IgA nephropathy) can cause more than one pattern of injury.

^aEach pattern could be caused by IgA nephropathy, lupus nephritis, postinfectious glomerulonephritis, and so forth.

of the GBM and mesangial matrix (Figs. 3.5 to 3.8). Abnormal deposits, such as electron-dense immune deposits (Figs. 3.5 and 3.6), or organized fibrillary or microtubular deposits, can be detected in subepithelial, intramembranous, and mesangial locations (see Figs. 3.5 to 3.8). Diagnostically informative ultrastructural abnormalities in GBMs include thickening, thinning, lamellation, and subendothelial electron-lucent expansion (see Fig. 3.7). Glomerular deposits with an organized (patterned) substructure are pathognomonic in some circumstances or at least narrow the differential diagnosis substantially (see Fig. 3.7 and Chapter 23). Abnormalities in cells can be readily detected, such as the effacement of podocyte foot processes seen with proteinuria or the swelling of endothelial cells seen with eclampsia/preeclampsia and the thrombotic microangiopathies.

Some diseases, such as fibrillary glomerulonephritis and immunotactoid glomerulopathy, can be diagnosed only by electron microscopy. More often, however, electron microscopy is an adjunct to light and IFM. Some diseases are more readily apparent by electron microscopy even though the diagnosis can be made by light microscopy. For example, noticing the striking intracellular zebra body myelin figures of Fabry disease may be unavoidable by electron microscopy while the pale intracellular vacuoles may be recognized by light microscopy only in retrospect once the diagnosis is made by electron microscopy. Certain ultrastructural features may lead to more precise diagnosis. For example, in a patient with a proliferative glomerulonephritis, identification of endothelial tubuloreticular inclusions raises the possibility of lupus nephritis, and microtubular configuration in the dense deposits raises the possibility of cryoglobulinemic glomerulonephritis. The bottom half of Figure 3.2 shows how observations by electron microscopy can guide the resolution of the differential diagnosis in a patient with glomerulonephritis. Electron microscopy is particularly useful in diagnosing glomerular diseases that have distinctive organized ultrastructural patterns in pathologic glomerular deposits, such as amyloidosis, fibrillary glomerulonephritis, immunotactoid glomerulopathy, cryoglobulinemia, monoclonal immunoglobulin deposition

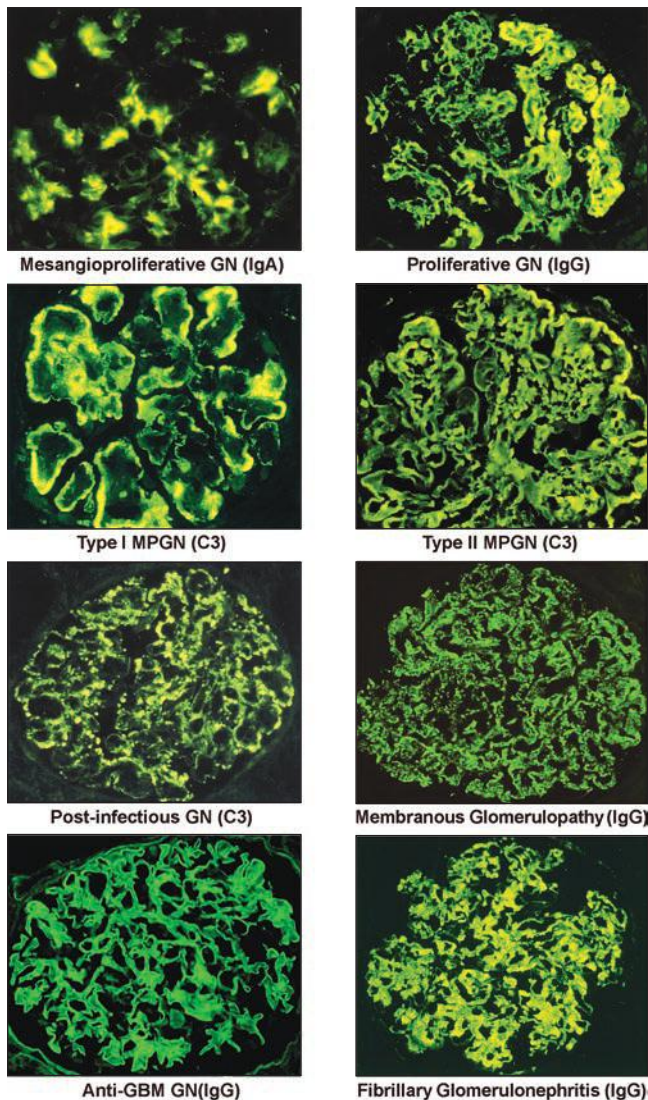


FIGURE 3.4 A sampling of staining patterns that must be discerned when evaluating glomerular diseases by direct immunofluorescence microscopy. Antibody specificity is shown in parentheses. The patterns of staining are mesangial in IgA nephropathy, granular mesangial and capillary wall in proliferative lupus GN, peripheral capillary wall granular in type I MPGN, bandlike capillary wall and coarsely granular mesangial in type II MPGN (dense-deposit disease), coarsely granular capillary wall in acute postinfectious GN, finely granular capillary wall in membranous glomerulonephritis, linear GBM staining in anti-GBM glomerulonephritis, and coarsely granular to chunky in fibrillary GN.

disease, collagenofibrotic glomerulopathy, and fibronectin glomerulopathy (see Chapter 23).

THE PATHOLOGIC DIAGNOSIS OF TUBULAR DISEASE

Diseases primarily affecting the renal tubules can be divided in a number of ways, but here are considered under the following morphologic headings (Table 3.6): acute tubular epithelial

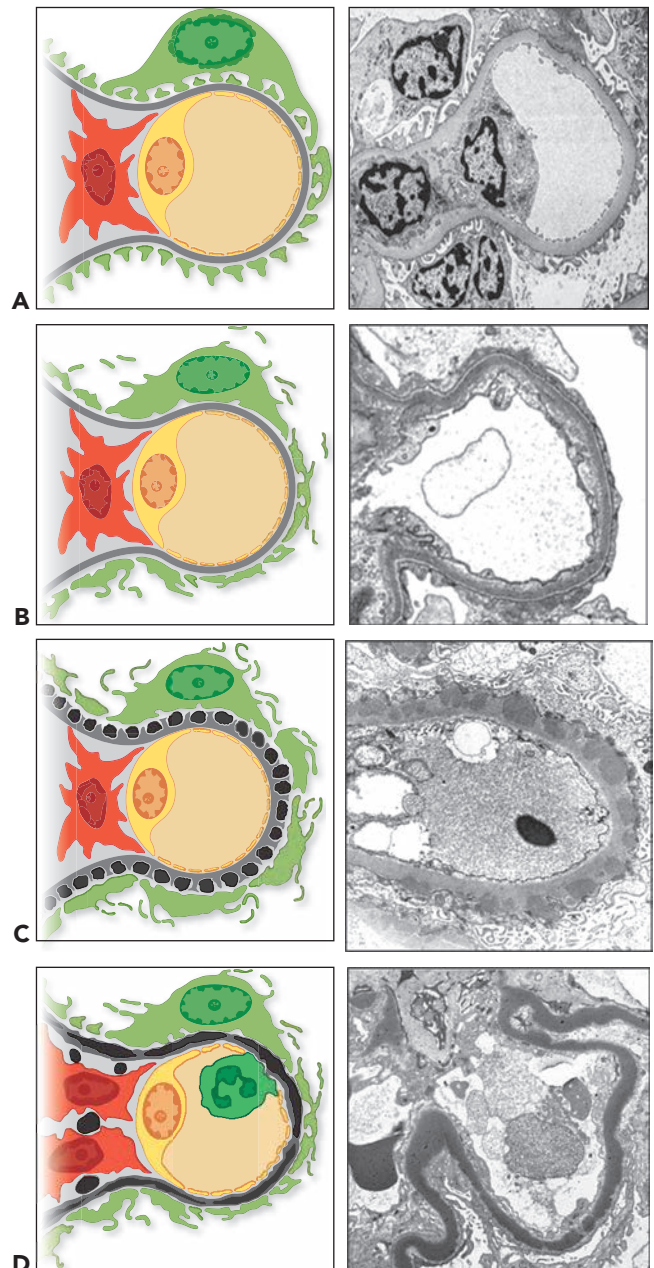


FIGURE 3.5 Diagrams and electron micrographs illustrating the characteristic ultrastructural changes in a glomerular capillary in selected causes for the nephrotic syndrome. **A:** Normal capillary with podocyte (green) with intact foot processes, normal thickness GBM (dark gray), fenestrated endothelium (yellow), mesangial cell (red), and mesangial matrix (light gray). **B:** Minimal change disease with extensive podocyte foot process effacement. **C:** Membranous glomerulonephritis (stage II) with numerous subepithelial dense deposits with adjacent projections of GBM and foot process effacement and microvillous transformation. **D:** Dense-deposit disease with extensive intramembranous dense deposits as well as mesangial dense deposits.

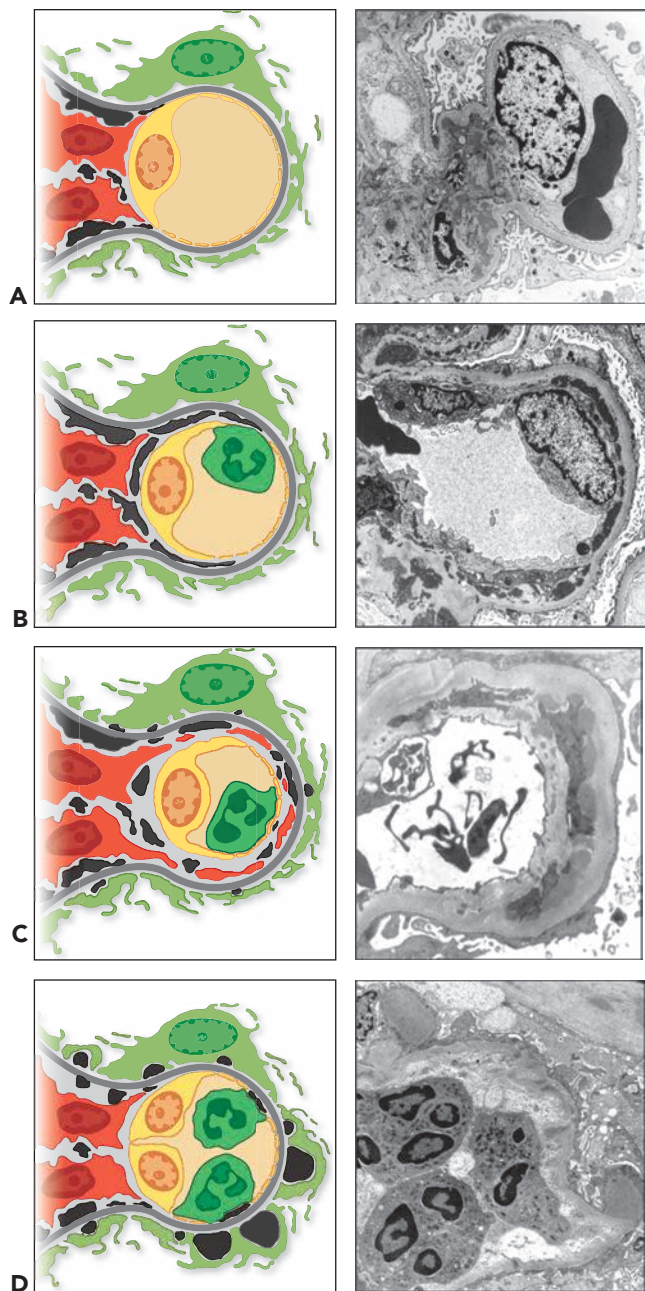


FIGURE 3.6 Diagrams and electron micrographs illustrating the characteristic ultrastructural changes in a glomerular capillary in selected causes for the nephritic syndrome. **A:** Immune complex–mediated mesangioproliferative glomerulonephritis with mesangial dense deposits, and mesangial hypercellularity. **B:** Immune complex–mediated proliferative glomerulonephritis with mesangial and subendothelial dense deposits, mesangial hypercellularity, and an endocapillary neutrophil (in the diagram but not electron micrograph.) **C:** MPGN with mesangial and subendothelial dense deposits, mesangial hypercellularity, interposition of mesangial cytoplasm into the subendothelial zone, and deposition of new basement membrane material in the subendothelial zone. **D:** Acute postinfectious glomerulonephritis with subepithelial humps, mesangial and small subendothelial dense deposits, mesangial and endothelial hypercellularity, and endocapillary neutrophils.

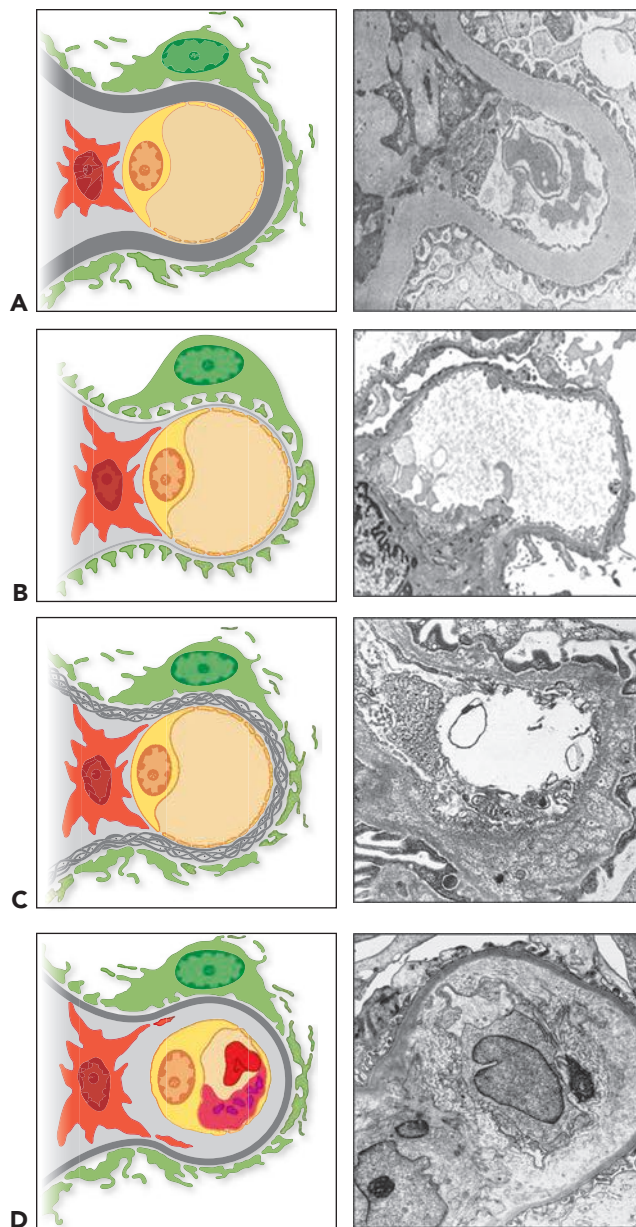


FIGURE 3.7 Diagrams and electron micrographs illustrating the characteristic ultrastructural changes in a glomerular capillary in selected diseases that cause ultrastructure alterations in GBMs (compare to Fig. 3.5A). **A:** Diabetic glomerulosclerosis with GBM thickening and increased mesangial matrix. **B:** Thin basement membrane lesion with markedly thinned lamina densa of the GBM. **C:** Hereditary nephritis (Alport syndrome) with “basket weave” GBM lamination. **D:** Hemolytic uremic syndrome–type thrombotic microangiopathy with electron-lucent expansion of the subendothelial zone, loss of endothelial fenestrations and platelet-rich thrombus (diagram only).

injury (including acute tubular necrosis) (see Chapter 26), tubulitis and tubulointerstitial inflammation (see Chapters 24 and 25), tubular casts, chronic changes (tubular atrophy), TBM changes, and other tubular changes. Table 3.7 contains a glossary of terms used to describe clinicopathologic and histopathologic lesions of the tubules.

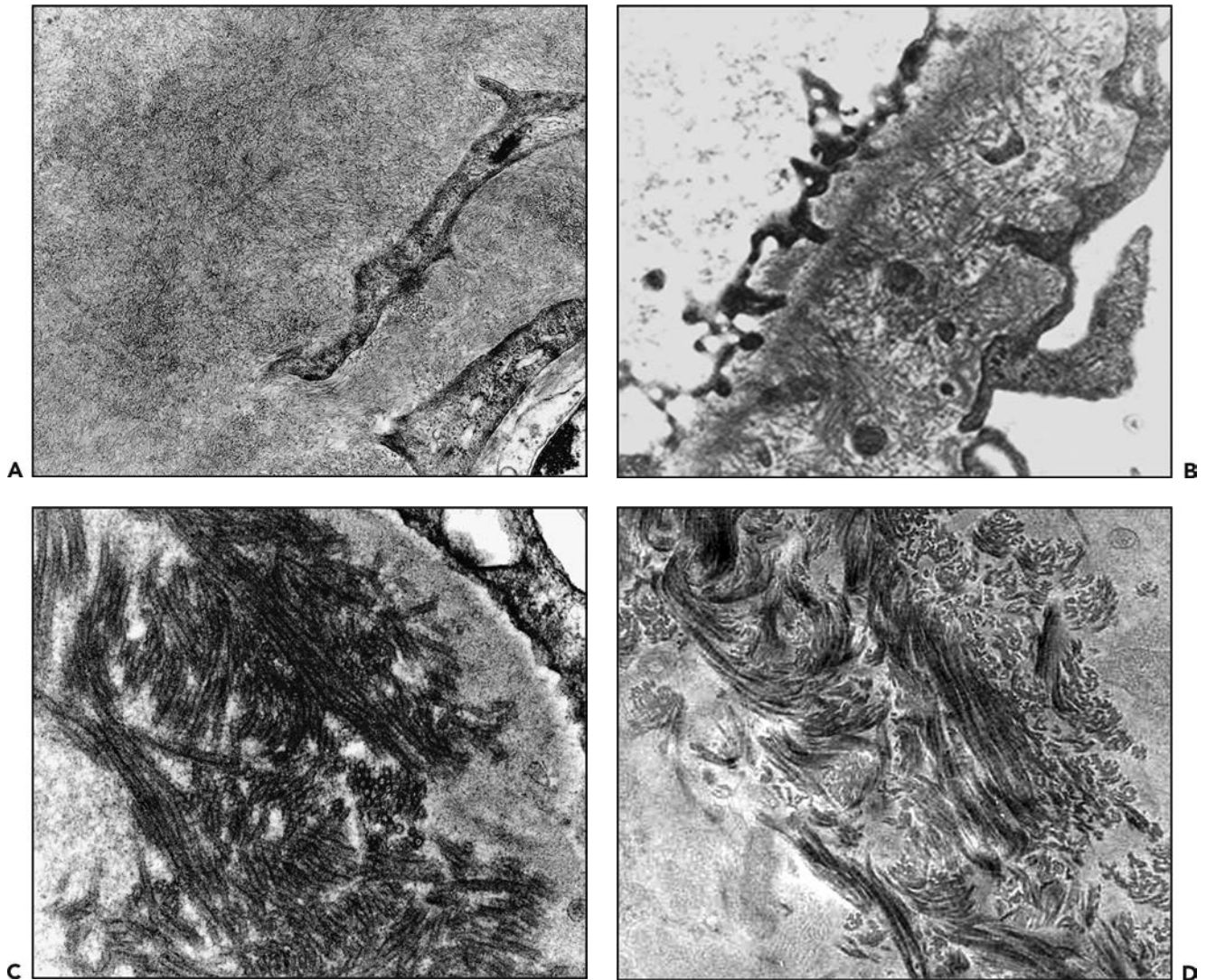


FIGURE 3.8 Electron micrographs of organized glomerular deposits. **A:** Amyloidosis with mesangial randomly arranged approximately 10 nm diameter fibrils. **B:** Fibrillary glomerulonephritis with capillary wall randomly arranged approximately 20 nm diameter fibrils. **C:** Immunotactoid glomerulopathy with capillary wall parallel stacks of approximately 50 nm diameter microtubules. **D:** Collagenofibrotic glomerulopathy with capillary wall curved type III collagen bundles with periodicity (striations). (All images are approximately 10,000 \times magnification.)

In the normal renal cortex, the tubules are back to back, virtually without any interstitium. In contrast, the tubules of the renal medulla are separated by varying amounts of interstitium, which is most abundant in the deep medulla. The tubular portions of each nephron can be divided morphologically and functionally into at least 16 different segments (15). However, for diagnostic purposes and in this section, we need only to recognize proximal convoluted tubules, the loops of Henle including the ascending thick and thin limbs, the distal convoluted tubules, and the cortical and medullary collecting ducts. Chapter 1 discusses tubular epithelial structure in detail.

The histologic differential diagnosis between primary acute tubular injury (ATI) with secondary interstitial

inflammation versus primary acute tubulointerstitial nephritis (TIN) is critical but often difficult. Because most inflammatory diseases affecting the tubules also involve the interstitium and because interstitial inflammation may be accompanied by tubulitis, the term *acute or chronic tubulointerstitial nephritis* is more appropriate than is *interstitial nephritis*. Because there may be histopathologic overlap between primary ATI with secondary interstitial inflammation versus primary tubulointerstitial inflammation, differentiation between these pathologic processes requires knowledgeable integration of the clinical and morphologic features. For example, extensive or severe interstitial inflammation and associated tubulitis (see “Tubulitis”) favors a primary acute TIN over primary ATI; a neutrophilic interstitial

TABLE 3.6 Tubular changes

Acute tubular epithelial cell injury (see Chapter 26)
Acute tubular epithelial necrosis
Nonnecrotic tubular epithelial cell injury
Acute simplification
Hyaline droplet formation
Vacuolar change
Hydropic change
Fatty change
Foam cells
Hypokalemic nephropathy
Pigments in tubular epithelium
Viruses in the tubular epithelium
Tubulitis and tubulointerstitial inflammation (see Chapters 24 and 25)
Tubular luminal casts
Tubular atrophy
TBM changes

infiltrate with abscesses and neutrophil casts favors an acute pyelonephritis or infection over ATI; and interstitial eosinophils admixed with lymphocytes and tubulitis suggests a primary allergic TIN.

Acute Tubular Injury

ATI causes ARF. The nomenclature for clinical and pathologic manifestations of acute renal injury has been evolving in recent years (16). The current trend is to use the generic term acute kidney injury (AKI) rather than ARF when there is kidney injury that causes a rise in serum creatinine over several days or weeks (see Chapter 26). Of course, AKI can result from injury not only to tubules but also to glomeruli or vessels. ATI can be caused by ischemic or nephrotoxic injury, and pathologically can result in overt acute tubular necrosis (ATN) or morphologic changes that are indicative of ATI but not ATN.

Acute Tubular Necrosis

ATN is a clinical-pathologic entity, characterized morphologically by destruction or severe injury of the renal tubular epithelium. The two major causes are toxins and ischemia. The toxic form is morphologically associated with more severe tubular epithelial injury including actual necrosis. The terms *acute tubular injury*, *acute vasomotor nephropathy*, *shock kidney*, *ischemic acute tubular nephropathy*, and *ischemic acute tubular necrosis* have been used for the more subtle morphologic changes associated with ischemia with minor or no morphologic evidence of overt necrosis. The major pathologic features of ATN are initially noted in the renal tubular epithelium, and they are listed in Table 3.8 and illustrated in Figure 3.9.

Acute Tubular Injury Without Overt Necrosis

Renal pathologic changes in patients with ATI may not include overt epithelial cell necrosis. Ischemic ATI often has little or no tubular epithelial necrosis but rather sublethal tubular injury in the form of epithelial simplification with loss of proximal

TABLE 3.7 Glossary of terms used to describe clinicopathologic and histologic lesions of the tubules

Term	Definition
Acute kidney injury	Abrupt onset of failure of renal function leading to retention of nitrogenous waste products; often anuric or oliguric.
Acute tubular injury	Acute cytoplasmic changes without overt necrosis, e.g., acute simplification with loss of brush border and flattening of cells.
Acute tubular necrosis	Necrosis of the tubular epithelium (often coagulation necrosis), usually secondary to toxins and/or ischemia.
Chronic renal failure	End result of a variety of progressive/irreversible renal diseases; accompanied by uremia.
Chronic renal insufficiency	Syndrome resulting from multitude of pathologic processes that lead to derangements of renal excretory and regulatory functions. Develops over period of months/years and ultimately lead to uremia.
Tubulitis	Presence of lymphocytes/other inflammatory cells infiltrating the tubular epithelium
Tubular atrophy	Wasting of tubules as a result of ischemia, obstruction, or severe cellular injury. The tubular cells are usually simplified, reduced in size, or dilated and filled with casts. The TBMs are often thickened.
Tubular casts	Various coagulated proteins and formed elements in the tubular lumens (e.g., RBC casts, WBC casts, hyaline or pigmented casts).
Hydropic change	Fine regular vacuolization of the proximal tubules.
Hyaline droplet formation	PAS/silver-positive resorption droplets in the proximal tubular epithelium, betraying glomerular permeability to proteins.
Fatty change	Small lytic vacuoles in the tubular epithelium in which the fat has been dissolved out by the formalin-fixation/paraffin embedding method. Usually seen in the nephrotic syndrome with hyperlipidemia.
Hypokalemic changes	Irregular-sized, coarse vacuoles occupying the renal epithelium.
Intranuclear inclusions	Dense inclusions in the nuclei often indicative of viral infection. Need to rule out lead nephropathy, tubular epithelial cell regeneration following ATN.

TABLE 3.8 Acute tubular injury

Necrosis of tubular epithelial cells (coagulation necrosis, karyorrhexis, pyknosis)
Swelling and clear vacuolation of tubular epithelium
Separation/detachment of tubular epithelium from underlying TBM
Simplification (loss/attenuation of PAS-positive brush border of proximal tubular epithelial cells and thinning of tubular epithelium)
Dilatation (ectasia) of the tubular lumina
Interstitial edema (clear widening of the normally sparse cortical interstitium by aqueous fluid)
Casts in tubule lumens (hyaline, cellular, granular, cellular debris, pigmented)
Crystals (e.g., oxalate)
Rupture of the TBMs (tubulorrhesis). There may be small adjacent granulomatous interstitial lesions.
Later, in the reactive/repairative/regenerative stage:
Basophilic flattened tubular epithelial cytoplasm
Large hyperchromatic nuclei (often with prominent nucleoli)
Mitotic figures in the tubular epithelial cells

tubule brush borders, sloughing of apical cytoplasm into the tubular lumen, and flattening of the epithelial cells with resultant widening of the tubular lumen (see Fig. 3.9A). These acute tubular changes typically are accompanied by interstitial edema. Nephrotoxic ATI more often has a component of overt ATN with localized denudation of TBMs by dropout of injured and necrotic cells, which subsequently can be replaced by regenerating cells with mitotic figures or hyperchromatic nuclei (see Fig. 3.9C).

Other Acute Renal Tubular Abnormalities

Some morphologic changes appear to be manifestations of disturbances of normal tubular functions such as trafficking and reabsorption of water, proteins, and lipids. Increased resorption of filtered protein and lipoprotein in patients with nephrotic syndrome results in numerous PAS-positive hyaline droplets (Fig. 3.10A) in the cytoplasm of proximal tubules that contain both proteins and lipids (see Fig. 3.10D). Clear cytoplasmic vacuolation (hydropic change) (see Fig. 3.10B and C) can result from many causes, including hypokalemia, cyclosporine A toxicity, and other drug toxicities.

Hyaline Droplet Change

This lesion of the proximal tubular epithelium consists of numerous lysosomal cytoplasmic protein droplets resulting from absorption of filtered plasma proteins. The droplets vary in size from small to large and are eosinophilic by H&E, PAS positive and silver positive (see Fig. 3.10A). By immunofluorescence, these droplets may stain for albumin, immunoglobulins, and other plasma proteins that have passed through the glomerular filter.

Vacuolar Change

Several conditions cause a foamy appearance of the tubular epithelium. *Hydropic change* is a generic term for fine, usually diffuse vacuolar clearing of the cytoplasm of the proximal tubular

epithelium (see Fig. 3.10B). These fine vacuoles contrast with the much coarser and irregular vacuolation seen with hypokalemia and some forms of toxic ATN. The brush border is generally well preserved. Hydropic change may be seen in patients who have received hypertonic solutions such as sucrose solutions, mannitol, high molecular weight dextrans, radiopaque contrast material, hydroxyethyl starch, or intravenous immunoglobulin. In the context of exposure to such hypertonic solutions, the synonym “osmotic nephrosis” can be used. Hydropic change is also seen in the renal allograft treated with cyclosporin A, and in this setting it has been called isometric or isotonic vacuolization. The optically clear vacuolation seen by light microscopy is a reflection of distended membrane-bound lysosomes, and there may also be dilatation of the endoplasmic reticulum by aqueous fluid. Especially in hypokalemia, clear vacuoles in the tubular epithelium seen by light microscopy are seen by electron microscopy to be the result of distention of the extracellular compartment between the interdigitating basement membranes of adjacent proximal tubular epithelial cells. When tubular epithelial cells have numerous vacuoles containing lipid (*fatty change*), the cytoplasm is filled with fine, small, clear vacuoles often best seen at the base of the proximal tubular epithelium (see Fig. 3.10C and D). Stains to demonstrate fat must be performed on the frozen sections because lipid is lost during preparation of paraffin sections. By electron microscopy, fatty vacuoles range in color from white-gray to electron lucent, contrasting with the electron dense appearance of protein resorption droplets. Fatty change is most commonly seen in patients with severe proteinuria or the nephrotic syndrome with hyperlipidemia and hyperlipiduria. Patients with Reye syndrome or phosphorus or carbon tetrachloride poisoning show similar changes. *Foam cells*, derived from monocyte/macrophages and containing cholesterol esters and other lipids, have abundant cytoplasm and centrally located round to oval nuclei. They are most commonly seen in the tubular epithelium and the renal interstitium in patients with long-standing nephrotic syndrome and hyperlipidemia/hyperlipiduria. In patients without significant proteinuria, interstitial foam cells suggest the diagnosis of Alport hereditary nephritis. *Hypokalemic nephropathy* is characterized by various-sized, clear cytoplasmic vacuoles in the renal tubular epithelium. The vacuolation is caused by both expansion of the extracellular spaces with ballooning of the space between the basal and lateral cell membranes and cytoplasmic vacuole formation. Hypokalemic nephropathy is caused by any chronic, long-standing loss of potassium including chronic laxative abuse, potassium-losing rectosigmoid polyps, various intrinsic renal conditions (such as chronic glomerulonephritis), or adrenal or metabolic conditions leading to hypokalemia. The clinical findings are reversible by potassium administration.

Hemosiderin, Other Pigments in Renal Tubular Epithelium, and Signs of Heavy Metal Poisoning

Hemosiderin collects in the renal tubular cytoplasm in various conditions that lead to intravascular hemolysis, such as erythrocyte destruction in hemolytic anemia (e.g., sickle cell disease) and by mechanical heart valves. It appears as coarse cytoplasmic granules of golden-brown pigment that stain positively with Prussian blue. It must be distinguished from other pigments such as melanin in patients with disseminated melanoma and bile pigments in icteric patients. In lead nephropathy, there are large

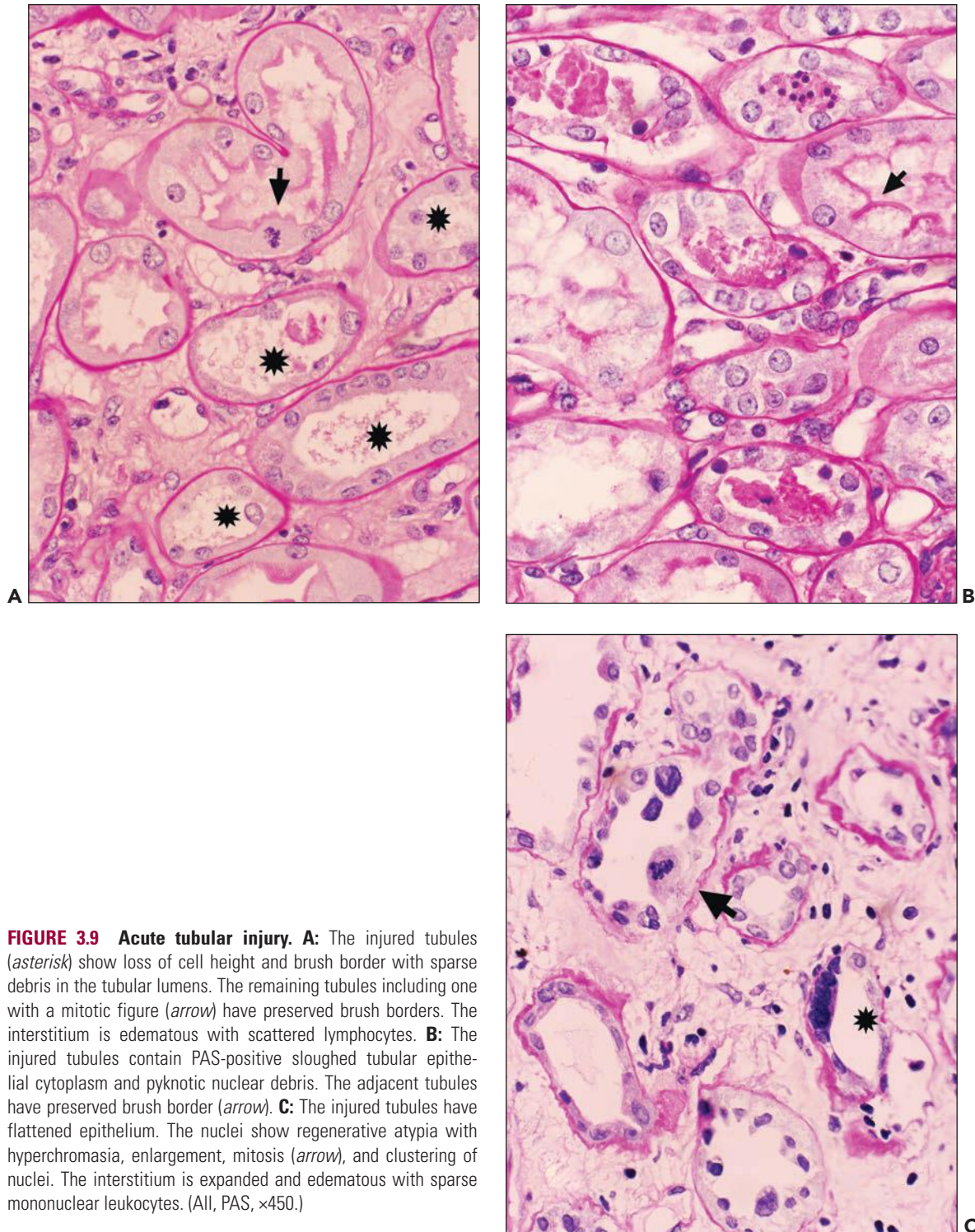


FIGURE 3.9 Acute tubular injury. **A:** The injured tubules (*asterisk*) show loss of cell height and brush border with sparse debris in the tubular lumens. The remaining tubules including one with a mitotic figure (*arrow*) have preserved brush borders. The interstitium is edematous with scattered lymphocytes. **B:** The injured tubules contain PAS-positive sloughed tubular epithelial cytoplasm and pyknotic nuclear debris. The adjacent tubules have preserved brush border (*arrow*). **C:** The injured tubules have flattened epithelium. The nuclei show regenerative atypia with hyperchromasia, enlargement, mitosis (*arrow*), and clustering of nuclei. The interstitium is expanded and edematous with sparse mononuclear leukocytes. (All, PAS, $\times 450$.)

PAS- and acid fast–positive intranuclear inclusions (Fig. 3.11A). Gold nephropathy is associated with filamentous inclusions seen by electron microscopy (EM) in the cytoplasm of tubular cells.

Viral Intranuclear Inclusions

Some viruses infect the renal tubular epithelium without leading to specific histologic changes whereas others produce typical cytopathic changes. Affected patients are

usually immunosuppressed, or the infection is noted in a renal transplant. The morphologic evidence of viral-induced renal tubular injury depends on the virus and the patient's response to the viral infection. For example, large intranuclear (Cowdry type A) and intracytoplasmic inclusions are characteristic of cytomegalovirus (CMV) (see Fig. 3.11B). Necrosis of tubular epithelium and large, sometimes smudgy nuclei are characteristic for adenovirus and polyoma (BK)

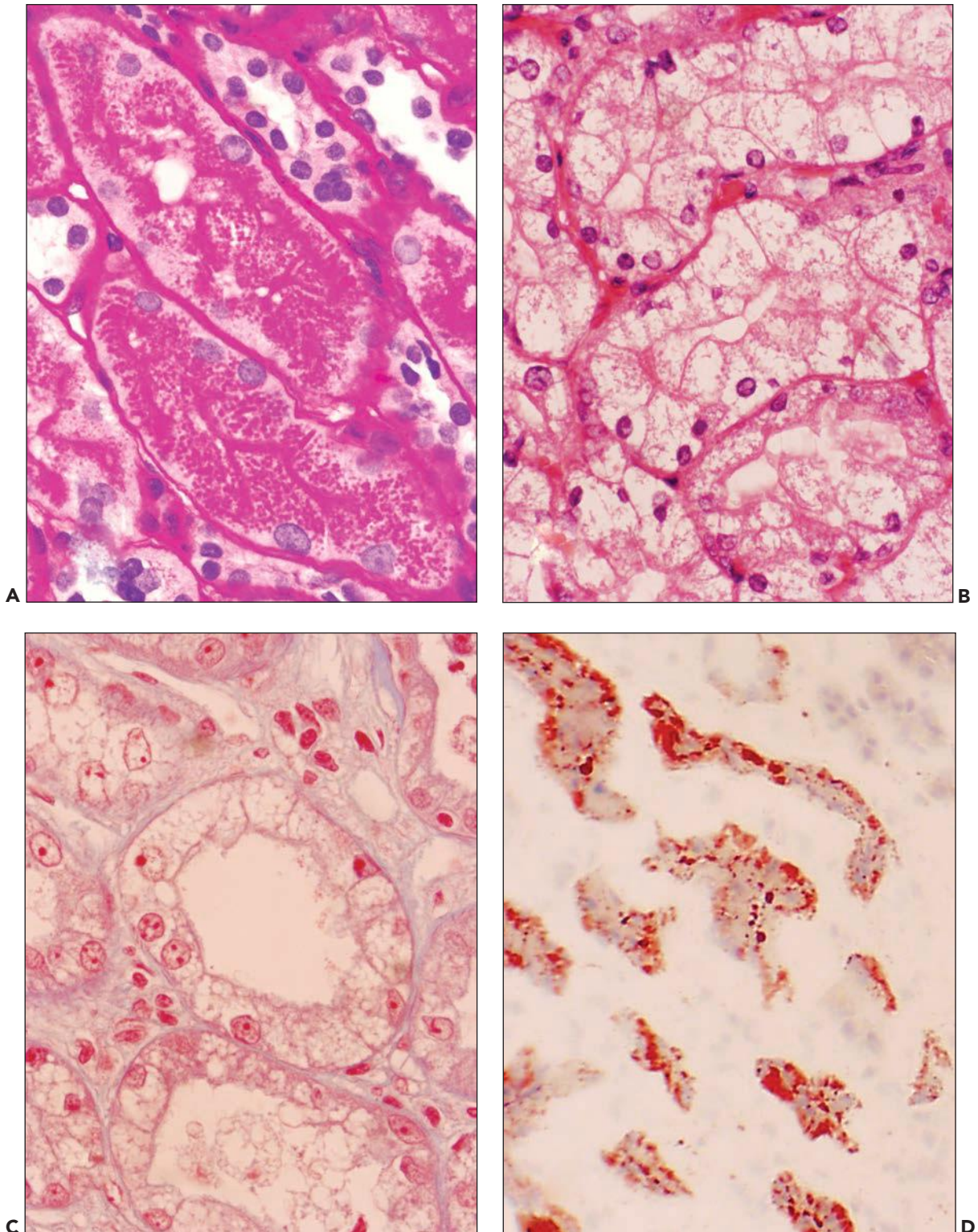


FIGURE 3.10 Other tubular changes. **A:** Hyaline droplet change (degeneration). Proteinuric patient with resorption droplets of filtered plasma proteins in the tubular cytoplasm. The droplets are prominent, PAS positive, and variable in size. ($\times 450$.) **B:** Hydropic change in a patient receiving mannitol for cerebral edema. The cytoplasm of the proximal tubules is filled with small and coalescing fluid-filled vacuoles. (H&E, $\times 450$.) **C** and **D:** Fatty change. Autopsy of patient with severe nephrotic syndrome. Grossly, the renal cortex contained discrete, golden-yellow infiltrates. **C:** The tubular cytoplasm is filled with small vacuoles. (Masson trichrome, $\times 540$.) **D:** Frozen section stained with oil red O demonstrates that the tubules contain droplets of neutral lipid. ($\times 90$.)

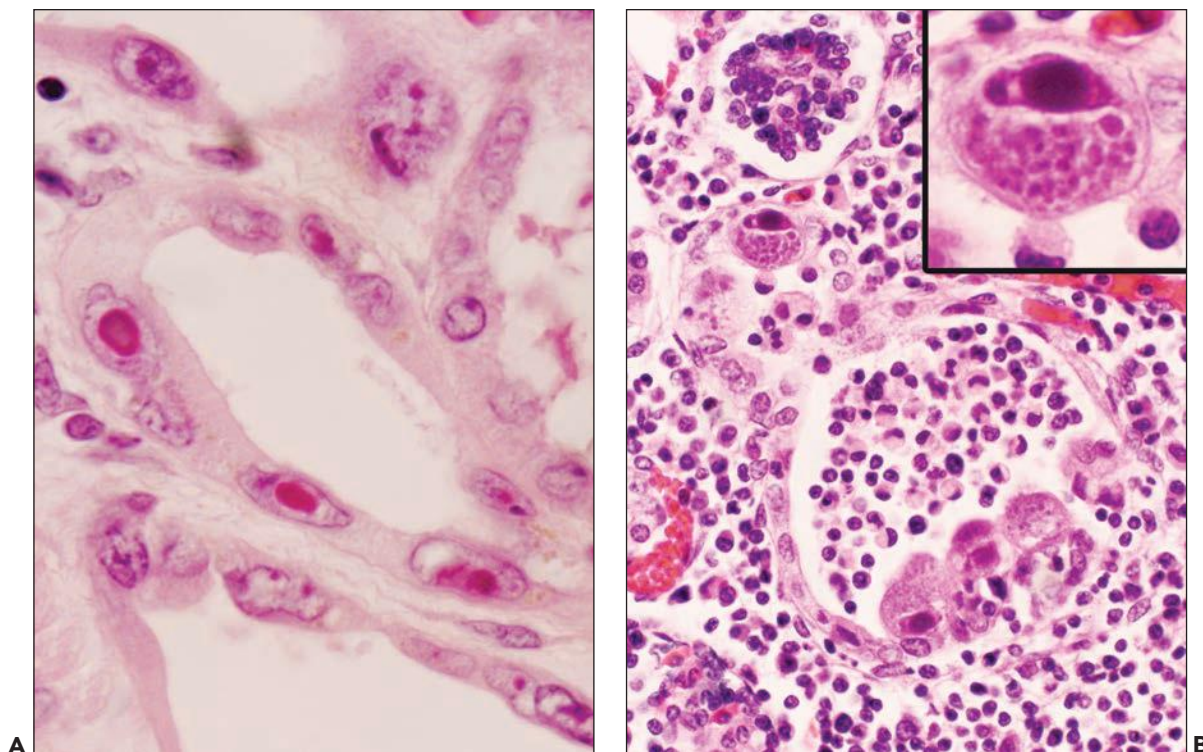


FIGURE 3.11 Nuclear inclusions. A: Experimental lead intoxication (monkey). The tubular epithelium is atrophic, and the nuclei contain prominent, intensely eosinophilic inclusions. The inclusions are also acid fast positive. (H&E, $\times 540$.) **B:** CMV tubulointerstitial nephritis in a newborn (note the immature glomerulus in the left upper corner). A mixed inflammatory infiltrate is expanding the interstitium and forming a pus cast in the center. Several tubular cells have enlarged, hyperchromatic atypical nuclei with viral changes. (H&E, $\times 540$.) **Inset.** Involved cell with a large nuclear and multiple cytoplasmic inclusions. (H&E, $\times 1370$.)

virus infections (see Chapter 29). However, large, hyperchromatic, crowded nuclei are also seen in regenerating renal tubular epithelial cells, and this condition should not be mistaken for a viral infection. Studies by electron microscopy, immunohistochemistry, and in situ hybridization using specific probes to the virus play a major role in the identification of these viruses and help to differentiate viral infection from regenerative atypia.

Tubulitis

Tubulitis is a marker of active tubulointerstitial inflammation and is defined as lymphocytes or other inflammatory cells on the epithelial side of the TBMs infiltrating the tubular epithelium (Fig. 3.12). Tubulitis has multiple causes. Most commonly, tubulitis is caused by either an acute cellular allograft rejection or acute or chronic TIN. It is also a common accompaniment to some glomerular diseases, such as lupus nephritis and pauci-immune (ANCA) crescentic glomerulonephritis, where the tubulitis tends to be mild and focal.

Tubular Casts

The different casts seen on microscopic examination of the urine sediment also are present in histologic sections. They include hyaline casts (seen in renal failure or low urine flow states), white blood cell (WBC) casts (tubular interstitial inflammation), epithelial cell and granular casts (ATI), red

blood cell (RBC) casts (glomerular sources of hematuria), and large hyaline, fractured casts associated with giant cells and polymorphonuclear leukocytes (immunoglobulin light chain casts). RBC casts due to biopsy trauma can be seen in percutaneous renal biopsies, and distinguishing them from RBC casts related to glomerular disease may be difficult. The correct interpretation of RBC casts requires integration of this feature with the clinical history and the other histologic biopsy findings. Dysmorphic and fragmented RBCs in casts favor glomerular origin. Aggregation of the red cells in a proteinaceous matrix, sometimes admixed with other cell types, and the presence of degenerating or dysmorphic RBCs helps to differentiate in vivo cast formation from the looser aggregates of intact RBCs that may occur following biopsy trauma. Coarsely granular, acidophilic (brick red) casts suggest the possibility of myoglobin or hemoglobin, which can be determined by immunocytochemistry. Tamm-Horsfall (uromodulin) casts may be distinguished by their bright staining with PAS and by their filamentous, heterogeneous texture. The presence and types of tubular casts should be noted; casts are the principal histologic features of light chain cast nephropathy, myoglobinuria, and hemoglobinuria. Oxalate nephropathy, urate nephropathy, nephrocalcinosis, phosphate nephropathy and forms of drug-induced tubular injury such as acyclovir toxicity have characteristic, extensive crystalline casts (often associated with interstitial crystalline deposits).

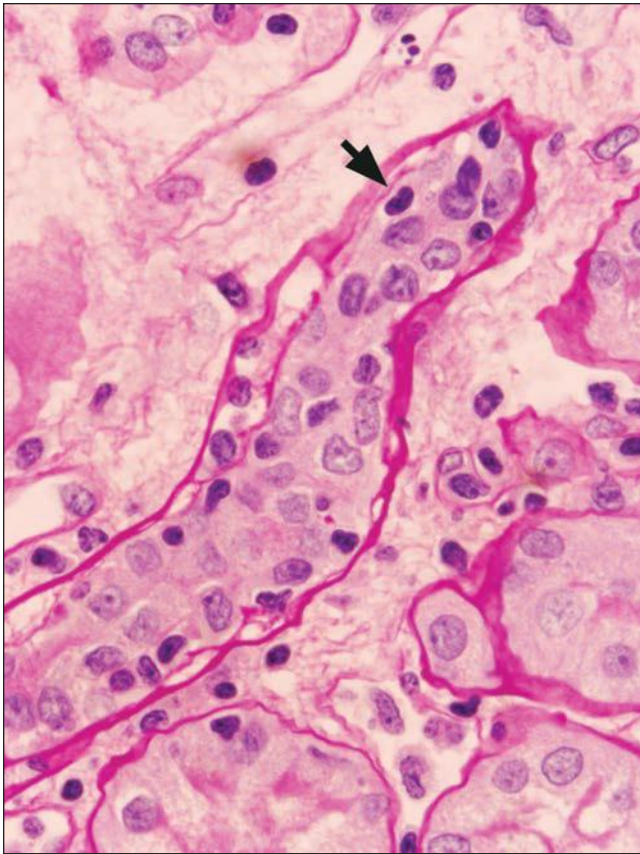


FIGURE 3.12 Tubulitis. The injured tubule in the center of the field contains many lymphocytes within the TBM. A typical lymphocyte (*arrow*) is identified by its small nucleus with compact chromatin compared with the larger, vesicular tubular nuclei and a clear surrounding halo. (PAS, $\times 540$.)

Tubular Atrophy

A diagnosis of tubular atrophy implies chronic tubular injury. The pathologist should distinguish the histologic signs of ATI from tubular atrophy. Both lesions show extensive epithelial changes, but tubular atrophy is usually accompanied by thickening and wrinkling of the TBMs whereas the TBMs are normal in ATI. Tubular atrophy is caused by all forms of chronic glomerular, tubular, interstitial, and vascular diseases. The TBMs are thickened and wrinkled, and the tubular epithelial cells are flattened and simplified with loss of histologic characteristics of different segments of the nephron. ATI also causes epithelial simplification, but is not accompanied by TBM thickening and wrinkling. Whereas the tubular lumen is often widened, or ectatic, in ATI, it is usually contracted in tubular atrophy (with the exception of atrophic tubules containing large hyaline casts). There is better correlation between renal function and chronic changes in the tubulointerstitial compartment than with glomerular or vascular pathology, irrespective of the underlying renal disease.

There are three histopathologic patterns of atrophic tubules. Classic atrophic tubules have thick, wrinkled, occasionally lamellated TBMs and simplified cuboidal non-descript tubular epithelium (Fig. 3.13A). Atrophic tubules showing an endocrinization pattern are small and have narrow

or no tubular lumina, cuboidal epithelial cells, and little or no basement membrane thickening (see Fig. 3.13B). There is minimal interstitial fibrosis and chronic inflammation. The small size of the tubules results in close approximation of glomeruli to each other (see Fig. 3.13B). Tubules with the endocrinization pattern of atrophy are reminiscent of endocrine (e.g., parathyroid or acinar pancreas) gland histology. The endocrinization pattern is caused by stenosis of the main renal artery or major arterial branches feeding large segments of the kidney. Tubules showing “thyroidization” have round tubules with simplified epithelium and uniform intratubular casts that mimic thyroid gland parenchyma (see Fig. 3.13B). This appearance is caused by fragmentation of tubules into short segments that round up into spherical profiles when cut in any plane of section. This can occur in any form of chronic kidney disease but is particularly common and extensive in chronic pyelonephritis.

In kidneys showing extensive tubular atrophy, nonatrophic functioning renal tubules may be enlarged with hypertrophied epithelial cells. These tubules are thought to develop as the consequence of compensatory hypertrophy. Because tubular disease characteristically has a focal or patchy distribution, the presence of tubular atrophy in a renal biopsy specimen may not be representative of the entire kidney. Extrapolation of this biopsy finding to the entire kidney should be done cautiously and with clinicopathologic correlation. Because there is a predilection for tubulointerstitial scarring to involve the subcapsular cortex early in the course of arterionephrosclerosis of hypertension or aging, biopsies that contain predominantly subcapsular cortex may overestimate the total renal injury, especially in older adults.

Mitochondrial Abnormalities

Certain drug toxicities and genetically determined mitochondrial cytopathies cause ATI secondary to mitochondrial dysfunction. For example, tenofovir causes ATN with pathologic mitochondrial abnormalities including swelling and dysmorphic cristae (17). Genetic mitochondrial cytopathies can cause tubular, glomerular, or cystic renal disease and may be accompanied by other organ system dysfunction. Renal tubular involvement often causes Fanconi syndrome when severe and may manifest pathologically as ATI with or without TIN.

Light microscopy may reveal abnormal eosinophilic cytoplasmic inclusions (giant mitochondria) in tubules, and electron microscopy will show ultrastructural mitochondrial abnormalities, such as enlargement, depletion, and dysmorphic structural alterations in cristae.

Tubular Basement Membrane Changes

Increased thickness with or without splitting or wrinkling is the major abnormality seen in TBMs, and this change is most commonly seen with tubular atrophy. Some diseases affecting the GBMs, such as diabetic nephropathy, hereditary nephritis (Alport syndrome), monoclonal immunoglobulin deposition disease, DDD and medullary cystic disease, and nephronophthisis have associated changes in the TBMs; thus, TBM are best studied in relation to pathology in the other renal structures. Calcium may be deposited in the TBMs in severe tubular atrophy or hypercalcemic conditions causing nephrocalcinosis. IFM and/or electron microscopy may reveal immune-type TBM deposits as seen

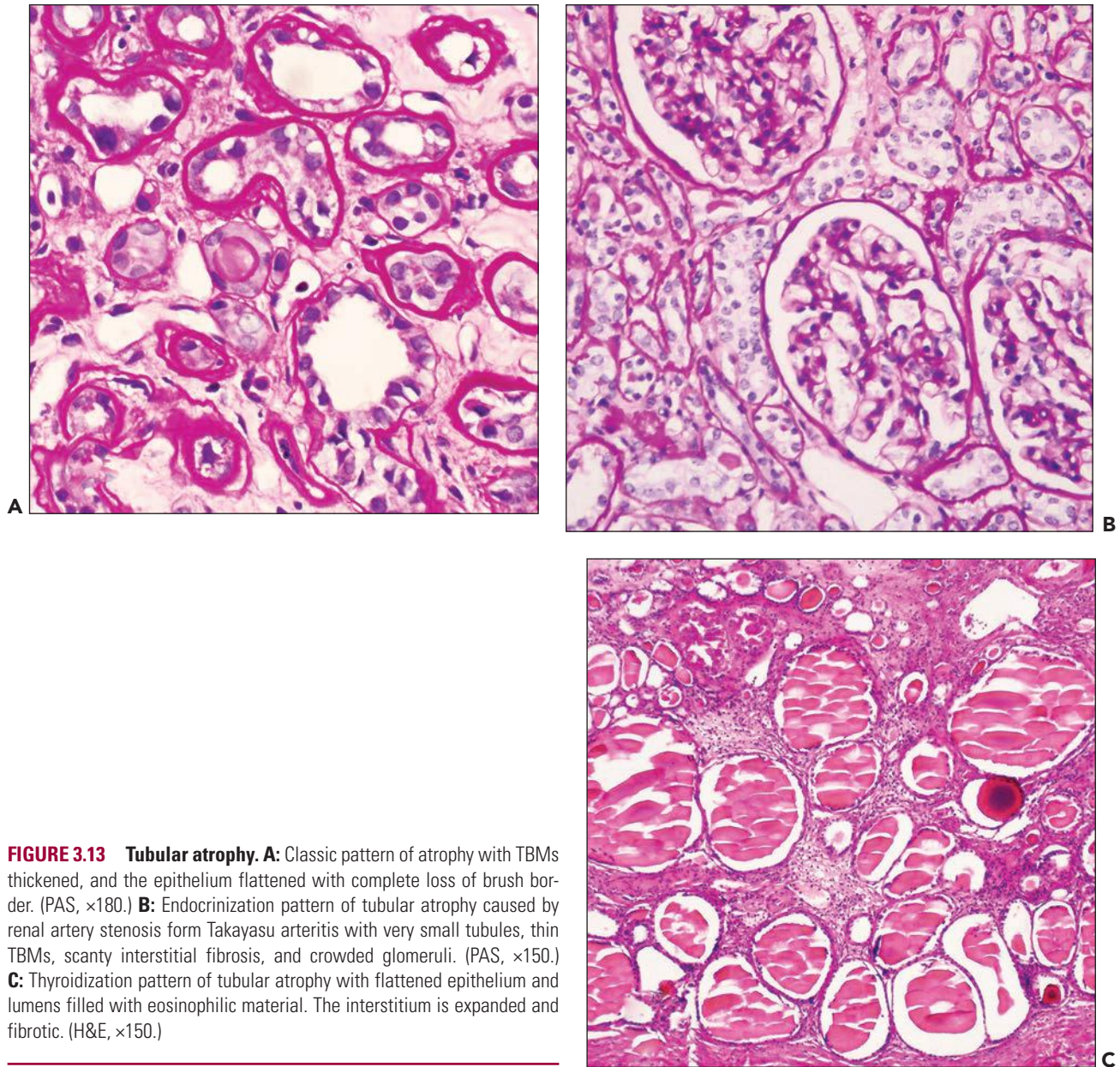


FIGURE 3.13 Tubular atrophy. **A:** Classic pattern of atrophy with TBMs thickened, and the epithelium flattened with complete loss of brush border. (PAS, $\times 180$.) **B:** Endocrinization pattern of tubular atrophy caused by renal artery stenosis from Takayasu arteritis with very small tubules, thin TBMs, scanty interstitial fibrosis, and crowded glomeruli. (PAS, $\times 150$.) **C:** Thyroidization pattern of tubular atrophy with flattened epithelium and lumens filled with eosinophilic material. The interstitium is expanded and fibrotic. (H&E, $\times 150$.)

in SLE, DDD, monoclonal immunoglobulin deposition disease, IgG4-related TIN, and other immune complex-mediated diseases (Fig. 3.14).

THE PATHOLOGIC DIAGNOSIS OF INTERSTITIAL DISEASE

The interstitium is that part of the renal parenchyma not occupied by glomeruli, tubules, and vessels. It is the smallest renal compartment. The interstitium occupies less than 5% of the cortex and outer medulla but occupies a greater percentage of the inner medulla where the tubules are more widely spaced (see Chapter 1). Interstitial expansion is the morphologic

sine qua non of interstitial disease. Increased interstitial volume due to fibrosis correlates with impaired renal function and is a negative prognostic indicator in diseases of the interstitium as well as in diseases involving the other renal compartments (17–19). However, interstitial expansion due to acute injury with edema and cellular infiltrates may be reversible, and its prognostic significance is less certain. Despite its small volume under normal circumstances, the interstitium is the principal site of pathology for many common diseases including allergic reactions to drugs and bacterial infections (acute pyelonephritis). By characterizing the cells and the material expanding the interstitium, the pathologist is able to determine the nature of the disease. Table 3.9 presents a glossary of terms used to describe interstitial pathology.

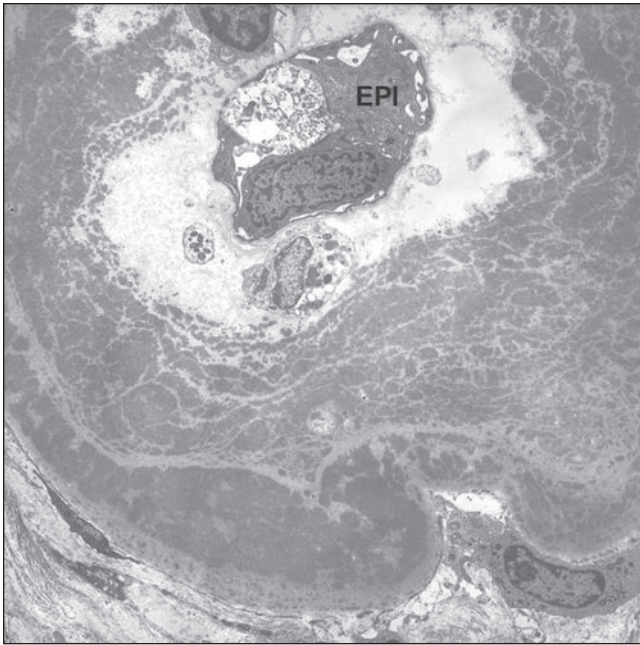


FIGURE 3.14 TBM deposits. Idiopathic, hypocomplementemic, immune complex–mediated TIN. The atrophic tubular epithelium (EPI) is surrounded by massive expansion of the TBMs by electron-dense deposits. The TBMs were intensely eosinophilic and thickened by light microscopy, and they stained for IgG, C3, and κ and λ by fluorescence microscopy. The patient had neither SLE nor Sjögren syndrome. (Uranyl acetate and lead citrate, $\times 2500$.)

Primary and Secondary Interstitial Disease

Many diseases express their primary pathology in the renal interstitium, but secondary interstitial involvement also occurs when diseases primarily target the other renal compartments. Injury to the glomeruli, tubules, or blood vessels frequently causes secondary interstitial disease by ischemia, inflammation, or some other mechanism. Because of these considerations, the diagnosis of primary renal interstitial disease requires that there is no pathology in the other renal compartments that is causing the interstitial lesions. This key distinction between primary and secondary interstitial disease requires a systematic examination of the other compartments to exclude primary pathology. The corollary is that in the presence of significant glomerular, vascular, or tubular disease, primary interstitial disease can be diagnosed only when an unrelated pathogenetic mechanism is acting in the interstitium or when the same mechanism is operative in the interstitium and at the primary site of injury (e.g., immune complex–mediated glomerular and TIN in SLE).

Acute and Chronic Tubulointerstitial Nephritis

There are two main forms of TIN based on the clinical presentation and pathologic manifestations. *Acute tubulointerstitial nephritis* has a relatively acute onset, and *chronic tubulointerstitial nephritis* has an insidious presentation that is followed by a chronic course. Unfortunately, these definitions are arbitrary, because there is clinical and temporal overlap between some

TABLE 3.9 Glossary of terms used to describe histologic findings in interstitial disease

Term	Definition
Interstitial	Space between the glomeruli, tubules, and blood vessels
Edema	Interstitial expansion by protein-poor, aqueous fluid
Interstitial foam cells	Interstitial macrophages with cytoplasmic lipid-containing vacuoles
Fibrosis	Interstitial expansion by collagen-rich matrix and increased fibroblasts
Granuloma	Inflammatory reaction characterized by coalescence of epithelioid macrophages with or without surrounding lymphocytes, fibroblasts, and giant cells
Primary interstitial disease	Renal injury with primary pathology in the interstitium
Secondary interstitial disease	Secondary pathologic changes in the interstitium caused by primary injury to the glomeruli, tubules, or blood vessels with
Tubulointerstitial nephritis	Inflammation of the interstitium and tubules
Acute TIN, clinical	Inflammatory interstitial and tubular disease of acute onset
Acute TIN, pathologic	Interstitial leukocyte infiltrates with or without edema and tubulitis in the absence of interstitial fibrosis and tubular atrophy
Chronic TIN, clinical	Interstitial and tubular disease of insidious onset and progressive course
Chronic TIN, pathologic	Interstitial inflammation with fibrosis and tubular atrophy
Acute pyelonephritis	Acute TIN caused by bacterial infection of the kidney
Chronic pyelonephritis	Chronic TIN caused by bacterial infection of the kidney

acute and some chronic forms of TIN that manifest similarly with silent, progressive loss of renal function. In contrast, the pathologic definitions of acute TIN and chronic TIN are more precise. The acute form may progress to chronic TIN. Acute TIN comprises interstitial edema and inflammatory cellular infiltrates, which include various leukocytes, alone or in combination. Tubulitis and ATI are characteristic features of the acute, active disease. Interstitial collagenous scars, usually associated with atrophic tubules and chronic inflammatory infiltrates, define chronic TIN. In chronic TIN, the inflammatory cells are generally fewer and more restricted in their distribution compared with acute TIN. In the chronic phase, there may be ongoing tubulitis involving predominantly the atrophic tubules. Thus, the pathology defines two patterns of TIN with functional implications: acute TIN implies a rapid onset and potentially reversible injury whereas chronic TIN implies chronicity and less likely reversibility (Table 3.10).

TABLE 3.10 Interstitial pathology

Acute (potentially reversible)
Edema
Cellular infiltrates (neutrophils, eosinophils, lymphocytes, monocytes, macrophages and plasma cells)
Infectious agents
Bacteria
Fungi
Immune aggregates and electron-dense deposits
Hemorrhage
Chronic
Fibrosis
Granulomas
Amyloidosis
Calcification
Crystals

Pathologic Processes Involving the Renal Interstitium

The remainder of this section covers the pathologic processes that involve the renal interstitium. Table 3.11 summarizes the different patterns of interstitial injury and lists the differential diagnosis of each.

Inflammation

The inflammatory process begins with injury, proceeds in a highly regulated fashion, and can result either in resolution, with return to normal histology and function, or in scarring and loss of function. Because of the stereotypic pathology associated with increased vascular permeability, recruitment, and exudation of leukocytes, and scar formation, the pathology of inflammation is not etiologically specific, and in the absence of a demonstrated pathogen or causative agent, the final diagnosis and the determination of cause usually require clinicopathologic correlation.

Edema

Interstitial edema is an early feature of inflammation, and it usually occurs in concert with cellular infiltration. Because humoral mediators of inflammation that alter vascular permeability cause edema, it may occur without significant exudation of leukocytes. In trichrome-stained sections, edema fluid is pale blue or optically clear, and at high magnification, the collagen fibers are widely separated (Fig. 3.15A). In contrast, trichrome staining of interstitial fibrosis is intensely blue with closely packed fibers (see Fig. 3.15F). Ultrastructural examination confirms the absence of increased interstitial collagen when edema is present.

Leukocytic Infiltrates

Leukocytic infiltrates are a component of acute TIN and chronic TIN, and they include neutrophils, eosinophils, lymphocytes, plasma cells, and monocytes/macrophages (see Fig. 3.15B). Table 3.12 lists the diseases associated with the different leukocytes and the chapter in which these diseases are discussed in detail. Although the cellular composition of the infiltrates is not pathognomonic, several associations deserve emphasis. *Neutrophils*, especially when they form microabscesses in the

TABLE 3.11 Patterns of interstitial injury observed by light microscopy and some but not all of the diseases that can cause each pattern of injury

Interstitial expansion by clear edema fluid
Acute tubular injury (without overt necrosis)
Acute tubular necrosis
Renal vein thrombosis
Nephrotic syndrome
Acute glomerulonephritis
Thrombotic microangiopathy
Interstitial expansion by extracellular eosinophilic material
Congo red negative (fibrosis)
Congo red positive (amyloid)
Interstitial expansion by leukocytes (see Table 3.12)
Interstitial foam cells
Hereditary nephritis (Alport syndrome)
Nephrotic syndrome with lipiduria
Interstitial hemorrhage
Severe glomerulonephritis with rupture of Bowman capsule
Malignant hypertension
Vasculitis, especially medullary angiitis
Acute rejection
Interstitial expansion by neoplastic cells
Lymphoma
Leukemia
Primary renal carcinomas
Metastases
Crystals and mineral deposits
Nephrocalcinosis
Phosphate nephropathy (calcium phosphate)
ARF (calcium oxalate)
Uric acid (gout)
Cholesterol (nephrotic syndrome with lipiduria)

interstitium and when they cause tubulitis and collect in the tubules (neutrophil casts) (see Fig. 3.15C), are highly suggestive of acute bacterial pyelonephritis, and in the presence of these histologic findings, clinical correlation and bacteriologic culture should be used to confirm the diagnosis. *Eosinophils* occur in various situations, but drug-induced TIN is one condition that is common in clinical nephrology. Identification and withdrawal of the causative agent often reverses drug-induced TIN.

Granulomas

Granulomatous tubulointerstitial nephritis (GIN) has a characteristic histology, especially when the granulomas have a classic appearance with a cuff of lymphocytes, epithelioid histiocytes, and giant cells (see Fig. 3.15D). Although drug reactions, infections, and sarcoidosis cause most renal granulomatous disease, like other inflammatory reactions, the granulomas are not pathognomonic. The differential diagnosis requires histochemical identification of acid-fast and fungal organisms, urine cultures to diagnose pyelonephritis, and clinical history and laboratory examination to identify drug reactions and sarcoidosis. In developed countries, most TIN with granulomatous inflammation is a later (subacute) phase of acute hypersensitivity TIN (see Chapter 25).

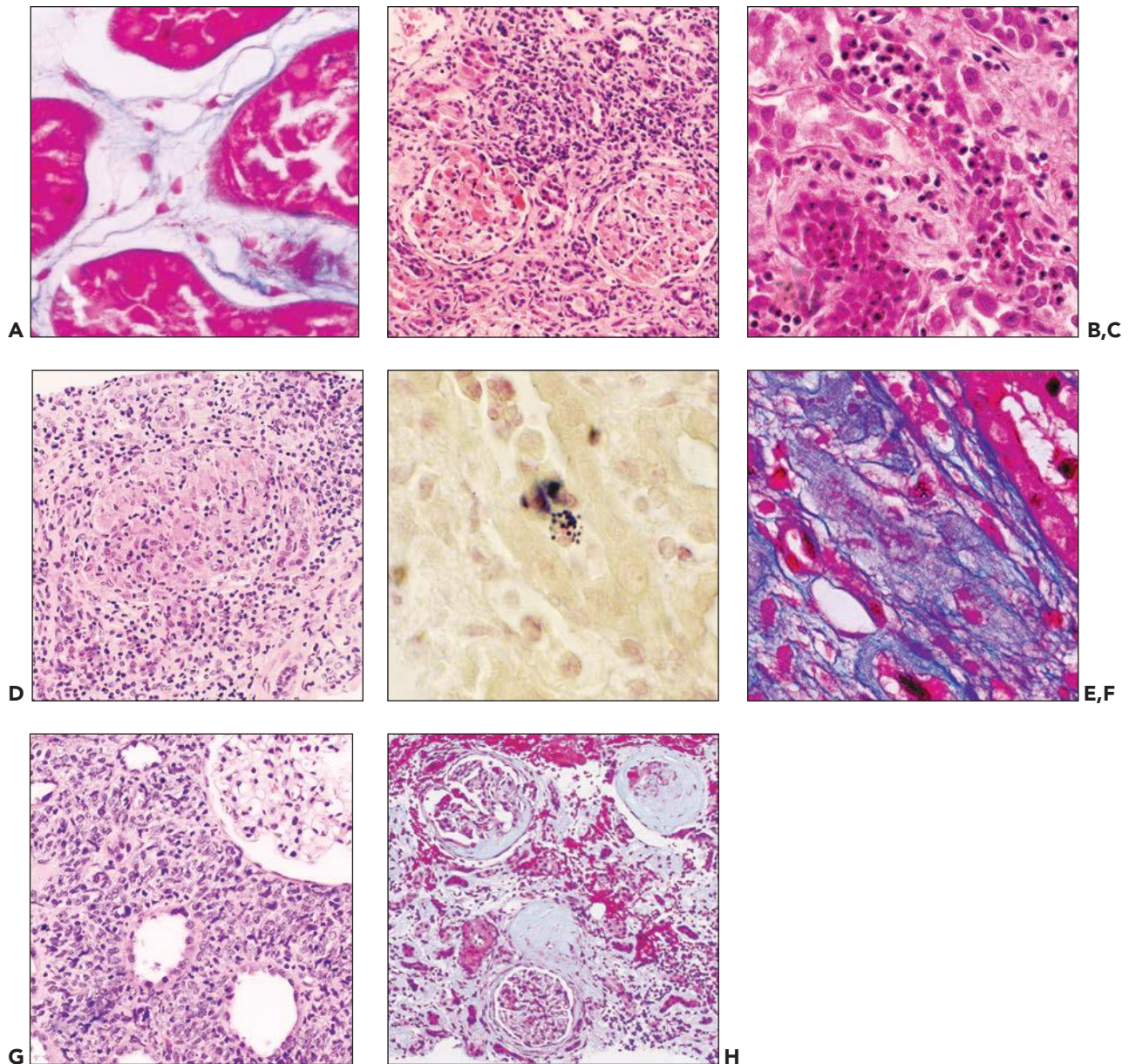


FIGURE 3.15 Patterns of interstitial injury observed by light microscopy. **A:** Interstitial edema. The renal tubules are separated by expanded interstitium containing distended vascular spaces and separation of the collagen fibers by edema fluid. (Masson trichrome, $\times 540$.) **B:** Acute TIN. This lesion is characterized by a predominantly lymphocytic infiltrate with preservation of the glomeruli and vascular structures. (H&E, $\times 150$.) **C:** Neutrophilic interstitial infiltrate with pus casts. Acute pyelonephritis. The tubules contain neutrophils (pus casts), and the edematous interstitium contains scattered neutrophils. (H&E, $\times 540$.) **D:** GIN caused by sarcoidosis. The granuloma comprises a central sheet of epithelioid macrophages with abundant eosinophilic cytoplasm surrounded by scattered lymphocytes. The biopsy also contained abundant multinucleated giant cells and active tubular and glomerular destruction (not illustrated). (H&E, $\times 540$.) **E:** *Staphylococcus aureus* pyelonephritis. Intracellular bacteria seen within a renal tubule. (Brown and Brenn stain [tissue Gram stain], $\times 1370$.) **F:** Chronic TIN. Atrophic tubules and epithelial cells are scattered within dense fibrous tissue. (Masson trichrome, $\times 540$.) **G:** Diffuse large cell B-cell lymphoma. The interstitium is diffusely expanded by neoplastic lymphocytes. The tubules are atrophic with thinned epithelium and loss of brush borders, and the glomeruli appear well preserved. (H&E, $\times 540$.) **H:** Chronic TIN with secondary glomerular pathology. The glomeruli show various degenerative changes including periglomerular fibrosis, hilar sclerosis, and global sclerosis. (Trichrome, $\times 150$.)

TABLE 3.12 The differential diagnosis of cellular interstitial infiltrates based on the predominant cell type

Disorder/Disease	Chapter
Neutrophils	
Bacterial infectious (acute pyelonephritis)	24
Eosinophils	
Drug-induced	25
ANCA vasculitis	16
Lymphoplasmacytic	
Drug-induced	25
Infectious	24
Anti-TBM (tubular basement membrane)	25
Immune complex TIN	25
Acute rejection, cellular	29
Autoimmune-associated	14
Macrophages/Granulomatous	
Drug-induced	25
Tuberculosis	24
Sarcoidosis	25
Xanthogranulomatous pyelonephritis	24
Malakoplakia	24
Neoplastic leukocytes	
Lymphoma	30
Leukemia	30
Posttransplant lymphoproliferative disorder	29

Infectious Agents

Bacteria, mycobacteria, fungi, and viruses can be observed in renal biopsies with special stains, immunohistochemistry, in situ hybridization and electron microscopy (see Fig. 3.15E). However, in many instances, documentation of an infection that is causing tubulointerstitial inflammation is made by clinical observations and microbiologic laboratory methods.

Immune Aggregates

Interstitial aggregates of immunoglobulin and complement components may accompany similar deposits in the TBMs or surrounding the peritubular capillaries. The immune aggregates activate complement and cause interstitial inflammation.

Fibrosis

Interstitial fibrosis is the scarring phase of the inflammatory process, and is invariably associated with tubular atrophy whether it is a primary interstitial disease or is secondary to glomerular or vascular disease. There often are scattered lymphocytes and macrophages associated with interstitial fibrosis. The interstitial expansion seen with fibrosis is eosinophilic with the hematoxylin and eosin stain, and it is dense blue with the trichrome stain (see Fig. 3.15F).

Neoplasia

There are rare benign tumors of the resident interstitial cells (medullary fibroma), but the most common interstitial neoplasms are metastatic epithelial tumors or hematologic lymphoproliferative disorders (see Fig. 3.15G) (see Chapter 30).

Other Causes of Interstitial Expansion

Accumulation of amyloid fibrils expands the interstitium in amyloidosis. In rare cases, the interstitial deposits predominate, but interstitial amyloid usually accompanies the more common glomerular and vascular deposits. The pathognomonic deposits are Congo red positive and appear as 10- to 12-nm randomly arranged fibrils by electron microscopy. Interstitial *hemorrhage*, indicating loss of vascular integrity, occurs in diverse diseases including severe hypertension, vasculitis, and acute humoral allograft rejection. *Crystals* with a characteristic appearance may blandly deposit in the interstitium (calcium oxalate) or they may excite a chronic granulomatous reaction (uric acid). Prominent interstitial collections of *foam cells* cause interstitial expansion in patients with long-standing, severe nephrotic syndrome with hyperlipidemia and patients with hereditary nephritis (Alport syndrome). The foam cells originate from macrophages, and the cytoplasmic vacuoles contain lipid. On occasion Tamm-Horsfall casts may rupture the tubules and incite an inflammatory reaction.

THE PATHOLOGIC DIAGNOSIS OF RENAL VASCULAR DISEASE

The kidney is a vascular organ receiving 20% of the cardiac output. In addition, much of the function of the kidney depends on careful regulation of blood flow to its various compartments. Different segments of the nephron have varying susceptibility to changes in hemodynamics including both pressure and flow.

Vessels can be damaged by hypertension, inflammation, deposition of material, toxins, and hypercoagulable states (Table 3.13). Each of these mechanisms of injury results in different forms of damage that may aid in the determination of the cause of injury. Vasculitis has mural infiltration by leukocytes, often with leukocytoclasia. Atheroemboli may lodge in the lumen and incite an inflammatory or thrombotic response. Materials such as amyloid or monoclonal light chain may be deposited in the wall of the vessel, interfering with its normal function. Toxic substances (e.g., cisplatin) may damage the endothelial layer, leading to thrombotic microangiopathy, or may injure the smooth muscle cells, leading to peripheral hyalin in the case of calcineurin inhibitor toxicity. Hypertension leads to several different alterations including hyaline deposits (glassy acidophilic PAS-positive material) in the walls of arterioles, replication of internal elastic lamina in arteries, medial hypertrophy, medial atrophy, medial sclerosis or, with severe hypertension, fibrinoid necrosis of arterioles and edematous (myxoid) intimal expansion in arteries. *Vasculitis* is defined as inflammation in a vessel wall. Any size of renal vessel may be affected. It is characterized by leukocytic infiltration, karyorrhexis, fibrin exudates, and, rarely granulomatous reaction (Fig. 3.16A). The internal elastic lamina may also be damaged, resulting in interruption, which may be determined with an elastic stain or Jones methenamine silver stain. Aneurysms may form, which usually are actually pseudoaneurysms caused by erosion of the necrotizing process through the vessel wall and into the perivascular tissue rather than dilation of the vessel wall. There may be hemorrhage into the interstitium. Arteritis is often complicated by thrombus formation, which with time may recanalize. The renal parenchyma distal to a thrombus may undergo infarction

TABLE 3.13 Mechanisms of vascular injury and their manifestations

Chronic Hypertension (Arterionephrosclerosis)
Hyaline arteriosclerosis
Arterial medial hypertrophy, atrophy, and sclerosis
Arterial fibrotic intimal thickening
Arterial replication of internal elastic lamina
Inflammation (Vasculitis)
Mural leukocyte infiltration and leukocytoclasia
Endothelialitis (Enderteritis)
Peritubular capillaritis
Medullary angiitis
Fibrinoid necrosis
Pseudoaneurysm
Thrombosis
Hypercoagulable States (Thrombotic Microangiopathy and Malignant Hypertension)
Thrombosis
Glomerular endothelial injury
GBM remodeling
Glomerular mesangiolysis
Arteriolar fibrinoid necrosis
Arterial edematous (myxoid) intimal thickening
Vasotoxins
Hyaline arteriopathy (e.g., calcineurin inhibitor toxicity)
Thrombotic microangiopathy (e.g., cisplatin)
Mural deposition of material
Hyaline arteriosclerosis
Amyloidosis
Abnormal metabolic products (e.g., Fabry disease)

followed by fibrosis. In the special case of vascular rejection, the inflammation may be limited to the subendothelial space of arteries (endarteritis) and may involve the peritubular capillaries (capillaritis). Veins may also be involved by inflammation in some forms of vasculitis. The medullary vasa recta can be affected, most often in ANCA-associated vasculitides, resulting in hemorrhagic leukocytoclastic angiitis (medullary angiitis) and rarely papillary necrosis.

Deposition of materials in vessel walls (e.g., amyloid) is recognized by loss of the normal structure (see Fig. 3.16B). Special stains, such as Congo red, PAS, or silver stain may help to determine its presence. Amyloid stains orange with Congo red and shows circular dichroism with apple green to yellow birefringence under polarized light. It does not stain well with either silver or PAS, giving a negative image in areas that normally would be positive.

Vasotoxic substances such as drugs (e.g., cisplatin) or *E. coli* toxins (Shiga toxin) may directly damage the endothelial cells, leading to thrombotic microangiopathy (see Fig. 3.16C), which is characterized by endothelial cell swelling and intimal edema with the formation of platelet fibrin thrombi with schistocytes (fragmented RBCs) in thrombi and injured vessel walls. The calcineurin inhibitors injure the arteriolar smooth muscle cells, resulting in myocyte dropout and the deposition of beaded peripheral hyaline material that projects outward from the adventitial side of the vessel (see Fig. 3.16D). This peripheral hyaline material should be distinguished from

hyaline arteriosclerosis (discussed below), which is more evenly distributed predominantly in a subendothelial location in the clinical setting of systemic hypertension or aging.

Hypertension leads to injury in all parts of the arterial wall and over time results in chronic changes. The arterial and arteriolar smooth muscle may become damaged by elevated blood pressure, resulting in signals that lead to remodeling of the wall to medial hypertrophy (see Fig. 3.16E). In these cases, the wall is thicker than expected for the overall size of the vessel. Endothelial injury is accompanied by hyaline arteriosclerosis (see Fig. 3.16F). On H&E, hyaline arteriosclerosis is glassy pink material. It stains magenta on PAS stain. It is thought to represent vascular insudation of plasma proteins. By immunofluorescence, hyaline often stains with antisera to IgM, C3, and C1q; by electron microscopy, it typically appears homogeneous and electron dense. This change interferes with the normal autoregulatory capacity of small vessels and when severe may compromise blood flow because of narrowing of the lumen. Very high levels of blood pressure may produce fibrinoid necrosis (see Fig. 3.16G), which is similar to that seen in other thrombotic microangiopathies but differs from vasculitis by virtue of the absence of inflammatory cells. Fibrinoid material in fibrinoid necrosis has a fibrillar texture that is different from the glassy, hard appearance of hyaline. Another helpful clue is that fibrin tends to stain more brightly red and hyaline more pink in H&E preparations.

Chronic hypertension in larger vessels leads to fibrointimal hyperplasia (see Fig. 3.16H), a change that may also be seen with aging. Prolonged hypertension may produce replication of the internal elastic lamina (see Fig. 3.16I).

Secondary effects of primary disease of the vascular bed cause varying patterns of injury in the remaining compartments. The extent of the alterations in other compartments may indicate the size of the vessel involved. Similarly, a pattern of injury within the distribution of a vessel suggests that the cause is vascular rather than the result of primary tubular, interstitial, or glomerular disease. For example, the recognition of a vascular pattern of focal injury called *striped fibrosis* is often associated with calcineurin inhibitor toxicity. The nature of the injury in a vessel can help resolve the differential diagnosis. For example, recognition that injury in an arteriole is fibrinoid necrosis rather than hyaline arteriosclerosis helps determine the cause of the injury.

CONCLUSIONS

The number of patterns of injury affecting the various renal compartments is limited; however, in most instances, a clinically informed and careful, knowledgeable evaluation of a properly prepared renal biopsy specimen that is examined by light, immunofluorescence, and electron microscopy renders the correct diagnosis. The acumen to make the most accurate and clinically useful diagnosis is not easily reduced to an algorithm, which by its nature depends on simplification. One disease may have different patterns or it may affect multiple histologic compartments so that it will appear in many places in any but the most simplistic scheme. Even well-defined patterns of glomerular damage are rarely specific for a single clinicopathologic entity. Therefore, the algorithmic approach is useful in specific instances, but in general, the renal diagnosis

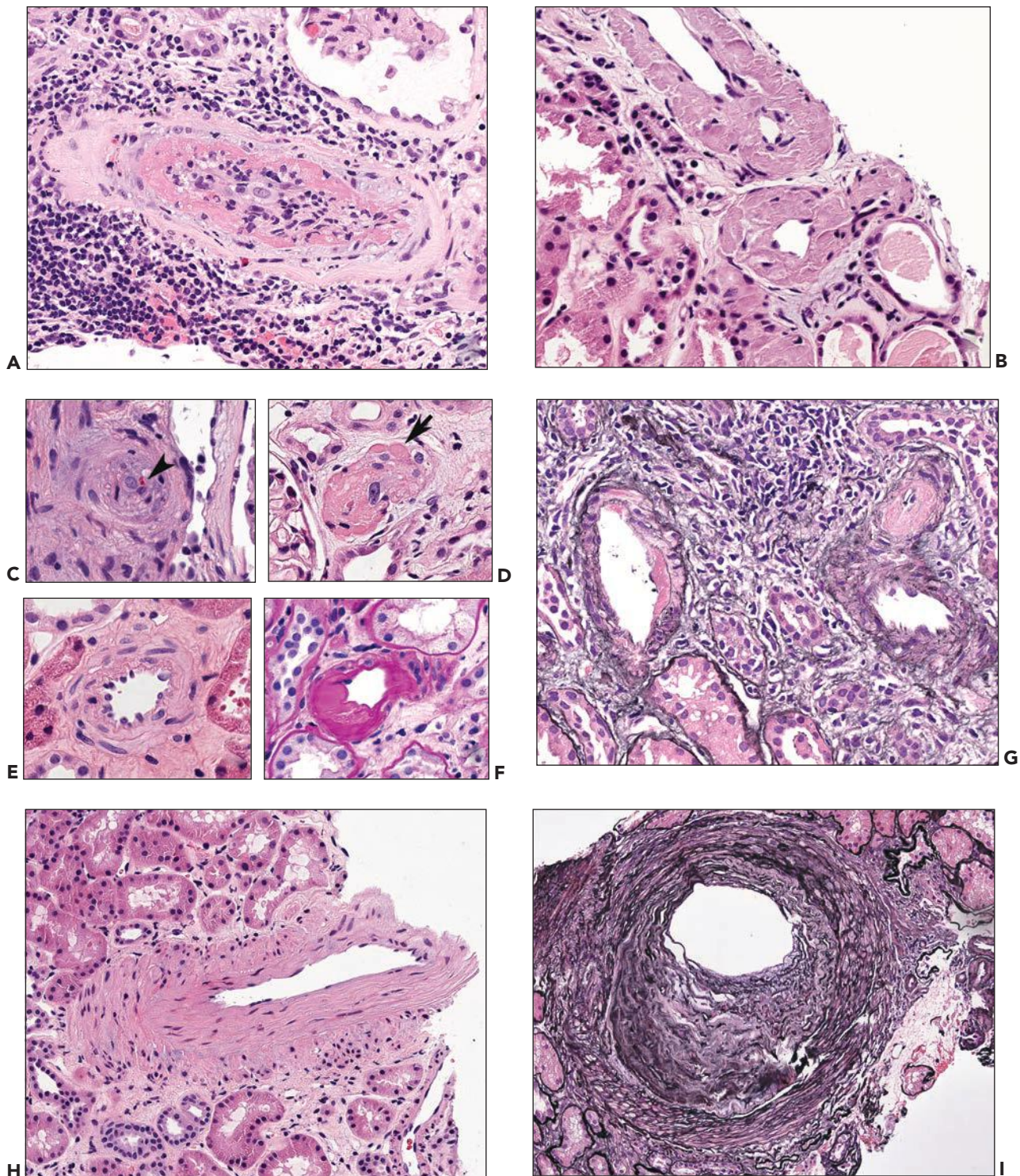


FIGURE 3.16 Patterns of vascular pathology observed by light microscopy. **A:** Vasculitis of an interlobular artery characterized by fibrinoid necrosis (*eosinophilic material expanding the intima*) with swollen endothelial cells accompanied by inflammation that extends into the wall. (H&E, $\times 260$.) **B:** Amyloid deposited in wall of an interlobular artery. Note portion of wall lacking cell nuclei with amorphous structure. (H&E, $\times 260$.) **C:** Arteriole with platelet fibrin thrombus and schistocytes (*arrowhead*) characteristic of thrombotic microangiopathy. (H&E, $\times 300$.) **D:** Afferent arteriole showing peripheral hyaline (*arrow*) extending out from the outside of the vessel filling smooth muscle cells. (H&E, $\times 325$.) **E:** Arteriole with medial hypertrophy showing too many layers of smooth muscle cells for the size of the vessel. (H&E, $\times 285$.) **F:** Vessel showing hyaline arteriosclerosis staining magenta with a glassy hard appearance. Note intimal location in contrast to peripheral location associated with calcineurin inhibitor toxicity. (PAS, $\times 315$.) **G:** Fibrinoid necrosis of two arterioles showing intimal accumulation of pink material with fibrillar texture. Note lack of inflammation. The vessel to the right has near occlusion of the lumen by this process. (PAS-Jones, $\times 260$.) **H:** Arcuate artery showing fibrointimal thickening resulting in a narrowed lumen. (H&E, $\times 165$.) **I:** Replication of the internal elastic lamina can be identified on H&E, but is more easily detected on silver or elastic stain. (PAS-Jones, $\times 125$.)

requires a more sophisticated integration of histology with immunopathology, ultrastructure, clinical information, and laboratory data.

The pathologic diagnosis of renal disease proceeds in a logical fashion from the histologic features to the diagnosis, and the correct interpretation of the pathology requires knowledge and experience. Because clinical history and laboratory findings are critical information, it is important to know the questions being asked of the biopsy. With the clinical information in mind, the pathologist must first determine which histologic compartments are involved and then must decide which one is the site of primary disease. In addition, the pathologist must identify the pathologic features and, when appropriate, estimate the extent of the abnormalities. When indicated, the pathologist should inquire about additional clinical details and issues raised by the pathologic findings. The final diagnosis results from the integration of all available data. In addition to a morphologic diagnosis, the renal pathology should answer clinically relevant questions concerning prognosis and therapy, and it should identify important secondary processes. Finally, the biopsy enhances understanding of renal pathophysiology and stimulates the study of renal disease with the ultimate goal of improved prevention and treatment of kidney diseases.

REFERENCES

1. Weening J, Jennette JC. Historical milestones in renal pathology. *Virchows Arch* 2012;461:3.
2. Heptinstall RH. *Pathology of the Kidney*, 1st ed. Boston: Little, Brown and Company, 1966.
3. Papper S. *Clinical Nephrology*, 2nd ed. Philadelphia: Little, Brown and Company, 1978.
4. Walker PD. The renal biopsy. *Arch Pathol Lab Med* 2009;133:181.
5. Walker PD, Cavallo T, Bonsib SM. Practice guidelines for the renal biopsy. *Mod Pathol* 2004;17:1555.
6. Corwin HL, Schwartz MM, Lewis EJ. The importance of sample size in the interpretation of the renal biopsy. *Am J Nephrol* 1988;8:85.
7. Pirani CL, Pollak VE, Schwartz FD. The reproducibility of semiquantitative analyses of renal histology. *Nephron* 1964;29:230.
8. Austin HA III, Muenz LR, Joyce KM, et al. Diffuse proliferative lupus nephritis: identification of specific pathologic features affecting renal outcome. *Kidney Int* 1984;25:689.
9. Solez K, Racusen LC. The Banff classification revisited. *Kidney Int* 2013;83:201.
10. Solez K, Colvin RB, Racusen LC, et al. Banff 07 classification of renal allograft pathology: updates and future directions. *Am J Transplant* 2008;8:753.
11. Working Group of the International IgA Nephropathy Network and the Renal Pathology Society, Cattran DC, Coppo R, et al. The Oxford classification of IgA nephropathy: rationale, clinicopathological correlations, and classification. *Kidney Int* 2009;76:534.
12. Working Group of the International IgA Nephropathy Network and the Renal Pathology Society, Roberts IS, Cook HT, et al. The Oxford classification of IgA nephropathy: pathology definitions, correlations, and reproducibility. *Kidney Int* 2009;76:546.
13. Jennette JC, Falk RJ. Glomerular clinicopathologic syndromes. In: Greenberg A, Cheung AK, Coffman TM, et al., eds. *National Kidney Foundation Nephrology Primer*, 5th ed. San Diego: Academic Press, 2009:148, Chapter 16.
14. Jennette JC, Falk RJ. Diagnosis and management of glomerular diseases. *Med Clin North Am* 1997;81:653.
15. Madsen K, Tischer C. Anatomy of the kidney. In: Brenner BM, Rector FC Jr, eds. *The Kidney*, 7th ed. Philadelphia, PA: WB Saunders, 2004:17.
16. Schrier RW. ARF, AKI, or ATN? *Nat Rev Nephrol* 2010;6:1250.
17. Kohler JJ, Hosseini SH, Hoying-Brandt A, et al. Tenofovir renal toxicity targets mitochondria of renal proximal tubules. *Lab Invest* 2009;89:513.
18. Chapman JR. Longitudinal analysis of chronic allograft nephropathy: clinicopathologic correlations. *Kidney Int Suppl* 2005;S108.
19. Coppo R, D'Amico G. Factors predicting progression of IgA nephropathies. *J Nephrol* 2005;18:503.

Cystic Diseases and Developmental Kidney Defects

Cystic kidney diseases 119

- Polycystic kidney disease 120
- Renal medullary cysts 136
- Molecular pathogenesis of cystic kidney diseases 139
- Renal cysts in hereditary syndromes 144
- Multilocular renal cyst (multilocular cystic nephroma) 147
- Localized cystic disease 147
- Simple cortical cysts 148
- Acquired cystic kidney disease 148
- Miscellaneous renal cysts 149

Developmental kidney defects 151

- Cell and molecular biology 153
- Genes controlling nephrogenesis 153
- Nongenetic causes of renal malformations 157
- Teratogens and altered maternal diet may contribute to renal malformations 157
- Pathology 158

CYSTIC KIDNEY DISEASES

Cystic kidney diseases are heterogeneous in origin, distribution, and pathogenesis. Cysts usually originate in the tubules but may also involve the glomeruli. Depending on patient age and/or heredity, cysts are focal or diffuse, unilateral or bilateral, occur as an isolated defect, or accompanied by cysts in other organs. For example, cysts in the liver are common in autosomal dominant polycystic kidney disease (ADPKD). Most kidney cysts are benign; some are malignant or neoplastic with malignant potential. Genetic studies reveal an increasing number of mutations accompanying kidney cysts. Furthermore, mutations are now detected in entities previously thought to be sporadic (e.g., multicystic renal dysplasia and multilocular cyst/cystic nephroma). Early pathologic classifications were based mainly on morphologic characteristics

(1) or incorporated clinical, radiologic, and genetic criteria (2). More recently, some authors proposed to classify cystic kidney diseases based exclusively on pathogenesis, for example, under “ciliopathies.” This option follows new discoveries that show protein products of gene mutation causing cysts to be localized on cilia or their basal bodies. There are two types of cilia: motile and nonmotile or primary cilia, which are ubiquitous on eukaryotic cells, including renal tubular epithelial cells (3). Which classification will prevail in the future remains to be seen, but the success of a classification scheme is generally measured by its precision (the degree of observer variability in assigning a specific case to a specific category) and accuracy (the degree to which a specific category correlates with specific defining features). The cilia classification is conceptually more precise; however, not all cysts have a genetic cause; therefore, accurate grouping of the latter entities is not possible on the basis of genetics alone (4). In addition, the cilia classification, even though more precise, is complicated by significant phenotypic variability and clinical or pathologic overlap among various mutation-defined entities (5). Furthermore, the biologic function of cystic disease–related mutations is not fully understood, even though the frequently observed multiorgan involvement in hereditary cystic kidney diseases is far better explained, because cilia are widespread in tissues; thus, mutations in ciliary genes may affect multiple organs (3). Considering that a molecular/genetic classification of cystic kidney diseases is a work in progress and no universally accepted classification currently exists, the classification in the previous edition of this book still is valid and therefore is used in this edition with only minor modifications (Table 4.1). However, the many discoveries about the genetic basis for cystic diseases are reviewed in the context of this classification.

In examining cystic kidneys, the gross morphology and radiologic appearance are very important. The following basic questions are a useful guide: (a) are the cysts bilateral or unilateral, (b) focal or diffuse? or (c) is the kidney enlarged or approximately normal size? Multiple bilateral renal cysts are frequently hereditary, in contrast to isolated, unilateral cysts that are most often acquired. The term “polycystic” is conventionally reserved for ADPKD and autosomal recessive polycystic kidney disease (ARPKD). Multicystic is a term used for a subcategory of renal

TABLE 4.1 Classification of cystic kidney diseases

- A. Polycystic kidney disease**
1. Autosomal dominant (ADPKD)
 - a. Classic ADPKD in adults
 - b. Early-onset ADPKD in children
 2. Autosomal recessive (ARPKD)
 - a. Classic ARPKD in neonates and infants
 - b. Delayed-onset ARPKD in older children and adults
 3. GCKD
 - a. **Primary**
 1. ADPKD
 2. ARPKD
 3. ADGCKD (UROM)
 4. HNF1 β
 5. TSC2
 6. NPHP
 - b. **Secondary**
 - Renal dysplasia
 - Sporadic
 - Obstructive
 - Syndromic
 - Ischemic
 - Drug induced
- B. Renal medullary cysts**
1. NPH, autosomal recessive
 2. Medullary cystic disease (MCKD), autosomal dominant
 - a. MCKD 1
 - b. MCKD 2
 - c. UROM-associated hyperuricemia
 - d. Renin
 - e. HPRT1
 - f. SLC2A9
 3. MSK
- C. Cysts in hereditary cancer syndromes**
1. von Hippel-Lindau disease
 2. TSC
- D. Multilocular renal cyst and variants**
- E. Localized cystic disease**
- F. Simple cortical cysts**
- G. Acquired (dialysis-induced) cysts**
- H. Miscellaneous**
1. Pyelocalyceal diverticuli
 2. Perinephric pseudocysts
 3. Hygroma renalis-lymphangiomas

Note: multiple cysts may also occur with renal dysplasia but are not considered "cystic disease" but primarily a developmental defect.

dysplasia characterized by diffuse cysts that may grossly mimic ADPKD in early childhood, but the dysplastic features are apparent microscopically. Most cysts are tubular in origin; when cysts involve the glomeruli, cystic dilation of the Bowman space (>twice normal) involving greater than 5% of glomeruli are involved, the diagnosis of glomerulocystic kidney disease (GCKD) is appropriate. GCKD can be primary or secondary; for example, childhood ADPKD may present as primary GCKD and vascular ischemia can cause secondary GCKD (6).

Medullary cystic disease is an autosomal dominant tubulointerstitial disease of adults with end-stage renal disease (ESRD) occurring in the fourth to seventh decade. Two genetic loci for medullary cystic kidney disease (MCKD) are described: MCKD1 and MCKD2. Symptoms are similar but neither imaging studies nor histopathologic findings are specific as discussed later (7). Notably, some patients do not have cysts at all. MCKD was once thought to be the same entity as juvenile nephronophthisis (NPHP) due to the overlapping phenotypes (5). Clearly, NPHP is genetically distinct from MCKD with about 13 different genes causing a variety of clinical NPHP phenotypes. The MCKD1 locus is mapped to chromosome 1q21, but the gene remains unknown. The MCKD2 locus on chromosome 16p12 is identified as the uromodulin (UMOD) gene. UROM mutations may present as GCKD. Therefore, some authors prefer the term uromodulin disorders. Other authors propose to reclassify MCKD as one of the four types of autosomal dominant interstitial kidney disease (ADIKD). UMOD mutations in the proposed ADIKD classification encompass (a) MCKD2, (b) familial juvenile hyperuricemic nephropathy (FJHN), (c) uromodulin-associated kidney disease (UAKD), and (d) GCKD. Once again, we believe that at this time, our classification may be preferable for the intended readership.

Medullary sponge kidney (MSK) is a disease of adults characterized by cysts in the collecting ducts. Cysts are often discovered incidentally by excretory urography in patients investigated for urinary tract infections or stones. On radiology, calcified collecting ducts appear as filling defects (8). Kidney cysts can be neoplastic (9). Renal cysts associated with hereditary cancer syndromes such as von Hippel-Lindau (VHL) disease and tuberous sclerosis (TSC) are typically bilateral and multiple. Nonneoplastic, multilocular renal cyst is a distinct tumor mainly of childhood, also called cystic nephroma. The terms multilocular cystic nephroma (MCN), polycystic nephroblastoma, and cystic differentiated nephroblastoma describe the same entity with nephroblastoma added in some neoplasms that mimic Wilms tumor. For example, an intermediate form between multilocular cyst and Wilms tumor is described as cystic partially differentiated nephroblastoma. MCN is typically unilateral; bilateral presentation is exceptionally rare (10). A new association of pediatric cystic nephroma with lung tumors such as pleuropulmonary blastoma was recently reported; some patients have familial disease, suggesting that cystic nephroma that was once considered a benign and sporadic tumor at least in part has a genetic basis (11). An entity called localized cystic disease of the kidney is also described, apparently with no hereditary basis (12).

Simple cortical cysts, extrarenal cysts (parapelvic lymphangiectasis and perinephric pseudocysts), and hemodialysis-induced cysts have distinct pathogeneses and are discussed as separate entities (Table 4.1).

Polycystic Kidney Disease

Autosomal Dominant Polycystic Kidney Disease

INCIDENCE, CLINICAL PRESENTATION, AND GENETICS

ADPKD is the most common inherited cystic kidney disease affecting 1:500 to 1000 individuals worldwide and 2.3% of patients on dialysis in the United States (13–15).

Both men and women are affected, but women have a less severe disease. ADPKD is a systemic disease, and patients

experience multiple renal and extrarenal complications. Clinical symptoms usually appear after the third decade, but the phenotypic spectrum ranges from in utero onset to adequate renal function at old age. Common complications include kidney stones, infections, flank pain, gross hematuria, and hypertension. Hypertension and gross hematuria are often diagnosed before the age of 30 and thought of as markers of progressive disease (15,16). ESRD is common with mean age at 59 years, while approximately 15% of ADPKD patients retain adequate renal function at 80 years (17). Family history of ESRD plays an important role in predicting ESRD. ESRD at an earlier age (before 55 years) in at least one family member correlates with PKD1 mutations; if at least one family member developed ESRD greater than 70 years of age, this family history was predictive of PKD2 with a 100% predictive value (18). The liver is involved in 94% of cases in the Consortium of Radiologic Imaging Studies of Polycystic kidney Disease (CRISP) study and eventually becomes palpable but is unusual to manifest as massive liver disease that requires surgical intervention. A separate polycystic liver disease without renal involvement exists and is caused by mutations in non-ADPKD genes as discussed later under polycystic liver disease. Women have different rates of occurrence of renal and extrarenal complications in ADPKD, including liver cyst growth and expansion. Women tend to have more severe liver disease stimulated by estrogens (17,19). Women develop renal insufficiency with smaller renal volume than men, whereas liver cystic disease occurs earlier and more frequently in women than in men (Table 4.1). Pancreatic cysts are rare (present in only around 10% of patients), which is a distinguishing feature from other multiorgan hereditary cysts such as VHL disease (20,21). Other extrarenal manifestations include increased incidence of intracranial aneurysms (approximately 8% of ADPKD patients) and extracranial aneurysms, colon diverticula, and mitral valve prolapse.

Genetics have brought unprecedented insights in ADPKD pathogenesis. Ninety percent of affected individuals have a parent with the disease, and their children have a 50% chance of inheriting the condition. De novo mutations may account for about 10% of cases. Mutations are found in two genes, PKD1 and PKD2. A third gene (PKD3) was suspected based on reported isolated cases (less than 1%) but is not yet confirmed. However, lack of evidence in spite of intense search for a third gene is now suggesting that it likely does not exist (22). Recent methodologic advances have improved mutation detection, and at least 700 PKD1 and over 100 PKD2 mutations are reported, most of which are private (17,23–25). PKD1 contains 4,302 amino acids and PKD2 968 amino acids. PKD1 mutations were thought to affect 80% to 85% of patients, and PKD2 mutations the remaining 10% to 15%, but new data show that PKD2 may be more common affecting 26% to 36% of ADPKD patients (22). Most mutations are missense and inactivating, but there is no good genotype/phenotype correlation suggesting complex mechanisms including factors that affect protein trafficking (26), the mutation type on cilia, its functionality, and dosage, factors that may explain the variable clinical manifestations. For example, experimental data show that mutation characteristics may predict ESRD and rate of cyst development/growth in humans. Hopp et al. (27) show that Pkd1+ mice with PKD1p.R3277C(RC) knockin develop rapidly progressive disease in contrast to Pkd1+/- mice that

are normal. This model in which the level of functionality of the mutation product (dosage) determines cystogenesis mimics in utero onset in humans and typical ADPKD presentation in adults, respectively. In addition, concurrent mutation in other genes may also play a role. For example, the protein product of the gene defective in cystic fibrosis (CF), cystic fibrosis transmembrane conductance regulator (CFTR), plays a crucial role in fluid accumulation promoting cyst swelling (28). Patients with PKD1 have earlier onset of symptoms, in contrast to patients carrying PKD2 mutations who tend to have delayed cyst formation, hypertension, and ESRD, by 10 to 20 years. Both PKD1 and PKD2 genes exhibit extensive allelic heterogeneity that correlates with variable clinical manifestations (Table 4.2); 18% to 59% of the phenotypic differences in PKD1 are attributed to inherited background genes and perhaps environmental factors that modify disease expression but have no significant difference in life expectancy.

The PKD1 gene is located on chromosome 16p13.3 and consists of a large 53-kb genomic DNA with 46 exons. It encodes a 460-kDa protein, polycystin 1. PKD2 maps to chromosome 4q13-q23 and consists of a smaller DNA sequence of 5.4 kb with 15 exons that encodes polycystin 2. The gene products are called polycystin 1 and 2, respectively. The precise role of mutated polycystins in cyst formation is still under investigation. It is proposed that individual cystogenesis requires biallelic inactivation of a polycystic disease gene through germ-line and somatic mutations within an epithelial cell (the second-hit hypothesis). In this model, the second hit is the limiting step. This hypothesis is supported by genetic studies of cystic epithelia from ADPKD patients and mouse models (25,29). Activated normal polycystin 1 is thought to be an epithelial cell membrane receptor sensing cues in the extracellular environment required for renal tubular epithelial cell division and differentiation. Mutated polycystin 1 is only detected in cytoplasmic pools in cystic cells. Polycystin 2 is a smaller molecule localized in the plasma membrane and the endoplasmic reticulum and has structural similarities with a family of sodium/calcium channels, thus thought to modulate intracellular levels of Ca²⁺ (30). Polycystin 1 and 2 have similar cellular distribution providing a biochemical basis for the identical phenotypes caused by PKD1 and PKD2 mutations.

TABLE 4.2 Phenotypic variability in ADPKD is gene dependent (17–21)

	ADPKD1 16p 13.3 (85% of all patients)	ADPKD2 4p21
Age at presentation	30 y	>50 y
Average kidney size	>1 kg	650 g
Number of cysts	More and earlier development	Fewer cysts but same growth rate
ESRD	50 y	70 y
Hypertension	Common and severe	Less severe
Liver cysts	Common	Common
Intracranial aneurysms	~8%	Yes
Pancreatic cysts	Yes	Yes
Gender	Men have worse disease	

However, other factors such as altered responsiveness to c-AMP may be more important inducers of cysts (31), and there may be an important role for effects on primary cilia (25).

Genetic testing is possible by either linkage analysis in large families with several affected members or direct mutation screening. Linkage analysis is limited by the fact that a minimum of four affected family members are required; in small families with a single individual member affected, this test cannot be performed. Direct sequencing is more sensitive and detects about 70% of ADPKD mutations (32). However, for various reasons in the remaining 30%, the results are ambiguous or negative. Therefore, this approach also has limitations, and there are patients subjected to genetic analysis without definitive results. Genetic analysis methods continue to evolve and include next-generation technologies. Preimplantation diagnosis is also possible (33).

RADIOLOGIC EVALUATION

Ultrasound, computed tomography (CT), and magnetic resonance imaging (MRI) are essential for ADPKD diagnosis, patient follow-up, and lately a choice for therapeutic intervention (interventional radiology to minimize cyst volume). Ultrasound is more frequently used for screening, but CT and MRI are more sensitive particularly in early detection of ADPKD when the cysts may be small and or few. Characteristic findings of classic ADPKD are bilaterally enlarged kidneys with multiple cysts with varying signal intensity (Fig. 4.1). Hemorrhage, tumors within a cyst, or infection generates a high-intensity signal on CT or MRI. Concurrent liver cysts are a frequent finding. Total kidney volume is a major indicator for disease progression, and new methods that reliably measure ADPKD progression were initiated by the CRISP (20). The CRISP study revealed that cyst enlargement contributed to renal impairment and correlated with hypertension; in contrast, smaller cysts on MRI were frequently found in normotensive patients. By 30 years of age, most ADPKD patients have radiologic evidence of kidney cysts. Adults less than 30 years of age and children may

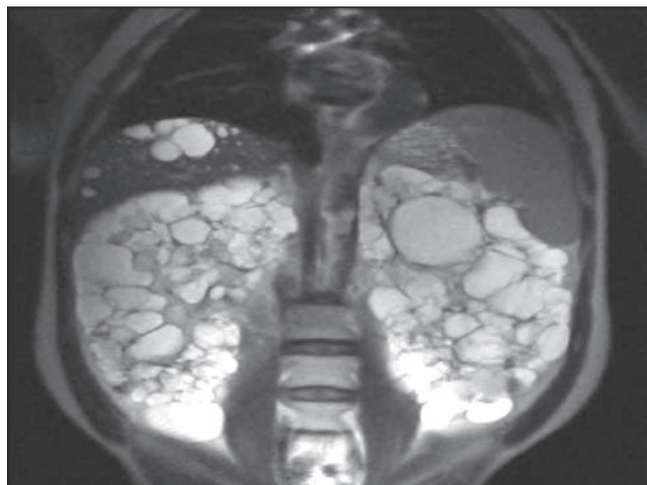


FIGURE 4.1 Coronal T2-weighted CT image shows innumerable bright-appearing cysts replacing both the kidneys and liver of a 54-year-old man with ADPKD. (Courtesy of Cary Lynn Siegel, Mallinckrodt Institute of Radiology, Washington University, Saint Louis, MO.)

have asymmetric kidney involvement (unilateral and few cysts). Diagnosis is not problematic in classic adult ADPKD, but phenotypic variability in early stages may hamper recognition and management of patients with only a few cysts, even when family history of ADPKD is known. Ultrasound lacks diagnostic accuracy particularly in infantile and childhood-onset ADPKD. On ultrasound, ADPKD mimics ARPKD and GCK, bilateral cystic dysplasia, and Meckel-Gruber syndrome (Fig. 4.2). Furthermore, the majority of fetuses screened by ultrasound show no apparent renal or extrarenal cysts, and children may be asymptomatic and not develop cysts for 10 to 20 years after birth. Ninety percent of patients have an affected parent, and diagnosis is highly likely if more than one generation has multiple large cysts with no other symptoms/signs. The traditional guide for family screening is that around 95% of affected individuals will have cysts by the time they reach 30, but Pei et al. (34) recently refined this algorithm because it tended to underdiagnose PKD2-affected families: three or more renal cysts establish a diagnosis of PKD between 15 and 39 years; two or more cysts in each kidney are sufficient for individuals aged 40 to 59 years; and four or more cysts in each kidney are required for individuals ≥ 60 years old (Table 4.3) (15,22,34). Nonetheless, a 19% to 38% false-negative rate is reported in age-specific radiologic analysis of patients with known ADPKD



FIGURE 4.2 Ultrasound from a young child shows nephromegaly with increased echogenicity and multiple discrete cysts with ADPKD. Features are indistinguishable from ARPKD. (Courtesy of Dr. Christine Menias, Mallinckrodt Institute of Radiology, Washington University, Saint Louis, MO.)

TABLE 4.3 Revised radiologic criteria for ADPKD (34,60)

Age	Number of Cysts	Positive predictive value	Negative predictive value
15–29	≥3 cysts unilateral or bilateral	100	85.5
30–39	≥3 cysts unilateral or bilateral	100	96.4
40–59	≥2 cysts in each kidney	100	94.8
≥60	≥4 cysts in each kidney	100	100

genotype (35). This does not include the small proportion (5% to 10%) of children with no apparent history of ADPKD at the time of first presentation and a presumed new mutation. The differential diagnosis includes ARPKD and malignancy, as discussed further below.

PATHOLOGY

Pathology of ADPKD can be divided into the typical adult presentation and atypical presentation in children (early-onset ADPKD). In adults, ADPKD kidneys are not routinely resected; when patients develop severe complications, such as recurrent and severe back pain, bleeding, or infection, or prior to renal transplantation, surgical removal reveals enormous bosselated kidneys. The kidneys weigh on average 2.5 kg each (mean normal kidney weight equals 0.150 kg). The smaller ADPKD kidneys in adults weighing less than 1 kg may represent PKD2 mutations (see Table 4.2 and Fig. 4.3). The reniform appearance of the kidneys is lost, and the kidney is distorted by multiple cysts that may contain clear, turbid, gelatinous, or hemorrhagic fluid. On sagittal sections, cysts are typically unilocular, oval, or spherical, vary in size from millimeters to several centimeters, and are randomly distributed. The renal pelvis and calyces cannot be identified, and

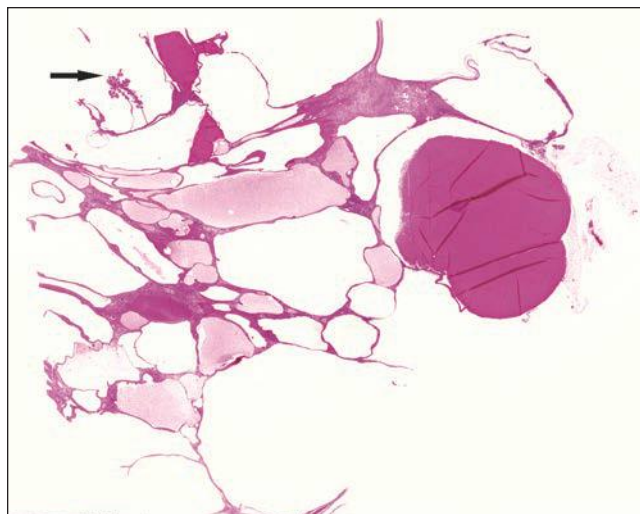


FIGURE 4.4 ADPKD microscopic pathology. Multiple, varying in size, cysts replace the kidney parenchyma. The cysts contain a characteristic dark staining fluid; focal papillary microadenomas (*arrow*) growing within the cysts are frequent (whole slide scanned).

replacement of the normal renal parenchyma is usually extensive. Residual renal parenchyma is compressed and eventually becomes atrophic by the enlarging cysts filled with eosinophilic fluid (Fig. 4.4). Interstitial fibrosis abounds in most specimens. Globally sclerosed glomeruli are increased; cystic glomeruli are also frequently present likely secondary to vascular ischemia as parenchymal arteries are thickened (Fig. 4.5). However, even at end stage, there is significant number of intact-appearing glomeruli, which may explain why these severely distorted kidneys may continue to function for a long time in spite of cyst expansion. The epithelium lining the cysts is denuded, flat, or hyperproliferative. Proliferating epithelium within ADPKD

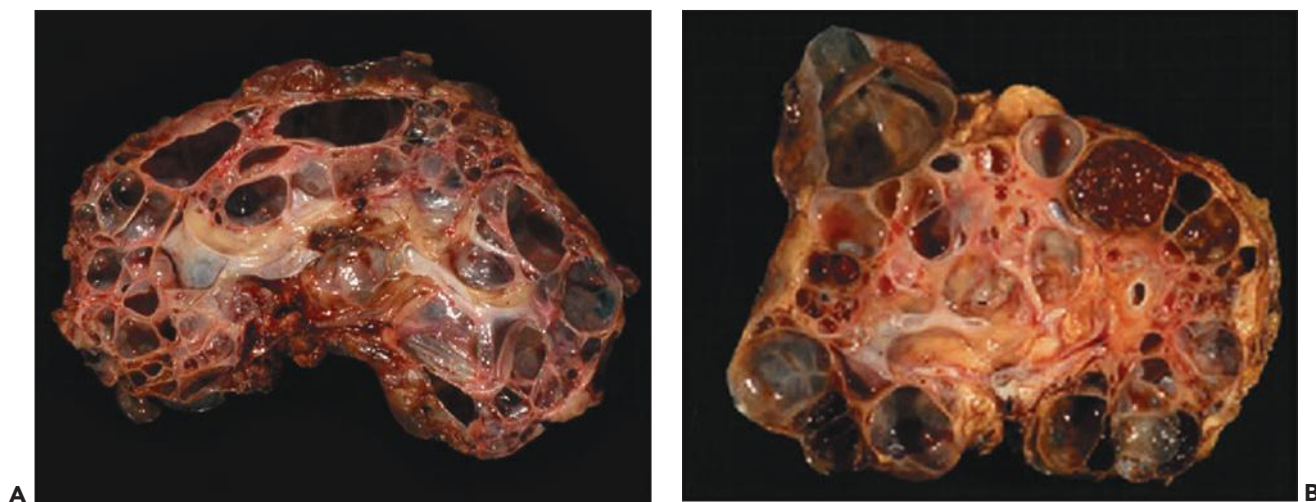


FIGURE 4.3 ADPKD gross pathology. **A:** A 1620-g left kidney from a 52-year-old woman. **B:** A 49-year-old woman with a 700-g right kidney.

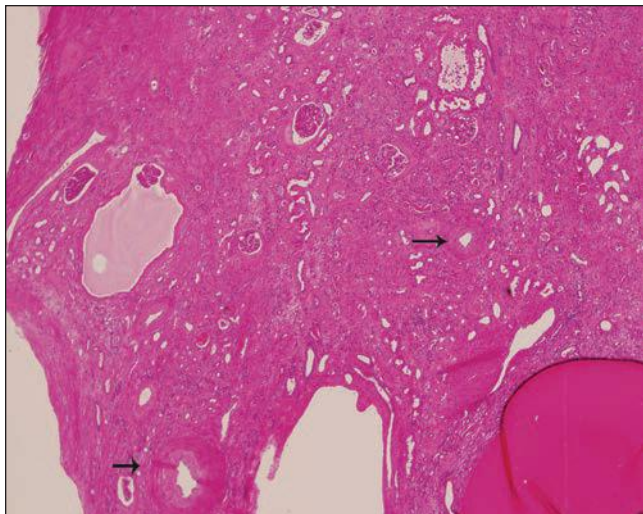


FIGURE 4.5 Advanced ADPKD with interstitial fibrosis, tubular atrophy partially preserved glomeruli (one with a glomerular cyst change), and thick interlobular arteries (arrows) between typical tubular cysts filled with eosinophilic fluid. (H&E $\times 40$)

cysts is indeed characteristic and not infrequently gives rise to papillary microadenomas that increased the risk for malignancy (Figs. 4.4 and 4.6). Micropolyps are present in as many as 90% of patients with ADPKD (36). They may be small with broad base or flower-like microadenomas.

ADPKD cysts arise in a small fraction (1% to 2%) of proximal and distal tubules early in childhood, and new cysts are unlikely to develop over a patient's lifetime. Cyst development follows gradual luminal dilation by tubular epithelial cell proliferation, apoptosis, and fluid accumulation. Eventually, cysts separate from the parent tubules and become a sac-like structure while their lining epithelial cells continue autonomous proliferation. Another feature of ADPKD epithelia is proliferation and loss of polarity and show characteristic

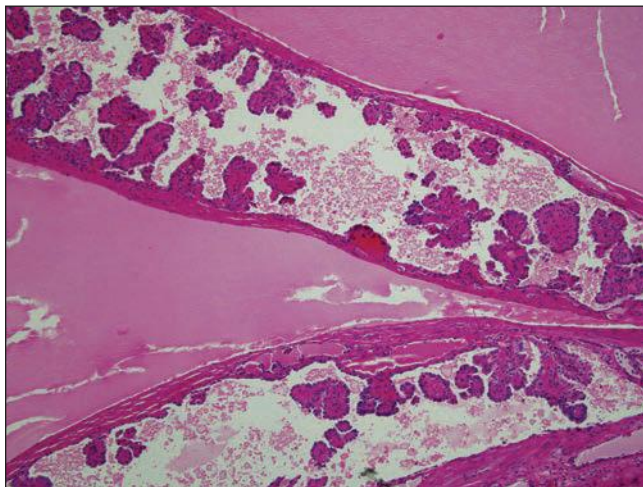


FIGURE 4.6 ADPKD with proliferating epithelia forming numerous micropapillae within fluid filled cysts. (H&E $\times 200$)

mis-polarization of proteins such as $\text{Na}^+\text{-K}^+\text{-ATPase}$ (37). Cell proliferation is accompanied by secretion of high amounts of electrolyte transport proteins that result in excessive secretion of solute and fluid into the cysts. These phenomena are consistent with a neoplastic-like phenotype in ADPKD epithelia, perhaps because the mutated polycystins are unable to maintain the normal state of epithelial differentiation and maturation (see under molecular biology of ADPKD). Other factors such as epidermal growth factor may also mediate cell proliferation and fluid secretion within the cysts (38). The observation that cyst formation involves a fraction and not all nephrons has immediate clinical implications and prompted intense research in designing clinical trials for early intervention to control cyst size (see Clinical Management, Prognosis, and Therapy). The relationship between kidney size and progression to renal failure is now clearly elucidated. In patients who develop renal failure, there is loss of noncystic parenchyma in association with nephron mass replacement by interstitial fibrosis. In fact, the size of the cysts correlates directly with the loss of renal function. Cysts prevent the drainage of urine from upstream tributaries, cause tubular atrophy, and release chemokines, cytokines, and growth factors resulting in the progression to fibrosis (39). Finally, while there is a lot of experimental evidence that implicates cilia in ADPKD, abnormal cilia in human disease is rarely demonstrated. Figure 4.7 shows cilia in normal and ADPKD tubular epithelial cells. Cells lining ADPKD cysts exhibit increased number of cilia and also supernumerary basal bodies compared to normal epithelial cells. These findings are similar to tubular epithelial spheroid cell cultures grown on Matrigel that form hollow structures mimicking tubule formation (40). Extra cilia derived from the same ciliary pocket (a specialized space in the root of cilia) suggest that the ciliary pocket may be the rate-limiting structure for trafficking of ciliary proteins in human ADPKD (see under Molecular Pathogenesis). However, additional studies in human tissues are required to derive definitive results on the pathology of cilia in human ADPKD.

MALIGNANCY IN ADPKD

There are numerous case reports of renal cell carcinoma (RCC) developing in ADPKD cystic kidneys and small patient series that show more than 10-fold increase of malignancy compared to the general population. Multifocal and bilateral RCC was reported by Jay Bernstein in as many as 20% of ADPKD kidneys enforcing the view that epithelial cells lining ADPKD cysts have neoplastic properties (41). However, others find no significantly increased risk. In the last 10 years, we have seen 6 RCCs in 22 resected ADPKD kidneys (that is equal to about 27% of resected ADPKD kidneys), but this number certainly represents a selection bias. Intracystic RCCs usually range from 1 to 4 cm and can be unilateral or bilateral. Histologically, tumors are typically RCCs, clear cell, papillary, or chromophobe type (Fig. 4.8). The predominant histologic type appears to be papillary RCC. Tumors are diagnosed on routine radiologic follow-up screening. Beyond RCC, other kidney malignancies, for example, transitional cell carcinoma, are found incidentally (Fig. 4.9).

EARLY-ONSET ADPKD

Early-onset ADPKD may start in utero and be apparent on fetal ultrasound. Postnatally, there is a spectrum of lesions ranging from unilateral cystic disease (Fig. 4.10) to just a few

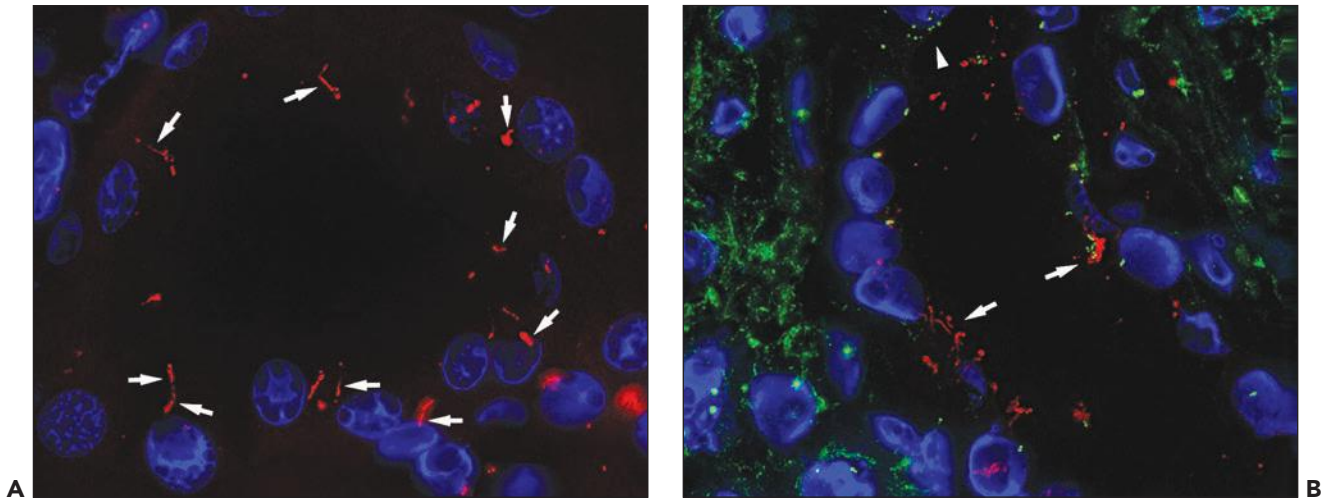


FIGURE 4.7 **A:** Normal human proximal tubule cilia stained with glutamylated tubulin (red) centrioles (green) and nuclei (blue). **B:** Cilia (arrows) from human ADPKD cyst lining epithelial cells are superciliated, and basal bodies are increased compared to control. (Courtesy of Moe Mahjoub, Renal Division, Washington University School of Medicine, Saint Louis, MO.)

isolated cysts (Fig. 4.11). This variability in ADPKD cyst development has prompted a revision of the previously established radiologic criteria for childhood ADPKD that lowered the threshold for at-risk individuals (34). A rare example of infantile ADPKD with gross pathology similar to adults is shown in Figure 4.12; cysts are filled with gelatinous fluid, and compared to Figure 4.3, this infantile kidney is nothing but a *miniature* image of adult ADPKD. In childhood ADPKD, concurrent liver or pancreas cysts facilitate the diagnosis (Fig. 4.13). However, more frequently than one may expect, a renal biopsy is performed to rule out early-onset ADPKD following ambiguous MRI or CT. Such cases also have unclear ADPKD

family history and absent extrarenal cysts. A constant and helpful finding is the finding of bilaterally enlarged kidneys (always a good indication for hereditary disease). The example shown in Figure 4.14 is from a 4.5-year-old boy who presented with acute renal failure, fever, and acute pyelonephritis. There was no family history of ADPKD. CT showed an infiltrating pattern suggestive of bilateral nephroblastomatosis or Wilms tumor. There were no liver lesions. Renal biopsy revealed cystic glomeruli and focal tubular dilation, but no evidence of blastema (Fig. 4.14B). There were no papillary proliferations. Tubular atrophy and chronic interstitial inflammation was minimal. Acute inflammatory cells were present in some



FIGURE 4.8 **ADPKD with intracystic RCC.** **A:** A distinct solid yellow tumor mass fills one of the cysts. **B:** The tumor consists of typical papillary RCC with focal microcalcifications.

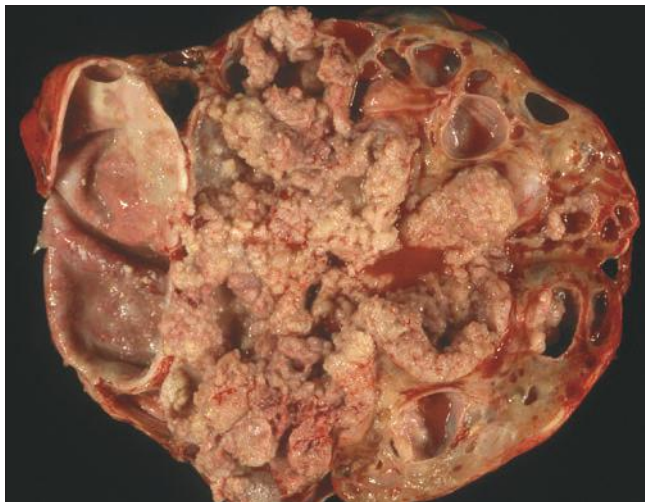


FIGURE 4.9 ADPKD with transitional cell carcinoma. Left nephrectomy from a 44-year-old woman. The kidney is enlarged (weight = 2,300 g). Multiple oval-shaped cysts are appreciated in the cortex. The tumor has a micropapillary gross appearance and infiltrates around the cysts. Microscopically, the tumor was transitional cell carcinoma arising in the renal pelvis. It involved the calyces and the ureter but did not extend into the cysts.

tubules consistent with the recent history of acute pyelonephritis. Features such as in this biopsy may be interpreted as nonspecific, but glomerular cysts in the renal biopsy of a young child with bilaterally enlarged kidneys raise the possibility of early-onset ADPKD to be confirmed with genetic testing. The differential diagnosis of glomerular cysts collectively known as GCKD includes ARPKD (discussed below). Genetic testing is helpful in the majority (greater than 70%) but not all cases. For example, in Figure 4.15 is a renal biopsy from a 7-year-old boy with no family history of ADPKD who presented with bilaterally enlarged kidneys and liver cysts radiologically thought to be polycystic kidney disease (PKD). Genetic testing was performed prior to renal biopsy, but the results were ambiguous. The biopsy shows numerous tubular cysts some filled with



FIGURE 4.10 ADPKD from a 16-year-old who presented with unilaterally enlarged cystic kidney.



FIGURE 4.11 A young child with early-onset ADPKD: enlarged kidney contains only a few cysts; adjacent parenchyma is intact.

pale fluid; cysts are oval and focally elongated. A few glomeruli were globally sclerosed, and others were immature (fetal glomeruli). There were no micropapillae. Given the history of liver cysts and in the exclusion of ARPKD, early-onset ADPKD was favored, perhaps due to de novo mutation.

Early-onset ADPKD is not only difficult to diagnose but also difficult to explain with the two-hit hypothesis that presupposes a time interval for the second hit. A “*third-hit* signaling” that is thought to promote aberrant cellular proliferation and kidney growth may in part explain the phenotypic variability including early-onset ADPKD (42). In addition, some patients may have concurrent mutations in other genes, for example, the CF gene (43), HNF β 1 (26), or TSC. Modifier genes that may accentuate the disease phenotype without a second hit remain a possibility to explain the presentation in young patients with early-onset ADPKD.



FIGURE 4.12 A rare example of early-onset ADPKD. Numerous cysts contain gelatinous fluid. (Courtesy Stephen Bonsib, Nephropathology Associates, Arkansas.)



FIGURE 4.13 Early-onset ADPKD presenting in utero. Fetal autopsy shows cysts in the pancreas. (Courtesy of Stephen Bonsib, Nephropathology Associates, Arkansas.)

DIFFERENTIAL DIAGNOSIS

The differential diagnosis of early-onset ADPKD is primarily from classic ARPKD and secondly from other cystic diseases of childhood such as TSC and malformation syndromes including renal cystic dysplasia, bilateral Wilms tumor, and lymphoma. A rare but very intriguing entity, the so-called contiguous TSC2/PKD1 gene syndrome, is characterized by concurrent ADPKD and TSC (44). The TSC2 gene locus is adjacent to PKD1 on chromosome 16p. The kidneys contain multiple cysts lined by flattered epithelium next to typical TSC lesions such as angiomyolipomas or intraglomerular hamartomas (see under Tuberous Sclerosis). In contrast to PKD, multicystic dysplastic kidneys are usually smaller or normal in size and tend to regress in early childhood rather than get larger, a feature that is distinctly helpful in the clinical differential diagnosis of cystic kidney disease of childhood. In addition, dysplastic kidneys in malformation syndromes often have extrarenal manifestation

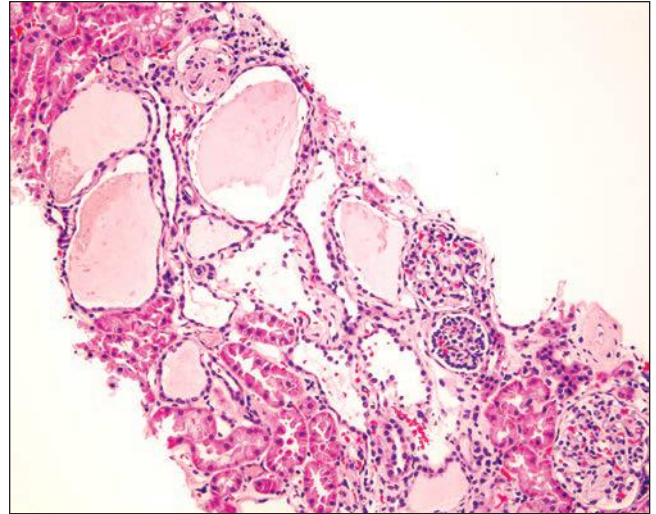


FIGURE 4.15 Renal biopsy from a 7-year-old boy who presented with bilateral renal cysts and concurrent liver cysts but no family history of ADPKD. Biopsy shows multiple tubular cysts filled with pale fluid; there is no interstitial fibrosis. The findings support ADPKD given the liver lesions. (H+E $\times 400$)

different than those seen in ADPKD (45). Malignancy is easy to rule out on renal biopsy.

Autosomal Recessive Polycystic Kidney Disease

INCIDENCE, CLINICAL PRESENTATION, AND GENETICS

ARPKD is much less common compared to ADPKD with an incidence of 1:20,000 live births. Typically, ARPKD starts in utero and presents at birth with large kidneys and liver fibrosis. Atypical ARPKD manifests in older children or young adults presenting predominantly with liver disease. About 50% of ARPKD is

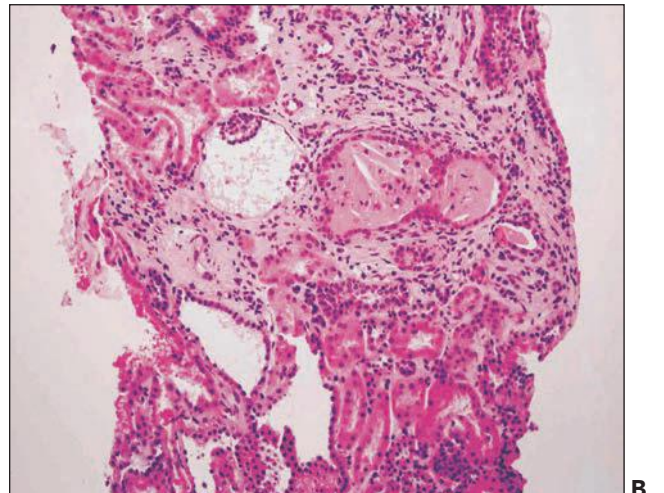
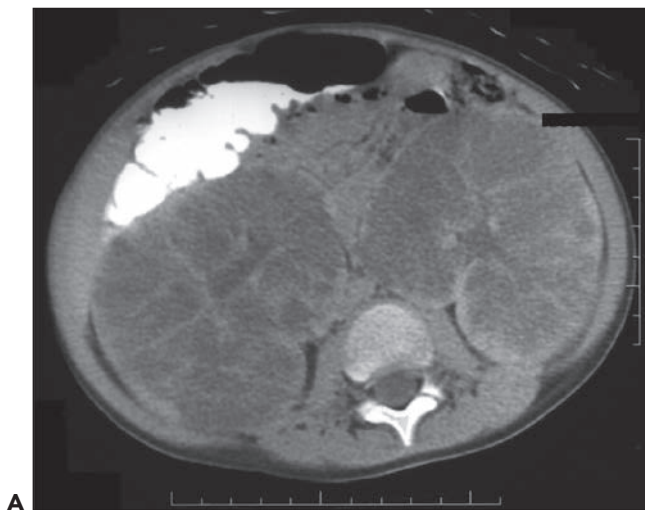


FIGURE 4.14 MRI shows bilaterally enlarged kidneys interpreted as diffuse nephroblastomatosis. **A:** The patient was a 4.5-year-old boy who presented with acute renal failure, hypertension, and acute pyelonephritis. **B:** Renal biopsy shows glomerular cysts and mild collecting duct ectasia but no evidence of blastema. The findings are consistent with early-onset ADPKD; ARPKD is in the differential diagnosis. (H+E $\times 400$)

perinatal; kidneys are echogenic, and babies develop oligohydramnios leading to lung hypoplasia and death in about 30% of cases. Bile duct dilation and cirrhosis complicated by sepsis are common immediate causes of neonatal death. In older children, liver complications also predominate. A database with clinical information of patients surviving infancy has accumulated data from 34 centers in America (46). More than 200 enrolled patients were categorized into two groups; 79.4% were born before 1990 and 20.35% after 1990; 85% were alive at 1 month, 78% at 1 year, and 75% at 5 years. Respiratory and chronic renal insufficiency was a significant predictor for mortality. Hypertension and liver disease did not affect survival. The most frequent complications were chronic lung disease, growth retardation, hyponatremia, and urinary tract infections. Hypertension was common but not seen in all patients. Ultrasound evaluation among 191 of the patients in the database, in about 50%, revealed echogenic kidneys without cysts (because masses of tiny cysts increase echogenicity but each individual cyst is below the limits of ultrasound resolution); the remaining had small cortical cysts. Liver imaging was normal in about 50% of patients; 16% had liver cysts consistent with Carol disease and of those 3 (13%) had episodes of acute cholangitis. These data and additional studies show that patients who survive infancy do much better than previously reported with a mean life expectancy of 27 years (range 18 to 55) (47). A minority of patients will not progress to ESRD, but most will have dialysis or transplantation. Complications may arise in women during pregnancy, such as acute decline of renal function and preeclampsia (48).

In ARPKD, neither parent has the disease; each child of parents who are both carriers has a 1:4 chance of inheriting the disease and 1:2 chance of being a carrier. All patients with ARPKD have mutations in the polycystic kidney and hepatic disease 1 gene (PKHD1), which is located on chromosome 6p21 and encodes a protein named fibrocystin/polyductin; greater than 300 mutations were identified in neonatal disease. There have been no new genes identified to explain infantile versus juvenile onset. Specific genotypes according to some authors affect the severity of renal and hepatic histologic abnormalities. For example, a study compared 54 fetuses with medical pregnancy termination to 20 neonates who died shortly after birth and found 55.5% of the mutations were truncated fibrocystin. Presence of two truncating mutations correlated with the most severe prenatal ARPKD (49). However, a different study of neonatal survivors (78 children and adults) identified 77 mutations (41 new), 19 of which were truncating in spite of postnatal onset (50,51). Haplotype-based diagnostic tests for at-risk pregnancies are available with a mutation detection rate of about 60% to 80% with those with kidney cysts and about 30% for those with liver disease but no renal cysts. In 12/78 cases, the criteria for ARPKD were not met, and GCKD, ADPKD, and other entities were thought possible but not confirmed. In spite of some limitations of genetic testing, preimplantation genetic methods are helpful and constantly improving (52).

RADIOLOGIC EVALUATION

Neonatal ARPKD is diagnosed by fetal ultrasound as early as 17 weeks of gestation. Kidneys are bilaterally enlarged and hyperechogenic, echogenicity attributed to innumerable 1- to 2-mm cysts in the collecting ducts that increase acoustic interface frequencies. MRI can be used for the evaluation of fetuses that have equivocal second-trimester ultrasound. In the last few decades, ARPKD occurring in older children is recognized

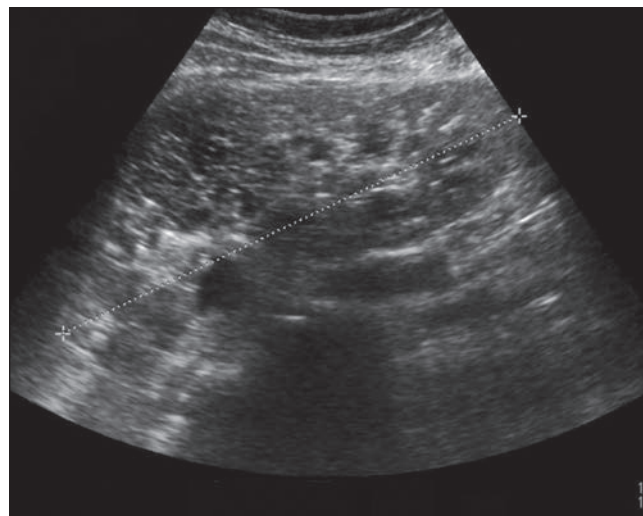


FIGURE 4.16 Ultrasound from a 24-year-old woman with ARPKD shows enlarged cystic kidneys. (Courtesy Cary Lynn Siegel.)

(50). Findings range from bile duct dilatation to portal hypertension to esophageal varices and enlarged liver and spleen. Figures 4.16 and 4.17 are from a 24- and a 23-year-old woman, respectively. Ultrasound shows enlarged cystic kidneys, and CT clearly demonstrates concurrent kidney enlargement, liver cirrhosis, and splenomegaly. Liver and kidney dysfunction appear independent in late-onset ARPKD; patients may present with liver symptoms first, and they may reach middle age without ESRD. Atypical cases with no liver lesions may be mistaken for ADPKD or malignancy.

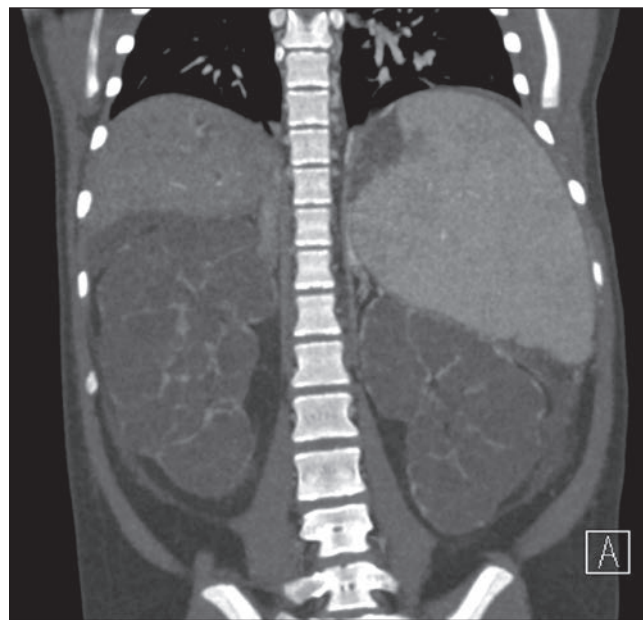


FIGURE 4.17 Postcontrast CT from a 23-year-old woman with end-stage ARPKD shows huge bilateral kidneys and both hepatomegaly and splenomegaly consistent with liver cirrhosis. (Courtesy Cary Lynn Siegel.)

PATHOLOGY

Neonatal ARPKD typically presents with congenital kidney enlargement and liver fibrosis. The kidneys show diffuse microcysts, which give these kidneys a sponge appearance (Fig. 4.4.18A). Sagittal sectioning reveals diffuse replacement of the renal parenchyma by cylindrical cysts (Fig. 4.18B). Microscopically, cysts involve the collecting ducts and typically extend to the cortex (Fig. 4.18C). There is no increased interstitial tissue. Autopsy studies showed that collecting duct dilatation and renal cortical involvement increase with gestational age (49). However, cysts may be entirely absent in early gestation, focally present in midgestation, or involving the kidney globally in late gestation. Type of mutation also affects the extent and time of cyst development. For example, in the study by Denamur et al., two severe (truncating) ARPKD mutations correlated with diffuse cylindrical cysts. Degenerating kidney cysts may present diagnostic difficulties as cysts may appear irregular with a branching pattern instead of cylindrical (Fig. 4.19). Histologic variability prompted some authors to devise a scoring system that takes into account the extent of collecting duct dilatation, loss of proximal tubules, cortical involvement,

and loss of the nephrogenic zone; four grades 1 to 4 were proposed. Based on this scoring, ARPKD in Figure 4.18 represents a grade 3 lesion. In the renal biopsy submitted from a 7-year-old boy with clinically unexpected ARPKD, we found medullary duct ectasia with normal lining and intact renal cortex; there were no typical cylindrical cysts extending into the cortex (Denamur grade 2) (Fig. 4.20A and B). This scoring system may not be applicable in all cases (e.g., Fig. 4.19) but raises awareness of the subtle findings in ARPKD and indicates that absence of typical long cylindrical cysts does not exclude ARPKD diagnosis. Liver biopsy was also performed in this 7-year-old boy and showed bile ductile proliferation (Fig. 4.20C). MRI imaging revealed an ambiguous infiltrative pattern suggestive of bilateral lymphoma (Fig. 4.20D).

The differential diagnosis of neonatal ARPKD includes early-onset ADPKD and bilateral cystic renal dysplasia sporadic or syndromic and Meckel-Gruber syndrome. Meckel syndrome is an autosomal recessive disease characterized by cystic kidneys associated with hepatic fibrosis, polydactyly, and central nervous system abnormalities such as encephaloceles. Both the kidneys are enlarged, but microscopically, the kidneys are dysplastic.

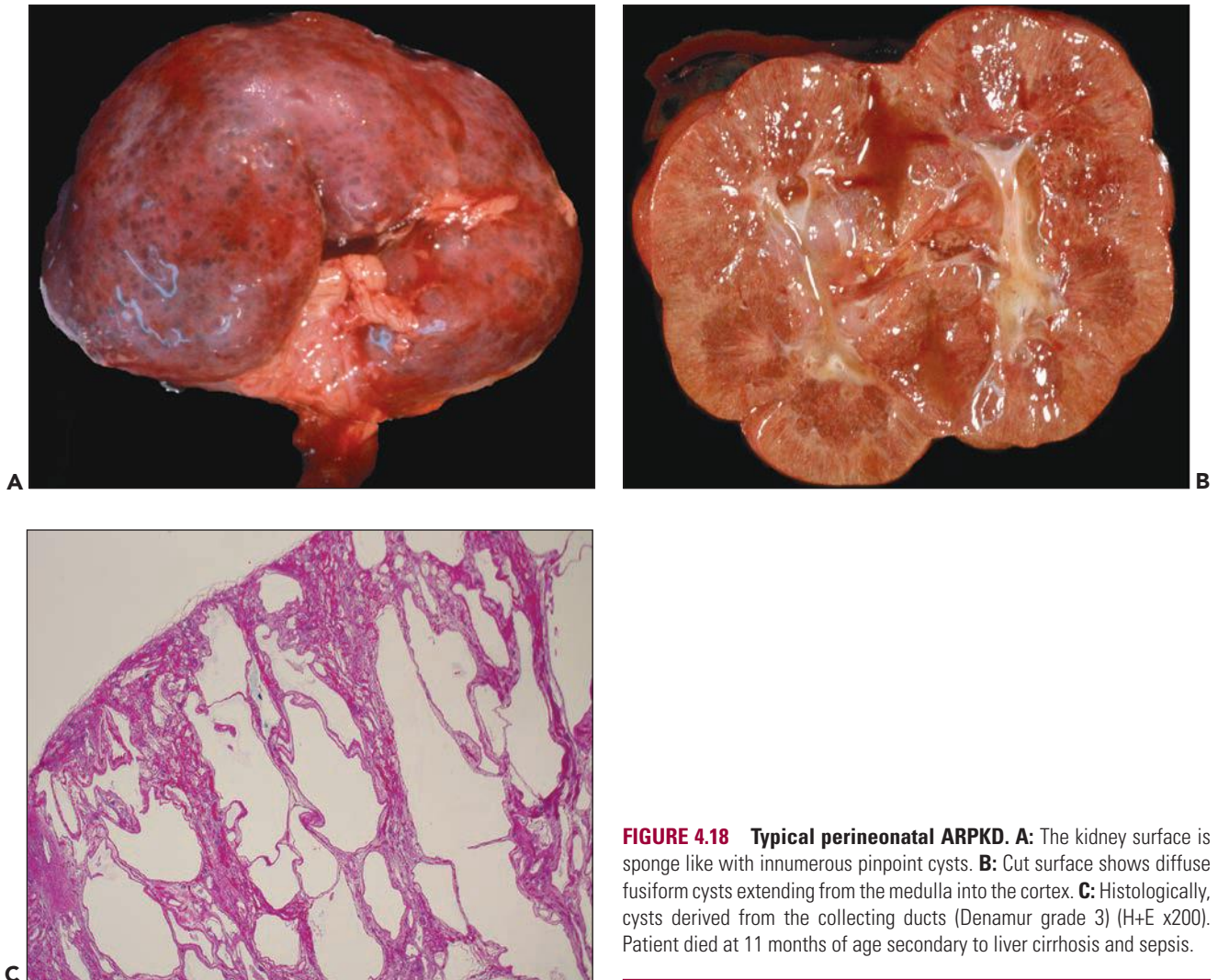


FIGURE 4.18 Typical perineonatal ARPKD. **A:** The kidney surface is sponge like with innumerable pinpoint cysts. **B:** Cut surface shows diffuse fusiform cysts extending from the medulla into the cortex. **C:** Histologically, cysts derived from the collecting ducts (Denamur grade 3) (H+E x200). Patient died at 11 months of age secondary to liver cirrhosis and sepsis.

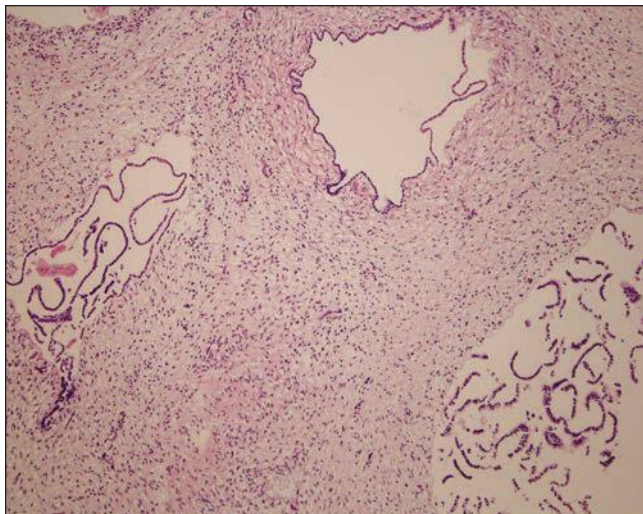


FIGURE 4.19 Atypical, irregular, and partly degenerating cysts in markedly enlarged kidney (weight = 35.1 g; normal for age and wt = 4.2 g) from stillborn male fetus with hypoplastic lungs and biliary dysgenesis consistent with fatal ARPKD. (H+E $\times 200$)

Polycystic Liver Disease and Hepatic Fibrosis

Polycystic liver disease encompasses three etiologies: (a) cysts associated with ADPKD, (b) a separate entity of autosomal dominant polycystic liver disease (ADPLD) that is not accompanied by kidney cysts, and (c) Caroli disease. The most frequent is extrarenal ADPKD. Liver cysts may cause severe liver dysfunction when they are multiple occupying a large liver segment (Fig. 4.21), but more frequently are focal and asymptomatic. Polycystic liver disease is arbitrarily defined as a liver that contains greater than 20 cysts (53–55). Cysts are intrahepatic or perihilar replacing the liver parenchyma (Fig. 4.22A). Microscopically, cysts appear disconnected from the biliary tree and composed of dilated bile ducts embedded in a fibrous stroma (known as von Meyenburg complex) (Fig. 4.22B). These are thought to derive from abnormal ductal plate formation in utero justifying the term biliary dysgenesis. In ARPKD, there is also abnormal formation of bile ducts and defective apoptosis of excess precursor cells leading to increased number of bile ducts, abnormal branching, and invariably periportal hepatic fibrosis (Fig. 4.23). Septic cholangitis and death from septicemia is a severe complication in neonates. Rarely, hepatic fibrosis instead of liver cysts may be seen in patients with ADPKD and or liver cysts are reported in children with ARPKD (56,57). These exceptions to the more typical kidney-liver phenotypes raise questions about the mechanisms of such crossover presentations, for example, the role of epithelial stromal interactions and or background gene modifiers. Malignancy is rare but at least one case of cholangiocarcinoma developing in polycystic liver disease in an adult is reported (53).

ADPLD is a heterogeneous entity; 80% of patients presumed to have ADPLD have no detectable gene mutations. A sizable minority has mutations in two genes: one on the short arm of chromosome 19 affecting protein kinase substrate

80K-H (PRKCSH) coding for a protein called hepatocystin and a second on chromosome 6 involves Sec63. These proteins localize in the endoplasmic reticulum of cholangiocytes and are thought to mediate cell proliferation and fluid secretion via increased 3',5'-cyclic adenosine monophosphate (cAMP). Evidence derives from studies that show secretin (a cAMP agonist) to increase fluid production in hepatic cysts and somatostatin analogs to suppress the size of liver cysts (58–60). These studies brought forth new compounds as therapeutic agents targeting reduction of cell proliferation and fluid secretion by liver cysts.

DIFFERENTIAL DIAGNOSIS

The differential diagnosis of polycystic liver disease includes Caroli disease. This is a rare congenital disease first described in 1958 by a French physician and characterized by sac-like or fusiform dilation of intrahepatic bile ducts not associated with obstruction, also known as communicating cavernous ectasia or congenital cystic dilatation of the intrahepatic biliary tree. It is common in Asia in young individuals and distinct from other diseases that cause ductal dilatation caused by obstruction. It usually affects the entire liver, but one lobe or a segment may be involved. Caroli disease is in the spectrum of ductal plate malformations representing persistence of embryologic structures at the ductal plate forming focal or diffuse anastomosing channels. Fibrosis and duct ectasia result from local tissue remodeling. Diagnosis of Caroli disease depends on demonstrating continuity of the cysts with the biliary tree by percutaneous cholangiography. In ARPKD, biliary cysts only rarely communicate with the bile ducts. However, some authors use the term “Caroli disease” generically to describe nonobstructive intrahepatic biliary dilatation on ultrasound or CT. Cysts in isolated ADPLD arise from biliary microhamartomas. Findings in isolated ADPLD may mimic liver involvement in ADPKD, and patients may also have mitral valve abnormalities, but there are “no kidney cysts.”

PATHOGENESIS

The pathogenesis of liver cysts is thought to be due to persistence or lack of remodeling of the embryonic ductal plate, which normally takes place during embryogenesis (61). Hepatic precursor cells normally migrate from the foregut and form a double layer around the portal veins, which is called the ductal plate. The ductal plate remodels into bile ducts and portal tracts over several weeks during embryonal development. The rest of the precursor cells undergo apoptosis. If precursor cells do not involute or do not respond to proper signals and remain unincorporated, they may lead to ductal plate dysgenesis. It is interesting that among other factors participating in biliary morphogenesis, liver-specific loss of HNF1 β produces immature ductal plates and loss of planar cell polarity of cholangiocytes (61). Other investigators have studied cilia of cholangiocytes and gene mutations that impair function of cilia. Cilia in small liver cysts (less than 1 cm) appear normal; larger cysts greater than 1 cm have shortened cilia, while larger cysts (greater than 3 cm) show no cilia. In addition, cyst epithelia show increased cell proliferation and increased expression of estrogen receptors, IGF1, IGF1-R, proliferating and pAKT (62). Furthermore, some patients with HNF1 β are reported to

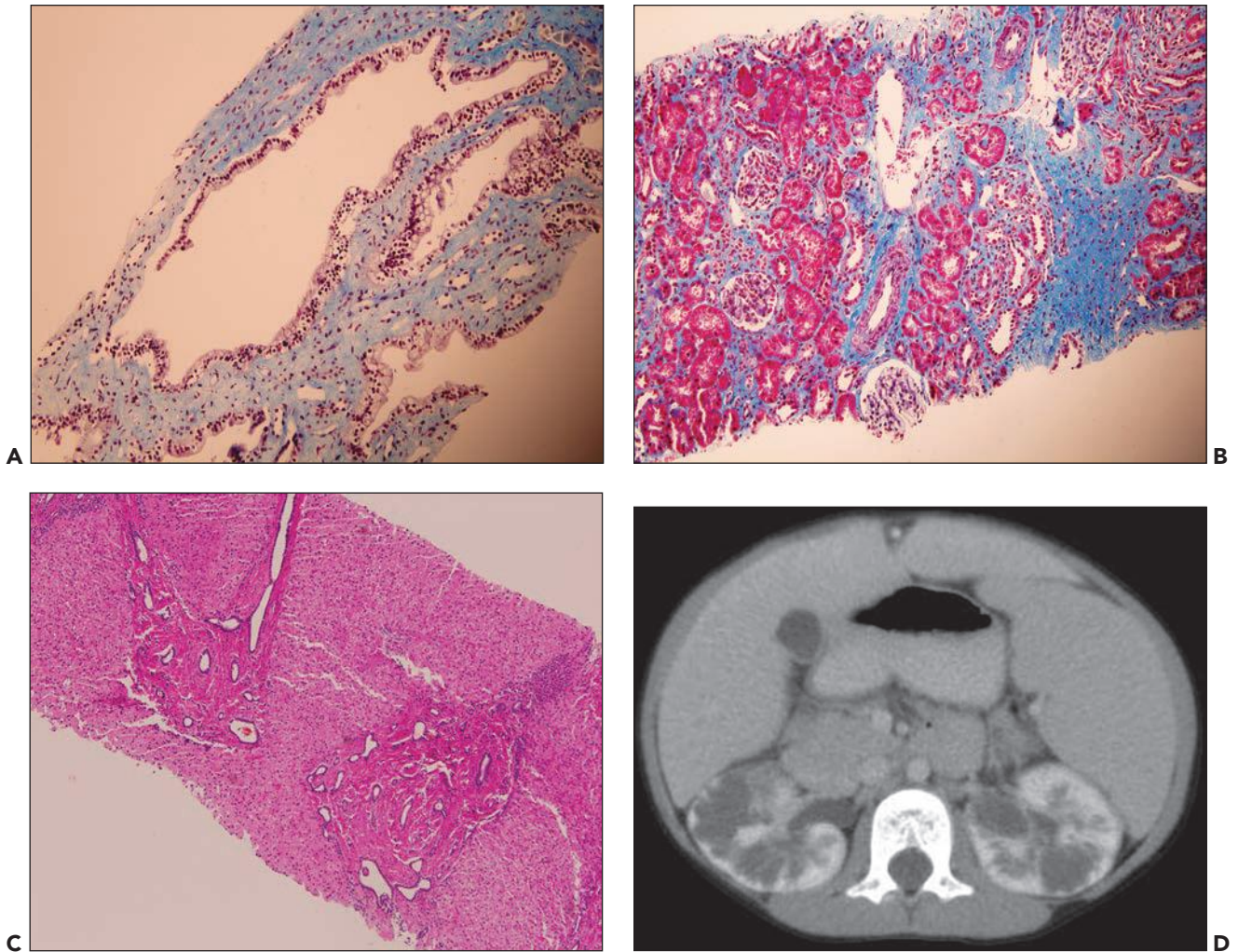


FIGURE 4.20 Renal biopsy from a 7-year-old with clinically unsuspected ARPKD shows **(A)** medullary duct ectasia and **(B)** uninvolved cortex (Denamur grade 1). Trichrome stain $\times 200$. **C:** Liver biopsy shows proliferation of bile ducts (H&E $\times 200$). **D:** MRI shows bilaterally enlarged kidneys with an infiltrative pattern interpreted as bilateral lymphoma.

lack cilia on cholangiocytes (63). These structural and functional ciliary defects are somewhat similar to ciliary dysfunction in kidney cyst formation.

Clinical Management, Prognosis, and Therapy

Recognition of treatable complications of ADPKD in recent decades facilitated early diagnosis and better management. Fast kidney enlargement detected by ultrasound occurs in some but not all individuals. Those with slower renal growth have less associated risk factors such as hypertension and decreased glomerular filtration rate. Progressive disease manifests with increased overall kidney and individual cyst size; therefore, new therapies target minimizing cyst size and renal growth by selective surgery (64) or with experimental drugs that exploit new molecules as revealed by clinical trials and animal studies. The latest is Tolvaptan (vasopressin V₂-receptor antagonist), which has a modest effect in slowing renal failure and kidney size (65). Renal transplantation is also a choice. Treatment of liver disease is similarly multifaceted

and includes partial liver resection, transplantation, and/or experimental drugs (15).

Glomerulocystic Kidney Disease

GCKD is not one disease but a heterogeneous group of entities with glomerular cysts as the common histologic finding (Table 4.4). By definition greater than 5% of glomeruli should be cystic. A glomerular cyst is defined by a dilated Bowman space greater than or equal to two times the normal (6,66). GCKD can be classified into primary and secondary types. Primary GCKD includes GCKD associated with heritable diseases such as (a) ADPKD, (b) ARPKD, (c) ADGCKD due to UROM, HNF1 β , and renin mutations; (d) TSC, and (e) NPHP. Secondary GCKD includes (a) renal dysplasia, sporadic/nonhereditary, obstructive, and syndromic and (b) ischemic GCKD. Kidneys may be enlarged, normal in size or small. ADGCKD is clinically heterogeneous and includes families that have mild chronic disease with hypoplastic kidneys in some individuals, or normal size kidneys in others,

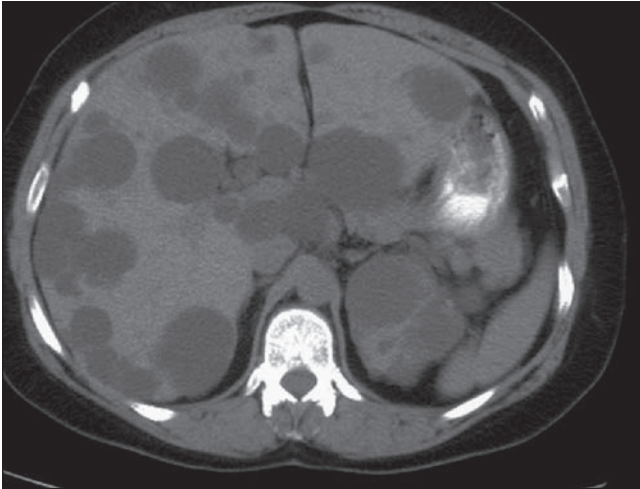


FIGURE 4.21 Abdominal CT, axial view shows multiple liver cysts as well as cysts in the left kidney upper pole; patient was a 62-year-old woman with advanced ADPKD.



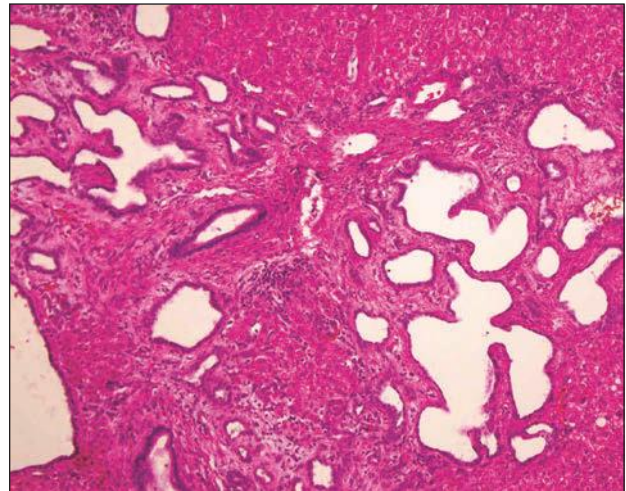
FIGURE 4.23 Liver cirrhosis in neonatal ARPKD. The liver is enlarged (weight = 560 g, normal for age = 331 g), firm, and diffusely nodular; the patient was a 15-month-old baby girl who died from acute cholangitis and sepsis due to *Pseudomonas aeruginosa*.

and separate families characterized by maturity-onset diabetes of the young (less than 25 years of age) (MODY) and renal cysts (67). ADGCKD with normal or smaller than normal kidneys was found in an Italian family with glomerular cysts, no extrarenal cysts, and an overall benign course with stable renal failure (68). A missense mutation (c315R) in the gene for uromodulin (UMOD), also known as Tamm-Horsfall protein, was found in some family members (69). Subsequently, a separate family with ADGCKD and UMOD mutations was reported independently (70). Interestingly, all members of this unique family had severe impairment of urine-concentrating ability and hyperuricemia resembling the phenotype of NPH-MCDK complex and severe reduction of excreted uromodulin.

Immunohistochemistry with antibodies to uromodulin revealed dense intracellular accumulation of uromodulin in tubular epithelia of the thick ascending limb of Henle loop in kidney biopsies. Confusion exists in the literature when it comes to the specific renal biopsy findings of patients with reported UMOD mutations because there is no microscopic description in all cases, and some authors prefer to categorize UROM mutations according to presenting symptoms, for example, hyperuricemia, or consider these in the spectrum of tubulointerstitial nephritis and NPHP. UMOD mutations are responsible for three autosomal dominant tubulointerstitial nephropathies including medullary cystic kidney disease type 2



A



B

FIGURE 4.22 **A:** Gross pathology of cystic liver disease: multiple thin-wall cysts replace the liver parenchyma; the patient was a 56-year-old man with ADPKD. **B:** Sections show multiple ectatic, angulated, and branching bile ducts (bile duct hamartomas/von Meyenburg complex). (H&E $\times 400$)

TABLE 4.4 Glomerulocystic kidney disease

Primary	Gene	Common findings/associations
1. ADPKD	PKD1,2	Family history, bilaterally enlarged kidneys, cysts in other organs
2. ARPKD	PKDH1	No family history, bilaterally enlarged kidneys, liver fibrosis
3. ADGCKD	UROM, HNF1 β	No family history, small or normal size kidneys, early type II diabetes
4. TSC2	TSC2	No family history, no cysts in other organs, small or normal kidneys
5. NPHP	Infantile	Phenotypic heterogeneity; polyuria, polydipsia, hyperuricemia, corticomedullary cysts
6. Other	?	Hyperuricemia
Secondary		
1. Renal dysplasia		
Sporadic	Unknown	Unilateral or bilateral, small or slightly enlarged kidneys, smooth muscle collars, cartilage
Obstructive		Urine flow obstruction
Syndromic	>100 syndromes	Associations vary with chromosomal anomaly
Ischemic		
HUS/TTP, vasculitis	None	Thrombi, coagulation defects
Vascular stenosis		Systemic sclerosis, skin abnormalities, and renal vasculitis
Drug induced		Renal artery or major branch stenosis Lithium

(Modified from Lennerz JK, Spence DC, Iskandar SS, et al. Glomerulocystic kidney: one hundred-year perspective. *Arch Pathol Lab Med* 2010;134:583.)

(MCKD2), FJHN, and GCKD. Nonetheless, it appears that most patients with UMOD mutations do not have glomerular cysts, and there are patients with hyperuricemia and glomerular cysts who upon genetic analysis show no evidence of UROM mutations. In MODY, hepatocyte nuclear factor (HNF) 1 β mutations in a fraction of patients cause early-onset type II diabetes and kidney cysts. Diabetes is overt in about half of the patients with documented mutations. In others, diabetes is found upon screening (71). Some patients have glomerular cysts, others have small kidneys with oligomeganephronia (few but large glomeruli), or renal dysplasia and anomalies of the lower genitourinary tract. The reasons for phenotypic variability in MODY remain unclear. However, HNF1 β plays an important role in nephron and biliary development in animal models and is a regulator of UROM transcription. Both HNF1 β and mutated UROM are implicated in abnormal cilia formation in human ADPKD/ARPKD (72,73).

PATHOLOGY AND DIFFERENTIAL DIAGNOSIS

Gross pathology of GCKD varies with the underlying etiology. Bilaterally enlarged kidneys in an infant or young child are likely ADPKD or ARPKD. In the remaining entities, shown in Table 4.4, the kidneys are either slightly larger or normal size. Glomerular cysts involve the Bowman space and sometimes the origin of the proximal tubule. They can be focal or diffuse. The wedge biopsy shown in Figure 4.24 is from a 2-year-old boy with rapid bilateral kidney enlargement. The great majority of glomeruli are cystic but interestingly orderly arranged in rows. There are no tubular cysts, and the intervening stroma is not fibrotic. Liver biopsy was also submitted to rule out liver mass diagnosed on ultrasound. Portal triads were expanded with prominent bile duct proliferation in a pattern of hepatic fibrosis. This case of GCKD associated with hepatic fibrosis is highly consistent with delayed-onset ARPKD. The example shown in Figure 4.25 is from a 35-week gestational age baby born to a 33-year-old G16P3576 mother who had a number of spontaneous abortions along with a number of

children born with congenital anomalies. A prenatal ultrasound showed hydrocephalus, bilateral echogenic kidneys, and oligohydramnios. Baby died at birth from respiratory failure due to hypoplastic lungs. At autopsy, the kidneys were grossly enlarged with minute cysts on the external surface. Histologic examination showed diffuse glomerular cysts in minute and immature glomeruli, absent nephrogenic zone, focal renal dysplasia, and no liver abnormalities (Fig. 4.25C). This case of bilateral renal dysplasia presenting as GCKD is an example of the spectrum of entities that enter the differential diagnosis of glomerulocystic kidneys. Dysplastic kidneys are often associated with urine flow obstruction and can be bilateral. Urine backflow may cause both tubular and Bowman space dilation

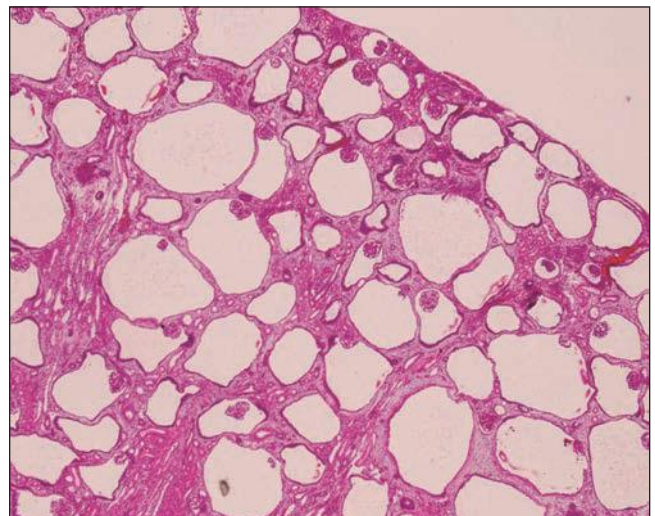


FIGURE 4.24 Glomerular cysts in wedge renal biopsy from a 2-year-old boy with rapid bilateral kidney enlargement and hepatic fibrosis on CT. (H&E \times 100)

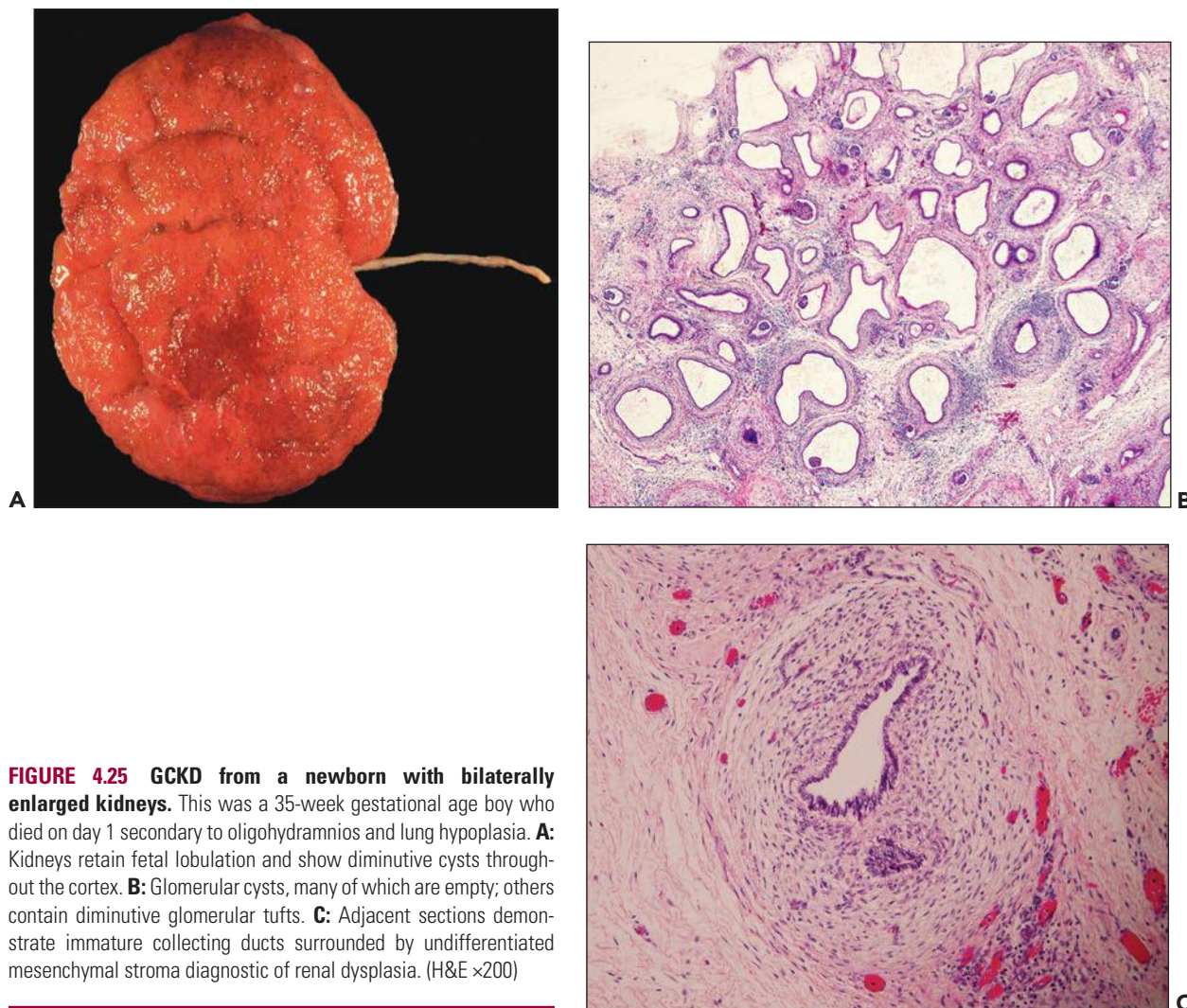


FIGURE 4.25 GCKD from a newborn with bilaterally enlarged kidneys. This was a 35-week gestational age boy who died on day 1 secondary to oligohydramnios and lung hypoplasia. **A:** Kidneys retain fetal lobulation and show diminutive cysts throughout the cortex. **B:** Glomerular cysts, many of which are empty; others contain diminutive glomerular tufts. **C:** Adjacent sections demonstrate immature collecting ducts surrounded by undifferentiated mesenchymal stroma diagnostic of renal dysplasia. (H&E $\times 200$)

inducing glomerular cysts and disruption of orderly glomerulogenesis. Evidence for such a mechanism derives from experimental ureteral ligation in neonatal animals (74).

GCKD occurs in patients with UROM mutations and hyperuricemia. Hyperuricemic nephropathies have overlapping symptoms with infantile or juvenile NPH. Therefore, GCKD can also be a feature of NPH. The patient whose biopsy is shown in Figure 4.26 developed hyperuricemia and increased creatinine. There was no family history of hyperuricemia or kidney disease. The kidney size and shape were within normal; there were no apparent cysts, and the liver was intact. Renal biopsy showed GCKD; moderate tubular atrophy suggested an ongoing process (Fig. 4.26B). However, this patient tested negative for known hyperuricemia-related mutations such as UROM, HNF1 β , and Renin mutations. These examples demonstrate genetic heterogeneity in GCKD and suggest that new genes are likely to be discovered in familial hyperuricemic nephropathy.

Glomerular cysts are also seen in the kidneys of children with chromosomal anomalies such as trisomy 21, trisomy 18, Turner syndrome, or heritable syndromes such as TSC, oral-facial-digital dysplasia, glutaric aciduria type II, and sporadic cystic renal dysplasia (Fig. 4.27). In such immature kidneys, it is not unusual to find dysplastic glomeruli containing three or

more nubs of residual glomerular tufts enclosed in the same cyst (discussed further under renal dysplasia and Figure 4.56A) (6).

In adults, sporadic GCKD is frequently secondary to ischemia, due to renal artery stenosis (Fig. 4.28), thrombotic microangiopathy associated with hemolytic uremic syndrome (HUS) or lupus nephritis (75).

Recognizing glomerular cysts can be difficult when the glomerular tuft degenerates as the cysts enlarge. Therefore, empty cysts may be misinterpreted as tubular (see Fig. 4.25B). Immunohistochemistry with segment-specific lectins, epithelial membrane antigen (EMA), a collecting duct marker, and PAX2, which stains parietal epithelial cells are helpful in defining cyst derivation (Fig. 4.29).

In summary, the significance of GCKD lies in (a) knowing the histopathologic criteria for diagnosis and (b) the significance of extrarenal associations in placing a case under a given category. The differential diagnosis in children includes early-onset ADPKD, late-onset ARPKD, certain mutations (e.g., in HNF-1 β , TSC, OFD1), slowly progressing autosomal dominant GCKD associated with or without UMOD mutations, and renal dysplasia (sporadic, obstructive, or syndromic). In adults, acquired ischemia (HUS) is the most common cause. Genetic counseling and molecular genetic testing

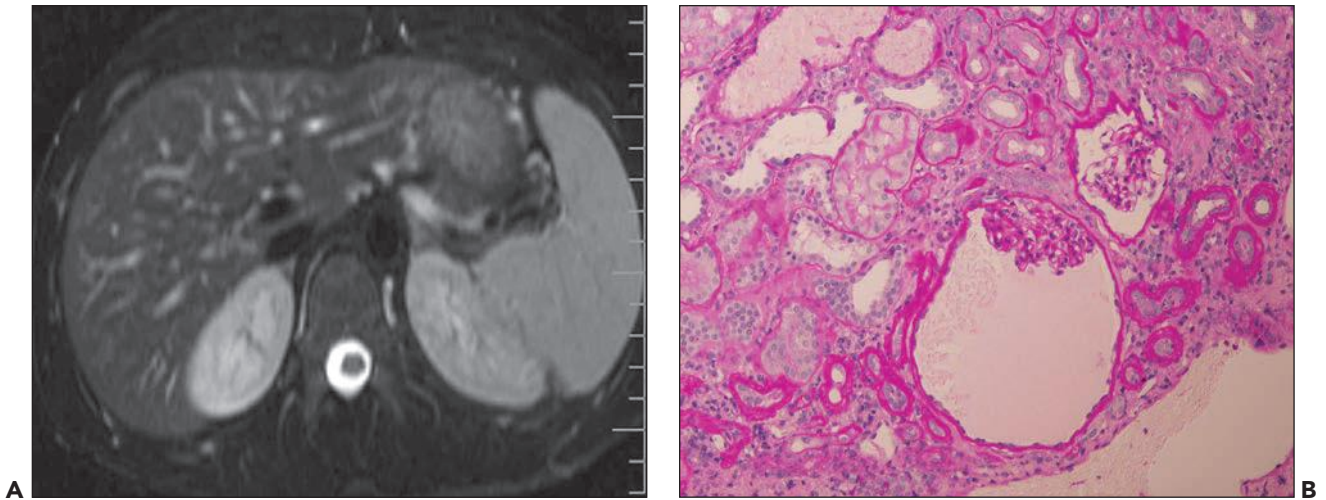


FIGURE 4.26 Abdominal CT from a young man with no family history of chronic kidney disease and hyperuricemic nephropathy. **A:** Kidneys are normal size with no cysts. **B:** Renal biopsy shows glomerular cysts and focal tubular atrophy.

to exclude heritable mutations (ADPKD/ARPKD, HNF1 β , UROM and currently unknown genes) are currently the standard of care.

PATHOGENESIS

Understanding of cystic renal disease has greatly advanced in the past few decades. However, the exact pathogenesis of GCKD is still unclear. At least four proposed mechanisms to explain glomerular cyst formation have been proposed: (a) intrarenal medullary inflammation or intrarenal medullary obstruction during the last 10 weeks of gestation, (b) altered collagen composition of the Bowman capsule, (c) stenosis at the glomerulotubular junction, and (d) ciliary dysfunction. However, intrarenal obstruction during fetal development does not explain the predominately cortical distribution of cysts; a

weak Bowman capsule that would facilitate dilatation of the urinary space as prourine is formed during kidney development has not been proven, and three-dimensional reconstruction and image analysis have excluded glomerulotubular junction stenosis/obstruction (6). The cilia hypothesis is currently the prevailing one to explain ADPKD/ARPKD and other hereditary cystic diseases based on data that support tubular epithelial proliferation, fluid accumulation, and remodeling of the extracellular matrix contributing to cyst formation. It is possible that the same factors underlie cyst formation in GCK. It is interesting that developing podocytes do have cilia in contrast to mature podocytes, but there is almost nothing known about their physiologic role or function (76). Environmental factors (e.g., gestational maternal phenacetin), toxin exposure, infections, or drugs (ego, lithium) have also been postulated. With

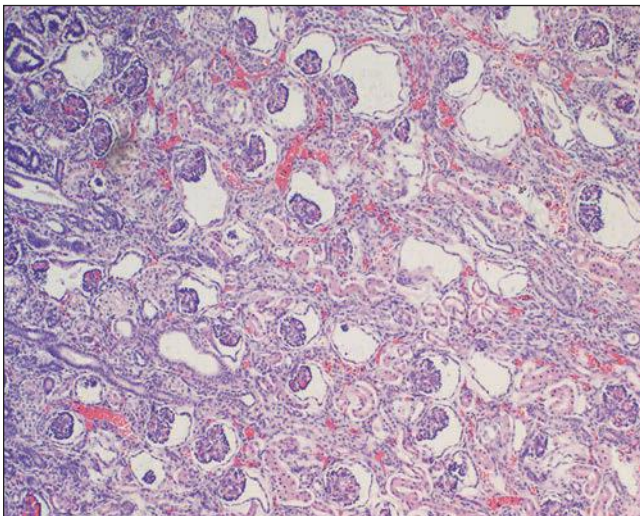


FIGURE 4.27 GCKD in a 17-week baby girl with Turner syndrome. Kidneys were bilaterally enlarged. (H&E $\times 200$)

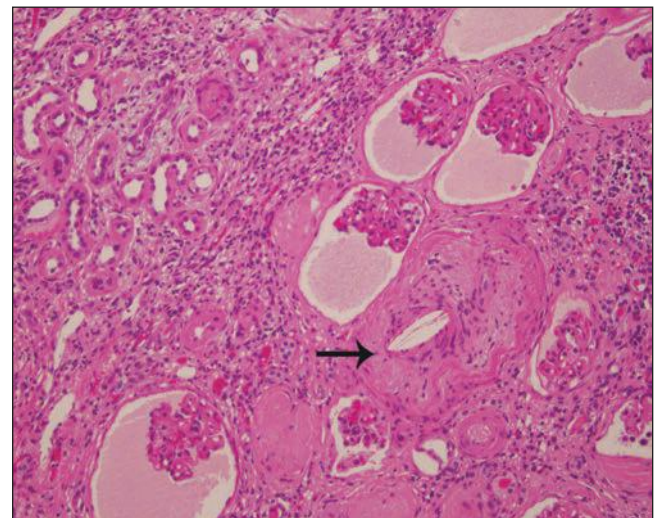


FIGURE 4.28 Ischemic GCKD shows cystic glomeruli adjacent to cholesterol emboli (*arrow*); the patient was a 64-year-old man with renal artery atherosclerosis. (H&E $\times 100$)

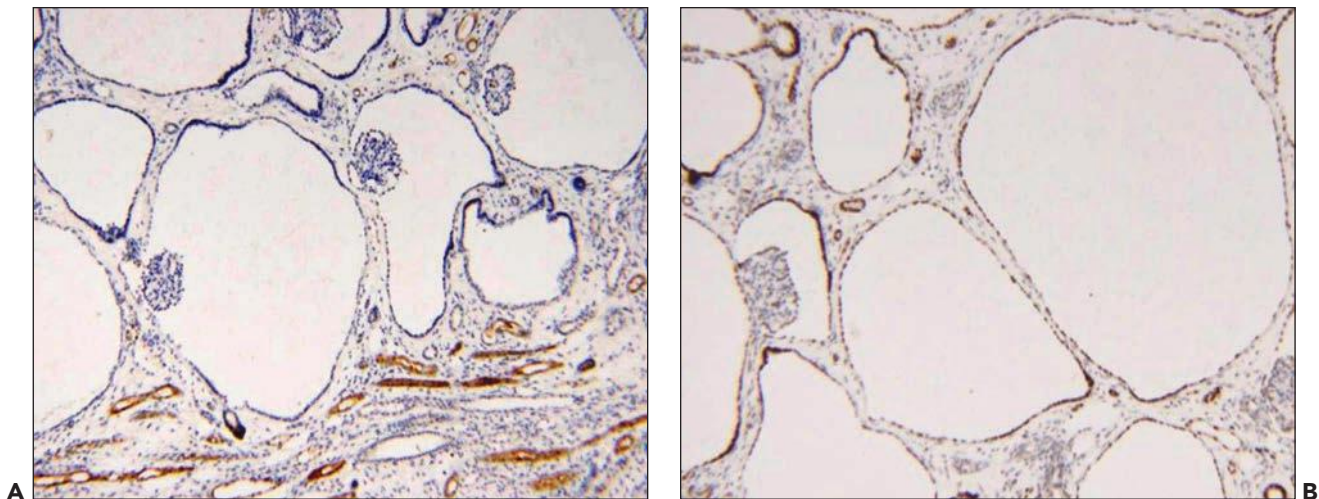


FIGURE 4.29 Immunohistochemistry for glomerular cysts. **A:** EMA highlights distal tubules and collecting ducts. **B:** PAX2 stains predominantly parietal epithelial cells indicating that the empty cysts represent the Bowman capsule.

the exception of lithium and even though GCKD in humans shows remarkable resemblance to cysts in the rabbit following long-standing corticosteroid treatment, the contribution of steroids in human disease is vague. Among numerous mouse models for cystic kidney diseases, GCKD is evident in 25% of aged *+/-jcpk* heterozygotes (66). This and other animal models offer an opportunity to study the enigma of GCKD.

Renal Medullary Cysts

Nephronophthisis and Medullary Cystic Kidney Disease

INCIDENCE, CLINICAL PRESENTATION, AND GENETICS

Taken together, the NPHP family of syndromes is the most frequent genetic inherited cause of ESRD in children and adolescents according to some authors (77). Inheritance is autosomal recessive, and traditional cloning and conditions include the original NPHP group and the associated Senior-Loken, Joubert, Meckel-Gruber, Cogan, and Mainzer-Saldino syndromes (78). NPHP and associated disorders are considered ciliopathies, as all NPHP gene products are expressed in the primary cilia, similarly to the PKD proteins (79). These are caused by mutations in over 18 genes, mostly highly conserved across evolution, with a striking common feature that their encoded proteins all appear to localize to the primary cilia or centrosomes. This is not just in renal epithelial cells, but in other affected sites such as the cerebellum, liver and bone, and the retina where rods and cones are modified cilia.

Classical juvenile NPHP is characterized by insidiously progressive tubulointerstitial nephritis that progresses to end-stage renal failure usually during adolescence. Increased thirst and urination are the typical first signs at around 3 years of age, secondary to a urinary concentrating defect, followed by failure to thrive and rising creatinine. Kidneys may be relatively normal size but loss of corticomedullary differentiation occurs as the disease progresses and cysts occur at the corticomedullary junction around the time children reach CKD V. NPHP1, 3, 4, 5, 6, 7, 8, and 9 mutations have been detected in juvenile NPHP, while NPHP2 accounts for the rarer infantile form that

is characterized by cortical microcysts and end-stage disease before the age of 5 (79).

Pathways disrupted in various NPHP include canonical and noncanonical Wnt signaling, Sonic hedgehog, and Hippo (80,81). Inversin, the gene product of NPHP1, illustrates the complexity and interactions within this group: inversin colocalizes with nephrocystin and β -tubulin in primary cilia (82) and acts as a molecular switch between different Wnt signaling cascades by inhibiting the canonical Wnt pathway via increased turnover of disheveled, which is downstream of the frizzled wnt receptor, while promoting noncanonical signaling required for convergent extension (at least in *Xenopus*) (83).

MCKD has autosomal dominant inheritance and is relatively rare with an annual incidence of 34 to 56 new cases per year reported at the United States Renal Database (www.usrds.org/request.asap). The main clinical symptoms that NPHP and MCKD share are decreased urine-concentrating capacity, polydipsia and polyuria, and renal cyst formation in the corticomedullary junction or the medulla. An association with hyperuricemia and gout is recognized. However, clinical presentation varies greatly across these groups. For example, polydipsia/polyuria may be mild or absent, and renal cysts may only be found at autopsy and not by ultrasound or CT (84). Ultrasound detects cysts in only 40% of the patients. Patients with no cysts may not be diagnosed until late in life or at autopsy. Cysts are unilateral or bilateral, and they vary in number. In a large 186 member Cypriot family, bilateral cysts were found in only 12.5% of carriers (84). Less than half of these patients had hyperuricemia, and clinical gout was only reported in five. Therefore, while clinical symptoms and presence of cysts are part of the disease phenotype, none are sensitive enough for diagnosis. Heredity may not be apparent at first either. There are two genes (and perhaps a third) designated as MCKD1 and MCKD2. ESRD in MCKD1 develops at about 62 years and in MCKD2 at about 32 years. A father-to-son transmission suggests an autosomal dominant mode. Patients often develop hypertension early but, paradoxically, some develop hypotension later due to salt wasting. There are

also associations such as hypogonadism, epilepsy, and spastic quadriplegia among others. A locus on chromosome 1q21 for MCKD 1 was identified in the Cypriot family presenting with very late onset of ESRD. A second locus on chromosome 16p12 for MCKD2 that encodes for uromodulin was found in an Italian family and confirmed by independent investigators in a Welsh family in the United Kingdom (85,86). A third MCKD gene is thought possible by Kroiss et al. Familial hyperuricemic nephropathy presenting during childhood was described in two Czech families and one Belgian family (87). The gene in these families is located close to 16q12 (16q11 locus in fact), suggesting that more loci will be identified in families with a combination of MCKD symptoms and variable ESRD onset.

Currently, hyperuricemia is the common finding in three clinical entities related to UROM gene mutations, also referred to as *uromodulin disorders*. These are MCKD2, FJHN, and GCKD. UMOD gene encodes for uromodulin, an 85-kDa glycoprotein involved in renal stone formation and urothelial cytoprotection. Patients often present in early adulthood with hyperuricemia or gout and normal blood pressure. ESRD develops in 15 to 20 years. At least 40 UMOD mutations are reported. Renal biopsy findings in most patients with UROM mutations do not show glomerular cysts but tubulointerstitial fibrosis, a phenotype seen in NPHP/MCKD diseases (88).

Pathology and Pathogenesis

The pathology of NPHP and MCKD is nonspecific. In juvenile NPHP, the kidneys are grossly normal or slightly decreased in size. Corticomedullary or medullary cysts are present in some patients (Fig. 4.30). Histopathologic findings consist of a triad of findings: tubular cysts, tubulointerstitial inflammation and fibrosis, and tubular basement membrane disruption. Glomerulosclerosis is invariably present but varies between 20% and 50%. Cystic dilation involves distal tubules and collecting ducts. Dilated tubules may contain acellular material that stains positive with antibodies to uromodulin (also known as Tamm-Horsfall protein). These histopathologic findings are more frequent in juvenile and adolescent NPHP, while infantile NPHP often presents with glomerular cysts. Uromodulin was initially proposed as an NPHP hallmark and the result of an intrinsic tubular defect that allows it to escape into the lumen or the interstitium (Fig. 4.31A). However, uromodulin accumulation in renal tubules is seen in association with increased intratubular pressure in obstructive and reflux nephropathy in which tubular basement membrane disruption is not the primary defect, as well as chronic nephropathy, stone disease, and other conditions (73). Nonetheless, disintegration of the tubular basement membrane is an important finding in NPHP-MCKD (Figs. 4.31B and 4.32A). Electron microscopy reveals dilated tubules with irregular out pouching and tubular basement membrane thickening, splitting, and replication, alternating with thin or entirely absent segments (Fig. 4.32B). Patients with some NPHP patients with detectable UROM mutations have distinct features on electron and light microscopy. These consist of uromodulin accumulation in the distal tubules (Fig. 4.33A) and hyperplastic rough endoplasmic reticulum (RER) and amorphous deposits within dilated RER cisternae (Fig. 4.33B).

Pathogenesis of cyst formation and predilection of the corticomedullary junction in NPHP-MCKD continues to be

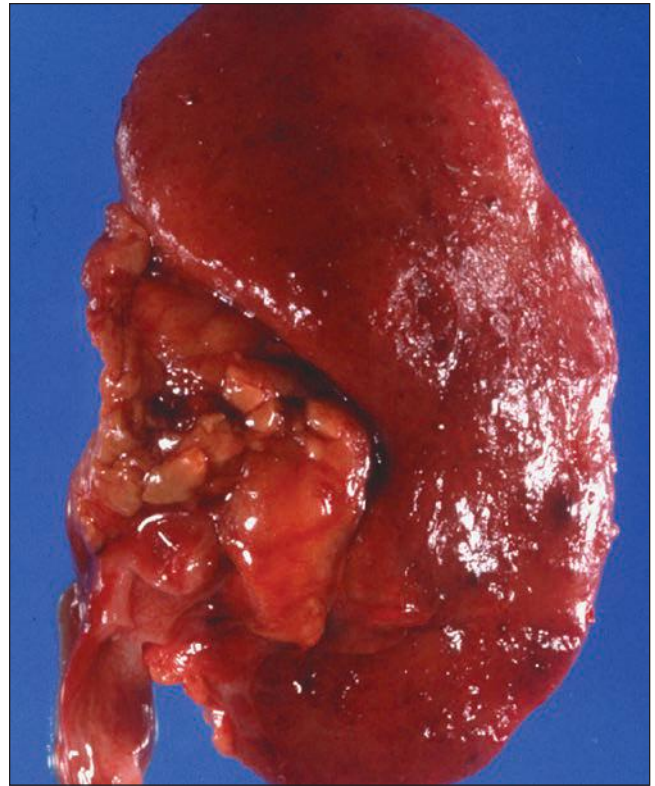


FIGURE 4.30 Gross pathology in NPHP. The kidney is slightly decreased in size with a few small cysts apparent on the external surface. The patient was an 8-year-old boy who first presented with cerebellar ataxia at the age of 2; at age 6, developed polyuria and polydipsia that progressed rapidly to ESRD. His mother had microphthalmia and extremely poor vision of unknown etiology.

an enigma, but several hypotheses are now actively explored. Once again the cilia hypothesis predominates and a wealth of information from animal models has brought unprecedented insights into these diseases (89). For example, inversin is thought to act as a molecular switch between the different Wnt signaling pathways and is associated with the accumulation of proteins within the cilia. Nephrocystin-1 is localized to centrosomes in interphase and the mitotic spindle pole during mitosis, while the product of NPHP9 localizes to the proximal region of the primary cilium and thought to modulate ciliary targeting of polycystin 1 and 2 (89). In animal models, the mutant forms of uromodulin cause the protein to be retained in the RER, which inhibits normal trafficking and expression at the cell surface. Accumulation within the RER may interfere with appropriate localization of the mutant protein within the physiologic site in the basal aspect of tubular epithelial cells.

DIFFERENTIAL DIAGNOSIS

The differential diagnosis of hyperuricemic disorders includes diseases due to mutations in genes other than UROM. These include Renin and SLC2A9 encoding for GLUT9, an important proximal tubule transporter of uric acid (90,91). Mutations of the latter lead to reduced renal excretion of urate, and patients also have gout. Renin mutations were identified

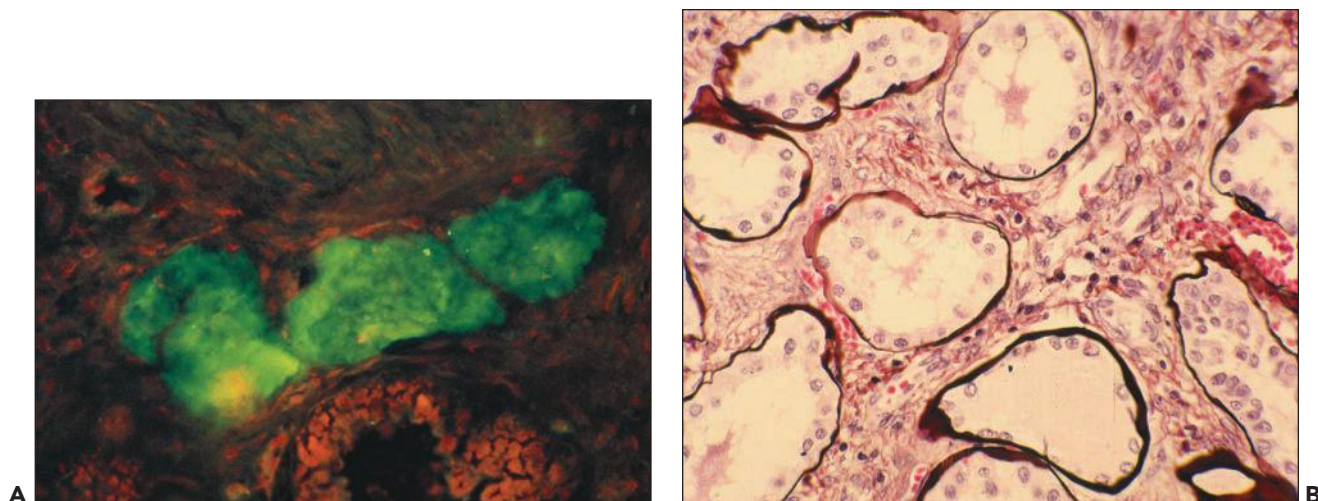


FIGURE 4.31 Renal biopsy of a patient with NPHP shown in previous figure shows positive uromodulin (THP) staining of tubular secretions (**A**; immunofluorescence $\times 200$) and tubulointerstitial injury with thinning and thickening of tubular basement membrane (**B**; silver stain, $\times 200$).

in 39 kindred with hyperuricemia who were previously tested negative for UROM mutations.

Children who lack active urinary sediment or heavy proteinuria and do not have polydipsia and polyuria may only be diagnosed if they have renal cysts detected by ultrasound. In adults who have nonspecific symptoms and a nondiagnostic renal ultrasound, diagnosis of NPHP-MCKD is very frequently missed. For example, in a pedigree of Native Americans living in North Carolina, the diagnosis was not made until family members of a middle-age man were screened for living related kidney donation (92). Similarly, in the Cypriot series, most patients were not diagnosed until late in life (84). Presence of renal cysts and history of familial kidney disease are very helpful, but cysts, as mentioned earlier, are usually few. Notably, NPHP-MCKD patients do not develop flank pain, hematuria,

or lithiasis as in ADPKD. Furthermore, kidneys in ADPKD are enlarged and in NPHP are small or normal.

Upon gross examination, cysts are in the corticomedullary or medullary region of the kidney in contrast to diffuse cysts in ADPKD that occupy the entire kidney. Microscopically, there are no papillary proliferations in the cysts of NPHP-MCKD. In fact, cysts in NPHP-MCKD form *ex vacuo* (degenerative cysts). The pathologic findings in NPHP-MCKD are of tubulointerstitial nephritis. Approximately one third of the patients have UROM mutations, inherited by autosomal dominant mode. Luminal uromodulin in a subset of patients may be a helpful hint. Anti-uromodulin antibodies strongly stain distal tubules (93). Hyperuricemia in children or young adults with NPHP-like presentation also raises the differential diagnosis of inherited deficiencies of purine degradation enzymes such

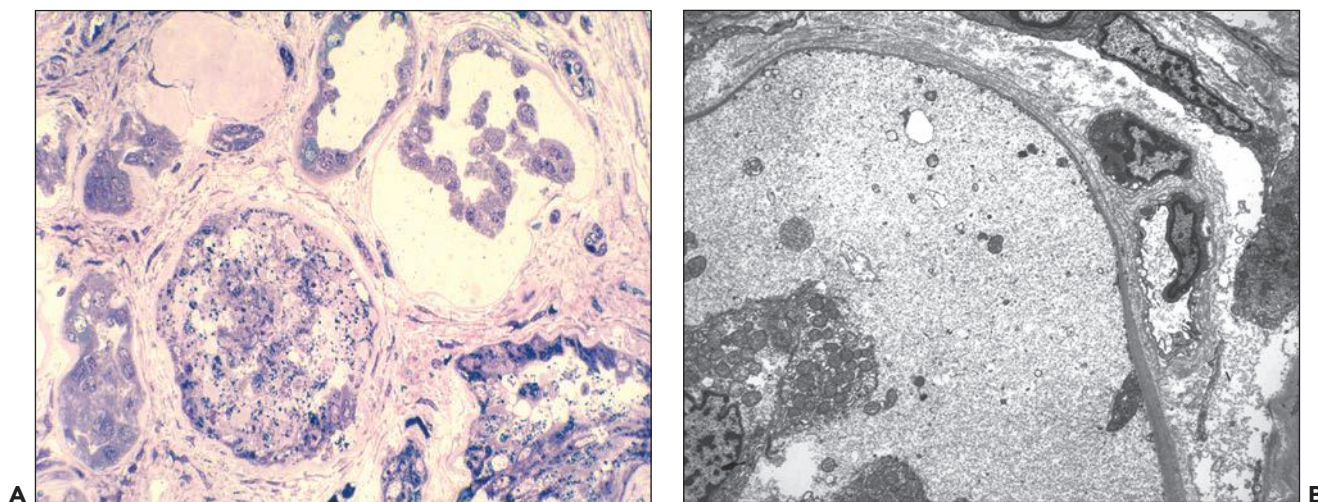


FIGURE 4.32 **A**: Thick sections show disrupted tubular epithelial lining with en masse detachment. **B**: Electron microscopy reveals thinning and lamellation of the tubular basement membrane and granular disintegration of the epithelial cell cytoplasm. (EM $\times 6000$.)

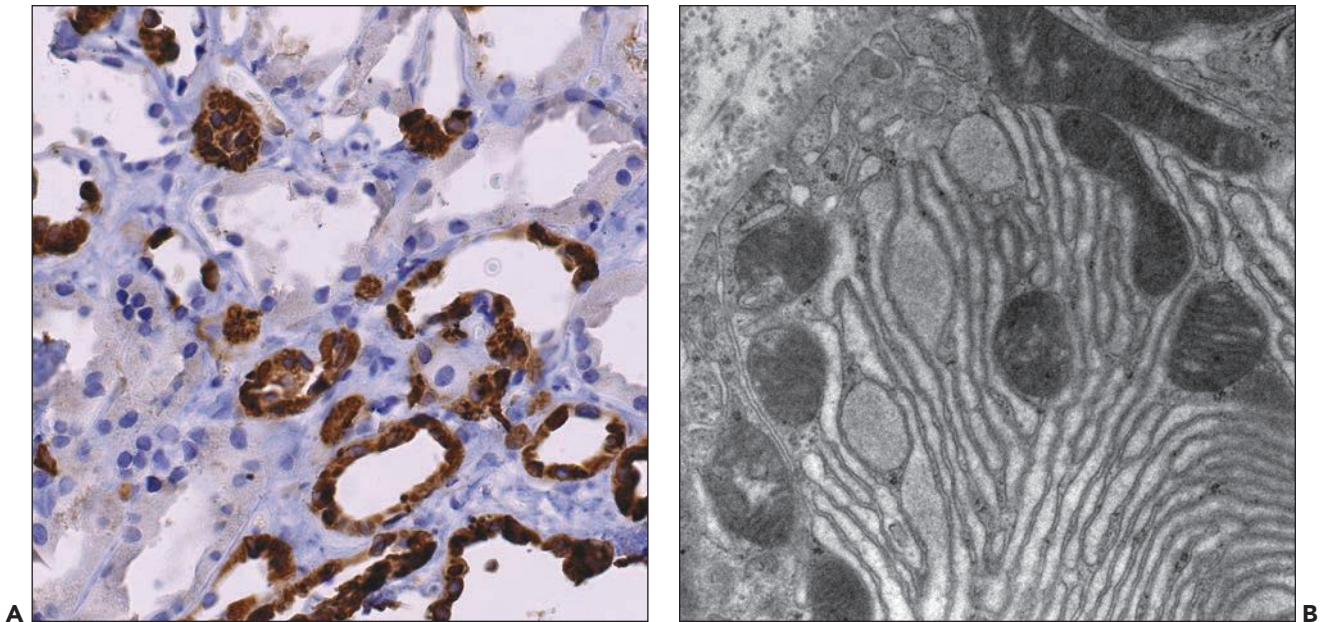


FIGURE 4.33 Renal biopsy from a patient with UROM mutation identified by linkage analysis. The biopsy showed nonspecific findings of tubulointerstitial disease. **A:** Uromodulin stain reveals strong accumulation in distal tubules. **B:** Electron microscopy shows the hyperplastic endoplasmic reticulum and accumulation of amorphous material in dilated cisternae. (Courtesy Sabine Leh, Haukeland University Hospital, Bergen, Norway.)

as X-Linked hypoxanthine-guanine and autosomal dominant adenine phosphoribosyltransferase (PP-ribose P synthase) deficiency (94).

Another entity in the spectrum of NPHP is Meckel-Gruber syndrome, in which autosomal recessive, often lethal, is characterized by encephalocele, cleft palate, dysplastic cystic kidneys, and abnormal digits. There is marked genetic variability with mutations in nine genes reported so far (95). The example shown in Figure 4.34 is from a 2-day-old baby girl with encephalocele and clinodactyly. Notably, Bardet-Biedl syndrome (BBS) shares some of the latter features (discussed briefly below). Table 4.5 lists the entities related to NPHP under the “ciliopathies” concept.

Medullary Sponge Kidney

MSK is a cystic disease of adults with cysts that arise in the medullary collecting ducts. Cysts contain numerous calcium deposits or stones and may reach 8 to 10 cm in diameter. Patients present with hematuria, infection of the urinary tract, or obstruction. Upon radiologic investigation, bilateral nephrolithiasis is found in most individuals (96). A typical example is shown in Figure 4.35. The excretory ureterogram shows filling defects in the medulla without hydronephrosis. Lithiasis often takes interesting shapes and has been likened to a flower bouquet or “papillary blush” by radiologists.

Unilateral or segmental disease is rare. MSK in the majority of patients is a nonhereditary disorder, but approximately 12% of patients appear to have familial disease. Italian investigators recently reported mutations in the glial cell-derived neurotrophic factor (GDNF), a ligand for RET receptor signaling and genitourinary development. Mutations in GDNF and RET cause urinary tract malformations collectively known as CAKUT

(discussed under renal malformations). How GDNF mutations may cause sponge kidney remains to be investigated (97).

Molecular Pathogenesis of Cystic Kidney Diseases

There has been an explosion in genetic information regarding the mutations underlying diverse cystic kidney diseases since the turn of the century, and the majority appear linked to a



FIGURE 4.34 Meckel-Gruber syndrome. The kidneys were enlarged and cystic with a combined weight of 60.2 g (normal for age = 26.1 ± 4.9 g) with histologic findings of renal dysplasia.

TABLE 4.5 NPHP and related ciliopathies: genes and protein products

Gene	Protein
PKD1	Polycystin 1
PKD2	Polycystin 2
PKHD1	Fibrocystin
GCKD	
UROM	Uromodulin
HNF1 β	LFB3
RENIN	Renin
NPHP1	Nephrocystin 1
NPHP2	Inversin
NPHP3	Nephrocystin 3 (Meckel-Gruber) ^a
NPHP4	Nephrocystin 4
NPHP5	Nephroretinin 5 <i>IQCB1</i> (Senior-Løken) ^a
NPHP6	Nephrocystin 6/CEP290 (Joubert) ^a
NPHP7	Nephrocystin 7/GLIS2
NPHP8	Nephrocystin 8/RPGRIP1 (Meckel-Gruber) ^a
NPHP9	Nephrocystin 9/NIMA-related kinase 8
NPHP10	Nephrocystin 10/SDCCAG8 (BBS) ^a
NPHP11	Nephrocystin 11/ <i>TMEM67/MKS3</i> (liver fibrosis) ^a
NPHP12-NPHP1L	Nephrocystin 12/ <i>XPNPEP3</i> (mitochondrial disease) ^a
NPHP13	Nephrocystin 13
MCKD1	Unknown
MCKD 2	Uromodulin, HNF1 β , Renin
MCKD3	Unknown
Bardet-Biedl syndrome BBS 1-12	BBS proteins
Renal dysplasia PAX2	Paxillin

^aEntities in parenthesis are in the NPHP phenotypic spectrum or the predominant clinical presentation.

previously underwhelming cellular organelle—the primary cilium. Hence, many apparently distinct conditions have now been ascribed to the new disease category termed ciliopathies (77,98). Primary cilia are finger-like projections from the cell, enclosed in the plasma membrane, that are involved in mechanosensation, calcium influx, hedgehog and Wnt signaling, and planar cell polarity (99). Cilia are anchored internally by a modified centriole, termed the basal body, and it is likely that the whole cilium/basal body/centriole complex is crucial for the normal maintenance of well-differentiated cells. Defects throughout this complex cause cystic kidney diseases in human and many experimental animal models (100), but it must be pointed out that many of cyst-related proteins also have important roles in other subcellular locations such as basolateral membranes, endoplasmic reticulum, and the Golgi apparatus; hence, despite the overwhelming rush of publications, defects in the cilia/centrosome complex may not be the sole cause of cystic kidneys. Irrespective of the underlying cause, there are several fundamental abnormalities in diseased renal epithelia that eventually generate cystic



FIGURE 4.35 Medullary sponge kidney. Intravenous urography (at 4 minutes) demonstrates markedly dilated collecting ducts greater in the right compared to left. The calyceal system is normal. There is no hydronephrosis or hydroureter. From a 34-year-old man who presented with flank pain. (Courtesy Cary Lynn Siegel.)

kidneys, including increased proliferation in cyst epithelia coupled with apoptosis of surrounding tissues, altered polarity of cyst epithelia with mislocalization of receptor and transporter proteins, and abnormal cell-cell/cell-matrix interactions. The net effect of these is to promote cyst growth while disrupting normal surrounding tissues and renal function. Here, we consider the genetics and biology of cystic kidneys, linking cilia, and diverse pathways to these fundamental other processes, first in relation to polycystic kidneys and ciliopathies and then in cystic dysplastic and multicystic dysplastic kidneys.

Autosomal Dominant Polycystic Kidney Disease

The *PKD1* gene is located on chromosome 16p13.3 and consists of a large 53-kb genomic DNA with 46 exons. Six pseudogenes caused by duplication of *PKD1* exons 1–33 are found on 16p13.1. These hampered the initial search for the gene, but they have suboptimal start codons, so they are not translated. *PKD1* encodes a 460-kDa protein with over 3,000 amino acids, polycystin 1. *PKD2* maps to chromosome 4q13-q23, consists of a smaller DNA sequence of 5.4 kb with 15 exons that encodes polycystin 2, a 110-kDa protein with 968 amino acids. Only one of the *PKD1* or 2 alleles is usually mutated when assessed in the blood of PKD patients, but it has long been supposed that loss of the second normal copy within the kidney is required to generate cysts (and similarly to generate PKD pathology in other organs). This is the two-hit hypothesis, but incomplete penetrance of homozygous variants and compound heterozygotes may also occur (101), and a potential third hit such as renal injury may accelerate PKD (102).

Polycystin 1 has (a) a large extracellular N-terminal region with many different domains including 12–15 PKD repeat motifs (immunoglobulin-like folds), two leucine-rich repeats, a region with homology to C-type lectins, and WSC, GPS, and REJ domains, (b) multiple transmembrane domains, and (c) a small intracellular 197-amino-acid cytoplasmic tail containing a coiled-coil- and G protein-binding domain. Polycystin 1

is strongly expressed in developing renal epithelia, particularly proximal tubules, and then at lower levels in the mature kidney. Expression has also been recorded in the brain, heart, and liver. At a subcellular level, polycystin 1 localizes to the cilium, lateral cell junctions, and the basolateral membrane (103). Immunohistochemistry can still pick up polycystin 1 protein in some ADPKD kidneys, but this tends to be in cytoplasmic pools rather than associated with the cell membrane.

Polycystin 2 contains six transmembrane domains, but both its N and C termini are intracellular. It localizes to distal tubules, collecting duct, and thick ascending limb in both developing and mature kidneys. Subcellular distribution includes cilia and some membrane overlap with polycystin 1, but it is also often found in the endoplasmic reticulum, suggesting additional possible intracellular roles.

Many different functions have been ascribed to polycystin 1 and 2, both acting together and individually. When first described, polycystin 1 was linked to cell-cell and cell-matrix adhesion, whereas polycystin 2 was predicted to be an ion channel. Interestingly, this latter function was later proven correct but it requires heterodimerization of polycystin 1 and 2 together via their coiled-coil domains for calcium-permeable nonselective cation currents. Mutation of either polycystin disrupts this channel activity, and polycystin 2 is only translocated to the plasma membrane when polycystin 1 is present in the cell (104). Other overlapping functions for the polycystins include activation of the JAK-STAT pathway by polycystin 1 with polycystin-2 acting as a critical cofactor (105), regulation of G protein signaling, and activation of the AP1 transcription factor (106).

Autosomal Recessive Polycystic Kidney Disease

Mutations in the polycystic kidney and hepatic disease 1 gene (*PKHD1*) cause ARPKD; this is located on chromosome 6p21, spanning 470 kb and produces a 16-kb transcript. The resulting protein, termed fibrocystin or polyductin by different authors, contains 4074 amino acids with a large N-terminal extracellular region, a single transmembrane section, and a short intracellular cytoplasmic domain. In the kidney, it is mainly localized on the primary cilium and in basal bodies and the plasma membrane, in renal epithelia. Expression has also been noted in cholangiocytes. Aside from potential roles in cilia, fibrocystin may have receptor-like function via the large extracellular domain, while the intracellular part can be cleaved and translocated to the nucleus in cells stimulated with protein kinase C or increased intracellular calcium (again linking back to cilia). Several authors have reported colocalization of fibrocystin with polycystin 2, which suggests the possibility of a large PKD complex involved in a common molecular pathway in vivo (107,108).

Large number of mutations spread throughout the *PKHD1* gene, and the majority of patients are compound heterozygotes. There is a high risk of fetal presentation and neonatal death if the child carries two truncating mutations (109). Cysts only derive from the collecting ducts in ARPKD but can come from all nephron segments in ADPKD (although 85% to 90% still arises from collecting ducts!). ARPKD typically presents antenatally because of ultrasonically bright, enlarged kidneys. There is a high chance of perinatal death from immature lung development if there is severe oligo- or anhydramnios before 24 weeks of gestation (110).

Other Ciliopathies with Renal Cysts

Pathways disrupted in various NPHP include canonical and noncanonical Wnt signaling, Sonic hedgehog, and Hippo (80,81). Inversin, the gene product of NPHP1, illustrates the complexity and interactions within this group: inversin localizes with Nephrocystin and β -tubulin in primary cilia (82) and acts as a molecular switch between different Wnt signaling cascades by inhibiting the canonical Wnt pathway via increased turnover of dishevelled, which is downstream of the frizzled Wnt receptor, while promoting noncanonical signaling required for convergent extension (at least in *Xenopus*) (83).

BARDET-BIEDL SYNDROME

BBS has distinctive clinical features comprising obesity, retinopathy, polydactyly, learning disabilities, and hypogonadism, plus diverse renal abnormalities of dysplasia and cystic tubular disease (98,111–113). Sixteen mutated genes (BBS1–16) have currently been described (98,112,114) and new ones being implicated such as LZTFL1 (115), which appears to be an upstream regulator of the BBSome (the collective name for the group of conserved proteins affected in BBS). Current estimates are that mutations can now be identified in over 80% of classical BBS patients (114). Clinical presentation is often via identification of the associated problems rather than renal disease. For example, children may present with night blindness then visual deterioration due to rod-cone or nonspecific learning difficulties and obesity. A history of postaxial polydactyly should always be sought because small appendages may have been tied off at birth and forgotten without specific questioning.

The BBS genes are intimately associated with cilia assembly and function (116–118). Most components of the BBSome localize to the base and transition fibers of the primary cilium, and they are essential for intraflagellar transport (IFT) within the organelle; mutations can therefore disrupt normal anterograde and/or retrograde movement (i.e., up and down; see below), which is essential for ciliary assembly and function. The BBS genes also modulate Sonic hedgehog signaling by ensuring regulated turnover of smoothened and patched 1 (113).

Potential Central Role of Primary Cilia in Polycystic Kidneys

Primary cilia are finger-like projections from the apical cell surface (Fig. 4.36), enclosed by a modified cell membrane (119,120). They have a microtubule cytoskeleton with nine peripheral doublets, the ciliary axome, in contrast to motile cilia that have nine peripheral and two central microtubules (9 + 0 vs. 9 + 2). Antonie Philips van Leeuwenhoek described them over 300 years ago. The term “primary cilia” was not used until Sorokin in 1968 (see historical review by Bloodgood) (121). The first link to PKD came from mating behavior in *Caenorhabditis elegans* in 1999. Barr and Sternberg (122) demonstrated that the *lov-1* gene, which encodes a transmembrane protein with homology to polycystin 1, is expressed in adult male sensory neuron cilia and is required for sensory response and vulva location. Moreover, the *PKD2* homologue also localized to these neurons and functions in male sensory behavior (123). In 2000, Murcia et al. linked PKD to cilia in the Oak Ridge Polycystic Kidney (*orp*) mouse. The gene mutated in these mice is *Tg737* (*polaris*), and mutants have defective cilia

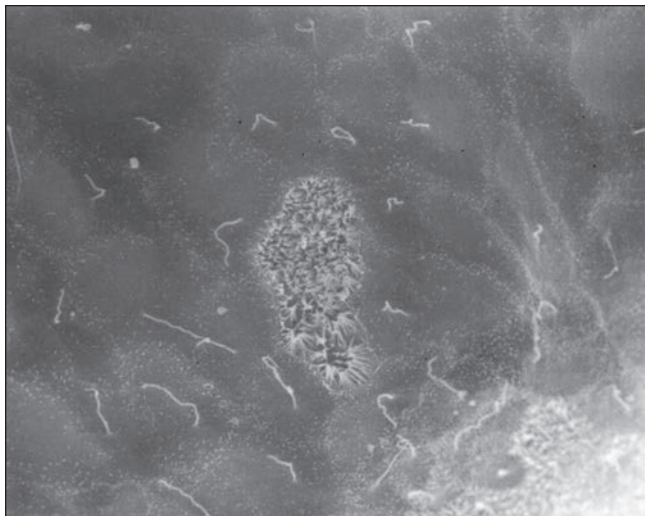


FIGURE 4.36 Transgenic PKD2 rat model shows cilia extending from epithelial cells lining the cyst wall. (Courtesy Ralph Witzgall, Institute for Molecular and Cellular Anatomy, University of Regensburg, Germany.)

in ventral node cells in early development that can disrupt left-right axis determination (124).

Structure and Assembly of Primary Cilia

Primary cilia are dynamic structures that are rapidly assembled and disassembled at different stages of the cell cycle. The centrosome migrates toward the cell surface as the cell enters G₀, the mother centriole attaches to a Golgi-derived vesicle mediated in part by the distal appendages of the centriole, also known as transition fibers, and the axoneme of the primary cilium grows from the cell surface into the lumen (125,126). The primary cilium is resorbed as cells reenter the cell cycle and divide but regrows as each daughter cell becomes quiescent. Proteins needed to build the cilium are moved up and down the cilium by the same processes as required to build flagella; hence, it is termed IFT, and speeds of around 1 $\mu\text{m/s}$ have been recorded (127). Movement toward the tip of the cilium is termed anterograde IFT and depends upon kinesin-2 microtubule motors, while the reverse retrograde transport requires dynein (128). Disruption of transport in either direction perturbs cilia formation. Defective anterograde movement blocks development, whereas disruption of the dynein motor results in short, stumpy cilia (129). Moreover, kidney-targeted inactivation of kinesin-2 not only inhibits renal ciliogenesis but also induces cystic kidney disease (130). Cilia are also shorter than normal in the *orpk* mouse (131). Cilia assembly may also be regulated by microRNAs because targeted disruption of the miRNA enzyme dicer in the collecting ducts disrupts cilia development and is associated with cysts (132).

Although the cilium arises from the cell, its membrane composition is subtly different because of regulated trafficking of proteins and lipids into it (133). A ciliary necklace (125) and “ciliary pore complex” (134) have been reported in various species, functioning as barriers through which only selected proteins are allowed passage into the ciliary compartment. There is also a ciliary pocket, a depression of the plasma membrane in which the primary cilium is rooted (135). The pocket

shares many morphologic features with the flagellar pocket of Trypanosomatids, which is a trafficking-specialized membrane domain at the base of the flagellum. The BBS genes have crucial roles in targeting to the cilium (136).

Fluid Flow and Calcium

Most “ciliopathy” patients and murine models have structurally normal cilia, with rare exceptions such as *orpk* mentioned above. Hence, if cilia are to have a role in cystic kidneys, their function must be affected by ciliopathy mutations. An obvious mechanism might involve dysregulation of calcium influx, based on the predicted function of polycystin 2 as a calcium channel and the observation that intracellular calcium levels are 20 nM lower in ADPKD cells versus normal human kidney epithelial cells. The first evidence supporting a ciliary role in sensing fluid flow and then modulating calcium influx came from nonrenal studies on left-right asymmetry. Loss of *Pkd2* and other ciliopathy genes can cause randomization of organ laterality both in mice and zebrafish (137,138). This is thought to result from abnormal signal transduction in peripheral monocilia of the organizing node during development (the mammalian “laterality organ”) (139). Mechanical bending of individual cilia using micropipettes induces calcium influx (140); hence, it was postulated that regulated fluid flow generated by cilia in the node bends these cilia to induce polycystin-dependent calcium signaling in the paraxial mesoderm to the left of the node (137,141,142). Moving to the kidney, fluid flow also induces calcium influx in cultured Madin-Darby canine kidney cells (derived from collecting duct epithelia) and requires polycystin 1 and 2. This influx leads to calcium-induced calcium release from the endoplasmic reticulum mediated via the ryanodine receptor (143,144). Downstream effects may include activation of map kinase signaling, leading to increased cell proliferation and abnormal fluid secretion, both contributing to cyst formation.

Cilia, Cyclic AMP, and DDAVP Antagonist Therapy

Lower intracellular calcium levels caused by aberrant ciliary function is likely to have many consequences, but a key event may be reduced clearance of intracellular cyclic AMP (cAMP) in ciliopathy renal epithelial cells, leading to accumulation of this factor (145–147). cAMP is an ubiquitous intracellular second messenger, generated by G protein-coupled receptors linked to adenylyl cyclases and broken down by cAMP phosphodiesterases (147). A key factor activated by cAMP is protein kinase A (pkA), which is linked to the apical CF transmembrane regulator (chloride channel). This has been implicated in one mechanism promoting cystogenesis, namely dysregulated fluid secretion (148). cAMP is also pivotal in the increased epithelial proliferation needed for cyst expansion. cAMP stimulates proliferation of epithelial cells from cysts in ADPKD via RAF1, MEK1, and ERK pathways, in contrast to normal epithelia where it is antimitotic (149).

Upward of 70% of cysts in ADPKD arise from collecting duct principal cells (150), and the main stimulator of cAMP in these is vasopressin via the V₂ receptor system. Hence, a number of vasopressin antagonists have been trailed in animal models of PKD, mainly by Vincente Torres et al.; these studies demonstrated effective lowering of cAMP levels, reduction in cyst formation, and preservation of renal function (151,152). The next step was human trials, and it has recently been

reported that Tolvaptan significantly reduced the expected increase in kidney size, ameliorated progressive loss of renal function, and decreased episodes of renal pain (65). This is encouraging news, although it must be noted that the major side effect of increased urine output did cause a 23% patient dropout from the study, versus 14% placebo.

Cilia and mTOR

The mammalian target of rapamycin (mTOR) is a serine/threonine kinase with roles in several processes deregulated in cystic kidneys including proliferation, survival, and polarity (153). mTOR is part of at least two multiprotein complexes, mTOR complex 1 (mTORC1) and mTORC2. The former promotes cell proliferation in response to stimuli such as growth factors, insulin, oxidative stress, and some amino acids (particularly leucine), and it is a target of the immunosuppressing antirejection drug rapamycin. mTORC2 is also sensitive to growth factors, insulin, and nutrient levels, but its main roles seem to be in regulating the cytoskeleton via F-actin stress fibers, paxillin, and the Rho/Rac system. It was initially thought unresponsive to rapamycin but may be affected after chronic use (153).

Components of the mTORC1 pathways are elevated in cystic epithelia in both human ADPKD and ARPKD and from mouse models of renal cystic disease including those with ciliary defects (154–157). The latter findings are consistent with recent data that bending of cilia down-regulates mTOR signaling, independent of calcium influx Akt (158); hence, defective cilia structure or function might be expected to raise mTOR levels. Rapamycin convincingly slows cyst progression in diverse rodent models of PKD (157,159–161), but some of the doses used are high with increased morbidity/mortality, and there is one report of longer-term glomerular and parenchymal hypertrophy after short-term pulse therapy at early cystic stages (160). Human studies are underway at present, but results from 18- to 24-month trials of sirolimus or everolimus are unconvincing (162,163). Part of the problem may be that toxic doses are needed for effective cyst therapy; hence, one group has developed folate-conjugated rapamycin in the hope that folate receptor-mediated endocytosis within the kidney will increase local reagent delivery. Results are promising in mice (164).

Cilia, Wnt, and Planar Cell Polarity

Diverse recent studies confirm that knockdown of ciliogenesis genes disrupts Wnt signal transduction in mouse, zebrafish, and frog. A number of Wnt signaling pathways have been described, which can be grouped into canonical or noncanonical pathways, but signaling is typically initiated by interaction of different Wnt ligands with specific frizzled (Fz) receptors, followed by recruitment of the intracellular protein, disheveled (Dvl), and activation of specific coreceptors (165,166). While canonical Wnt signaling results in activation of β -catenin-mediated transcription, noncanonical pathways are, by definition, β -catenin independent. The Wnt/ Ca^{2+} noncanonical pathway may be linked to calcium influx via bending the cilium but a better studied pathway is the Wnt/planar cell polarity (PCP), which regulates cell migration and polarity.

In the canonical pathway, mice overexpressing β -catenin in renal epithelia develop cysts, owing to defects in cell turnover and aberrant localization of ion channels (167). The cytoplasmic tail of polycystin 1 interacts with β -catenin and may

modulate Wnt signaling, although there are conflicting results over whether this is stimulatory or inhibitory (168,169). Secreted Frizzled-related protein 4, which specifically inhibits canonical Wnt signaling, is up-regulated in human ADPKD and several mouse models of renal cystic disease, and genetic variation of *DKK3*, encoding a Wnt/ β -catenin antagonist, may modify the severity of ADPKD (170,171). Therefore, canonical Wnt signaling is directly implicated in renal cystic disease.

The PCP pathway has recently come to prominence because of several lines of evidence that regulated cell polarity is abnormal in PKD cells (172,173). All cells have three axes: apical-basal and, when looked at from above, North-South, and East-West. It is the latter two axes that are considered in PCP diseases. Precisely orientated cell division is critical for convergent extension, which promotes tubule development in lower animals such as *Drosophila* and *Xenopus*. Similar processes occur in mammals too, although this does not seem to be only mechanism involved and noncanonical signaling may also play a role (99). PCP signaling is activated by ligands, such as Wnt11 and Wnt9b, that are essential for normal kidney development. Wnt11 is expressed in the ureteric ampullae, where it activates Gdnf/Ret signaling and branching morphogenesis (174), and loss of Wnt9b or the PCP protein Fat4 causes renal cysts with abnormal epithelial polarity, orientation of cell division, and tubule elongation (175,176). Epithelial cell intercalation drives elongation of renal tubules in embryonic development, whereas direction of cell division is more important postnatally since the mitotic spindles are orientated in the direction of tubule elongation after birth. Both of these processes are disrupted in mouse models of renal cystic disease, including mice with mutations in *Hnf1 β* , *Tsc1/2*, and *Pkd1* (172,173). Several ciliopathy genes have been implicated in the regulation of the Wnt/ β -catenin and Wnt/PCP signaling pathways, and work in zebrafish and frogs suggests that these components may regulate the balance between canonical and noncanonical signaling, possibly through regulation of Dvl, which is common to both pathways; furthermore, this balance may be regulated by fluid flow (83,128). Therefore, cilia may coordinate Wnt signaling pathways, and deregulated Wnt signaling may contribute to cyst formation.

Cilia and Hedgehog Signaling

Cilia play a central role in hedgehog (Hh) signal transduction. There are three activators of Hh signaling: Sonic (Shh), Indian (Ihh), and Desert (Dhh) hedgehog. These function via a single major receptor, Patched 1 (Ptch1) (177,178), which inhibits a second transmembrane protein, Smoothed (Smo), until stimulated by one of the three hedgehog ligands when Smo repression is lifted. This leads to accumulation of Smo in cilia, which changes the Gli transcription factors, Gli2 and Gli3, from transcriptional repressors to transcriptional activators (179,180). Several cilia mutants have dysregulated Hh activity, ranging from elevated signaling in tissues not normally eliciting a Hh response and reduced signaling in tissues normally showing high levels of Hh signal transduction, for example, the Joubert syndrome gene, *Arl13b* (181). It is likely that cilia represent a site at which many components of the Hh and other signaling pathways become concentrated, making it a “molecular meeting place” that promotes targeted interactions owing to the juxtaposition of the ciliary axoneme and specialized membrane.

Abnormal Hh signaling causes ectopic and cystic kidneys in Smith-Lemli-Opitz syndrome, caused by mutations in *DHCR7* that may affect HH signaling via defective cholesterol biosynthesis (182). Reduced Hh signaling has been linked to kidney cysts in mice *in vivo* (183), but it is interesting that *Ihh* is the most highly up-regulated gene in a renal explant model of corticosteroid-induced renal cyst formation (184); moreover, treatment with the Smo antagonist cyclopamine reduced cysts, which implicates canonical Hh signaling in pathogenesis.

Renal Cysts in Hereditary Syndromes

von Hippel-Lindau Disease

INCIDENCE, CLINICAL PRESENTATION, AND GENETICS

VHL disease is an autosomal dominant hereditary disorder with an incidence of 1:30,000 to 1: 50,000 live births (185). VHL is caused by germ-line mutations of the *VHL* tumor suppressor gene located on 3p25-26 chromosome. Both men and women are affected. The hallmarks of the disease are cysts and benign and malignant tumors in multiple organs. Tumors involve the central nervous system (hemangioblastomas), retina (angiomas), inner ear (endolymphatic sac tumor), kidney, pancreas (islet cell tumors), epididymis in men or broad ligament in women (cystadenomas), and pheochromocytomas (186). A characteristic feature of all tumors associated with VHL is the high degree of vascularization and the presence of a clear cell component. The frequency of lesions varies in different families, and at a minimum, one characteristic tumor (CNS hemangioblastoma or clear cell tumor in a visceral organ) suffices for diagnosis if definitive family history exists. In the absence of family history, two characteristic (clear cell) tumors are required for diagnosis. Kidney cysts predominate and are found in approximately 70% of the cases. Pancreatic cysts affect 26% of patients, but cysts in the liver are rare.

The most common imaging finding in VHL is renal cysts (187). VHL kidneys are usually either normal or slightly enlarged. Renal failure is rare, but when it occurs is because of diffuse replacement of the renal parenchyma by multiple cysts.

Other organs that may develop cysts include the pancreas, spleen, lungs, bone, and skin. Kidney tumors are typically RCC clear cell type arising within the cysts (Fig. 4.37A). RCC is the main cause of morbidity and mortality and affects 75% of patients by the age of 60 years; it may also be the first manifestation of the disease. Other symptoms are hematuria and urinary tract infections, but hypertension is rare unless there is a pheochromocytoma. Most studies show that only a minority of patients have the full set of manifestations. More than 100 germ-line mutations have been identified; phenotypic variability is in part due to mutation type. For example, renal disease is more frequent in patients with truncating mutations of the protein (pVHL) or large rearrangements as opposed to patients who have missense mutations (188). Patients with truncating mutations are designated as having VHL type 1 and characteristically develop all manifestations except pheochromocytoma. Patients with missense mutations have a predominant risk to develop pheochromocytoma and are designated as VHL type 2. VHL type 2 is further subdivided into type 2A (low risk for RCC and pancreas tumors), B (susceptible to all tumors from the VHL menu), and C (almost exclusively developing pheochromocytomas) (189). Other studies find that renal cysts are independent of mutation type, while pancreatic cysts and hemangioblastomas correlate with gene deletions (190).

PATHOLOGY

VHL cysts are grossly small and do not transform the kidneys into the giant organs as in ADPKD (Fig. 4.37B). Bilateral or unilateral cysts are few in number ranging from microscopic to a few centimeters. Histologically, cysts may be denuded or lined by low epithelium. Intracystic tumor nodules are typically clear cell type RCC (Fig. 4.38). Papillary RCC is sometimes found, but cells lining the papillae are clear cell type. Kidney tumors are usually found upon routine screening for occult disease. A lesion in the CNS or the spinal cord is more likely to be hemangioblastoma than RCC. If abdominal lesions originate outside the kidney, pheochromocytoma should be excluded. Distinguishing VHL from ADPKD and TSC as

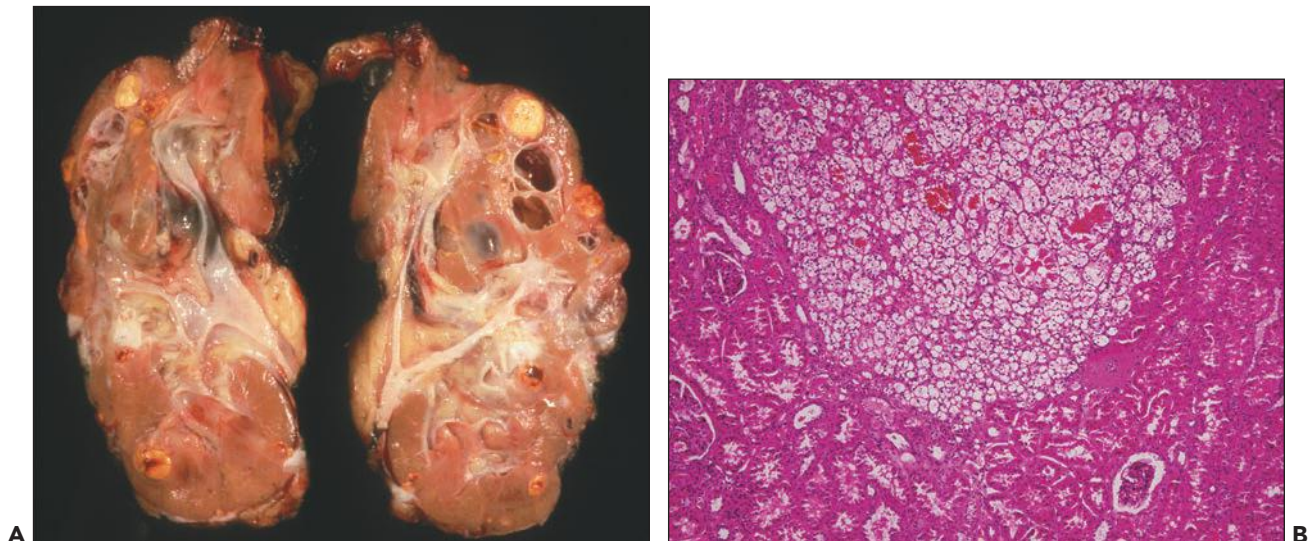


FIGURE 4.37 VHL kidneys with (A) grossly apparent bilateral RCCs. B: RCC, clear cell type in one of the cysts.

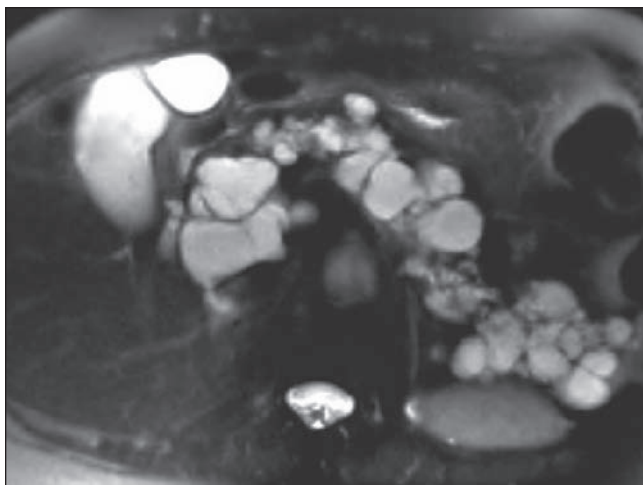


FIGURE 4.38 Axial T2-weighted fat-saturated image demonstrates innumerable cysts in the pancreas of a patient with VHL. (Courtesy Dr. Cary Lynn Siegel.)

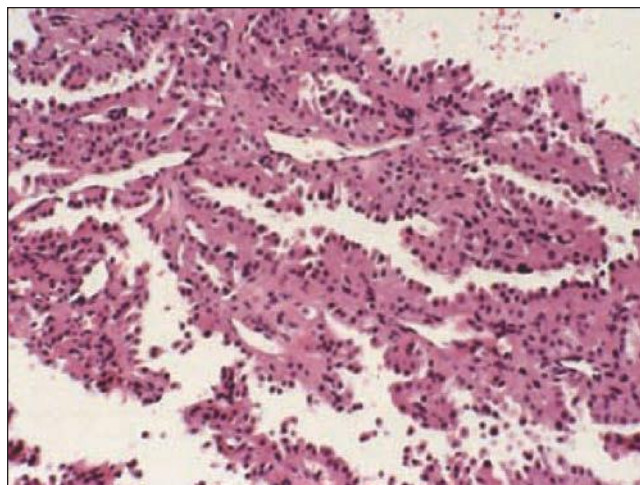


FIGURE 4.39 Low-grade papillary RCC from renal biopsy of a young child who presented with bilaterally enlarged kidneys. Tumor cell nuclei are low grade and difficult to distinguish from renal tubules.

well as other hereditary cystic diseases may at times be difficult (187). Differences such as kidney size, frequency of cysts, and extrarenal associations are helpful diagnostic clues. For example, cysts primarily in the pancreas are characteristic of VHL (Fig. 4.38). Solid nodules within cysts are common in VHL and rare in ADPKD. Liver cysts are rare in VHL in contrast to ADPKD. Distinguishing VHL from adult TSC is easier based on the fact that the most common tumor is angiomyolipoma, and extrarenal manifestations are distinct from VHL (see below). Diagnosis may be particularly difficult in young children when the first presentation is bilateral RCC. Such tumors may be very low histologic grade with individual tumor cells resembling closely normal tubules or tubular hyperplasia (10). An example of a case from a 7-year-old boy is shown in Figure 4.39. Kidneys were bilaterally enlarged, occupied by heterogeneous masses with cystic and solid components. CT confirmed multiple renal cysts 1 to 4 cm in diameter. Renal biopsy revealed benign-appearing papillary proliferations. Nuclei had very low-grade atypia (Fig. 4.39). Family history was negative for VHL and TSC in this child, but one should be aware of the possibility of *de novo* mutations and/or newly described types of hereditary clear cell RCC that are not related to VHL or TSC genes (10,191).

PATHOGENESIS

The *VHL* gene targets the hypoxia-inducible factor (HIF)-1 that regulates expression of hypoxia-inducible genes including the vascular endothelial growth factors such as VEGF, platelet-derived growth factor B, Flik-1, and Tie-2, and also erythropoietin and transforming growth factor α (TGF α). VHL also regulates genes related to cell cycle, epithelial cell differentiation, and fibronectin assembly in the extracellular matrix (reviewed in (192)). As a tumor suppressor gene, biallelic *VHL* inactivation leads to uncontrolled cell growth, neoplastic transformation and overexpression of VEGF in tumor cells and neoangiogenesis. A two-hit mechanism is thought to operate in this disease similar to ADPKD and TSC. The *VHL* gene has only three exons and codes for three proteins, two of which are

due to an internal translational initiation start site at codon 54. Both proteins are thought to be wild (functional) type. A third protein is derived from exon 1 spliced into exon 3 and is not a tumor suppressor. However, there are at least 3 HIF α subunits (1a, 2a, and 3a) that are targeted by pVHL; hence, regulation of hypoxia-inducible genes is not straightforward. One thing appears to be clear: RCC in VHL derives from cyst epithelia with VHL gene deletion (193). Furthermore, through studies on VHL pathogenesis, sporadic RCC and a cystic variety of RCC called multilocular cystic RCC are understood to be in part due to VHL mutations and related dysregulated pathways (194).

PROGNOSIS AND MANAGEMENT

Optimization of surgical treatment has changed the long-term prognosis of VHL patients. Nephron-sparing procedures for lesions over 3.5 cm that have solid intracystic nodules are preferred in patients with a few lesions. Bilateral nephrectomy and transplantation is an acceptable alternative in those with multiple lesions. New innovative approaches in VHL management include radiofrequency ablation or cryosurgery and needle ablation for small primary or recurrent lesions (187).

Tuberous Sclerosis

INCIDENCE, CLINICAL PRESENTATION, AND GENETICS

TSC is a systemic phacomatosis characterized by hamartomatous proliferative lesions in almost every organ, including the brain, skin, retina, heart, endocrine glands, digestive system, lung, and kidney. Renal lesions include angiomyolipomas, cysts, and RCC. It is estimated to affect 1/10,000 to 1/15,000 live births and is inherited as an autosomal dominant trait. Up to 60% of cases are sporadic with no family history of TSC and are thought to represent new mutations. Both men and women are affected. Development of symptoms varies, but most patients are diagnosed in the first two decades. The heart, kidney, skin, and brain are frequently affected. The kidney is affected in about 50% of the cases (195). Angiomyolipomas are present in approximately 85%, cysts in 45%, and RCC in

approximately 4%. Angiomyolipomas are more frequent in women and TSC2 mutations. They are composed of variable combinations of fat, vessels, and smooth muscle, and they tend to be numerous and bilateral in TSC in contrast to sporadic tumors. Unusual nuclear pleomorphism or epithelioid variants should be considered potentially malignant. RCCs are usually clear cell type, but rarely papillary or chromophobe types occur. Renal cysts usually coexist with tumors and are simple and few. Cystic-only kidney involvement is less frequent affecting about 17% of patients, and these cysts are often asymptomatic (196). Renal failure and hypertension may develop because of enlarging lesions and replacement of the renal parenchyma. Pulmonary lymphangiomyomatosis is one of TSC manifestations that may on occasion be concurrent with renal cysts (197).

Two tumor suppressor genes, TSC1 and TSC2, located at 9q34 and 16p13.3, respectively, are identified (198). Development of tumors requires a second (somatic) mutation in addition to the germ-line mutation. Truncating intragenic mutations that affect the corresponding allele were also detected by genetic analysis of hamartomas and malignant tumors of TSC patients. Mutations spanning the entire length of the genes are reported. TSC2 mutations are more frequent in patients who have no family history of TSC (new mutations) and are associated more with mental retardation. Lung disease (lymphangiomas) occurs with both TSC1 and TSC2 mutations but is very rare (only 3/150 patients in one study) (197).

CT and MRI are commonly used for follow-up of patients who carry TSC diagnosis (199). Cysts are detected more frequently in children. Both cysts and angiomyolipomas increase in size with age. MRI demonstrates coexisting bright and dark signal intensities that correspond to cysts and fat, respectively. TSC tumors are usually treated conservatively, unless they are complicated by bleeding. Rapid growth and young age are an exception to watchful waiting. The fact that both VHL and TSC are complicated by RCC may at times cause diagnostic difficulties in patients who lack extra renal stigmata. A potential perplexing differential diagnosis in children is the exclusion of the contiguous gene TSC/ADPKD syndrome (see above under ADPKD). Such children may present with bilaterally enlarged kidneys, negative family ADPKD history, and CNS lesions of TSC.

PATHOLOGY

Kidney resection is performed for enlarging angiomyolipoma, RCC, or persistent hematuria. Cystic kidneys from TSC patients are very rarely seen in surgical pathology. In such cases, diagnosis is often a surprise, because cystic kidneys may be the only and first manifestation of TSC. Cysts may be unilateral or bilateral, diffuse, or localized. Kidneys may appear segmentally or diffusely cystic containing cysts of variable size and shape (Fig. 4.40). In childhood TSC, gross pathology is nonspecific. Multicystic renal dysplasia is the most likely presumptive clinical diagnosis in the absence of relevant history. However, TSC cysts have unique microscopic features that set them apart from all other cystic diseases, including VHL disease and renal dysplasia. The lining epithelium is composed of cuboidal large cells with deeply eosinophilic cytoplasm in either a single or multiple layers (Fig. 4.41). Cysts may contain eosinophilic thyroid-like secretions and or intracystic masses resembling neoplastic proliferations. Nuclear pleomorphism and atypia

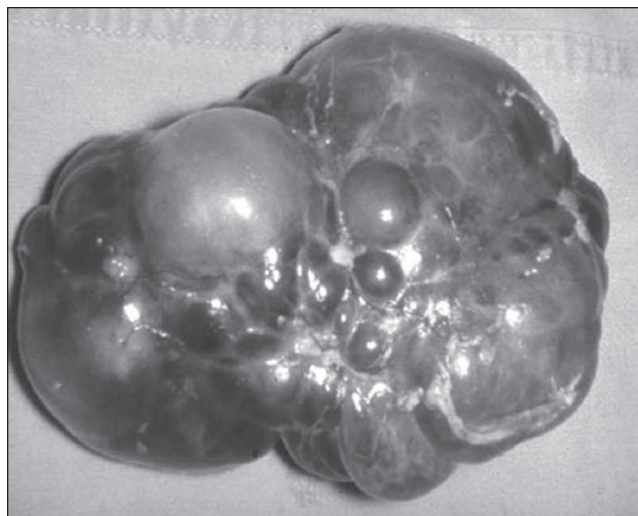


FIGURE 4.40 Cystic kidney from a child with tuberous sclerosis (TSC).

may be present, suggesting that these are likely precursors of RCC. Tubular and glomerular cysts (GCKD) with cuboidal or polygonal proliferating epithelial cells filled with lipid vacuoles (glomerular microhamartomas) are rarely seen (200).

Cystic disease is usually mild in adults. Cysts are small and focal and are often adjacent to angiomyolipomas (Fig. 4.42). These cysts may resemble cysts in VHL disease, but concurrent angiomyolipomas make the distinction easy. However, TSC cysts are not always associated with angiomyolipomas.

In summary, histopathologic features that suggest TSC include characteristic cuboidal eosinophilic cyst-lining epithelium, glomerular cysts, glomerular hamartomas, multifocal or bilateral angiomyolipomas, cysts associated with angiomyolipomas or RCC, and or extrarenal findings (pulmonary lymphangiomas).

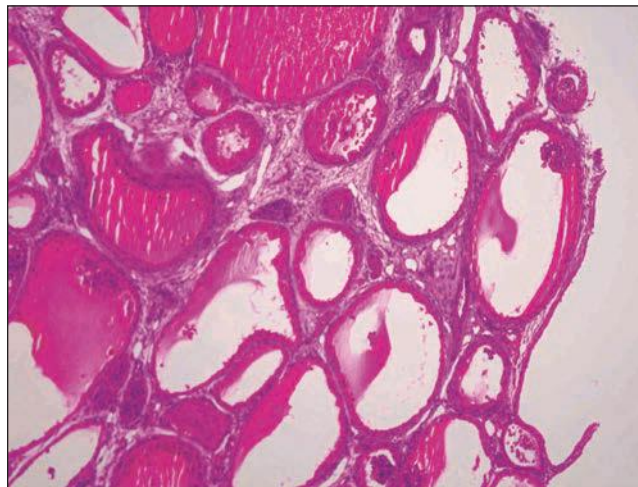


FIGURE 4.41 TSC cysts are lined by proliferating epithelium composed of large eosinophilic cells with atypical nuclei; some cysts are glomerular in origin. (H&E $\times 100$)

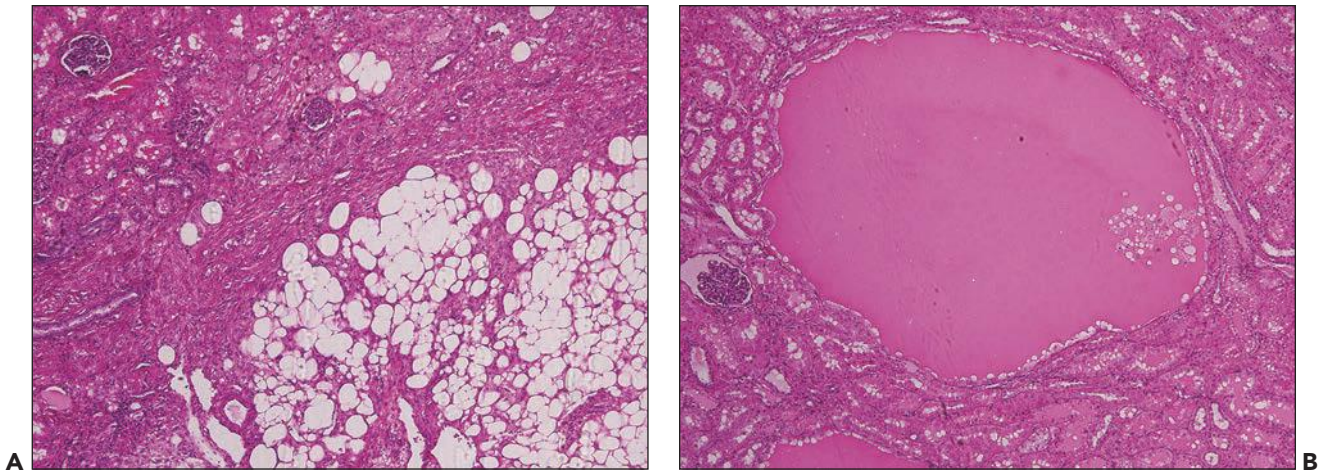


FIGURE 4.42 TSC cysts in an adult adjacent to (A) angiomyolipoma; (B) a small cyst lined by a single epithelial layer ($\times 200$).

DIFFERENTIAL DIAGNOSIS

In children, multicystic renal dysplasia, early-onset ADPKD, and contiguous gene TSC-ADPKD syndrome are the main entities to consider. VHL disease also enters the differential diagnosis, and it may be impossible at times to exclude without molecular genetics.

Pathogenesis

TSC1 encodes for hamartin and TSC2 for tuberin, a putative GTPase that appears to interact with hamartin in vitro suggests that they function in the same cellular pathway. The mechanisms through which TSC1 and TSC2 mediate cellular growth control are only partially understood. TSC2 was directly linked to cell size regulation by the discovery that mutation in *dTsc2* leads to the gigas (large cell) phenotype in the fly (201). Recent genetic studies suggest that TSC2 targets the rapamycin (TOR) pathway via phosphatidylinositol-3-kinase (PI3K), while the TSC1-TSC2 complex functions downstream of Akt and upstream of TOR to restrict cell growth and cell proliferation. While a role in cell cycle control is found for tuberin, similar cellular-specific roles are not proven for hamartin. The fact that the two interact in vivo suggests similar functions and is consistent with the phenotypic manifestations in patients who carry mutations of either TSC1 or TSC2. Phenotype-genotype correlations and current work into the molecular signaling of these genes suggest that abnormalities in additional pathways, for example, β -catenin signaling, may be responsible for variability in TSC manifestations (202).

Multilocular Renal Cyst (Multilocular Cystic Nephroma)

Clinical Presentation

MCN is an infrequent lesion seen both in children and adults. Overall, MCN accounts for about 5% of pediatric neoplasms. Children less than 4 years of age and men and women greater than 30 years of age are affected (203). Most cases are sporadic and unilateral, even though recent studies suggest that some cases are familial (11). Congenital presentation in newborns and young infants is usually with an abdominal mass, abdominal pain, and hematuria mimicking Wilms tumor, a much

more frequent entity in infancy. MCN is a slow growing lesion in both children and adults, but occasionally rapid growth is observed. Ultrasound, CT, or MRI is helpful in revealing the cystic nature of the lesion and its multilocular consistency but cannot distinguish it from entities with similar presentation such as unilateral early-onset ADPKD, multicystic dysplasia, malignancy, and a benign, nonfamilial condition known as “localized cystic disease.” Pathologic evaluation is the best approach to diagnosis.

Pathology

MCN is usually a large lesion occupying most of the kidney. The tumor is often encapsulated and consists of noncommunicating multiloculated lobules that are filled with gelatinous or clear fluid (Fig. 4.43A). The lobules measure a few millimeters to 3 to 4 cm and are separated by thin septae. Septae may fold into the cysts, but nodular proliferations within the cysts are not a feature of MCN. The renal pelvis may be involved. Microscopically, cyst lining is quite characteristic composed of a single layer of flat or “hobnail”-appearing cells. The septae contain connective tissue and focally atrophic tubules (Fig. 4.43B). Presence of undifferentiated mesenchymal cells (blastema) is not part of benign MCN and is considered to confer malignant potential. The term partially differentiated nephroblastoma is coined for these lesions. In spite of the worrisome features, there have been no reported metastases or recurrences following surgical resection in this variant. Recently, MCN and variants showing variable amount of stromal and epithelial components were reclassified and the term renal epithelial and stromal tumor was proposed (203). An example is shown in Figure 4.44. Another interesting recent finding is the association of MCN with pulmonary blastoma, an entity that in some patients is hereditary (11,204).

Localized Cystic Disease

This is an uncommon presentation of renal cystic disease that has been mistaken for unilateral ADPKD, MCN, and cystic neoplasms. Some of the described cases have been mistaken diagnoses (12). Clinically, localized cystic disease may present with flank pain, hematuria, as an abdominal mass or be an



FIGURE 4.43 **A:** MCN in a young infant consists of **(A)** multiloculated cysts filled with gelatinous fluid. **B:** Tumor consists of slender connective tissue septae lined by a single layer of epithelial cells with a flat or hobnail appearance. (H&E $\times 200$)

incidental finding. More than half of the reported cases were treated conservatively and only 4/18 (approximately 20%) had a nephrectomy. Most patients are men. The median age of diagnosis is 50 years (range 24 to 83 years). It may involve a segment or the entire kidney. Depending on the extent of renal involvement, it has been called segmental cystic disease of the kidney, unilateral cystic disease, or unilateral polycystic disease. Obviously, the latter term is to be avoided, because this entity is not familial; it involves only the kidney and bears no resemblance to ADPKD, which is a hereditary and systemic disease. We have seen a couple cases in adults. Both kidneys showed microcysts without fluid. The intervening renal parenchyma was normal. Microscopically, the cysts were denuded of epithelium. None of the patients had stigmata to suggest hereditary

cysts. Nonetheless, such cases are interesting, and teach us that there are yet unsolved mysteries in cystic kidney disease.

Simple Cortical Cysts

Simple cysts are discrete lesions that may develop within the kidney or on its surface. Their prevalence is reported to be 12% to 25% in the adult population (205). These are common findings in autopsy of older men, but they are a rare phenomenon in children. For example, in a study of 6521 consecutive pediatric autopsies, only 7 cases were identified (less than 1%). A predominant male occurrence is documented in the literature (205).

Simple cysts are usually oval or round with a smooth outline and are filled with clear or yellow fluid. They are acquired and thought to originate from the diverticula of the distal convoluted or collecting tubules. The proposed pathogenesis is that diverticula increase in number with age, probably as a result of weakening of tubular basement membranes. Enlargement of size and number of cortical cysts was found to increase with age from 5.1% in the fourth to 36.1% in the eighth decade of life (205). The average increase in size and the rate of enlargement were 2.82 mm and 6.3% yearly, respectively. An interesting observation by Terada et al. was that cysts in patients younger than 50 years grew more rapidly than in patients over 50 years. However, the results of this study may have been flawed by including patients with multilocular cysts, which reportedly progressed more rapidly than simple cysts.

Histopathologic features of a simple cortical cyst are typically of an empty space, often without lining surrounded by compressed, fibrotic interstitium (Fig. 4.45).

Acquired Cystic Kidney Disease

Acquired renal cysts by definition occur in the native kidneys of patients with ESRD treated for uremia with hemo- or peritoneal dialysis that did not have hereditary cystic kidney disease prior to dialysis. Diagnostic criteria require three or more cysts per kidney in a dialysis patient (206). The number of cysts increases with time on dialysis and is estimated that

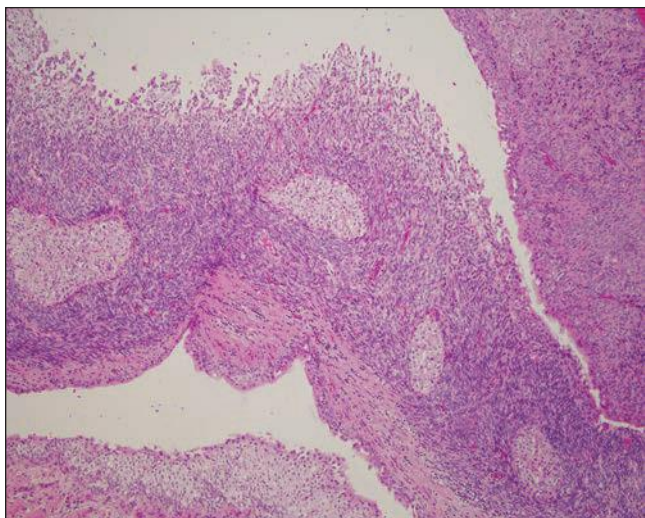


FIGURE 4.44 **Variant of MCN in a 55-year-old woman.** Cysts are lined by flat or low proliferative epithelium and an adjacent epithelial component (mixed renal epithelial and stromal tumor). (H&E $\times 200$)

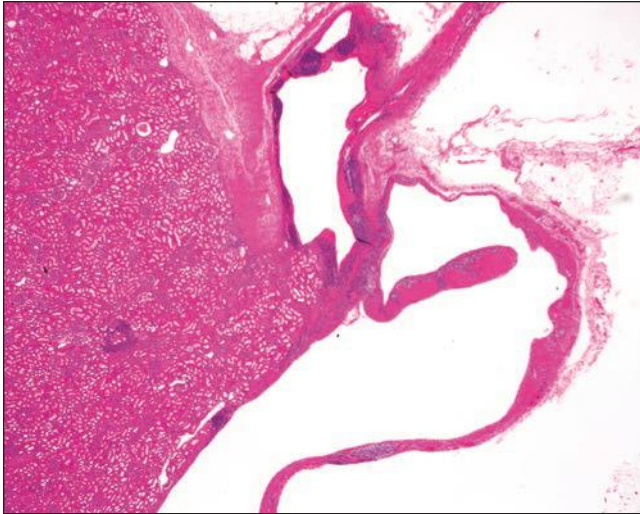


FIGURE 4.45 Simple cortical cyst devoid of epithelial lining located at the cortical surface. (H&E $\times 40$)

greater than 50% of patients develop cysts within 5 years of dialysis and about 90% by 10 years. Once again, men are more susceptible than women. Children on dialysis are not exempt from this risk: in one study, 25% acquired cysts over a period of 16 years (207).

Two to seven percent of patients with acquired renal cystic disease develop intracystic RCC (Fig. 4.46C). These tumors are often bilateral and may be metastatic at the time of diagnosis. The risk of developing RCC is estimated to be 40 to 100 times higher compared to the general population. Tumors tend to be more aggressive in younger men on dialysis. Periodic radiologic evaluation of all patients on dialysis is recommended to prevent fatal complications (208).

Pathology

Cysts often involve greater than 25% of the renal parenchyma, (Fig. 4.46A) but, in contrast to PKD, kidneys with acquired renal cystic disease tend to be either normal size or slightly smaller. The cysts often display fresh intracystic bleeding and are lined by cuboidal or hobnail epithelial cells arranged in single or multiple layers. Flat epithelium and micropapillary proliferation forming small adenomas (less than 5 mm in diameter) are frequent findings in the same specimen, suggesting a malignant predisposition of the lining epithelial cells. Papillary RCC is the most common type when overt intracystic malignancy develops (Fig. 4.46C). In addition, oxalate crystals are common within the cysts and/or in the interstitium and appear to be a distinct finding of dialysis-acquired cysts with carcinoma (Fig. 4.47) (209). It is proposed that oxalate deposits may promote malignancy or alternatively that the genetic changes that predispose to oxalate crystal formation also promote malignant transformation in acquired cystic epithelia. It is generally thought that pathogenesis of acquired renal cystic disease is a consequence of sustained uremia, but recognition of oxalate crystals as a hallmark of this disease brings a new insight that irrespective of its pathogenetic significance may be a helpful radiologic feature in the follow-up of dialysis patients at risk of developing aggressive tumors.

Miscellaneous Renal Cysts

Pyelocalyceal diverticuli, perinephric pseudocysts, and hygroma renalis are conditions that may present diagnostic difficulty on radiologic examination and sometimes clinically but rarely require the pathologist's attention and therefore are briefly discussed here.

Pyelocalyceal Diverticuli

These appear as circular or ovoid filling defects of the renal pelvis or the calyces on intravenous pyelogram (Fig. 4.48). They are more common in children and often solitary (210). They may be found incidentally during excretory urography or provoke severe acute flank pain and gross hematuria or urinary infection. Isolated pyelocalyceal diverticuli are rare in adults, if one excludes postoperative damage of the lining epithelium. Their presence in young children has prompted speculation that they represent ureteric bud branches that failed to induce nephrons and/or to be integrated into the normal tubulocalyceal system. An association with xanthogranulomatous pyelonephritis was reported (211). Current management of pyelocalyceal diverticuli has evolved from open surgery to a minimally invasive retroperitoneal laparoscopic ablation with good results. Histologically, the cavity is lined by flat epithelium surrounded by a thin layer of smooth muscle. Inflammation and squamous metaplasia or calcifications may be present.

Perinephric Pseudocysts

Perinephric pseudocysts represent urine accumulation within the perinephric fat. They consist of reactive variably inflamed fibrous tissue and fat without a lining epithelium. These lesions are usually localized and rarely cause kidney displacement in the retroperitoneal space. Blunt trauma to the kidney or a surgical procedure that caused damage to the renal capsule is the most frequent cause. Clinically, they may present with flank or abdominal pain or be discovered incidentally long after the event as localized calcified lesions in the perinephric fat.

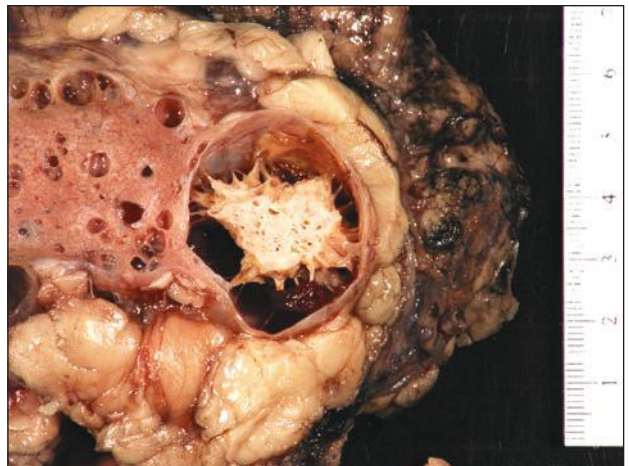
Hygroma Renalis

This condition consists of ectasia of the lymphatics in the renal capsule and is also known as pericalyceal lymphangiomatosis. It presents as a circumscribed cystic mass that consists of dilated lymphatics containing eosinophilic fluid, encircles the renal pelvis or extends to the renal capsule. The kidney may appear enlarged and diffusely cystic resembling cysts in polycystic kidneys. However, cysts consist of thin fibrous walls lined by endothelial cells. The disease affects men and women, children and adults, and can be bilateral or unilateral.

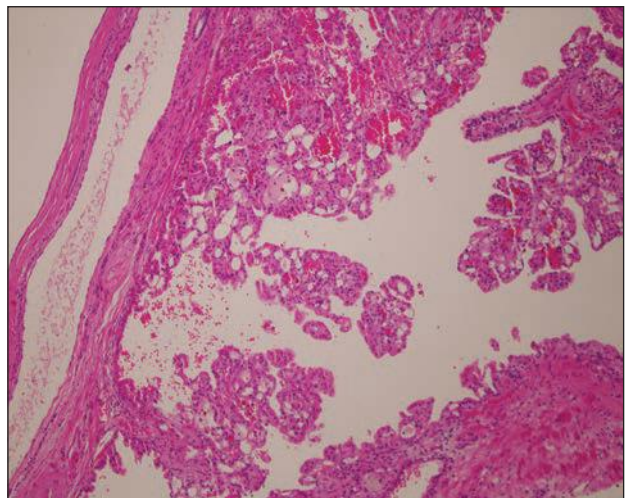
Pericalyceal lymphangiomatosis is primarily diagnosed in adults who may be asymptomatic or experience symptoms of urinary obstruction. The condition resembles cystic hygroma of the head and neck. In fact, there is an interesting case report of hygroma renalis affecting one sibling in a single family and hygroma of the face affecting her sister (212). Some familial cases are reported (213,214). The case shown in Figure 4.49 was from a young woman who presented with hematuria and flank pain. The MRI shows enlarged right kidney with indistinct miniscule cysts extending from the renal pelvis to the cortex. A biopsy was performed and showed thin wall cysts with flat lining consistent with endothelium. The case shown in Figure 4.50 is abdominal CT from a middle-age man who



A



B



C

FIGURE 4.46 Hemodialysis acquired cystic kidney disease. **A:** Abdominal CT shows bilateral cystic kidneys. **B:** RCC is present in one of the cysts. **C:** The tumor is papillary clear cell carcinoma (H&E $\times 200$).

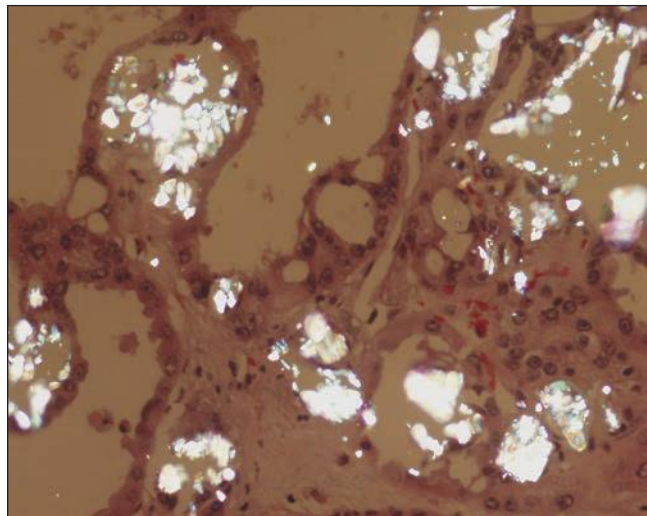


FIGURE 4.47 Oxalate deposits in acquired cystic kidney RCC. (Courtesy Dr. Luan Truong, Baylor College of Medicine, Texas.) ($\times 40$.)



FIGURE 4.48 Calyceal diverticulum. IVU tomogram shows a collection of contrast material above the upper pole calyces.

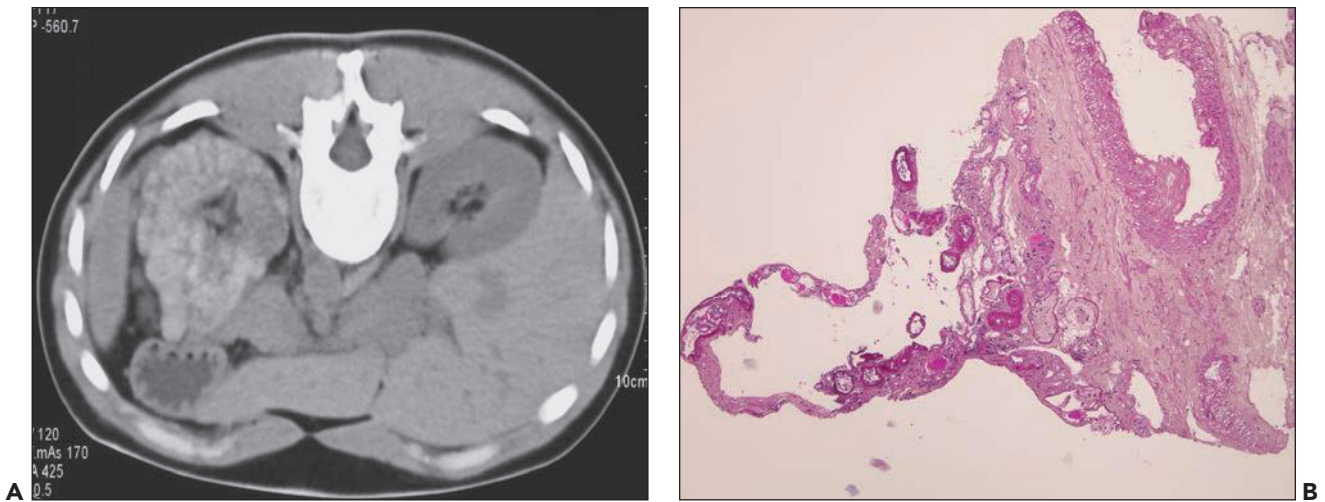


FIGURE 4.49 Renal lymphangiectasia. **A:** Abdominal CT shows an enlarged right kidney with innumerable, minute cysts; contralateral kidney is normal. The patient was a 35-year-old woman who presented with hematuria. **B:** Histologically, cysts have thin wall and flat lining.

was thought to have PKD because of bilaterally enlarged cystic kidneys. Arrows indicate perirenal and peripelvic fluid accumulation but no cysts.

DEVELOPMENTAL KIDNEY DEFECTS

Developmental kidney defects are a major subset of congenital anomalies of the kidney and urinary tract (CAKUT spectrum), which can affect up to 1 in 20 births although the majority are not severe (215). Kidney anomalies within

CAKUT include aplasia, hypoplasia, adysplasia, dysplasia with and without cysts, and multicystic dysplasia (Table 4.6). Other parts of the spectrum encompass ureteric anomalies such as megaureter, ureteropelvic junction (UPJ) obstruction, ureterovesical junction (UVJ) obstruction or incompetence, duplex kidneys/ureters, and anomalies of the bladder and urethra (216). Approximately half of the CAKUT cases associated with end-stage renal failure in children have patent urinary tracts, whereas the rest have obstructive nephropathy; the latter are mainly boys with bladder outflow obstruction (BOO) and posterior urethral valves (217). Some renal functional impairment may be superimposed postnatally from bacterial pyelonephritis and/or persistent urinary flow impairment causing renal atrophy and fibrosis, but the primary “hit” in CAKUT is clearly a developmental one. UPJ, UVJ, and related anomalies are discussed in Chapter 24. This part of the chapter focuses mainly on developmental anomalies of the kidney proper. There is no accepted classification scheme for these anomalies, many of which are now linked to specific gene mutations (Table 4.7).

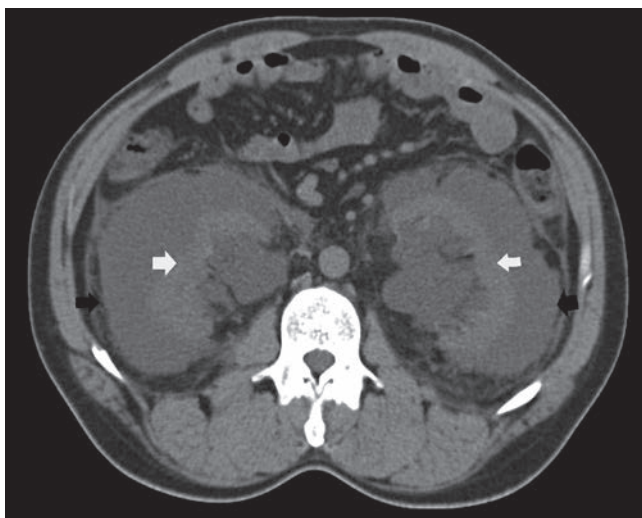


FIGURE 4.50 Bilateral lymphangiectasia mimicking PKD. Abdominal CT shows bilateral ectatic perirenal (*black arrows*) and peripelvic (*white arrows*) fluid accumulation in lymphatics. The patient was a 47-year-old man with hematuria.

TABLE 4.6 Developmental kidney defects

- A. Renal agenesis/aplasia
- B. Adysplasia
- C. Renal dysplasia
- D. Renal hypoplasia
 - Oligomeganephronia
 - Simple hypoplasia
- E. Renal ectopia/malrotation
- F. Renal fusion
- G. Renal duplication
- H. Supernumerary kidney
- I. Tubular dysgenesis

TABLE 4.7 Genetic renal and urinary tract malformation syndromes

Alagille syndrome (predominantly *JAG1* mutation—ligand for Notch signaling pathway; occasionally *NOTCH2* mutation where renal anomalies are more common): dysplastic or multicystic kidneys, vesicoureteric reflux; cholestasis, cardiac disease, skeletal abnormalities, ocular abnormalities, and characteristic facial phenotype

Apert syndrome (*FGFR2* mutation—growth factor receptor): hydronephrosis and duplicated renal pelvis with premature fusion of cranial sutures and digital anomalies, particularly syndactyly

Bardet-Biedl syndrome (BBS1-16 mutations—mostly involved in cilia or basal body assembly or function): renal dysplasia and calyceal malformations with retinopathy, digit anomalies, obesity, diabetes mellitus, and male hypogonadism

Beckwith-Wiedemann syndrome (*p57KIP2 (CDKN1C)* mutation in a small minority of patients—cell cycle gene; 50% due to methylation defects affecting a region on chromosome 11 containing *CDKN1C* plus *H19*, *IGF2*, and *KCNQ10T1* genes): large kidneys, cysts, and dysplasia; predilection to Wilms tumor; widespread somatic overgrowth

Branchiootorenal syndrome (*EYA1*, *SIX1*, and *SIX5* mutations—transcription factors): renal agenesis and dysplasia with deafness and branchial arch defects such as cysts and fistulae in the neck (branchial arch region)

Campomelic dysplasia (*SOX9* mutation—transcription factor): diverse renal and skeletal malformations

Carnitine palmitoyltransferase II deficiency (*CPT2* mutation in the enzyme): renal dysplasia, structural brain abnormalities

CHARGE association (*CHD7* mutation—chromodomain helicase DNA-binding protein; rarely *SEMA3E* mutation): diverse urinary tract malformations; coloboma, heart malformation, choanal atresia, retardation, genital and ear anomalies

Denys-Drash, Frasier, and WAGR syndromes (*WT1* mutations—transcription/splicing factor; can be contiguous gene defect with *PAX6* in WAGR): renal malformations, mesangial cell sclerosis, and calyceal defects; Wilms tumor, aniridia, and streak gonads

Di George syndrome (microdeletion at 22q11 with the loss of function of several genes including *TBX1* and/or *COMT* and perhaps others): renal agenesis, dysplasia, vesicoureteric reflux, with heart and branchial arch defects

Fanconi anemia (at least 15 mutant genes reported—involved in DNA repair pathway): renal agenesis, ectopic/horseshoe kidney, anemia, and limb malformations

Fraser syndrome (*FRAS1* or *FREM2* mutations—cell adhesion): renal agenesis and dysplasia, digit and ocular malformations

Glutaric acidemia type II (*ETF A*, *ETFB*, or *ETFDH* mutations—enzymes involved in flavoprotein metabolism): cystic and dysplastic disease; brain malformations; enlarged liver; dilated cardiomyopathy; metabolic crisis

Hypoparathyroidism, deafness, and renal anomalies (HDR or Barakat) syndrome (*GATA3* mutation—zinc finger transcription factor): renal agenesis, dysplasia, and vesicoureteric reflux; hypoparathyroidism; sensorineural deafness

Kallmann syndrome (X-linked form—*KAL1* mutation—cell adhesion molecule; autosomal form—*FGFR1* mutation—growth factor receptor): renal agenesis and dysplasia in X-linked form

Mayer-Rokitansky-Küster-Hauser syndrome (*WNT4* mutation—growth factor signaling pathway): renal agenesis, ectopic kidneys, and absence of müllerian-derived structures in females

Meckel syndrome (mutation in at least eight genes including *B9D1*, *B9D2*, *CC2D2A*, *CEP290*, *MKS1*, *RPGRIP1L*, *TMEM216*, and *TMEM67*): cystic renal dysplasia; occipital encephalocele; polydactyly; liver fibrosis

Nail-patella syndrome (*LMX1B* mutation—transcription factor): renal agenesis, malformation of the glomerulus; abnormalities of the nails, knees, elbows, and pelvis; glaucoma

Okihiro (Duane-radial ray) syndrome (*SALL4* mutation—transcription factor): ectopic kidneys and lower urinary tract malformation; malformed finger-like or absent thumbs and partial or complete absence of bones in the forearm

Oral facial digital syndrome type 1 (*OFD1* mutation—centrosomal protein): glomerular cysts with facial and digital anomalies

Pallister-Hall syndrome (*GLI3* mutation—transcription factor): renal agenesis and dysplasia; polydactyly; and/or syndactyly

Posterior urethral valves (PUV; loci and genes unknown): nonsyndromic cases in siblings and male relatives (full phenotype not possible because of urethral differences in females)

Prune belly (Eagle-Barrett) syndrome (*CHRM3* mutation—muscarinic cholinergic receptor): functional bladder outlet obstruction/prune belly syndrome

Renal coloboma syndrome (*PAX2* mutation—paired box-containing transcription factor): renal hypoplasia; vesicoureteric reflux with coloboma

RCAD syndrome (*TCF2/HNF1B* mutation—transcription factor): renal dysplasia, cysts and hypoplasia; urogenital abnormalities; MODY; gout

Simpson-Golabi-Behmel syndrome (*GPC3* mutation—glypican-3 proteoglycan): renal overgrowth, cysts, and dysplasia

Smith-Lemli-Opitz syndrome (*DHCR7* (7-dehydrocholesterol reductase)—cholesterol biosynthesis): renal cysts and dysplasia; microcephaly, malformations of the heart, lungs, gut, and genitalia

Townes-Brocks syndrome (*SALL1* mutation—transcription factor): renal dysplasia and lower urinary tract malformations; imperforate anus, ear and hand malformations (usually affecting the thumb)

Urofacial (Ochoa) syndrome (*HPSE2* mutations—heparanase 2): urine flow impairment linked to hydronephrosis, vesicoureteric reflux, bladder emptying difficulty; abnormal facial expression

Ulnar-mammary syndrome (*TBX3* mutation—T-box contacting transcription factor): renal dysplasia; ulnar ray defects, obesity, hypoplasia of the nipples, and uterine anomalies

von Hippel-Lindau disease (*VHL* mutation—tumor suppressor gene): renal and pancreatic cysts, renal tumors

Vesicoureteric reflux (rarely *ROBO2* or *SOX17* mutation but genetically heterogeneous): nonsyndromic familial cases with no secondary cause (e.g., urinary flow impairment) are recognized

Zellweger spectrum (at least 12 *PEX* gene family mutations—peroxisomal proteins): cystic dysplastic kidneys; hypotonia, hearing and visual loss, and seizures

Cell and Molecular Biology

In the last 20 years, there have been major advances in the understanding of cellular and molecular pathogenesis of CAKUT, with new genes being reported frequently to clarify developmental pathways. In order to interpret these, it is a prerequisite to understand the processes involved in normal nephrogenesis. This is described fully in Chapter 2, but a brief overview is given here. Kidney formation involves a balance between basic cellular and tissue processes such as proliferation, death, differentiation, and morphogenesis, all normally controlled by regulated gene expression but easily disrupted as we discussed later. Cell proliferation predominates as the kidney develops from less than a thousand cells at its inception to many millions in the mature organ. After the initial stages, proliferation is mainly confined to the periphery of the kidney, particularly the narrow rim of outer cortex containing actively branching ureteric bud tips and adjacent condensing mesenchyme (218). Fine tuning of cell numbers occurs by apoptosis, with at least 50% of the cells produced in the developing kidney eventually deleted by this programmed cell death (218,219). Apoptosis occurs in different sites, primarily in early nephron precursors such as comma and S-shaped bodies and the medulla, locations in which cell death may be important for morphogenesis and collecting duct remodeling. Several levels of differentiation occur during normal nephrogenesis ranging from early mesenchymal-epithelial differentiation to form renal vesicles through to terminal differentiation where different cells in the same nephron segments acquire different functions (e.g., α - and β -intercalated and principal cells in the collecting ducts). Morphogenesis is the process whereby groups of cells acquire complex three-dimensional shapes. This is clearly important in the kidney where there is such an intimate relationship between different nephron and collecting duct segments and the renal vasculature, but little is known about controlling factors.

Direct perturbation of expression of important nephrogenic genes secondary to mutations is an important cause of CAKUT in man, and many renal malformations can be replicated to examine the pathogenesis more fully by transgenic technology in mice. Similar disrupted expression may also occur as a chance (stochastic) event and can be generated by extrinsic, nongenetic factors, such as teratogens or maternal diet, and physical or functional obstruction of the developing urinary tract. To make the situation even more complex, all of these mechanisms can overlap to generate compound effects. Genetic factors might generate urinary flow impairment, for example, with secondary effects in the kidney, or there may be altered gene activity in both upper and lower urinary tract. The latter gives rise to a “field effect” and has been postulated for genes such as the BMP4 and AT2/angiotensin pathways that have widespread expression in the developing kidney and urinary tract (220,221). Similarly, in the renal cysts and diabetes (RCAD) syndrome, there are genetic defects in HNF-1 β , which is expressed in nephrogenesis, and there is a predisposition to diabetes, with consequent poorly regulated blood sugars during pregnancy, if the mother is a carrier. Similarly, although around half of the CAKUT cases associated with childhood chronic kidney disease (CKD) stage V in children have patent urinary tracts, the remainder have a lower urinary tract flow problem such as BOO with posterior urethral valves (222).

Some renal functional impairment may be superimposed postnatally from bacterial pyelonephritis and/or persistent urinary flow impairment causing renal atrophy and fibrosis. However, the primary “hit” in CAKUT is clearly a developmental one.

The proposed pathogenesis of dysplastic kidneys is represented schematically in Figure 4.51, with a central mechanism being disruption of mutual induction between ureteric bud and mesenchymal lineages in many cases. This leads to abnormal collecting duct development/branching and loss of potential functioning nephrons, plus formation of aberrant structures such as cysts and metaplastic cartilage and stromal expansion, with the net effect being a major nephron deficit. Parts of this pathogenic process may also apply to other renal malformations and to adult diseases where existing nephrons may be lost, and there is expansion of the stromal compartment.

Genes Controlling Nephrogenesis

Outgrowth of the ureteric bud into a specific area of the metanephric mesenchyme is a one-off event that must occur at the right time and place for normal development. The kidney may not form without it, or the whole pattern of nephrogenesis can be disrupted. Many later events are reiterated multiple times; however, so there is still scope for defects in these processes to cause maldevelopment, but these are more likely to affect nephron number rather than disrupt kidney development completely. These are processes such as mutual ureteric bud-mesenchyme induction, repeated branching of the bud ampullae with condensation of the mesenchyme followed by mesenchymal-epithelial transition, and differentiation of specialized nephron segments.

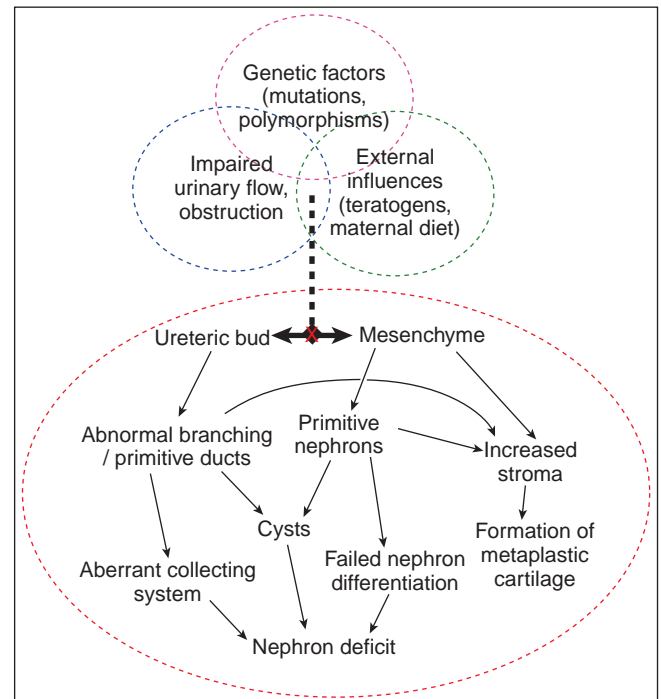


FIGURE 4.51 Proposed mechanisms of developmental kidney disease.

Twenty years ago, the molecular controls of each of these steps were virtually unknown, but we are now beginning to understand some of them, although often the understanding is better in mice and other animals than in humans because there are better experimental models. It is assumed that the same factors are important across mammalian species in the following descriptions, but this is not always the case; for example, the X-linked Kallmann syndrome has a high frequency of renal dysplasia/agenesis, and it is caused by mutations in *KALI*, but there is no mouse ortholog of this factor (223,224). Also, even when nearly all of the genes expressed in a developing structure are known, this does not mean that a genetic explanation can always be found for developmental defects involving that pathway (225).

THE GDNF/RET SYSTEM

Initiation and growth of the ureteric bud involves a fine balance between positive inducers/stimulating signals and negative repressor molecules (226,227). The GDNF/Ret pathway is one of the most important positive initiators. Genes such as *Spry1*, *Slit2/Robo*, and semaphorins act as negative regulators, and many of these effects occur by modulating GDNF/Ret.

GDNF is secreted by the mesenchyme adjacent to the Wolffian duct at the site of the presumptive ureteric bud and binds to the Ret receptor tyrosine kinase in the duct in association with an adapter molecule, GDNF receptor α (*GFR α*) (228,229). Genetic ablation of any of these factors causes either complete failure of metanephric development or severe dysplasia (230–232). Ret and *GFR α* are expressed along the entire nephric/mesonephric duct, in the ureteric bud, which arises from it, and also in branching bud tips in the metanephros. GDNF, on the other hand, is initially restricted to the mesenchyme in the vicinity of the nascent ureteric bud and is then expressed in the condensing renal mesenchyme adjacent to actively branching bud tips in the metanephros (233). GDNF expression is under the control of a cascade of transcription factors including the *PAX2*, *EYA1*, and several *Six* and *Sall* genes (226,234–236). Ret expression requires vitamin A (237), but there are fewer other known regulatory factors than GDNF. There is strong evidence for at least two functions of the GDNF/Ret signaling system in nephrogenesis: (a) initiation of ureteric outgrowth from the mesonephric duct and (b) promoting branching of the ureteric tree in the metanephros. Several teams have demonstrated that excess GDNF stimulates ectopic ureteric bud formation in vitro (238,239), and *Foxc1* mutant mice have anterior expansion of the GDNF mesenchymal expression domain leading to a greater incidence of duplex ureters (240). *Slit2/Robo* signaling, another pathway identified in neural development, appears to normally restrict GDNF expression to the more posterior nephrogenic mesenchyme (241).

GDNF has equally potent effects within later metanephric development: excess growth factor increases ureteric bud branching in organ culture and stimulates branching morphogenesis of a ureteric bud-derived cell line (242), while, conversely, GDNF neutralizing antibodies inhibit branching morphogenesis, and heterozygous GDNF mutant mice have decreased ureteric bud branches (229). GDNF may also promote ureteric bud survival, since it prevents experimental apoptosis of ureteric bud cultured as a monolayer. *SOX* genes, such as *Sox8* and *Sox9*, act downstream of RET signaling in the ureteric bud tips and ablation of these causes severe

malformation of the collecting duct tree (243). *Wnt11* expression in the bud is also strongly linked to GDNF/Ret function in the developing metanephros, and it has been postulated that there is an autoregulatory feedback loop involving these factors that coordinates ureteric branching (174).

Several factors restrict ureteric bud outgrowth, mostly by effects on GDNF/RET signaling. *SLIT2* and its receptor *ROBO2* are important for axon guidance and cell migration within the developing nervous system, but they also regulate GDNF expression at initiation of ureteric bud outgrowth: mice lacking these factors have a wider swathe of GDNF expression that extends anteriorly, and this allows extra buds to grow forward from the Wolffian duct (241). Moreover, mutations in *ROBO2* have been linked to vesicoureteric reflux in humans, which may reflect aberrant origin or development of the lower ureter (244,245). *Spry1* null mutant mice also have supernumary ureteric buds (246), and this has again been linked to dysregulation (i.e., expansion) of the normally restricted GDNF/Ret signaling domain. *Spry1* also appears to restrict later branching of the ureteric bud lineage, being negatively regulated by angiotensin II via the angiotensin II type 1 receptor, although this also promotes some aspects of development by stimulating *PAX2* via the angiotensin II type 2 receptor (227). *Semaphorin3a* is another factor that down-regulates both GDNF signaling (and hence ureteric branching) and growth of the vascular tree, while the related *Semaphorin3c* promotes branching of these systems (247).

Other systems involved in both ureteric bud outgrowth and ureter formation include fibroblast growth factors (FGFs) and their receptors (248,249). *Fras1* is mutated in Fraser syndrome (250) and linked to *Sprouty* (251), *ETV4* and *5* (252), the bone morphogenetic protein (BMP)/*Gremlin* system (253) and *Teashirt* genes (254).

PAX GENES

The *PAX* family of transcription factors control diverse aspects of embryonic patterning and cell specification in organisms from *Drosophila*, through zebrafish to human (255), but only *PAX2*, *3*, and *8* are expressed in the developing kidney. *PAX2* is expressed in intermediate mesoderm, the nephric duct, then the mesonephric duct, and finally in the tips of the ureteric bud and the condensing mesenchyme in the metanephros, and it has critical roles during mesenchymal condensation and epithelial transformation since perturbed expression causes renal malformations (218,234). *Pax2* expression correlates with the sites of rapid cell division in the ureteric bud tips and condensing mesenchyme, and lack of *pax2* is associated with increased apoptosis (218,256,257). *PAX2* mutations occur in the human “renal-coloboma” syndrome, which consists of optic nerve colobomas, renal anomalies, and vesicoureteral reflux (258). Mice with decreased levels of *Pax2* have aberrant kidney development. Heterozygous mutations cause hypoplastic kidneys with reduced branching of the ureteric bud and reduced numbers of nephrons and cortical thinning, while homozygous null mutants lack mesonephric tubules and the metanephroi fail to form because the ureteric buds are absent (259). Overexpression of *pax2* also causes murine kidney abnormalities, including cystic tubular changes, proteinuria, and renal failure (260).

Control of *PAX2* expression is poorly understood, but *Yin Yang 1*, another transcription factor, binds to part of the

Pax2 promoter leading to increased expression (261), and the vascular endothelial growth factor (VEGF) receptor Flk1 up-regulates Pax2 in the metanephric mesenchyme (262). The Wilms tumor gene WT1, on the other hand, down-regulates PAX2 in a negative feedback loop since PAX2 binds to two sites in the WT1 promoter sequence and causes up to a 35-fold increase in expression, as assessed using reporter genes (263,264). PAX2 also modulates GDNF signaling (238), again demonstrating the complex interactions of many of the key factors in nephrogenesis.

PAX8 is expressed in the developing mesonephric tubules and then in the condensing mesenchyme of the murine metanephros (265) and is down-regulated in maturing nephron epithelia (266). Its roles in nephrogenesis are uncertain, since null mutants have thyroid rather than kidney defects (267). PAX8 may be important as a cofactor in very early kidney development; however, because the mesenchymal-epithelial transformation required for nephric duct formation does not occur in double PAX8/PAX2 mutants (268). Pax3 expression is in the metanephric mesenchyme and stroma, and it is up-regulated in some Wilms tumors, again suggesting a PAX-WT1-negative regulatory loop (269).

WT1

The WT1 gene was first discovered in Wilms tumors but is only mutated in about 15% with several other factors involved in a greater proportion including WTX, CTNNB1, and IGF2 (270). WT1 encodes a transcription factor protein containing four zinc-finger DNA-binding motifs that is expressed in the mesonephric glomeruli and at low levels in the condensing metanephric mesenchyme. As the metanephric comma and S-shaped bodies develop, WT1 levels increase but become restricted to the visceral glomerular epithelia, with podocytes remaining strongly positive in the mature kidney (218). Complete lack of WT1 causes death in utero because of defects in mesothelial-derived components where WT1 is normally expressed, including the heart and lungs (271). Renal development is also severely disrupted: small numbers of normal-appearing mesonephric tubules form, but the ureteric bud fails to branch from the Wolffian duct and the intermediate mesoderm, which should form the metanephric blastema, dies by apoptosis. Several human syndromes are associated with WT1 mutations. Denys-Drash syndrome consists of genitourinary abnormalities, including ambiguous genitalia in 46 XY males, nephrotic syndrome with mesangial sclerosis leading to renal failure, and a predisposition to Wilms tumor (272). This is caused by point mutations of WT1, predominantly affecting the zinc finger DNA-binding domains. WAGR syndrome consists of Wilms tumor, aniridia, genitourinary abnormalities including gonadoblastoma, and mental retardation. Frasier syndrome is characterized by focal glomerular sclerosis with progressive renal failure and gonadal dysgenesis. This is caused by intronic point mutations of WT1 that affect the balance between different WT1 splice isoforms (273).

WT1 has multiple isoforms generated by alternative splicing, RNA editing, and alternative translation initiation sites (274). Functions as a transcription factor are mainly mediated via the isoform lacking the amino acids lysine, threonine, and serine between zinc fingers 3 and 4, which is known as the KTS form. PAX2 is a major downstream repression target, but other classical nephrogenic molecules include Wnt/ β -catenin,

IGFs, Spry1, Sall1, and Bmps (275–277). Several novel potential targets have also been identified in mice using chromatin immunoprecipitation coupled to promoter microarray, including Cxnc5, Lsp1, Pbx2, Plexdc2, Rps6ka3 (Rsk2), Scx, and Sox11 (278).

WNT GENES

The WNT gene family consists of over 20 members, and many are expressed in normal nephrogenesis where they have key roles in both mesenchymal and epithelial lineages (279,280). Wnt signaling occurs via canonical or noncanonical pathways, but signaling is typically initiated by interaction of different Wnt ligands with specific Frizzled (Fz) receptors, followed by recruitment of the intracellular protein, disheveled (Dvl), and activation of specific coreceptors (166). Canonical Wnt signaling results in activation of β -catenin-mediated transcription, but this is not involved in the Wnt/ Ca^{2+} or Wnt/planar cell polarity (PCP) noncanonical pathways.

WNT4 is up-regulated during mesenchymal-epithelial differentiation, stimulated by PAX2 (281), and mice lacking wnt4 do not progress beyond the condensate stage (282). Wnt4 alone is sufficient to induce tubulogenesis in the isolated metanephric mesenchyme (283). A loss-of-function WNT4 mutation has been described in Mayer-Rokitansky-Küster-Hauser syndrome, which comprises defects in müllerian-derived structures and renal agenesis (284). Wnt11 is expressed at the tips of the ureteric bud (285) but is not sufficient to induce tubulogenesis (283). Wnt11 mutations disrupt ureteric branching morphogenesis, which leads to kidney hypoplasia, perhaps by disrupting Wnt11/GDNF/Ret feedback (174). These effects are likely to result from disruption of canonical signaling since Dickkopf-1, a canonical inhibitor, disrupts ureteric bud branching in a similar pattern (286). The Townes-Brocks syndrome (ear, limb, heart, and renal anomalies) results from mutations in SALL1, which is known to activate canonical Wnt signaling and regulate ureteric bud tip differentiation (235,287). Wnt9b is also expressed by the ureteric bud, but there are data for both canonical and planar cell polarity signaling for this factor (175,288) and for the latter pathways in both ureteric branching morphogenesis and glomerular maturation (289). One effect of Wnt9b is to stimulate wnt4 expression in the mesenchyme, leading to mesenchymal-epithelial transformation. Both wnts can be replaced by activating the Notch pathway, which is normally involved in specifying proximal epithelial fate during later nephron differentiation (and differentiation of principal cells in collecting ducts) (290,291).

BMPs

BMPs are a large subgroup within the TGF β family, and they are often expressed alongside wnts in kidney development (292,293). Several functions have been ascribed to BMPs including (a) control of ureteric bud outgrowth and elongation, (b) prevention of apoptosis in the metanephric mesenchyme, and (c) promotion of smooth muscle development in the ureters (221,253,294,295). BMP2 is expressed in the condensing mesenchyme, and null mutants die early in development. Excess BMP2 inhibits metanephric growth and ureteric branching in vitro (296). BMP4 is initially expressed in stromal cells surrounding the mesonephric duct, including at the site of ureteric bud outgrowth and then in the mesenchyme around the stalk of the ureteric bud. BMP4 knockout mice

also die early, but heterozygotes survive with hypoplastic or dysplastic kidneys. BMP7 is more widely expressed in the kidney, encompassing the ureteric bud, loose and condensed mesenchyme, and primitive nephrons (297). BMP7 null mutants survive until birth but then die from renal failure as a result of defective mesenchymal differentiation and increased apoptosis leading to a severe nephron deficit (298,299). BMP7 is involved in initial ureteric bud outgrowth (253) and may then have concentration-dependent roles because, at least in vitro, low levels increase ureteric bud branching, whereas higher doses inhibit it (300).

BMPs signal via the BMP type 1 (BMPRIA, BMPRIB) and type 2 (BMPRII) receptors. In vitro studies have identified roles of BMP2 and BMPRIA (also known as activin-like kinase 3, ALK3) in inhibiting branching morphogenesis, with downstream signaling via cytoplasmic SMAD1 (300). Moreover, transgenic mice expressing constitutively active BMPRIA in the ureteric bud develop medullary cystic dysplasia with increased β -catenin/SMAD1 complexes (301), and this receptor has recently been reported to be important in kidney regeneration and fibrosis (302). BMP signaling is modulated by antagonists such as gremlin (Grem1): null mutants have renal agenesis caused by defective ureteric bud outgrowth/branching, a failure to establish GDNF/WNT11 feedback signaling and apoptotic death of the metanephric mesenchyme (294). Another BMP antagonist, Cerberus homologue (Cer1), has recently been implicated in fine tuning the spatial organization of the ureteric tree, again by affecting GDNF and WNT11 (303).

FORKHEAD/WINGED HELIX TRANSCRIPTION FACTORS

The conserved forkhead/winged helix transcription factor gene family has several members implicated in kidney and urinary tract development. Mutations in the *Foxc1* gene are responsible for the classical congenital hydrocephalus mouse, and homozygous mutants have markedly abnormal early nephrogenesis with ectopic mesonephric tubules and anterior ureteric buds, often leading to duplex kidneys and ureters (240). *Foxc1* also appears to interact with *Foxc2* during renal (and heart) development since most *Foxc1/Foxc2* compound heterozygotes have hypoplastic kidneys and a single hydroureter, while all heterozygotes are normal.

Foxd1, previously known as BF2, is one of the few genes known to be implicated in interstitial differentiation. *Foxd1* is expressed in the cells immediately surrounding condensed mesenchyme cells that express *Pax2*, and mice with null mutations have rudimentary, fused kidneys and die soon after birth (304). Interestingly, the mesenchyme condenses in the null mutant mice but does not develop any further and neither comma nor S-shaped bodies are formed. The ureteric bud also fails to branch normally, and *ret* is widely distributed in the bud epithelium, rather than confined to the bud tips. *Foxd1* is also expressed in the renal capsule, and deletion from this sites leads to loss of early patterning and an aberrant ureteric tree (305).

HEPATOCYTE NUCLEAR FACTOR 1 β

Mutations of the *TCF2* gene, encoding the transcription factor HNF1 β , cause the RCAD syndrome and are a major cause of human congenital kidney malformations (306). HNF1 β is expressed in the mesonephric duct, ureteric bud lineage

and early nephron epithelia, and adjacent paramesonephric ducts, which should differentiate into the uterus and fallopian tubes (307). Renal malformations in RCAD are highly variable, ranging from grossly cystic dysplastic kidneys, through hypoplasia with oligomeganephronia to apparent unilateral agenesis and, in females, is accompanied by similarly diverse uterine abnormalities. Absence of HNF1 β expression at the very tips of the branching ureteric tree has led to speculation that it is a "maturation factor" rather than a "branching factor," but investigation of this potential role has been difficult since null mutants die in early embryogenesis (308). More subtle abnormalities do occur with *TCF2* mutations and experimentally perturbed function including defects in primary cilia and renal magnesium handling (306,309). Potential factors regulated by HNF1 β include DCoH, E4F1, and ZFP36L1 (310), and a recent study suggests a link between TGF- β , HNF1 β , and microRNA-192 (miR-192) (311) as well as a direct link to *PKD2*, which may provide further explanation for the cystic phenotype (312).

FURTHER IMPORTANT GENES

There is insufficient space to discuss all of the known nephrogenesis factors in as much detail as those above, but the brief synopsis of several further important groups/factors follows.

Osr1 (Odd skipped related1; otherwise termed *Odd1*) is expressed in early intermediate mesoderm and necessary for metanephric kidney development, with highest expression in the cap mesenchyme (313). *Osr1*-positive cells contribute to most nephron segments and direct cells toward kidney rather than a vascular phenotype (314). *Osr1* is necessary for correct expression of *GDNF*, *PAX2*, *Six2*, *Sall1*, and *Eya1* (313).

Cited1 is a transcriptional cofactor important in early nephron patterning that is expressed in self-renewing epithelial progenitor cells in the cap mesenchyme (315). FGF and EGF signaling systems are crucial to maintain these progenitors (316).

Six genes. *Six1* forms a developmental pathway comprising *Six1:Eya1:Pax2* important for up-regulating *GDNF* and also mediates ureteral smooth muscle formation (317). *Six2* expression maintains a proportion of undifferentiated progenitors in the renal mesenchyme so that there are self-renewing progenitors throughout nephrogenesis (318).

EYA1 is the mammalian homologue of the *Drosophila* transcriptional coactivator "eyes absent" gene, and *EYA1* mutations occur in a quarter of branchiootorenal syndrome patients (319), while others may have *Six1* mutations disrupting the *Six1:Eya1:Pax2* pathway (320). Homozygous *eya1* null mutant mice die at birth with multiple abnormalities including renal agenesis because of defective ureteric bud outgrowth and subsequent metanephric induction (321).

FGFs have multiple roles throughout nephrogenesis. They bind the receptor tyrosine kinases, *FGFR1* and 2, activating Ras-GTPase and ERK and promoting cell proliferation (322). FGF 2 is expressed in the renal mesenchyme and protects it from apoptosis (323,324), while FGF7 and 10 signaling is important in ureteric bud branching (322). Perturbed FGF8 expression disrupts nephron epithelialization, and deletions of this or *FGFR1* account for a small proportion of Kallmann syndrome (223).

Hox genes encode homeodomain transcription factors that specify positional information along the anterior-posterior

axis. *Hoxb7* is expressed throughout the ureteric bud, and *Hoxb7*-GFP mice are an elegant way to investigate branching morphogenesis (325). *Hoxa11* and *Hoxd11* combined mutants have renal agenesis, while single mutants do not, which may be explained by several *Hox11* analogous proteins forming a complex with *Pax2* and *Eya1* to directly activate expression of *Six2* and *Gdnf* in the metanephric mesenchyme (326). Recent data have implicated *Hox10* genes in a similar patterning role (327).

Kidney development requires supporting matrix, glycosaminoglycans, and adhesion molecules, and aberrant expression of these can perturb nephrogenesis. Glypican-3 mutations occur in Simpson-Golabi-Behmel syndrome (328), and heparan sulfate has a regulatory role in ureteric patterning via modulation of FGF signaling (329).

Nongenetic Causes of Renal Malformations

Renal malformations are associated with urinary tract obstruction. Isolated renal dysplasia is the most important single cause of CKD V in early childhood, but the second commonest diagnosis is dysplasia secondary to urinary tract obstruction such as posterior urethral valves (222). Other associations include urethral atresia, obstructive lesions at the pelviureteric and ureterovesical junctions, and the latter category including obstructive megaureters and ureterocoeles (330). Moreover, multicystic dysplastic kidneys are classically reported to be connected to “atretic” (i.e., nonpatent ureters), and obstruction has been invoked in the early etiopathogenesis of the prune belly syndrome, a condition in boys with urinary tract dilatation and dysplasia plus cryptorchidism and incomplete development of the abdominal wall muscles.

Experimental renal malformations can be generated by obstruction of the developing urinary tract. Over 40 years ago, Beck demonstrated that surgical obstruction of fetal sheep kidneys perturbed nephrogenesis and generated many features of dysplasia (331), and this has been reiterated in many subsequent studies (332–334). It is intriguing that common patterns of dysregulation of proliferation/apoptosis plus up-regulation of key nephrogenic molecules such as *PAX2* and *TGF- β 1* occur in these models and both sporadic and obstructed human cases since this implies a common sequence of maldevelopment, irrespective of the underlying cause (334,335). There are several other obstruction models too. Opossum metanephroi have been experimentally obstructed in neonates in the marsupial pouch to generate broadly similar changes to the ovine studies (74), but these experiments also allowed therapeutic intervention: administration of IGF, for example, ameliorates renal fibrosis, tubular cystic changes, and calyceal dilation that follow obstruction (336). The problem with Sheep and opossums is the lack of readily available molecular reagents to modulate gene expression; hence, a major advance in the last 10 years has been development of rodent obstruction models. Chevalier et al. have extensively investigated ureteric obstruction in neonatal rats where nephrogenesis continues for 2 weeks after birth; once again obstructive nephropathy is attenuated by EGF or IGF (220,337,338). Animal models have also been used to assess whether decompression of the developing urinary tract can improve renal outcome. In the sheep, Glick et al. (339) found that in utero decompression prevents renal dysplasia, but this conflicts with Chevalier's reports in neonatal rats where relief of obstruction attenuated but did not reverse

renal injury resulting from 5 days ureteric obstruction (340). These data are consistent with the generally poor results for in utero intervention to relieve obstruction in humans where shunting may improve perinatal survival but does not significantly improve the poor renal function (341). The assumption is that the kidneys may be too far along the path of maldevelopment before the intervention.

Teratogens and Altered Maternal Diet May Contribute to Renal Malformations

Diverse drugs and chemicals can be teratogenic to the developing kidney (342,343). They can be divided into two broad categories: exogenous factors such as drugs and endogenous factors that become teratogenic when present in excess. A classic example occurs with the renin-angiotensin system, which is targeted by angiotensin-converting enzyme inhibitors and receptor blockers to treat hypertension. If used during pregnancy, these can cause skull malformations, termed hypocalvaria plus neonatal renal failure from a combination of hemodynamic compromise and renal tubular dysgenesis (RTD) (220,344).

High glucose levels in diabetic mothers are associated with an increased incidence of kidney and lower urinary tract malformations, plus abnormalities in the nervous, cardiovascular, and skeletal systems (345,346). Experimental exposure of embryonic kidneys to high glucose alters the expression of laminin β 2 in the basement membrane (347) and expression of IGF receptors (348), but there are at least two other factors that may contribute to congenital diabetic nephropathy. Firstly, there is often an association with caudal regression syndrome, which causes reduction of distal structures such as the sacrum and hind limbs and might clearly affect the lower urinary tract, and secondly, it is likely that many of the cases ascribed to maternal diabetes had *HNF1 β* mutations as reported in the RCAD syndrome above. High doses of vitamin A and its derivative retinoids have also been linked to human and rodent renal malformations such as renal agenesis (349), although these are also sometimes associated with caudal regression (350). Too little vitamin A also perturbs renal development, however, via multiple effects including modulation of *GDNF/Ret*, *Wnt11*, and *WT1* signaling in the metanephros (351,352) and interaction with the *GDNF* receptor *Ret* which patterns distal ureter and bladder trigone development (353). Intriguingly, some of these effects are potentially, reversible at least in vitro (351). Fetal kidney development is abrogated when pregnant mice are exposed to all-trans retinoic acid or the retinoic acid receptor agonist Am580, but nephrogenesis can be rescued by culture in serum-containing media (351).

Maternal diet may have a more subtle effect on nephrogenesis, affecting nephron number rather than inducing gross changes (346). This hypothesis arose from epidemiologic data suggesting that fetal life can “program” the child for later diseases: individuals born to mothers with poor diets appear much more likely to develop hypertension, cardiovascular disease, and diabetes in adulthood (354,355), and the proposed link between congenital “nephron deficits” and later hypertension (356). Using animal experiments, it is now well established that moderate to severe dietary protein restriction during pregnancy impairs somatic growth and reduces numbers of glomeruli per kidney, and this has been linked to early deletion of renal mesenchymal cells by apoptosis, with subsequent reduction in the

pool of renal precursor cells (357). Vitamin A may also have a regulatory effect on nephron number (358), while other factors such as dietary iron may be important: maternal iron restriction, for example, causes hypertension that has been linked in part to a deficit in nephron number and aberrant kidney development (359,360).

Pathology

Renal Agenesis and Renal Aplasia

Renal agenesis is defined as complete unilateral or bilateral absence of the kidney. Studies in animals and human embryos indicate that this anomaly results from failure of initiation of the pronephros-mesonephros sequence and failure of the ureteric bud to develop. In contrast, *renal aplasia* is defined as absent kidneys that were initially induced, but further stages of nephrogenesis were halted and the kidney eventually involuted. These definitions appear distinct in their pathogenesis and cell biology, but, in reality, there is crossover when discussed clinically because an absent kidney in any given patient may result from either process.

BILATERAL RENAL AGENESIS

Absence of both kidneys is rare with a suggested incidence of 1:7000 to 1:10,000 births occurring more frequently in boys (361,362). It is almost always incompatible with life, with a sharply increased incidence of premature labor and miscarriage. Neonatal death is due to severe lung hypoplasia secondary to oligohydramnios. Kidneys produce most of the amniotic fluid from the second trimester of pregnancy, which is essential for lung and skin development. Oligohydramnios is associated with multiple other anomalies to include limb and face deformities such as wide set eyes, prominent epicanthic folds, receding chin, flat nose and ears. These abnormalities are known as Potter sequence (oligohydramnios sequence). The facial/limb features are thought to result from pressure of the uterine wall on the fetus because of decreased amniotic fluid. Typically, the adrenal glands appear enlarged and disc-like probably from the lack of compression from the kidney below. Occasionally, the adrenal glands are completely absent. Bilateral renal agenesis is often accompanied by genital anomalies including absent phallus, ectopic testes, hypospadias, small or abnormal uterus and imperforate anus and urethral, and bladder agenesis. These anomalies may form part of a "developmental field effect" involving the entire caudal end of the embryo including the hindgut and lower extremities to cause sirenomelia.

Renal agenesis can be diagnosed by ultrasound as early as the first trimester. Therapeutic abortion is often considered at this stage because of dismal prognosis. It should be noted, however, that there are two reported cases of postnatal survivors demonstrating that lung development and survival of the fetus may proceed without kidneys in some cases (363).

UNILATERAL RENAL AGENESIS

Unilateral absence of the kidney is common, affecting up to 1:1000 individuals (364). It occurs equally in both sexes, with the left kidney affected more often. Uncomplicated unilateral agenesis may not be diagnosed until later in life when it is found incidentally or because of a palpable contralateral kidney due to compensatory hypertrophy. However, a great number of patients (50% to 70%) have an associated urogenital anomaly and are diagnosed early in life either by fetal

ultrasound or because of genitourinary complications after birth.

Clinical studies using pre- and postnatal ultrasound show that in humans, most solitary kidneys represent cases of unilateral renal aplasia that regresses rapidly after birth. For example, small reniform kidneys could be demonstrated by fetal ultrasound that disappeared in a short period after birth (365).

The most frequent association of unilateral renal agenesis is reflux nephropathy. In one study of 46 consecutive cases of unilateral renal agenesis, approximately half had UVJ or UPJ obstruction in the contralateral kidney (364). Other associated anomalies include contralateral renal dysplasia, absence of vas deference, absent adrenals, and pelvic renal ectopy. In adults, solitary kidneys are frequently found incidentally. The high incidence in the general population dictates that presence of two kidneys be documented prior to required nephrectomy. The outcome for solitary kidneys has been regarded as benign with only a moderately increased long-term risk of proteinuria and hypertension. The benign prognosis only applies when there are no abnormalities in the "normal" opposite kidney. Solitary kidneys are not immune to random kidney disease. For example, membranous glomerulonephritis, autosomal ADPKD, RCC, and renal failure accelerated by obesity and or hypertension have been reported in solitary kidneys (366–368).

Bilateral or unilateral renal agenesis accompanies many syndromes such as the branchiootorenal syndrome, RCAD and the hypoparathyroidism, sensorineural deafness and renal anomalies (HDR) syndrome, Fanconi anemia, Fraser and Kallmann syndrome, Di George, Smith-Lemli-Opitz, and Klinefelter syndrome (47,XXY) (Table 4.7).

Perhaps the most intriguing type of renal agenesis is familial disease, occurring either as bilateral or unilateral agenesis/aplasia or in combination with contralateral dysplasia in members of the same family known as hereditary renal adysplasia (369).

Hereditary Renal Adysplasia

Renal adysplasia is defined as unilateral renal agenesis in association with dysplasia of the contralateral kidney (Fig. 4.52). The term adysplasia is often used more broadly to include dysplasia, absent kidneys, and almost any other structural or positional kidney/lower urinary tract defect. However, hereditary renal adysplasia should be confined to renal dysplasia, renal adysplasia, or renal agenesis in any combination, in different members of the same family. The genetic link between renal agenesis and some types of renal dysplasia points to a common pathogenetic mechanism for these anomalies and perhaps relates to the degree of failure of the ureteric bud in its inductive function on the metanephric blastema. The dysplastic kidneys in renal adysplasia are usually small and multicystic (Fig. 4.52). Most cases of hereditary adysplasia are recognized at an autopsy performed for investigation of perinatal death. Retrospective family studies then reveal unilateral renal agenesis or dysplasia in parents or living siblings. Deaths from bilateral renal agenesis also may have occurred in siblings and sometimes in other generations of the same family. An autosomal dominant mode of inheritance with variable expression in familial renal adysplasia is reported, but the occasional cases of agenesis or dysplasia affecting siblings with normal parents suggests that there are other types of inheritance. Some patients with adysplasia have PAX2 mutations (370,371).



FIGURE 4.52 Renal adysplasia. The right kidney is multicystic dysplastic. The left kidney is a nub-like (aplastic).

Renal Dysplasia

In the strictest terms, renal dysplasia can only be diagnosed on the basis of histology. The malformed kidney can be either larger or smaller than normal and diffusely or partly cystic (Fig. 4.53). The distinct features are disrupted organization of normal nephrons, abundance of undifferentiated cells, thick vessels, metaplastic cartilage, and primitive, poorly branched ducts with smooth muscle collars (Figs. 4.54 to 4.57). Cartilage is only present in one third of the cases, but smooth muscle collars enclosing primitive ducts are invariably present. The latter two features are the most sensitive and specific histologic findings that are essential for the diagnosis of renal dysplasia. Glomeruli may be focally or even diffusely cystic imitating GCKD (see Fig. 4.56). Such cases are perplexing, but first,



FIGURE 4.53 Multicystic dysplastic kidney from a 2-year-old.

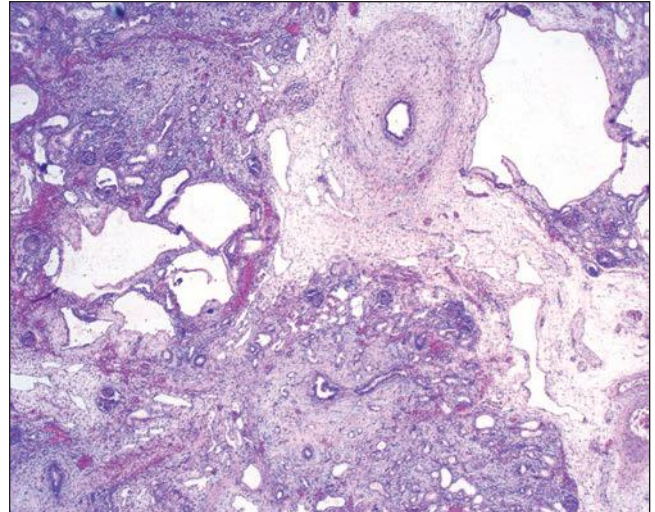


FIGURE 4.54 Renal dysplasia is characterized by disorganized renal parenchyma, immature glomeruli and tubules, cysts, and smooth muscle collars surrounding aborted and primitive collecting ducts. ($\times 40$)

the kidneys lack the enormous size of polycystic kidneys, and second careful search and additional sections almost invariably show dysplastic features (Fig. 4.56B). The degree of dysplasia within the kidney can vary; for example, it may affect cortex and medulla or predominantly the medulla alone, and it may involve a segment or the entire kidney. Segmental dysplasia is most frequently seen in children with duplicate ureters immediately above the duplication (Fig. 4.58) and very rarely in adults (372). Renal cortex is reduced in thickness due to decreased nephron formation. Nephrogenic rests are sometimes found in dysplastic kidneys (Fig. 4.59), but Wilms tumor is a very rare occurrence. RCC developing in an atrophic kidney was the subject of a single case report (373). Atrophic and rudimentary dysplastic kidneys are sometimes erroneously called hypoplastic from which they should be distinguished (see below).

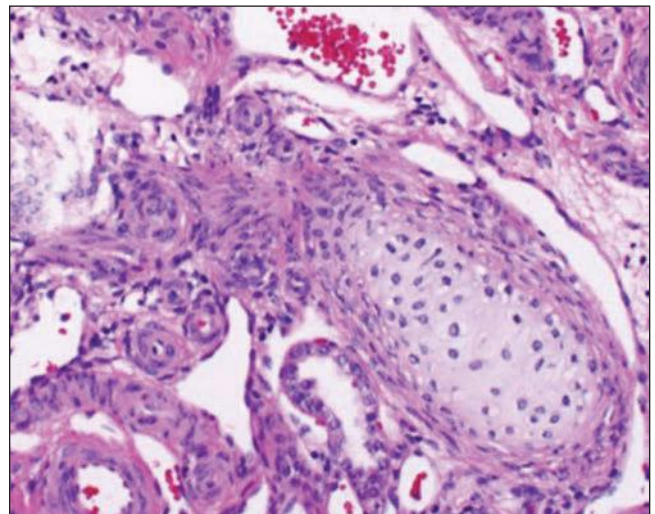


FIGURE 4.55 Dysplastic kidney with metaplastic cartilage. ($\times 100$)

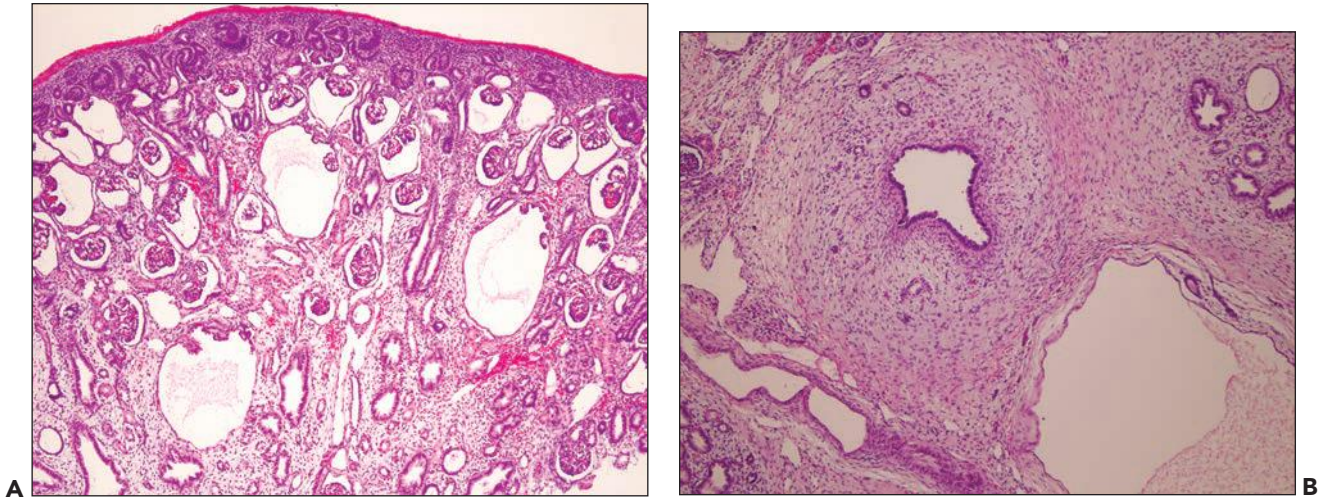


FIGURE 4.56 Dysplastic kidney from a 32-week male fetus with unilateral renal aplasia, no hydronephrosis, or extrarenal abnormalities or **(A)** shows glomerular cysts and dysplastic glomeruli with supernumerary tufts. **B:** Fibromuscular collars around a primitive collecting duct were found in adjacent sections (H&E $\times 100$). The findings are diagnostic of GCKD secondary to renal dysplasia.

Variations in gross appearance have prompted investigators to distinguish dysplasia in different types such as cystic (multicystic), hypoplastic, hypodysplastic, segmental, or obstructive dysplasia when associated with urine flow obstruction. Such distinctions and terminology may have clinical value, but with an ever increasing new literature from cell biology, seem to have lost their luster.

Unilateral dysplasia is more common than bilateral. Both can be associated with Potter syndrome because of frequent anomalies in the contralateral kidney. Coexisting abnormalities of the urinary tract occur in 50% to 75% of patients with unilateral dysplasia; hence, they fall into the CAKUT spectrum; some of these cases are now found to have a genetic

basis (374,375). Renal dysplasia is frequently found in renal ectopias including the horseshoe kidney, kidneys with ureteral duplication, hydroureters, UPJ, and UVJ obstruction, reflux, and superimposed pyelonephritis also referred to as obstructive nephropathy (see Chapter 22). The role of obstruction in the pathogenesis of human renal dysplasia is substantiated by numerous studies that show tubular dilation and cyst formation due to fluid accumulation in humans and animal

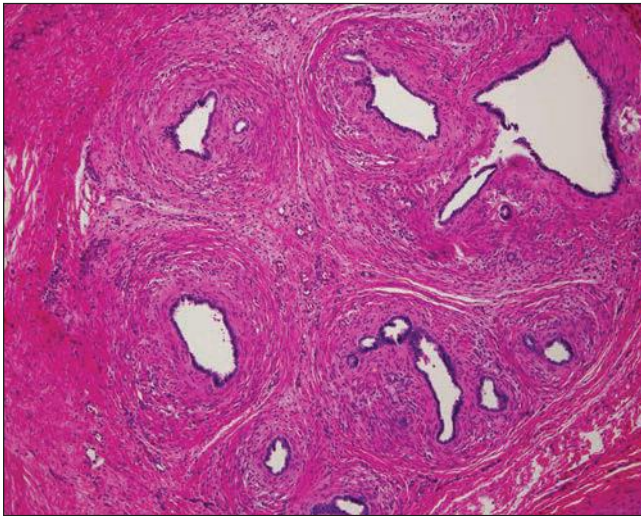


FIGURE 4.57 Advanced renal dysplasia with aborted nephrogenesis; fibromuscular collarettes replace the renal parenchyma. (H&E $\times 100$)

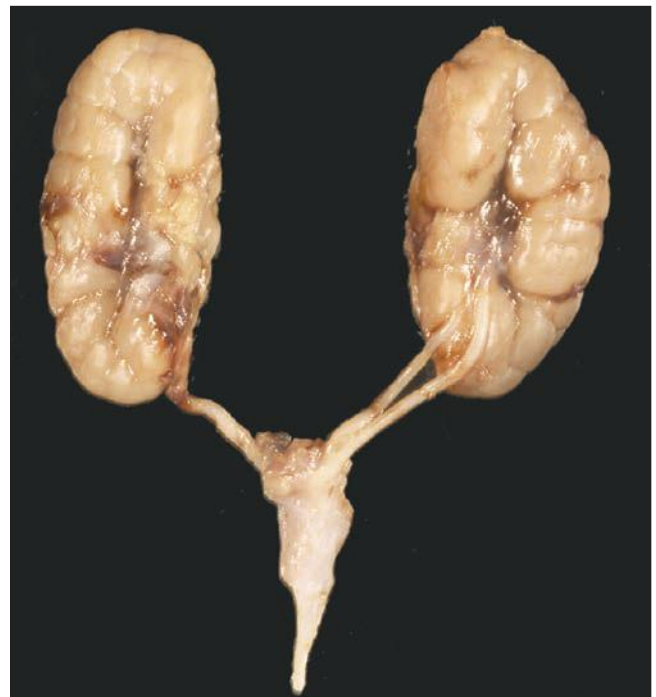


FIGURE 4.58 Ureteral duplication in the left kidney.

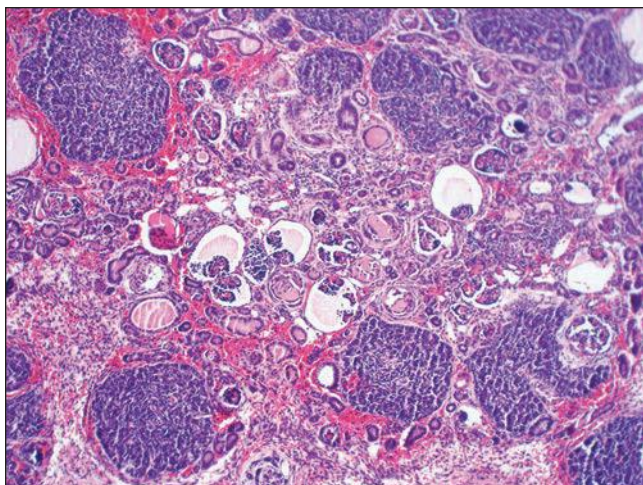


FIGURE 4.59 Nephrogenic rests in the dysplastic kidney; glomerular cysts are also present. ($\times 200$)

models (discussed under cell biology). In obstructed kidneys, the main differential diagnosis is from pure hydronephrosis. In pure hydronephrosis, thinning of the medulla is usually more extreme than that of the cortex, whereas in a hydronephrotic dysplastic kidney, the reverse is more frequent. In addition, primitive, comma shaped ducts and smooth muscle collars are not a feature of pure hydronephrosis (discussed in Chapter 22).

The fact that dysplasia occurs in kidneys without evidence of obstruction has raised alternative hypotheses to include loss of local gene transcriptions (376,377). As discussed under adysplasia, multicystic dysplasia can be part of related familial kidney anomalies, but unilateral dysplasia without other genitourinary anomalies has been reported with an autosomal dominant mode of inheritance. For example, Srivastava reported a woman with unilateral multicystic dysplasia who presented with abdominal mass in infancy. Both of her children had unilateral dysplasia with prenatal ultrasound (378). A father to son transmission is found in independent families with isolated unilateral cystic dysplasia, further supporting an autosomal dominant mode of inheritance (379,380). Search for specific genes revealed mutations in *PAX2* independently of or with renal coloboma syndrome (370,371). These genetic studies reveal complex and variant genetic pathogenesis and are important for genetic counseling of affected individuals, but most often unilateral renal dysplasia appears sporadic rather than familial.

The differential diagnosis of multicystic dysplastic kidneys in childhood includes unilateral or bilateral tumors. The overall prognosis of unilateral dysplasia depends on the presence of other anomalies that sometimes may be more severe and overshadow the kidney problem. Isolated unilateral disease has good prognosis with appropriate conservative management to prevent infections or treat hypertension. A small number of patients may experience renin-dependent hypertension due to increased ectopic renin production in the dysplastic kidney that is curable with surgery (Fig. 4.60) (381–383). However, renin is generally decreased in dysplastic kidneys. Since Renin participates in vasculogenesis during kidney development, decreased

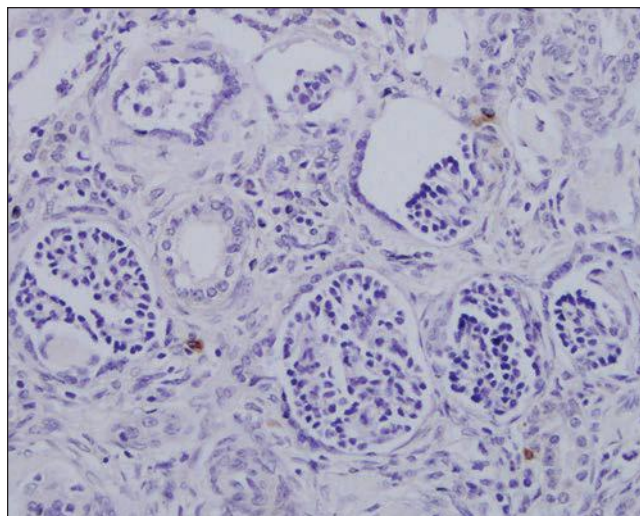


FIGURE 4.60 Renin immunohistochemistry shows decreased renin in afferent arterioles and ectopic renin in interstitial cells within dysplastic kidney parenchyma; from a child with renin-dependent hypertension.

renin in dysplastic kidneys may contribute to abnormally thick and malformed vessels. Routine surgical removal of the dysplastic kidney is not recommended. At least one third of dysplastic kidneys undergo rapid involution postnatally (384,385). However, in children with renin dependent hypertension, removal of the dysplastic kidney cures hypertension.

Renal Hypoplasia

Hypoplastic kidneys are defined as small kidneys that weigh less than 50% of the normal mean for age and have no histologic abnormality other than secondary focal segmental glomerulosclerosis (FSGS). Renal hypoplasia is classified as simple hypoplasia or hypoplasia with hypertrophy of nephrons (oligomeganephronic hypoplasia). Hypoplasia is difficult to distinguish from secondary atrophy or segmental pyelonephritic scarring, all of which may interfere with renal growth. Excluding secondary renal damage (atrophy) in a small kidney requires radiographic examination with contrast media to exclude segmental scarring and calyceal clubbing, a change diagnostic of reflux and congenital renal artery stenosis. A narrow renal artery in acquired renal disease retains a wide, funnel-shaped segment at its origin from the aorta as an indication of its previously wider overall caliber (386). Adequate histologic examination of the kidney is required to exclude evidence of dysplasia. Parenchymal maldifferentiation is lacking in the purely hypoplastic kidney (Fig. 4.61). Kidneys that are small entirely because of acquired disease should not be described as hypoplastic but as atrophic. An entity that may be relevant at this point is the so-called Ask-Upmark kidney, a type of small kidney associated with hypertension in childhood (discussed in Chapter 22).

Although the true incidence of renal hypoplasia is difficult to establish, apparently it is much rarer than formerly thought, and most cases are bilateral. Two main varieties can be distinguished: oligonephronic hypoplasia (oligomeganephronia) and simple hypoplasia.



FIGURE 4.61 Hypoplastic kidneys from a 4-month-old girl with feeding difficulty and kidney, brain, and other anomalies due to 4p deletion (Wolf-Hirschhorn syndrome). Kidneys show profound decrease in renal lobulation but otherwise normal parenchyma.

OLIGOMEGANEPHRONIA

This is a distinct form of nonfamilial bilateral renal hypoplasia in which the combined kidneys weigh 12 to 45 g and always less than 50% of the expected weight. The number of renal lobes is reduced, and sometimes only one or two pyramids can be identified. The parenchyma is typically firm and pale, and renal surfaces are smooth or finely granular. Microscopically, the striking feature is reduced number of nephrons, but those present are hypertrophied. The glomeruli are clearly enlarged by up to three times the normal diameter, and the tubules are dilated and lined by enlarged epithelial cells. Children with oligonephronia develop polyuria and polydipsia, a urine-concentrating defect, and often salt wasting in the first 2 years of life. Dehydration, vomiting, unexplained fever, and growth retardation are also common features, and the clinical picture may resemble that of juvenile NPHP. However, significant proteinuria is more frequent with oligonephronia, and the absence of a family history may help to distinguish it from familial juvenile NPHP, which is inherited as an autosomal recessive trait. Although oligonephronia is usually a sporadic-isolated anomaly, Salomon et al. (387) found PAX2 mutations implicated in three patients with oligomeganephronia. This rare disease characterized by nephron deficit in premature babies and/or infants is gaining increasing interest particularly in regard to the association of low birth weight with low nephron numbers and subsequent increased risk for hypertension and heart disease in adulthood (388). Premature babies or small for age infants have a high incidence of cardiovascular disease, hypertension, hyperlipidemia, diabetes, and renal failure in adulthood. Computer-assisted histomorphometry and radial glomerular counts in one premature infant with low birth weight revealed approximately 50% decrease in glomerular generations compared to normal control and a significant increase in the size of glomeruli. Glomerulomegaly, a hallmark of hyperfiltration, appears to play a role in the low birth weight premature babies and may be due to decreased renal mass (389).

SIMPLE HYPOPLASIA

Simple hypoplasia may be bilateral or, much less frequently, unilateral, and it differs from oligonephronic hypoplasia chiefly in that nephronic hypertrophy is not a feature. Histologic examination reveals a reduced volume of normally differentiated renal parenchyma. Secondary FSGS with focal tubulointerstitial damage may be apparent, particularly with more extreme reduction in renal size (Fig. 4.61).

Bilateral small kidneys with less than 50% of the expected mean combined renal mass are sometimes encountered in children with multiple congenital malformations, Down syndrome, or long-standing disease or anomalies of the central nervous system. In this situation, the number of renal lobes is often normal, and the reduced renal size possibly represents a failure of normal postnatal growth, rather than an intrinsic deficiency in renal parenchymal mass. Some ectopic or malrotated kidneys may be smaller than expected, even when histologic signs of dysplastic parenchymal differentiation are absent. The blood supply to such kidneys is often anomalous.

Ectopia and Malrotation

Permanent malposition of the kidney outside its normal lumbar site constitutes renal ectopia, a condition that may affect one or both kidneys or a solitary kidney in unilateral agenesis. Ectopia is seen in about 1 in 800 radiologic examinations of the kidney. Ectopic kidneys need to be distinguished from abnormally mobile, ptotic (“droopy”) kidneys that are less firmly anchored than normal to the posterior abdominal wall by their peritoneal covering and may therefore change position excessively during respiration. They are not permanently displaced, however, and they have a normal blood supply.

During development, the kidneys ascend to a progressively higher level from the pelvis and ultimately end in the lumbar region between the 12th thoracic and 3rd lumbar vertebral bodies. During the ascent, which is largely a result of differential growth of the caudal end of the embryo, the kidney rotates medially through 90 degrees, so the renal hilum and pelvis, which are at first located anteriorly, come to be on the medial aspect. Interference with this process results in renal ectopia below the normal position, usually in the pelvis. Such ectopic kidneys are almost always malrotated, with an anteriorly directed pelvis, and their shape is often discoid or lumpy rather than reniform. Rarely, reversed (lateral) rotation of the kidney occurs, with a laterally facing renal pelvis, and exceptionally, the kidney may rotate through 180 degrees, so the pelvis is anterior (Fig. 4.62). Ectopic kidneys are very rarely found at a higher level than normal, although they have been described in the thorax in association with a diaphragmatic defect. The blood supply to ectopic kidneys is generally anomalous and is derived from single or multiple branches of the common iliac artery or lower abdominal aorta.

Renal ectopia may be simple or crossed. In simple ectopia, the kidney and ureter are on the correct side of the body. The ureter is short and may be inserted ectopically in the bladder neck, urethra, seminal vesicle, or vagina; sometimes, it is subject to vesicoureteral reflux. In crossed ectopia, the kidney is situated on the opposite side of the body of the urethral orifice with the ureter crossing the midline. The two kidneys are thus



FIGURE 4.62 A malrotated left kidney with the renal pelvis facing anteriorly instead of laterally. Also note the kidney has a discoid instead of reniform shape. (Courtesy John Kissane Washington University, Saint Louis.)

located on the same side of the body, with the ectopic kidney generally below the orthotropic kidney. The two kidneys may be fused together, a condition known as crossed fused ectopia. Ectopic kidneys are often dysplastic, and distortion or kinking of the renal pelvis or obstruction by blood vessels crossing anterior to the renal pelvis may lead to intermittent obstruction and hydronephrosis. This condition, particularly if accompanied by vesicoureteral reflux, predisposes to renal infection. In about 25%, renal calculi are present. Pelvic renal ectopia can be associated with anorectal anomalies, particularly rectal atresia, or with congenital absence or atresia of the vagina in female patients.

Renal Fusion

In renal fusion, the two kidneys are joined, and the parenchyma is continuous between them. Each kidney has a separate collecting system and ureter that are inserted orthotopically on the two sides. Renal fusion should be distinguished from ureteral duplication, in which two ureters, even if completely separate, are inserted on the same side of the bladder. Most commonly, the kidneys are fused by their lower poles across the midline, the “horseshoe kidney,” which is seen in approximately 1 in 600 radiologic examinations. Horseshoe kidneys are often situated lower than normal and so can be regarded as ectopic as well as fused (Fig. 4.63). The renal pelvis is usually located anteriorly, and hydronephrosis resulting from a high ureteropelvic junction or compression by aberrant renal arteries is not uncommon. Midline fusion is about twice as common in males as in females. It is not infrequently associated with other congenital malformations and is common in Turner syndrome. Although usually asymptomatic, the presence of hydronephrosis predisposes to renal infection and calculus formation. Occasionally, the fused renal tissue may be palpable as an apparently pulsatile midline mass that has been mistaken for an aortic aneurysm.

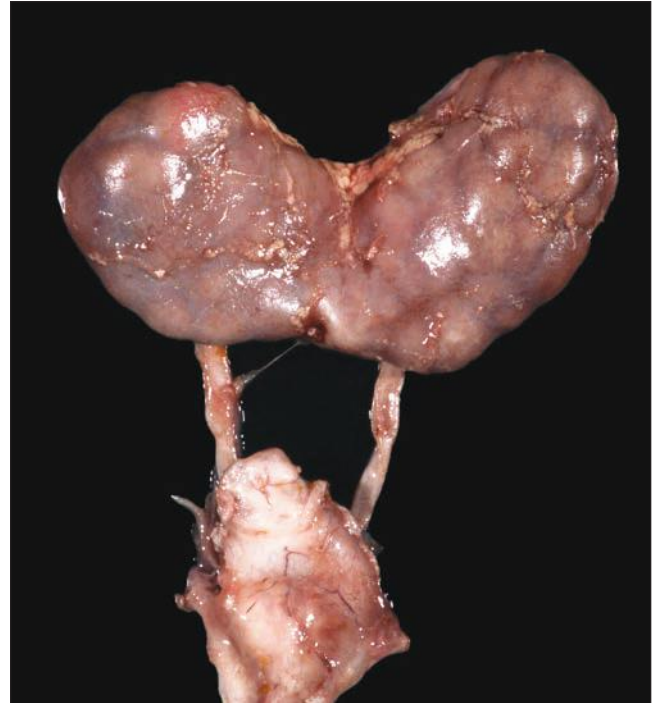


FIGURE 4.63 The horseshoe kidney is a pelvic kidney, both fused and ectopic.

Renal Duplication

Some degree of duplication of the renal pelvis and ureter (duplex kidney) is common, occurring in about 5% of unselected autopsies. The extent of the duplication varies from mere bifurcation of the extrarenal renal pelvis to complete duplication of the whole system with two completely separate ureters with separate orifices (see Fig. 4.58). Complete ureteral duplication is rare (1% of all duplications) and may be associated with segmental renal dysplasia, ectopia of one of the ureters, and ureterocele. The conjoint ureter, in which separate renal pelvises and upper ureters join to form a single lower ureter, is relatively common. Rarely, triplication and even quadruplication of the ureter occur.

Supernumerary Kidney

This rare anomaly is characterized by the presence of a third kidney morphologically separate from the other two, with its own pelvicalyceal system and blood supply. The extra kidney is ectopic, usually situated beneath the lower pole of a normal kidney, and its ureter may join one of the other two or may drain separately. Sometimes, it is inserted ectopically. Exceptionally, multiple supernumerary kidneys have been described. The condition is usually asymptomatic, but renal infection, obstruction, and stone formation may occur.

Renal Tubular Dysgenesis

This syndrome is characterized clinically by oligohydramnios, widely separated cranial sutures and fontanelles, Potter sequence, and premature stillbirth or neonatal death from respiratory failure. Originally described in two stillborn siblings, RTD was subsequently reported in more than 70 cases. Recent studies by Gribouval et al. (390) demonstrated mutations in

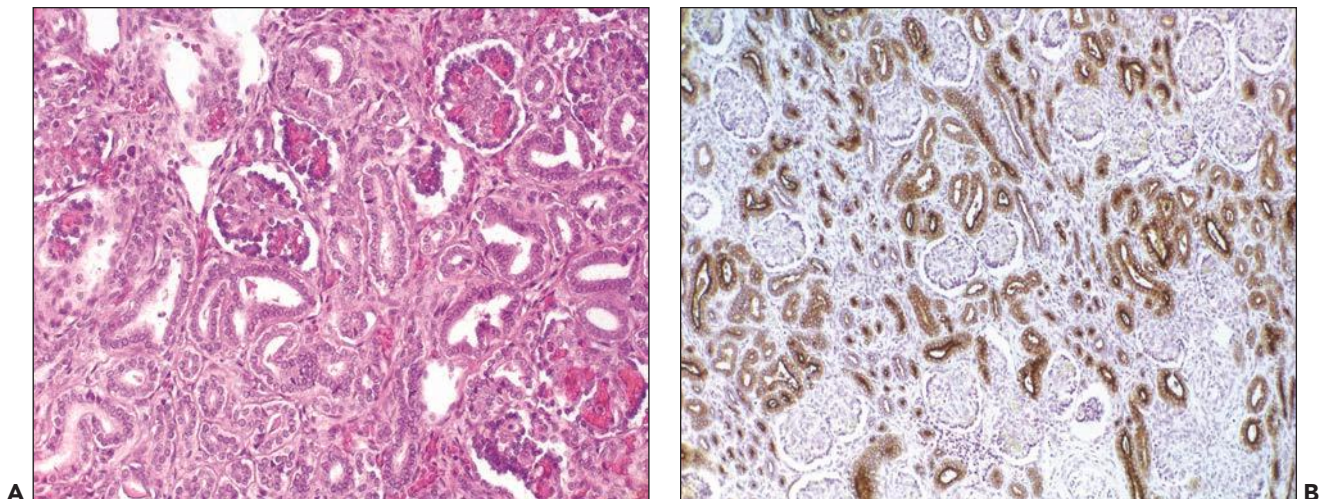


FIGURE 4.64 Renal tubular dysgenesis. **A:** The glomeruli appear crowded. Proximal tubules lack brush borders and cannot be distinguished from distal tubules. **B:** Epithelial membrane antigen (EMA) stains all tubules (normally only distal tubules stain) ($\times 200$). (Courtesy Dr. David Brink, Department of Pathology, St. Louis University, St. Louis.)

the genes coding for renin, angiotensin-converting enzyme, or angiotensin II receptor type 1. Eleven individuals from nine families (some consanguineous) had RTD (390). Histologically, all kidneys had typical findings of RTD with absent proximal tubule differentiation, and some had intense renin expression detected by immunohistochemistry. Additionally, the same authors reported 54 distinct mutations in 48 unrelated families, most of which were ACE mutations found in two thirds of families (391). In the infants of mothers given ACE inhibitors, some degree of glomerular and tubular dilatation similar to RTD, but the condition is not necessarily fatal. The variability of the drug-related lesions, with recovery in some patients, suggests a possible dose-related effect. Most authors believe that the underlying mechanism for RTD is renal hypoperfusion, whether genetic or secondary, and precludes normal development and differentiation of proximal tubules (391,392).

PATHOLOGY

Grossly, the kidneys are normal size or enlarged. Histologically, the glomeruli appear crowded, and the tubules are lined by small, darkly staining cells that cannot be differentiated histologically into proximal and distal convoluted tubules (Fig. 4.64). Lack of differentiation is highlighted by immunohistochemical staining for EMA that normally stains only distal tubules. In RTD, there is uniform positive staining of all tubules (Fig. 4.64B). Similarly, lectin staining with *Arachis hypogaea* (peanut) lectin shows uniform apical staining of tubular cells, while normally, this staining is characteristic of distal tubules and collecting ducts. Electron microscopy may demonstrate occasional tubular segments with brush borders.

REFERENCES

1. Foucar E. Classification in anatomic pathology. *Am J Clin Pathol* 2001;116(Suppl):S5.
2. Bonsib SM. The classification of renal cystic diseases and other congenital malformations of the kidney and urinary tract. *Arch Pathol Lab Med* 2010;134:554.
3. Hildebrandt F, Benzing T, Katsanis N. Ciliopathies. *N Engl J Med* 2011;364:1533.
4. Loftus H, Ong AC. Cystic kidney diseases: many ways to form a cyst. *Pediatr Nephrol* 2013;28:33.
5. Chaki M, Hoefele J, Allen SJ, et al. Genotype-phenotype correlation in 440 patients with NPHP-related ciliopathies. *Kidney Int* 2011;80:1239.
6. Lennerz JK, Spence DC, Iskandar SS, et al. Glomerulocystic kidney: one hundred-year perspective. *Arch Pathol Lab Med* 2010;134:583.
7. Wolf MT, Mucha BE, Hennies HC, et al. Medullary cystic kidney disease type 1: mutational analysis in 37 genes based on haplotype sharing. *Hum Genet* 2006;119:649.
8. McPhail EF, Gettman MT, Patterson DE, et al. Nephrolithiasis in medullary sponge kidney: evaluation of clinical and metabolic features. *Urology* 2012;79:277.
9. Truong LD, Choi YJ, Shen SS, et al. Renal cystic neoplasms and renal neoplasms associated with cystic renal diseases: pathogenetic and molecular links. *Adv Anat Pathol* 2003;10:135.
10. Moch H. Cystic renal tumors: new entities and novel concepts. *Adv Anat Pathol* 2010;17:209.
11. Boman F, Hill DA, Williams GM, et al. Familial association of pleuropulmonary blastoma with cystic nephroma and other renal tumors: a report from the International Pleuropulmonary Blastoma Registry. *J Pediatr* 2006;149:850.
12. Slywotzky CM, Bosniak MA. Localized cystic disease of the kidney. *AJR Am J Roentgenol* 2001;176:843.
13. Collins AJ, Foley RN, Chavers B, et al. United States Renal Data System 2011 Annual Data Report: atlas of chronic kidney disease and end-stage renal disease in the United States. *Am J Kidney Dis* 2012;59:A7.
14. Neumann HP, Jilg C, Bacher J, et al. Epidemiology of autosomal-dominant polycystic kidney disease: an in-depth clinical study for south-western Germany. *Nephrol Dial Transplant* 2013;28(6):1472-1487.
15. Torres VE, Harris PC, Pirson Y. Autosomal dominant polycystic kidney disease. *Lancet* 2007;369:1287.
16. Helal I, Reed B, Schrier RW. Emergent early markers of renal progression in autosomal-dominant polycystic kidney disease patients: implications for prevention and treatment. *Am J Nephrol* 2012;36:162.
17. Harris PC, Rossetti S. Determinants of renal disease variability in ADPKD. *Adv Chronic Kidney Dis* 2010;17:131.
18. Barua M, Cil O, Paterson AD, et al. Family history of renal disease severity predicts the mutated gene in ADPKD. *J Am Soc Nephrol* 2009;20:1833.
19. Chapman AB. Cystic disease in women: clinical characteristics and medical management. *Adv Ren Replace Ther* 2003;10:24.

20. Chapman AB, Guay-Woodford LM, Grantham JJ, et al. Renal structure in early autosomal-dominant polycystic kidney disease (ADPKD): the Consortium for Radiologic Imaging Studies of Polycystic Kidney Disease (CRISP) cohort. *Kidney Int* 2003;64:1035.
21. Chatha RK, Johnson AM, Rothberg PG, et al. Von Hippel-Lindau disease masquerading as autosomal dominant polycystic kidney disease. *Am J Kidney Dis* 2001;37:852.
22. Pei Y. Practical genetics for autosomal dominant polycystic kidney disease. *Nephron Clin Pract* 2011;118:c19.
23. Audrezet MP, Corne-Le Gall E, Chen JM, et al. Autosomal dominant polycystic kidney disease: comprehensive mutation analysis of PKD1 and PKD2 in 700 unrelated patients. *Hum Mutat* 2012;33:1239.
24. Fain PR, McFann KK, Taylor MR, et al. Modifier genes play a significant role in the phenotypic expression of PKD1. *Kidney Int* 2005;67:1256.
25. Ong AC, Wheatley DN. Polycystic kidney disease—the ciliary connection *Lancet* 2003;361:774.
26. Bergmann C, Weiskirchen R. It's not all in the cilium, but on the road to it: genetic interaction network in polycystic kidney and liver diseases and how trafficking and quality control matter. *J Hepatol* 2012;56:1201.
27. Hopp K, Ward CJ, Hommerding CJ, et al. Functional polycystin-1 dosage governs autosomal dominant polycystic kidney disease severity. *J Clin Invest* 2012;122:4257.
28. Li H, Yang W, Mendes F, et al. Impact of the cystic fibrosis mutation F508del-CFTR on renal cyst formation and growth. *Am J Physiol Renal Physiol* 2012;303:F1176.
29. Harris PC. What is the role of somatic mutation in autosomal dominant polycystic kidney disease? *J Am Soc Nephrol* 2010;21:1073.
30. Gallagher AR, Germino GG, Somlo S. Molecular advances in autosomal dominant polycystic kidney disease. *Adv Chronic Kidney Dis* 2010;17:118.
31. Calvet JP, Grantham JJ. The genetics and physiology of polycystic kidney disease. *Semin Nephrol* 2001;21:107.
32. Rossetti S, Consugar MB, Chapman AB, et al. Comprehensive molecular diagnostics in autosomal dominant polycystic kidney disease. *J Am Soc Nephrol* 2007;18:2143.
33. Verlinsky Y, Rechitsky S, Verlinsky O, et al. Preimplantation genetic diagnosis for polycystic kidney disease. *Fertil Steril* 2004;82:926.
34. Pei Y, Obaji J, Dupuis A, et al. Unified criteria for ultrasonographic diagnosis of ADPKD. *J Am Soc Nephrol* 2009;20:205.
35. Avni FE, Guissard G, Hall M, et al. Hereditary polycystic kidney diseases in children: changing sonographic patterns through childhood. *Pediatr Radiol* 2002;32:169.
36. Bernstein J, Evan AP, Gardner KD Jr. Epithelial hyperplasia in human polycystic kidney diseases. Its role in pathogenesis and risk of neoplasia. *Am J Pathol* 1987;129:92.
37. Barisoni L, Trudel M, Chretien N, et al. Analysis of the role of membrane polarity in polycystic kidney disease of transgenic SBM mice. *Am J Pathol* 1995;147:1728.
38. Grantham JJ. Mechanisms of progression in autosomal dominant polycystic kidney disease. *Kidney Int Suppl* 1997;63:S93.
39. Grantham JJ, Mulamalla S, Swenson-Fields KI. Why kidneys fail in autosomal dominant polycystic kidney disease. *Nat Rev Nephrol* 2011;7:556.
40. Mahjoub MR, Stearns T. Supernumerary centrosomes nucleate extra cilia and compromise primary cilium signaling. *Curr Biol* 2012;22:1628.
41. Bernstein J, Evan AP, Gardner KD Jr. Human cystic kidney diseases: epithelial hyperplasia in the pathogenesis of cysts and tumors. *Pediatr Nephrol* 1987;1:393.
42. Bell PD, Fitzgibbon W, Sas K, et al. Loss of primary cilia upregulates renal hypertrophic signaling and promotes cystogenesis. *J Am Soc Nephrol* 2011;22:839.
43. Xu N, Glockner JF, Rossetti S, et al. Autosomal dominant polycystic kidney disease coexisting with cystic fibrosis. *J Nephrol* 2006;19:529.
44. Martignoni G, Bonetti F, Pea M, et al. Renal disease in adults with TSC2/PKD1 contiguous gene syndrome. *Am J Surg Pathol* 2002;26:198.
45. Avni FE, Hall M. Renal cystic diseases in children: new concepts. *Pediatr Radiol* 2010;40:939.
46. Guay-Woodford LM, Desmond RA. Autosomal recessive polycystic kidney disease: the clinical experience in North America. *Pediatrics* 2003;111:1072.
47. Fonck C, Chauveau D, Gagnadoux MF, et al. Autosomal recessive polycystic kidney disease in adulthood. *Nephrol Dial Transplant* 2001;16:1648.
48. Parfrey PS. Autosomal-recessive polycystic kidney disease. *Kidney Int* 2005;67:1638.
49. Denamur E, Delezoide AL, Alberti C, et al. Genotype-phenotype correlations in fetuses and neonates with autosomal recessive polycystic kidney disease. *Kidney Int* 2010;77:350.
50. Gunay-Aygun M, Font-Montgomery E, Lukose L, et al. Characteristics of congenital hepatic fibrosis in a large cohort of patients with autosomal recessive polycystic kidney disease. *Gastroenterology* 2013;144:112.
51. Gunay-Aygun M, Tuchman M, Font-Montgomery E, et al. PKHD1 sequence variations in 78 children and adults with autosomal recessive polycystic kidney disease and congenital hepatic fibrosis. *Mol Genet Metab* 2010;99:160.
52. Malek J, Daar J. The case for a parental duty to use preimplantation genetic diagnosis for medical benefit. *Am J Bioeth* 2012;12:3.
53. Everson GT, Taylor MR, Doctor RB. Polycystic disease of the liver. *Hepatology* 2004;40:774.
54. Gevers TJ, Drenth JP. Diagnosis and management of polycystic liver disease. *Nat Rev Gastroenterol Hepatol* 2013;10(2):101–108.
55. Levy AD, Rohrmann CA Jr. Biliary cystic disease. *Curr Probl Diagn Radiol* 2003;32:233.
56. Lipschitz B, Berdon WE, Defelice AR, et al. Association of congenital hepatic fibrosis with autosomal dominant polycystic kidney disease. Report of a family with review of literature. *Pediatr Radiol* 1993;23:131.
57. Zingg-Schenk A, Caduff J, Azzarello-Burri S, et al. Boy with autosomal recessive polycystic kidney and autosomal dominant polycystic liver disease. *Pediatr Nephrol* 2012;27:1197.
58. Davila S, Furu L, Gharavi AG, et al. Mutations in SEC63 cause autosomal dominant polycystic liver disease. *Nat Genet* 2004;36:575.
59. Drenth JP, Martina JA, Te Morsche RH, et al. Molecular characterization of hepatocystin, the protein that is defective in autosomal dominant polycystic liver disease. *Gastroenterology* 2004;126:1819.
60. Torres VE, Harris PC. Autosomal dominant polycystic kidney disease: the last 3 years. *Kidney Int* 2009;76:149.
61. Raynaud P, Tate J, Callens C, et al. A classification of ductal plate malformations based on distinct pathogenic mechanisms of biliary dysmorphogenesis. *Hepatology* 2011;53:1959.
62. Alvaro D, Onori P, Alpini G, et al. Morphological and functional features of hepatic cyst epithelium in autosomal dominant polycystic kidney disease. *Am J Pathol* 2008;172:321.
63. Roelandt P, Antoniou A, Libbrecht L, et al. HNF1B deficiency causes ciliary defects in human cholangiocytes. *Hepatology* 2012;56:1178.
64. Chapman AB, Bost JE, Torres VE, et al. Kidney volume and functional outcomes in autosomal dominant polycystic kidney disease. *Clin J Am Soc Nephrol* 2012;7:479.
65. Torres VE, Chapman AB, Devuyst O, et al. Tolvaptan in patients with autosomal dominant polycystic kidney disease. *N Engl J Med* 2012;367:2407.
66. Bissler JJ, Siroky BJ, Yin H. Glomerulocystic kidney disease. *Pediatr Nephrol* 2010;25:2049.
67. Bingham C, Bulman MP, Ellard S, et al. Mutations in the hepatocyte nuclear factor-1beta gene are associated with familial hypoplastic glomerulocystic kidney disease. *Am J Hum Genet* 2001;68:219.
68. Gusmano R, Caridi G, Marini M, et al. Glomerulocystic kidney disease in a family. *Nephrol Dial Transplant* 2002;17:813.
69. Scolari F, Caridi G, Rampoldi L, et al. Uromodulin storage diseases: clinical aspects and mechanisms. *Am J Kidney Dis* 2004;44:987.
70. Rampoldi L, Caridi G, Santon D, et al. Allelism of MCKD, FJHN and GCKD caused by impairment of uromodulin export dynamics. *Hum Mol Genet* 2003;12:3369.
71. Bellanne-Chantelot C, Chauveau D, Gautier JF, et al. Clinical spectrum associated with hepatocyte nuclear factor-1beta mutations. *Ann Intern Med* 2004;140:510.
72. Choi YH, Suzuki A, Hajarnis S, et al. Polycystin-2 and phosphodiesterase 4C are components of a ciliary A-kinase anchoring protein complex that is disrupted in cystic kidney diseases. *Proc Natl Acad Sci U S A* 2011;108:10679.

73. Vyletal P, Bleyer AJ, Kmoch S. Uromodulin biology and pathophysiology— an update. *Kidney Blood Press Res* 2010;33:456.
74. Liapis H, Yu H, Steinhardt GF. Cell proliferation, apoptosis, Bcl-2 and Bax expression in obstructed opossum early metanephroi. *J Urol* 2000;164:511.
75. Emma F, Muda AO, Rinaldi S, et al. Acquired glomerulocystic kidney disease following hemolytic uremic syndrome. *Pediatr Nephrol* 2001;16:557.
76. Ichimura K, Kurihara H, Sakai T. Primary cilia disappear in rat podocytes during glomerular development. *Cell Tissue Res* 2010;341:197.
77. Hildebrandt F, Attanasio M, Otto E. Nephronophthisis: disease mechanisms of a ciliopathy. *J Am Soc Nephrol* 2009;20:23.
78. Otto EA, Ramaswami G, Janssen S, et al. Mutation analysis of 18 nephronophthisis associated ciliopathy disease genes using a DNA pooling and next generation sequencing strategy. *J Med Genet* 2011;48:105.
79. Salomon R, Saunier S, Naudet P. Nephronophthisis. *Pediatr Nephrol* 2009;24:2333.
80. Habbig S, Bartram MP, Sagmuller JG, et al. The ciliopathy disease protein NPHP9 promotes nuclear delivery and activation of the oncogenic transcriptional regulator TAZ. *Hum Mol Genet* 2012;21:5528.
81. Lienkamp S, Ganner A, Wälz G. Inversin, Wnt signaling and primary cilia. *Differentiation* 2012;83:S49.
82. Otto EA, Schermer B, Obara T, et al. Mutations in INVS encoding inversin cause nephronophthisis type 2, linking renal cystic disease to the function of primary cilia and left-right axis determination. *Nat Genet* 2003;34:413.
83. Simons M, Gloy J, Ganner A, et al. Inversin, the gene product mutated in nephronophthisis type II, functions as a molecular switch between Wnt signaling pathways. *Nat Genet* 2005;37:537.
84. Stavrou C, Koptides M, Tombazos C, et al. Autosomal-dominant medullary cystic kidney disease type 1: clinical and molecular findings in six large Cypriot families. *Kidney Int* 2002;62:1385.
85. Hateboer N, Gumbs C, Teare MD, et al. Confirmation of a gene locus for medullary cystic kidney disease (MCKD2) on chromosome 16p12. *Kidney Int* 2001;60:1233.
86. Kroiss S, Huck K, Berthold S, et al. Evidence of further genetic heterogeneity in autosomal dominant medullary cystic kidney disease. *Nephrol Dial Transplant* 2000;15:818.
87. Dahan K, Devuyt O, Smaers M, et al. A cluster of mutations in the UMOD gene causes familial juvenile hyperuricemic nephropathy with abnormal expression of uromodulin. *J Am Soc Nephrol* 2003;14:2883.
88. Bollee G, Dahan K, Flamant M, et al. Phenotype and outcome in hereditary tubulointerstitial nephritis secondary to UMOD mutations. *Clin J Am Soc Nephrol* 2011;6:2429.
89. Norris DP, Grimes DT. Mouse models of ciliopathies: the state of the art. *Dis Model Mech* 2012;5:299.
90. Beck BB, Trachtman H, Gitman M, et al. Autosomal dominant mutation in the signal peptide of renin in a kindred with anemia, hyperuricemia, and CKD. *Am J Kidney Dis* 2011;58:821.
91. Gibson T. Hyperuricemia, gout and the kidney. *Curr Opin Rheumatol* 2012;24:127.
92. Kiser RL, Wolf MT, Martin JL, et al. Medullary cystic kidney disease type 1 in a large Native-American kindred. *Am J Kidney Dis* 2004;44:611.
93. Christiansen RE, Fiskerstrand T, Leh S, et al. A mother and daughter with unexplained renal failure. *Nephron Clin Pract* 2011;119:c1.
94. Cameron JS, Simmonds HA. Hereditary hyperuricemia and renal disease. *Semin Nephrol* 2005;25:9.
95. Szymanska K, Berry I, Logan CV, et al. Founder mutations and genotype-phenotype correlations in Meckel-Gruber syndrome and associated ciliopathies. *Cilia* 2012;1:18.
96. EL-Merhi FM, Bae KT. Cystic renal disease. *Magn Reson Imaging Clin N Am* 2004;12:449.
97. Torregrossa R, Anglani F, Fabris A, et al. Identification of GDNF gene sequence variations in patients with medullary sponge kidney disease. *Clin J Am Soc Nephrol* 2010;5:1205.
98. Zaghoul NA, Katsanis N. Mechanistic insights into Bardet-Biedl syndrome, a model ciliopathy. *J Clin Invest* 2009;119:428.
99. Lienkamp SS, Liu K, Karner CM, et al. Vertebrate kidney tubules elongate using a planar cell polarity-dependent, rosette-based mechanism of convergent extension. *Nat Genet* 2012;44:1382.
100. Pan J, Seeger-Nukpezah T, Golemis EA. The role of the cilium in normal and abnormal cell cycles: emphasis on renal cystic pathologies. *Cell Mol Life Sci* 2013;70(11):1849–1874.
101. Rossetti S, Kubly VJ, Consugar MB, et al. Incompletely penetrant PKD1 alleles suggest a role for gene dosage in cyst initiation in polycystic kidney disease. *Kidney Int* 2009;75:848.
102. Takakura A, Contrino L, Zhou X, et al. Renal injury is a third hit promoting rapid development of adult polycystic kidney disease. *Hum Mol Genet* 2009;18:2523.
103. Wilson PD. Polycystic kidney disease: new understanding in the pathogenesis. *Int J Biochem Cell Biol* 2004;36:1868.
104. Hanaoka K, Qian F, Boletta A, et al. Co-assembly of polycystin-1 and -2 produces unique cation-permeable currents. *Nature* 2000;408:990.
105. Bhunia AK, Piontek K, Boletta A, et al. PKD1 induces p21(waf1) and regulation of the cell cycle via direct activation of the JAK-STAT signaling pathway in a process requiring PKD2. *Cell* 2002;109:157.
106. Chauvet V, Tian X, Husson H, et al. Mechanical stimuli induce cleavage and nuclear translocation of the polycystin-1 C terminus. *J Clin Invest* 2004;114:1433.
107. Wang S, Zhang J, Nauli SM, et al. Fibrocystin/polyductin, found in the same protein complex with polycystin-2, regulates calcium responses in kidney epithelia. *Mol Cell Biol* 2007;27:3241.
108. Zhang J, Wu M, Wang S, et al. Polycystic kidney disease protein fibrocystin localizes to the mitotic spindle and regulates spindle bipolarity. *Hum Mol Genet* 2010;19:3306.
109. Bergmann C, Senderek J, Windelen E, et al. Clinical consequences of PKHD1 mutations in 164 patients with autosomal-recessive polycystic kidney disease (ARPKD). *Kidney Int* 2005;67:829.
110. Winyard P, Chitty L. Dysplastic and polycystic kidneys: diagnosis, associations and management. *Prenat Diagn* 2001;21:924.
111. Forsythe E, Beales PL. Bardet-Biedl syndrome. *Eur J Hum Genet* 2013;21:8.
112. Tobin JL, Beales PL. Bardet-Biedl syndrome: beyond the cilium. *Pediatr Nephrol* 2007;22:926.
113. Zhang Q, Seo S, Bugge K, et al. BBS proteins interact genetically with the IFT pathway to influence SHH-related phenotypes. *Hum Mol Genet* 2012;21:1945.
114. Redin C, Le Gras S, Mhamdi O, et al. Targeted high-throughput sequencing for diagnosis of genetically heterogeneous diseases: efficient mutation detection in Bardet-Biedl and Alstrom syndromes. *J Med Genet* 2012;49:502.
115. Marion V, Stutzmann F, Gerard M, et al. Exome sequencing identifies mutations in LZTFL1, a BBSome and smoothed trafficking regulator, in a family with Bardet-Biedl syndrome with situs inversus and insertional polydactyly. *J Med Genet* 2012;49:317.
116. Blacque OE, Reardon MJ, Li C, et al. Loss of *C. elegans* BBS-7 and BBS-8 protein function results in cilia defects and compromised intraflagellar transport. *Genes Dev* 2004;18:1630.
117. Reiter JF, Blacque OE, Leroux MR. The base of the cilium: roles for transition fibres and the transition zone in ciliary formation, maintenance and compartmentalization. *EMBO Rep* 2012;13:608.
118. Wei Q, Zhang Y, Li Y, et al. The BBSome controls IFT assembly and turnaround in cilia. *Nat Cell Biol* 2012;14:950.
119. Pelucchi B, Aguiari G, Pignatelli A, et al. Nonspecific cation current associated with native polycystin-2 in HEK-293 cells. *J Am Soc Nephrol* 2006;17:388.
120. Satir P, Christensen ST. Structure and function of mammalian cilia. *Histochem Cell Biol* 2008;129:687.
121. Bloodgood RA. From central to rudimentary to primary: the history of an underappreciated organelle whose time has come. The primary cilium. *Methods Cell Biol* 2009;94:3.
122. Barr MM, Sternberg PW. A polycystic kidney-disease gene homologue required for male mating behaviour in *C. elegans*. *Nature* 1999;401:386.
123. Barr MM, DeModena J, Braun D, et al. The *Caenorhabditis elegans* autosomal dominant polycystic kidney disease gene homologs lov-1 and pkd-2 act in the same pathway. *Curr Biol* 2001;11:1341.
124. Murcia NS, Richards WG, Yoder BK, et al. The Oak Ridge Polycystic Kidney (orpk) disease gene is required for left-right axis determination. *Development* 2000;127:2347.

125. Gilula NB, Satir P. The ciliary necklace. A ciliary membrane specialization. *J Cell Biol* 1972;53:494.
126. Sorokin S. Centrioles and the formation of rudimentary cilia by fibroblasts and smooth muscle cells. *J Cell Biol* 1962;15:363.
127. Zhou J. Polycystins and primary cilia: primers for cell cycle progression. *Annu Rev Physiol* 2009;71:83.
128. Goetz SC, Anderson KV. The primary cilium: a signalling centre during vertebrate development. *Nat Rev Genet* 2010;11:331.
129. Pedersen LB, Veland IR, Schroder JM, et al. Assembly of primary cilia. *Dev Dyn* 2008;237:1993.
130. Lin F, Hiesberger T, Cordes K, et al. Kidney-specific inactivation of the KIF3A subunit of kinesin-II inhibits renal ciliogenesis and produces polycystic kidney disease. *Proc Natl Acad Sci U S A* 2003;100:5286.
131. Pazour GJ, Dickert BL, Vucica Y, et al. Chlamydomonas IFT88 and its mouse homologue, polycystic kidney disease gene *tg737*, are required for assembly of cilia and flagella. *J Cell Biol* 2000;151:709.
132. Nagalakshmi VK, Ren Q, Pugh MM, et al. Dicer regulates the development of nephrogenic and ureteric compartments in the mammalian kidney. *Kidney Int* 2011;79:317.
133. Rohatgi R, Snell WJ. The ciliary membrane. *Curr Opin Cell Biol* 2010;22:541.
134. Rosenbaum JL, Witman GB. Intraflagellar transport. *Nat Rev Mol Cell Biol* 2002;3:813.
135. Molla-Herman A, Ghossoub R, Blisnick T, et al. The ciliary pocket: an endocytic membrane domain at the base of primary and motile cilia. *J Cell Sci* 2010;123:1785.
136. Jin H, White SR, Shida T, et al. The conserved Bardet-Biedl syndrome proteins assemble a coat that traffics membrane proteins to cilia. *Cell* 2010;141:1208.
137. Pennekamp P, Karcher C, Fischer A, et al. The ion channel polycystin-2 is required for left-right axis determination in mice. *Curr Biol* 2002;12:938.
138. Sarmah B, Latimer AJ, Appel B, et al. Inositol polyphosphates regulate zebrafish left-right asymmetry. *Dev Cell* 2005;9:133.
139. Schottenfeld J, Sullivan-Brown J, Burdine RD. Zebrafish curly up encodes a Pkd2 ortholog that restricts left-side-specific expression of southpaw. *Development* 2007;134:1605.
140. Praetorius HA, Spring KR. Bending the MDCK cell primary cilium increases intracellular calcium. *J Membr Biol* 2001;184:71.
141. AbouAlaiwi WA, Takahashi M, Mell BR, et al. Ciliary polycystin-2 is a mechanosensitive calcium channel involved in nitric oxide signaling cascades. *Circ Res* 2009;104:860.
142. Nonaka S, Shiratori H, Saijoh Y, et al. Determination of left-right patterning of the mouse embryo by artificial nodal flow. *Nature* 2002;418:96.
143. Nauli SM, Alenghat FJ, Luo Y, et al. Polycystins 1 and 2 mediate mechanosensation in the primary cilium of kidney cells. *Nat Genet* 2003;33:129.
144. Praetorius HA, Spring KR. Removal of the MDCK cell primary cilium abolishes flow sensing. *J Membr Biol* 2003;191:69.
145. Antoni FA. Interactions between intracellular free Ca²⁺ and cyclic AMP in neuroendocrine cells. *Cell Calcium* 2012;51:260.
146. Cowley BD Jr. Calcium, cyclic AMP, and MAP kinases: dysregulation in polycystic kidney disease. *Kidney Int* 2008;73:251.
147. Wang X, Ward CJ, Harris PC, et al. Cyclic nucleotide signaling in polycystic kidney disease. *Kidney Int* 2010;77:129.
148. Yang B, Sonawane ND, Zhao D, et al. Small-molecule CFTR inhibitors slow cyst growth in polycystic kidney disease. *J Am Soc Nephrol* 2008;19:1300.
149. Yamaguchi T, Pelling JC, Ramaswamy NT, et al. cAMP stimulates the in vitro proliferation of renal cyst epithelial cells by activating the extracellular signal-regulated kinase pathway. *Kidney Int* 2000;57:1460.
150. Verani RR, Silva FG. Histogenesis of the renal cysts in adult (autosomal dominant) polycystic kidney disease: a histochemical study. *Mod Pathol* 1988;1:457.
151. Gattone VH II, Wang X, Harris PC, et al. Inhibition of renal cystic disease development and progression by a vasopressin V2 receptor antagonist. *Nat Med* 2003;9:1323.
152. Torres VE, Wang X, Qian Q, et al. Effective treatment of an orthologous model of autosomal dominant polycystic kidney disease. *Nat Med* 2004;10:363.
153. Lieberthal W, Levine JS. Mammalian target of rapamycin and the kidney. I. The signaling pathway. *Am J Physiol Renal Physiol* 2012;303:F1.
154. Becker JU, Opazo Saez A, Zerres K, et al. The mTOR pathway is activated in human autosomal-recessive polycystic kidney disease. *Kidney Blood Press Res* 2010;33:129.
155. Dere R, Wilson PD, Sandford RN, et al. Carboxy terminal tail of polycystin-1 regulates localization of TSC2 to repress mTOR. *PLoS One* 2010;5:e9239.
156. Fischer DC, Jacoby U, Pape L, et al. Activation of the AKT/mTOR pathway in autosomal recessive polycystic kidney disease (ARPKD). *Nephrol Dial Transplant* 2009;24:1819.
157. Shillingford JM, Murcia NS, Larson CH, et al. The mTOR pathway is regulated by polycystin-1, and its inhibition reverses renal cystogenesis in polycystic kidney disease. *Proc Natl Acad Sci U S A* 2006;103:5466.
158. Boehlke C, Kotsis F, Patel V, et al. Primary cilia regulate mTORC1 activity and cell size through Lkb1. *Nat Cell Biol* 2010;12:1115.
159. Shillingford JM, Piontek K.B, Germino GG, et al. Rapamycin ameliorates PKD resulting from conditional inactivation of Pkd1. *J Am Soc Nephrol* 2010;21:489.
160. Wu M, Arcaro A, Varga Z, et al. Pulse mTOR inhibitor treatment effectively controls cyst growth but leads to severe parenchymal and glomerular hypertrophy in rat polycystic kidney disease. *Am J Physiol Renal Physiol* 2009;297:F1597.
161. Zafar I, Ravichandran K, Belibi FA, et al. Sirolimus attenuates disease progression in an orthologous mouse model of human autosomal dominant polycystic kidney disease. *Kidney Int* 2010;78:754.
162. Serra AL, Poster D, Kistler AD, et al. Sirolimus and kidney growth in autosomal dominant polycystic kidney disease. *N Engl J Med* 2010;363:820.
163. Walz G, Budde K, Mannaa M, et al. Everolimus in patients with autosomal dominant polycystic kidney disease. *N Engl J Med* 2010;363:830.
164. Shillingford JM, Leamon CP, Vlahov IR, et al. Folate-conjugated rapamycin slows progression of polycystic kidney disease. *J Am Soc Nephrol* 2012;23:1674.
165. Grumolato L, Liu G, Mong P, et al. Canonical and noncanonical Wnts use a common mechanism to activate completely unrelated coreceptors. *Genes Dev* 2010;24:2517.
166. Lancaster MA, Gleeson JG. Cystic kidney disease: the role of Wnt signaling. *Trends Mol Med* 2010;16:349.
167. Saadi-Kheddouci S, Berrebi D, Romagnolo B, et al. Early development of polycystic kidney disease in transgenic mice expressing an activated mutant of the beta-catenin gene. *Oncogene* 2001;20:5972.
168. Kim E, Arnold T, Sellin LK, et al. The polycystic kidney disease 1 gene product modulates Wnt signaling. *J Biol Chem* 1999;274:4947.
169. Lal M, Song X, Pluznick JL, et al. Polycystin-1 C-terminal tail associates with beta-catenin and inhibits canonical Wnt signaling. *Hum Mol Genet* 2008;17:3105.
170. Liu M, Shi S, Senthilnathan S, et al. Genetic variation of DKK3 may modify renal disease severity in ADPKD. *J Am Soc Nephrol* 2010;21:1510.
171. Romaker D, Puetz M, Teschner S, et al. Increased expression of secreted frizzled-related protein 4 in polycystic kidneys. *J Am Soc Nephrol* 2009;20:48.
172. Bonnet CS, Aldred M, von Ruhland C, et al. Defects in cell polarity underlie TSC and ADPKD-associated cystogenesis. *Hum Mol Genet* 2009;18:2166.
173. Fischer E, Legue E, Doyen A, et al. Defective planar cell polarity in polycystic kidney disease. *Nat Genet* 2006;38:21.
174. Majumdar A, Vainio S, Kispert A, et al. Wnt11 and Ret/Gdnf pathways cooperate in regulating ureteric branching during metanephric kidney development. *Development* 2003;130:3175.
175. Karner CM, Chirumamilla R, Aoki S, et al. Wnt9b signaling regulates planar cell polarity and kidney tubule morphogenesis. *Nat Genet* 2009;41:793.
176. Saburi S, Hester I, Fischer E, et al. Loss of Fat4 disrupts PCP signaling and oriented cell division and leads to cystic kidney disease. *Nat Genet* 2008;40:1010.
177. Cohen MM Jr. Hedgehog signaling update. *Am J Med Genet A* 2010;152A:1875.
178. Pathi S, Pagan-Westphal S, Baker DP, et al. Comparative biological responses to human Sonic, Indian, and Desert hedgehog. *Mech Dev* 2001;106:107.

179. Kim J, Kato M, Beachy PA. Gli2 trafficking links Hedgehog-dependent activation of Smoothened in the primary cilium to transcriptional activation in the nucleus. *Proc Natl Acad Sci U S A* 2009;106:21666.
180. Rohatgi R, Milenkovic L, Scott MP. Patched1 regulates hedgehog signaling at the primary cilium. *Science* 2007;317:372.
181. Caspary T, Larkins CE, Anderson KV. The graded response to Sonic Hedgehog depends on cilia architecture. *Dev Cell* 2007;12:767.
182. Kelley RI, Hennekam RC. The Smith-Lemli-Opitz syndrome. *J Med Genet* 2000;37:321.
183. Hu MC, Mo R, Bhella S, et al. GLI3-dependent transcriptional repression of Gli1, Gli2 and kidney patterning genes disrupts renal morphogenesis. *Development* 2006;133:569.
184. Chan SK, Riley PR, Price KL, et al. Corticosteroid-induced kidney dysmorphogenesis is associated with deregulated expression of known cystogenic molecules, as well as Indian hedgehog. *Am J Physiol Renal Physiol* 2010;298:F346.
185. Lonsler RR, Glenn GM, Walther M, et al. von Hippel-Lindau disease. *Lancet* 2003;361:2059.
186. Chauveau D, Duvic C, Chretien Y, et al. Renal involvement in von Hippel-Lindau disease. *Kidney Int* 1996;50:944.
187. Northrup BE, Jokerst CE, Grubb RL III, et al. Hereditary renal tumor syndromes: imaging findings and management strategies. *AJR Am J Roentgenol* 2012;199:1294.
188. Gallou C, Chauveau D, Richard S, et al. Genotype-phenotype correlation in von Hippel-Lindau families with renal lesions. *Hum Mutat* 2004;24:215.
189. Richard S, Lidereau R, Giraud S. The growing family of hereditary renal cell carcinoma. *Nephrol Dial Transplant* 2004;19:2954.
190. Taylor SR, Singh J, Sagoo MS, et al. Clinical and molecular features associated with cystic visceral lesions in von hippel-lindau disease. *Open Ophthalmol J* 2012;6:83.
191. Linehan WM, Vasselli J, Srinivasan R, et al. Genetic basis of cancer of the kidney: disease-specific approaches to therapy. *Clin Cancer Res* 2004;10:6282S.
192. Brannon AR, Rathmell WK. Renal cell carcinoma: where will the state-of-the-art lead us? *Curr Oncol Rep* 2010;12:193.
193. Montani M, Heinimann K, von Teichman A, et al. VHL-gene deletion in single renal tubular epithelial cells and renal tubular cysts: further evidence for a cyst-dependent progression pathway of clear cell renal carcinoma in von Hippel-Lindau disease. *Am J Surg Pathol* 2010;34:806.
194. von Teichman A, Comperat E, Behnke S, et al. VHL mutations and dysregulation of pVHL- and PTEN-controlled pathways in multilocular cystic renal cell carcinoma. *Mod Pathol* 2011;24:571.
195. Rakowski SK, Winterkorn EB, Paul E, et al. Renal manifestations of tuberous sclerosis complex: Incidence, prognosis, and predictive factors. *Kidney Int* 2006;70:1777.
196. Ewalt DH, Sheffield E, Sparagana SP, et al. Renal lesion growth in children with tuberous sclerosis complex. *J Urol* 1998;160:141.
197. Hancock E, Tomkins S, Sampson J, et al. Lymphangioleiomyomatosis and tuberous sclerosis. *Respir Med* 2002;96:7.
198. Jones AC, Shyamsundar MM, Thomas MW, et al. Comprehensive mutation analysis of TSC1 and TSC2-and phenotypic correlations in 150 families with tuberous sclerosis. *Am J Hum Genet* 1999;64:1305.
199. Casper KA, Donnelly LF, Chen B, et al. Tuberous sclerosis complex: renal imaging findings. *Radiology* 2002;225:451.
200. Nagashima Y, Ohaki Y, Tanaka Y, et al. A case of renal angiomyolipomas associated with multiple and various hamartomatous microlesions. *Virchows Arch A Pathol Anat Histopathol* 1988;413:177.
201. Potter CJ, Huang H, Xu T. Drosophila Tsc1 functions with Tsc2 to antagonize insulin signaling in regulating cell growth, cell proliferation, and organ size. *Cell* 2001;105:357.
202. Mak BC, Kenerson HL, Aicher LD, et al. Aberrant beta-catenin signaling in tuberous sclerosis. *Am J Pathol* 2005;167:107.
203. Turbiner J, Amin MB, Humphrey PA, et al. Cystic nephroma and mixed epithelial and stromal tumor of kidney: a detailed clinicopathologic analysis of 34 cases and proposal for renal epithelial and stromal tumor (REST) as a unifying term. *Am J Surg Pathol* 2007;31:489.
204. Hill DA, Ivanovich J, Priest JR, et al. DICER1 mutations in familial pleuropulmonary blastoma. *Science* 2009;325:965.
205. Terada N, Ichioka K, Matsuta Y, et al. The natural history of simple renal cysts. *J Urol* 2002;167:21.
206. Choyke PL. Acquired cystic kidney disease. *Eur Radiol* 2000;10:1716.
207. Mattoo TK, Greifer I, Geva P, et al. Acquired renal cystic disease in children and young adults on maintenance dialysis. *Pediatr Nephrol* 1997;11:447.
208. Ishikawa I, Saito Y, Asaka M, et al. Twenty-year follow-up of acquired renal cystic disease. *Clin Nephrol* 2003;59:153.
209. Sule N, Yakupoglu U, Shen SS, et al. Calcium oxalate deposition in renal cell carcinoma associated with acquired cystic kidney disease: a comprehensive study. *Am J Surg Pathol* 2005;29:443.
210. Casale P, Grady RW, Feng WC, et al. The pediatric caliceal diverticulum: diagnosis and laparoscopic management. *J Endourol* 2004;18:668.
211. DeMarco RT, Cain MP, Davis MM. Xanthogranulomatous pyelonephritis associated with a congenital caliceal diverticulum. *Urology* 2001;57:168.
212. Mullins JR, Shield CF III, Porter MG. Hygroma renalis: two cases within a family and a literature review. *Surgery* 1992;111:339.
213. Antonopoulos P, Charalampopoulos G, Constantinidis F, et al. Familial renal retroperitoneal lymphangiomas: personal experience and review of literature. *JBR-BTR* 2010;93:258.
214. Karkouche R, Rocher L, Guettier C, et al. Bilateral renal lymphangiomas: imaging and histopathologic findings. *Abdom Imaging* 2013;38(4):858–862.
215. Winyard P, Chitty LS. Dysplastic kidneys. *Semin Fetal Neonatal Med* 2008;13:142.
216. Renkema KY, Winyard PJ, Skovorodkin IN, et al. Novel perspectives for investigating congenital anomalies of the kidney and urinary tract (CAKUT). *Nephrol Dial Transplant* 2011;26:3843.
217. Caskey CF, Hu X, Ferrara KW. Leveraging the power of ultrasound for therapeutic design and optimization. *J Control Release* 2011;156:297.
218. Winyard PJ, Nauta J, Lirenman DS, et al. Deregulation of cell survival in cystic and dysplastic renal development. *Kidney Int* 1996;49:135.
219. Coles HS, Burne JF, Raff MC. Large-scale normal cell death in the developing rat kidney and its reduction by epidermal growth factor. *Development* 1993;118:777.
220. Chevalier RL. Mechanisms of fetal and neonatal renal impairment by pharmacologic inhibition of angiotensin. *Curr Med Chem* 2012;19:4572.
221. Miyazaki Y, Oshima K, Fogo A, et al. Evidence that bone morphogenetic protein 4 has multiple biological functions during kidney and urinary tract development. *Kidney Int* 2003;63:835.
222. Penna FJ, Elder JS. CKD and bladder problems in children. *Adv Chronic Kidney Dis* 2011;18:362.
223. Hardelin JR, Dode C. The complex genetics of Kallmann syndrome: KAL1, FGF1, FGF8, PROKR2, PROKR2, et al. *Sex Dev* 2008;2:181.
224. Kirk JM, Grant DB, Besser GM, et al. Unilateral renal aplasia in X-linked Kallmann's syndrome. *Clin Genet* 1994;46:260.
225. van Eerde AM, Duran K, van Riel E, et al. Genes in the ureteric budding pathway: association study on vesico-ureteral reflux patients. *PLoS One* 2012;7:e31327.
226. Costantini F. GDNF/Ret signaling and renal branching morphogenesis: from mesenchymal signals to epithelial cell behaviors. *Organogenesis* 2010;6:252.
227. Yosypiv IV, Boh MK, Spera MA, et al. Downregulation of Spry-1, an inhibitor of GDNF/Ret, causes angiotensin II-induced ureteric bud branching. *Kidney Int* 2008;74:1287.
228. Jain S. The many faces of RET dysfunction in kidney. *Organogenesis* 2009;5:177.
229. Vega QC, Worby CA, Lechner MS, et al. Glial cell line-derived neurotrophic factor activates the receptor tyrosine kinase RET and promotes kidney morphogenesis. *Proc Natl Acad Sci U S A* 1996;93:10657.
230. Michos O, Cebrian C, Hyink D, et al. Kidney development in the absence of Gdnf and Spry1 requires Fgf10. *PLoS Genet* 2010;6:e1000809.
231. Pichel JG, Shen L, Sheng HZ, et al. GDNF is required for kidney development and enteric innervation. *Cold Spring Harb Symp Quant Biol* 1996;61:445.
232. Schuchardt A, D'Agati V, Larsson-Blomberg L, et al. Defects in the kidney and enteric nervous system of mice lacking the tyrosine kinase receptor Ret. *Nature* 1994;367:380.
233. Pachnis V, Mankoo B, Costantini F. Expression of the c-ret proto-oncogene during mouse embryogenesis. *Development* 1993;119:1005.

234. Harshman LA, Brophy PD. PAX2 in human kidney malformations and disease. *Pediatr Nephrol* 2012;27:1265.
235. Kiefer SM, Robbins L, Stumpff KM, et al. Sall1-dependent signals affect Wnt signaling and ureter tip fate to initiate kidney development. *Development* 2010;137:3099.
236. Reidy KJ, Rosenblum ND. Cell and molecular biology of kidney development. *Semin Nephrol* 2009;29:321.
237. Batourina E, Gim S, Bello N, et al. Vitamin A controls epithelial/mesenchymal interactions through Ret expression. *Nat Genet* 2001;27:74.
238. Brophy PD, Ostrom L, Lang KM, et al. Regulation of ureteric bud outgrowth by Pax2-dependent activation of the glial derived neurotrophic factor gene. *Development* 2001;128:4747.
239. Sainio K, Suvanto P, Davies J, et al. Glial-cell-line-derived neurotrophic factor is required for bud initiation from ureteric epithelium. *Development* 1997;124:4077.
240. Kume T, Deng K, Hogan BL. Murine forkhead/winged helix genes Foxc1 (Mfl) and Foxc2 (Mfh1) are required for the early organogenesis of the kidney and urinary tract. *Development* 2000;127:1387.
241. Grieshammer U, Le M, Plump AS, et al. SLIT2-mediated ROBO2 signaling restricts kidney induction to a single site. *Dev Cell* 2004;6:709.
242. Qiao J, Sakurai H, Nigam SK. Branching morphogenesis independent of mesenchymal-epithelial contact in the developing kidney. *Proc Natl Acad Sci U S A* 1999;96:7330.
243. Reginin A, Clarkson M, Neirijnck Y, et al. SOX9 controls epithelial branching by activating RET effector genes during kidney development. *Hum Mol Genet* 2011;20:1143.
244. Bertoli-Avella AM, Conte ML, Punzo F, et al. ROBO2 gene variants are associated with familial vesicoureteral reflux. *J Am Soc Nephrol* 2008;19:825.
245. Lu W, van Eerde AM, Fan X, et al. Disruption of ROBO2 is associated with urinary tract anomalies and confers risk of vesicoureteral reflux. *Am J Hum Genet* 2007;80:616.
246. Basson MA, Akbulut S, Watson-Johnson J, et al. Sprouty1 is a critical regulator of GDNF/RET-mediated kidney induction. *Dev Cell* 2005;8:229.
247. Reidy K, Tufro A. Semaphorins in kidney development and disease: modulators of ureteric bud branching, vascular morphogenesis, and podocyte-endothelial crosstalk. *Pediatr Nephrol* 2011;26:1407.
248. Hains D, Sims-Lucas S, Kish K, et al. Role of fibroblast growth factor receptor 2 in kidney mesenchyme. *Pediatr Res* 2008;64:592.
249. Sims-Lucas S, Di Giovanni V, Schaefer C, et al. Ureteric morphogenesis requires Fgfr1 and Fgfr2/Frs2alpha signaling in the metanephric mesenchyme. *J Am Soc Nephrol* 2012;23:607.
250. Pitera JE, Scambler PJ, Woolf AS. Fras1, a basement membrane-associated protein mutated in Fraser syndrome, mediates both the initiation of the mammalian kidney and the integrity of renal glomeruli. *Hum Mol Genet* 2008;17:3953.
251. Pitera JE, Woolf AS, Basson MA, et al. Sprouty1 haploinsufficiency prevents renal agenesis in a model of Fraser syndrome. *J Am Soc Nephrol* 2012;23:1790.
252. Lu BC, Cebrian C, Chi X, et al. Etv4 and Etv5 are required downstream of GDNF and Ret for kidney branching morphogenesis. *Nat Genet* 2009;41:1295.
253. Goncalves A, Zeller R. Genetic analysis reveals an unexpected role of BMP7 in initiation of ureteric bud outgrowth in mouse embryos. *PLoS One* 2011;6:e19370.
254. Lye CM, Fasano L, Woolf AS. Ureter myogenesis: putting Teashirt into context. *J Am Soc Nephrol* 2010;21:24.
255. Halder G, Callaerts P, Gehring WJ. Induction of ectopic eyes by targeted expression of the eyeless gene in Drosophila. *Science* 1995;267:1788.
256. Cohen T, Loutochin O, Amin M, et al. PAX2 is reactivated in urinary tract obstruction and partially protects collecting duct cells from programmed cell death. *Am J Physiol Renal Physiol* 2007;292:F1267.
257. Ostrom L, Tang MJ, Gruss P, et al. Reduced Pax2 gene dosage increases apoptosis and slows the progression of renal cystic disease. *Dev Biol* 2000;219:250.
258. Bower M, Salomon R, Allanson J, et al. Update of PAX2 mutations in renal coloboma syndrome and establishment of a locus-specific database. *Hum Mutat* 2012;33:457.
259. Torres, M, Gomez-Pardo E, Dressler GR, et al. Pax-2 controls multiple steps of urogenital development. *Development* 1995;121:4057.
260. Dressler GR, Wilkinson JE, Rothenpieler UW, et al. Deregulation of Pax-2 expression in transgenic mice generates severe kidney abnormalities. *Nature* 1993;362:65.
261. Patel SR, Dressler GR. Expression of Pax2 in the intermediate mesoderm is regulated by YY1. *Dev Biol* 2004;267:505.
262. Gao X, Chen X, Taglienti M, et al. Angioblast-mesenchyme induction of early kidney development is mediated by Wt1 and Vegfa. *Development* 2005;132:5437.
263. McConnell MJ, Cunliffe HE, Chua LJ, et al. Differential regulation of the human Wilms tumour suppressor gene (WT1) promoter by two isoforms of PAX2. *Oncogene* 1997;14:2689.
264. Ryan G, Steele-Perkins V, Morris JE, et al. Repression of Pax-2 by WT1 during normal kidney development. *Development* 1995;121:867.
265. Plachov D, Chowdhury K, Walther C, et al. Pax8, a murine paired box gene expressed in the developing excretory system and thyroid gland. *Development* 1990;110:643.
266. Poleev A, Fickenscher H, Mundlos S, et al. PAX8, a human paired box gene: isolation and expression in developing thyroid, kidney and Wilms' tumors. *Development* 1992;116:611.
267. Mansouri A, Chowdhury K, Gruss P. Follicular cells of the thyroid gland require Pax8 gene function. *Nat Genet* 1998;19:87.
268. Bouchard M, Pfeffer P, Busslinger M. Functional equivalence of the transcription factors Pax2 and Pax5 in mouse development. *Development* 2000;127:3703.
269. Hueber PA, Fukuzawa R, Elkares R, et al. PAX3 is expressed in the stromal compartment of the developing kidney and in Wilms tumors with myogenic phenotype. *Pediatr Dev Pathol* 2009;12:347.
270. Md Zin R, Murch A, Charles A. Pathology, genetics and cytogenetics of Wilms' tumour. *Pathology* 2011;43:302.
271. Kreidberg JA, Sariola H, Loring JM, et al. WT-1 is required for early kidney development. *Cell* 1993;74:679.
272. Little M, Wells C. A clinical overview of WT1 gene mutations. *Hum Mutat* 1997;9:209.
273. Klamt B, Koziell A, Poulat F, et al. Frasier syndrome is caused by defective alternative splicing of WT1 leading to an altered ratio of WT1 +/-KTS splice isoforms. *Hum Mol Genet* 1998;7:709.
274. Kreidberg JA, Hartwig S. Wilms' tumor-1: a riddle wrapped in a mystery, inside a kidney. *Kidney Int* 2008;74:411.
275. Gross I, Morrison DJ, Hyink DP, et al. The receptor tyrosine kinase regulator Sprouty1 is a target of the tumor suppressor WT1 and important for kidney development. *J Biol Chem* 2003;278:41420.
276. Kim MS, Yoon SK, Bollig F, et al. A novel Wilms tumor 1 (WT1) target gene negatively regulates the WNT signaling pathway. *J Biol Chem* 2010;285:14585.
277. Kreidberg JA. WT1 and kidney progenitor cells. *Organogenesis* 2010;6:61.
278. Hartwig S, Ho J, Pandey P, et al. Genomic characterization of Wilms' tumor suppressor 1 targets in nephron progenitor cells during kidney development. *Development* 2010;137:1189.
279. Schmidt-Ott KM, Barasch J. WNT/beta-catenin signaling in nephron progenitors and their epithelial progeny. *Kidney Int* 2008;74:1004.
280. Vainio SJ. Nephrogenesis regulated by Wnt signaling. *J Nephrol* 2003;16:279.
281. Torban E, Dziarmaga A, Iglesias D, et al. PAX2 activates WNT4 expression during mammalian kidney development. *J Biol Chem* 2006;281:12705.
282. Stark K, Vainio S, Vassileva G, et al. Epithelial transformation of metanephric mesenchyme in the developing kidney regulated by Wnt-4. *Nature* 1994;372:679.
283. Kispert A, Vainio S, McMahon AP. Wnt-4 is a mesenchymal signal for epithelial transformation of metanephric mesenchyme in the developing kidney. *Development* 1998;125:4225.
284. Biason-Lauber A, Konrad D, Navratil F, et al. A WNT4 mutation associated with Mullerian-duct regression and virilization in a 46, XX woman. *N Engl J Med* 2004;351:792.
285. Lako M, Strachan T, Bullen P, et al. Isolation, characterisation and embryonic expression of WNT11, a gene which maps to 11q13.5 and has possible roles in the development of skeleton, kidney and lung. *Gene* 1998;219:101.
286. Iglesias DM, Hueber PA, Chu L, et al. Canonical WNT signaling during kidney development. *Am J Physiol Renal Physiol* 2007;293:F494.

287. Sato A, Kishida S, Tanaka T, et al. Sall1, a causative gene for Townes-Brocks syndrome, enhances the canonical Wnt signaling by localizing to heterochromatin. *Biochem Biophys Res Commun* 2004;319:103.
288. Karner CM, Das A, Ma Z, et al. Canonical Wnt9b signaling balances progenitor cell expansion and differentiation during kidney development. *Development* 2011;138:1247.
289. Yates LL, Papakrivopoulou J, Long DA, et al. The planar cell polarity gene Vangl2 is required for mammalian kidney-branching morphogenesis and glomerular maturation. *Hum Mol Genet* 2010;19:4663.
290. Boyle SC, Kim M, Valerius MT, et al. Notch pathway activation can replace the requirement for Wnt4 and Wnt9b in mesenchymal-to-epithelial transition of nephron stem cells. *Development* 2011;138:4245.
291. Sirin Y, Susztak K. Notch in the kidney: development and disease. *J Pathol* 2012;226:394.
292. Itasaki N, Hoppler S. Crosstalk between Wnt and bone morphogenic protein signaling: a turbulent relationship. *Dev Dyn* 2010;239:16.
293. Martinez G, Bertram JF. Organisation of bone morphogenetic proteins in renal development. *Nephron Exp Nephrol* 2003;93:e18.
294. Michos O, Goncalves A, Lopez-Rios J, et al. Reduction of BMP4 activity by gremlin 1 enables ureteric bud outgrowth and GDNF/WNT11 feedback signalling during kidney branching morphogenesis. *Development* 2007;134:2397.
295. Miyazaki Y, Oshima K, Fogo A, et al. Bone morphogenetic protein 4 regulates the budding site and elongation of the mouse ureter. *J Clin Invest* 2000;105:863.
296. Piscione TD, Yager TD, Gupta IR, et al. BMP-2 and OP-1 exert direct and opposite effects on renal branching morphogenesis. *Am J Physiol* 1997;273:F961.
297. Dudley AT, Robertson EJ. Overlapping expression domains of bone morphogenetic protein family members potentially account for limited tissue defects in BMP7 deficient embryos. *Dev Dyn* 1997;208:349.
298. Dudley AT, Lyons KM, Robertson EJ. A requirement for bone morphogenetic protein-7 during development of the mammalian kidney and eye. *Genes Dev* 1995;9:2795.
299. Luo G, Hofmann C, Bronckers AL, et al. BMP-7 is an inducer of nephrogenesis, and is also required for eye development and skeletal patterning. *Genes Dev* 1995;9:2808.
300. Piscione TD, Phan T, Rosenblum ND. BMP7 controls collecting tubule cell proliferation and apoptosis via Smad1-dependent and -independent pathways. *Am J Physiol Renal Physiol* 2001;280:F19.
301. Hu MC, Piscione TD, Rosenblum ND. Elevated SMAD1/beta-catenin molecular complexes and renal medullary cystic dysplasia in ALK3 transgenic mice. *Development* 2003;130:2753.
302. Sugimoto H, LeBleu VS, Bosukonda D, et al. Activin-like kinase 3 is important for kidney regeneration and reversal of fibrosis. *Nat Med* 2012;18:396.
303. Chi L, Saarela U, Railo A, et al. A secreted BMP antagonist, Cer1, fine tunes the spatial organization of the ureteric bud tree during mouse kidney development. *PLoS One* 2011;6:e27676.
304. Hatini V, Huh SO, Herzlinger D, et al. Essential role of stromal mesenchyme in kidney morphogenesis revealed by targeted disruption of Winged Helix transcription factor BF-2. *Genes Dev* 1996;10:1467.
305. Levinson RS, Batourina E, Choi C, et al. Foxd1-dependent signals control cellularity in the renal capsule, a structure required for normal renal development. *Development* 2005;132:529.
306. Adalat S, Woolf AS, Johnstone KA, et al. HNF1B mutations associate with hypomagnesemia and renal magnesium wasting. *J Am Soc Nephrol* 2009;20:1123.
307. Kolatsi-Joannou M, Bingham C, Ellard S, et al. Hepatocyte nuclear factor-1beta: a new kindred with renal cysts and diabetes and gene expression in normal human development. *J Am Soc Nephrol* 2001;12:2175.
308. Barbacci E, Reber M, Ott MO, et al. Variant hepatocyte nuclear factor 1 is required for visceral endoderm specification. *Development* 1999;126:4795.
309. Zhang Y, Wada J, Yasuhara A, et al. The role for HNF-1beta-targeted collectrin in maintenance of primary cilia and cell polarity in collecting duct cells. *PLoS One* 2007;2:e414.
310. Dudziak K, Mottalebi N, Senkel S, et al. Transcription factor HNF1beta and novel partners affect nephrogenesis. *Kidney Int* 2008;74:210.
311. Jenkins RH, Martin J, Phillips AO, et al. Transforming growth factor beta1 represses proximal tubular cell microRNA-192 expression through decreased hepatocyte nuclear factor DNA binding. *Biochem J* 2012;443:407.
312. Mancusi S, La Manna A, Bellini G, et al. HNF-1beta mutation affects PKD2 and SOCS3 expression causing renal cysts and diabetes in MODY5 kindred. *J Nephrol* 2013;26:207.
313. James RG, Kamei CN, Wang Q, et al. Odd-skipped related 1 is required for development of the metanephric kidney and regulates formation and differentiation of kidney precursor cells. *Development* 2006;133:2995.
314. Mudumana SP, Hentschel D, Liu Y, et al. odd skipped related1 reveals a novel role for endoderm in regulating kidney versus vascular cell fate. *Development* 2008;135:3355.
315. Plisov S, Tsang M, Shi G, et al. Cited1 is a bifunctional transcriptional cofactor that regulates early nephronic patterning. *J Am Soc Nephrol* 2005;16:1632.
316. Brown AC, Adams D, de Caestecker M, et al. FGF/EGF signaling regulates the renewal of early nephron progenitors during embryonic development. *Development* 2011;138:5099.
317. Nie X, Sun J, Gordon RE, et al. SIX1 acts synergistically with TBX18 in mediating ureteral smooth muscle formation. *Development* 2010;137:755.
318. Self M, Lagutin OV, Bowling B, et al. Six2 is required for suppression of nephrogenesis and progenitor renewal in the developing kidney. *EMBO J* 2006;25:5214.
319. Abdelhak S, Kalatzis V, Heilig R, et al. A human homologue of the Drosophila eyes absent gene underlies branchio-oto-renal (BOR) syndrome and identifies a novel gene family. *Nat Genet* 1997;15:157.
320. Ruf RG, Xu PX, Silvius D, et al. SIX1 mutations cause branchio-oto-renal syndrome by disruption of EYA1-SIX1-DNA complexes. *Proc Natl Acad Sci U S A* 2004;101:8090.
321. Xu PX, Adams J, Peters H, et al. Eya1-deficient mice lack ears and kidneys and show abnormal apoptosis of organ primordia. *Nat Genet* 1999;23:113.
322. Bates CM. Role of fibroblast growth factor receptor signaling in kidney development. *Pediatr Nephrol* 2007;22:343.
323. Barasch J, Qiao J, McWilliams G, et al. Ureteric bud cells secrete multiple factors, including bFGF, which rescue renal progenitors from apoptosis. *Am J Physiol* 1997;273:F757.
324. Poladia DP, Kish K, Kutay B, et al. Role of fibroblast growth factor receptors 1 and 2 in the metanephric mesenchyme. *Dev Biol* 2006;291:325.
325. Watanabe T, Costantini F. Real-time analysis of ureteric bud branching morphogenesis in vitro. *Dev Biol* 2004;271:98.
326. Gong KQ, Yallowitz AR, Sun H, et al. A Hox-Eya-Pax complex regulates early kidney developmental gene expression. *Mol Cell Biol* 2007;27:7661.
327. Yallowitz AR, Hrycaj SM, Short KM, et al. Hox10 genes function in kidney development in the differentiation and integration of the cortical stroma. *PLoS One* 2011;6:e23410.
328. Cano-Gauci DF, Song HH, Yang H, et al. Glypican-3-deficient mice exhibit developmental overgrowth and some of the abnormalities typical of Simpson-Golabi-Behmel syndrome. *J Cell Biol* 1999;146:255.
329. Steer DL, Shah MM, Bush KT, et al. Regulation of ureteric bud branching morphogenesis by sulfated proteoglycans in the developing kidney. *Dev Biol* 2004;272:310.
330. Woolf AS, Price KL, Scambler PJ, et al. Evolving concepts in human renal dysplasia. *J Am Soc Nephrol* 2004;15:998.
331. Beck AD. The effect of intra-uterine urinary obstruction upon the development of the fetal kidney. *J Urol* 1971;105:784.
332. Attar R, Quinn F, Winyard PJ, et al. Short-term urinary flow impairment deregulates PAX2 and PCNA expression and cell survival in fetal sheep kidneys. *Am J Pathol* 1998;152:1225.
333. Peters CA, Carr MC, Lais A, et al. The response of the fetal kidney to obstruction. *J Urol* 1992;148:503.
334. Yang SP, Woolf AS, Quinn F, et al. Deregulation of renal transforming growth factor-beta1 after experimental short-term ureteric obstruction in fetal sheep. *Am J Pathol* 2001;159:109.
335. Yang SP, Woolf AS, Yuan HT, et al. Potential biological role of transforming growth factor-beta1 in human congenital kidney malformations. *Am J Pathol* 2000;157:1633.
336. Steinhart GF, Liapis H, Phillips B, et al. Insulin-like growth factor improves renal architecture of fetal kidneys with complete ureteral obstruction. *J Urol* 1995;154:690.
337. Chevalier RL, Goyal S, Wolstenholme JT, et al. Obstructive nephropathy in the neonatal rat is attenuated by epidermal growth factor. *Kidney Int* 1998;54:38.

338. Thornhill BA, Chevalier RL. Variable partial unilateral ureteral obstruction and its release in the neonatal and adult mouse. *Methods Mol Biol* 2012;886:381.
339. Glick PL, Harrison MR, Adzick NS, et al. Correction of congenital hydronephrosis in utero IV: in utero decompression prevents renal dysplasia. *J Pediatr Surg* 1984;19:649.
340. Chevalier RL, Thornhill BA, Chang AY, et al. Recovery from release of ureteral obstruction in the rat: relationship to nephrogenesis. *Kidney Int* 2002;61:2033.
341. Morris RK, Malin GL, Khan KS, et al. Systematic review of the effectiveness of antenatal intervention for the treatment of congenital lower urinary tract obstruction. *BJOG* 2010;117:382.
342. Shepard T. *Catalog of Teratogenic Agents*, 13th ed. Baltimore, MD: The Johns Hopkins University Press, 2010.
343. Solhaug MJ, Bolger PM, Jose PA. The developing kidney and environmental toxins. *Pediatrics* 2004;113:1084.
344. Polifka JE. Is there an embryopathy associated with first-trimester exposure to angiotensin-converting enzyme inhibitors and angiotensin receptor antagonists? A critical review of the evidence. *Birth Defects Res A Clin Mol Teratol* 2012;94:576.
345. Chugh SS, Wallner EI, Kanwar YS. Renal development in high-glucose ambience and diabetic embryopathy. *Semin Nephrol* 2003;23:583.
346. Woolf AS. Environmental influences on renal tract development: a focus on maternal diet and the glucocorticoid hypothesis. *Klin Padiatr* 2011;223(Suppl 1):S10.
347. Abrass CK, Spicer D, Berfield AK, et al. Diabetes induces changes in glomerular development and laminin-beta 2 (s-laminin) expression. *Am J Pathol* 1997;151:1131.
348. Duong Van Huyen JP, Amri K, Belair MF, et al. Spatiotemporal distribution of insulin-like growth factor receptors during nephrogenesis in fetuses from normal and diabetic rats. *Cell Tissue Res* 2003;314:367.
349. Rothman KJ, Moore LL, Singer MR, et al. Teratogenicity of high vitamin A intake. *N Engl J Med* 1995;333:1369.
350. Padmanabhan R. Retinoic acid-induced caudal regression syndrome in the mouse fetus. *Reprod Toxicol* 1998;12:139.
351. Tse HK, Leung MB, Woolf AS, et al. Implication of Wt1 in the pathogenesis of nephrogenic failure in a mouse model of retinoic acid-induced caudal regression syndrome. *Am J Pathol* 2005;166:1295.
352. Vilar J, Lalou C, Duong Van Huyen JP, et al. Midkine is involved in kidney development and in its regulation by retinoids. *J Am Soc Nephrol* 2002;13:668.
353. Batourina E, Choi C, Paragas N, et al. Distal ureter morphogenesis depends on epithelial cell remodeling mediated by vitamin A and Ret. *Nat Genet* 2002;32:109.
354. Barker DJ. The developmental origins of well-being. *Philos Trans R Soc Lond B Biol Sci* 2004;359:1359.
355. Fisher RE, Steele M, Karrow NA. Fetal programming of the neuroendocrine-immune system and metabolic disease. *J Pregnancy* 2012;2012:792934.
356. Brenner BM, Garcia DL, Anderson S. Glomeruli and blood pressure. Less of one, more the other? *Am J Hypertens* 1988;1:335.
357. Welham SJ, Wade A, Woolf AS. Protein restriction in pregnancy is associated with increased apoptosis of mesenchymal cells at the start of rat metanephrogenesis. *Kidney Int* 2002;61:1231.
358. Gilbert T, Merlet-Benichou C. Retinoids and nephron mass control. *Pediatr Nephrol* 2000;14:1137.
359. Lisle SJ, Lewis RM, Petry CJ, et al. Effect of maternal iron restriction during pregnancy on renal morphology in the adult rat offspring. *Br J Nutr* 2003;90:33.
360. Swali A, McMullen S, Hayes H, et al. Processes underlying the nutritional programming of embryonic development by iron deficiency in the rat. *PLoS One* 2012;7:e48133.
361. Carbillon L, Seince N, Largilliere C, et al. First-trimester diagnosis of sirenómelia. A case report. *Fetal Diagn Ther* 2001;16:284.
362. Favorito LA, Cardinot TM, Morais AR, et al. Urogenital anomalies in human male fetuses. *Early Hum Dev* 2004;79:41.
363. Murphy JJ, Fraser GC, Blair GK. Sirenómelia: case of the surviving mermaid. *J Pediatr Surg* 1992;27:1265.
364. Cascio S, Paran S, Puri P. Fetalized urological anomalies in children with unilateral renal agenesis. *J Urol* 1999;162:1081.
365. Hiraoka M, Tsukahara H, Ohshima Y, et al. Renal aplasia is the predominant cause of congenital solitary kidneys. *Kidney Int* 2002;61:1840.
366. Ghavamian R, Chevillie JC, Lohse CM, et al. Renal cell carcinoma in the solitary kidney: an analysis of complications and outcome after nephron sparing surgery. *J Urol* 2002;168:454.
367. Jeong GH, Park BS, Jeong TK, et al. Unilateral autosomal dominant polycystic kidney disease with contralateral renal agenesis: a case report. *J Korean Med Sci* 2003;18:284.
368. Watanabe T. Membranous glomerulonephritis in a patient with unilateral renal agenesis. *Nephron* 2002;91:159.
369. Gerard M, Layet V, Costa T, et al. Sirenómelia and caudal malformations in two families. *Am J Med Genet A* 2012;158A:1801.
370. Fletcher J, Hu M, Berman Y, et al. Multicystic dysplastic kidney and variable phenotype in a family with a novel deletion mutation of PAX2. *J Am Soc Nephrol* 2005;16:2754.
371. Martinovic-Bouriel J, Benachi A, Bonniere M, et al. PAX2 mutations in fetal renal hypodysplasia. *Am J Med Genet A* 2010;152A:830.
372. Suzuki K, Kurokawa S, Muraishi O, et al. Segmental multicystic dysplastic kidney in an adult woman. *Urol Int* 2001;66:51.
373. Rackley RR, Angermeier KW, Levin H, et al. Renal cell carcinoma arising in a regressed multicystic dysplastic kidney. *J Urol* 1994;152:1543.
374. Damen-Elias HA, Stoutenbeek PH, Visser GH, et al. Concomitant anomalies in 100 children with unilateral multicystic kidney. *Ultrasound Obstet Gynecol* 2005;25:384.
375. Chatterjee R, Ramos E, Hoffman M, et al. Traditional and targeted exome sequencing reveals common, rare and novel functional deleterious variants in RET-signaling complex in a cohort of living US patients with urinary tract malformations. *Hum Genet* 2012;131:1725.
376. Liapis H. Biology of congenital obstructive nephropathy. *Nephron Exp Nephrol* 2003;93:e87.
377. Shibata S, Nagata M. Pathogenesis of human renal dysplasia: an alternative scenario to the major theories. *Pediatr Int* 2003;45:605.
378. Srivastava T, Garola RE, Hellerstein S. Autosomal dominant inheritance of multicystic dysplastic kidney. *Pediatr Nephrol* 1999;13:481.
379. Li Volti S, Faiella A, Perrotta S, et al. Non-allelic heterogeneity in familial unilateral renal adysplasia. *Ann Genet* 2002;45:123.
380. Sekine T, Namai Y, Yanagisawa A, et al. A familial case of multicystic dysplastic kidney. *Pediatr Nephrol* 2005;20:1245.
381. Konda R, Sato H, Ito S, et al. Renin containing cells are present predominantly in scarred areas but not in dysplastic regions in multicystic dysplastic kidney. *J Urol* 2001;166:1910.
382. Liapis H, Doshi RH, Watson MA, et al. Reduced renin expression and altered gene transcript profiles in multicystic dysplastic kidneys. *J Urol* 2002;168:1816.
383. Narchi H. Risk of hypertension with multicystic kidney disease: a systematic review. *Arch Dis Child* 2005;90:921.
384. Eckoldt F, Woderich R, Wolke S, et al. Follow-up of unilateral multicystic kidney dysplasia after prenatal diagnosis. *J Matern Fetal Neonatal Med* 2003;14:177.
385. Ylinen E, Ahonen S, Ala-Houhala M, et al. Nephrectomy for multicystic dysplastic kidney: if and when? *Urology* 2004;63:768.
386. Norton KI. New imaging applications in the evaluation of pediatric renal disease. *Curr Opin Pediatr* 2003;15:186.
387. Salomon R, Tellier AL, Attie-Bitach T, et al. PAX2 mutations in oligomeganephronia. *Kidney Int* 2001;59:457.
388. Drukker A. Oligonephropathy: from a rare childhood disorder to a possible health problem in the adult. *Isr Med Assoc J* 2002;4:191.
389. Rodriguez MM, Gomez A, Abitbol C, et al. Comparative renal histomorphometry: a case study of oligonephropathy of prematurity. *Pediatr Nephrol* 2005;20:945.
390. Gribouval O, Gonzales M, Neuhaus T, et al. Mutations in genes in the renin-angiotensin system are associated with autosomal recessive renal tubular dysgenesis. *Nat Genet* 2005;37:964.
391. Gribouval O, Moriniere V, Pawtowski A, et al. Spectrum of mutations in the renin-angiotensin system genes in autosomal recessive renal tubular dysgenesis. *Hum Mutat* 2012;33:316.
392. Sequeira Lopez ML, Pentz ES, Nomasa T, et al. Renin cells are precursors for multiple cell types that switch to the renin phenotype when homeostasis is threatened. *Dev Cell* 2004;6:719.

The Nephrotic Syndrome and Minimal Change Disease

Filtration of macromolecules 173

- Brief review of anatomy 173
- Factors involved in glomerular filtration 174
- Mechanisms of proteinuria and the effacement of foot processes 176
- Effects of proteinuria on the tubules and interstitium 177

Pathophysiology and complications of the nephrotic syndrome 177

- Pathophysiology of the nephrotic syndrome 177
- Complications of the nephrotic syndrome 179

Causes and conditions associated with the nephrotic syndrome 180

- Frequency of glomerular diseases causing nephrotic syndrome 180
- Age differences in disease prevalence 180
- Geographic and racial differences in disease prevalence 181

Minimal change disease 182

- Terminology 182
- Clinical presentation and laboratory findings 182
- Pathology 184
- Pathogenesis 188
- Differential diagnosis 190
- Course of disease, prognosis, therapy, and clinicopathologic correlation 191
- Secondary causes of minimal change disease 193

Nephrotic syndrome in the first year of life 194

- Congenital nephrotic syndrome due to mutation in *NPHS1* (Finnish type) 195
- Diffuse mesangial sclerosis 196

The kidney is an efficient ultrafilter, and urinary protein loss is only 80 to 150 mg per day in the normal adult: 60% of the excreted protein is filtered by the glomeruli, with the remaining portion, chiefly Tamm-Horsfall protein, derived from tubular secretion (1). The nephrotic syndrome (NS) comprises heavy proteinuria, edema, hypoalbuminemia, and hyperlipidemia. Nephrotic-range proteinuria is defined as ≥ 3.5 g/d/1.73 m² surface area. Pathologic proteinuria is the defining feature and the most readily quantitated sign of the NS, and heavy proteinuria represents a profound departure from homeostasis.

The NS is associated with a spectrum of primary and secondary glomerular diseases. It is important to make a distinction among the various causes of NS, because these diverse glomerular lesions have different clinical courses, treatments, and prognoses. Furthermore, investigators are now beginning to understand the molecular basis for many of these diseases leading to more specific therapeutic strategies. This chapter is concerned primarily with minimal change disease (MCD) and its variants although other causes of NS are mentioned, and the basic pathogenetic mechanisms of the NS are reviewed. Briefer mention is made of other glomerular diseases that cause the NS, with references to discussions of them in other chapters of this book.

FILTRATION OF MACROMOLECULES

Because the major characteristic of the NS is heavy proteinuria, it would be helpful at this point to review our understanding of the filtration of macromolecules.

Brief Review of Anatomy

The anatomy of the glomerular capillary wall is discussed in detail in Chapter 1, and only the salient points are emphasized here. Traditionally, the glomerular filter has been considered to be composed of three components: the endothelial layer of the glomerular capillary, the glomerular basement membrane (GBM), and the podocytes with their interdigitating foot processes and slit diaphragms. More recently, two additional components, namely, the glycocalyx of the endothelial cells and the subpodocyte space (SPS), have been found to contribute to

glomerular permselectivity (2,3). Starting on the luminal side and proceeding outward, the glomerular capillary wall consists of the following structures. First, there is a fenestrated endothelial cell layer with a negatively charged glycocalyx coat. The glycocalyx is composed of proteoglycans with a core of perlecan, syndecan, and versican and covalently bonded side chains of glycosaminoglycans such as heparan sulfate (3). Various serum proteins may become adsorbed to this surface. The endothelial fenestrations occupy between 20% and 50% of the endothelial surface and are maintained by vascular endothelial growth factor (VEGF) secreted by the podocytes (3,4). The basement membrane can be resolved into three layers: the lamina rara interna, the lamina densa, and the lamina rara externa. The GBM is composed of type IV collagen (with a triple helix of $\alpha 3$, $\alpha 4$, and $\alpha 5$ chains) forming a three-dimensional framework that serves as a lattice for the remaining components (2,5). Laminin that is bound to the collagen by entactin and nidogen anchors both endothelial and epithelial cells via the $\alpha_3\beta_1$ -integrin (2,6,7) and contributes additional structural support to the collagen. The negative charge of the GBM is imparted by the heparan sulfate proteoglycans, primarily perlecan and agrin (2,7,8).

The podocyte or visceral epithelial cell is recognized as a major player in glomerular filtration. The foot processes—which interdigitate—are attached to the outer aspect of the GBM by both laminin and fibronectin (5). The dystroglycan complex links $\alpha_3\beta_1$ -integrin to the actin cytoskeleton in the foot processes, and its proper glycosylation is important in maintaining the foot processes (9). Additional proteins involved in the development and maintenance of the foot processes include podocalyxin, podoplanin, glomerular epithelial protein 1 (GLEPP-1), and glucocorticoid-induced transcript 1 (7,10,11). MicroRNAs also play a role in podocyte function (12). Synaptopodin and actin are important in podocyte motility, and megalin plays a role in endocytosis at the base of the foot processes (7). Chloride intracellular protein 5 may act as an adapter between the actin cytoskeleton and the plasma membrane of the podocyte (13). Filtration slits are located between adjacent foot processes and are bridged by the slit diaphragm. Since the description of nephrin in 1998 (14), more than 15 different gene products have been localized to or near the slit diaphragm (2,15,16). These proteins also help maintain the shape of the foot processes, are important in signaling pathways, and function in regulation of cytoskeleton, polarized sorting and endocytosis, cell differentiation, suppression of differentiation, mechanotransduction, and podocyte viability (15). The exact shape and size of the pores in the slit diaphragm are not known. The original description posited a zipper-like structure (17). A more recent study suggests the possibility of a heteroporous structure (18). The anatomy of the podocyte and the slit diaphragm is more fully described in Chapter 1. Three-dimensional reconstruction has demonstrated the presence of a flow-restrictive SPS (3). This is discussed below in the section on the effect of hemodynamic factors.

Factors Involved in Glomerular Filtration

Numerous factors control the filtration of macromolecules, and they are best considered under the following headings: the various properties of the molecules themselves, the principal ones being size, charge, and shape; the properties of the capillary wall; and hemodynamic factors, chief of which are

the glomerular plasma flow rate and transcapillary hydraulic pressure difference.

Properties of Molecules

Fractional clearance studies have determined how size affects the ability of molecules to cross the glomerular filter. When tritiated neutral dextrans were used to test glomerular permeability in the rat, their fractional clearance was 1 (no measurable restriction of filtration) when the effective hydrodynamic radius, a_e , was ≤ 20 Å; but with increasing a_e values, the fractional clearance decreased progressively until it approached 0 with radii greater than approximately 40 Å (19,20). Numerous studies over the years have confirmed that for neutral solutes, the sieving coefficient decreases with increasing molecular size (21). Charge also plays a role in controlling the transglomerular passage of macromolecules as suggested by the observation of Michael et al. (22) that there was a reduction in negative charge in the glomerular capillaries associated with proteinuria in rats with aminonucleoside nephrosis and in humans with MCD. Since these initial observations were made, fractional clearance studies using different sizes of neutral dextran and comparing their fractional clearances with those of negatively charged dextran sulfate of similar size and cationic dextran molecules supported the importance of electrostatic charge (23,24). However, others have argued that there is no charge selectivity and that negatively charged molecules of small size such as albumin may pass freely through the glomerulus to be reabsorbed by tubules (25). A raging controversy developed that is discussed below in the context of the properties of the capillary wall. Shape of the molecule undergoing filtration is another important determinant of filtration (26,27).

Properties of the Capillary Wall

The various elements of the glomerular capillary wall act together in series to control the filtration of macromolecules forming both size and charge barriers. The barrier is dynamic with cross talk between the epithelial and endothelial cells (28,29). The size-selective barrier resides in all layers of the glomerular filtration barrier. Originally, the GBM was thought to be the principal size-selective barrier (7), but this is no longer the prevailing opinion (29). Nonetheless, the occurrence of proteinuria associated with mutations in laminin (a protein found only in GBM) supports a contribution of the GBM to the size selectivity of the barrier (29). The role of the filtration slit diaphragm, first described by Rodewald and Karnovsky (17), was confirmed by Kestila et al. (14) following their discovery of nephrin mutations in congenital nephrotic syndrome (CNS) of the Finnish type in association with a loss of the slit diaphragms. More recent work shows a heteroporous structure in the slit diaphragms with variation in the size of the pores under pathologic conditions (18). Edwards et al. found that the sieving curve was highly dependent on changes in filtration slit width and not in changes in the GBM (30). They concluded that size selectivity is most sensitive to the size of the slit diaphragm and the hindrance coefficient of the GBM (30). Most recently, a role for the endothelial surface layer has also been described for size restriction (31). This layer is composed of glycocalyx composed of proteoglycans bound to the cell membrane and an endothelial cell coat attached to the glycocalyx. This cell coat consists of proteoglycans, glycosaminoglycans, glycoproteins, and various plasma proteins such as

albumin and orosomuroid (31). Deen (32) using mathematical modeling suggested that the endothelial and epithelial cell layers are most important for size selectivity.

Originally, it was believed that the charge barrier resided chiefly in the anionic sites of the GBM (33). It is now generally accepted that the charge barrier also resides in the endothelial and/or epithelial cells (7,21,28,29). Jeansson and Haraldsson (34) gave hyaluronidase and heparitinase III to mice and measured glomerular selectivity in both in vivo and isolated perfused kidneys. They found evidence for both size and charge selectivity using a heterogeneous charged fiber model. Treatment with hyaluronidase increased albumin permeability fourfold without changing the selectivity of similar sized neutral molecules. Additional evidence for the presence of both size and charge barriers was obtained from a study of adriamycin-induced NS in the mouse. The investigators demonstrated increased clearance of larger Ficolls in treated mice as compared to control mice (35). Furthermore, loss of charge selectivity was also established by comparison of the clearance of neutral as compared to anionic albumin (35). These changes were associated with a thinning of the glycocalyx of the endothelial cells and down-regulation of synthesis of the heparan sulfate proteoglycans (35). However, it has also been suggested that no charge barrier exists. Some investigators believe that albumin passes through the capillary wall but is then returned to the plasma by a proximal tubular albumin retrieval pathway in which megalin, a low-affinity albumin-binding receptor, directs albumin to lysosomes or via transcytosis to the basolateral membrane and cubilin, a higher-affinity albumin receptor, directs albumin to lysosomes (25). These authors suggest that proteinuria is due to inhibition of this retrieval pathway rather than increased glomerular permeability. This group using in vivo two-photon microscopy demonstrated that the glomerular sieving coefficient for albumin was higher than expected to a degree that supported lack of a charge barrier (36). This raised a storm of controversy with contentious articles and editorials. Several other investigators using the same two-photon technique demonstrated a glomerular sieving coefficient for albumin that was close to or at the expected value (37,38) supporting the presence of a charge-selective barrier. Most recently, Sandoval et al. (39) have shown that the glomerular sieving coefficient may vary in different strains of rats and under different conditions. Thus, the controversy is not yet entirely resolved and requires further consideration as our understanding evolves (40). Nonetheless, most investigators agree that a charge-selective barrier is present in the glomerulus. Additional evidence for the presence of a glomerular charge barrier is supported by the association of proteinuria with glomerular injury particularly the accumulating evidence of mutations to various elements of the glomerular filter and the occurrence of proteinuria (28).

Hemodynamic and Other Biophysical Factors

Hemodynamic factors, including blood flow, convection, diffusion, transcapillary hydraulic pressure difference, and intraglomerular pressure, have been shown to play an important role in the passage of macromolecules across the glomerulus (19). Fractional clearance of a solute depends on the relative transport of water and the molecule in question. The latter takes place by both convection and diffusion for intermediate-sized macromolecules (an α_c value between approximately 20 and 34 Å). For small and large macromolecules, convection

is the predominant mode of solute transport. An increase in the glomerular filtration rate (GFR) results in comparable increments in water flux and solute transport by convection so that no change in fractional clearance occurs when diffusion is not a factor. However, in the case of intermediate-sized molecules, an increase in GFR produces a decrease in diffusion and, therefore, a reduction of fractional clearance. Afferent arteriolar plasma protein concentration may also affect these factors. These findings, predicted on theoretical grounds (20), were confirmed using dextran under conditions of different glomerular plasma flow rates, one of the determinants of the GFR. Other evidence that glomerular hemodynamics may affect glomerular permeability is provided by the observation that angiotensin-converting enzyme (ACE) inhibition reduces proteinuria. Another structural feature that may affect water or macromolecular flux through the glomerulus is the SPS first demonstrated in three-dimensional reconstruction of the glomerulus (41). This space is bounded by the podocyte cell body and the filtration barrier. Filtrate leaves the SPS and enters the urinary space through small exit pores between cell bodies, which produces a high-resistance space that may be controlled by the podocyte (3,41,42).

A recent contribution from Hausmann et al. (43) suggests the possibility that extracellular potential differences could be a determinant of glomerular filtration. They studied the *Necturus maculosus* (common mudpuppy), which has sufficiently large glomeruli to undertake such a study, and found a potential difference of 0.09 mV at a perfusion pressure of 20 cm H₂O that could be eliminated by perfusion with a cation such as protamine. They explained this phenomenon as a streaming potential. This concept was further elucidated in an accompanying editorial in which a dilute ionic solution passes through a negatively charged filter, the positive ions will distribute in a uniform fashion (44). However, application of flow under pressure will cause the positive ions to flow through the filter where some will stick to the nonplasma side. Some of the negative ions will be reflected resulting in a streaming potential difference. Another editorial in the same issue suggests caution in the interpretation of these results (45).

Summary

The current view of the glomerular barrier to filtration has become more complex and gained several contentious issues since the previous edition of this book. Several reviews outline what is known as well as discussing some of these (3,21,28,29). In brief, most investigators agree that the barrier has both size- and charge-selective properties. Furthermore, it is now thought that these barriers are located across the entire structure of the glomerular capillary wall residing in the endothelial surface layer, the endothelial cell, the GBM, the podocytes and their slit diaphragms, and, perhaps, in the SPS (3,21,28,29). The capillary wall as a whole should be considered a dynamic structure with interactions between the cells. This cross talk is best illustrated by the role of VEGF-A produced by podocytes that influences the endothelial fenestrae and contributes to their maintenance (4,28). Additional evidence for the role of such paracrine signaling has been demonstrated by Schumacher et al. (46) who recently found that the transcription factor WT-1 modulates both VEGF-A and fibroblast growth factor 2 to increase expression of various sulfatases such that the heparan sulfate in the matrix is altered.

Mechanisms of Proteinuria and the Effacement of Foot Processes

In general, proteinuria may result when there is addition of protein to tubular fluid (Tamm-Horsfall protein), altered tubular reabsorption, or altered glomerular permeability. We discuss only the last in this section and specifically address mechanisms that apply to those glomerular diseases that primarily have the NS as the initial manifestation.

Numerous experimental models have been used to study possible mechanisms of proteinuria. The model of puromycin aminonucleoside nephrosis (PAN) has been used extensively over the years. This model shares many features of human MCD, and it is produced in rats by administering puromycin aminonucleoside (PA), either in a single injection or in several injections. A considerable proteinuria ensues that is due to increased glomerular permeability. Studies of the glomerular lesion using transmission and scanning electron microscopy (47,48) have revealed a replacement of foot processes by continuous sheets of flattened cytoplasm, epithelial vacuoles, a reduction in the number of epithelial slits with formation of occluding junctions, and focal areas where the epithelium has detached from the outside of the basement membranes (Fig. 5.1). Other experimental models of proteinuric diseases as well as in human disease associated with proteinuria have similar changes.

The association between glomerular foot process effacement (FPE) and proteinuria is well known, but the mechanism of this effacement is complex and dynamic. In fact, podocyte motility is a term that is now used to reflect this dynamic view of the filtration barrier and changes in podocyte conformation (49). Maintenance of foot processes may be deranged by alteration in negative charge of the apical domain of the podocyte, alterations in slit diaphragm, or interference with GBM-podocyte interaction (50,51). All three of these are functionally linked by the actin cytoskeleton (52). The association between loss of negative charge from the podocyte and FPE has been known for some time. Seiler et al. (53) showed that

neutralization of glomerular polyanion by infusion of protamine, a polycation, produced the same flattening of epithelium, which was reversible by perfusion of polyanions. Loss of polyanion has also been demonstrated in PAN (48) and following administration of anti-podoplanin antibody to rats (54). Podoplanin is a mucin-like substance expressed on the surface of rat podocytes that contributes to the negative charge. Its removal by specific antibody results in massive proteinuria and FPE (54). Additional evidence for a role for changes in the negative charge of the glomerular barrier was demonstrated by the recognition that angiopoietin-like protein 4 is up-regulated in the podocyte in MCD and is associated with both a loss of charge in the GBM and FPE mediated at least in part by a decrease in sialylation (55,56). This alteration is discussed in greater detail in the section on Pathogenesis of MCD.

The disruption of the components of the slit diaphragm in association with proteinuria and FPE has been demonstrated in CNS of the Finnish type (57) as well as in knockout models for nephrin and CD2AP (58,59). FPE is always seen in these models accompanied by loss of the slit diaphragms. The proteins of the slit diaphragm are connected to the actin cytoskeleton by adapter proteins. Using the PAN model, Ito et al. (60) demonstrated that activation of the mammalian target of rapamycin complex 1 preceded the occurrence of endoplasmic reticulum stress and the unfolded protein response that resulted in cytoplasmic location of nephrin and disruption of the filtration slit diaphragm.

Attachment of the foot processes to the GBM is mediated by laminin, dystroglycan, and $\alpha 3\beta 1$ -integrin (61). Noakes et al. (62) examined a mouse model with a null mutation for laminin- $\beta 2$. The mice developed massive proteinuria associated with FPE and died by 1 month of age. Others have examined the role of abnormalities in dystroglycan in detachment of the podocyte from the GBM. The dystroglycan complex mediates adhesion at the basal cell membrane of the foot process by connecting matrix protein of the GBM and the actin network of

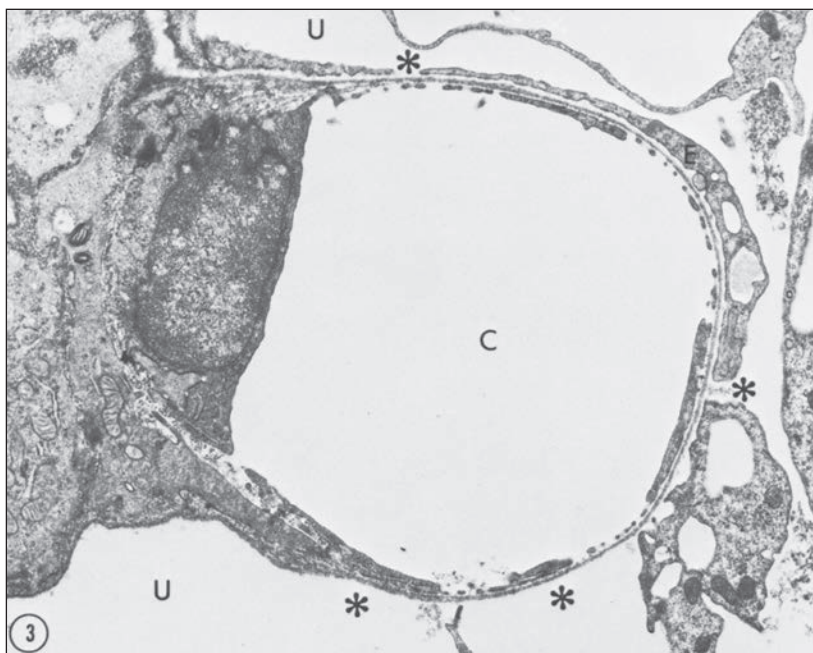


FIGURE 5.1 Electron micrograph of glomerular capillary (C) in a nephrotic rat that was subjected to aminonucleoside 5 days earlier. There is spread of epithelial cytoplasm and focal loss of covering on the outside of the GBM (asterisks). U, urinary space ($\times 6000$). (From Ryan GB, Karnovsky MJ. An ultrastructural study of the mechanisms of proteinuria in aminonucleoside nephrosis. *Kidney Int* 1975;8:219, with permission.)

the podocyte. Vogtlander et al. (63) noted that reactive oxygen species can cause deglycosylation of dystroglycan that may be associated with FPE. Reductions in dystroglycan have been seen in both MCD and focal segmental glomerulosclerosis (FSGS) (61,64).

As stated above, the three membrane domains on the podocyte are linked by the actin cytoskeleton, which has become a central focus in the concept of changing podocyte phenotype from stationary identified by the presence of intact foot processes to motile as associated with FPE. Prominent actin filaments are frequently seen in the effaced foot processes in human disease. Changes in the actin cytoskeleton have also been noted in PAN (48) as well as in an autosomal dominant form of FSGS that has mutations in α -actinin (65). The regulation of the actin cytoskeleton is complex and is not yet completely understood. Nephrin in the slit diaphragm interacts with the actin cytoskeleton via various adapter proteins, notably CD2AP, Nck, and Crk (52,66). B7-1 (CD80) is a transmembrane molecule regularly found on B cells and antigen-presenting cells that may also be expressed on podocytes (67). It is up-regulated by lipopolysaccharide (LPS), and such up-regulation was associated with actin reorganization in podocytes as well as a loss of slit diaphragms *in vitro* (67). Cathepsin L-mediated proteolysis particularly of dynamin and synaptopodin, important in maintaining podocyte stability, has been demonstrated to play a critical role in changing podocyte phenotype to motility (52,68). Activation of RhoA, a member of the family of small GTPases, is associated with actin polymerization, but its inhibition also resulted in actin polymerization, suggesting that RhoA must be tightly regulated (49,69).

Several investigators have found that the onset of heavy proteinuria coincides with epithelial detachment (70). Furthermore, ultrastructural tracer techniques have shown penetration of anionic ferritin into the urinary space at these detachment sites (48). Use of the technique of multiphoton fluorescence imaging *in vivo* in the PAN model confirmed areas of increased glomerular permeability near damaged podocytes as well as real-time shedding of podocytes (37). FPE is a reversible change, but if it progresses to foot process detachment, then irreversible injury may result (52).

Effects of Proteinuria on the Tubules and Interstitium

For many years, the question of damaging effects of proteinuria on the tubules and interstitium has been raised. The fact that patients with steroid-dependent MCD could suffer from nephrotic-range proteinuria for years and not show such injury spoke against the idea. However, mounting evidence suggests that at least nonselective proteinuria may result in such injury. Albumin, various vitamins, and other substances in tubular fluid are normally nearly completely reabsorbed by the tubular epithelium by receptor-mediated endocytosis (71). Uptake of albumin requires cubilin with endocytosis of the albumin-cubilin complex and transport to the lysosome necessitating the presence of megalin (72). It has been proposed that the various substances may directly cause tubular toxicity, that growth factors and other substances may cause up-regulation of cytokines/chemokines, or that complement may be activated (73–76). Theilig et al. (77) induced

crescentic glomerulonephritis (GN) in transgenic megalin-deficient mice. The lack of expression of megalin was mosaic so that megalin-deficient tubules could be compared to those that expressed megalin. This comparison showed endocytosis and an up-regulation of TGF β in the megalin-positive cells, while those deficient in megalin demonstrated apoptosis. However, neither group of tubules showed surrounding interstitial fibrosis. Kriz (77,78) believes that this experiment supports his contention that it is severe glomerular damage that is associated with downstream tubulointerstitial injury rather than tubular reabsorption of leaked proteins. Further experiments are necessary to dissect these possibilities.

PATHOPHYSIOLOGY AND COMPLICATIONS OF THE NEPHROTIC SYNDROME

The primary defect in the NS is loss of protein in the urine. Earley and Forland (79) calculated that complete failure to reabsorb filtered protein could account for proteinuria in humans of ≤ 0.5 to 2.5 g/24 hours at a GFR of 100 L/24 hours. It is now considered that proteinuria in excess of 2 to 2.5 g/24 hours indicates that at least some of the increased urinary protein has been derived from enhanced glomerular permeability. The nature of the protein lost in the urine may provide some information regarding the severity of the glomerular injury. Highly selective proteinuria—in which case only the smallest molecules are filtered in excess—indicates less injury to the glomerulus. Most glomerular diseases are manifest by poorly selective proteinuria.

Pathophysiology of the Nephrotic Syndrome

In addition to excessive loss of protein in the urine, the hallmarks of the NS include depression of certain serum proteins, edema formation, and a rise in serum lipids. Loss of protein in the urine is the basic defect, and the fall in serum protein, production of edema fluid, and hyperlipidemia stem from it (Fig. 5.2). Hypoalbuminemia in the NS is due to the combination of increased urinary loss and increased catabolism of albumin, chiefly in the kidney (80). The liver reacts to the low serum albumin levels by increasing albumin synthesis, but in the NS, the response is inadequate (80). The hypoalbuminemia then leads to both hyperlipidemia and edema formation.

Hyperlipidemia in the NS stems from several different mechanisms. A higher level of low-density lipoprotein (LDL) cholesterol is the principal alteration in the lipid profile, with increases chiefly in very low-density lipoproteins (VLDL) and apolipoproteins B, C-II, and C-III (81–83). The increase in apolipoprotein B is probably related to both hypoalbuminemia and changes in colloid oncotic pressure. The increase in LDL and VLDL is due to decreased catabolism secondary to decreased binding of lipoprotein lipase to endothelial cells (82,84), to reduced clearance of VLDL, and to a decrease in the VLDL receptor. In addition, lecithin cholesterol acyltransferase is lost in the urine so that there is limited uptake of surplus cholesterol (83). High-density lipoprotein (HDL) cholesterol shows little change so that the LDL/HDL is increased. However, the function of HDL in reverse cholesterol/lipid transport by the liver is impaired in NS due to deficiency of lecithin cholesterol acyltransferase, decreased docking receptor

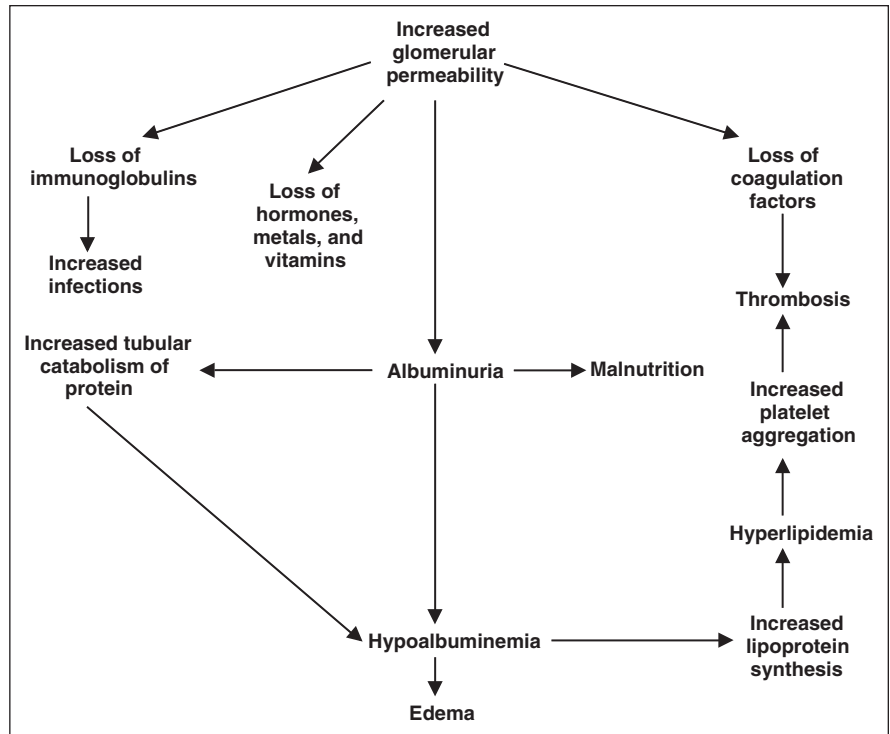


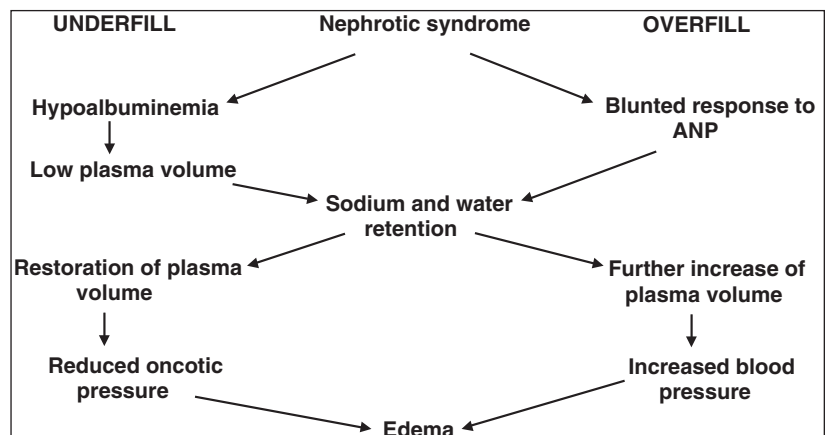
FIGURE 5.2 Pathophysiology of the nephrotic syndrome and its major complications.

for HDL in the liver, and increase in the hepatic HDL endocytic receptor (81). Triglycerides increase due to decreased clearance secondary to decrease in a number of lipases and up-regulation of hepatic diacylglyceride acyltransferase, the rate-limiting step in triglyceride synthesis (81). The increased synthesis of fibrinogen, transferrin, albumin, and apoA-1 is regulated transcriptionally (82).

Edema formation is the symptom of the NS that usually brings the patient to clinical attention. Our understanding of the mechanism of edema formation in the NS has expanded. In the classic mechanism, known as the underfill hypothesis, hypovolemia is the primary stimulus driving the kidney to retain sodium and water and eventually resulting in edema formation as the result of the Starling forces (Fig. 5.3) (85). However, most patients with NS are either normovolemic or hypervolemic. In an alternate theory, the overfill hypothesis, sodium retention by the kidney is primary. Sodium retention leads to increased blood volume and results in increased

blood pressure. These changes then lead to alterations in the Starling forces, which result in edema. Recent investigations have demonstrated that the primary cause of sodium retention in the NS is hyperactivity of the epithelial sodium channel (ENaC) in the cortical collecting duct (86–88). The ENaC is activated by proteolysis of its γ subunit by plasmin, which has been found in the urine of nephrotic patients (87–89). Other possible contributors to sodium retention in this setting include increased renal efferent sympathetic activity, atrial natriuretic peptide (ANP), or increased $\text{Na}^+\text{-K}^+$ ATPase activity (86,88). It is no longer believed that the renin-angiotensin system plays the major role. Thus, hypoalbuminemia is only one potential contributor to edema formation. Rostoker et al. (90) showed abnormal capillary permeability in patients with NS that resolved with steroid therapy. Current thinking still holds that increased capillary permeability and/or increased capillary-interstitial oncotic pressure gradient may participate in edema formation (86).

FIGURE 5.3 Mechanisms of edema formation in the nephrotic syndrome. *Left:* The classic view of edema formation, in which a low blood volume (underfill) serves as the signal for secondary renal sodium retention. *Right:* The mechanism of edema formation in most patients with the nephrotic syndrome who have normal or slightly elevated blood volumes (overfill). The blunted response to atrial natriuretic peptide observed in patients with the nephrotic syndrome may be the stimulus for primary renal sodium retention that plays a central role in edema formation.



Complications of the Nephrotic Syndrome

Hypercoagulability leading to thrombosis, increased susceptibility to infection, and cardiovascular disease are the principal nonrenal complications of the NS. Other complications are related to urinary losses of critical elements and include malnutrition, hormonal syndromes, and trace metal and vitamin deficiencies (see Fig. 5.2) (91).

Hypercoagulability and Renal Vein Thrombosis

Thromboembolic episodes occur in 20% to 42% of adults and in 1% to 9.2% of children with NS (92) and constitute the most life threatening of the complications of the NS. Deep venous thrombosis, renal vein thrombosis (RVT), and pulmonary embolism are the most common forms, but there are reports of arterial thrombosis and coronary thrombosis. Arterial thrombosis accounts for a higher percentage of thrombotic complications in children than in adults and results in a high rate of limb loss/death (93). In one study, the incidence of RVT in patients with NS was 35%, while the overall incidence of thrombotic complications outside the kidneys was 20% (94).

The pathogenesis of hypercoagulability in NS is multifaceted, stemming from an imbalance between coagulation and fibrinolysis (92). First, one must consider the presence of a genetic predisposition such as antithrombin deficiency that would increase the likelihood of thrombus formation (92). Many procoagulant factors are increased secondary to the lower serum albumin to which they are usually bound. These include fibrinogen; factors V, VII, and VIII; and von Willebrand factor (7,92,95). Increased fibrinogen leads to increased platelet aggregation and β -thromboglobulin. On the other hand, some anticoagulant substances are lost in the urine, including factors XI and XII, plasminogen, and antithrombin III (ATIII) (7,92,95). The loss of ATIII is thought to be particularly important as patients with NS who have such a deficiency have a 50% to 70% risk for thromboembolism (93). The fibrinolytic system is tilted toward decreased fibrinolysis with decreased plasminogen and plasminogen activator (92). It has been shown that the fibrin clot structure in NS may be less porous so that the thrombi are more resistant to fibrinolysis (92). Furthermore, prothrombotic microparticles, formed from various blood cells, may be increased in NS (92).

In children, the risk for thromboembolism is greater in those patients with CNS or with secondary forms of NS (92). In adults, the risk of RVT is higher in patients with membranous GN with 37% as compared to 24% for other forms of glomerular disease (92). Presentation of RVT varies with age. In young adults, it presents with flank pain and microscopic hematuria, whereas in older adults, presentation is characterized by a chronic syndrome. Furthermore, extrarenal thrombosis is also more common in older adults (92). Other clinical signs include acute renal enlargement, hematuria, oliguria, and acute renal failure (ARF) (96). Thromboembolic events occur early in the course of NS, usually within the first 6 months after diagnosis (97).

Infection

Infections were a major cause of mortality in patients with NS in the era before antibiotics (98), and bacterial infections remain a significant cause of morbidity. The prevalence of

infections ranges from 8% to 38% in children (99), and one adult series reports a prevalence of 19%. Types of infections include sepsis, peritonitis, cellulitis, pneumonia, urinary tract infection (UTI), and meningitis (100–102). In 340 French children hospitalized with NS, severe bacterial infection was diagnosed 48 times (14%) in 32 patients. One half of the patients had spontaneous peritonitis, most often as the result of *Streptococcus pneumoniae* infection (99). The frequency of different types of infection varies by geographic location. A recent study from China found that 19% of admissions to a hospital for NS were also attended by infection (102). Pneumonia was most common followed by UTI, sepsis, peritonitis, and cellulitis. Age also affected the type of infection with children under 10 years suffering from pneumonia, while those older than 10 years had UTI most commonly (102). Infections with *S. pneumoniae* are sufficiently common that it is recommended that children with NS should be vaccinated against capsular antigens (100).

Comparisons of patients with NS with and without infections have cited risk factors for infection that include elevated levels of serum cholesterol (95), a serum IgG concentration of less than 600 mg/dL, a serum creatinine level of more than 2.0 (103), and increased fragility of the skin as a portal of entry (7). The heightened susceptibility to infection in patients with NS is usually attributed to hypogammaglobulinemia owing to urinary losses of immunoglobulin, increased catabolism, and a reduced rate of synthesis (7,95,100,101). Cellular immunity is also abnormal in the NS (95,100,101). These defects include a reduction in the numbers of circulating T lymphocytes and a depressed blastogenic response to mitogens (95). An increased incidence of infection results from these abnormalities in immunity and from inhibition of leukocyte chemotaxis (95). It has also been suggested that zinc deficiency resulting from urinary losses may contribute to an abnormal immune response in patients with NS (95). Loss of serum complement and opsonizing factors also contribute to the increased frequency of infection (95).

Atherosclerosis

Hypercholesterolemia and hyperlipidemia are almost always present in patients with NS, and these biochemical abnormalities may contribute to the progression of glomerular disease (104). Hyperlipidemia in patients with NS may also cause systemic atherosclerosis. The lipid profile seen in patients with NS is characterized by hypercholesterolemia, elevated plasma LDLs and lipoprotein (a), hypertriglyceridemia, and alterations in HDL metabolism (81,105). The increases in cholesterol and LDL are due to increased synthesis of both moieties and decreased catabolism of cholesterol (83,105). Hypertriglyceridemia is due to decreased clearance of VLDLs and chylomicrons and due to the up-regulation of hepatic diacylglyceride acyltransferase (81,106). The changes in HDL metabolism are described in the section above on pathophysiology of hyperlipidemia. Increased lipoproteins and oxidized lipoproteins have also been described in children with NS (107). Recent evidence suggests that increased oxidative stress, a known risk factor for atherosclerosis, in NS may be due at least in part to decreased paraoxonase-1 activity in patients with NS (108). Paraoxonase-1 prevents oxidation of serum lipoproteins and reduces risk of atherosclerosis.

Ordóñez et al. (109) compared the risk of coronary heart disease in 142 nondiabetic adults (older than 15 years old) with

NS (proteinuria more than 3.5 g per day) and nonproteinuric control subjects matched for age and sex. Neither the subjects nor the controls had a preexisting coronary heart disease. The authors estimated that the risk of myocardial infarction (MI) is between five- and sixfold higher for the patients with NS than for the controls and that all coronary heart disease events (MI, angina pectoris, and coronary insufficiency) and deaths from coronary heart disease are two- to threefold higher in these patients. Exclusion of 17 patients with MCD from the analysis did not substantially alter the results. The increase in MIs may be related to increased LDL, resulting in decreased nitric oxide-mediated vasodilation (110). Another possible mechanism of increased MIs is related to loss of lysophosphatidylcholine resulting in decreased deformability of erythrocytes and increased platelet adhesion (110). Given the apparent risk of catastrophic complications, patients with prolonged NS and hyperlipidemia should be considered for pharmacologic or dietary treatment aimed at lowering the plasma lipid levels (109).

CAUSES AND CONDITIONS ASSOCIATED WITH THE NEPHROTIC SYNDROME

Clinical and pathologic observations have associated many different diseases with the NS, and the frequency and the consistency of the clinical association usually establish the validity of the relationship. Occasionally, there may be a direct relationship between a glomerular lesion and an etiologic agent. For example, finding of tumoral or microbial antigens in the immune deposits of membranous GN strongly supports an etiologic relationship between the agent and the underlying glomerular condition (reviewed in Chapter 7). The more common causes of the NS are listed in Table 5.1. When associations are only occasional, caution should prevail before making cause-and-effect assumptions from anecdotal experiences.

Frequency of Glomerular Diseases Causing Nephrotic Syndrome

The NS has been associated with myriad clinical disorders, but there are only a few forms of glomerular pathologic lesions that are responsible for most cases of the NS. One of the most important contributions of the renal biopsy has been to identify these different glomerular diseases. Table 5.2 summarizes the series that studied mainly adults, while Table 5.3 comprises series of children only. It is apparent from these tables that certain diseases are common causes of the NS.

Table 5.2 shows the relative incidence of the major histologic diagnoses among adults with the NS, taken from studies in which there was a clear distinction made between MCD and FSGS. Many variables affect the relative proportions of the diseases, such as the referral patterns and biopsy indications in different practice settings, and it is likely that these differences contributed to the patterns of disease in the different studies.

Series that come from referral centers are likely to contain patients with more serious or therapeutically difficult features. Such referral populations contain smaller numbers of patients with MCD and larger numbers of those with more serious conditions. This is brought out clearly by the study of White et al. (118). In a population of referred children, they found

TABLE 5.1 Major causes of NS

Primary glomerular diseases presenting with nephrotic syndrome
Minimal change disease
Focal segmental glomerulosclerosis
Membranous glomerulonephritis
IgM nephropathy
C1q nephropathy
Fibrillary/immunotactoid glomerulopathy
Membranoproliferative glomerulonephritis
C3 glomerulonephritis
Dense deposit disease
Congenital nephrotic syndrome of Finnish type
Diffuse mesangial sclerosis
Primary glomerular diseases presenting with hematuria sometimes accompanied by NS
IgA nephropathy
Postinfectious glomerulonephritis
Systemic diseases
Diabetic nephropathy
Amyloidosis
Immunoglobulin deposition diseases
Henoch-Schönlein purpura
Lupus nephritis

that MCD, FSGS, and membranoproliferative GN accounted for 64%, 11%, and 11%, respectively, of the cases of the NS. In contrast, a population of unselected patients yielded figures of 88%, 5%, and 1% for the same conditions (118). For these reasons, the prevalence of the less severe disease and, in the context of the NS, MCD will tend to be underestimated. MCD is further undercounted because standards of care do not require biopsy before initiating treatment in children with NS. Nevertheless, the frequency of FSGS relative to other causes of the NS is increasing in both adults (113) and children (119,120). The patients' ages, geographic differences, and racial differences influence the prevalence of the diseases causing the NS, and they are discussed in turn.

Age Differences in Disease Prevalence

The distribution of glomerular lesions in children with NS differs from that in adults. Table 5.3 deals with a series made up of children only, and two thirds of these patients in the studies prior to 1990 have MCD. The incidence of MCD in children who had renal biopsies ranges between 34.1% and 52.7% (117,120,121). The incidence is higher in children less than 6 years of age relative to older children, 71.1% and 24.1%, respectively (120). The other relatively common lesions in children are FSGS and membranoproliferative GN. Membranous GN affects only small numbers of pediatric patients, except in Habib and Kleinknecht's series (114). More recent series (117,121) show a lower percentage of patients with MCD, reflecting the current practice of not performing biopsies in young children with NS unless they are steroid unresponsive or resistant. Boyer et al. (121) examined 201 consecutive children who presented with idiopathic NS. Of those patients, 95 were steroid sensitive and were not biopsied. If one assumes that those patients had MCD, then the incidence of MCD

TABLE 5.2 Incidence of glomerular lesions most commonly appearing in the form of nephrotic syndrome in adults

	Cameron 1979 (111)	Tiebosch et al. 1987 (112)	Haas et al. 1976–1979 (113)	Haas et al. 1995–1997 (113)
Minimal change disease	25%	20.5%	23%	15%
Focal segmental glomerulosclerosis	9%	13.6%	15%	35%
Membranous GN	21%	31.8%	36%	33%
Membranoproliferative GN	14%	4.5%	6%	2%
Other proliferative GN	13%	20.5%	3%	9%
Other lesions	18%	9.1%	7%	4%
Total study population	500	44	199	233

rises to 72%, which is closer to the figures from the 1970s (see Table 5.3). However, the percentage with FSGS is 24%, which is double the numbers for that entity from the earlier studies confirming the observations of others regarding an apparent increase in the incidence of FSGS (117,122).

The prevalence of the various glomerular lesions in *older children and adults* with NS is quite different from that in young children; significant proportions have membranous GN, MCD, FSGS, and various forms of proliferative GN, with significant contributions from systemic lupus erythematosus, diabetes mellitus, and amyloidosis (123–125). This morphologic diversity dictates a different clinical approach in adults with idiopathic NS in whom the morphologic diagnosis often cannot be deduced from the clinical history or the laboratory examination. The different forms of glomerular disease have very different therapeutic and prognostic implications, and lesion-specific therapy based upon a renal biopsy is the foundation for optimal treatment of these patients.

Studies of the NS in the *elderly* have found that membranous GN is the most common lesion in people between 65 and 79 years of age, with MCD as the most common lesion in the very elderly (Table 5.4) (126–128). Other lesions seen in biopsies in the elderly with NS include benign nephrosclerosis, diabetes, FSGS, IgA nephropathy, and amyloid. MPGN associated with hematologic neoplasms is also seen more frequently in the elderly (126). It is worth noting that in evaluating renal disease in the elderly, age-related changes may confuse the unwary (126). For example, the number of functioning glomeruli decreases by 30% to 50% in the seventh decade. In addition, there is a loss of capillaries within

glomeruli accompanied by an increase in mesangial cell number, a decrease in epithelial cells, and a loss of filtering surface. Interstitial volume remains the same. Diverticula may form in distal tubules. Arteries spiral and become tortuous with the shrinking of the cortex (129). These morphologic changes are accompanied by physiologic alterations and a gradual loss of renal functional reserve. Furthermore, MCD may be superimposed on these changes so that it may be difficult to establish the diagnosis (127,128).

Geographic and Racial Differences in Disease Prevalence

The country of origin may also affect the proportions of the diseases causing the NS. For example, in Thailand, the incidence of common glomerular lesions in children is as follows: MCD, 16.5%; FSGS, 12%; mesangioproliferative GN (mostly IgM), 33%; membranoproliferative GN, 30.8%; and membranous GN, 7.7% (130). The high rate of membranoproliferative GN is attributed to a combination of infectious disease and malnutrition. In China, in a study of 1523 patients 14 years or older with NS, the frequency of these lesions was MCD 20.4%, FSGS 4.1%, mesangioproliferative GN (including IgA) 18.3%, membranoproliferative GN 10%, membranous GN 20.7%, amyloidosis 2.5%, lupus nephritis 16%, and other 8% (125). Additional differences were seen in a study using the Italian National Registry of Renal Biopsies. In that study, the frequency of these diseases in all ages was MCD 16.7%, FSGS 16.9%, mesangioproliferative GN (non-IgA) 5.3%, membranoproliferative GN 8.1%, membranous GN 44.1%, IgA nephropathy 8.1%, postinfectious GN 0.7%, and crescentic GN 1.4% (131).

TABLE 5.3 Histologic diagnosis of nephrotic syndrome, exclusive of systemic disease, in children

Diagnosis	Habib and Kleinknecht (114)	International Study (115)	Chen et al. (116)	Gulati et al. (117)	Boyer et al. (121)
Minimal change disease	51.5%	76.4%	66.8%	34.2%	72%
Focal segmental glomerulosclerosis	11.6%	8.6%	11.6%	39.1%	24%
Membranous GN	9.1%	1.5%	2.1%	1.8%	2%
Membranoproliferative GN	9.4%	7.5%	1.7%	16.2%	2%
Diffuse mesangial sclerosis	1.5%	0%	0.4%	0.9%	
Other lesions	16.9%	6%	17.4%	7.6%	
Total	406	521	232	222	201

TABLE 5.4 Comparison of frequency of common lesions producing nephrotic syndrome by age

Diagnosis	Children	Adults	Elderly	Very elderly
			65–79 y	80–91 y
Minimal change disease	58%	26%	20%	46%
Focal glomerulosclerosis	36%	39%	39%	36%
Membranous GN	6%	35%	41%	15%

Data from Nair R, Bell JM, Walker PD. Renal biopsy in patients aged 80 years and older. *Am J Kidney Dis* 2004;44:618.

Within a country, the frequency of lesions may be different among various races or ethnicity. For example, in South Africa, Bhimma et al. (132) studied the frequency of causes of NS in black, Indian, and mixed-race children. They found that the frequency differed as shown in Table 5.5. In addition, the course of the disease varied among the groups. For example, only 37.5% of the blacks with MCD were steroid sensitive compared to 96.2% of the Indian children (132).

Membranous GN is the most common cause of NS in European and North American adults, but observations suggest that this is not the case for African Americans. The most common cause of NS in African Americans is FSGS (113,133,134). In a series of 340 adult patients with idiopathic NS, Korbet et al. found that the incidence of FSGS was 57% among 121 African Americans compared with 23% among 123 Caucasians. Membranous GN remained the most common cause of NS in white adults (134).

MINIMAL CHANGE DISEASE

Terminology

After the introduction of the concept of nephrosis by Müller (135), the term *lipoid nephrosis* was coined by Munk (136) to describe the presence of fat bodies in the urine and fatty changes in the tubules seen at autopsy. The term *lipoid nephrosis* implies a degenerative appearance of the tubules as well as

suggesting a possible role for abnormalities of lipid metabolism in the pathogenesis of the renal lesion, but in the era before the widespread application of percutaneous renal biopsy, it was applied to many different clinical situations and pathologic lesions linked primarily by the presence of the NS. Series of patients in whom lipid nephrosis was defined clinically or without evidence from immunofluorescence and electron microscopy undoubtedly had other lesions. As lipid nephrosis evolved to imply a specific glomerular lesion, many terms have been suggested in its place, including another obsolete term “nil disease.” Most authors now use the word minimal as part of the name of this lesion. Thus, such terms as *minimal change NS*, *minimal lesion*, and *minimal change glomerulopathy* are commonly seen. MCD is currently the most widely used and accepted term for this disease entity.

Clinical Presentation and Laboratory Findings

Clinical Presentation in Children

MCD is more common in boys than in girls; the ratio of boys to girls is approximately 2:1 (114,115,118). It is most commonly a condition of young children; with biopsy verification, the peak incidence was between 2 and 4 years (114,118). Almost 80% of histologically verified cases of MCD in the International Study of Kidney Diseases in Children (115) were found in children under the age of 6 years, with a median age of 3 years. However, MCD can occur at any age and is a common cause of NS in adults. It is more common among Caucasians, Asians, and Hispanics than among African Americans (137). The incidence is 2 to 16/100,000 per year in children under 16 years (137).

The clinical manifestations are similar to those seen in other forms of the idiopathic NS, and edema is the most common presenting sign (114). Microscopic hematuria was found in 36% of histologically confirmed cases in one study (114) and in 13% in another (118). Macroscopic hematuria was rare. Hypercholesterolemia is seen more frequently and is often elevated to very high levels. Blood pressure is usually normal at onset, and <20% of patients have hypertension (114,115,118). Transient depression of renal function has been recorded in 0.8% (138), 9.6% (114), and 19% (118) of children with MCD. In those cases in which the clearance is depressed initially, there is a return to normal with remission. The significance of decreased renal function in patients with MCD is discussed later (see “Acute Renal Failure in Minimal Change Disease”). Serum complement levels are not usually depressed (114,115,118). Proteinuria is almost always of the selective type (114,118). In fact, Adamson et al. (139) have suggested that the presence of higher levels of gamma globulins (greater

TABLE 5.5 Frequency of lesions associated with nephrotic syndrome in South African children according to race-ethnicity

Diagnosis	Black	Indian	Mixed
Minimal change disease	13.5%	46.8%	21.7%
Focal segmental glomerulosclerosis	28.4%	20.6%	43.5%
Membranous (including hepatitis B)	39.8%	2.4%	26.1%
Membranoproliferative GN	5.1%	0%	3.1%
Mesangioproliferative GN	7.2%	2.4%	8.7%
Total subjects	263	263	20

Data from Bhimma R, Coovadia HM, Adhikari M. Nephrotic syndrome in South African children: changing perspectives over 20 years. *Pediatr Nephrol* 1997;11(4):429.

than 4.3%) on urine protein electrophoresis in conjunction with a normal GFR predicts an increased risk of FSGS.

MCD was defined in patients with NS, and there is a reluctance to make the diagnosis in patients with asymptomatic proteinuria. Hiraoka et al. (140) addressed the issue of “asymptomatic MCD” by reporting the cases of eight children with proteinuria discovered by chance on urinary screening. Two of the eight children underwent renal biopsy for coexistent hematuria, and the histopathologic diagnosis was MCD. None of the eight asymptomatic children relapsed for ≥ 1 year after completion of treatment, and only two experienced steroid-responsive relapses in greater than 6 years of follow-up. The authors concluded that among patients with steroid-responsive NS and a clinical diagnosis of MCD, those with mild manifestations without edema will have a favorable clinical course without relapse. Branten et al. (141) reported on a mother and two daughters with persistent proteinuria for 20 years in the mother but without any abnormality on biopsy including normal foot processes. These authors suggested the possibility that this represented a familial nephropathy different from MCD. On occasion, isolated FPE is found in patients with slightly elevated urine protein or no proteinuria. Because the relationship of isolated FPE to MCD is unknown and it is uncertain that the patients require treatment with steroids, I recommend that such patients be classified as having nondiagnostic glomerular changes. It is important to note that patients with MCD may have less than widespread FPE if the biopsy is performed when the patient is entering spontaneous remission or following treatment.

Clinical Presentation in Adults

MCD is a major cause of the NS in adults (see Table 5.2), but in contrast to the situation with children, it is not the most common glomerular pathologic manifestation (111,142–146). The clinical presentation is usually similar to that seen in children (142,144), although some studies report a higher incidence of hypertension, ARF (111,142–146), and nonselectivity of proteinuria (111), particularly in the elderly (128). The condition is identical to MCD of childhood so far as the appearances by light, immunofluorescence, and electron microscopy are concerned, except that obsolete glomeruli, focal tubular loss and atrophy, and thickening of arterioles and arteries are seen more often in adults. Children have more frequent relapses (137). Secondary cases of MCD are more common in adults, and in some 10% of cases, it is associated with a drug reaction or a lymphoproliferative disorder (142,144). A familial form of steroid-responsive NS, likely representing MCD, has been reported in a Bedouin kindred (147).

De novo MCD has been described (148–150). In one series of 67 patients with posttransplant NS, five had MCD (150). Fifteen cases have now been reported, and eight were in living-related donor kidneys (148,150). Many of these cases occurred within a few months following transplantation. None of the recipients had FSGS as a primary disease. Most remitted with appropriate therapy. It is critical to exclude other possible causes of NS prior to making this diagnosis.

Laboratory Findings

The proteinuria in MCD is usually highly selective; that is, it is composed largely of albumin rather than larger molecules such as IgG (151). The selectivity index is a measure of the permeability of albumin relative to IgG with a value greater

than 0.2 indicating nonselective proteinuria (152). This may be used as a measure of likelihood of response to therapy as well as a possible indication of MCD rather than FSGS. However, not all investigators found a correlation between the index and response to therapy (153).

Variations in a number of different interleukins (ILs) have been described in MCD (137,153,154). Circulating soluble IL-receptor-2 is increased with MCD and decreases on complete remission (154). Increases in IL-4, IL-8, IL-13, IL-18, and IL-19 have also been described (137,153,154). An increase in urinary IL-6 is associated with steroid-resistant MCD (154). Other substances found to be increased in MCD include tumor necrosis factor- α and beta receptors and hemopexin (153). Most recently, an increase in urinary soluble CD80 (sCD80) has been detected in patients with MCD in relapse but not in patients with FSGS (155,156). CD80 is a transmembrane protein that is expressed on podocytes and can provide a costimulatory signal for T lymphocytes (155). This aspect is discussed below in the section on Pathogenesis. If this result is validated by others in a wider population, it may be very useful in distinguishing between MCD and early cases of FSGS in which damaged glomeruli may not be sampled.

Acute Renal Failure in Minimal Change Disease

MCD is usually associated with an excellent prognosis for resolution of proteinuria and preservation of renal function. However, it imparts some degree of renal insufficiency in between 1% and 17% of children and adults (138,157,158). The ARF may occur at presentation or during a relapse (157,159). These patients tended to have lower serum albumin and higher degrees of proteinuria (157,159). Renal biopsy demonstrated tubular injury consistent with acute tubular necrosis including loss of brush border, attenuation of the epithelial cells, occasional mitoses, and tubular dilatation (157,159,160). The complication of ARF in patients with MCD, especially when associated with acute interstitial nephritis, should prompt a careful search for an etiologic agent, such as nonsteroidal anti-inflammatory drugs (NSAIDs), that also may cause FPE (see Chapter 25), or the concomitant administration of a potentially nephrotoxic drug, such as a diuretic or antibiotic. In these cases, the renal insufficiency is reversed by discontinuing the drug.

The pathogenesis of ARF in the setting of MCD has several possible explanations. In adults with MCD, ARF is associated with older age and vascular disease (157,158,160), but this association cannot explain all cases. Direct tubular toxicity from the increased glomerular permeability has been suggested (159). The origin of tubular injury and dysfunction may reside in the altered hemodynamics seen in patients with NS. It has been suggested that this form of tubular damage is the result of hypovolemia due to low plasma oncotic pressure, but the absolute and relative blood volumes and the renal plasma flow are well preserved in most patients with NS (138,160). Chen et al. (161) found that immunohistochemical staining for endothelin 1 (ET-1) was stronger in patients with MCD and ARF than in patients with MCD and normal renal function. They also found more severe interstitial edema and more widespread FPE in the patients with ARF. They hypothesized that the cytokines that are increased in MCD (see below “Pathogenesis”) may induce ET-1 production. ET-1 may induce mesangial cell contraction, which may result in reduced filtration surface area and GFR.

Pathology

Gross Pathology

It is uncommon today to see kidneys as specimens in untreated patients with MCD. In reports dating from before the availability of effective therapy or in patients dying of complications of the NS, both kidneys are enlarged, sometimes to twice their normal size. They are extremely pale, with a smooth subcapsular surface and, when cut across, appear swollen and edematous. Lipid-filled tubules with a golden yellow color are present in discrete clusters separated by uninvolved tubules or diffusely involving the cortex. The striking color of the tubules gave rise to the descriptive diagnosis of lipid nephrosis. The characteristic appearance of the tubules is not specific to MCD and is observed at autopsy and occasionally in needle biopsy cores from patients with severe NS caused by diverse glomerular diseases.

Light Microscopic Findings

GLOMERULI

Simply stated, light microscopy of this disease shows no or minimal glomerular abnormality (Figs. 5.4 and 5.5). The glomerular capillaries are patent, with neither thickening nor irregularity of the capillary wall. Although some specimens show a slight increase in the mesangial matrix or cellularity (114,118), the presence of focal segmental glomerular collapse or scarring, endocapillary proliferation, or adhesions is not supportive of the diagnosis of MCD. In contrast to FSGS, where the visceral epithelial cells frequently are hypertrophied, epithelial cell pathologic features are not seen by light microscopy. In most patients, mesangial cellularity is normal, but mesangial hypercellularity has been described in either a segmental or global pattern (114,162–165) (Fig. 5.6). Hematuria is more frequently seen in this variant (166). In addition, immature glomeruli may be seen in

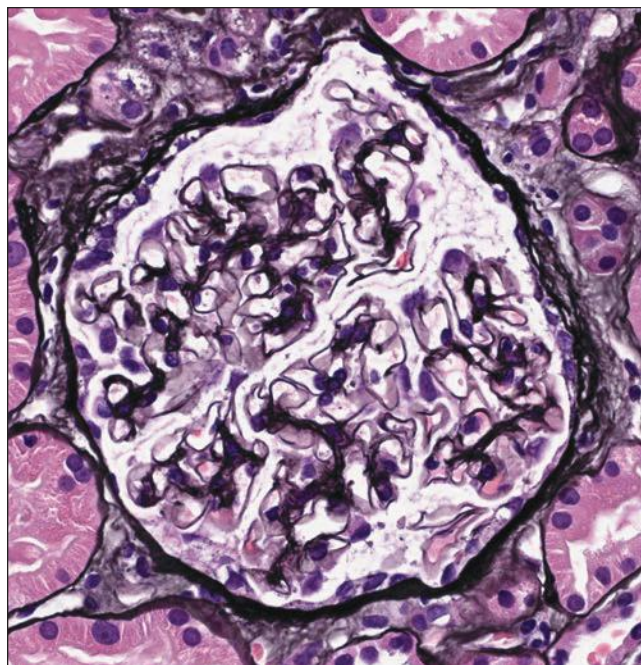


FIGURE 5.5 Light micrograph of glomerulus stained with silver showing thin and delicate capillary walls. (PAS-Jones, $\times 390$.)

MCD, particularly in association with mesangial hypercellularity (167). The therapeutic and prognostic implications of this and other renal findings are discussed in the section Clinicopathologic Correlation.

Focal hyalinized/obsolete glomeruli (focal global glomerular sclerosis), in contrast to segmental glomerulosclerosis, may

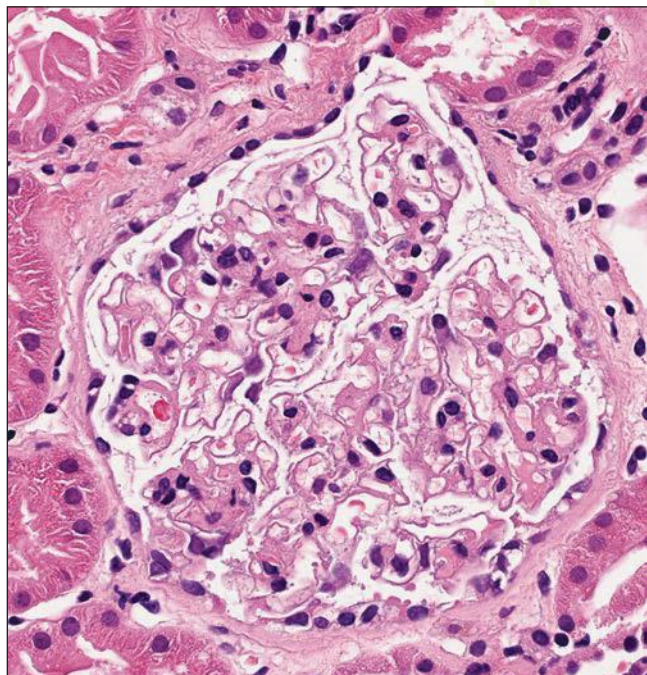


FIGURE 5.4 Light micrograph of glomerulus from a child showing no glomerular changes. (H&E, $\times 370$.)

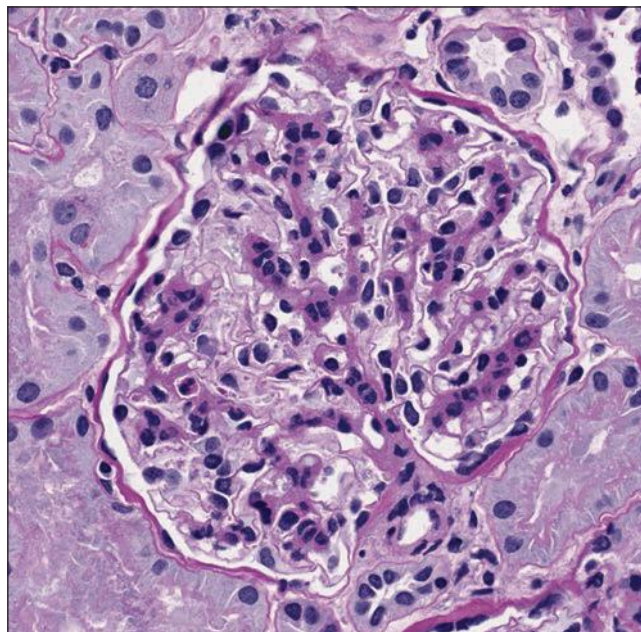


FIGURE 5.6 Light micrograph of glomerulus from a patient with the nephrotic syndrome showing diffuse mesangial hypercellularity and mild matrix increase. (PAS stain, $\times 450$.)

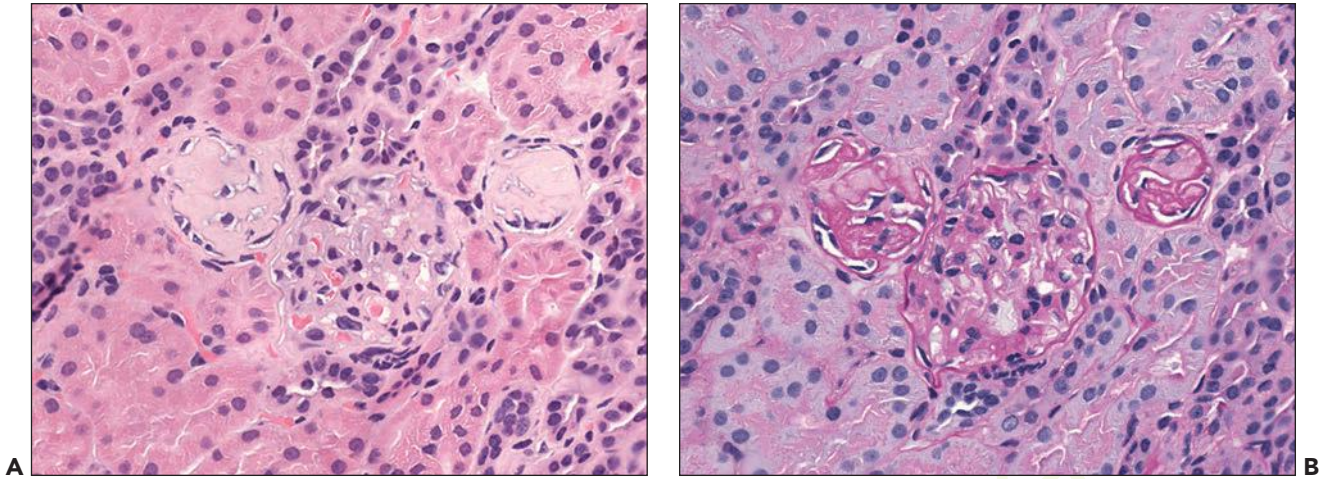


FIGURE 5.7 Light micrograph of involuted glomeruli from a patient with minimal change disease. (A: H&E, $\times 240$; B: PAS, $\times 240$.)

be present in a renal biopsy suggestive of MCD, especially if such glomeruli are not associated with interstitial fibrosis and tubular atrophy (118,163) (Fig. 5.7). Dijkman et al. (168) believe that such glomeruli represent a different form of glomerulosclerosis, which they named involuted glomeruli. These glomeruli are characterized by a strong staining matrix forming a network and accompanied by a few vital appearing cells. These cells stained for podocyte or parietal cell markers. These glomeruli increased in number with interval since diagnosis. They found them in most of their patients with MCD but not in patients with other diseases.

Globally, sclerotic glomeruli are occasionally seen in normal children's kidneys, and they increase in number as a person ages. The number of glomeruli so affected in normal subjects as a function of age varies between 1% and 10% up to age 40 (169,170), and that percentage increases to 30% by age 80. Smith et al. (170) provide a figure of less than 3% as the mean expected obsolete glomeruli up to age 56 and, in addition, provide a quick formula to determine the figure for the 90th percentile at any particular age. The upper limit of the expected number of obsolete glomeruli should not exceed the age of the patient divided by 2 minus 10. Korbet et al. (144) reported the cases of 40 adult patients with MCD (mean age, 40.7 ± 19.8 [mean \pm SD] years) and 19 ± 16 glomeruli per biopsy. Ten biopsies contained globally sclerotic glomeruli (2.2 ± 1.1 sclerotic glomeruli/involved biopsy; range, 1 to 5). These observations indicate that small numbers of hyalinized glomeruli may be found in normal kidneys, even in younger age groups, and in studies that address the significance of global glomerular sclerosis in MCD, its presence did not affect prognosis (114,163) and was not related to mesangial proliferation and mesangial IgM deposition.

TUBULES

Tubular and interstitial pathologic lesions are not classic features of MCD, but clear vacuoles or hyaline droplets may be seen in the tubular epithelial cells. Fine vacuolation, representing fat droplet deposition, is evident in frozen sections, and much of it is doubly refractile and responsible for the characteristic oval fat bodies that appear in the urine. Hyaline droplets, representing resorbed protein, often are quite prominent, particularly in the context of heavy proteinuria. Eosinophilic

casts may be present in the collecting ducts. Acute tubular injury with degenerative and regenerative activity and associated interstitial changes may be seen when acute renal insufficiency is superimposed upon NS in patients with MCD (Fig. 5.8) (see above "Acute Renal Failure in Minimal Change

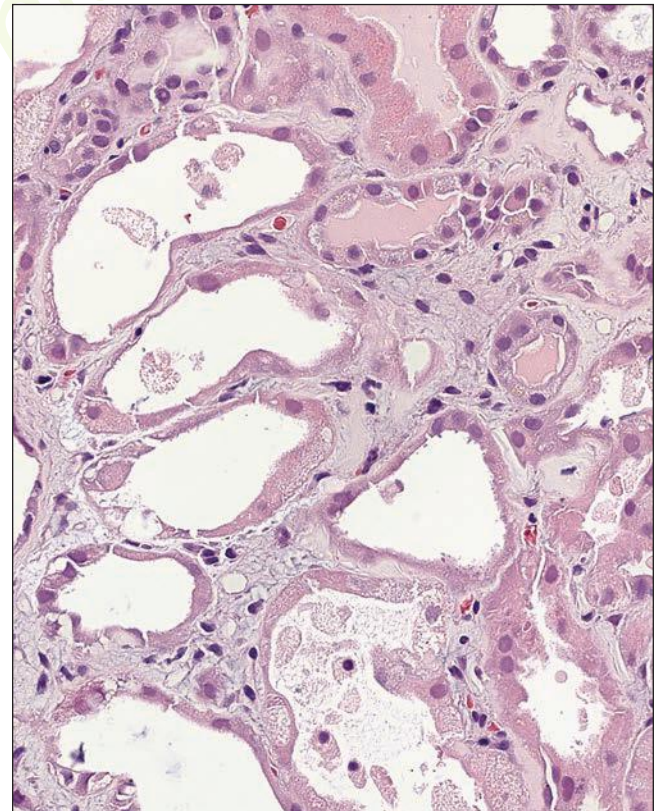


FIGURE 5.8 Light micrograph from an elderly patient with nephrotic syndrome and acute renal failure. The tubules are dilated with patchy marked attenuation of epithelial cells. Some tubules contain sloughed epithelial cells. Moderate interstitial edema is also present with only a few scattered inflammatory cells. (H&E, $\times 530$.)

Disease”) (158,160). Tubular atrophy is not a usual feature of the disease, but it may be seen in a focal distribution in older patients. In them, it is thought not to be a part of the MCD but is considered instead to be related to glomerular obsolescence and ischemia. However, focal tubular changes, including atrophy, thickening of the tubular basement membrane, and focal calcified casts, are also described in children with MCD (163,171). In children, nephrocalcinosis is seen particularly in association with furosemide treatment, a finding that also can be induced in rats (171).

INTERSTITIUM AND BLOOD VESSELS

Edema of the interstitium is seen in a few patients with MCD, and focal fibrosis is present, along with tubular atrophy, in older patients. Repeat biopsies in patients who have been treated with cyclosporine or other calcineurin inhibitors may show interstitial fibrosis as a complication of that therapy (172). Chronic inflammatory cells may be seen in association with acute tubular damage, but they are not usually plentiful. Interstitial foam cells are uncommon in my experience. Blood vessels show no characteristic pathologic features, but intimal arterial thickening may be present in older patients.

Immunofluorescence Findings

Immunofluorescence studies have generally reported that immunoglobulins are absent from the glomeruli (114,144), and in most cases, the presence of significant glomerular immune deposits excludes a diagnosis of MCD. Immunoglobulins, particularly IgM, and complement (C3), when present, are of low intensity and localized to the mesangium, and they are not associated with corresponding electron-dense deposits (144). Studies that compared patients with such minor positive findings on immunofluorescence against those who had negative findings found no difference in their response to steroid treatment, and the authors were inclined to consider the focal deposition of immunoglobulin as secondary to the proteinuria and not of primary pathogenic importance (173). A recent study has reexamined the presence of IgM in a mesangial pattern and found that children with such an immunofluorescence pattern in the setting of MCD had a poorer response to steroids and a greater likelihood of developing renal insufficiency even in the absence of deposits by electron microscopy (174). This is discussed further in the section on IgM nephropathy below. Hyaline droplets in the tubular epithelial cells may give positive staining for albumin and other serum proteins.

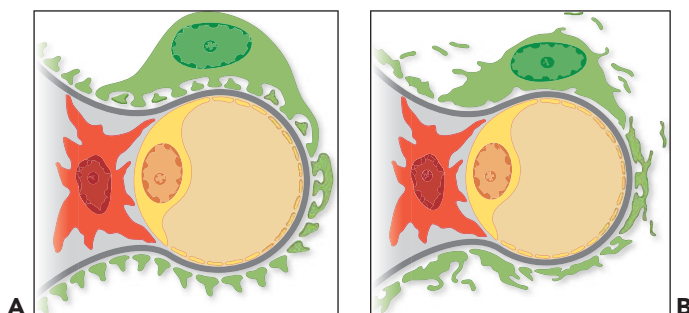
The picture is complicated when patients with NS have clinical features suggesting MCD but are found to have widespread, intense deposits of immunoglobulins and

complement and when evidence of glomerular immune reactants is supported by the presence of electron-dense deposits. There have been reports of children with NS with the appearance of MCD on light microscopy but with prominent *mesangial IgA* deposits by immunofluorescence studies (175–178) and mesangial electron-dense deposits together with extensive FPE on ultrastructural examination (when it was available) (176,178). The NS is present in only approximately 5% of patients with IgA (175), and among the 15 children in these four studies, only 5 had hematuria, the usual presenting feature of IgA nephropathy. At the last follow-up, all were in remission, although some had suffered relapses at various points during the course of their disease. Some groups (176,179) consider these cases to represent a variant of IgA nephropathy. Several other investigators (175,177,178,180,181) regard them as MCD with incidental mesangial IgA deposits because the clinical course more closely resembles MCD, and there is extensive FPE in the absence of peripheral capillary wall deposits. Other authors believe these patients have both MCD and IgA nephropathy (182). Similarly, *IgM and C1q nephropathy* are primary glomerular diseases in which mesangial immune deposits may be seen in patients with NS and normal or nearly normal glomeruli by light microscopy. Since the renal outcome and response to therapy may be different in patients with MCD, IgM and C1q nephropathy are discussed later in this chapter.

Electron Microscopic Findings

The only consistent glomerular pathologic characteristic in MCD is simplification of the shape of the visceral epithelial cells (podocytes), a change seen by electron microscopy as effacement of the discrete foot processes (Figs. 5.9 and 5.10). Effacement is usually extensive (183). Coarsening, defined as foot processes that are twice normal in width, may also be seen. In all cases, FPE and/or coarsening should be widespread and at a minimum should involve more than half of the surface area of capillary loops. The relationship between the degree of effacement and the amount of protein excretion has proved inconstant. It is now generally accepted that no correlation is present between measured foot process width and the severity of proteinuria (184–186). Deegens et al. (184) found that mean foot process width was greater in patients with FSGS than in those with MCD; however, there was sufficient overlap that such measurements cannot be used to distinguish between these entities. Remission of NS in MCD is associated with return of the foot processes to normal. Partial response to treatment will also result in a lessening of the effacement and appearance of coarsened foot processes. Effacement of the foot

FIGURE 5.9 Diagram depicting one normal glomerular capillary (**A**) and one glomerular capillary with extensive podocyte foot process effacement and podocyte microvilli (**B**). (Green, podocyte; dark gray, GBM; yellow, endothelial cell; red, mesangial cell; light gray, mesangial matrix.)



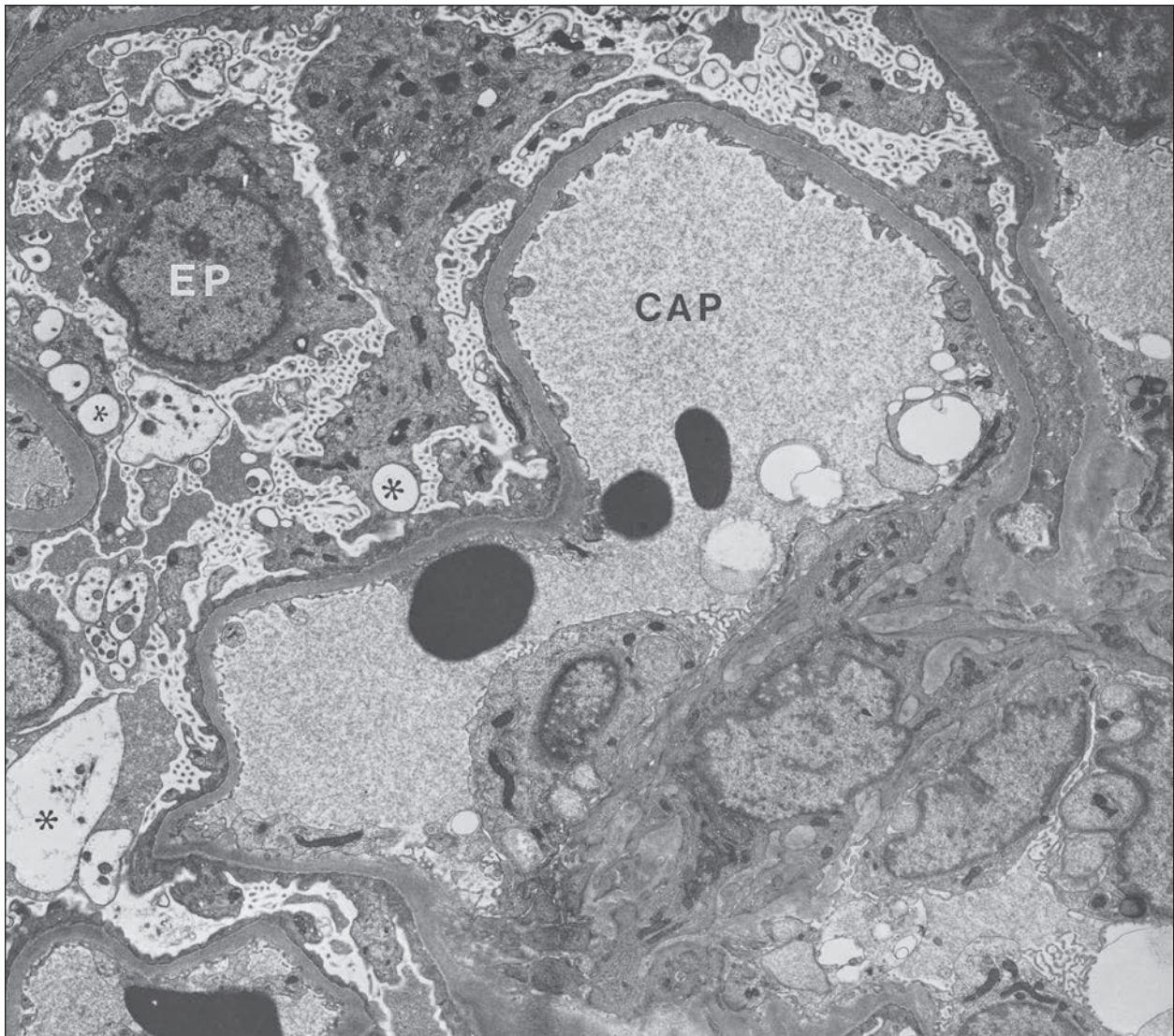


FIGURE 5.10 Electron micrograph of a portion of a glomerulus from a 22-year-old woman with minimal change disease. The pathologic changes are confined to the epithelial cells that show diffuse foot process effacement, vacuolization (*asterisks*), and microvillous transformation. EP, glomerular epithelial cell; CAP, glomerular capillary. (Uranyl acetate and lead citrate; $\times 5000$.)

processes is also associated with aggregation of microfilaments at the base of the epithelial cells (Fig. 5.11). Loss of the foot processes is accompanied by distortion of the filtration slits with reduction in number of the slit diaphragms (187,188). Patrakka et al. (187) found that 50% of slit pores contained slit diaphragms in patients with MCD compared to 87% of slit pores in patients with tubulointerstitial disease without glomerular disease. Some slits showed a displacement of the diaphragms in a ladder-like formation toward the apex of the pore (187,188). Other epithelial cell changes include hypertrophy, microvillous transformation, formation of vacuoles (see Figs. 5.9 and 5.10), and the presence of protein and lipid resorption droplets (183,189). Chiang et al. (190) found more glomerular epithelial cell vacuoles in biopsies from patients with FSGS and from patients with apparent MCD who had FSGS in a subsequent biopsy, when compared with patients with

MCD alone. Although the authors suggested that epithelial cell vacuolization is a marker for FSGS, this alteration did not predict the renal outcome. Small focal areas of detachment of the foot processes from the GBM may be observed in MCD (191). However, other authors did not see areas of epithelial cell detachment using either transmission or scanning electron microscopy (186).

The GBM is usually of normal thickness and texture. Thin GBM was observed in 10% of cases of MCD, but thin GBM (Fig. 5.12) was present in 7.8% of the normal controls in this study (192). Furthermore, patients with thin GBM are not more likely to have hematuria than those with normal thickness of GBM (192). Granules and lucency have been described in the GBM (191). Duplication and wrinkling have also been noted in the GBM (191). Other miscellaneous changes in the components of the capillary wall have been described to

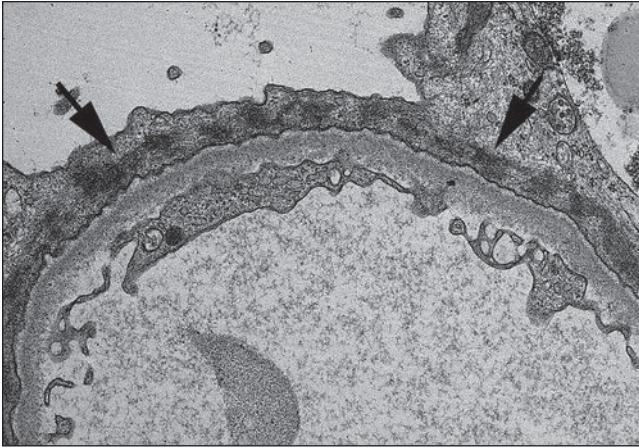


FIGURE 5.11 Electron micrograph of a portion of a glomerular epithelial cell with foot process effacement shows aggregation of microfilaments (arrowheads). (Uranyl acetate and lead citrate; $\times 10,000$.)

include swelling of the endothelial cells, lipid droplets in the mesangial cells, microfilaments, and curved striated bodies in the mesangial matrix (191,193). On occasion, investigators have described small deposits in the mesangial matrix or in the subendothelial space. It is doubtful that they represent true immune complexes (191,193).

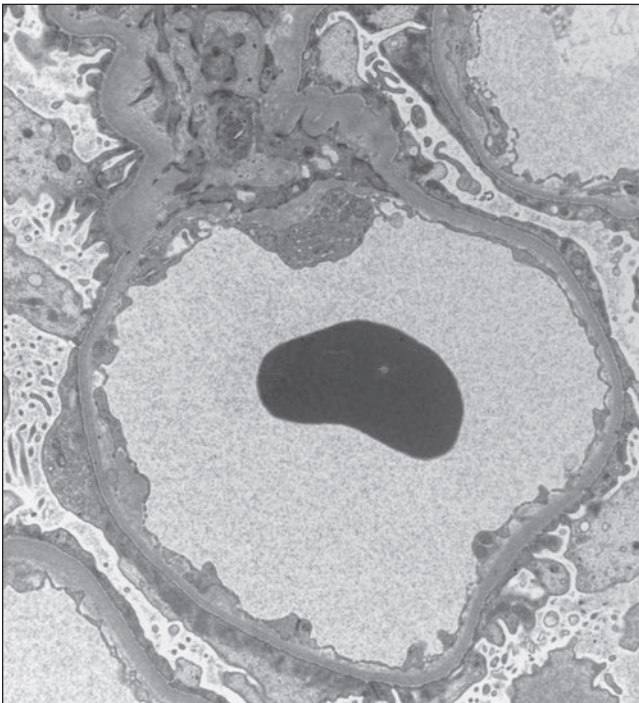


FIGURE 5.12 Electron micrograph of a glomerular capillary loop showing thin glomerular basement membrane with extensive effacement of foot processes. (Uranyl acetate and lead citrate, $\times 9500$.)

Immunohistochemical and Molecular Findings

Oomura et al. (194), in their histochemical study of the GBM and mesangial matrix, did not detect any differences between patients with MCD and controls with respect to the various collagens tested, heparan sulfate core protein, laminin, or fibronectin. Decreased anionic staining sites in the GBM have been noted in MCD using polyethyleneimine as a cationic probe (195).

More recently, investigators have turned their attention to an examination of alterations in the visceral epithelial cells. Barisoni et al. (196) showed that podocytes in MCD retain their differentiated phenotype. Schmid et al. (197) measured mRNA for α -actinin-4, GLEPP-1, WT-1, synaptopodin, dystroglycan, nephrin, podoplanin, and podocin in microdissected glomeruli and found no difference from controls. Other investigators have also confirmed that α -actinin (198), podocin, synaptopodin (199), podoplanin, and podocalyxin (200) were similar to controls. Using microarray technology following laser capture microdissection of glomeruli from patients with MCD, Hodgkin et al. (201) found that mRNA expression of podocyte differentiation markers was similar to normal controls and clustered apart from FSGS samples. Kavoura et al. (202) showed reduced podocalyxin using histochemical techniques in patients with MCD. Synaptopodin was slightly decreased in MCD when measured by quantitative image analysis (203). Furthermore, the glomerular epithelial cells are in growth arrest, as expected (203). Nephrin, one of the major proteins found in the filtration slit diaphragm, is unchanged in amount in MCD (204–206). Kim et al. (205) used immunogold to detect nephrin and found that the number of particles per filtration slit was unchanged in MCD as compared to controls but that the number of slits was decreased secondary to the effacement of foot processes. Lahdenkari et al. (207) studied 25 adult Finns with MCD as children. Twenty were steroid sensitive although nine had frequent relapses, and five were steroid resistant. Three of the patients continued to have proteinuria, but all had normal renal function. Twelve patients had sequence variations in 11 exons in the gene for nephrin. They found that there was a correlation between the mean number of nucleotide changes and the severity of the disease. Five of the patients had nonconservative amino acid changes that lead to a conformational alteration in the protein. Four of these five patients showed a poor initial response with remission occurring more than 5 years after onset of greater than 10 relapses. They suggested that mutations in nephrin may affect the course of MCD. Caridi et al. (208) found podocin mutations in 2 of 30 patients with MCD. Galectin-1 colocalizes with nephrin at the slit diaphragm and has been shown to be reduced in patients with MCD (209).

Complement receptor 1, a complement regulatory protein, is reduced in many glomerular diseases, including MCD (210). The α and β dystroglycan subunits are normally present at the basal cell membrane of the foot processes with the α subunit binding to matrix proteins and the β subunit linking to actin (61,64). Both subunits are decreased in MCD (61,64). Steroid therapy restored dystroglycan to normal levels (61). Caveolin-1 is increased in endothelial cells in a number of glomerular diseases including MCD and correlates to the degree of urinary protein (211).

Pathogenesis

The precise pathogenesis of MCD remains unknown. Several possible pathogenetic mechanisms have been suggested. Abnormalities in the immune system have been considered for

many years in view of the sensitivity of this disease to steroid therapy. Some of the possible immune mechanisms include circulating factor(s), T-cell dysfunction, in particular alterations in the T-regulatory (T-reg) cells, alterations in T-cell differentiation, and abnormal regulation of T cells by B cells. Other investigations suggest that podocyte abnormalities and epigenetic mechanisms are important. It seems likely that the pathogenesis of MCD is due to a complex interplay of several of these possible mechanisms (212).

One of the first pieces of evidence for a role for cell-mediated immunity in the pathogenesis of MCD was the occurrence of NS with the pathologic features of MCD in certain patients with Hodgkin disease (213). On the basis of this observation, coupled with the beneficial effects on MCD of measles, steroids, and cyclophosphamide—all of which are modifiers of cell-induced immunity—an early hypothesis was put forward by Shalhoub (214), who suggested that an episodic activation of a clone of T cells, in response to an unknown antigen, produced a circulating lymphokine with the ability to render capillary walls unduly permeable. Several cases of the NS with pathologic findings of both MCD and interstitial inflammatory infiltrates support a role for T lymphocytes in the pathogenesis of MCD (215–217). In those cases associated with the administration of fenopufen, a nonsteroidal anti-inflammatory agent, the interstitial infiltrate was mainly composed of cytotoxic T cells (217). Other studies cited MCD in association with various neoplasms of leukocytes, including mycosis fungoides with visceral involvement that resolved with treatment of the neoplasm (215) and angiotropic large cell lymphoma (216). In the latter case, effacement of foot processes of the epithelial cells was present only in areas proximate to large neoplastic cells within glomerular capillaries. The foot processes were discrete in areas away from the tumor cells. It was again suggested that a lymphokine may have been secreted by the tumor that injured the epithelial cells in some way.

The search for lymphokine(s) and other substances capable of producing the structural and functional changes associated with MCD has been under way for several years. Tomizawa et al. (218) found that the T lymphocytes of patients with MCD produced a vascular permeability factor. Other investigators isolated a variety of proteins from the urine or plasma of patients with MCD but not from patients whose NS was associated with other glomerular lesions (219,220). Recombinant hemopexin reduces the charge of the GBM and induces proteinuria after renal perfusion in rats (221). Furthermore, hemopexin has been shown to cause nephrin-dependent actin remodeling within podocytes *in vitro* resulting in membrane ruffling (222). Holt et al. (223) studied plasma and urinary levels of heparanase in children with MCD as well as in adults with NS including four with MCD. They found that plasma heparanase was decreased in children with active disease as compared to normal children. Adults also showed decreases in plasma heparanase but no change in urinary heparanase. The authors hypothesized that at least in children, the heparanase bound to the endothelial cells resulting in degradation of heparan sulfate glycosaminoglycan and increased glomerular permeability. The idea is supported by an animal model in which overexpression of heparanase leads to an MCD phenotype (224).

The search for circulating factors led to an examination of the levels of various cytokines in MCD as a number of ILs are able to alter glomerular permeability (225–227). However, the

production of cytokines by T cells is controlled by T-reg cells that suppress the production of cytokines by the T-effector cells, leading Araya et al. (228) to examine the question of whether the T-reg mechanism is deficient in MCD, allowing increased amounts of circulating cytokines. They found that the T-reg cells in patients with MCD in relapse were impaired in their ability to suppress the release of cytokines from T-effector cells. Furthermore, the ability to suppress such cells returned when the patients went into remission (228). This reduced ability to suppress T-effector cells was not due to a decrease in the number of T-reg cells. One possible mechanism is a reduction in IL-10 release. Another factor may be the balance between T-reg cells and T helper (Th)-17 cells (229). The balance between Th17 and T-reg cells is important in autoimmunity and control of inflammation. Liu et al. (229) examined adult patients with MCD and found an increase in the number of Th17 cells, their cytokines (IL-23 and IL-17), and their transcription factor (retinoic acid receptor–related orphan receptor γ T) with a corresponding decrease in the number of T-reg cells, their cytokines (IL-10 and TGF β), and transcription factor (fork-head/winged helix). Thus, these authors found an increase in the ratio of Th17/T-reg cells, and this increase correlated to the degree of proteinuria (229). The transcription factor NF- κ B plays a role in the development of both T-reg cells and Th17 cells (230). The NF- κ B pathway has been shown to be deregulated in MCD with increased activation in relapse (231). The pathway is repressed during remission (231).

Many authors cite the relationship between atopy or an increase in IgE that may be seen in MCD with an expansion of the T_H2 subset of CD4⁺ T lymphocytes (227,232,233). Cho et al. (232) looked for relationships between the levels of ILs and the activity of disease. They studied 22 children with MCD using CD23 as a molecular marker of IL-4 activity. They found that CD23 was elevated as compared to control patients. Eleven of the patients (232) who maintained high levels of CD23 relapsed quickly. Sahali et al. (234) demonstrated down-regulation of the IL-12R β 2 chain in MCD, which supports T_H2 polarization. Alterations in the mRNA splicing/transcription machinery may account for the T_H2 polarization (212). Additional mechanisms may involve changes in maturation of T cells in the thymus related to the autoimmune regulator protein (212). The recent successful use of rituximab, a monoclonal anti-CD20 antibody, to treat steroid-dependent idiopathic NS (235) suggests a possible role of B cells in the immune dysregulation in MCD acting through abnormal regulation of T-cell function by B cells or via abnormal communication between B and T cells (212).

The primary pathology in MCD is effacement of foot processes in the podocyte. Thus, we should also consider the role of this cell in the pathogenesis of this disease. CD80 is a transmembrane protein usually found on B cells and antigen-presenting cells where it acts as a costimulatory protein binding to CD28 (67). Reiser et al. (67) showed that CD80 (also known as B7-1) is expressed on podocytes and that its up-regulation by exposure to LPS results in reorganization of the actin cytoskeleton, disruption of the slit diaphragm, and FPE. Furthermore, they found that this up-regulation occurs following binding of the LPS to Toll-like receptor (TLR)-4, which is constitutively expressed on podocytes (67). This action was independent of T and B cells as SCID mice had FPE on exposure to LPS. Shimada et al. (236) found that TLRs 1 to 6 and

9 are also expressed on podocytes with TLR-3 most highly expressed. Polyinosinic-polycytidylic acid (PolyIC), the TLR-3 ligand, induced CD80 up-regulation associated with actin reorganization and decreased synaptopodin. In addition, they demonstrated that the signaling mechanism for the PolyIC involved interferon pathways and NF- κ B. Finally, since NF- κ B is targeted by corticosteroids, these investigators administered dexamethasone and showed that it decreased PolyIC-mediated CD80 expression and reduced podocyte injury (236). They hypothesized that the corticosteroids used to treat MCD may act on the podocyte as well as on T cells (236). Further credence to the idea that CD80 plays a role in the pathogenesis of MCD is provided by the finding that urinary excretion of sCD80 is increased in MCD in relapse as compared to patients with MCD in remission or with other proteinuric glomerular diseases as well as to normal healthy controls (155). However, these effects of LPS and PolyIC including up-regulation of CD80 are transient suggesting that they may represent a first hit, perhaps due to a viral infection in the case of MCD (237). CTLA-4 and IL-10 are able to inhibit CD80 expression. As described above, T-reg cells secrete IL-10 and may be dysfunctional in MCD. Shimada et al. (237) suggest that this inability to suppress the CD80 may represent the second hit that results in MCD.

Recent evidence implicates proteins secreted by podocytes in the pathogenesis of MCD (55,212,238–240). Angiopoietin-like-4 (Ang-4) is a glycoprotein that was found in highest concentration in adipose tissue and liver where it inhibited lipoprotein lipase (241). It is also secreted by podocytes and is up-regulated following injection of rats with a specific fraction of nephrotoxic serum (55,238). On further investigation, Clement et al. (55) found that Ang-4 colocalized with CD2 adaptor protein in a capillary loop pattern in normal rats. They also noted progressive up-regulation of the mRNA for Ang-4 in rats following a single dose of PA, a model for MCD. They demonstrated increased Ang-4 in serum, glomeruli, and urine of patients with MCD (55). They could reproduce the NS with selective proteinuria, effacement of foot processes, and loss of GBM charge in a rat model with transgenic expression of Ang-4. Furthermore, they found that GBM showed a loss of charge associated with a hyposialylated Ang-4, which they showed was specifically derived from podocytes. Taken together, these results as well as other confirmatory experiments suggested that Ang-4 likely plays a role in the pathogenesis of human MCD (55,238).

Two other proteins secreted by podocytes may also play a role in the pathogenesis of MCD. Ang-3 has also been found to be up-regulated using gene chips and tissues from various nephrotic diseases (239). Gao et al. showed that Ang-3 was up-regulated in an *in vitro* model of Adriamycin administration to podocytes associated with increased motility and permeability of the podocytes (239). A genome-wide association study has found an association between a variant of glypican-5 (GPC-5) and acquired NS of various types (240). GPC-5 is localized to the podocyte in the kidney and is involved in various signaling pathways (240). The studies on this protein are preliminary at this point.

Recent investigations suggest that epigenetic mechanisms play a role in the pathogenesis of MCD (212,242,243). Epigenetics refers to inherited modifications that alter gene expression or phenotype without altering the sequence of the

DNA. Such changes occur via DNA methylation, alterations in histones by acetylation/deacetylation, and gene silencing by interfering RNA (212). The possibility that epigenetic mechanisms may be important is suggested by the recognition that MCD relapses may be triggered by environmental factors, the relapsing/remitting pattern, the presence of epigenetic alterations in other autoimmune diseases, and the finding that remission following steroid therapy is attended by reversal of epigenetic alterations (212). Audard et al. (242) found that nuclear factor-related kappa B (NFRKB), a component of the chromatin-remodeling complex, is increased in amount in MCD in relapse when compared to patients in remission in CD4⁺ T cells and in B cells. Furthermore, the NFRKB was present in the nucleus during relapse, whereas it was restricted to the cytoplasm during remission. NFRKB also activated the AP-1 signaling pathway, which could result in increased secretion of some cytokines. Finally, it induced hypomethylation of genomic DNA indicating a role in gene regulation via increased binding of certain transcription factors (242). Kobayashi et al. (243) found that DNA methylation was decreased in several genes in Th0 cells but not in monocytes. They hypothesized that this may influence the differentiation of Th0 cells to Th effector cells or alter gene expression after such differentiation.

Differential Diagnosis

The differential diagnosis of MCD includes IgM nephropathy, C1q nephropathy, CNS, and FSGS. IgM nephropathy is a clinicopathologic entity that shows either no glomerular changes by light microscopy or mild mesangial hypercellularity accompanied by bright staining of the mesangium by antiserum to IgM on immunofluorescence (244,245). Tejani and Nicastrì (246) noted the frequent presence of hematuria in the clinical presentation as well as a less responsive result to therapy. However, the lesion became controversial because IgM is frequently seen in biopsies as a nonspecific finding. As summarized by Border (247), confusion arose due to variance in the definition of significant IgM deposits. I restrict the diagnosis of IgM nephropathy to those cases with bright staining (at least 2+ out of 3) and with demonstrable mesangial deposits on electron microscopy. Al-Eisa et al. (248) found no difference in relapse rates or response to therapy for children with IgM deposition as compared to those with MCD without IgM. Another study in 110 adults and children with IgM nephropathy and 15-year follow-up showed that 22.7% progressed to end-stage renal disease with another 13.7% manifesting renal insufficiency (249). More recent studies have examined differences in response to therapy. Swartz et al. (174) found that children with an MCD pattern of histology and IgM on immunofluorescence had a poorer prognosis with 17% developing chronic kidney disease or end-stage renal disease. Furthermore, they had a poorer response to cyclophosphamide. Geier et al. (250) did not see a difference in response to cyclophosphamide for patients with IgM nephropathy. Kanemoto et al. (251) found an increase in steroid resistance in patients with IgM mesangial positivity on immunofluorescence but a good response to cyclosporine A (CSA) equivalent to patients without IgM.

Jennette and Hipp (252) first described C1q nephropathy in 15 patients with predominant mesangial C1q localization along with C3 and immunoglobulins in patients without evidence of systemic lupus erythematosus. Light microscopic

examination revealed changes that ranged from normal to mesangial proliferative to active GN. Iskandar et al. (253) studied 15 patients between 2 and 16 years of age with a female predominance of 2:1. Eight had a light microscopic appearance of MCD, while the others showed either mesangial proliferation or a picture similar to FSGS. Most had well-defined mesangial deposits on electron microscopy. Patients who presented with NS and/or who had FSGS-like picture on biopsy were less likely to respond to steroids. Markowitz et al. (254) studied 19 patients between the ages of 3 and 42 with a female predominance. Fourteen of their patients were African American. The authors believe that this represents a variant of FSGS since the majority of their patients had that microscopic picture. More recent studies, including one review of the literature have examined the relationship between histologic pattern and course of the disease (255–257). Hisano et al. studied 61 patients (255). Most showed an MCD pattern with only eight having an FSGS pattern on light microscopy. The only patients requiring dialysis were two of the patients with FSGS. Vizjak et al. (256) examined 82 biopsies from 72 patients with mesangial C1q on immunofluorescence and discerned differences in both presentation and course with differing histologic features. They found that those patients who presented with NS had either an MCD or FSGS pattern on histology. Seventy-seven percent of the patients with MCD remitted, while 33% with FSGS progressed to end-stage renal disease. The patients with a proliferative GN presented with either chronic kidney disease or simply hematuria/mild proteinuria. More than half of this group maintained stable renal function. A review of the literature not including the last two studies discussed above found a similar correlation between presentation and histologic appearance and course (257). These studies suggest that the pathogenesis may vary according to different histologic appearances, a concept that will require further study (255–257).

The clinical presentation of FSGS is frequently identical to MCD so that the most common question asked of the renal pathologist in biopsies of children with the NS is to distinguish between these two entities. When classic segmental sclerosis lesions are present (see Chapter 6), then there is no problem, and the diagnosis of FSGS can be made. However, since by its nature FSGS affects only some glomeruli, it may be impossible to distinguish between these two with certainty particularly if the biopsy is small. Several features can favor one or the other. These include glomerular size, presence of tubular atrophy, and sample of deep cortex. Fogo et al. (258) examined glomerular size in the initial biopsy of children with NS. Of the 42 initial biopsies, 23 showed a glomerular area less than that of controls, and only 1 of these patients proved to have FSGS on subsequent biopsy. In contrast, FSGS was confirmed at the second biopsy in 5 of 15 patients with initial biopsies that showed a glomerular area up to 1.75 times that of controls and in all 4 patients with a glomerular area greater than 1.75 times that of controls. These findings were confirmed in another study that showed that the glomerular volumes were greater in children with FSGS and diffuse mesangial sclerosis (DMS) than in patients with MCD (259). The presence of tubular atrophy suggests the possibility of a glomerulus with a segmental lesion in the tissue near the biopsy especially in children. It is useful to have a sample of juxtamedullary cortex as that is the first location of such lesions in FSGS.

Dissection of possible pathogenetic mechanisms for MCD has led to the finding of elevation of CD80 in the urine of patients with MCD in relapse (155,156) but not in the urine of patients with FSGS (156). Other investigators found oligomers of Ang-4 in the urine of patients with MCD in preliminary studies (55). Additional experiments have demonstrated a reduction in a podocyte protein pdlim-2 in glomeruli of patients with MCD and membranous GN but not FSGS using immunoelectron microscopy (260). Clinical tests have not yet been validated for any of these substances in the diagnosis of MCD. Genetic testing is now available for a number of genes involved in CNS, DMS, FSGS, and a number of other different conditions presenting with NS in childhood (261–265). The genes involved in CNS and DMS are discussed at the end of this chapter. The genes involved in FSGS are discussed in Chapter 6. An approach for genetic testing in steroid-resistant NS is provided by Santin et al. (265).

Course of Disease, Prognosis, Therapy, and Clinicopathologic Correlation

Clinical Course in Children

Remission from the NS occurs in MCD within 8 weeks of onset of therapy with a frequency of 90% to 95% (114,118,163,266,267). However, sustained remission has been reported to vary between 10% and 60% (266,267). Remissions may occur spontaneously, be brought on by infections, or follow treatment with steroids (114).

Several studies have evaluated the clinical course in children with MCD. Trompeter et al. (268) reported on the long-term follow-up into adulthood of 152 patients who were seen initially when less than 10 years old for treatment of the NS. Biopsy showed MCD in each case. They were treated with prednisone therapy. At the last follow-up, 131 were in remission. One hundred of those in remission had not relapsed in greater than 4 years. Only 5.5% of the total number continued to have relapses as adults. It is interesting to note that those who continued to relapse had been less than 6 years old at the initial presentation. Eleven patients had died, seven from complications of the NS. More recent studies show higher rates and frequency of relapse extending into adulthood (269–271). A study from India in 1071 patients with steroid-sensitive NS (70% had MCD on biopsy) demonstrated that more than 50% were frequent relapsers in the early period after onset (272). Risk factors for relapse included younger age at onset, initial therapy for less than 8 weeks, and short time of initial remission (272). Relapses may follow minor upper respiratory tract infections. Treatment with prednisolone during such intercurrent infections cut relapse rates in half (273). In a separate study, low birth weight was associated with an adverse effect on the course and prognosis of MCD (274). Other investigators have found that as many as 25% of patients with biopsy-proven MCD continue to relapse into adulthood while maintaining normal renal function (270). Such patients suffer from the complications of the various therapeutic agents with which they are treated including infections (the most common cause of mortality), hypertension, osteoporosis, decreased visual acuity, infertility, obesity, and short stature (270,271). The role of polymorphisms in such genes as *NPSH1* and *NPSH2* in determining the risk for relapses is being studied, but definitive results have yet to be reported (207,270,271).

Clinical Course in Adults

The response to steroids of MCD in adults is similar in many aspects to that of children, but it is distinguished by a significantly longer interval from initiation of therapy to response. Older series reported a good response to steroids (164,275) and a high incidence of relapse. This finding is in contrast to later studies (143–145) in which the patients took longer to respond to steroids but suffered fewer relapses than children.

Nolasco et al. (145) studied 89 patients with adult-onset NS and MCD. Results of conventional prednisone therapy were examined in 75 patients. After an 8-week course, only 45 of 75 (60%) patients were in remission. However, continuation of therapy for an additional 8 weeks resulted in a remission rate of 81%. Long-term follow-up showed continued remission in 24%, infrequent relapse in 58%, and frequent relapses in only 21%. Treatment with cyclophosphamide in those who were resistant to steroids showed a similar trend toward a longer period of time for induction of remission but with a more stable result. Korbet et al. (144) studied 40 adults with MCD. They found that it often took longer than 16 weeks to induce the first remission, but remission was achieved in 91% of those so treated. At the last follow-up, 72.5% of patients remained in complete remission, 7.5% were in partial remission, and 20% continued to have NS. Similar results were found in a recent study in China (143). These investigators saw complete remission in 42%, 80%, and 94% at 4, 8, and 12 weeks, respectively. Relapses occurred in 42%. Because most adults with NS have a glomerular disease that is not responsive to steroids, achievement of an acceptable therapeutic risk/benefit ratio is predicted upon the demonstration by renal biopsy of MCD.

Prognosis and Therapy

Several clinical factors affect prognosis. The International Study (163) examined 218 patients with a biopsy-based diagnosis of MCD and an initial response to steroids. They found that the number of relapses occurring in the first 6 months best predicted the number of subsequent relapses. Another predictor of prognosis is the degree of selectivity of the proteinuria. Bazzi et al. (276) studied the selectivity index defined as $SI = uIgG/slGg \times (sTf/uTf)$, where Tf is transferrin. Nine had MCD; the remainder had FSGS or membranous GN. High selectivity was defined as an index less than 0.1 with nonselectivity having a value 0.2 or higher. Six of the MCD patients had high selectivity, two had moderate selectivity, and one had nonselective proteinuria. Prognosis was determined by the degree of selectivity as all patients with high selectivity went into remission. Fifty-nine percent of those with moderate selectivity went into remission with 25% progressing to renal failure. The group with nonselective proteinuria had only 29% in remission and 35% went on to renal failure. Recently, it has been shown that serum IgE levels are elevated in patients with MCD as compared to patients with other diseases associated with the NS including membranous GN, IgA nephropathy, and membranoproliferative GN (277). Within the group of patients with MCD, IgE levels were higher in those who were steroid resistant and during relapse (277).

Steroids remain the first drug used to treat MCD at the initial presentation (278). In children with the first or infrequent relapses, steroids continue as the recommended therapy (278). The development of immunosuppressive drugs for

use in transplantation has provided new therapies to treat patients with MCD who have failed their course of steroids. In adults, the addition of CSA to prednisolone on the first relapse has been shown to shorten the time to remission and lessen the dose of steroids required for therapy (279). CSA may also be used in patients with frequent relapses although proteinuria often returns on cessation of therapy (280). Furthermore, CSA has the unfortunate side effect of causing interstitial fibrosis with possible progression to renal insufficiency (280,281). Independent risk factors for the occurrence of fibrosis include therapy for greater than 24 months and heavy proteinuria for more than 30 days during the treatment period (281). Mycophenolate mofetil (MMF) has been used as a steroid-sparing agent in patients with frequent relapses or in steroid-dependent NS particularly if they have failed CSA treatment (278,280,282). Oral cyclophosphamide (CYT) has been recommended for use in children with frequent relapses (278,283). In such cases, response is more likely in older children and in those with lower degrees of steroid dependence. CYT has not been found to be as useful in steroid-dependent cases (278,283). Steroid-resistant NS is the most difficult to treat. Many of the papers discussing this form of NS include patients with FSGS as well as MCD, and additional discussion of this topic is found in Chapter 6. One recent paper in adults with steroid-resistant biopsy-proven MCD compared the use of tacrolimus (TAC) to intravenous pulse CYT and found them both efficacious (284). The remission rate was 76% after 6 months of therapy in the TAC group and 50% in the CYT group. However, 40% of the TAC patients relapsed on cessation of therapy as compared to one out of seven in the CYT group who had remitted (284). As it is now believed that B cells may also play a role in the pathogenesis of MCD, agents such as rituximab, a monoclonal antibody that inhibits CD20-mediated B-cell proliferation and differentiation, have now been added to the list of useful therapeutic agents to be used in treating steroid-resistant forms of the disease (285,286). In children, small studies have shown excellent results in steroid-dependent forms of MCD with four of five children having complete remission with relapse in two of those four (285). Most of the children with steroid-resistant NS had FSGS in this review. Nonetheless, some had at least partial remission. Takei and Nitta (286) reviewed seven case reports of patients with frequently relapsing or steroid-dependent MCD and found that six had complete and one patient had partial remission with three relapses. Both groups of authors caution about possible adverse effects such as increased risk of infection and suggest that controlled clinical trials are needed to fully assess this new therapy (285,286).

Clinicopathologic Correlation

RELATIONSHIP BETWEEN MCD AND FSGS

Progression of MCD to chronic renal failure and death from uremia occurs in less than 1% of patients with biopsy findings interpreted as MCD at the onset of proteinuria, before the initiation of therapy (114,268). However, subsequent identification of FSGS has been documented in a few patients, especially among those with a frequently relapsing course (114). This may be interpreted as progression of MCD to FSGS. However, it is possible in those cases that FSGS was not diagnosed in the initial biopsy because a sclerotic glomerulus was not included in the biopsy sample (see Chapter 6). However, as we now

understand more about the genetics and pathogenesis of these diseases, it has become clear that they are separate entities.

MESANGIAL HYPERCELLULARITY

Investigators have tried to define predictors of clinical behavior in MCD—chiefly steroid responsiveness—by analyzing histologic features seen on renal biopsy and clinical presentation. The International Study of Kidney Disease in Children (163) divided 389 children with MCD into five histologic groups. There were 219 children with MCD without either glomerular or tubular abnormality, 98 with focal glomerular obsolescence (focal global glomerular sclerosis), 16 with mild mesangial thickening (increased matrix without hypercellularity), 29 with focal tubular changes, 27 with mild mesangial hypercellularity (up to 3 cells per mesangial area), and 12 with diffuse mesangial hypercellularity (more than 4 cells per mesangial area) (see Fig. 5.6). These investigators found that the level of initial nonresponse to steroids in the children with tubular changes (14.3%), mild mesangial hypercellularity (14.8%), and diffuse mesangial hypercellularity (45.5%), taken as a group, was greater than in children with nil disease (4.7%), focal glomerular obsolescence (7.8%), and mild mesangial thickening (6.3%) ($P < 0.02$). The children with diffuse mesangial hypercellularity also showed a higher rate of initial nonresponse compared with the children with mild mesangial hypercellularity. However, there were no differences among the groups with respect to either relapses or deaths, and by 52 weeks, the differences in the proportions of patients who remained proteinuric were no longer statistically significant.

Other groups have found that increased mesangial hypercellularity correlated with more frequent relapses. Siegel et al. (287) studied 38 such children who initially had uncomplicated NS. They all had a good initial response to steroids, but steroid-dependent, frequently relapsing NS developed in all of them. Before initiation of cyclophosphamide therapy, each had a renal biopsy that showed a spectrum of glomerular pathologic changes: MCD in 47%, mesangial hypercellularity in 24%, and FSGS in 29%. They all responded to cyclophosphamide, but relapses occurred at a rate of 22% in the children with MCD, 56% in those with mesangial hypercellularity, and 73% for the children with FSGS. Although the glomerular pathologic lesion at presentation was unknown, histologic information obtained at the time when the patients showed signs of steroid dependence clearly predicted subsequent behavior.

Long-term prognosis does not seem to vary with the degree of mesangial hypercellularity. The Southwest Pediatric Nephrology Study Group (162) found that there was a correlation between the degree of mesangial hypercellularity and the initial response to steroid therapy. However, long-term follow-up of the five children with the most severe mesangial hypercellularity showed variable responses. Additional groups have confirmed these findings (166,288). Thus, children with the NS and diffuse mesangial hypercellularity had an overall good prognosis despite a tendency toward initial nonresponse to steroid therapy.

FOCAL GLOBAL GLOMERULAR SCLEROSIS

As stated above, the International Study of Kidney Disease in Children (163) found that focal global obsolescence did not seem to have an effect on prognosis. However, Figure 2 in that manuscript shows the involuted type of glomerular

obsolescence described by Dijkman et al. (168) that is not associated with tubulointerstitial lesions. It appears that this type of glomerular change does not affect prognosis. Querfeld et al. (289) defined focal global sclerosis as the presence of greater than 15% of glomeruli with complete obsolescence accompanied by tubular atrophy and interstitial fibrosis. Out of 238 patients with idiopathic NS, 5 had focal global sclerosis (2.1%). At their last evaluation, three were in complete remission, one was in partial remission, and one patient had persistent proteinuria. The last two also had hypertension. A larger study with a reasonable follow-up period is required to determine whether this alteration has an effect on therapeutic response and/or long-term outlook.

GLOMERULAR TIP LESION

The glomerular tip lesion was first described by Howie and Brewer (290) and defined as the presence of glomeruli with a segmental lesion at the outer 25% with adhesion or prominence of podocytes at the tubular neck. This change is usually accompanied by endocapillary hypercellularity with or without foam cells or sclerosis (290,291). On the basis of their observation of these lesions in patients dying of MCD prior to 1950 due to the lack of steroid therapy, Haas and Yousefzadeh suggested that this lesion could be seen in MCD particularly in the setting of heavy proteinuria (292). Howie et al. (293) in a review of 50 biopsies previously classified as MCD found the tip lesion in four patients. Three were in remission on follow-up, but one developed FSGS. Stokes et al. (291) have suggested that it represents a distinct entity that lies somewhere between MCD and FSGS with respect to prognosis. This lesion is more fully discussed in Chapter 6.

Secondary Causes of Minimal Change Disease

Secondary forms of MCD can be the result of treatment with various therapeutic agents particularly, NSAIDs, lymphomas and other neoplasms, allergic reactions, infections, and transplants. The glomerular lesion is indistinguishable from idiopathic MCD, and the diagnosis of secondary MCD is based upon the clinical history.

Nonsteroidal Anti-inflammatory Drugs and Other Pharmacologic Agents

The usual pattern of nephrotoxicity with this family of anti-inflammatory agents is interstitial nephritis, as is discussed in Chapter 25. However, nephrotoxicity may also manifest as the NS (217,294). When this occurs, the biopsy shows MCD that may or may not be accompanied by interstitial infiltrates (Fig. 5.13), usually consisting of T cells (217,294). Warren et al. (294) found that 5 of their 55 adult patients with MCD used NSAIDs. Two patients showed signs of ARF in addition to the NS. All had complete remission on withdrawal of the offending agent. Four of the five patients went into remission in 15 days, which represents an unusually rapid response to therapy for idiopathic MCD in adults. The patients were followed for 1 to 10 years and suffered no relapses. A case of interstitial nephritis and MCD with the COX-2 inhibitor, celecoxib, has been reported (295). NS secondary to drug toxicity from NSAIDs may also be accompanied by acute tubular necrosis (296).

Several other drugs have now been associated with MCD (297–301). In each case, the NS has resolved with withdrawal

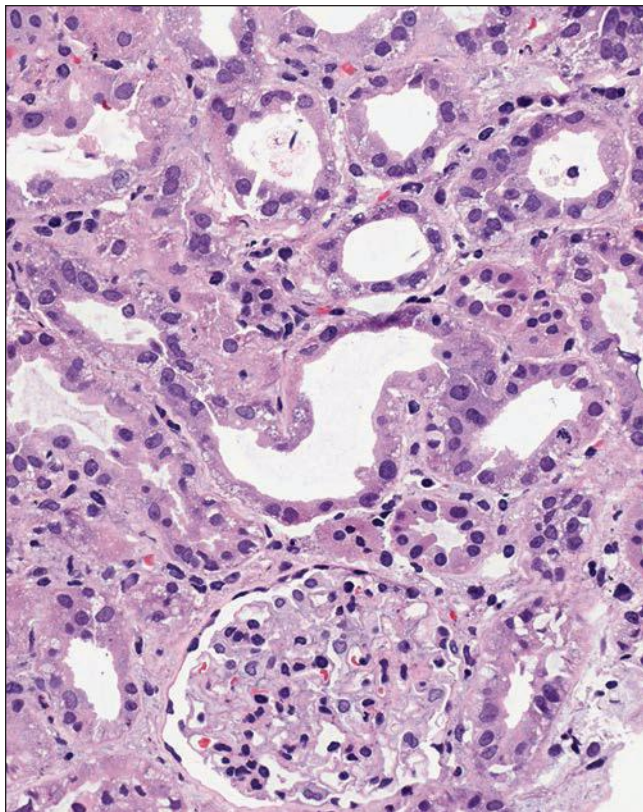


FIGURE 5.13 Light micrograph of kidney biopsy from a patient who had used NSAIDs and presented with nephrotic syndrome and acute renal failure. The glomerulus shows no abnormalities. Diffuse tubular injury is present with mild tubular dilatation, chronic inflammatory infiltrate, and mild interstitial edema. (H&E, $\times 300$.)

of the offending agent. Interferon- α was used to treat hepatitis C virus infection (299). Interferon- β was used to treat malignant melanoma (300). The NS disappeared with withdrawal and reappeared with reinstatement of the drug. Barri et al. (298) reported five cases of NS associated with pamidronate, a bisphosphonate used to treat bone-related complications in multiple myeloma. Two showed MCD, two had FSGS, and one had the collapsing variant of FSGS. All but the patient with the collapsing lesion resolved on discontinuation of the drug, although one had persistent proteinuria. Lithium and a mercury-containing skin-lightening cream have also been associated with MCD (297,301).

Lymphoma and Other Neoplasia

The NS has been described in patients with a variety of neoplasms (302,303). Approximately 11% of patients with the NS have an associated neoplasm. This percentage increases to 22% in patients older than 60 years with the NS (303). Most cases with MCD have been associated with lymphomas, most commonly Hodgkin disease (213,302,304). However, only 0.4% of patients with Hodgkin disease develop MCD (303). Dabbs et al. (305) compiled 63 cases of Hodgkin disease complicated by the NS and found 41 cases of MCD with remaining cases representing a variety of different glomerular lesions. The severity of the renal disease often parallels the course of the tumor,

and proteinuria may herald a recurrence (305). The NS occurs in Hodgkin disease with greater frequency than if it were a chance association. In favor of a causal relationship is the fact that there is usually a rapid clearing of the NS when irradiation or chemotherapy is instituted (304,306). In addition, NS may recur upon relapse of Hodgkin disease (305,306). The mechanism producing MCD in Hodgkin lymphoma is not yet known, but it is of interest that there is T_H2 polarization in both conditions suggesting the possibility of a link through a cytokine common to both (302).

The picture of MCD, while predominating in Hodgkin disease, is not found so frequently in non-Hodgkin lymphomas and leukemias, where several different types of lesions have been described. For example, in the series of Dabbs et al. (305), there were 32 patients with non-Hodgkin lymphomas associated with the NS. Of these, five had MCD, but the remaining had other glomerular lesions. Case reports of other types of leukemias and/or lymphoproliferative disorders have also shown an association with the NS, often with MCD as the glomerular lesion (302,303).

Rare association has been reported with rectal carcinoma, bronchogenic carcinoma, and renal cell carcinoma (302,307,308). Two cases have been reported showing an association between MCD and bronchogenic carcinoma (308). A case of renal cell carcinoma with MCD that remitted on removal of the tumor has also been reported (307). In the case of the rectal carcinoma, the patient had increased levels of VEGF that returned to normal on resection of the tumor (309). Proteinuria also disappeared with resection.

Bee Sting, Hypersensitivity, and Autoimmune Disorders

Atopy has been reported in up to 50% of children with MCD and is thought to be a possible inciting factor by some (101,310). As mentioned in the section on Pathogenesis of MCD, T_H2 polarization is thought to play a role in the evolution of MCD (212), and an expansion of the T_H2 compartment is also seen in allergy. However, IL-4 is the cytokine released by T cells in allergy, whereas IL-13 is the more critical factor in MCD (310). Nevertheless, bee stings have been temporally associated with an abrupt onset of NS (311–313). In these cases, the NS has responded promptly to steroid therapy, and no relapses have occurred (311–313). The histologic picture has been that of MCD.

A variety of other case reports have been published of patients with MCD and with a range of associations including hypersensitivity, autoimmune disorders, and parasitic diseases. In most cases, the MCD remitted with appropriate therapy of the underlying condition. These associations include postvaccination (314), Guillain-Barre syndrome (315,316), Hashimoto thyroiditis (317,318), pemphigus (319), ehrlichiosis (320), *Strongyloides* (321), pertussis (322), and hydatid disease (323).

NEPHROTIC SYNDROME IN THE FIRST YEAR OF LIFE

Hinkes et al. (324) demonstrated that mutations in *NPHS1*, *NPHS2*, *WT-1*, or *LAMB2* accounted for two thirds of cases in 975 infants presenting with the CNS prior to their first

birthday. NS present at birth or developing within the first 3 months has been termed CNS. The most frequent disease in this group is CNS of the Finnish type and is now known to be caused by mutations in *NPHS1*, the gene that codes for nephrin (14,325). The preferred terminology is now CNS type 1 (325). NS presenting between 4 and 12 months of age has been called infantile NS and is due to a number of other mutations (Table 5.6) that frequently show DMS on biopsy. Mutations in *PLCE1* are associated with either isolated DMS or FSGS. Mutations in *WT-1* and *LAMB2* are associated with syndromic DMS and are discussed below. Mutations in *NPHS2* are associated with the pathology of FSGS and are discussed in Chapter 6. It is becoming evident that patients who develop NS in the first year of life require mutational analysis as well as renal biopsy in order to determine prognosis and appropriate treatment (261,326). Novel mutations can be expected in the future, and additional analysis may provide better therapeutic options.

Congenital Nephrotic Syndrome due to Mutation in *NPHS1* (Finnish Type)

The congenital nephrotic syndrome of the Finnish type (CNF), now termed CNS type 1, is phenotypically and genetically distinct from the other causes of the NS that develop during the first postnatal year. Proteinuria begins during gestation, and it is always present at birth, which is often premature, accompanied by a large placenta (327,328). The neonates may show muscular hypotonia and cardiac hypertrophy (327). Microscopic hematuria is often present, and mild degrees of aminoaciduria and glucosuria are commonly found, presumably owing to tubular changes. Serum creatinine is typically normal during the first few months.

CNF has an autosomal recessive mode of inheritance, and it occurs in various ethnic groups and races. However, more than half of the published cases are from Finland where the gene frequency is 1:200 with an incidence of 10 to 12.5 per 100,000 live births (327,329). The responsible gene (*NPHS1*) was identified by genome-wide screening of affected Finnish families and was localized to the long arm of chromosome 19 (19q13). In Finland, two *NPHS1* mutations are responsible for most of the cases of CNS: Fin-major is a deletion of nucleotides 121–122, and Fin-minor encodes a premature termination (14). More than 173 mutations have now been recorded involving most of the exons (330,331). Nephrin, the protein product of *NPHS1*, is a major component of the slit diaphragm (332,333), and intact nephrin is required for the stability and normal function of the glomerular filter (14). Defective nephrin synthesis leads to a lack of slit diaphragms and podocyte

dysfunction resulting in proteinuria. Nephrin also functions as a regulator of cell signaling and of the actin cytoskeleton (334). In fact, nephrin interacts with many of the other proteins that are products of genes mutated in the other forms of NS that will be discussed later in this chapter and in Chapter 6 (334). Interference with nephrin function in mice by injecting anti-slit diaphragm antibody (335) or absence of the gene in knockout mice (336) results in proteinuria, ultrastructural pathology in or absence of the slit diaphragm, and FPE.

The kidneys are usually increased in size, and some show minute cortical cysts, confined to the deeper cortex (328,337,338). The glomerular pathology is not diagnostic of CNS, and the most common pathologic finding is tubular dilatation (Fig. 5.14). Few glomerular abnormalities may be present at birth, but fetal glomeruli, mesangial sclerosis, and global glomerular sclerosis are seen in varying proportions as the disease develops (339). The mesangial expansion is due to an increase in both number of mesangial cells and matrix (340). The proximal convoluted tubules in many cases are dilated, with a low, lipid-containing epithelium (337). Nephron dissection (338) confirmed that the tubular dilatation is in the proximal convoluted segment, and it has been called microcystic disease. The tubule is segmented like a string of sausages, and in some of the affected nephrons, the capsular space of the glomerulus is dilated.

Electron microscopy (341–344) shows wide-spread effacement of the glomerular epithelial cell foot processes. Slit diaphragms are not seen between the adjacent pedicels (Fig. 5.15), and nephrin is not usually expressed (344). Rare exceptions include one infant with the mutation Fin-major/R743C in whom slit diaphragms and glomerular nephrin expression were seen (343). Subendothelial widening was observed in some cases. The GBM is ultrastructurally and biochemically normal (345). Immunoglobulins and complement components are inconsistently present in the glomeruli where they are concentrated in scars (346).

The CNS is unresponsive to treatment, and without renal replacement therapy, survival beyond 10 years of age is rare (261,326,327). Management consists of albumin infusions, use of ACE inhibitors to reduce proteinuria, and parenteral nutrition as needed (261,326,327). In some cases, unilateral nephrectomy is performed in order to reduce protein loss (327). Others perform bilateral nephrectomy followed by peritoneal dialysis to avoid the complications of the NS and allow the child to reach sufficient size for transplantation (327). As genetic testing has expanded in childhood NS, numerous mutations in *NPHS1* have been identified with several of these

TABLE 5.6 Mutations causing nephrotic syndrome in the first year of life

Gene	Inheritance	Protein	Phenotype	Chapter
<i>NPHS1</i>	AR	Nephrin	CNS; loss of slit diaphragms	5
<i>NPHS2</i>	AR	Podocin	CNS or early or late SRNS; FSGS	6
<i>PLCe1</i>	AR	Phospholipase Ce	Early SRNS; DMS or FSGS	6
<i>LAMB 2</i>	AR	Laminin β 2	CNS; Pierson DMS	5
<i>WT-1</i>	AD	Wilms tumor 1	Denys-Drash, Frasier; WAGR; DMS	5

AR, autosomal recessive; AD, autosomal dominant; CNS, congenital nephrotic syndrome; SRNS, steroid-resistant nephrotic syndrome; FSGS, focal segmental glomerulosclerosis; DMS, diffuse mesangial sclerosis; WAGR, Wilms tumor, aniridia, genitourinary malformations, and mental retardation

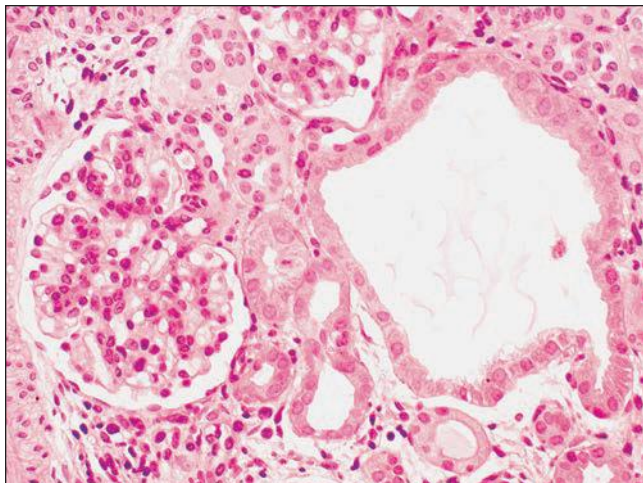


FIGURE 5.14 Light micrograph of congenital nephrotic syndrome of the Finnish type. The glomerulus shows diffuse mesangial hypercellularity. Note the tubular cyst. (H&E, $\times 330$.)

showing milder phenotypes (325,331,343). Several missense variants trafficked to the plasma membrane and were able to form dimers (347). Patients with these variants presented at an older age and had a milder form of the disease (347). In a similar vein, Machuca et al. (348) examined genotype-phenotype correlations for mutations in *NPHS1* and found that patients with milder cases had either mutations in the cytoplasmic tail or missense mutations in extracellular domain that retained function.

Transplants are usually performed in patients between 1 and 2 years of age with 5-year patient survival of 90% and graft survival of 80% (327). Recurrent disease following transplantation is not expected, but Patrakka et al. (349) observed NS in 13 of 51 grafts in children with *NPHS1* mutations: The

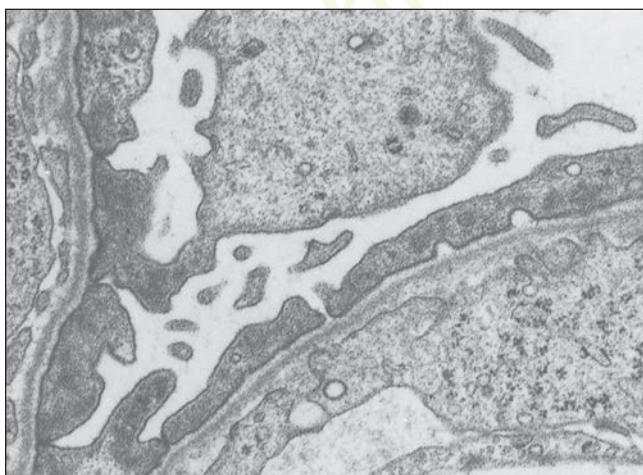


FIGURE 5.15 Electron micrograph from congenital nephrotic syndrome of the Finnish type. Note the absent slit diaphragm between the z pedicels. (Uranyl acetate and lead citrate, $\times 12,000$.)

nephrotic grafts showed FPE and decreased slit diaphragms, and nephrin mRNA and protein were decreased in some biopsies but never absent. All the patients had the Fin-major/Fin-major genotype that is associated with absent nephrin in the native kidneys, and antinephrin antibodies developed in four of nine patients supporting an immune pathogenesis. Seven episodes in this series responded to cyclophosphamide therapy, but six grafts were lost. Chaudhuri et al. (350) reported the successful use of rituximab in a single case of recurrence of NS. Decrease in B cells was associated with decrease in antinephrin antibodies. The child remained in remission at the time of publication. Thus, recurrent NS in patients transplanted for CNS appears to have a different pathogenesis from the original disease.

Diffuse Mesangial Sclerosis

Most of the remaining forms of NS presenting in the first year of life are due to specific mutations and are associated with the pathologic picture of DMS (see Table 5.6). The pathology of DMS and these syndromes was described long before the underlying genetic defects were identified, and the syndromes and their interrelationships will be considered.

Habib and Bois (328) reported six cases of DMS in nephrotic infants, and they later collected and analyzed 40 patients with DMS (including 14 with the Denys-Drash syndrome) (351). The NS develops early in patients with DMS, and when it is present at birth, DMS may be confused with the CNS type 1 (Finnish type). However, its rapid course to end-stage renal disease and its characteristic glomerular pathology establish the diagnosis. All the glomeruli show mesangial sclerosis, and the matrix initially has a fibrillar appearance with the deeper glomeruli least affected. Later, in the course, accumulation of mesangial matrix obliterates the capillary lumens (Fig. 5.16). At advanced stages, the tuft contracts, but the epithelial cell hypertrophy persists. The tubules are dilated and atrophic, and they may contain hyaline casts. Nondiagnostic deposits of IgM and C3 are seen in the mesangium of the less affected glomeruli and at the periphery of the sclerotic glomeruli (351). Electron microscopy shows mesangial collagen fibrils, and the GBM is split and wavy because of zones of subepithelial lucent widening (Fig. 5.17). The patients presented by Habib et al. (351) generally progressed to end-stage renal disease in a few months, usually before 4 years of age; 10 patients received transplants, and none developed recurrent disease. Habib (351) reported 26 patients with DMS who did not have the other features of the Denys-Drash syndrome (see below), but their clinical presentation suggested that they were associated with an inherited systemic syndrome. Mutational analysis of 35 patients with isolated DMS found mutations in *PLCE1* in 10 patients (352). *PLCE1* codes for phospholipase C ϵ 1, which catalyzes the hydrolysis of phosphoinositides resulting in second messengers that are involved in growth and differentiation (352). The mutations in this study were frame shift, stop codon, or splice shift mutations. Missense mutations in this gene have been associated with more slowly progressing disease and FSGS on pathology (326).

WT1

This section focuses on the syndromes related to mutations in *WT1*: the Denys-Drash and Frasier syndromes. WT1 is a zinc finger transcription factor that plays a major role in kidney and

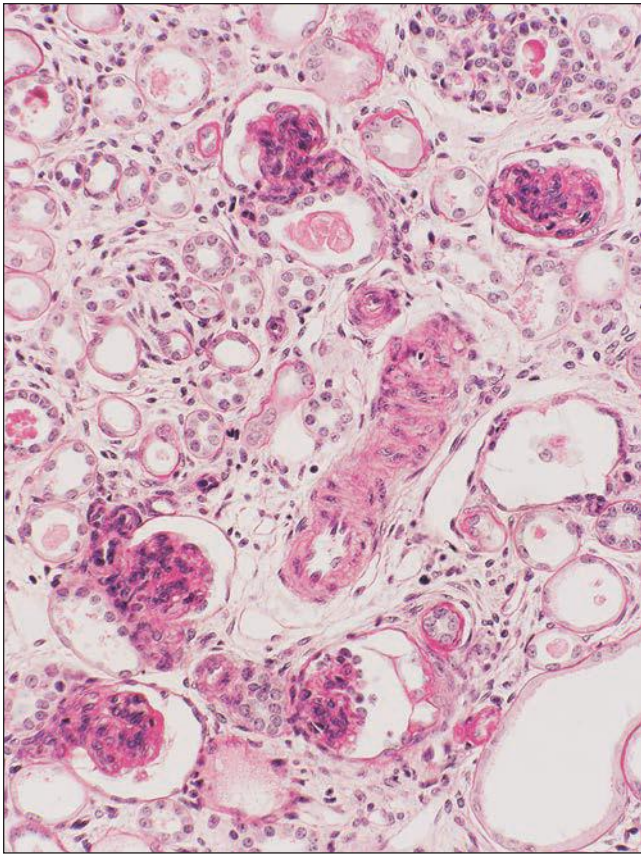


FIGURE 5.16 Light micrograph from patient with isolated diffuse mesangial sclerosis and nephrotic syndrome. The patient was an XX female who was nephrotic at birth. The glomeruli in this illustration are representative of the more than 100 glomeruli present on the biopsy. They show mesangial expansion with obliteration of the capillaries without adhesions or global sclerosis. The patient progressed to end-stage renal disease by 3 months of age. (PAS, $\times 330$). (Courtesy of Dr. Marie-Claire Gubler, Hôpital Necker-Enfants Malades, Paris.)

gonad development and maintenance of podocyte function (353,354). *WT1* was initially identified as a Wilms tumor suppressor gene in children presenting with the WAGR syndrome (Wilms tumor, aniridia, genitourinary malformations, mental retardation), and these children have large germ-line mutations in one allele of *WT1* rendering it nonfunctional. Patients with the WAGR syndrome have an increased risk of progressive renal disease and end-stage renal disease after 20 years (38.3%) compared with patients with unilateral Wilms tumor with no associated syndrome (no germ-line mutation) (less than 1.0%) (355).

THE DENYS-DRASH SYNDROME

The glomerular pathology of the Denys-Drash syndrome (Fig. 5.18) is identical with DMS, and it progresses rapidly to end-stage renal disease. In addition to the glomerular pathology, the Denys-Drash triad (356,357) includes male pseudohermaphroditism and a predisposition to develop Wilms tumor (261,326). The Denys-Drash syndrome is caused by missense mutations in exons 8 or 9 of *WT1* that reduce the

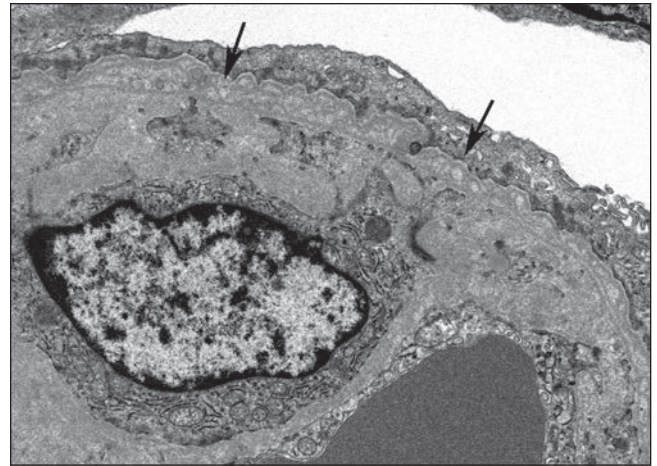


FIGURE 5.17 Electron micrograph from diffuse mesangial sclerosis. Note splitting of glomerular basement membrane (arrows) and extensive effacement of foot processes. (Uranyl acetate and lead citrate $\times 10,200$.)

DNA-binding capacity of the protein (261,358). Missense and nonsense mutations in these exons have been associated with a high risk of Wilms tumor, which usually presents at a younger age when seen in Denys-Drash syndrome as compared to Wilms tumor patients without the NS (358). Prophylactic bilateral nephrectomy may be performed when the children reach chronic kidney disease stage V (261,358). All components of the syndrome are not always seen in affected individuals, and even in individuals with the same specific germ-line mutation in *WT1*, various phenotypes have been reported (358,359). Ratelade et al. (360) characterized a mouse model

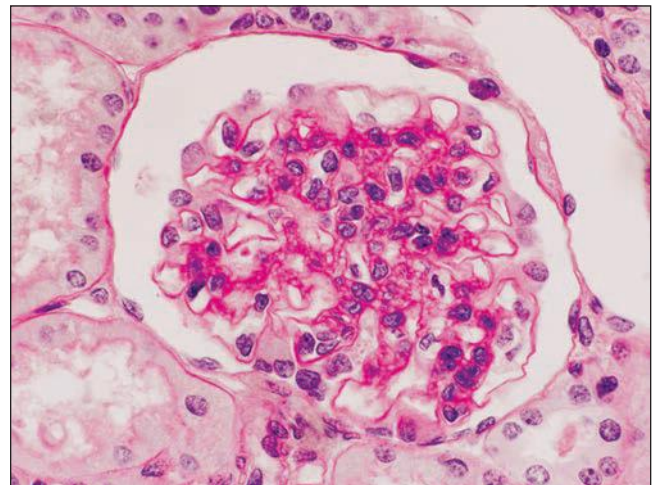


FIGURE 5.18 Light micrograph from the Denys-Drash syndrome. The patient had proteinuria at 6 months and bilateral Wilms tumor detected at 9 months with the classical R394W mutation in *WT1*. This representative glomerulus from the nephrectomy specimen shows diffuse mesangial expansion by PAS-positive matrix. There were no segmental scars in the 38 glomeruli present in the specimen. (PAS, $\times 660$.) (Courtesy of Dr. Marie-Claire Gubler, Hôpital Necker-Enfants Malades, Paris.)

with a missense mutation in *WT1* that produced DMS. They demonstrated that two gene targets of *WT1* not known previously to be expressed in the podocyte were down-regulated in this model. *Scel* encodes sciellin, a protein that is present in cornified epithelium and is thought to help those tissues withstand mechanical and biochemical stress. These authors showed that it colocalizes with nephrin, but its function in the kidney has not yet been determined (360). *Sulf1* is also down-regulated, which may lead to changes in the regulation of growth factor signaling (360).

FRASIER SYNDROME

Frasier syndrome comprises male pseudohermaphroditism (XY chromosomes, female external genitalia, and streak ovaries), progressive nephropathy, and ovarian tumors (gonadoblastoma) (361). The Frasier syndrome is caused by mutations in the *WT1* donor splice site of intron 9 leading to defective alternative splicing of *WT1* and an altered ratio of *WT1*-positive/negative KTS isoforms (362,363). In contrast with the glomerular lesion of the Denys-Drash syndrome and DMS, FSGS is the characteristic glomerular pathology (Fig. 5.19) (261,363). Thus, this lesion is also discussed in Chapter 6. However, phenotypic heterogeneity is seen with other glomerular pathology and is also described in this syndrome (261,326,364). McTaggart et al. (364) reviewed all the reported phenotypes associated with intron 9 *WT1* mutations. They found phenotypic variability: in 22 cases, the renal diagnosis was FSGS in 16, DMS in 4, and membranoproliferative GN in 1. The onset of symptoms was at age older than 2 years in 17 of 22 patients, but 4 patients were younger than 2 years including 1 who was symptomatic at birth. In general, end-stage renal disease occurred in older children and adults, but one patient developed end-stage renal disease at 14 months and 8 patients had

not developed end-stage renal disease. Twenty-six patients had an XY karyotype, and six had an XX karyotype. The external genitalia were female in 19 patients and male in 1. Five patients had a variety of ovarian tumors, and 14 had no tumor (or a bilateral gonadectomy).

The Denys-Drash and Frasier syndromes are caused by different mutations in *WT1*, but there is phenotypic and genotypic overlap. However, the clinical classification remains prognostically important: Patients classified clinically as Denys-Drash syndrome patients have a rapidly progressive form of DMS and a high incidence of Wilms tumor, whereas patients with Frasier syndrome have a more slowly progressive form of FSGS, a low incidence of Wilms tumor, and a higher risk of gonadal tumors (364). Mutational analysis should be performed in any child with DMS seen on renal biopsy (261,326).

LAMB2 (Pierson Syndrome)

Pierson syndrome is characterized by microcoria and abnormal lens shape and cataract that presents with NS at birth or within the first months of life (365,366). The glomerular pathology shows DMS and rapid progression to end-stage renal disease is typical. Truncating mutations in *LAMB2*, which codes for laminin $\beta 2$, are responsible for this syndrome (366). Laminin is a critical component of the GBM. Milder forms may also be seen with missense mutations with later presentation and with DMS or FSGS as the pathology (326,367). Chen et al. (368) produced three transgenic lines with an R246Q-mutant laminin $\beta 2$ that replaced the wild-type laminin. These mice had a milder form of the disease than mice that were deficient. Furthermore, mice with a higher level of expression of the mutant laminin had less severe disease (368).

REFERENCES

1. Robinson RR. Isolated proteinuria in asymptomatic patients. *Kidney Int* 1980;18:395.
2. Garg P, Rabelink T. Glomerular proteinuria: a complex interplay between unique players. *Adv Chronic Kidney Dis* 2011;18(4):233.
3. Salmon AH, Neal CR, Harper SJ. New aspects of glomerular filtration barrier structure and function: five layers (at least) not three. *Curr Opin Nephrol Hypertens* 2009;18(3):197.
4. Eremina V. Glomerular-specific alterations of VEGF-A expression lead to distinct congenital and acquired renal diseases. *J Clin Invest* 2003;111(5):707.
5. Abrahamson DR. Structure and development of the glomerular capillary wall and basement membrane. *Am J Physiol* 1987;253:F783.
6. Yurchenco PD, Schittny JC. Molecular architecture of basement membranes. *FASEB J* 1990;4:1577.
7. Tesar V, Zima T, Kalousova M. Pathobiochemistry of nephrotic syndrome. *Adv Clin Chem* 2003;37:173.
8. Kanwar YS, Farquhar MG. Isolation of glycosaminoglycans (heparan sulfate) from glomerular basement membranes. *Proc Natl Acad Sci U S A* 1979;76:4493.
9. Kojima K, Nosaka H, Kishimoto Y, et al. Defective glycosylation of alpha-dystroglycan contributes to podocyte flattening. *Kidney Int* 2011;79(3):311.
10. Kerjaschki D, Sharkey DJ, Farquhar MG. Identification and characterization of podocalyxin, the major sialoprotein of the renal glomerular epithelial cell. *J Cell Biol* 1984;98:1591.
11. Nishibori Y, Katayama K, Parikka M, et al. *Glci1* deficiency leads to proteinuria. *J Am Soc Nephrol* 2011;22(11):2037.
12. Zhdanova O, Srivastava S, Di L, et al. The inducible deletion of *Drosna* and microRNAs in mature podocytes results in a collapsing glomerulopathy. *Kidney Int* 2011;80(7):719.



FIGURE 5.19 Light micrograph from Frasier syndrome in an XY female with an intronic *WT1* mutation. Proteinuria was detected at 2 years of age, and nephrotic syndrome developed at age 14 years. This glomerulus is representative of 5 segmental scars seen in a biopsy containing 67 glomeruli. Note the area of capillary collapse and glomerular sclerosis involving the hilum with hyalinosis indicated by the arrow. The patient went into end-stage renal disease at 35 years of age. (PAS, $\times 330$.) (Courtesy of Dr. Marie-Claire Gubler, Hôpital Necker-Enfants Malades, Paris.)

13. Pierchala BA, Munoz MR, Tsui CC. Proteomic analysis of the slit diaphragm complex: CLIC5 is a protein critical for podocyte morphology and function. *Kidney Int* 2010;78(9):868.
14. Kestila M, Lenkkeri U, Mannikko M, et al. Positionally cloned gene for a novel glomerular protein—nephrin—is mutated in congenital nephrotic syndrome. *Mol Cell* 1998;1(4):575.
15. Benzing T. Signaling at the slit diaphragm. *J Am Soc Nephrol* 2004;15:1382.
16. Johnstone DB, Holzman LB. Clinical impact of research on the podocyte slit diaphragm. *Nat Clin Pract Nephrol* 2006;2(5):271.
17. Rodewald R, Karnovsky MJ. Porous substructure of the glomerular slit diaphragm in the rat and mouse. *J Cell Biol* 1974;60(2):423.
18. Gagliardini E, Conti S, Benigni A, et al. Imaging of the porous ultrastructure of the glomerular epithelial filtration slit. *J Am Soc Nephrol* 2010;21(12):2081.
19. Brenner BM, Bohrer MP, Baylis C, et al. Determinants of glomerular permselectivity: insights derived from observations in vivo. *Kidney Int* 1977;12:229.
20. Chang RLS, Robertson CR, Deen WM, et al. Permselectivity of the glomerular capillary wall to macromolecules. I. Theoretical considerations. *Biophys J* 1975;15:861.
21. Haraldsson B, Nystrom J, Deen WM. Properties of the glomerular barrier and mechanisms of proteinuria. *Physiol Rev* 2008;88:451.
22. Michael AF, Blau E, Vernier RL. Glomerular polyanion: alteration in aminonucleoside nephrosis. *Lab Invest* 1970;23:649.
23. Chang RLS, Deen WM, Robertson CR, et al. Permselectivity of the glomerular capillary wall. III. Restricted transport of polyanions. *Kidney Int* 1975;8:212.
24. Bohrer MP, Baylis C, Humes HD, et al. Permselectivity of the glomerular capillary wall: facilitated filtration of circulating polycations. *J Clin Invest* 1978;61:72.
25. Russo LM, Bakris GL, Comper WD. Renal handling of albumin: a critical review of basic concepts and perspective. *Am J Kidney Dis* 2002;39:899.
26. Ohlson M, Sorensson J, Lindstrom K, et al. Effects of filtration rate on the glomerular barrier and clearance of four differently shaped molecules. *Am J Physiol Renal Physiol* 2001;281(1):F103.
27. Rennke HG, Venkatachalam MA. Glomerular permeability of macromolecules: effect of molecular configuration on the fractional clearance of uncharged dextran and neutral horseradish peroxidase in the rat. *J Clin Invest* 1979;63:713.
28. Haraldsson B, Jeansson M. Glomerular filtration barrier. *Curr Opin Nephrol Hypertens* 2009;18(4):331.
29. Jarad G, Miner JH. Update on the glomerular filtration barrier. *Curr Opin Nephrol Hypertens* 2009;18:226.
30. Edwards A, Daniels BS, Deen WM. Ultrastructural model for size selectivity in glomerular filtration. *Am J Physiol Renal Physiol* 1999;276(6):F892.
31. Friden V, Oveland E, Tenstad O, et al. The glomerular endothelial cell coat is essential for glomerular filtration. *Kidney Int* 2011;79(12):1322.
32. Deen WM. Cellular contributions to glomerular size-selectivity. *Kidney Int [Comment]* 2006;69(8):1295.
33. Kanwar YS, Farquhar MG. Anionic sites in the glomerular basement membrane: in vivo and in vitro localization to the laminae rarae by cationic probes. *J Cell Biol* 1979;81:137.
34. Jeansson M, Haraldsson B. Glomerular size and charge selectivity in the mouse after exposure to glycosaminoglycan-degrading enzymes. *J Am Soc Nephrol* 2003;14:1756.
35. Jeansson M, Bjorck K, Tenstad O, et al. Adriamycin alters glomerular endothelium to induce proteinuria. *J Am Soc Nephrol* 2009;20(1):114.
36. Russo LM, Sandoval RM, McKee M, et al. The normal kidney filters nephrotic levels of albumin retrieved by proximal tubule cells: retrieval is disrupted in nephrotic states. *Kidney Int* 2007;71(6):504.
37. Peti-Peterdi J, Sipos A. A high-powered view of the filtration barrier. *J Am Soc Nephrol* 2010;21(11):1835.
38. Tanner GA. Glomerular sieving coefficient of serum albumin in the rat: a two-photon microscopy study. *Am J Physiol Renal Physiol* 2009;296(6):F1258.
39. Sandoval RM, Wagner MC, Patel M, et al. Multiple factors influence glomerular albumin permeability in rats. *J Am Soc Nephrol* 2012;23(3):447.
40. Fissell WH. Illuminating the glomerular filtration barrier, two photons at a time. *J Am Soc Nephrol* 2012;23(3):373.
41. Neal CR, Crook H, Bell E, et al. Three-dimensional reconstruction of glomeruli by electron microscopy reveals a distinct restrictive urinary subpodocyte space. *J Am Soc Nephrol* 2005;16(5):1223.
42. D'Agati V. And you thought the age of anatomic discovery was over. *J Am Soc Nephrol* 2005;16(5):1166.
43. Hausmann R, Kuppe C, Egger H, et al. Electrical forces determine glomerular permeability. *J Am Soc Nephrol* 2010;21(12):2053.
44. Harper SJ, Bates DO. Glomerular filtration barrier and molecular segregation: guilty as charged? *J Am Soc Nephrol* 2010;21(12):2009.
45. Thomson SC, Blantz RC. A new role for charge of the glomerular capillary membrane. *J Am Soc Nephrol* 2010;21(12):2011.
46. Schumacher VA, Schlotzer-Schrehardt U, Karumanchi SA, et al. WT1-dependent sulfatase expression maintains the normal glomerular filtration barrier. *J Am Soc Nephrol* 2011;22(7):1286.
47. Andrews PM. A scanning and transmission electron microscopic comparison of puromycin aminonucleoside-induced nephrosis to hyperalbuminemia induced proteinuria with emphasis on kidney podocyte pedicel loss. *Lab Invest* 1977;36:183.
48. Olson JL, Rennke HG, Venkatachalam MA. Alterations in the charge and size selectivity barrier of the glomerular filter in aminonucleoside nephrosis in rats. *Lab Invest* 1981;44:271.
49. Kistler AD, Altintas MM, Reiser J. Podocyte GTPases regulate kidney filter dynamics. *Kidney Int* 2012;81(11):1053.
50. Asanuma K, Mundel P. The role of podocytes in glomerular pathobiology. *Clin Exp Nephrol* 2003;7:255.
51. Mundel P, Shankland SJ. Podocyte biology and response to injury. *J Am Soc Nephrol* 2002;13:3005.
52. Mundel P, Reiser J. Proteinuria: an enzymatic disease of the podocyte? *Kidney Int* 2010;77(7):571.
53. Seiler MW, Venkatachalam MA, Cotran RS. Glomerular epithelium: structural alterations induced by polycations. *Science* 1975;189:390.
54. Matsui K, Breiteneder-Geleff S, Kerjaschki D. Epitope-specific antibodies to the 43-kD glomerular membrane protein podoplanin cause proteinuria and rapid flattening of podocytes. *J Am Soc Nephrol* 1998;9(11):2013.
55. Clement LC, Avila-Casado C, Mace C, et al. Podocyte-secreted angio-poitin-like-4 mediates proteinuria in glucocorticoid-sensitive nephrotic syndrome. *Nat Med* 2011;17(1):117.
56. Reiser J. Filtering new facts about kidney disease. *Nat Med* 2011;17(1):44.
57. Tryggvason K. Unraveling the mechanisms of glomerular ultrafiltration: nephrin, a key component of the slit diaphragm. *J Am Soc Nephrol* 1999;10(11):2440.
58. Donoviel DB, Freed DD, Vogel H, et al. Proteinuria and perinatal lethality in mice lacking NEPH1, a novel protein with homology to NEPHRIN. *Mol Cell Biol* 2001;21:4829.
59. Shih NY, Li J, Karpitskii V, et al. Congenital nephrotic syndrome in mice lacking CD2-associated protein. *Science* 1999;286:225.
60. Ito N, Nishibori Y, Ito Y, et al. mTORC1 activation triggers the unfolded protein response in podocytes and leads to nephrotic syndrome. *Lab Invest* 2011;91(11):1584.
61. Regele HM, Fillipovic E, Langer B, et al. Glomerular expression of dystroglycans is reduced in minimal change nephrosis but not in focal segmental glomerulosclerosis. *J Am Soc Nephrol* 2000;11(3):403.
62. Noakes PG, Miner JH, Gautam M. The renal glomerulus of mice lacking s-laminin/lamininbeta2:Nephrosis despite molecular compensation by laminin beta1. *Nat Genet* 1995;10:400.
63. Vogtlander NP, Tamboer WP, Bakker MA, et al. Reactive oxygen species deglycosilate glomerular alpha-dystroglycan. *Kidney Int* 2006;69(9):1526.
64. Kojima K, Davidovits A, Poczewski H, et al. Podocyte flattening and disorder of glomerular basement membrane are associated with splitting of dystroglycan-matrix interaction. *J Am Soc Nephrol* 2004;15:2079.
65. Kaplan JM, Kim SH, North KN, et al. Mutations in ACTN4, encoding alpha-actinin-4, cause familial focal segmental glomerulosclerosis. *Nat Genet* 2000;24(3):251.
66. George B, Verma R, Soofi AA, et al. Crk1/2-dependent signaling is necessary for podocyte foot process spreading in mouse models of glomerular disease. *J Clin Invest* 2012;122(2):674.

67. Reiser J, von Gersdorff G, Loos M, et al. Induction of B7-1 in podocytes is associated with nephrotic syndrome. *J Clin Invest* 2004;113(10):1390.
68. Sever S, Altintas MM, Nankoe SR, et al. Proteolytic processing of dynamin by cytoplasmic cathepsin L is a mechanism for proteinuric kidney disease. *J Clin Invest* 2007;117(8):2095.
69. Wang L, Ellis MJ, Gomez JA, et al. Mechanisms of the proteinuria induced by Rho GTPases. *Kidney Int* 2012;81(11):1075.
70. Messina A, Davies DJ, Dillane PC, et al. Glomerular epithelial abnormalities associated with the onset of proteinuria in aminonucleoside nephrosis. *Am J Pathol* 1987;126:220.
71. Christensen EI, Verroust PJ, Nielsen R. Receptor-mediated endocytosis in renal proximal tubule. *Pflügers Arch* 2009;458(6):1039.
72. Amsellem S, Gburek J, Hamard G, et al. Cubilin is essential for albumin reabsorption in the renal proximal tubule. *J Am Soc Nephrol* 2010;21(11):1859.
73. Abbate M, Zoja C, Remuzzi G. How does proteinuria cause progressive renal damage? *J Am Soc Nephrol* 2006;17(11):2974.
74. Nielsen R, Christensen EI. Proteinuria and events beyond the slit. *Pediatr Nephrol* 2010;25(5):813.
75. Satirapoj B, Nast CC, Adler SG. Novel insights into the relationship between glomerular pathology and progressive kidney disease. *Adv Chronic Kidney Dis* 2012;19(2):93.
76. Vernon KA, Cook HT. Complement in glomerular disease. *Adv Chronic Kidney Dis* 2012;19(2):84.
77. Theilig F, Kriz W, Jerichow T, et al. Abrogation of protein uptake through megalin-deficient proximal tubules does not safeguard against tubulointerstitial injury. *J Am Soc Nephrol* 2007;18(6):1824.
78. Kriz W, LeHir M. Pathways to nephron loss starting from glomerular diseases—insights from animal models. *Kidney Int* 2005;67(2):404.
79. Earley LE, Forland M. Nephrotic syndrome. In: Earley LE, Gottschalk CW, eds. *Strauss and Welt's Diseases of the Kidney*. Boston: Little, Brown, and Co., 1979:765.
80. Bernard DB. Extrarenal complications of the nephrotic syndrome. *Kidney Int* 1988;33:1184.
81. Vaziri ND, Gollapudi B, Han S, et al. Nephrotic syndrome causes upregulation of HDL endocytic receptor and PDZK-1-dependent downregulation of HDL docking receptor. *Nephrol Dial Transplant* 2011;26(10):3118.
82. Kaysen GA, De Sain-Van der Velden MGM. New insights into lipid metabolism in the nephrotic syndrome. *J Am Soc Nephrol* 1999;10(Suppl 71):S18.
83. Vaziri ND. Molecular mechanisms of lipid disorders in nephrotic syndrome. *Kidney Int* 2003;63:1964.
84. Shearer GC, Stevenson FT, Atkinson DN, et al. Hypoalbuminemia and proteinuria contribute separately to reduced lipoprotein catabolism in the nephrotic syndrome. *Kidney Int* 2001;59:179.
85. Rodriguez-Iturbe B, Herrera-Acosta J, Johnson RJ. Interstitial inflammation, sodium retention, and the pathogenesis of nephrotic edema: a unifying hypothesis. *Kidney Int* 2002;62(4):1379.
86. Siddall EJ, Radhakrishnan J. The pathophysiology of edema formation in the nephrotic syndrome. *Kidney Int* 2012;82(6):635.
87. Svenningsen P, Bistrup C, Friis UG, et al. Plasmin in nephrotic urine activates the epithelial sodium channel. *J Am Soc Nephrol* 2009;20(2):299.
88. Svenningsen P, Skott O, Jensen BL. Proteinuric diseases with sodium retention: Is plasmin the link? *Clin Exp Pharmacol Physiol* 2012;39(1):117.
89. Carattino MD, Hughey RP, Kleyman TR. Proteolytic processing of the epithelial sodium channel gamma subunit has a dominant role in channel activation. *J Biol Chem* 2008;283(37):25290.
90. Rostoker G, Behar A, Lagrue G. Vascular hyperpermeability in nephrotic edema. *Nephron* 2000;85(3):194.
91. Kaysen GA. Nonrenal complications of the nephrotic syndrome. *Annu Rev Med* 1994;45:201.
92. Kerlin BA, Ayoob R, Smoyer WE. Epidemiology and pathophysiology of nephrotic syndrome-associated thromboembolic disease. *Clin J Am Soc Nephrol* 2012;7(3):513.
93. Chuang CH, Lee CT, Cheng YF, et al. Bilateral renal infarctions and lower limbs artery thrombosis in a patient with nephrotic syndrome. *J Nephrol* 2004;17(2):311.
94. Llach F. Hypercoagulability, renal vein thrombosis, and other thrombotic complications of nephrotic syndrome. *Kidney Int* 1985;28:429.
95. Abbrasc C. Clinical spectrum and complications of the nephrotic syndrome. *J Invest Med* 1997;45:143.
96. Schlegel N. Thromboembolic risks and complications in nephrotic children. *Semin Thromb Hemost* 1997;23(3):271.
97. Mahmoodi BK, ten Kate MK, Waanders F, et al. High absolute risks and predictors of venous and arterial thromboembolic events in patients with nephrotic syndrome: results from a large retrospective cohort study. *Circulation* 2008;117(2):224.
98. Rich AR. A hitherto undescribed vulnerability of the juxtamedullary glomeruli in lipid nephrosis. *Bull Johns Hopkins Hosp* 1957;100:173.
99. Liponski I, Cochat P, Gagnadoux MF, et al. Bacterial complications of nephrotic syndrome in children [in French]. *Presse Med* 1995;24:19.
100. Park SJ, Shin JI. Complications of nephrotic syndrome. *Korean J Pediatr* 2011;54(8):322.
101. Gordillo R, Spitzer A. The nephrotic syndrome. *Pediatr Rev* 2009;30(3):94.
102. Wei CC, Yu IW, Lin HW, et al. Occurrence of infection among children with nephrotic syndrome during hospitalizations. *Nephrology (Carlton)* 2012;17(8):681.
103. Ogi M, Yokoyama H, Tomosugi N, et al. Risk factors for infection and immunoglobulin replacement therapy in adult nephrotic syndrome. *Am J Kidney Dis* 1994;24:427.
104. Kim HJ, Vaziri ND. Sterol regulatory element-binding proteins, liver X receptor, ABCA1 transporter, CD36, scavenger receptors A1 and B1 in nephrotic kidney. *Am J Nephrol* 2009;29(6):607.
105. Lacquaniti A, Bolignano D, Donato V, et al. Alterations of lipid metabolism in chronic nephropathies: mechanisms, diagnosis and treatment. *Kidney Blood Press Res* 2010;33(2):100.
106. Vaziri ND, Kim CH, Phan D, et al. Up-regulation of hepatic Acyl CoA: diacylglycerol acyltransferase-1 (DGAT-1) expression in nephrotic syndrome. *Kidney Int* 2004;66(1):262.
107. Li HQ, Wu J, Niu DM, et al. The level of native and oxidized lipoprotein(a) in children with nephrotic syndrome. *Clin Biochem* 2012;45(1-2):101.
108. Soyoral YU, Aslan M, Emre H, et al. Serum paraoxonase activity and oxidative stress in patients with adult nephrotic syndrome. *Atherosclerosis* 2011;218(1):243.
109. Ordóñez JD, Hiatt RA, Killebrew EJ, et al. The increased risk of coronary heart disease associated with nephrotic syndrome. *Kidney Int* 1993;44:638.
110. Joles JA, Stroes ESG, Rabelink TJ. Endothelial function in proteinuric renal disease. *Kidney Int* 1999;56(Suppl 71):S57.
111. Cameron JS. The natural history of glomerulonephritis. In: Kincaid-Smith P, d'Apice AJF, Atkins RC, eds. *Progress in Glomerulonephritis*. New York: Wiley, 1979:209.
112. Tiebosch AT, Wolters J, Frederik PF, et al. Epidemiology of idiopathic glomerular disease: a prospective study. *Kidney Int* 1987;32:112.
113. Haas M, Meehan SM, Karrison TG, et al. Changing etiologies of unexplained adult nephrotic syndrome: a comparison of renal biopsy findings from 1976–1979 and 1995–1997. *Am J Kidney Dis* 1997;30(5):621.
114. Habib R, Kleinknecht C, eds. *The Primary Nephrotic Syndrome of Childhood: Classification and Clinicopathologic Study of 406 Cases*. New York: Appleton Century Crofts, 1971.
115. International Study of Kidney Disease in Children. Nephrotic syndrome in children: prediction of histopathology from clinical and laboratory characteristics at time of diagnosis. A Report from the International Study of Kidney Disease in Children. *Kidney Int* 1978;13:159.
116. Chen WP, Lin CY, Hsu HC, et al. Childhood nephrotic syndrome and heavy proteinuria in Taiwan: a retrospective clinicopathologic study. *Child Nephrol Urol* 1988;9:57.
117. Gulati S, Sharma AP, Sharma RK, et al. Do current recommendations for kidney biopsy in nephrotic syndrome need modifications? *Pediatr Nephrol* 2002;17(6):404.
118. White RH, Glasgow EF, Mills RJ. Clinicopathological study of nephrotic syndrome in childhood. *Lancet* 1970;1:1353.
119. Chesney R. The changing face of childhood nephrotic syndrome. *Kidney Int* 2004;66:1294.
120. Srivastava T, Simon SD, Alon US. High incidence of focal segmental glomerulosclerosis in nephrotic syndrome of childhood. *Pediatr Nephrol* 1999;13(1):13.

121. Boyer O, Moulder JK, Somers MJ. Focal and segmental glomerulosclerosis in children: a longitudinal assessment. *Pediatr Nephrol* 2007;22(8):1159.
122. Borges FF, Shiraichi L, da Silva MP, et al. Is focal segmental glomerulosclerosis increasing in patients with nephrotic syndrome? *Pediatr Nephrol* 2007;22(9):1309.
123. Mubarak M, Kazi JI, Lanewala A, et al. Pathology of idiopathic nephrotic syndrome in children: are the adolescents different from young children? *Nephrol Dialysis Transpl* 2012;27:722.
124. Rivera F, Lopez-Gomez JM, Perez-Garcia R. Clinicopathologic correlations of renal pathology in Spain. *Kidney Int* 2004;66(3):898.
125. Zhou FD, Shen HY, Chen M, et al. The renal histopathological spectrum of patients with nephrotic syndrome: an analysis of 1523 patients in a single Chinese centre. *Nephrol Dial Transplant* 2011;26(12):3993.
126. Pincon E, Rioux-Leclercq N, Frouget T, et al. Renal biopsies after 70 years of age: a retrospective longitudinal study from 2000 to 2007 on 150 patients in Western France. *Arch Gerontol Geriatr* 2010;51(3):e120.
127. Nair R, Bell JM, Walker PD. Renal biopsies in patients aged 80 years and older. *Am J Kidney Dis* 2004;44(4):618.
128. Glasscock RJ. Glomerular disease in the elderly population. *Geriatr Nephrol Urol* 1998;8(3):149.
129. Frocht A, Fillit H. Renal disease in the geriatric patient. *J Am Geriatric Soc* 1984;32:28.
130. Kirdpon S, Vuttivirojana A, Kovitangkoon K, et al. The primary nephrotic syndrome in children and histopathologic study. *J Med Assoc Thai* 1989;72(Suppl 1):26.
131. Gesualdo L, Di Palma AM, Morrone LF, et al. The Italian experience of the national registry of renal biopsies. *Kidney Int* 2004;66(3):890.
132. Bhimma R, Coovadia HM, Adhikari M. Nephrotic syndrome in South African children: changing perspectives over 20 years. *Pediatr Nephrol* 1997;11(4):429.
133. Bonilla-Felix M, Parra C, Dajani T, et al. Changing patterns in the histopathology of idiopathic nephrotic syndrome in children. *Kidney Int* 1999;55(5):1885.
134. Korbet SM, Genchi RM, Borok RZ, et al. The racial prevalence of glomerular lesions in nephrotic adults. *Am J Kidney Dis* 1996;27:647.
135. Müller F. Morbus brightii. *Verh Dtsch Ges Pathol* 1905;9:64.
136. Munk F. Klinische diagnostik der degenerativen Nietenkrankungen. *Z Klin Med* 1913;78:1.
137. van den Berg JG, Weening JJ. Role of the immune system in the pathogenesis of idiopathic nephrotic syndrome. *Clin Sci (Lond)* 2004;107(2):125.
138. Vande Walle J, Mauel R, Raes A, et al. ARF in children with minimal change nephrotic syndrome may be related to functional changes of the glomerular basal membrane. *Am J Kidney Dis* 2004;43(3):399.
139. Adamson O, Trachtman H, Tejani A. Urinary protein electrophoresis patterns in childhood idiopathic nephrotic syndrome. *Int J Pediatr Nephrol* 1986;7:181.
140. Hiraoka M, Takeda N, Tsukahara H, et al. Favorable course of steroid responsive nephrotic children with mild initial attack. *Kidney Int* 1995;47:1392.
141. Branten AJ, van den Born J, Jansen JL, et al. Familial nephropathy differing from minimal change nephropathy and focal glomerulosclerosis. *Kidney Int* 2001;59(2):693.
142. Colattur SN, Korbet SM. Long-term outcome of adult minimal change disease. *Saudi J Kid Dis Transplant* 2000;11:334.
143. Huang JJ, Hsu SC, Chen FF, et al. Adult-onset minimal change disease among Taiwanese—clinical features, therapeutic response, and prognosis. *Am J Nephrol* 2001;21(1):28.
144. Korbet SM, Schwartz MM, Lewis EJ. Minimal change glomerulopathy of adulthood. *Am J Nephrol* 1988;8:291.
145. Nolasco F, Cameron JS, Heywood EF, et al. Adult onset minimal change nephrotic syndrome: a long term follow up. *Kidney Int* 1986;29:1215.
146. Tse KC, Lam MF, Yip PS, et al. Idiopathic minimal change nephrotic syndrome in older adults: steroid responsiveness and pattern of relapses. *Nephrol Dial Transplant* 2003;18(7):1316.
147. Landau D, Oved T, Geiger D, et al. Familial steroid-sensitive nephrotic syndrome in Southern Israel: clinical and genetic observations. *Pediatr Nephrol* 2007;22(5):661.
148. Madhan KK, Temple-Camp CRE. Late de novo minimal change disease in a renal allograft. *Saudi J Kid Dis Transplant* 2009;20:266.
149. Markowitz GS, Stemmer CL, Croker BP, et al. De novo minimal change disease. *Am J Kidney Dis* 1998;32(3):508.
150. Zafarmand AA, Baranowska-Daca E, Ly PD, et al. De novo minimal change disease associated with reversible post-transplant nephrotic syndrome. A report of five cases and review of literature. *Clin Transplant* 2002;16(5):350.
151. Bazzi C, Pettrini C, Rizza V, et al. Characterization of proteinuria in primary glomerulonephritides: urinary polymers of albumin. *Am J Kidney Dis* 1997;30(3):404.
152. D'Amico G, Bazzi C. Pathophysiology of proteinuria. *Kidney Int* 2003;63:809.
153. Trachtman H, Greenbaum LA, McCarthy ET, et al. Glomerular permeability activity: prevalence and prognostic value in pediatric patients with idiopathic nephrotic syndrome. *Am J Kidney Dis* 2004;44(4):604.
154. Schnaper HW. Primary nephrotic syndrome of childhood. *Curr Opin Pediatr* 1996;8(2):141.
155. Garin EH, Diaz LN, Mu W, et al. Urinary CD80 excretion increases in idiopathic minimal-change disease. *J Am Soc Nephrol* 2009;20(2):260.
156. Garin EH, Mu W, Arthur JM, et al. Urinary CD80 is elevated in minimal change disease but not in focal segmental glomerulosclerosis. *Kidney Int* 2010;78(3):296.
157. Waldman M, Crew RJ, Valeri A, et al. Adult minimal-change disease: clinical characteristics, treatment, and outcomes. *Clin J Am Soc Nephrol* 2007;2(3):445.
158. Bargman JM. Management of minimal lesion glomerulonephritis: evidence-based recommendations. *Kidney Int* 1999;55(Suppl 70):S3.
159. Stellato T, Capalleri A, Farina M, et al. Severe reversible acute renal failure in idiopathic nephrotic syndrome. *J Nephrol* 2010;23:717.
160. Smith JD, Hayslett JP. Reversible renal failure in the nephrotic syndrome. *Am J Kidney Dis* 1992;19:201.
161. Chen C-L, Fang H-C, Chou K-J, et al. Increased endothelin 1 expression in adult-onset minimal change nephropathy with acute renal failure. *Am J Kidney Dis* 2005;45:818.
162. Southwest Pediatric Nephrology Study Group. Childhood nephrotic syndrome associated with diffuse mesangial hypercellularity. A report for the Southwest Pediatric Nephrology Study Group. *Kidney Int* 1983;24:87.
163. International Study of Kidney Disease in Children. Primary nephrotic syndrome in children: clinical significance of histopathologic variants of minimal change and of diffuse mesangial hypercellularity. A report for the International Study of Kidney Disease in Children. *Kidney Int* 1981;20:765.
164. Cameron JS, Turner DR, Ogg CS, et al. The nephrotic syndrome in adults with "minimal change" glomerular lesions. *Q J Med* 1974;43:461.
165. Waldherr R, Gubler MC, Levy M, et al. The significance of pure diffuse mesangial proliferation in idiopathic nephrotic syndrome. *Clin Nephrol* 1978;10:171.
166. Joh K, Matsuyama N, Kanetsuna Y, et al. Nephrotic syndrome associated with diffuse mesangial hypercellularity: is it a heterogeneous disease entity? *Am J Nephrol* 1998;18(3):214.
167. Ostalska-Nowicka D, Zachwieja J, Maciejewski J, et al. The prognostic value of glomerular immaturity in the nephrotic syndrome in children. *Pediatr Nephrol* 2004;19(6):633.
168. Dijkman HB, Wetzels JF, Gemmink JH, et al. Glomerular involution in children with frequently relapsing minimal change nephrotic syndrome: an unrecognized form of glomerulosclerosis? *Kidney Int* 2007;71(1):44.
169. Kappel B, Olsen S. Cortical interstitial tissue and sclerosed glomeruli in the normal human kidney, related to age and sex: a quantitative study. *Virchows Arch [Pathol Anat]* 1980;387:271.
170. Smith SM, Hoy WE, Cobb L, et al. Low incidence of glomerulosclerosis in normal kidneys. *Arch Pathol Lab Med* 1989;113:1253.
171. Mocan H, Yildiran A, Camlibel T, et al. Microscopic nephrocalcinosis and hypercalciuria in nephrotic syndrome. *Hum Pathol* 2000;31(11):1363.
172. Seikaly MG, Prashner H, Nolde-Hurlbert B, et al. Long-term clinical and pathological effects of cyclosporin in children with nephrosis. *Pediatr Nephrol* 2000;14(3):214.
173. Prasad DR, Zimmerman SW, Burkholder PM. Immunohistologic features of minimal change nephrotic syndrome. *Arch Pathol Lab Med* 1977;101:345.

174. Swartz SJ, Eldin KW, Hicks MJ, et al. Minimal change disease with IgM+ immunofluorescence: a subtype of nephrotic syndrome. *Pediatr Nephrol* 2009;24(6):1187.
175. Gallego N, Gonzalo A, Mampaso F, et al. Steroid dependent nephrotic syndrome with minimal glomerular changes and mesangial IgA deposits. *Child Nephrol Urol* 1988;9:98.
176. Lai KN, Lai FM, Chan KW, et al. An overlapping syndrome of IgA nephropathy and lipid nephrosis. *Am J Clin Pathol* 1986;86:716.
177. Sinnassamy P, O'Regan S. Mesangial IgA deposits with steroid responsive nephrotic syndrome: probable minimal lesion nephrosis. *Am J Kidney Dis* 1985;5:267.
178. Wu G, Katz A, Cardella C, et al. Spontaneous remission of nephrotic syndrome in IgA glomerular disease. *Am J Kidney Dis* 1985;6:96.
179. Han SH, Kang EW, Park JK, et al. Spontaneous remission of nephrotic syndrome in patients with IgA nephropathy. *Nephrol Dial Transplant* 2011;26(5):1570.
180. Clive DM, Galvanek EG, Silva FG. Mesangial immunoglobulin A deposits in minimal change nephrotic syndrome: a report of an older patient and review of the literature. *Am J Nephrol* 1990;10(1):31.
181. Philibert D, Cattran D, Cook T. Clinicopathologic correlation in IgA nephropathy. *Semin Nephrol* 2008;28(1):10.
182. Kim SM, Moon KC, Oh KH, et al. Clinicopathologic characteristics of IgA nephropathy with steroid-responsive nephrotic syndrome. *J Korean Med Sci* 2009;24(Suppl):S44.
183. Rivera A, Magliato S, Meleg-Smith S. Value of electron microscopy in the diagnosis of childhood nephrotic syndrome. *Ultrastruct Pathol* 2001;25(4):313.
184. Deegens JK, Dijkman HB, Borm GF, et al. Podocyte foot process effacement as a diagnostic tool in focal segmental glomerulosclerosis. *Kidney Int* 2008;74(12):1568.
185. Fries JW, Rumpelt HJ, Thoenes W. Alterations of glomerular podocytic processes in immunologically mediated glomerular disorders. *Kidney Int* 1987;32:742.
186. Lahdenkari AT, Lounatmaa K, Patrakka J, et al. Podocytes are firmly attached to glomerular basement membrane in kidneys with heavy proteinuria. *J Am Soc Nephrol* 2004;15(10):2611.
187. Patrakka J, Lahdenkari AT, Koskimies O, et al. The number of podocyte slit diaphragms is decreased in minimal change nephrotic syndrome. *Pediatr Res* 2002;52(3):349.
188. Van Den Berg JG, Weerman MAV, Assmann KJ, et al. Podocyte foot process effacement is not correlated with the level of proteinuria in human glomerulopathies. *Kidney Int* 2004;66:1901.
189. Silva FG, Pirani CL. Electron microscopic study of medical diseases of the kidney: update—1988. *Mod Pathol* 1988;1:292.
190. Chiang ML, Hawkins EP, Berry PL, et al. Diagnostic and prognostic significance of glomerular epithelial cell vacuolization and podocyte effacement in children with minimal lesion nephrotic syndrome and focal segmental glomerulosclerosis: an ultrastructural study. *Clin Nephrol* 1988;30:8.
191. Yoshikawa N, Cameron AH, White RH. Ultrastructure of the non sclerotic glomeruli in childhood nephrotic syndrome. *J Pathol* 1982;136:133.
192. Sue YM, Huang JJ, Hsieh RY, et al. Clinical features of thin basement membrane disease and associated glomerulopathies. *Nephrology (Carlton)* 2004;9(1):14.
193. Rosenberg HG. Primary glomerular diseases (primary glomerulopathies). *Pathol Res Pract* 1986;181:489.
194. Oomura A, Nakamura T, Arakawa M, et al. Alterations in the extracellular matrix components in human glomerular diseases. *Virchows Arch [Pathol Anat]* 1989;415:151.
195. Kitano Y, Yoshikawa N, Nakamura H. Glomerular anionic sites in minimal change nephrotic syndrome and focal segmental glomerulosclerosis. *Clin Nephrol* 1993;40:199.
196. Barisoni L, Kriz W, Mundel P, et al. The dysregulated podocyte phenotype: a novel concept in the pathogenesis of collapsing idiopathic focal segmental glomerulosclerosis and HIV-associated nephropathy. *J Am Soc Nephrol* 1999;10(1):51.
197. Schmid H, Henger A, Cohen CD, et al. Gene expression profiles of podocyte-associated molecules as diagnostic markers in acquired proteinuric diseases. *J Am Soc Nephrol* 2003;14(11):2958.
198. Goode NP, Shires M, Khan TN, et al. Expression of alpha-actinin-4 in acquired human nephrotic syndrome: a quantitative immunoelectron microscopy study. *Nephrol Dial Transplant* 2004;19(4):844.
199. Horinouchi I, Nakazato H, Kawano T, et al. In situ evaluation of podocin in normal and glomerular diseases. *Kidney Int* 2003;64(6):2092.
200. Koop K, Eikmans M, Baelde HJ, et al. Expression of podocyte-associated molecules in acquired human kidney diseases. *J Am Soc Nephrol* 2003;14:2063.
201. Hodgins JB, Borczuk AC, Nasr SH, et al. A molecular profile of focal segmental glomerulosclerosis from formalin-fixed, paraffin-embedded tissue. *Am J Pathol* 2010;177(4):1674.
202. Kavoura E, Gakiopoulou H, Paraskevaku H, et al. Immunohistochemical evaluation of podocalyxin expression in glomerulopathies associated with nephrotic syndrome. *Hum Pathol* 2011;42(2):227.
203. Srivastava T, Garola RE, Whiting JM, et al. Synaptopodin expression in idiopathic nephrotic syndrome of childhood. *Kidney Int* 2001;59(1):118.
204. Hingorani S, Finn LS, Kowalewska J, et al. Expression of nephrin in acquired forms of nephrotic syndrome in childhood. *Pediatr Nephrol* 2004;19:300.
205. Kim BK, Hong HK, Kim JH, et al. Differential expression of nephrin in acquired human proteinuric diseases. *Am J Kidney Dis* 2002;40:964.
206. Patrakka J, Ruotsalainen V, Ketola I, et al. Expression of nephrin in pediatric kidney diseases. *J Am Soc Nephrol* 2001;12(2):289.
207. Lahdenkari AT, Kestila M, Holmberg C, et al. Nephrin gene (NPHS1) in patients with minimal change nephrotic syndrome (MCNS). *Kidney Int* 2004;65(5):1856.
208. Caridi G, Bertelli R, Di Duca M, et al. Broadening the spectrum of diseases related to podocin mutations. *J Am Soc Nephrol* 2003;14:1278.
209. Shimizu M, Khoshnoodi J, Akimoto Y, et al. Expression of galectin-1, a new component of slit diaphragm, is altered in minimal change nephrotic syndrome. *Lab Invest* 2009;89(2):178.
210. Moll S, Miot S, Sadallah S, et al. No complement receptor 1 stumps on podocytes in human glomerulopathies. *Kidney Int* 2001;59(1):160.
211. Moriyama T, Tsuruta Y, Shimizu A, et al. The significance of caveolae in the glomeruli in glomerular disease. *J Clin Pathol* 2011;64(6):504.
212. Elie V, Fakhoury M, Deschenes G, et al. Physiopathology of idiopathic nephrotic syndrome: lessons from glucocorticoids and epigenetic perspectives. *Pediatr Nephrol* 2012;27(8):1249.
213. Ghosh L, Muehrcke RC. Nephrotic syndrome: a prodrome to lymphoma. *Ann Int Med* 1970;72:379.
214. Shalhoub RJ. Pathogenesis of lipoid nephrosis: a disorder of T cell function. *Lancet* 1974;2:556.
215. Allon M, Campbell WGJ, Nasr SA, et al. Minimal change glomerulonephropathy and interstitial infiltration with mycosis fungoides. *Am J Med* 1988;84:756.
216. D'Agati V, Sablay LB, Knowles DM, et al. Angiotropic large cell lymphoma (intravascular malignant lymphomatosis) of the kidney: presentation as minimal change disease. *Hum Pathol* 1989;20:263.
217. Finkelstein A, Fraley DS, Stachura I, et al. Fenoprofen nephropathy. lipoid nephrosis and interstitial nephritis: a possible T lymphocyte disorder. *Am J Med* 1982;72:81.
218. Tomizawa S, Maruyama K, Nagasawa N, et al. Studies of vascular permeability factor derived from T lymphocytes and inhibitory effect of plasma on its production in minimal change nephrotic syndrome. *Nephron* 1985;41:157.
219. McCarthy ET, Sharma M, Savin VJ. Circulating permeability factors in idiopathic nephrotic syndrome and focal segmental glomerulosclerosis. *Clin J Am Soc Nephrol* 2010;5(11):2115.
220. Cheung PK, Stulp B, Immenschuh S, et al. Is 100KF an isoform of hemopexin? Immunohistochemical characterization of the vasoactive plasma factor 100KF. *J Am Soc Nephrol* 1999;10(8):1700.
221. Bakker WW, Borghuis T, Harnesen MC, et al. Protease activity of plasma hemopexin. *Kidney Int* 2005;68:603.
222. Lennon R, Singh A, Welsh GI, et al. Hemopexin induces nephrin-dependent reorganization of the actin cytoskeleton in podocytes. *J Am Soc Nephrol* 2008;19(11):2140.
223. Holt RCL, Webb NJ, Ralph S, et al. Heparanase activity is dysregulated in children with steroid-sensitive nephrotic syndrome. *Kidney Int* 2005;67:122.

224. Zcharia E, Metzger S, Chajek-Shaul T, et al. Transgenic expression of mammalian heparanase uncovers physiological functions of heparan sulfate in tissue morphogenesis, vascularization, and feeding behavior. *FASEB J* 2004;18:252.
225. Garin EH. Circulating mediators of proteinuria in idiopathic minimal lesion nephrotic syndrome. *Pediatr Nephrol* 2000;14(8–9):872.
226. Garin EH, West L, Zheng W. Interleukin-8 alters glomerular heparan sulfate glycosaminoglycan chain size and charge in rats. *Pediatr Nephrol* 2000;14(4):284.
227. Van den Berg JG, Aten J, Chand MA, et al. Interleukin-4 and interleukin-13 act on glomerular visceral epithelial cells. *J Am Soc Nephrol* 2000;11(3):413.
228. Araya C, Diaz L, Wasserfall C, et al. T regulatory cell function in idiopathic minimal lesion nephrotic syndrome. *Pediatr Nephrol* 2009;24(9):1691.
229. Liu LL, Qin Y, Cai JF, et al. Th17/Treg imbalance in adult patients with minimal change nephrotic syndrome. *Clin Immunol* 2011;139(3):314.
230. Ruan Q, Chen YH. Nuclear factor-kappaB in immunity and inflammation: the Treg and Th17 connection. *Adv Exp Med Biol* 2012;946:207.
231. Sahali D, Pawlak A, LeGouvello S, et al. Transcriptional and post-transcriptional alterations in IkBa in active minimal change nephrotic syndrome. *J Am Soc Nephrol* 2001;12:1648.
232. Cho BS, Yoon SR, Jang JY, et al. Up-regulation of interleukin-4 and CD23/FcepsilonRII in minimal change nephrotic syndrome. *Pediatr Nephrol* 1999;13(3):199.
233. Yap HK, Cheung W, Murugasu B, et al. Th1 and Th2 cytokine mRNA profiles in childhood nephrotic syndrome: evidence for increased IL-13 mRNA expression in relapse. *J Am Soc Nephrol* 1999;10(3):529.
234. Sahali D, Pawlak A, Valanciute A, et al. A novel approach to the investigation of the pathogenesis of active minimal change nephrotic syndrome using subtracted cDNA library screening. *J Am Soc Nephrol* 2002;13:1238.
235. Sellier-Leclerc AL, Baudouin V, Kwon T, et al. Rituximab in steroid-dependent idiopathic nephrotic syndrome in childhood—follow-up after CD19 recovery. *Nephrol Dial Transplant* 2012;27(3):1083.
236. Shimada M, Ishimoto T, Lee PY, et al. Toll-like receptor 3 ligands induce CD80 expression in human podocytes via an NF-kappaB-dependent pathway. *Nephrol Dial Transplant* 2012;27(1):81.
237. Shimada M, Araya C, Rivard C, et al. Minimal change disease: a “two-hit” podocyte immune disorder? *Pediatr Nephrol* 2011;26(4):645.
238. Chugh SS, Clement LC, Mace C. New insights into human minimal change disease: lessons from animal models. *Am J Kidney Dis* 2012;59(2):284.
239. Gao X, Xu H, Liu H, et al. Angiotensin-like protein 3 regulates the motility and permeability of podocytes by altering nephrin expression in vitro. *Biochem Biophys Res Commun* 2010;399(1):31.
240. Okamoto K, Tokunaga K, Doi K, et al. Common variation in GPC5 is associated with acquired nephrotic syndrome. *Nature Gen* 2011;43(5):459.
241. Yoshida K, Shimizugawa T, Ono M, et al. Angiotensin-like protein 4 is a potent hyperlipidemia-inducing factor in mice and inhibitor of lipoprotein lipase. *J Lipid Res* 2002;43(11):1770.
242. Audard V, Pawlak A, Candelier M, et al. Upregulation of nuclear factor-related kappa B suggests a disorder of nuclear regulation in minimal change disease. *PLoS ONE* 2012;7:e30523.
243. Kobayashi Y, Aizawa A, Takizawa T, et al. DNA methylation changes between relapse and remission of minimal change nephrotic syndrome. *Pediatr Nephrol* 2012;27(12):2233–2241.
244. Bhasin HK, Abuelo JG, Nayak R, et al. Mesangial proliferative glomerulonephritis. *Lab Invest* 1978;39:21.
245. Cohen AH, Border WA, Glassock RJ. Nephrotic syndrome with mesangial IgM deposits. *Lab Invest* 1978;38:610.
246. Tejani A, Nicastri AD. Mesangial IgM nephropathy. *Nephron* 1983;35:1.
247. Border WA. Distinguishing minimal change disease from mesangial disorders. *Kidney Int* 1988;34:419.
248. Al-Eisa A, Carter JE, Lirenman DS, et al. Childhood IgM nephropathy: comparison with minimal change disease. *Nephron* 1996;72(1):37.
249. Myllymaki J, Saha H, Mustonen J, et al. IgM nephropathy: clinical picture and long-term prognosis. *Am J Kidney Dis* 2003;41:343.
250. Geier P, Roushdi A, Skalova S, et al. Is cyclophosphamide effective in patients with IgM-positive minimal change disease? *Pediatr Nephrol* 2012;27:2227.
251. Kanemoto K, Ito H, Anzai M, et al. Clinical significance of IgM and C1q deposition in the mesangium in pediatric idiopathic nephrotic syndrome. *J Nephrol* 2013;26(2):306.
252. Jennette JC, Hippi CG. C1q nephropathy: a distinct pathologic entity usually causing the nephrotic syndrome. *Am J Kidney Dis* 1985;6:103.
253. Iskandar SS, Browning MC, Lorentz WB. C1q nephropathy: a pediatric clinicopathologic study. *Am J Kidney Dis* 1991;18:459.
254. Markowitz GS, Schwimmer JA, Stokes MB, et al. C1q nephropathy: a variant of focal segmental glomerulosclerosis. *Kidney Int* 2003;64:1232.
255. Hisano S, Fukuma Y, Segawa Y, et al. Clinicopathologic correlation and outcome of C1q nephropathy. *Clin J Am Soc Nephrol* 2008;3(6):1637.
256. Vizjak A, Ferluga D, Rozic M, et al. Pathology, clinical presentations, and outcomes of C1q nephropathy. *J Am Soc Nephrol* 2008;19(11):2237.
257. Wenderfer SE, Swinford RD, Braun MC. C1q nephropathy in the pediatric population: pathology and pathogenesis. *Pediatr Nephrol* 2010;25(8):1385.
258. Fogo A, Hawkins EP, Berry PL, et al. Glomerular hypertrophy in minimal change disease predicts subsequent progression to focal glomerular sclerosis. *Kidney Int* 1990;38:115.
259. Nyberg E, Bohman SO, Berg U. Glomerular volume and renal function in children with different types of the nephrotic syndrome. *Pediatr Nephrol* 1994;8:285.
260. Sistani L, Duner F, Udumala S, et al. Pdlim2 is a novel actin-regulating protein of podocyte foot processes. *Kidney Int* 2011;80(10):1045.
261. Buscher AK, Weber S. Educational paper: the podocytopathies. *Eur J Pediatr* 2012;171(8):1151.
262. Kleta R, Kloorwijk E, Stanescu H, et al. Filtering the genes and sorting the glomerular filter: a new piece in the puzzle? *Nephrol Dial Transplant* 2011;26(9):2743.
263. Machuca E, Benoit G, Antignac C. Genetics of nephrotic syndrome: connecting molecular genetics to podocyte physiology. *Hum Mol Genet* 2009;18(R2):R185.
264. Sanna-Cherchi S, Burgess KE, Nees SN, et al. Exome sequencing identified MYO1E and NEIL1 as candidate genes for human autosomal recessive steroid-resistant nephrotic syndrome. *Kidney Int* 2011;80(4):389.
265. Santin S, Bullich G, Tazon-Vega B, et al. Clinical utility of genetic testing in children and adults with steroid-resistant nephrotic syndrome. *Clin J Am Soc Nephrol* 2011;6(5):1139.
266. Ahmad H, Tejani A. Predictive value of repeat renal biopsies in children with nephrotic syndrome. *Nephron* 2000;84(4):342.
267. Constantinescu AR, Shah HB, Foote EF, et al. Predicting first-year relapses in children with nephrotic syndrome. *Pediatrics* 2000;105(3):492.
268. Trompeter RS, Lloyd BW, Hicks J, et al. Long term outcome for children with minimal change nephrotic syndrome. *Lancet* 1985;1:368.
269. Banaszak B, Banaszak P. The increasing incidence of initial steroid resistance in childhood nephrotic syndrome. *Pediatr Nephrol* 2012;27(6):927.
270. Kyrieleis HA, Lowik MM, Pronk I, et al. Long-term outcome of biopsy-proven, frequently relapsing minimal-change nephrotic syndrome in children. *Clin J Am Soc Nephrol* 2009;4(10):1593.
271. Lemley KV. How ‘minimal’ are the adult consequences of childhood MCNS? *Nat Rev Nephrol* 2010;6:70.
272. Sinha A, Hari P, Sharma PK, et al. Disease course in steroid sensitive nephrotic syndrome. *Indian Pediatr* 2012;49(11):881.
273. Gulati A, Sinha A, Sreenivas V, et al. Daily corticosteroids reduce infection-associated relapses in frequently relapsing nephrotic syndrome: a randomized controlled trial. *Clin J Am Soc Nephrol* 2011;6(1):63.
274. Teeninga N, Schreuder MF, Bokenkamp A, et al. Influence of low birth weight on minimal change nephrotic syndrome in children, including a meta-analysis. *Nephrol Dial Transplant* 2008;23(5):1615.
275. Hopper JJ, Ryan P, Lee JC, et al. Lipoid nephrosis in 31 adult patients: renal biopsy study by light, electron, and fluorescence microscopy with experience in treatment. *Medicine (Baltimore)* 1970;49:321.
276. Bazzi C, Petrini C, Rizza V, et al. A modern approach to selectivity of proteinuria and tubulointerstitial damage in nephrotic syndrome. *Kidney Int* 2000;58(4):1732.

277. Tan Y, Yang D, Fan J, et al. Elevated levels of Immunoglobulin E may indicate steroid resistance or relapse in adult primary nephrotic syndrome, especially in minimal change nephrotic syndrome. *J Int Med Res* 2011;39:2307.
278. Gipson DS, Massengill SF, Yao L, et al. Management of childhood onset nephrotic syndrome. *Pediatrics* 2009;124(2):747.
279. Eguchi A, Takei T, Yoshida T, et al. Combined cyclosporine and prednisolone therapy in adult patients with the first relapse of minimal-change nephrotic syndrome. *Nephrol Dial Transplant* 2010;25(1):124.
280. Cattran DC, Alexopoulos E, Heering P, et al. Cyclosporin in idiopathic glomerular disease associated with the nephrotic syndrome : workshop recommendations. *Kidney Int* 2007;72(12):1429.
281. Iijima K, Hamahira K, Tanaka R, et al. Risk factors for cyclosporine-induced tubulointerstitial lesions in children with minimal change nephrotic syndrome. *Kidney Int* 2002;61:1801–1805.
282. Gargah TTG, Lakhous MR. Mycophenolate mofetil in treatment of childhood steroid-resistant nephrotic syndrome. *J Nephrol* 2011;24(2):203.
283. Zagury A, de Oliveira AL, de Moraes CA, et al. Long-term follow-up after cyclophosphamide therapy in steroid-dependent nephrotic syndrome. *Pediatr Nephrol* 2011;26(6):915.
284. Li H, Shi X, Shen H, et al. Tacrolimus versus intravenous pulse cyclophosphamide therapy in Chinese adults with steroid-resistant idiopathic minimal change nephropathy: a multicenter, open-label, nonrandomized cohort trial. *Clin Ther* 2012;34(5):1112.
285. Haffner D, Fischer DC. Nephrotic syndrome and rituximab: facts and perspectives. *Pediatr Nephrol* 2009;24(8):1433.
286. Takei T, Nitta K. Rituximab and minimal change nephrotic syndrome: a therapeutic option. *Clin Exp Nephrol* 2011;15(5):641.
287. Siegel NJ, Gaudio KM, Krassner LS, et al. Steroid dependent nephrotic syndrome in children: histopathology and relapses after cyclophosphamide treatment. *Kidney Int* 1981;19:454.
288. Kirpekar R, Yorgin PD, Tune BM, et al. Clinicopathologic correlates predict the outcome in children with steroid-resistant idiopathic nephrotic syndrome treated with pulse methylprednisolone therapy. *Am J Kidney Dis* 2002;39(6):1143.
289. Querfeld U, Waldherr R, Scharer K. The significance of focal global sclerosis in idiopathic nephrotic syndrome. Long-term clinical observations. *Acta Paediatr Scand* 1985;74(6):913.
290. Howie AJ, Brewer DB. The glomerular tip lesion: a previously undescribed type of segmental glomerular abnormality. *J Pathol* 1984;142:205.
291. Stokes MB, Markowitz GS, Lin J, et al. Glomerular tip lesion: a distinct entity within the minimal change disease/focal segmental glomerulosclerosis spectrum. *Kidney Int* 2004;65(5):1690.
292. Haas M, Yousefzadeh N. Glomerular tip lesion in minimal change nephropathy: a study of autopsies before 1950. *Am J Kidney Dis* 2002;39(6):1168.
293. Howie AJ, Agarwal A, Sebire NJ, et al. Glomerular tip changes in childhood minimal change nephropathy. *Pediatr Nephrol* 2008;23(8):1281.
294. Warren GV, Korbet SM, Schwartz MM, et al. Minimal change glomerulopathy associated with nonsteroidal antiinflammatory drugs. *Am J Kidney Dis* 1989;13:127.
295. Alper AB, Jr, Meleg-Smith S, Krane NK. Nephrotic syndrome and interstitial nephritis associated with celecoxib. *Am J Kidney Dis* 2002;40(5):1086.
296. Galesic K, Ljubanovic D, Bulimbasic S, et al. Minimal change disease and acute tubular necrosis caused by diclofenac. *Nephrology (Carlton)* 2008;13(1):87.
297. Petersen CE, Amaral S, Frosch E. Lithium-induced nephrotic syndrome in a prepubertal boy. *J Child Adolesc Psychopharmacol* 2008;18(2):210.
298. Barri YM, Munshi NC, Sukumalchandra S, et al. Podocyte injury associated glomerulopathies induced by pamidronate. *Kidney Int* 2004;65(2):634.
299. Dizer U, Beker CM, Yavuz I, et al. Minimal change disease in a patient receiving IFN-alpha therapy for chronic hepatitis C virus infection. *J Interferon Cytokine Res* 2003;23(1):51.
300. Nakao K, Sugiyama H, Makino E, et al. Minimal change nephrotic syndrome developing during postoperative beta-interferon therapy for malignant melanoma. *Nephron* 2002;90:498.
301. Tang HL, Chu KH, Mak YF, et al. Minimal change disease following exposure to mercury-containing skin-lightening cream. *Hong Kong Med J* 2006;12:316.
302. Lien YH, Lai LW. Pathogenesis, diagnosis and management of paraneoplastic glomerulonephritis. *Nat Rev Nephrol* 2011;7(2):85.
303. Ronco PM, Harrington JT, Preud'homme JL, et al. Paraneoplastic glomerulopathies: new insights into an old entity. *Kidney Int* 1999;56(1):355.
304. Moorthy AV, Zimmerman SW, Burkholder PM. Nephrotic syndrome in Hodgkin's disease: evidence for pathogenesis alternative to immune complex deposition. *Am J Med* 1976;61:476.
305. Dabbs DJ, Striker LM, Mignon F, et al. Glomerular lesions in lymphomas and leukemias. *Am J Med* 1986;80:63.
306. Audard V, Larousserie F, Grimbert P, et al. Minimal change nephrotic syndrome and classical Hodgkin's lymphoma: report of 21 cases and review of the literature. *Kidney Int* 2006;69(12):2251.
307. Auguet T, Lorenzo A, Colomer E, et al. Recovery of minimal change nephrotic syndrome and acute renal failure in a patient with renal cell carcinoma. *Am J Nephrol* 1998;18(5):433.
308. Moorthy AV. Minimal change glomerular disease: a paraneoplastic syndrome in two patients with bronchogenic carcinoma. *Am J Kidney Dis* 1983;3:58.
309. Taniguchi K, Fujioka H, Torashima Y, et al. Rectal cancer with paraneoplastic nephropathy: association of vascular endothelial growth factor. *Dig Surg* 2004;21(5–6):455.
310. Abdel-Hafez M, Shimada M, Lee PY, et al. Idiopathic nephrotic syndrome and atopy: is there a common link? *Am J Kidney Dis* 2009;54(5):945.
311. Olivero JJ, Ayus JC, Eknoyan G. Nephrotic syndrome developing after bee stings. *South Med J* 1981;74:82.
312. Tareyeva IE, Nikolaev AJ, Janushkevitch TN. Nephrotic syndrome induced by insect sting. *Lancet* 1982;2:825.
313. Tasic V. Nephrotic syndrome in a child after a bee sting. *Pediatr Nephrol* 2000;15(3–4):245.
314. Kikuchi Y, Imakiire T, Hyodo T, et al. Minimal change nephrotic syndrome, lymphadenopathy and hyperimmunoglobulinemia after immunization with a pneumococcal vaccine. *Clin Nephrol* 2002;58(1):68.
315. Chen JK, Wu MS, Yang CW, et al. Guillain-Barre syndrome associated with minimal change glomerulopathy and tubular dysfunction - related to acetone-based organic solvent? *Am J Nephrol* 2002;22(5–6):560.
316. Kitamura H, Nakano T, Kakihara M, et al. A case of Guillain-Barre syndrome developed minimal change nephrotic syndrome simultaneously. *Am J Nephrol* 1998;18(2):151.
317. Kuzmanovska DB, Shahpazova EM, Kocova MJ, et al. Autoimmune thyroiditis and vitiligo in a child with minimal change nephrotic syndrome. *Pediatr Nephrol* 2001;16(12):1137.
318. Nishimoto A, Tomiyoshi Y, Sakemi T, et al. Simultaneous occurrence of minimal change glomerular disease, sarcoidosis and Hashimoto's thyroiditis. *Am J Nephrol* 2000;20(5):425.
319. Herron MD, Kohan DE, Hansen CD. Minimal change nephropathy associated with pemphigus vulgaris: a new relationship? *J Am Acad Dermatol* 2004;50(4):645.
320. Scaglia F, Vogler LB, Hymes LC, et al. Minimal change nephrotic syndrome: a possible complication of ehrlichiosis. *Pediatr Nephrol* 1999;13(7):600.
321. Miyazaki M, Tamura M, Kabashima N, et al. Minimal change nephrotic syndrome in a patient with strongyloidiasis. *Clin Exp Nephrol* 2010;14(4):367.
322. Kim JJ, Clothier J, Sebire NJ, et al. Nephrotic syndrome in infancy can spontaneously resolve. *Pediatr Nephrol* 2011;26(10):1897.
323. Gelman R, Brook G, Green J, et al. Minimal change glomerulonephritis associated with hydatid disease. *Clin Nephrol* 2000;53(2):152.
324. Hinkes BG, Mucha B, Vlangos CN, et al. Nephrotic syndrome in the first year of life: two thirds of cases are caused by mutations in 4 genes (NPHS1, NPHS2, WT1, and LAMB2). *Pediatrics* 2007;119(4):e907.
325. Godefroid N, Dahan K. Expanding the clinical spectrum of congenital nephrotic syndrome caused by NPHS1 mutations. *Nephrol Dial Transplant* 2010;25(9):2837.
326. Caridi G, Trivelli A, Sanna-Cherchi S, et al. Familial forms of nephrotic syndrome. *Pediatr Nephrol* 2010;25(2):241.
327. Jalanko H. Congenital nephrotic syndrome. *Pediatr Nephrol* 2009;24(11):2121.

328. Habib R, Bois E. Heterogeneity of early onset nephrotic syndromes in infants (nephrotic syndrome “in infants”). Anatomical, clinical and genetic study of 37 cases. *Helv Paediatr Acta* 1973;28(2):91.
329. Norio R. The nephrotic syndrome and heredity. *Hum Hered* 1969;19(2):113.
330. Ovunc B, Ashraf S, Vega-Warner V, et al. Mutation analysis of NPHS1 in a worldwide cohort of congenital nephrotic syndrome patients. *Nephron Clin Pract* 2012;120(3):c139.
331. Schoeb DS, Chernin G, Heeringa SE, et al. Nineteen novel NPHS1 mutations in a worldwide cohort of patients with congenital nephrotic syndrome (CNS). *Nephrol Dial Transplant* 2010;25(9):2970.
332. Holzman LB, St John PL, Kovari IA, et al. Nephrin localizes to the slit pore of the glomerular epithelial cell. *Kidney Int* 1999;56(4):1481.
333. Ruotsalainen V, Ljungberg P, Wartiovaara J, et al. Nephrin is specifically located at the slit diaphragm of glomerular podocytes. *Proc Natl Acad Sci U S A* 1999;96(14):7962.
334. Welsh GI, Saleem MA. Nephrin-signature molecule of the glomerular podocyte? *J Pathol* 2010;220(3):328.
335. Orikasa M, Matsui K, Oite T, et al. Massive proteinuria induced in rats by a single intravenous injection of a monoclonal antibody. *J Immunol* 1988;141(3):807.
336. Putaala H, Soininen R, Kilpelainen P, et al. The murine nephrin gene is specifically expressed in kidney, brain and pancreas: inactivation of the gene leads to massive proteinuria and neonatal death. *Hum Mol Genet* 2001;10(1):1.
337. Huttunen NP, Rapola J, Vilksa J, et al. Renal pathology in congenital nephrotic syndrome of Finnish type: a quantitative light microscopic study on 50 patients. *Int J Pediatr Nephrol* 1980;1(1):10.
338. Oliver J. Microcystic renal disease and its relation to “infantile nephrosis”. *Am J Dis Child* 1960;100:312.
339. Liapis H. Molecular pathology of nephrotic syndrome in childhood: a contemporary approach to diagnosis. *Pediatr Dev Pathol* 2008;11(4):154.
340. Kaukinen A, Kuusniemi AM, Helin H, et al. Changes in glomerular mesangium in kidneys with congenital nephrotic syndrome of the Finnish type. *Pediatr Nephrol* 2010;25(5):867.
341. George CR, Hickman RO, Stricker GE. Infantile nephrotic syndrome. *Clin Nephrol* 1976;5(1):20.
342. Hallman N, Hjelt L. Congenital nephrotic syndrome. *J Pediatr* 1959;55(2):152.
343. Patrakka J, Kestila M, Wartiovaara J, et al. Congenital nephrotic syndrome (NPSH1): features resulting from different mutations in Finnish patients. *Kidney Int* 2000;58:972.
344. Patrakka J, Martin P, Salonen R, et al. Proteinuria and prenatal diagnosis of congenital nephrosis in fetal carriers of nephrin gene mutations. *The Lancet* 2002;359(9317):1575.
345. Tryggvason K. Composition of the glomerular basement membrane in the congenital nephrotic syndrome of the Finnish type. *Eur J Clin Invest* 1977;7(3):177.
346. Kobayashi N. An immunohistochemical study on renal biopsies in children. *Arch Dis Child* 1966;41(219):477.
347. Philippe A, Nevo F, Esquivel EL, et al. Nephrin mutations can cause childhood-onset steroid-resistant nephrotic syndrome. *J Am Soc Nephrol* 2008;19(10):1871.
348. Machuca E, Benoit G, Nevo F, et al. Genotype-phenotype correlations in non-Finnish congenital nephrotic syndrome. *J Am Soc Nephrol* 2010;21(7):1209.
349. Patrakka J, Ruotsalainen V, Reponen P, et al. Recurrence of nephrotic syndrome in kidney grafts of patients with congenital nephrotic syndrome of the Finnish type: role of nephrin. *Transplantation* 2002;73(3):394.
350. Chaudhuri A, Kambham N, Sutherland S, et al. Rituximab treatment for recurrence of nephrotic syndrome in a pediatric patient after renal transplantation for congenital nephrotic syndrome of Finnish type. *Pediatr Transplant* 2012;16(5):E183.
351. Habib R. Nephrotic syndrome in the 1st year of life. *Pediatr Nephrol* 1993;7(4):347.
352. Gbadegesin R, Hinkes BG, Hoskins BE, et al. Mutations in PLCE1 are a major cause of isolated diffuse mesangial sclerosis (IDMS). *Nephrol Dial Transplant* 2008;23(4):1291.
353. Gubler MC. WT1, a multifunctional protein. Contribution of genetic models to the understanding of its various functions. *J Am Soc Nephrol* 2002;13(8):2192.
354. Parsa A. Genotype-phenotype correlations: filling the void. *Clin J Am Soc Nephrol* 2010;5(9):1542.
355. Breslow NE, Takashima JR, Ritchey ML, et al. Renal failure in the Denys-Drash and Wilms’ tumor-aniridia syndromes. *Cancer Res* 2000;60(15):4030.
356. Denys P, Malvaux P, Van Den Berghe H, et al. Association of an anatomopathological syndrome of male pseudohermaphroditism, Wilms’ tumor, parenchymatous nephropathy and XX/XY mosaicism. *Arch Fr Pediatr* 1967;24(7):729.
357. Drash A, Sherman F, Hartmann WH, et al. A syndrome of pseudohermaphroditism, Wilms’ tumor, hypertension, and degenerative renal disease. *J Pediatr* 1970;76(4):585.
358. Chernin G, Vega-Warner V, Schoeb DS, et al. Genotype/phenotype correlation in nephrotic syndrome caused by WT1 mutations. *Clin J Am Soc Nephrol* 2010;5(9):1655.
359. Ruf RG, Schultheiss M, Lichtenberger A, et al. Prevalence of WT1 mutations in a large cohort of patients with steroid-resistant and steroid-sensitive nephrotic syndrome. *Kidney Int* 2004;66(2):564.
360. Ratelade J, Arrondel C, Hamard G, et al. A murine model of Denys-Drash syndrome reveals novel transcriptional targets of WT1 in podocytes. *Hum Mol Genet* 2010;19(1):1.
361. Frasier SD, Bashore RA, Mosier HD. Gonadoblastoma associated with pure gonadal dysgenesis in monozygous twins. *J Pediatr* 1964;64:740.
362. Barboux S, Niaudet P, Gubler MC, et al. Donor splice-site mutations in WT1 are responsible for Frasier syndrome. *Nat Genet* 1997;17(4):467.
363. Klamt B, Koziell A, Poulat F, et al. Frasier syndrome is caused by defective alternative splicing of WT1 leading to an altered ratio of WT1 +/-KTS splice isoforms. *Hum Mol Genet* 1998;7(4):709.
364. McTaggart SJ, Algar E, Chow CW, et al. Clinical spectrum of Denys-Drash and Frasier syndrome. *Pediatr Nephrol* 2001;16(4):335.
365. Pierson M, Cordier J, Hervouet F, et al. An unusual congenital and familial congenital malformative combination involving the eye and kidney. *J Genet Hum* 1963;12:184.
366. Zenker M, Aigner T, Wendler O, et al. Human laminin beta2 deficiency causes congenital nephrosis with mesangial sclerosis and distinct eye abnormalities. *Hum Mol Genet* 2004;13(21):2625.
367. Lehnhardt A, Lama A, Amann K, et al. Pierson syndrome in an adolescent girl with nephrotic range proteinuria but a normal GFR. *Pediatr Nephrol* 2012;27(5):865.
368. Chen YM, Kikkawa Y, Miner JH. A missense LAMB2 mutation causes congenital nephrotic syndrome by impairing laminin secretion. *J Am Soc Nephrol* 2011;22(5):849.

Focal Segmental Glomerulosclerosis

Background and history 208

Relationship of FSGS to minimal change disease 209

Primary FSGS 209

Epidemiology and clinical presentation 209

Pathologic features of FSGS 210

Morphologic variants of FSGS 217

Collapsing variant (also known as collapsing glomerulopathy) 218

Tip variant 221

Cellular variant 221

Perihilar variant 221

NOS variant 221

Pathologic differential diagnosis of FSGS 225

Clinical-pathologic correlation of histologic variants of primary FSGS 225

Clinical course and prognostic factors 228

Etiology and pathogenesis 228

Primary FSGS: Treatment 231

Recurrence of primary FSGS in the renal allograft 232

Genetic causes and familial forms of FSGS 232

Clinical presentation 235

Pathologic features 235

Pathogenesis 235

Autosomal recessive steroid-resistant nephrotic syndrome 236

Autosomal dominant FSGS 237

Syndromic FSGS 238

Mitochondriopathies associated with FSGS 239

Mitochondrial tRNA^{Leu(URR)} 239

Coenzyme Q10 synthesis defects 239

Risk alleles in patients of African descent 240

Adaptive FSGS 240

Clinical features 241

Pathologic features 241

Pathologic differential diagnosis 242

Etiology and pathogenesis of adaptive FSGS 242

Animal models prove podocyte depletion theory of FSGS 242

Treatment and prognosis of adaptive FSGS 243

Virus-associated FSGS 243

Clinical features and pathogenesis 243

Pathologic findings 243

Drug-associated FSGS 244

Clinical features 244

Pathologic features 244

Pathogenesis 244

FSGS in systemic lupus erythematosus (lupus podocytopathy) 244

C1q nephropathy 245

Definition 245

Clinical features 245

Pathologic features 246

Differential diagnosis 246

Etiology and pathogenesis 246

Treatment and prognosis 247

Focal segmental glomerulosclerosis (FSGS) refers to a pattern of glomerular scarring that affects a subset of glomeruli (i.e., focal) and involves only a portion of the glomerular tuft (i.e., segmental) (Fig. 6.1) (1). FSGS is not a single disease but encompasses a group of distinct clinical-pathologic syndromes with diverse etiologies and disease associations. Most cases of FSGS are primary or idiopathic; these are generally characterized by

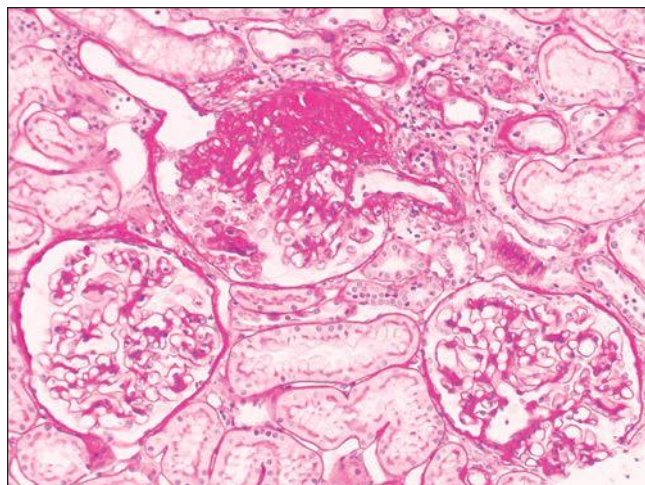


FIGURE 6.1 Primary FSGS. Focal segmental distribution of glomerulosclerosis lesions. The glomerulus at the top shows a discrete segmental scar with adhesion to the Bowman capsule. The two glomeruli at the bottom of the picture are normal. (Periodic acid-Schiff [PAS], $\times 150$.)

heavy proteinuria and frequent progression to end-stage renal disease (ESRD) (1). Secondary causes of FSGS include genetic defects, viral infections, drugs, toxins, and adaptive responses mediated by altered glomerular hemodynamics (referred to as glomerular hypertension) (Table 6.1). Focal and segmental glomerular scarring also occurs as a nonspecific pattern of injury in the course of progression of diverse inflammatory, proliferative, and thrombotic glomerular diseases.

Since publication of the sixth edition of *Heptinstall's Pathology of the Kidney*, our understanding of the pathogenesis of FSGS has expanded and continues to be elucidated at the cellular, molecular, and genetic levels (2,3). Data from human and experimental studies indicate that podocyte injury and depletion (podocytopenia) are pivotal events in many if not all forms of FSGS and that parietal epithelial cells also play a role in the morphogenesis of the segmental lesions (1). The presence of circulating permeability factors in primary FSGS and secondary FSGS due to genetic disorders is increasingly apparent (4,5). Finally, evidence supports that the morphologic variants of primary and secondary FSGS differ with respect to their presenting clinical and demographic features, prognoses, and associations with potential pathogenetic mechanisms.

This chapter reviews the clinical-pathologic characteristics of primary FSGS and the major secondary forms of FSGS. C1q nephropathy (C1qN), an entity that often presents with nephrotic syndrome and shows histologic features of FSGS, is also discussed (6). Congenital nephrotic syndrome (CNS) and genetic conditions typically associated with diffuse mesangial sclerosis are reviewed in Chapter 5.

BACKGROUND AND HISTORY

The first morphologic depiction of FSGS lesions in patients with nephrotic syndrome was published by Fahr in 1925 (7) (Fig. 6.2). Fahr attributed the focal segmental hyalinization to capillary degeneration in patients with lipoid nephrosis. Subsequently, in a 1957 autopsy study of children with the

TABLE 6.1 Etiologic classification of FSGS

FSGS classification	Etiology
Primary FSGS	Specific cause unknown; mediated by putative circulating permeability factors
Secondary FSGS	
Familial or genetic	Mutations in specific podocyte genes (expanded in Table 6.5)
Virus associated	Human immunodeficiency virus type 1, parvovirus B19, simian virus 40, cytomegalovirus, Epstein-Barr virus
Drug induced	Heroin; interferons alpha, beta, and gamma; lithium; pamidronate; sirolimus; calcineurin inhibitor nephrotoxicity; anabolic steroids
Adaptive	Mediated by adaptive structural-functional responses to glomerular hypertension caused by elevated glomerular capillary pressures and flows.
	<i>Conditions with reduced functioning nephrons:</i>
	Oligomeganephronia, very low birth weight, unilateral renal agenesis, renal dysplasia, reflux nephropathy, sequela to cortical necrosis, surgical renal ablation, renal allograft, aging kidney, any advanced renal disease with reduced functioning nephrons
	<i>Conditions with initially normal renal mass:</i>
	Systemic hypertension, acute or chronic vasoocclusive processes (atheroembolization, thrombotic microangiopathy, renal artery stenosis), elevated body mass index (obesity, increased lean body mass [e.g., bodybuilding]), cyanotic congenital heart disease, sickle cell anemia

Adapted from D'Agati VD, Kaskel FJ, Falk RJ. Focal segmental glomerulosclerosis. *N Engl J Med* 2011;365(25):2398–2411.

nephrotic syndrome, Rich (8) noted that children dying acutely of infectious complications, mostly within the 1st year of diagnosis, either showed no FSGS lesions or had only a few lesions involving the juxtamedullary glomeruli, whereas children dying with uremia and hypertension displayed more extensive cortical involvement by FSGS. These findings suggested that FSGS was a progressive kidney disease that initially affected the juxtamedullary glomeruli (8). In 1970, Churg et al. (9) described the pathologic features of FSGS in children with idiopathic nephrotic syndrome for the International Study of Kidney Diseases in Children (ISKDC) and noted that FSGS was usually steroid resistant and had a poor renal prognosis. Since that time, morphologic variants of FSGS have been recognized, and numerous secondary causes of FSGS, including genetic and acquired forms, have been identified. Meanwhile, the incidence

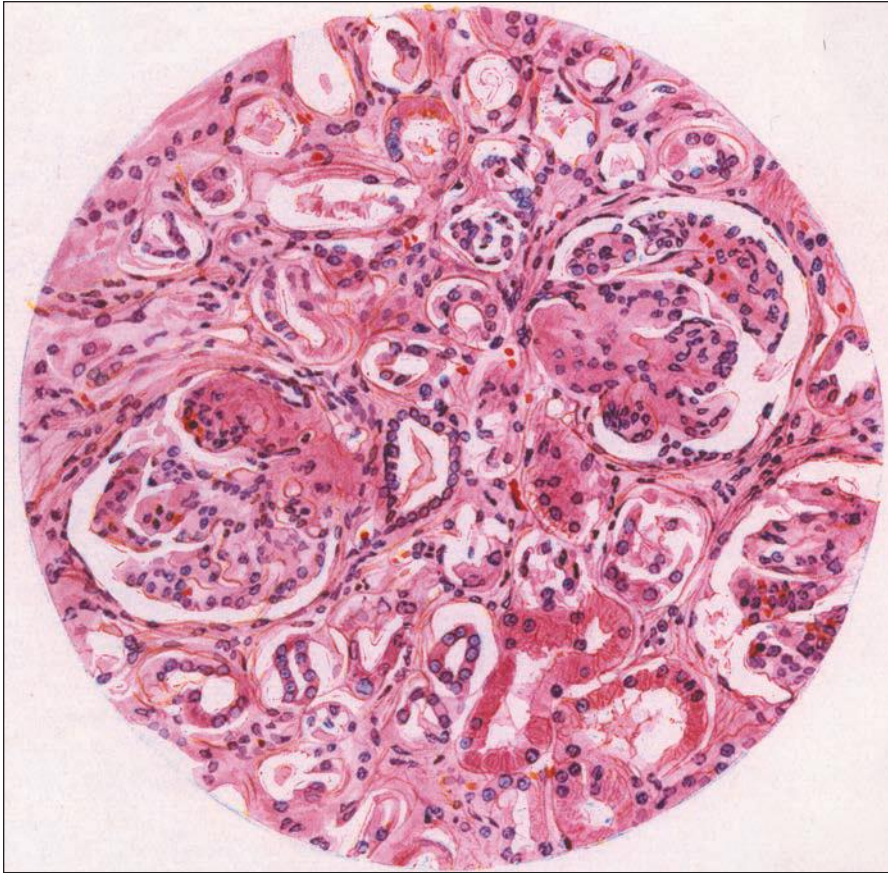


FIGURE 6.2 The first illustration of focal segmental glomerulosclerosis in a patient with nephrotic syndrome (lipoid nephrosis).

Two glomeruli show segmental obliteration of capillary lumina with accumulation of matrix. (From Fahr T. Pathologische Anatomie des morbus brightii. In: Henke F, Lubarsch O, eds. *Handbuch der speziellen pathologischen Anatomie und Histologie*. Berlin: Springer, 1925:156.)

of primary FSGS has grown, and it is now the leading cause of steroid-resistant nephrotic syndrome (SRNS) in both children and adults (10) and the most common primary glomerular disease causing ESRD in the United States (11,12).

Relationship of FSGS to Minimal Change Disease

Because both primary FSGS and minimal change disease (MCD) manifest the nephrotic syndrome and foot process effacement, it has been suggested that these conditions might represent a spectrum of podocytopathies that differ mainly with respect to the greater reversibility of podocyte injury in MCD. In support of this hypothesis are the findings of potential circulating permeability factors in both of these conditions and the development of either MCD or FSGS lesions in the puromycin aminonucleoside (PAN) model, depending on the cumulative dose of toxin, suggesting a related pathomechanism. The nonsclerotic glomeruli in human FSGS typically exhibit podocyte foot process effacement resembling MCD. In addition, transition from MCD-like glomerular disease (extensive foot process effacement without sclerosis) to FSGS has been noted in some sequential human biopsy samples and in the setting of recurrent FSGS following kidney transplantation (13). Of note, global glomerulosclerosis is seen with increased frequency in relapsing or steroid-dependent childhood MCD, suggesting that these sclerotic glomeruli may result from involution of immature glomeruli that may be more prone to develop global, rather than segmental, sclerosis (14). By analogy,

PAN given to neonatal mice leads to impaired glomerular maturation and resorption of the underdeveloped glomeruli, possibly reflecting loss of critical podocyte functions necessary for normal glomerular maturation (15). Despite these similarities, the weight of evidence from recent immunohistochemical (16), molecular (17), and permeability factor (4,5) studies favors that MCD and FSGS are distinct entities with different pathogenesis and pathobiology (3). MCD is discussed separately in Chapter 5.

PRIMARY FSGS

Epidemiology and Clinical Presentation

The incidence of FSGS is estimated at seven cases per million per year (10). However, data from renal biopsy studies and national registries of patients with nephrotic syndrome and ESRD may be subject to detection bias, as biopsy indications are influenced by the patient's age and clinical presentation and vary among geographic regions. Most adults with idiopathic nephrotic syndrome undergo renal biopsy on first clinical presentation because the potential causes are diverse. By contrast, in the pediatric age group, most nephrotic children will have steroid-responsive MCD; thus, a biopsy is performed only in those children who fail to respond to an empiric course of glucocorticoids or who relapse after treatment. The clinical threshold for biopsy may vary, and patients with proteinuria less than 1 g/d are more likely to undergo renal biopsy in Australia and New Zealand than in the United States and Europe (10).

The majority of children (75% to 90%) (18,19) and fewer adults (50% to 60%) with primary FSGS present with the nephrotic syndrome (i.e., nephrotic-range proteinuria, edema, hypoalbuminemia, and hypercholesterolemia); the rest have subnephrotic proteinuria. The pathophysiology of the nephrotic syndrome is discussed in detail in Chapter 5. In adults, the nephrotic syndrome is defined by urine protein excretion greater than 3.5 g/d and serum albumin levels less than 3.5 g/dL. In children with the nephrotic syndrome, urine protein excretion exceeds 1 g/m² of body surface area per day and serum albumin is less than 2.5 g/dL. In both children and adults, serum cholesterol level exceeds 200 mg/dL and peripheral edema is present. Renal insufficiency is present at the time of biopsy in approximately 20% of children and 30% of adults; hypertension is identified in 30% of children and 45% of adults; and microhematuria is seen in 57% to 68% of cases (20). Serum complement levels are normal, and the standard serologic tests for autoimmune connective tissue diseases and viral hepatitis are negative.

The proportion of childhood nephrotic syndrome due to FSGS increases with age, from less than 10% before 6 years of age up to 50% in adolescence (21). Given that as many as 20% of primary FSGS cases are steroid responsive (20), FSGS is probably underdiagnosed in patients less than 18 years of age with nephrotic syndrome, who typically receive empiric therapy without resort to biopsy (22). In the ISKDC study of children who underwent renal biopsy between 1967 and 1974, FSGS was diagnosed in 6.9% of children with primary nephrotic syndrome (20). In more recent studies, the frequency of FSGS in children with nephrotic syndrome undergoing renal biopsy has ranged from 18% to 23%, while the incidence of nephrotic syndrome in children ranged from two to four cases per 100,000 children per year (23,24). In a study of Canadian children (most of whom were Caucasian) biopsied between 1985 and 2002, the incidence of FSGS ranged from 0.37 to 0.94 new cases per 100,000 children, with a higher incidence in more recent cases (23). Male children are more commonly affected than females (20,25,26).

In adults, the renal biopsy prevalence of primary FSGS has increased from 2.5% to 4% of all biopsies in the 1970s to 12.2% to 18.7% in the 1990s (27). In patients over 60 years of age, 5.4% of those with nephrotic syndrome had FSGS (28), while in the very elderly (greater than 80 years of age), the renal biopsy prevalence of primary FSGS was 4% (29). Between 2004 and 2008 in the United States, the incidence of ESRD caused by FSGS was 2.2%, although it is likely that FSGS also accounted for some cases of ESRD that were never biopsied and classified as either glomerulonephritis or hypertensive kidney disease (11).

Among adults with nephrotic syndrome undergoing renal biopsy, the frequency of FSGS is 10% in Asia, 20% in Europe and among North American whites, and up to 78% among North American blacks (10). In Africa, the biopsy frequency of FSGS ranges from 23% to 40% (10). Both the incidence of ESRD from FSGS and rate of progression to ESRD are higher in black children than in whites (20,30,31). In all children with ESRD, the prevalence of FSGS is 14.4%, ranging from 11.7% in whites to 23.7% in blacks (31).

The incidence of FSGS and the proportion of ESRD caused by FSGS have increased over the past few decades in both children and adults and in blacks and whites

(10,21,23,30,32–36). This increase has been reported in some (37) but not all other countries (10) and is particularly striking in African Americans, in whom FSGS is now the leading cause of nephrotic syndrome and, in children, the leading cause of ESRD (31,38,39). The incidence of ESRD due to FSGS is approximately 5 cases per million in Caucasians and 30 to 40 cases per million in African Americans (21). The incidence of FSGS as a cause of ESRD has increased nearly fivefold in African Americans since the early 1980s. The incidence in Caucasians has also increased, albeit more slowly. This rising incidence is probably due largely to a true increase in disease incidence, as well as potential detection bias (e.g., changes in renal biopsy practice or pathologic diagnostic criteria).

Pathologic Features of FSGS

Gross Pathology

In early studies of children dying of nephrosis (some of whom presumably had primary FSGS), the kidneys were described as enlarged and swollen, with fat-filled cortices (7). This fatty appearance is attributable to the abundant lipid resorption droplets seen histologically in proximal tubular epithelial cells. In cases where FSGS has progressed to ESRD, the kidneys show bilateral symmetric shrinkage.

Light Microscopy

The “classic” lesion of FSGS consists of segmental solidification of the glomerular capillary tuft by an acellular extracellular matrix that is eosinophilic, periodic acid-Schiff (PAS) reactive, and argyrophilic (Fig. 6.3). This may be accompanied by hyalinosis, the accumulation of a glassy, eosinophilic material caused by entrapment of plasma proteins (Figs. 6.4 to 6.6). Hyalinosis lesions may contain extracellular lipid vacuoles that appear as sharply delineated, round, empty spaces. FSGS lesions are often associated with adhesion to the Bowman capsule (see Fig. 6.4), and the smallest lesions may consist of a simple synchial attachment, without prominent matrix accumulation in the underlying glomerular tuft. A single lesion (Fig. 6.7) or

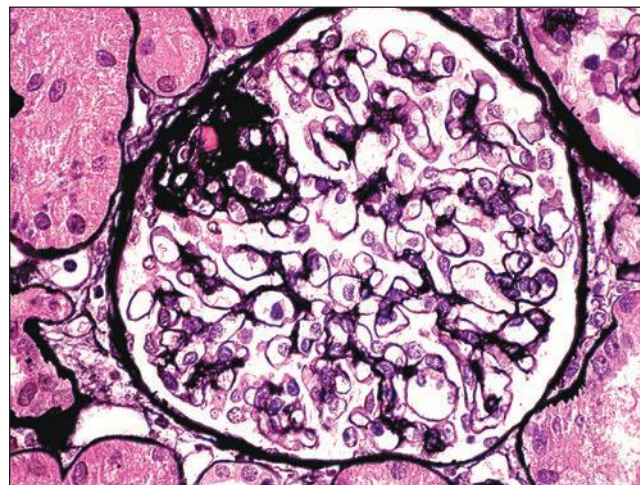


FIGURE 6.3 Primary FSGS, NOS. With a silver stain, the extracellular matrix is argyrophilic (black), whereas hyaline is pink. (Jones methenamine silver [JMS] stain, $\times 600$.)

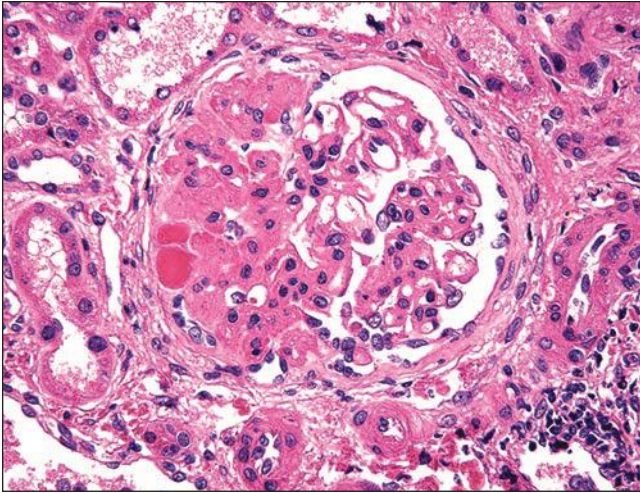


FIGURE 6.4 Primary FSGS, NOS. The left half of the glomerulus shows segmental obliteration of capillary lumina by the matrix and hyalinosis with broad adhesion to the Bowman capsule. Hyaline has a glassy, more eosinophilic appearance than the adjacent matrix material. (H&E, $\times 400$.)

multiple individual lesions (Fig. 6.8) may exist in a given glomerulus, as revealed by serial sectioning and three-dimensional reconstructions (40). Juxtamedullary glomeruli appear to be more vulnerable to developing FSGS than superficial glomeruli, likely because of their greater single-nephron glomerular filtration rate (GFR) and higher glomerular capillary pressures and flow rates (41,42).

In addition to matrix and hyaline accumulation, FSGS lesions demonstrate variable degrees of cellularity. Hypercellularity can affect the extracapillary and/or the

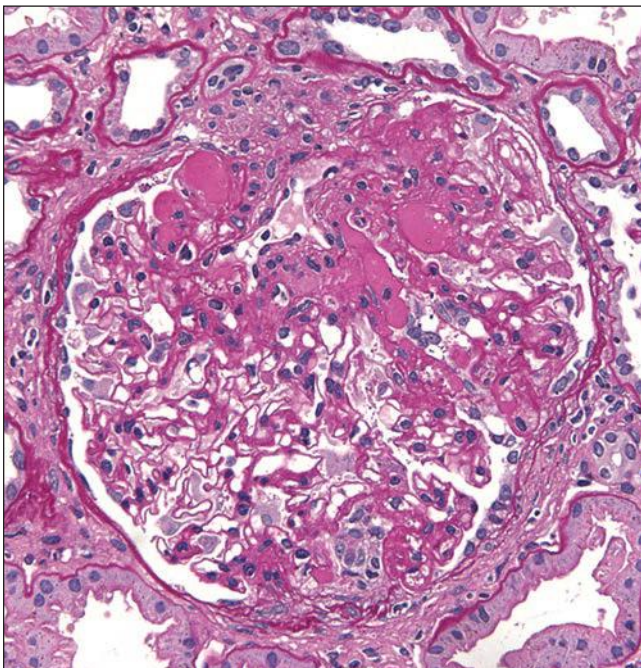


FIGURE 6.5 Primary FSGS. Hyalinosis and matrix both stain pink with PAS, but hyaline has a glassy appearance. (PAS, $\times 400$.)

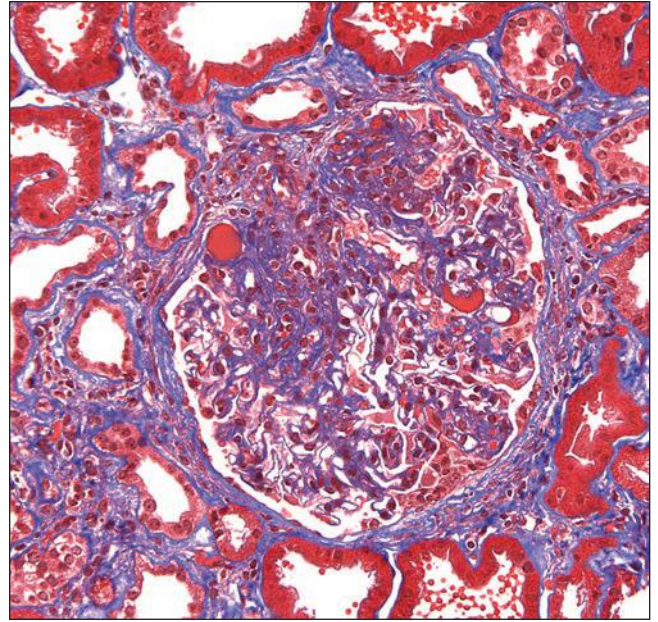


FIGURE 6.6 Primary FSGS. Hyalinosis stains bright red and extracellular matrix stains blue with trichrome stain. (Trichrome stain, $\times 400$.)

endocapillary zones. This most commonly consists of mild swelling and hyperplasia of visceral epithelial cells, forming a single layered “cap” or “cobble-stone” appearance overlying the segmental sclerosis lesion (Figs. 6.9 and 6.10). A halo-like effect of a looser pale matrix between the capped visceral cells and the original glomerular basement membrane (GBM) reflects the deposition of the extracellular matrix produced by parietal cells that migrate over the sclerotic lesions (43). In other examples, the glomerular epithelial cell hyperplasia is more exuberant with confluence of the visceral and parietal cell layers. The swollen epithelial cells often display PAS-positive cytoplasmic protein resorption droplets. Intracapillary foam

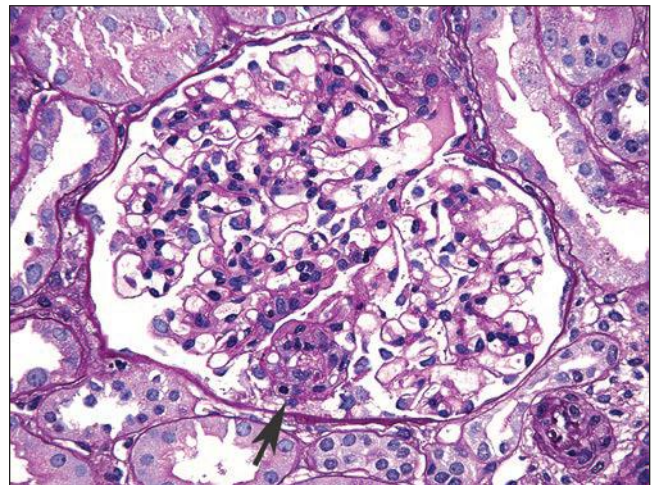


FIGURE 6.7 Primary FSGS. A single segmental lesion (arrow) with endocapillary hypercellularity and mild hyalinosis involves the periphery of the glomerular tuft. (PAS, $\times 400$.)

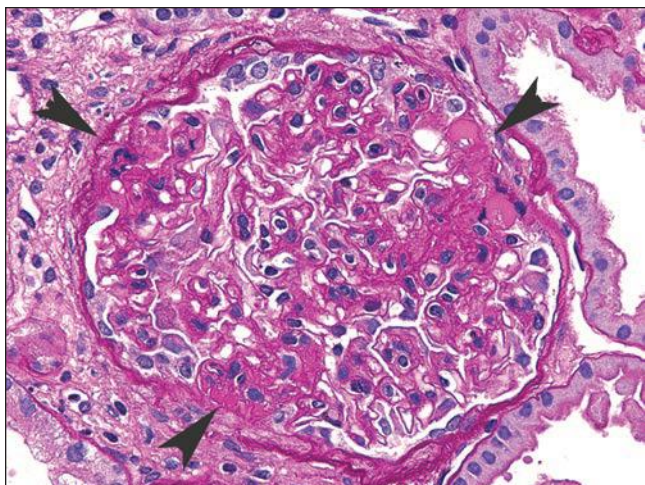


FIGURE 6.8 Primary FSGS. Three discrete lesions (*arrowheads*) of the matrix and/or hyaline are present in the same glomerulus. (PAS, $\times 400$.)

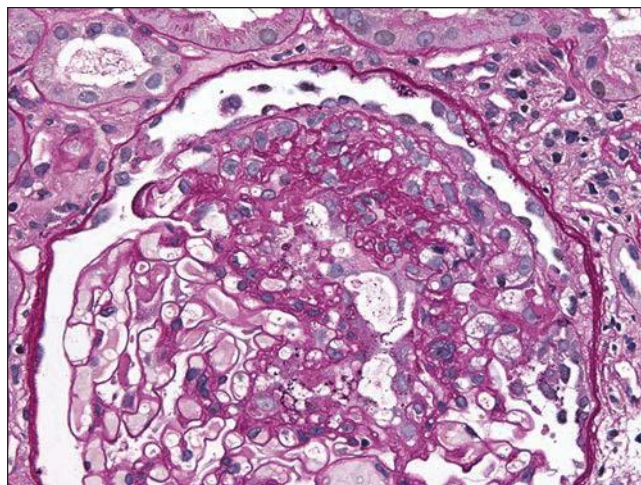


FIGURE 6.10 Primary FSGS. A segmental sclerosis lesion with "capping" of overlying visceral epithelial cells. (PAS, $\times 400$.)

cells may be seen in areas of segmental sclerosis (Figs. 6.11 and 6.12) and are sometimes numerous, leading to expansion of the glomerular tuft (Fig. 6.13). These cells express monocyte markers, such as CD68, but it is unclear if they derive from circulating macrophages or from transdifferentiation of resident glomerular endothelial or mesangial cells.

Glomerular capillaries may also show an implosive, collapsed appearance, accompanied by severe hyperplasia of epithelial cells in the Bowman space (Fig. 6.14). In some cases, capillary collapse is accompanied by endocapillary hypercellularity causing expansion of the glomerular tuft (see Fig. 6.13). Segmental lesions may localize to the hilar region (vascular pole), to the paratubular region (adjacent to the origin of the proximal tubule), or have an indeterminate relationship to these landmarks in the plane of section (Figs. 6.15 and 6.16) (see Morphologic Variants of FSGS below). Focal and

segmental lesions of sclerosis tend to evolve into diffuse and global lesions with chronicity. The degree of global glomerulosclerosis is variable and depends on disease severity, the timing of the biopsy, and the rate of disease progression. The finding of only global glomerulosclerosis, without segmental lesions, is nonspecific and increases with age, reflecting coexistent arterionephrosclerosis related to senescence and/or hypertension. Although the nonsclerotic glomeruli may appear normal, morphometric analysis shows an increase in the glomerular area and mesangial matrix in both childhood (44) and adult primary FSGS (45); these features are more prominent in cases of secondary adaptive FSGS (see section on Adaptive FSGS below). Glomeruli unaffected by sclerosis may exhibit diffuse podocyte swelling.

Proximal tubules often display PAS-positive protein resorption droplets and clear lipid vacuoles (Fig. 6.17). Tubular atrophy and interstitial fibrosis are often present, ranging from

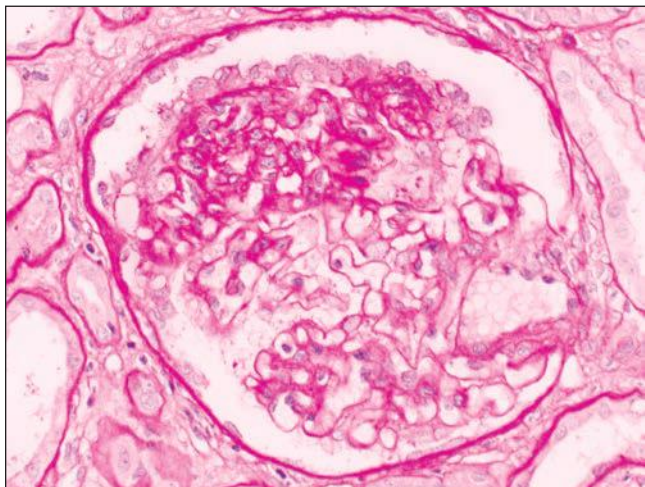


FIGURE 6.9 Primary FSGS. There is a monolayer of podocytes overlying a sclerotic portion of a glomerulus ("cobblestone pattern"). The podocytes are cuboidal with abundant cytoplasm, vesicular nuclei, and prominent nucleoli. (PAS, $\times 330$.)

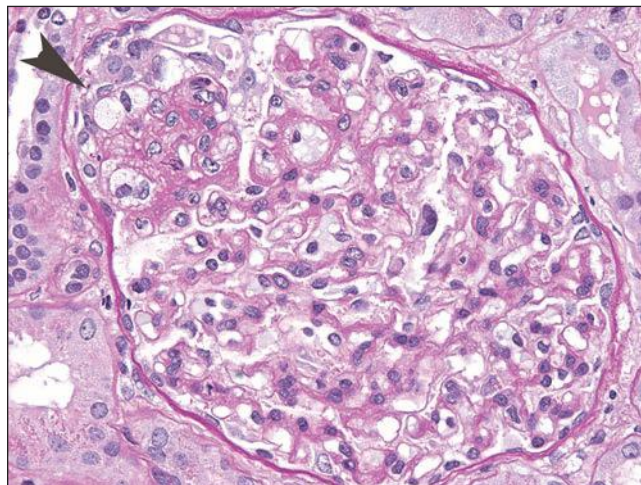


FIGURE 6.11 Primary FSGS. A segmental lesion contains endocapillary foam cells (*arrowhead*). (PAS, $\times 400$.)

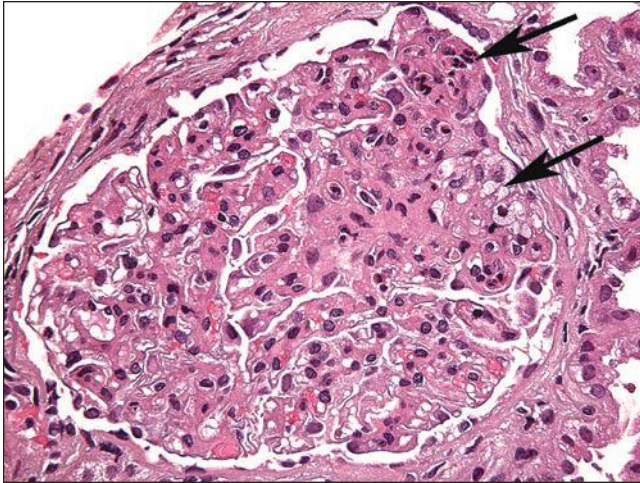
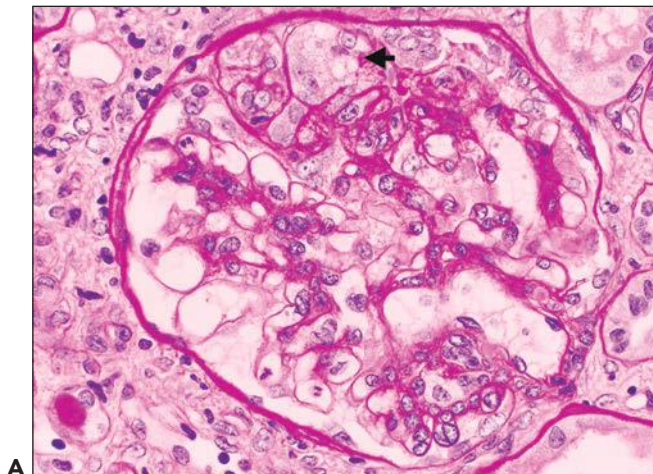


FIGURE 6.12 Primary FSGS. A segmental sclerosis lesion contains endocapillary foam cells, as well as some infiltrating leukocytes (arrows) (H&E, $\times 400$)

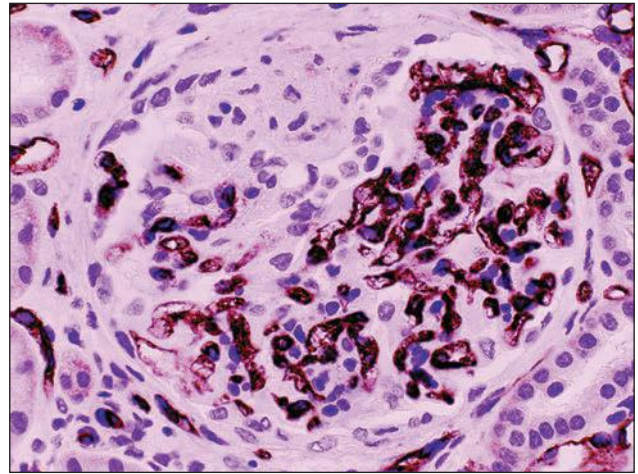
mild to severe, but are generally commensurate with the degree of glomerulosclerosis (Fig. 6.18). Interstitial foam cells may be seen, either singly or in aggregates, in cases with long-standing proteinuria. In the setting of severe unremitting nephrotic syndrome and marked hypoalbuminemia, proximal tubules

may exhibit degenerative and regenerative changes resembling acute tubular necrosis (Fig. 6.19). Arterial vessels show changes related to hypertension and/or aging.

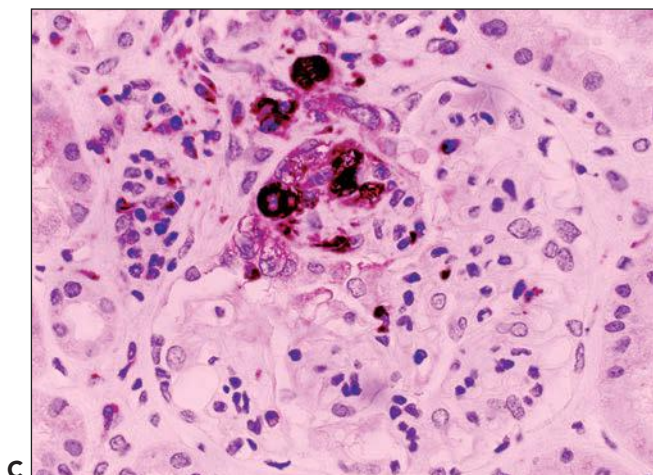
Importantly, the likelihood of identifying a diagnostic glomerular lesion in a biopsy sample is determined by both the proportion of glomeruli affected by the disease and by the sample size, and FSGS lesions may be missed in small biopsy samples (46). FSGS lesions may also be missed in early disease if only the superficial renal cortex is sampled, or if the glomerular scarring has become diffuse and global, in the later stages of disease. It has been estimated that a sample of at least 20 glomeruli is required to confidently exclude the presence of disease affecting 10% of glomeruli (46). While the percentage of glomerular involvement by FSGS lesions is difficult to ascertain in small biopsies, one study showed frequencies of 11.7% in children and 31.5% in adults, increasing to 23.2% and 48%, respectively, after serial sectioning (47). In adults with primary FSGS, the prevalence of glomeruli with segmental lesions increased from 31.5% to 71.8% after exhaustive serial sectioning (48). Therefore, additional tissue sections should be performed if there is a high clinical suspicion of FSGS. Biopsy findings of focal tubular atrophy and interstitial fibrosis without sclerosing glomerular lesions should also prompt a more exhaustive search for unsampled FSGS. In such cases, the portions of the biopsy allocated for immunofluorescence and electron microscopy should be examined carefully by light microscopy for possible FSGS lesions.



A



B



C

FIGURE 6.13 Primary FSGS with cellular and collapsing features.

A: Several glomerular capillaries at the top of the glomerulus are expanded and occluded by foam cells (arrow). The overlying podocytes are hyperplastic. Adjacent capillaries display segmental collapse. (PAS, $\times 330$.) **B:** The same glomerulus illustrated in (A) is stained for the endothelial marker, CD31. The glomerular capillaries are stained everywhere except in the segmental lesion, indicating that the capillary endothelium has been obliterated. (CD31 immunoperoxidase, $\times 330$.) **C:** The endocapillary foam cells stain with the macrophage marker, CD68. (CD68 immunoperoxidase, $\times 330$.)

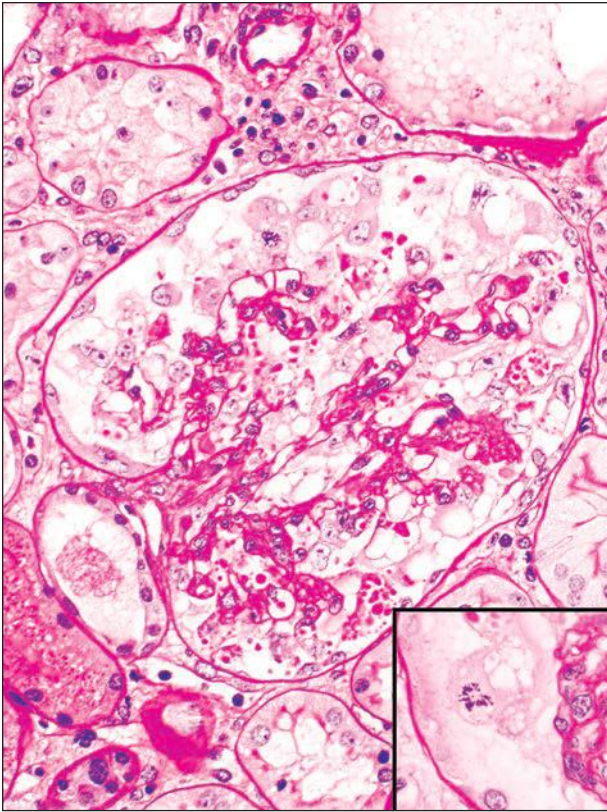


FIGURE 6.14 Primary FSGS, collapsing variant. There is global implosive collapse of capillaries with wrinkling of the glomerular basement membranes, accompanied by swelling and proliferation of glomerular epithelial cells that contain cytoplasmic vacuoles and PAS-positive cytoplasmic droplets. One epithelial cell (*inset*) displays a mitotic figure. (PAS, $\times 330$.)

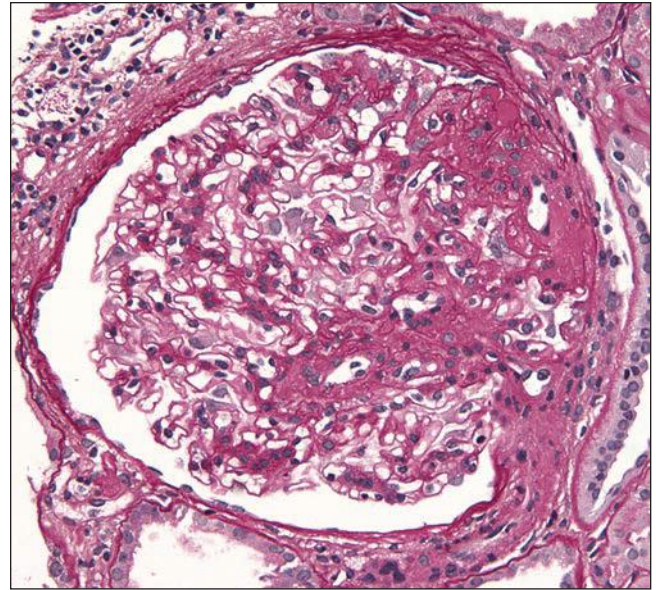


FIGURE 6.16 Primary FSGS, perihilar variant. Segmental sclerosis and hyalinosis located in the perihilar region (vascular pole). (PAS, $\times 600$.)

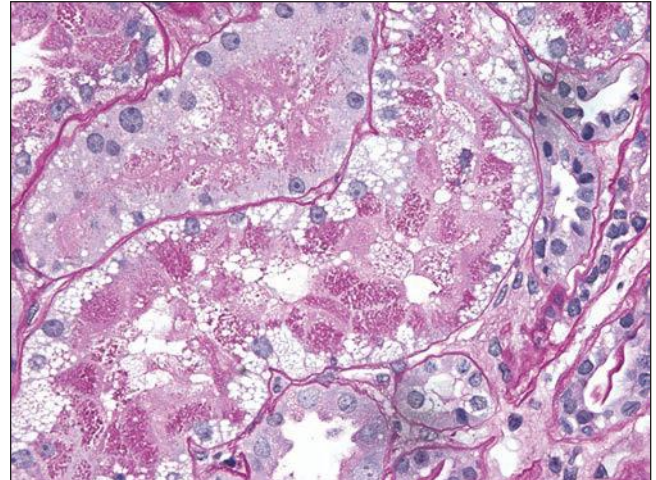


FIGURE 6.17 Proximal tubules display cytoplasmic protein and lipid droplets. (PAS, $\times 600$.)

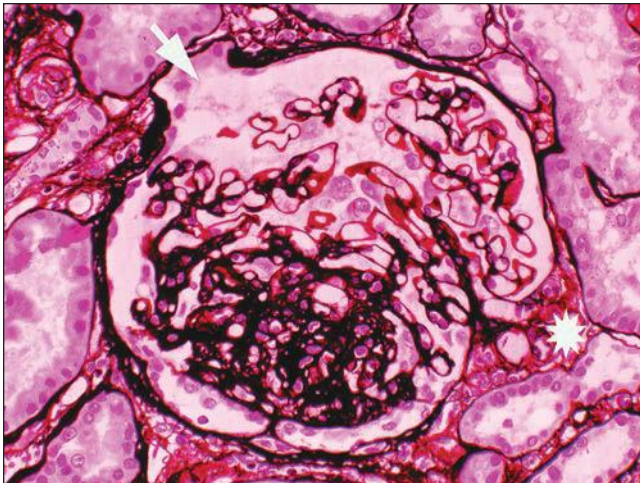


FIGURE 6.15 Primary FSGS, NOS. A segmental sclerosis lesion with a small adhesion involves neither the hilum (*asterisk*) nor the tubular pole of the glomerulus (*arrow*). (JMS stain, $\times 330$.)

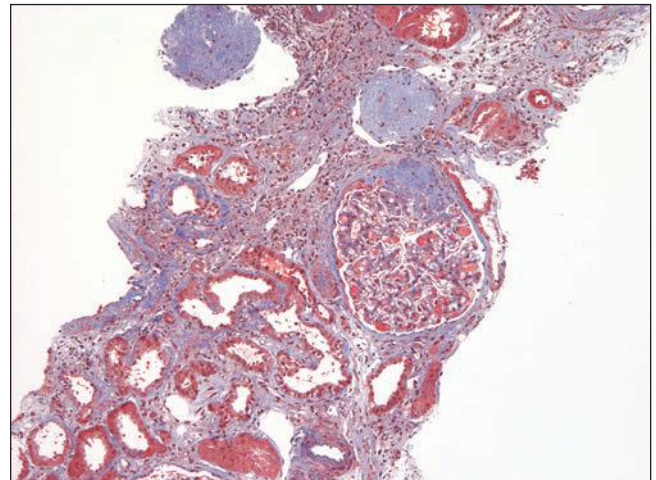


FIGURE 6.18 Primary FSGS. One glomerulus shows segmental sclerosis, and the other two are globally sclerotic, consistent with advanced chronicity. There are prominent tubular atrophy and interstitial fibrosis. (Trichrome stain, $\times 100$.)

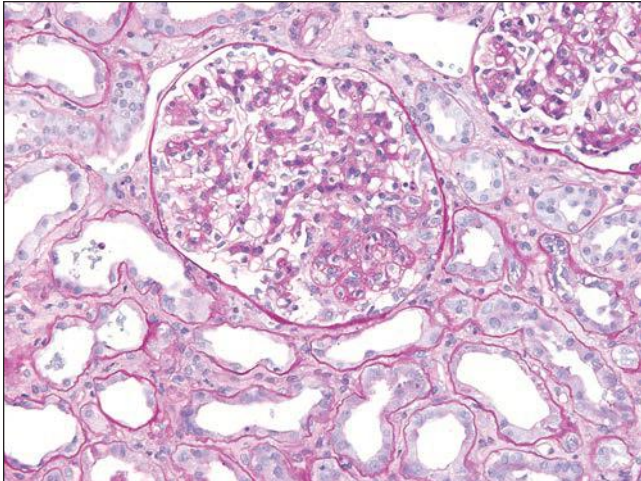


FIGURE 6.19 Primary FSGS, with severe acute tubular injury. Proximal tubules display epithelial simplification with loss of brush border. (PAS, $\times 200$.)

Immunofluorescence Microscopy

There is often segmental glomerular staining for IgM and C3 (and to a lesser extent C1q), consistent with nonspecific trapping in areas of sclerosis and/or hyalinosis (Fig. 6.20). Less intense and more delicate mesangial staining for IgM and C3 may also be observed involving the mesangium of nonsclerotic segments (Fig. 6.21). Protein resorption droplets in podocytes and proximal tubular cells commonly stain for albumin and IgG, as well as IgA. Tubular epithelial cytoplasmic staining for C3 may also be observed. Staining for other immune reactants is negative.

Electron Microscopy

Electron microscopy typically demonstrates effacement of podocyte foot processes overlying areas of segmental sclerosis and in more than 50% of the capillary surface area in the nonsclerotic

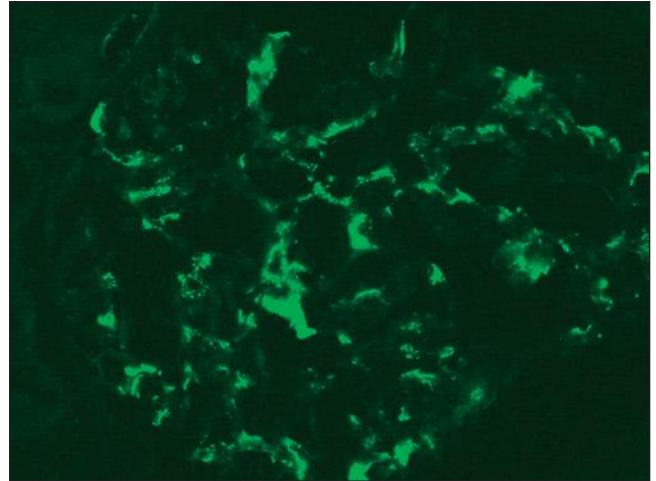


FIGURE 6.21 Immunofluorescence microscopy shows finely granular mesangial staining for IgM. (FITC anti-human IgM, $\times 330$.)

glomeruli (Fig. 6.22). The effacement process is thought to involve retraction of podocyte foot processes (or pedicels) into the cell body or primary processes. Foot process effacement is also seen in other proteinuric diseases and is thus a nonspecific podocyte response. However, the finding of effacement involving patent glomerular capillaries in the absence of immune deposits or other ultrastructural abnormalities of the GBM should suggest a podocytopathy. A recent morphometric study showed that the mean foot process width was significantly greater in primary FSGS compared to MCD and secondary (adaptive) FSGS (49), suggesting that the degree of foot process effacement is a helpful clue in distinguishing primary FSGS from adaptive forms. Podocytes may be swollen and show increased organelar content, microvillous surface projections, and loss of primary processes. In some cases, the podocyte cell body appears to sit directly on the GBM, without recognizable primary processes.

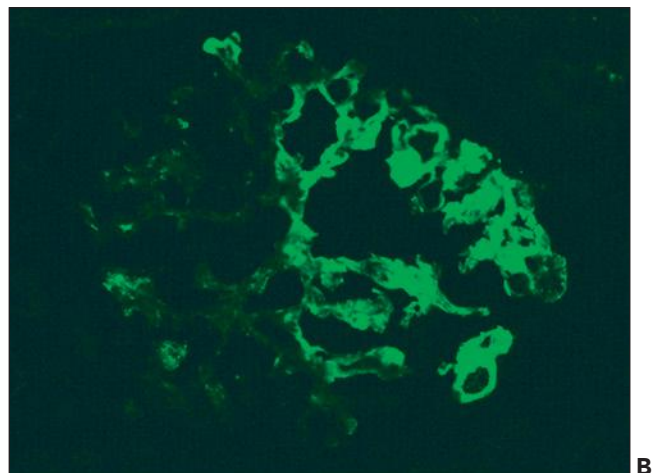
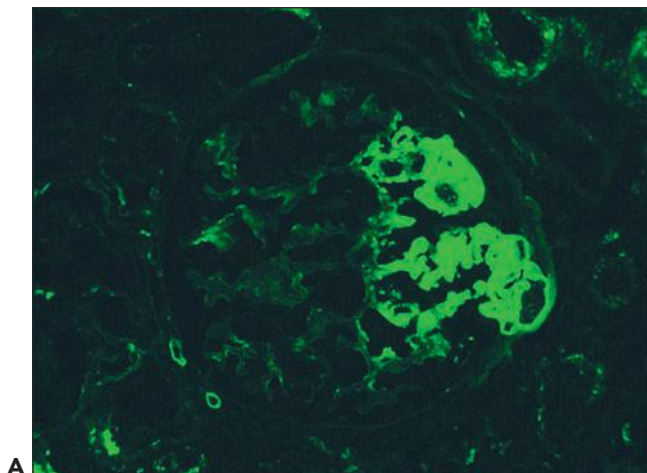


FIGURE 6.20 Immunofluorescence microscopy shows segmental glomerular tuft staining for IgM (**A**) and C3 (**B**). (FITC anti-human IgM [**A**] and FITC anti-human C3 [**B**], $\times 330$.)

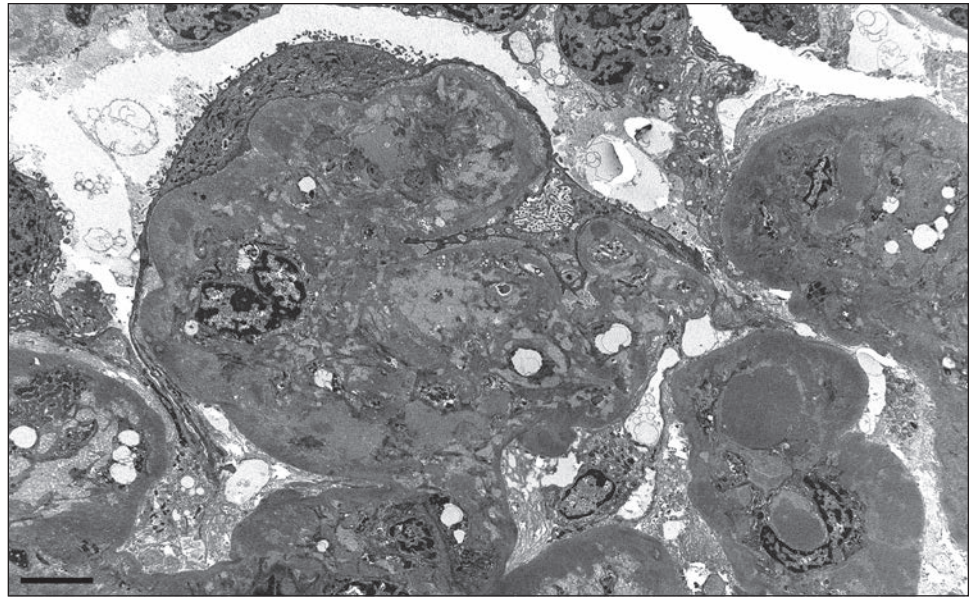


FIGURE 6.22 Primary FSGS.

Segmental solidification of the glomerular tuft with wrinkling of basement membranes and inframembranous hyaline is accompanied by diffuse effacement of the overlying podocyte foot processes. (Electron photomicrograph, original magnification $\times 6000$.)

Many filtration slit diaphragms become displaced or lost. Podocyte actin filaments typically undergo rearrangement to form a dense cytoskeletal “mat” parallel to the direction of the GBM, in the basal cytoplasm above the effaced foot processes. Detachment and lifting of injured podocytes from the GBM may be seen (Fig. 6.23). These changes are often followed by the laying down of a lamellated neomembrane between detached visceral epithelial cells and the underlying GBM. Recent studies suggest that this looser matrix, which is less electron dense

than the normal GBM, is derived from parietal cells that have replaced lost podocytes (43). Cytoplasmic electron dense protein droplets are common in cases with severe proteinuria. Hyalinosis lesions are characterized by accumulation of amorphous electron dense material, sometimes containing clear, rounded inclusions representing entrapped lipid and typically localize to the inframembranous region (i.e., between the endothelial cell and the GBM). Endocapillary foam cells are rounded cells with electron-lucent lipid-rich cytoplasmic vacuolization (Fig. 6.24).

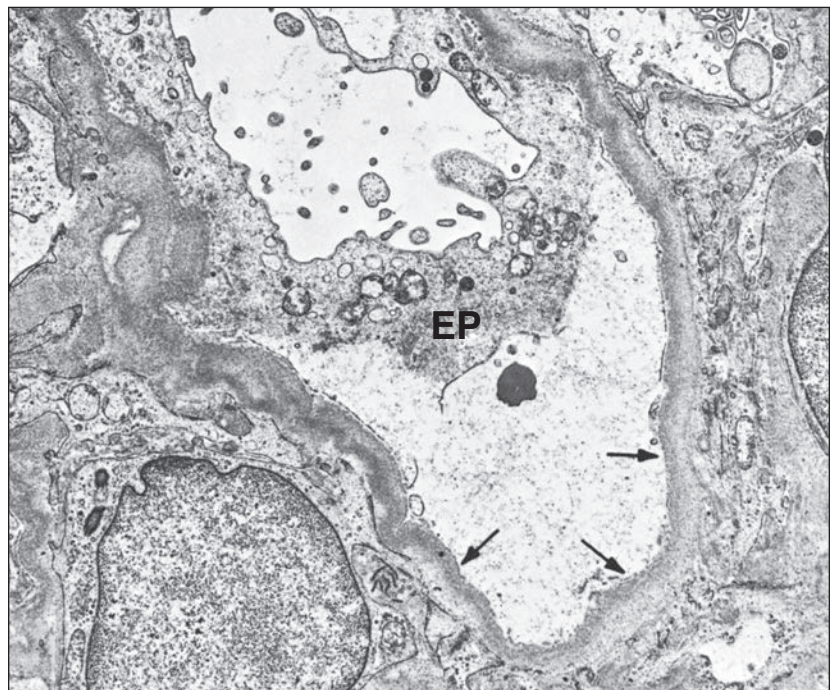


FIGURE 6.23 Electron micrograph shows epithelial cell (EP) detachment from the underlying glomerular capillary basement membrane (arrows). The intervening area contains finely granular material. (Original magnification, $\times 5000$.) (Courtesy of Drs. Jacob Churg and Edith Grishman.)

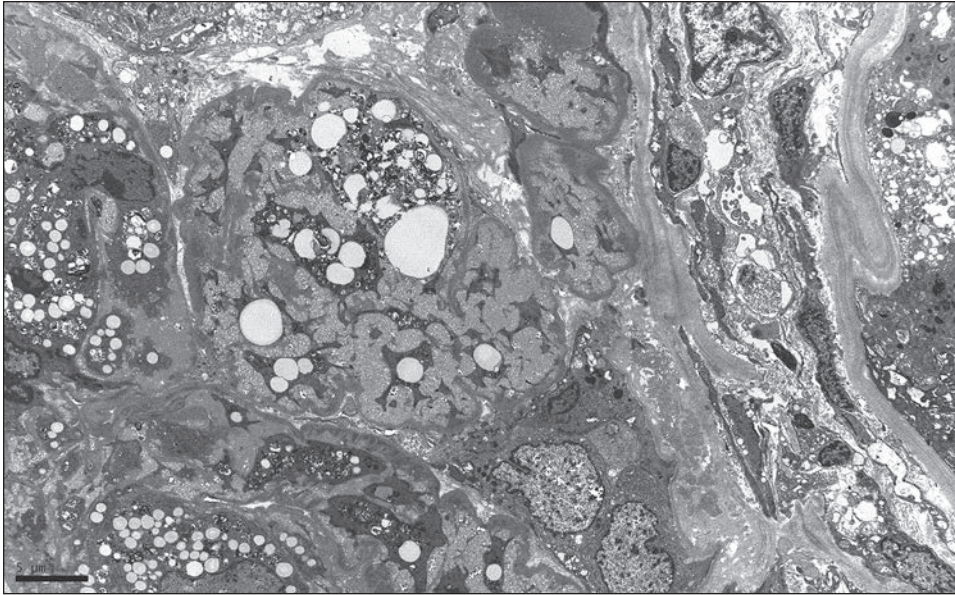


FIGURE 6.24 Primary FSGS, tip variant. Endocapillary foam cells and extracellular matrix obliterate the glomerular capillary lumina. (Electron photomicrograph, original magnification $\times 3000$.)

Morphologic Variants of FSGS

Since the early descriptions of FSGS by Churg et al. (9), it was recognized that FSGS lesions were morphologically heterogeneous with respect to the degree of cellularity and their location within the glomerular globe. In 1984, Howie and Brewer (50) coined the term “glomerular tip lesion” for a distinctive finding in some patients with idiopathic nephrotic syndrome. This lesion consisted of small segmental lesions at the tubular pole (i.e., the glomerular “tip”), which either prolapsed into the proximal tubule or adhered to the Bowman capsule at the tubular outlet, accompanied by signs of injury in the adjacent proximal tubular epithelium. Tip lesions showed prominent swelling of overlying visceral epithelial cells and contained endocapillary foam cells (and less commonly hyaline); other glomeruli showed no pathologic alterations other than foot process effacement. Cases of glomerular tip lesion had an excellent response to steroids and favorable outcome, similar to MCD and distinct from FSGS (50). Subsequently, it was suggested that glomerular tip lesion might also represent an early stage in the evolution of FSGS, not otherwise specified (NOS) (51).

In 1985, Schwartz and Lewis used the term “cellular lesion” for cases of FSGS that were characterized by prominent visceral epithelial cell abnormalities, including swelling and hyperplasia. Cellular lesions might also display endocapillary hypercellularity with foam cells and infiltrating leukocytes or collapse of the underlying capillaries (52). The cellular lesion was associated with heavier proteinuria, more frequent nephrotic syndrome, and a shorter time from onset of symptoms to biopsy, suggesting that it might represent an early stage in the development of FSGS (52). However, it did not correlate with initial serum creatinine or rate of ESRD (53).

In 1986, Weiss et al. (54) described FSGS with features of glomerular collapse and epithelial hypercellularity in patients who had severe nephrotic syndrome and rapid progression to ESRD. This entity was subsequently called collapsing

glomerulopathy (or collapsing FSGS), and its aggressive clinical course was confirmed by other investigators (55–57). Thus, collapsing FSGS can be considered a subset of the “cellular lesion” originally described by Schwartz and Lewis. Lesions of collapsing FSGS were noted in patients with human immunodeficiency virus type 1 (HIV-1) infection who presented with severe nephrotic syndrome and rapid-progression renal failure (58), and this secondary form of collapsing FSGS was subsequently termed HIV-associated nephropathy (HIVAN) (59,60). Other secondary viral and drug-induced causes of collapsing glomerulopathy have since been described.

The prognostic significance of FSGS variants and their relationship to each other have been controversial (61). Indeed, some investigators have questioned whether collapsing glomerulopathy and glomerular tip lesion should even be considered as forms of FSGS, given their frequent lack of *bona fide* extracellular matrix accumulation (i.e., sclerosis). However, as both of these entities usually present with nephrotic syndrome and often coexist with “classic” FSGS lesions, either within the same biopsy or in sequential biopsies (56), they can be considered within the spectrum of FSGS.

The lack of a standardized approach to definition and classification has hindered study of these morphologic variants of FSGS, a working classification (hereafter referred to as the “Columbia Classification”) was proposed in 2004 (62). This classification sets forth defining criteria and a stepwise, hierarchical approach to distinguish five mutually exclusive morphologic variants of FSGS: collapsing, tip lesion, cellular, perihilar variant, and NOS variant (62). Importantly, this classification is applicable to primary and secondary forms of FSGS and does not imply that these variants per se represent specific disease entities.

A summary of the Columbia Classification is provided in Table 6.2 and drawings of four of the variants are provided in Figure 6.25. In this schema, a segmental lesion is defined as “less than 100% of the glomerular tuft involvement with

TABLE 6.2 Histologic variants of FSGS

Histologic subtype	Defining features	Clinical features	Associations
Collapsing	Implosive collapse of glomerular capillaries with hyperplasia of overlying visceral epithelial cells. Severe tubular injury and tubular microcysts may be seen. Podocyte foot process effacement is usually severe.	Primary or secondary to viruses (notably HIV), drugs (pamidronate, interferon), and vasoocclusive disease.	Usually presents with severe nephrotic syndrome and renal insufficiency. Black racial predominance. Worst prognosis, with poor responsiveness to steroids and rapid progression to kidney failure.
Tip	Segmental lesion involving the tubular pole, with adhesion to the tubular outlet or confluence of podocytes and tubular epithelial cells. Tubular atrophy and interstitial fibrosis are generally mild. Podocyte foot process effacement is usually severe.	Usually primary. Tip lesions may also be seen in other diseases with heavy proteinuria (e.g., membranous glomerulonephritis, diabetic nephropathy, and preeclampsia).	Usually presents with abrupt onset of full nephrotic syndrome. Predominance in Caucasian adults. Usually responds to steroids and has the lowest risk of progression.
Cellular	Expansile segmental lesion with endocapillary hypercellularity, often including foam cells and infiltrating leukocytes, with variable glomerular epithelial cell hyperplasia. Podocyte foot process effacement is variable but often severe.	Usually primary. Least common variant. May be an early stage in the evolution of sclerotic lesions.	Typically presents with the nephrotic syndrome.
Perihilar	Segmental hyalinosis and sclerosis involving the vascular pole (perihilar region) in the majority of glomeruli with segmental lesions. Often may be accompanied by glomerulomegaly in cases of adaptive FSGS. Foot process effacement tends to be mild and focal.	Common in adaptive FSGS associated with obesity, elevated lean body mass, hypertensive nephrosclerosis, reflux nephropathy, renal agenesis, sickle cell anemia, and oligomeganephronia.	In adaptive FSGS, usually presents with subnephrotic proteinuria and normal serum albumin levels.
NOS	Does not meet defining features of the above variants. Foot process effacement is variable and may be severe.	Primary or secondary (including genetic forms). Most common variant in most studies. Other variants may evolve into NOS over time.	May present with the nephrotic syndrome or subnephrotic proteinuria.

Adapted from D'Agati VD, Kaskel FJ, Falk RJ. Focal segmental glomerulosclerosis. *N Engl J Med* 2011;365(25):2398–2411.

some residual patent capillaries,” whereas a global lesion affects the entire glomerular tuft (62). The finding of segmental (Fig. 6.26A) or global (Fig. 6.26B) glomerular capillary collapse with overlying visceral epithelial cell hypertrophy and hyperplasia in at least one glomerulus warrants a diagnosis of the collapsing variant of FSGS, irrespective of the findings in other glomeruli. Excluding collapsing lesions, the finding of a single segmental lesion involving the tip domain (outer 25% of the tuft next to the proximal tubule origin) where the tubular pole is identified is diagnostic of the tip variant (Fig. 6.27). After excluding collapsing and tip lesions, the finding of one glomerulus with segmental expansile endocapillary hypercellularity obliterating capillary lumina (with or without foam cells, hyalinosis, infiltrating leukocytes, karyorrhexis, and epithelial cell hyperplasia) is classified as cellular variant (Figs. 6.13 and 6.28). Perihilar variant is defined as segmental hyalinosis and sclerosis contiguous with the glomerular hilum affecting the majority ($\geq 50\%$) of glomeruli with segmental lesions, excluding collapsing, cellular, and tip lesions (Fig. 6.29). All other

cases are classified as FSGS NOS variant, which by default represents the common, “classic” or generic lesion of segmental sclerosis.

Although the Columbia Classification is essentially heuristic, reflecting the collective experience of the participating pathologists and evidence from the literature, subsequent studies have confirmed significant differences in presenting clinical and demographic features and patient outcomes among the FSGS variants (see Clinical-Pathologic Correlation of Histologic Variants of Primary FSGS and Tables 6.3 and 6.4).

Collapsing Variant (Also Known as Collapsing Glomerulopathy)

Collapsing lesions of sclerosis may be focal and segmental but are more typically diffuse and global in distribution. Capillary collapse is best appreciated with silver or PAS stains, which demonstrate wrinkling of the GBMs, leading to luminal obliteration (Fig. 6.30). There is usually little if any extracellular

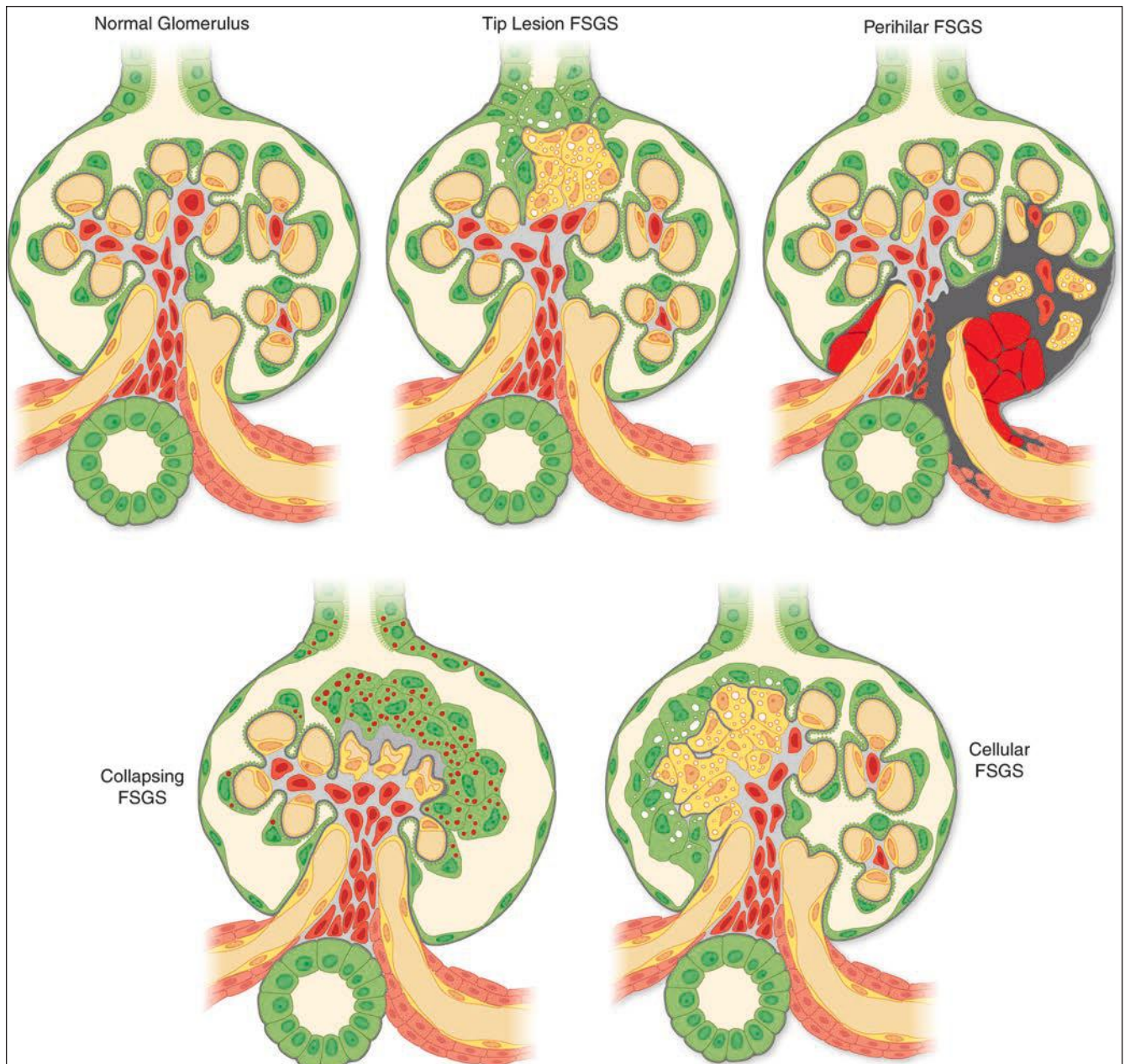


FIGURE 6.25 Drawings of the histologic features of the Columbia Classification variants of FSGS (NOS not shown).

Top Row: Normal glomerulus for comparison with epithelial cells green, endothelial cells yellow, mesangial and smooth muscle cells orange, foam cells yellow with clear vacuoles, and basement membranes gray. Tip lesion variant FSGS with segmental lesion involving the tubular pole, confluence of podocytes, and tubular epithelial cells, an endocapillary foam cell (yellow with clear vacuoles) and slight increase in the extracellular matrix. Perihilar variant FSGS with segmental hyalinosis (red) and sclerosis (dark gray) involving the vascular pole (perihilar region). **Bottom Row:** Collapsing variant FSGS with segmental collapse of capillaries, separation of podocytes from the glomerular basement membrane, accumulation of subepithelial extracellular matrix and hyperplasia and swelling of overlying epithelial cells that have abundant cytoplasmic protein droplets. Cellular variant FSGS with segmental obliteration of capillary lumens by endocapillary hypercellularity caused by foam cells (yellow with vacuoles) and adjacent epithelial hypertrophy and mild hyperplasia.

matrix accumulation in the acute collapsing lesions, but this may be present in other glomeruli. Hyalinosis lesions are rare in this variant. Capillary collapse is accompanied by prominent epithelial cell hypertrophy and hyperplasia within the Bowman space. The epithelial cells typically line the external

surface of the glomerular tuft but may fill the Bowman space, forming a “pseudocrescent” (Fig. 6.31). Serial sections have shown that these lesions are often continuous with the parietal epithelial cell layer; however, these cells usually lack the spindled morphology, intercellular matrix, and pericellular

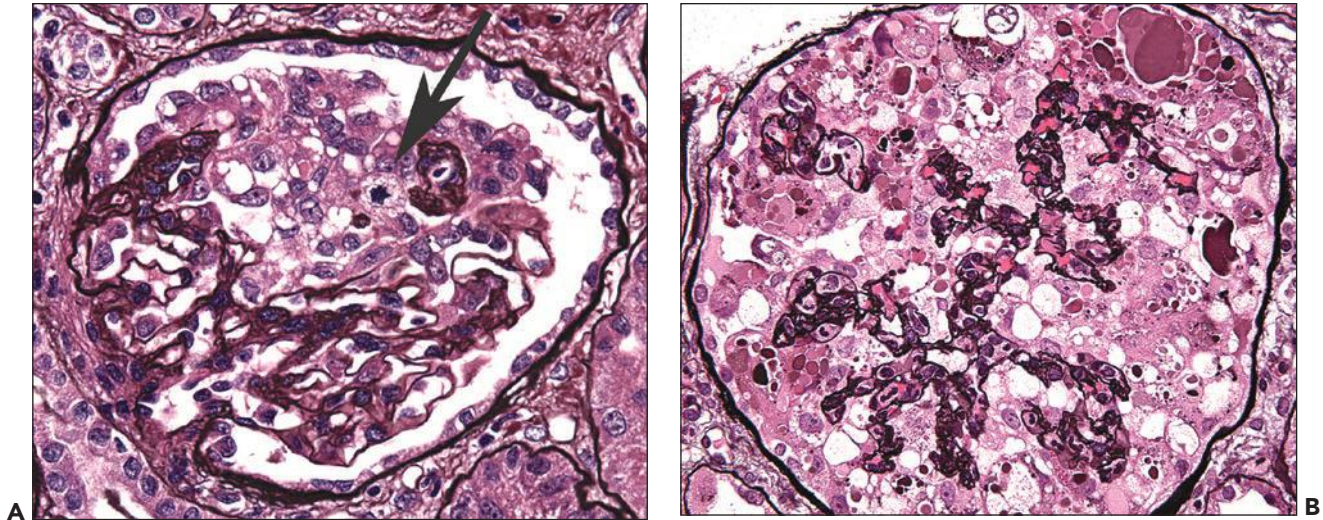


FIGURE 6.26 **A:** Primary FSGS, collapsing variant. A glomerulus shows segmental collapse of capillaries, associated with marked hyperplasia and swelling of overlying epithelial cells, one of which is undergoing mitosis (*arrow*). (PAS, $\times 400$.) **B:** Primary FSGS, collapsing variant. There is global collapse of capillaries, associated with hyperplasia and swelling of overlying epithelial cells, many of which display abundant cytoplasmic protein droplets and vacuoles. (JMS stain, $\times 400$.)

fibrin seen in true inflammatory crescents. Features of fibrinoid necrosis and ruptures of the GBM or Bowman capsule, which are often identified in crescentic glomerulonephritis, are absent. Visceral epithelial cell nuclei are typically enlarged and show vesicular chromatin and prominent nucleoli; rarely, mitotic figures or binucleated cells are evident (see Fig. 6.25) (56). The swollen epithelial cells often contain large cytoplasmic protein droplets, coarse cytoplasmic vacuoles, and lipid droplets; they may have prominent subpodocyte, tunnel-like spaces that raise the cell bodies off the underlying

basement membrane (Fig. 6.32). Proximal tubules frequently show degenerative and regenerative changes (Fig. 6.33), and tubular microcysts (dilated tubules filled with proteinaceous casts) are commonly seen (Fig. 6.34). Tubular atrophy and interstitial fibrosis are often severe and disproportionate to the degree of glomerulosclerosis. Foot process effacement is usually severe. Endothelial tubuloreticular inclusions (TRIs) are not a feature of primary collapsing FSGS but may be seen in secondary collapsing glomerulopathy associated with interferon therapy (71), HIV infection (60), or the podocytopathy of systemic lupus erythematosus (SLE) (72).

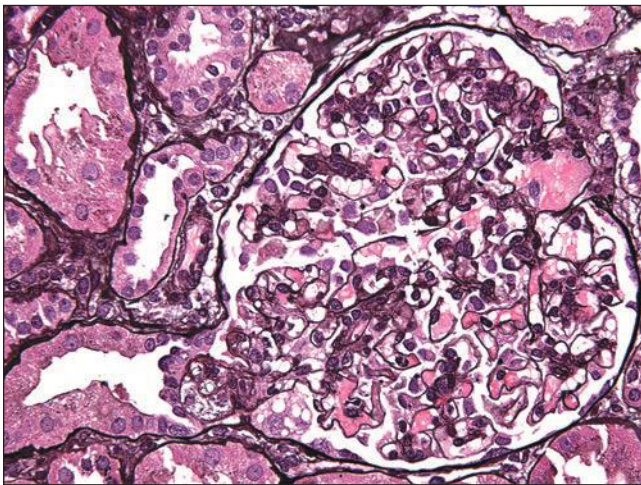


FIGURE 6.27 **Primary FSGS, tip variant.** Segmental endocapillary foam cell accumulation is seen at the origin of the proximal tubule. The affected segment has prolapsed into the tubular orifice with confluence of overlying podocytes with proximal tubular epithelium. The remainder of the glomerular tuft appears normal in cellularity. (JMS stain, $\times 400$.)

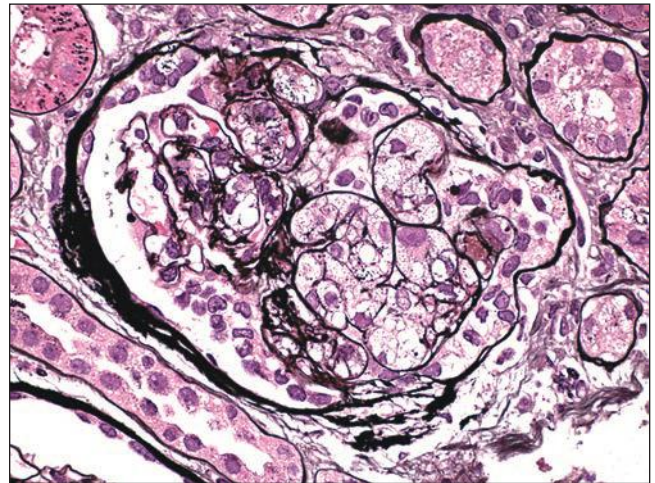


FIGURE 6.28 **Primary FSGS, cellular variant.** There is segmental expansion of the glomerular tuft by endocapillary foam cells, occluding capillary lumina. (Jones stain, $\times 600$.)

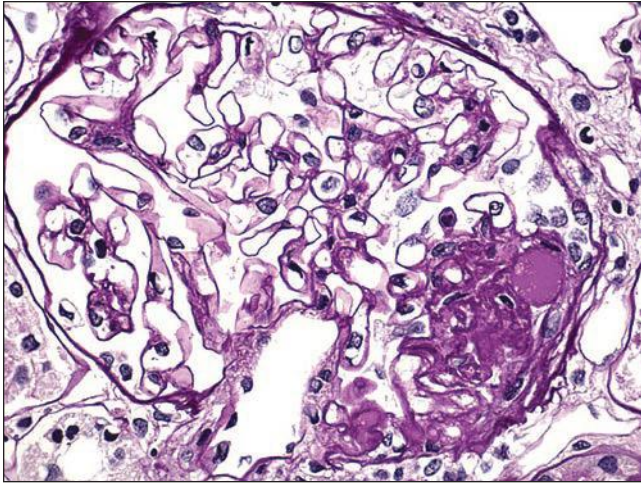


FIGURE 6.29 FSGS, perihilar variant. A glomerulus shows segmental perihilar sclerosis and hyalinosis. (PAS, $\times 600$.)

Tip Variant

As originally described by Howie and Brewer in 1984 (50), the glomerular tip lesion consists of a small segmental lesion in the glomerular tuft adjacent to the origin of the proximal tubule with intracapillary foam cells and/or PAS-positive hyaline, hyperplasia and vacuolization of overlying podocytes, tuft adhesion to the Bowman capsule, and confluence of podocytes with proximal tubular epithelial cells (50). The remaining glomerulus showed no pathologic alteration, except diffuse foot process effacement on electron microscopy. In the Columbia Classification, tip lesion is defined as a segmental lesion in the tip domain (the outer 25% of the glomerular tuft adjacent to the tubular orifice) and where the tubular pole is identified, with either adhesion or confluence of podocytes with parietal or tubular cells at the tubular lumen or neck (Figs. 6.35 to 6.37). The outer 25% of the tuft was chosen to identify lesions originating in the tip domain and exclude segmental lesions originating elsewhere that impinge on the tip as they enlarge. Glomerular tip lesions are typically cellular (81% in one series) (73) and contain prominent endocapillary foam cells, but they may also be sclerosing and contain hyaline (see Fig. 6.36). “Classic”/NOS lesions are more common in repeat biopsies, suggesting evolution from tip lesions (73). In the largest study of primary tip variant using the Columbia Classification, most biopsies (74%) also contained nontip segmental lesions involving the periphery of the tuft, but none showed perihilar segmental sclerosis or diffuse mesangial hypercellularity (73).

In two studies of primary adult FSGS using the Columbia Classification, tip lesions were identified in 12% (73) and 24% (61) of glomeruli, respectively, while in an autopsy study of children dying with nephrosis, Haas and Yousefzadeh identified tip lesions in 0.3% to 4.4% of glomeruli (74). In a recent report from Howie et al. (51), tip lesions involved more than 50% of glomeruli in only 2 of 15 cases, neither of which showed 100% glomerular involvement (51). Thus, glomerular tip lesions are typically focal and may be missed subject to sampling error, particularly in limited biopsy specimens.

Interestingly, glomerular tip lesions were identified retrospectively in 10% of children initially diagnosed with MCD (75) and in five of eight autopsies of children dying with nephrosis prior to 1950 (74). These findings suggest that tip variant may be underrecognized in children with steroid-responsive nephrotic syndrome, as renal biopsy is typically reserved for children whose nephrotic syndrome is resistant to steroid therapy.

Compared to the collapsing, cellular, and NOS variants, the tip variant shows the least amount of chronic tubulointerstitial injury (3,64,70,76) and arteriosclerosis (64). A subset of cases demonstrate acute tubular injury, patchy interstitial edema, and mononuclear interstitial inflammatory cell infiltrates, which are associated with reversible acute renal failure, analogous to the reversible acute tubular injury occurring in adult MCD. Foot process effacement is typically severe (Figs. 6.38 and 6.39).

Cellular Variant

The cellular lesion is characterized by focal segmental expansion of the glomerular tuft by endocapillary foam cells and infiltrating leukocytes, with or without endocapillary fibrin, hyaline, karyorrhexis, pyknosis, and hyperplasia of overlying epithelial cells (Figs. 6.13, 6.28, and 6.40). As noted previously, mild prominence of visceral epithelial cells and a few intracapillary foam cells are not uncommon in cases of “typical” (i.e., NOS) FSGS (Figs. 6.11 and 6.12); the key diagnostic feature of the cellular lesion is *expansion* of the glomerular tuft by the endocapillary hypercellularity without an accompanying matrix (sclerosis). Such cases may lack any evidence of segmental scars, mimicking a focal proliferative glomerulonephritis. Cellular lesions are most commonly located in the peripheral tuft (70). Additional sectioning of the biopsy may reveal unsampled glomerular tip lesions or collapsing lesions, either of which would change the variant designation.

Perihilar Variant

The perihilar variant is characterized by segmental hyalinosis and sclerosis lesions contiguous with the glomerular hilum (i.e., at the vascular pole) involving the majority (at least 50%) of glomeruli with segmental lesions (Figs. 6.16, 6.29, 6.41, and 6.42). There may be extension of hyalinosis to involve the adjacent incoming afferent arteriole. Visceral epithelial cell hyperplasia is uncommon in this variant. Podocyte loss is often obvious, associated with adhesions to the Bowman capsule. There are only limited descriptions of the glomerular pathology and ultrastructural features in cases of primary perihilar FSGS. However, in adaptive FSGS (which typically shows perihilar features), the glomeruli are usually enlarged and foot process effacement is mild (Fig. 6.43).

NOS Variant

The defining lesion of NOS variant is segmental obliteration of the glomerular capillaries by the extracellular matrix. As a diagnosis of exclusion, it requires that a biopsy does not meet defining features for any of the other variants. In children and young adults in the FSGS Clinical Trial, NOS was the most common variant in all age groups (3). Of note, the degree of

TABLE 6.3 Frequency of Columbia Classification morphologic variants in primary FSGS

References	N	Age ^a	Ethnicity or race	Time to biopsy ^a	Nephrotic syndrome	FSGS variant frequency				
						Collapsing	Tip	Cellular	Perihilar	NOS
Paik et al. (19)	92	80.4 ± 42.4 mo (12–171)	Korean	22.1 ± 29 mo (1–127)	92%	10.6%	6.1%	1.5%	9.1%	72.7%
Silverstein and Craver (63)	41	10.9 ± 0.9 y	Black, 80.5%; White, 19.5%	Unknown	63.4%	29%	0	37%	0	44%
El-Refaeey et al. (26)	72	6.3 y (1–16)	Egyptian	8 ± 14.6 mo	100%	6%	2%	0	7%	85%
Thomas et al. (64)	197	49 ± 15 y	Black, 40%	Unknown	70%	11%	17%	3%	26%	42%
Deegens et al. (65)	93	49 ± 16 y	White, 96%	3.8 mo	63%	5%	37%	0	26%	32%
Nada et al. (66)	210	>17 y	Indian	(0.1–303)	Unknown	2%	13.5%	8%	4%	72.5%
Taneda et al. (67)	85	39.4 ± 1.7 y (18–77)	Japanese	57.8 ± 8.8 mo	44.7%	16%	30%	14%	16%	24%
Gipson et al. (68)	138 ^b	<18 y, 67%; >18 y, 33%	Black, 38%; White, 57%; Other, 5%	Unknown	UPC >2: 76%; UPC 1–1.99: 24%	12%	10%	3%	7%	68%
Canaud et al. (69)	77 ^c	<16 y, 73%; >16 y, 27%	Unknown	Unknown	100%	13%	8%	22%	8%	49%

^aAge and time from disease onset to biopsy; mean ± standard error of mean (range).

^bAll steroid resistant.

^cAll with end-stage kidney disease.

N, number of cases; UPC, urine protein-to-creatinine ratio; NOS, not otherwise specified variant.

TABLE 6.4 Renal outcomes in primary FSGS by histologic variant

References	Follow-up mean \pm SEM (range)	Outcomes ^a	Overall rates	Collapsing	Tip lesion	Cellular	Perihilar	NOS
Silverstein and Craver (63)	3.9 \pm 0.5 y (1–17)	CR/PR ESRD	70.7% 4.9%	45.4% 18.2%	NS	75% 0%	NS	72.2% 0%
Thomas et al. (64)	1.8 y (0–16)	CR/PR ESRD ^b	19%/5% 33%	14%/4% 67%	50%/3% 24%	33%/0% NS	10%/9% 25%	13%/3% 35%
Deegens et al. (65)	66 mo (1–273)	CR/PR ESRD	44% 34%	50% 70%	57% 22%	NS NS	25% 37%	38% 45%
D'Agati et al. (76)	78 wk	CR/PR ^c ESRD ^{b,c}	14% 25%	NS 47%	NS 7%	NS NS	NS NS	NS 20%
Taneda et al. (67)	55.9 \pm 8.8 mo	CR/PR ESRD	56.9% 18.2%	44% 30%	84.2% 10.5%	60% 33.3%	30% 0%	47.1% 22.2%
Stokes et al. (70)	33.7 \pm 2.7 mo	CR/PR ESRD	38.5% 30.7%	13.2% 65.3%	75.8% 5.7%	44.4% 27.8%	NS NS	38.6% 34.5%

^aCR/PR, complete remission/partial remission.^bThree-year renal survival.^cAll steroid resistant, subsequently treated with either cyclosporine or mycophenolate and dexamethasone. ESRD, end-stage renal disease; NS, not studied or not applicable.

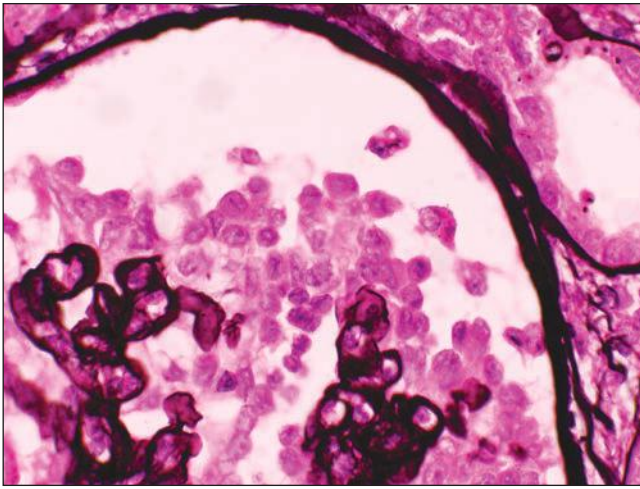


FIGURE 6.30 Primary FSGS, collapsing variant. Hyperplastic and hypertrophied epithelial cells overlie a collapsed glomerular segment, forming a pseudocrescent. Some of these epithelial cells are detached, lying free within the Bowman space. (JMS stain, $\times 660$.)

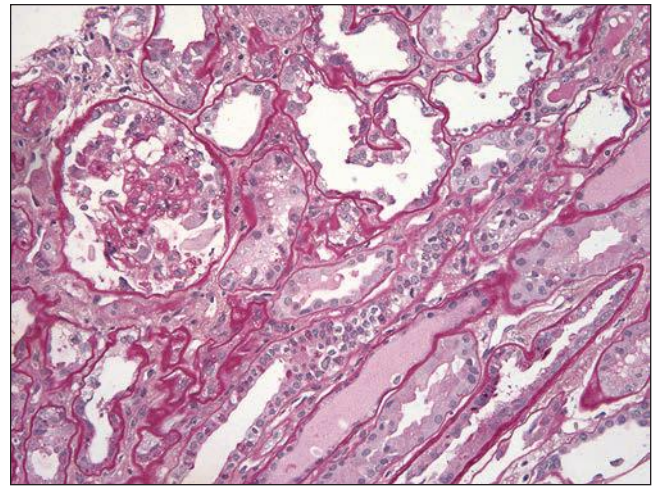


FIGURE 6.33 Primary FSGS, collapsing variant. Severe tubular degenerative changes are seen. (PAS, $\times 100$.)

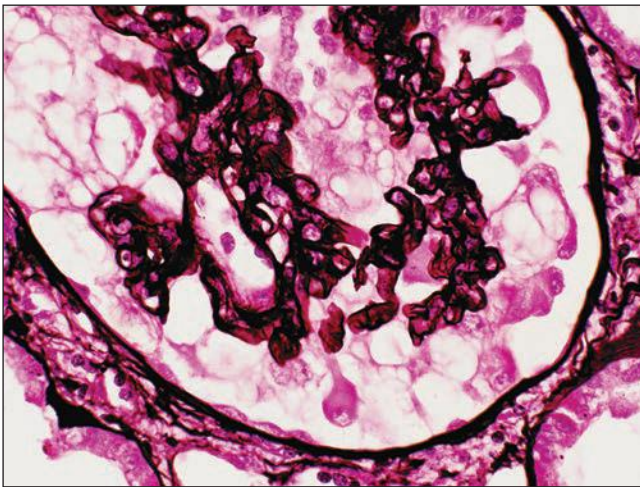


FIGURE 6.31 Primary FSGS, collapsing variant. Visceral epithelial cells have copious, vacuolated cytoplasm, and the nuclei are vesicular with prominent nucleoli. (JMS stain, $\times 660$.)

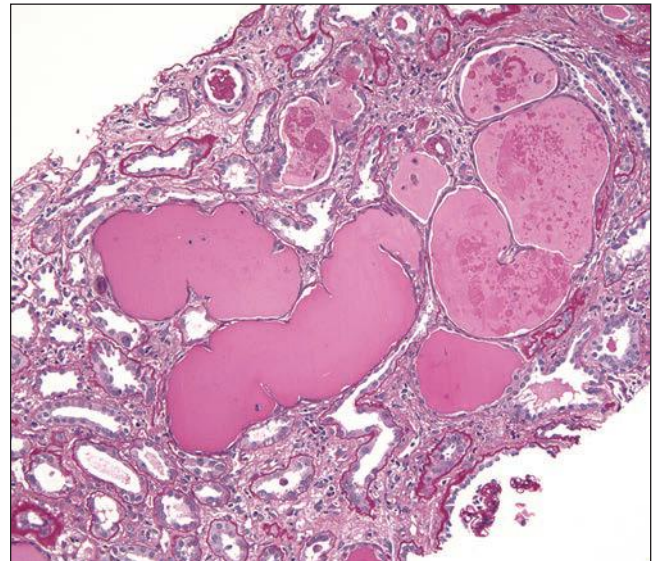


FIGURE 6.34 Primary FSGS, collapsing variant. Tubular ectasia with microcyst formation is seen. (PAS, $\times 100$.)

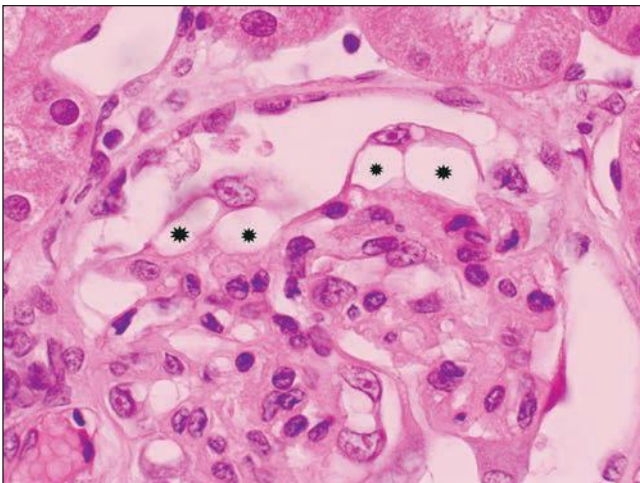


FIGURE 6.32 Primary FSGS, collapsing variant. Podocytes separate from the basement membrane forming tunnel-like pseudocysts between the cell and the basement membrane (*asterisks*). (H&E, $\times 660$.)

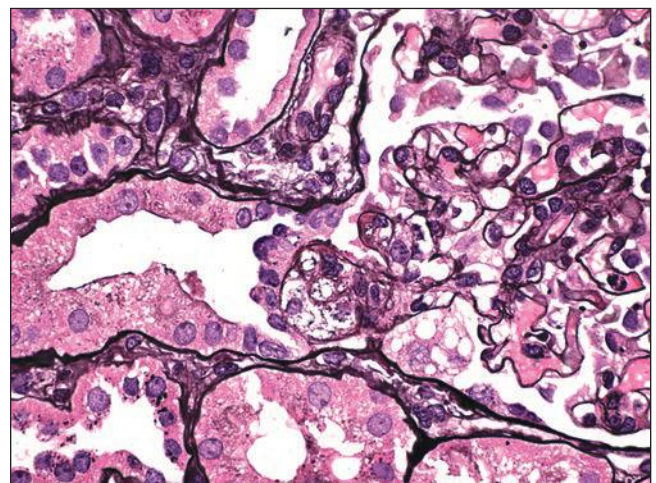


FIGURE 6.35 Primary FSGS, tip variant. A higher power magnification of Figure 6.30 demonstrates confluence of visceral epithelial cells and proximal tubular epithelial cells. (JMS stain, $\times 600$.)

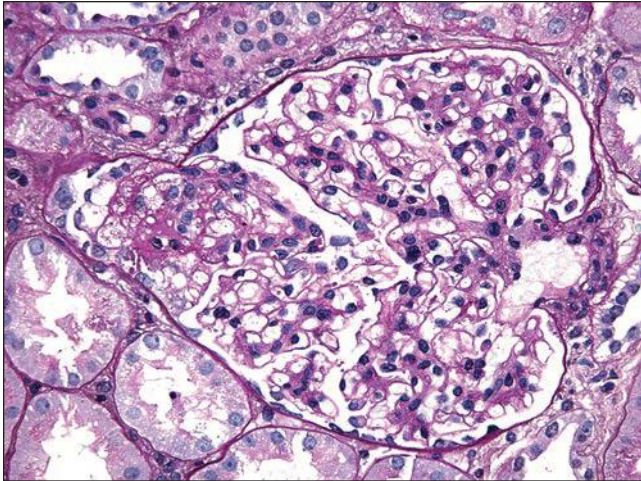


FIGURE 6.36 Primary FSGS, tip variant. Segmental endocapillary foam cell accumulation and PAS-positive hyaline are seen at the origin of the proximal tubule. The remainder of the glomerular tuft appears normal in cellularity. (PAS, $\times 400$.)

tubulointerstitial scarring is not significantly worse in NOS compared to the other variants, implying that NOS is not just an advanced stage of the other variants (64). Thus, the NOS variant may occur *ab initio* or other variants may evolve into NOS over time.

Pathologic Differential Diagnosis of FSGS

The pathologic differential diagnosis of FSGS includes postinflammatory scarring from immune complex-mediated glomerulonephritis (e.g., IgA nephropathy or lupus nephritis) and

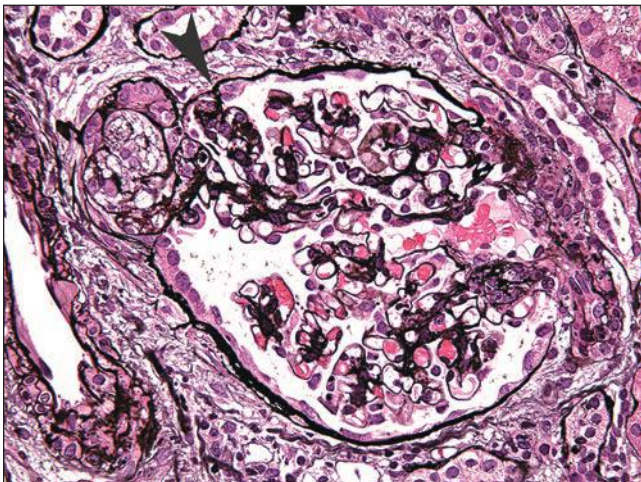


FIGURE 6.37 Primary FSGS, tip variant. A segmental lesion containing endocapillary foam cells has prolapsed into the origin of the proximal tubule. There is synechial attachment between the glomerular tuft and Bowman capsule at the tubular pole. (JMS stain, $\times 400$.)

pauci-immune glomerulonephritis or progression from other nonproliferative glomerulopathies, such as hereditary nephritis. Careful correlation with clinical history and immunofluorescence and electron microscopic findings is usually sufficient to exclude these conditions.

The extracapillary hypercellularity seen in collapsing, cellular, and tip variants (and to a lesser degree in the NOS variant) may suggest crescent formation. However, the hyperplastic visceral epithelial cells in FSGS lack the spindled morphology, intercellular matrix, and pericellular fibrin typically seen in true inflammatory crescents; in addition, features of fibrinoid necrosis and rupture of the GBMs or Bowman capsule are absent. Moreover, the typical clinical history of nephrotic syndrome with negative antineutrophil cytoplasmic antigen (ANCA) serologies and absence of signs of extrarenal vasculitis help distinguish FSGS from pauci-immune crescentic glomerulonephritis.

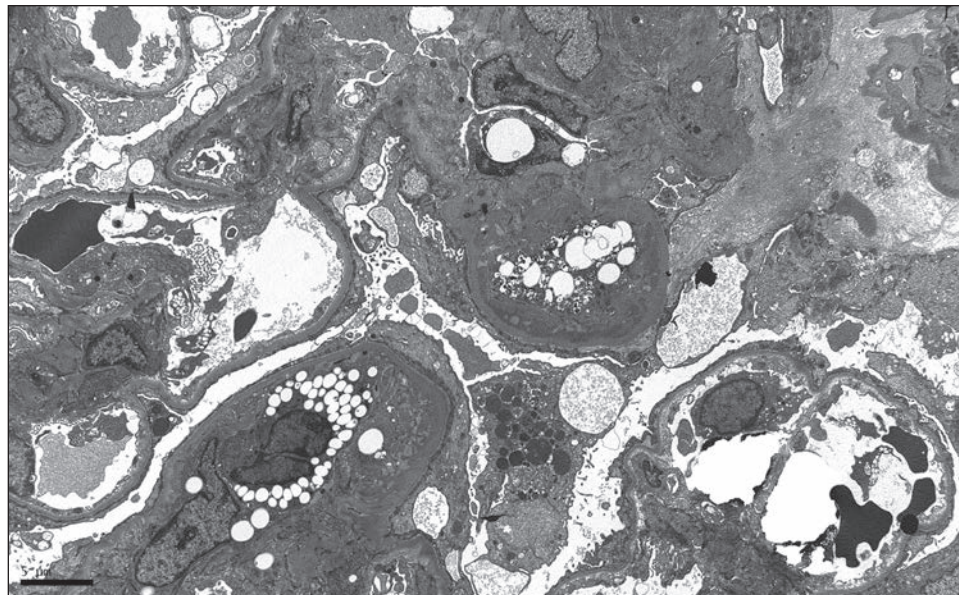
Glomerular tip changes have been described in diverse glomerular diseases characterized by heavy proteinuria, including membranous glomerulonephritis, diabetic glomerulosclerosis, and preeclampsia (77). The clinical history and other biopsy findings usually make this differential diagnosis straightforward. Cellular variant FSGS may mimic focal proliferative glomerulonephritis. However, the absence of immune complex deposits and the findings of heavy proteinuria and diffuse foot process effacement favor a diagnosis of a primary podocytopathy.

Clinical-Pathologic Correlation of Histologic Variants of Primary FSGS

The frequencies and clinical characteristics of the Columbia Classification variants of primary FSGS are summarized in Table 6.3. In most series, NOS was the most common variant, ranging from 32% to 73% of cases, although tip variant was predominant in two studies of adult FSGS (one European (65) and one Japanese (67)). The frequencies of the other variants ranged from 2% to 29% (collapsing), 0% to 37% (tip), 0% to 37% (cellular) and 0% to 26% (perihilar) (19,26,63,65–69). In a French series of 77 cases with ESRD from primary FSGS (comprising 56 children and 21 adults), the frequencies were as follows: NOS variant, 49%; cellular variant, 22%; collapsing variant, 13%; tip variant, 8%; and perihilar variant, 8% (69). These differences in frequency may reflect demographic differences (age and ethnicity), genetic factors, duration of disease, previous treatment (i.e., steroid-resistant vs. untreated nephrotic syndrome), and the frequency of nephrotic syndrome (which ranged from 44.7% to 100%).

The first reports of primary collapsing glomerulopathy described a strong association with African ancestry and a male predominance (55–57), and similar associations have been identified with the Columbia Classification definition of collapsing variant primary FSGS (64,70,76). This variant usually presents with severe nephrotic syndrome and renal insufficiency, despite a shorter duration of symptoms compared to NOS variant, suggesting more acute injury rather than delayed diagnosis (56,70). Compared to the other variants, adults with collapsing variant tend

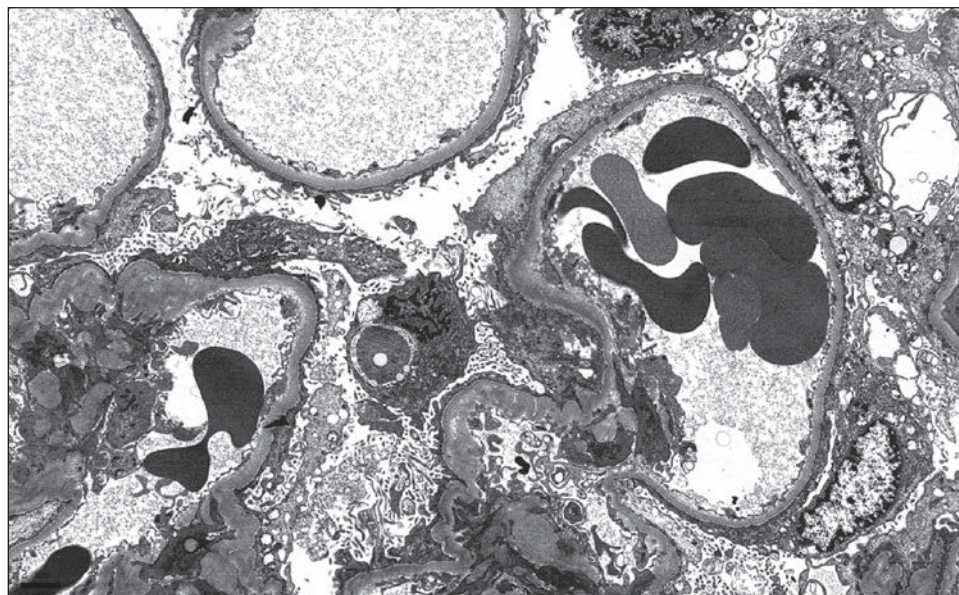
FIGURE 6.38 Primary FSGS, tip variant. Podocytes display diffuse foot process effacement and focal cytoplasmic vacuoles. Endocapillary foam cells are seen. (Electron photomicrograph, original magnification $\times 6000$.)



to be younger, have a higher serum creatinine at presentation, heavier proteinuria, and lower serum albumin (64,70). In one pediatric study, the collapsing variant was associated with higher blood pressures than cellular variant or NOS, but outcomes were similar (67). The collapsing variant has the lowest percentage of remissions (complete and partial) and highest rate of ESRD (64,70,76) and the shortest median renal survival, ranging from 13 to 15 months (54–57). Much of the recent increase in the incidence of FSGS in the United States appears due to an increase in collapsing FSGS (56).

By comparison, tip variant predominantly affects older adults and generally has a benign clinical course (64,65,73). This variant occurs in all ethnic groups but predominantly afflicts Caucasians in most North American studies; however, in one series, the majority of patients were African American (61). Tip variant typically presents with sudden onset of severe nephrotic syndrome, similar to MCD, and has better initial kidney function than collapsing or NOS variants (73). Some patients have acute kidney injury that resolves with remission of nephrotic syndrome, suggesting a role for hemodynamic factors associated with severe nephrotic syndrome, resembling

FIGURE 6.39 Primary FSGS, tip variant. A glomerulus that did not contain a tip lesion also displays diffuse podocyte foot process effacement. (Electron photomicrograph, original magnification $\times 6000$.)



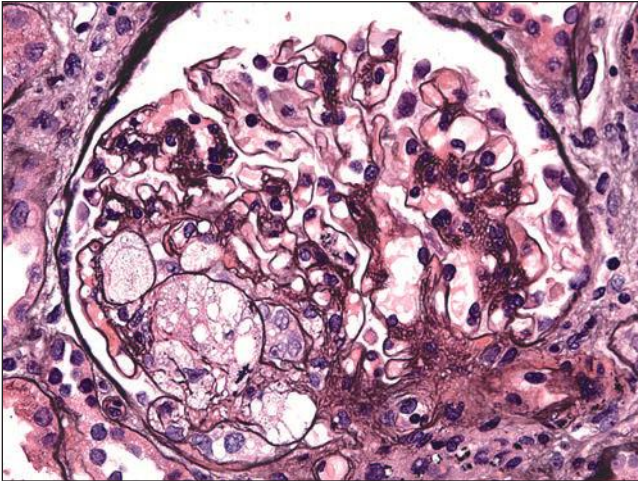


FIGURE 6.40 Primary FSGS, cellular variant. There is segmental expansion of the glomerular tuft by endocapillary foam cells. (JMS stain, $\times 400$.)

adult MCD. Tip variant has the best initial and final renal function and the highest rate of complete remission and renal survival at 5 years (64). However, progression to end-stage kidney disease may occur and recurrence in the renal allograft has been described (51).

Factors that predict poor renal outcome in tip variant include failure of remission of proteinuria (61) and greater number of nontip segmental lesions in the initial biopsy (51,73). Some studies have shown higher remission rates and less ESRD compared to FSGS NOS (64,73), whereas others (including two pediatric series) did not show any relationship between final outcome and any FSGS variant (19,61,67). In one study of children with SRNS, the prognosis for tip variant was no different than NOS variant (78). Whether tip variant in children is biologically different from the disease in adults is uncertain. Renal biopsy in children with idiopathic nephrotic

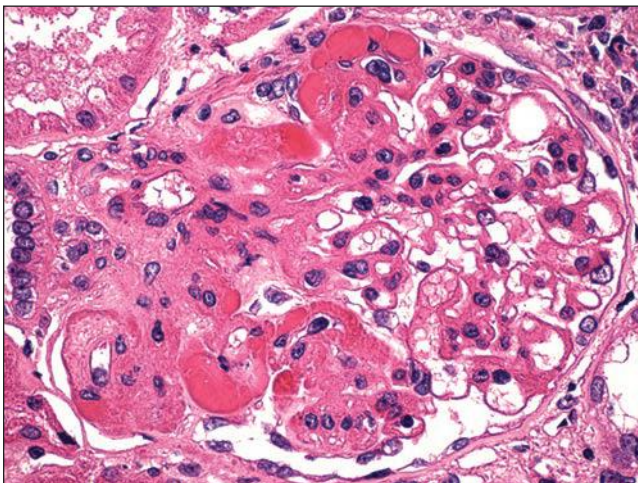


FIGURE 6.41 FSGS, perihilar variant. Segmental accumulation of matrix and hyaline involving the perihilar region (vascular pole). (PAS, $\times 200$.)

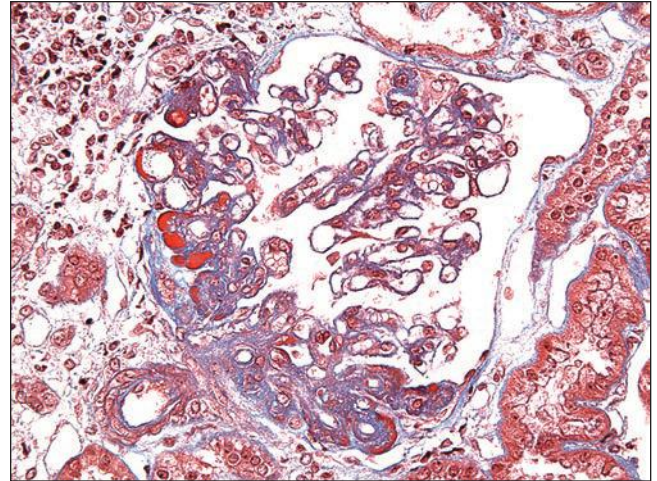


FIGURE 6.42 FSGS, perihilar variant. Hyalinosis stains red with trichrome stain. (Trichrome, $\times 400$.)

syndrome is usually restricted to cases that do not respond to empiric steroid therapy, thus may identify cases that have an inherently worse prognosis compared to adults, in whom steroid responsiveness is typical (73). On the other hand, the results of the NIH-sponsored FSGS Clinical Trial showed that, even among 138 steroid-resistant children and young adults, those with tip variant had better renal survival than patients with NOS and collapsing variants (76). In the NIH trial, rates of progression to ESRD at 3 years were highest for collapsing variant (47%), intermediate for NOS (20%), and lowest for tip variant (7%).

Cellular variant is rare in adults (3% to 4.6% of primary FSGS cases) (64,70) but has been reported in up to 37% of pediatric FSGS cases (67). In a study of 22 patients with cellular variant (only 1 of whom was less than 18 years old), patients had heavier proteinuria, more frequent nephrotic syndrome, lower serum albumin, and shorter interval from onset of symptoms to biopsy compared to NOS variant, suggesting a more acute disease (70). In a pediatric study, cellular variant showed less chronic injury, less hypertension, and better remission rates than collapsing variant, and 75% entered remission (67). There are limited data regarding long-term prognosis in cellular variant, reflecting its relative infrequency, but this appears to be intermediate between collapsing variant and FSGS (NOS) (70).

In the Chapel Hill series of primary FSGS, the perihilar variant had the lowest frequency of nephrotic syndrome, lowest initial serum creatinine, and highest association with hypertension (64). Despite infrequent use of steroids and low rates of complete or partial remission (approximately 10% for each), renal survival was good (75% at 3 years) and better than NOS and collapsing variants (64). However, in the Dutch cohort of mostly Caucasian adults with FSGS, the 5-year survival for perihilar variant was 55%, compared to 63% for NOS and 78% for tip variant (65). The relatively poor prognosis of perihilar variant in this study was associated with more severe glomerular scarring, suggesting more advanced disease at diagnosis (65). Of note, there were no significant differences in age and frequency of hypertension among the FSGS variants in this cohort.

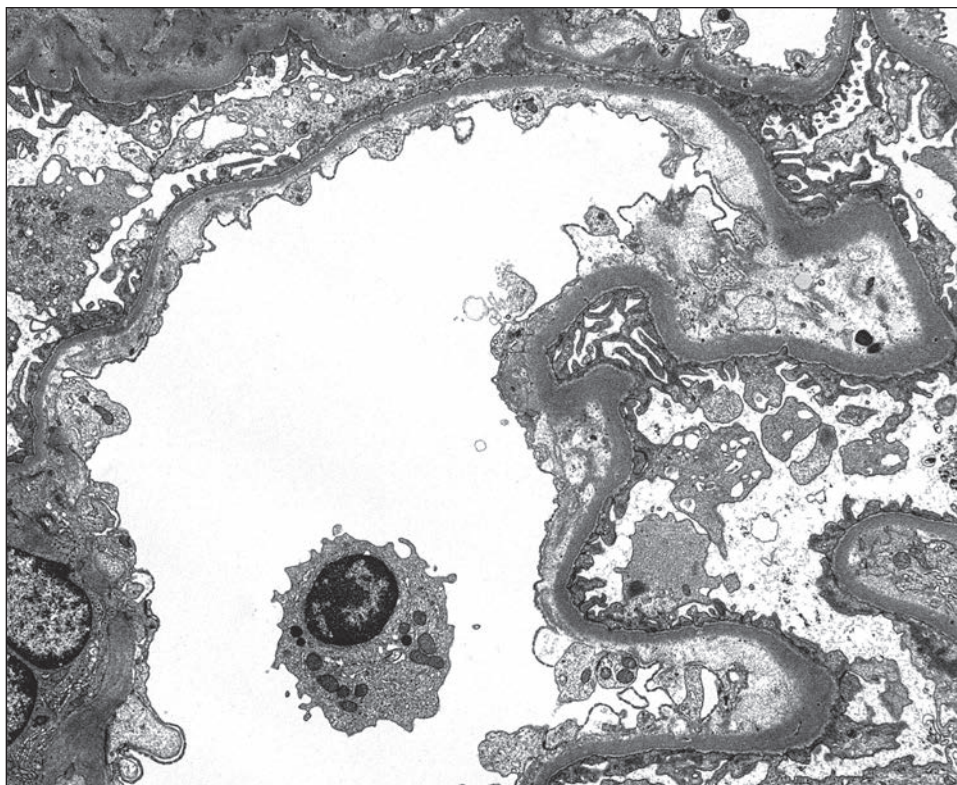


FIGURE 6.43 FSGS, perihilar variant. In this case of hypertensive nephrosclerosis, podocyte foot processes are mostly preserved, with only mild and focal effacement. There is widening of the subendothelial space with accumulation of ill-defined electron lucent material (“fluff”), consistent with prior endothelial cell injury due to hypertension. (Electron photomicrograph, original magnification $\times 5000$.)

Clinical Course and Prognostic Factors

Primary FSGS progresses to ESRD in approximately 50% of patients within 10 years of clinical onset. The presence of nephrotic syndrome (vs. asymptomatic proteinuria) is an important prognostic factor, as patients with asymptomatic proteinuria rarely develop ESRD (79) (Fig. 6.44). Persistence of nephrotic syndrome following therapy is associated with a high rate of progression, whereas reduction in proteinuria (whether complete or partial remission) is associated with much better outcomes (61,80,81) (Fig. 6.45). Spontaneous remissions are rare (65,79,82). Up to 100% 5-year renal survival has been identified for complete remissions (generally defined as proteinuria less than 0.2 g/d) versus 90% survival for partial remission (0.2 to 2 g/d) and 60% survival for nonremitters (81). Other factors that are associated with worse prognosis include black race (30), heavier proteinuria (79), greater renal insufficiency (30,79,83), more severe tubular atrophy and interstitial fibrosis (84), and collapsing variant (64,70). By contrast, most studies in adult FSGS show that tip variant has the highest remission rates (64,65,70) and the lowest risk of ESRD (65,70).

Etiology and Pathogenesis

Loss of the Glomerular Filtration Barrier: Role of Podocyte Injury

The specific etiology of primary FSGS is unknown but believed to involve one or more circulating permeability factors that cause podocyte injury and a migratory phenotype, leading to effacement and eventual podocytopenia, as occurs in other forms of FSGS. This reflects the central role of the podocyte in

maintaining the normal glomerular filtration barrier and providing structural support to the glomerular capillary architecture. Podocyte function and the glomerular filtration barrier are discussed in detail in Chapters 1 and 5 and are reviewed briefly here.

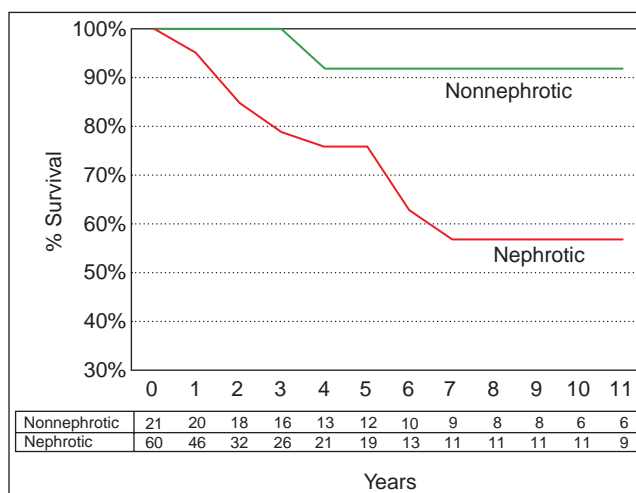


FIGURE 6.44 Cumulative renal survival for patients with and without the nephrotic syndrome ($P < 0.05$ by the log-rank test). Numbers in the table represent patients at risk at each time point. (Adapted from Rydel JJ, Korbet SM, Borok RZ, et al. Focal segmental glomerular sclerosis in adults: Presentation, course and response to treatment. *Am J Kidney Dis* 1995;25:534.)

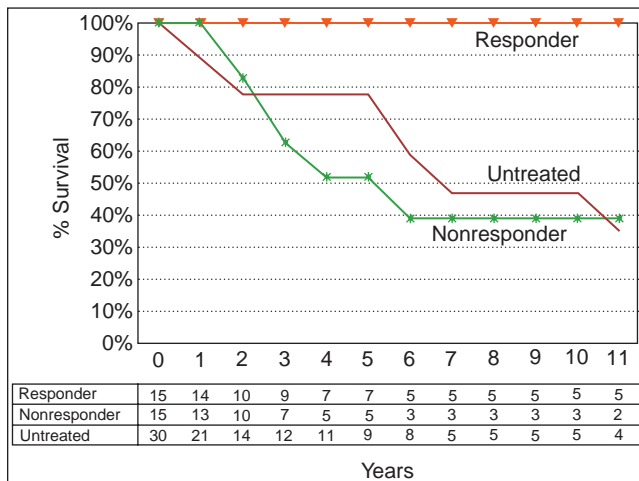


FIGURE 6.45 Cumulative renal survival for nephrotic patients based on treatment and response ($P < 0.05$ by the log-rank test). Numbers in the table represent patients at risk at each time point. (Adapted from Rydel JJ, Korbet SM, Borok RZ, et al. Focal segmental glomerular sclerosis in adults: Presentation, course and response to treatment. *Am J Kidney Dis* 1995;25:534.)

The glomerular filtration barrier is a trilaminar complex with net negative charge that progressively restricts the passage of macromolecules based on their size, molecular weight, charge, and molecular conformation. The major structural components consist of the podocyte cell layer, the GBM, and the endothelial cell layer. Adjacent podocytes form a complex network of interdigitating foot processes that are connected by slit diaphragms that resemble modified zona adherens junctions. The slit diaphragm is the anatomic basis of the most restrictive size selectivity of the glomerular filtration barrier and also functions as a signal transduction complex, affecting downstream cellular responses including actin remodeling, prosurvival pathways, cell polarity, endocytosis, and differentiation. Podocytes also synthesize the extracellular matrix components of the GBM and produce survival factors, such as vascular endothelial growth factor (VEGF), which are essential to maintain normal endothelial structure and function. The net negative charge of the filtration barrier reflects the anionic structural elements, including heparan sulfate proteoglycans (predominantly agrin and perlecan) within the GBM and sialoproteins (predominantly podocalyxin) forming the glycocalyx on the surfaces of podocytes and endothelial cells.

The podocyte is a motile cell endowed with mechanosensors that respond to positional stimuli and shear stress and has a complex actin cytoskeleton that controls many of its specialized properties, including motility and maintenance of the mature podocyte phenotype. The highly differentiated foot process architecture depends on complex interactions between the actin cytoskeleton and podocyte proteins governing signal transduction networks required for normal structure and homeostasis (85). Interference of signaling from any of the specialized podocyte domains, including the slit diaphragm, apical or basal membranes,

nucleus, or cytoskeleton itself can lead to reorganization of the actin cytoskeleton and the generalized response of foot process effacement seen in FSGS (86). The number of podocyte genes known to be mutated in genetic forms of FSGS is rapidly expanding (see Genetic causes and familial forms of FSGS). Some of the most common genetic defects target integral proteins comprising the slit diaphragm, such as nephrin and podocin (87–89). The importance of apical membrane proteins is demonstrated in mice that express hyposialated podocalyxin, leading to effacement and proteinuria, and the development of human FSGS in patients carrying mutations in the apical membrane protein glomerular epithelial protein-1 (GLEPP-1) (90,91). Disruption of the basal membrane-GBM interface due to mutations in integrins, laminins, or tetraspanins causes proteinuria in humans and mice (22,92–95). Dysregulated enzymatic cleavage of cytoskeletal dynamin by cytosolic cathepsin L leads to an abnormally motile podocyte phenotype, effacement, and proteinuria, and cathepsin L up-regulation has been identified in several human proteinuric diseases, including MCD and FSGS (96,97). Podocytes whose adherence to the GBM has been weakened by effacement may be more vulnerable to detachment in the course of normal filtration pressures. Because mature podocytes are terminally differentiated cells with limited regenerative capacity, any injury that leads to irreversible podocyte stress and loss through detachment, apoptosis, or necrosis will inevitably impair the glomerular filtration barrier and may potentially cause glomerulosclerosis (98). Evidence from animal models suggests that loss of podocytes can promote strain on adjacent podocytes, perhaps through mechanical stretch tension or loss of survival signaling, leading to local propagation of podocyte injury. Such local spread of podocyte loss might explain the segmental nature of the lesions (99).

Cellular Phenotypic Alterations in Primary FSGS

Immunohistochemical and molecular studies in human disease and experimental models have provided insights into cellular events involved in the pathogenesis of FSGS. Mature podocytes are quiescent cells that express cyclin-dependent kinase inhibitors p27 and p57, Wilms tumor protein-1 (WT-1), CD10/common acute lymphoblastic leukemia antigen (CALLA), C3b receptor, glomerular epithelial protein-1 (GLEPP-1), podocalyxin, synaptopodin, and vimentin, while proliferation markers (PCNA and Ki67) are not expressed. In FSGS characterized by prominent visceral epithelial cell hyperplasia, the proliferating cells have an altered phenotype. This process has been variously termed podocyte dysregulation, dedifferentiation, transdifferentiation, and epithelial-mesenchymal transformation (100–102). The dysregulated visceral epithelial cells show loss of mature markers (e.g., nephrin and WT-1), down-regulation of p21 and p57, expression of PCNA and Ki67 (indicating reentry into the cell cycle), and expression of cytokeratin and macrophage markers (100,103). Importantly, cellular and collapsing variants display a similar immature or dysregulated phenotype, reflecting their characteristic glomerular epithelial cell hyperplasia (103). All FSGS variants show reduced podocyte expression of WT-1, consistent with the common feature of podocyte depletion;

interestingly, the prognostically poor collapsing variant shows the greatest increase in interstitial fibroblast-specific protein-1 (FSP-1) (16).

Initially it was assumed based on their anatomic location that the visceral epithelial cell proliferation in FSGS was derived from podocytes, but new evidence supports an origin from parietal epithelial cells and facultative stem cells lining the Bowman capsule (104–107). The proliferating cells express cytokeratin 8, cadherin, claudin, and PAX-2, which are present in normal parietal cells but not in mature podocytes. In several animal models of FSGS, as well as in humans, activated parietal cells express CD44 and form cellular adhesions in areas of podocyte loss, where they synthesize a Bowman capsule–type extracellular matrix (43). Mice lacking the cell cyclin inhibitor p21 develop cellular and collapsing FSGS associated with podocytopenia and proliferation of parietal epithelial cells (108). On the other hand, reversible podocyte cell cycle entry has been demonstrated in a model of collapsing FSGS caused by conditional podocyte expression of the telomerase protein component TERT, suggesting that podocytes may be induced to proliferate under rare circumstances (109).

Many of the proliferating visceral epithelial cells in FSGS appear to derive from precursor cells lining the Bowman capsule. Ronconi et al. (110) have demonstrated the hierarchical distribution of three different cell populations lining the normal human Bowman capsule. The least differentiated cells are located at the urinary pole and express CD133+ and CD24+ (human stem cell markers) but are negative for the podocyte marker podocalyxin (PCX–). These cells are capable of transforming into podocytes and tubular epithelial cells (110). Mature, terminally differentiated podocytes (CD133–, CD24–, and PCX+) are present at the vascular pole. An intermediate population of CD133+, CD24+, and PCX+ cells is present in the midcapsule between urinary and vascular poles. When these three different cell populations were injected into severe combined immune deficiency (SCID) mice with adriamycin-induced injury, only the CD133+, CD24+, and PCX– cells were associated with reduced glomerular injury. Another study demonstrated recruitment of podocytes from precursor cells lining the Bowman capsule with capacity to switch to a podocyte phenotype and migrate onto the glomerular tuft (107). Bone marrow–derived stem cells have also been shown to be a source of regenerating podocytes in a murine model of Alport syndrome (111). However, bone marrow–derived stem cells have not been reported to replenish lost podocytes in experimental ablation or toxin models of FSGS (112). Microarray studies performed on glomeruli microdissected from human renal biopsies with primary collapsing FSGS show reduced expression of podocyte maturity markers and slit diaphragm proteins, along with increased expression of parietal cell markers and genes involved in development and differentiation, consistent with podocyte dysregulation and the recruitment of parietal cells and progenitor cells (113). In summary, there is evidence that immature podocytes, facultative stem cells, and parietal cells may contribute to the extracapillary proliferation seen in FSGS. It remains to be determined, however, if these proliferating cells are capable of differentiating into mature podocytes replete with foot

processes and slit diaphragms needed to reconstitute a normal filtration barrier.

Reduced staining for α_3 and β_1 integrin subunits is seen in human FSGS NOS and precedes the development of FSGS lesions in the PAN model (114). Podocyte detachment from the GBM results in shedding and podocytopenia (114). Urinary excretion of podocytes (detected with an immunostain for podocalyxin) is higher in patients with FSGS compared to those with MCD or membranous glomerulonephritis (115) and podocyturia may be a marker of FSGS disease activity (116).

The predisposition to formation of segmental lesions at the tubular pole, producing tip lesions, likely involves mechanical factors particular to this region. It is possible that injured, effaced podocytes may be more susceptible to mechanical strain at the glomerular tip, where there is convergence of protein-rich ultrafiltrate originating from all portions of the glomerular globe. An *in vitro* study suggests that increased shear stress and turbulence in the paratubular region could draw podocytes toward the tubular lumen, promoting detachment (117). Tuft prolapse itself likely causes physical trauma to podocytes at the tip domain, promoting their detachment and adhesion formation at this site. The presence of prominent intracapillary foam cells may be a response to localized defects in the tuft caused by mechanical trauma, podocyte loss, and/or reverse filtration of ultrafiltrate enriched in proteins and lipid in areas of podocyte injury. In some cases of glomerular tip lesion and cellular FSGS, there is segmental endothelial cell proliferation, perhaps reflecting localized disturbance of podocyte-endothelial interactions following podocyte injury, as shown in neonatal mice exposed to PAN (15). Similar mechanisms of podocyte stress in the tip domain could explain the reports of tip lesion (and other FSGS lesions) in other glomerular diseases associated with tuft enlargement and heavy proteinuria (including membranous glomerulonephritis (77), diabetic glomerulosclerosis, and IgA nephropathy (118)) in addition to several experimental models of glomerular proteinuria (119).

Circulating Glomerular Permeability Factors in Primary FSGS

Historically, primary FSGS has long been postulated to arise from one or more circulating permeability factors or cytokines of possible immune origin. In the 1970s, Shalhoub et al. (120) postulated the presence of a T-cell–derived factor that could alter glomerular permeability. Indirect evidence for circulating permeability factors includes the dramatic recurrence of proteinuria in patients with ESRD due to FSGS within minutes or hours of renal transplantation and the reduction in proteinuria following plasmapheresis (121). Sera from patients with recurrent FSGS caused proteinuria and foot process effacement when injected into rats and increased permeability to albumin (P_{alb}) in isolated rat glomeruli (5,122). Higher levels of P_{alb} were associated with recurrent FSGS and other risk factors for recurrence (e.g., previous recurrence and rapid progression to ESRD) and with collapsing FSGS in the native kidney (5,123). Recently, the kidney from a transplanted patient with early recurrent FSGS in the allograft was surgically removed and

retransplanted into another (non-FSGS) recipient, followed by swift recovery of proteinuria, providing the ultimate proof of concept that the circulating factor is specific to the FSGS patient (124).

Several candidate factors, measuring approximately 30 to 50 kDa in size, have been identified by affinity chromatography and fractionation of plasma proteins removed by protein A immunoadsorption from permeability-causing FSGS sera (125). Recently, Savin's group identified candidate factor cardiotrophin-like cytokine 1 (CLC-1), a member of the interleukin 6 family with molecular weight of less than 30 kDa, which has 100-fold higher concentrations in FSGS than in normal sera and can be enriched by galactose affinity chromatography, providing a rationale for trials of galactose to treat primary FSGS (5,125). Moreover, this cytokine induces glomerular permeability in functional assays and decreases nephrin expression by glomeruli and podocytes *in vitro*, effects that are blocked by a monoclonal antibody to CLC-1 (5).

Another candidate is soluble urokinase receptor (suPAR) (4,126). Elevated serum levels of suPAR (greater than 3000 pg/mL) have been identified in the majority of patients with primary FSGS in three different cohorts (55.3% (4,126), 70% (3), and 84.3% (126), respectively), but not in healthy subjects or patients with MCD, membranous glomerulonephritis, or preeclampsia (4,126). Increased serum levels of suPAR before renal transplantation were associated with an increased risk of recurrent disease in the allograft, and mouse models that overexpress suPAR developed an FSGS-like disease. Circulating suPAR induces foot process effacement through the activation of podocyte β_3 integrin, one of the major proteins binding podocytes to the GBM. Activation of β_3 integrin on podocytes promotes cell motility via activation of the small GTPases Cdc42 and Rac1, which could theoretically promote podocyte effacement and detachment (127). This effect can be blocked in humans by using plasmapheresis to lower the circulating levels of suPAR and in animal models by neutralizing antibodies or genetic mutations that interfere with suPAR- β_3 integrin interactions (4,127). Recent evidence indicates that suPAR levels can also be elevated in patients with reduced GFR, secondary forms of FSGS and various other acute and chronic renal diseases and inflammatory conditions. Thus, at present the role of suPAR in FSGS patients remains uncertain.

How permeability factors lead to proteinuria remains obscure, but experimental evidence supports reorganization of the actin cytoskeleton. Studies of conditionally immortalized podocytes exposed to plasma from nephrotic patients showed reallocation of nephrin, podocin, and CD2AP from the slit diaphragm to the cytoplasm and increased calcium influx, effects that were dependent on the presence of nephrin (128). Similarly, the protease hemopexin, which has been identified in patients with MCD, also induces nephrin-dependent reorganization of the actin cytoskeleton in cultured podocytes (129).

The diagnostic specificity and prognostic significance of P_{alb} levels remain unproven. Not all patients with primary FSGS have a demonstrable circulating permeability factor, and these factors have also been identified in some patients with genetic forms of FSGS (130) or MCD (131). One study showed no correlation between P_{alb} and therapeutic response

to cyclosporine A (CsA) in steroid-resistant primary FSGS (132). In another study, P_{alb} was identified in nearly 50% of children with idiopathic nephrotic syndrome but did not predict clinical response to steroid treatment, histologic findings (i.e., MCD or FSGS), or clinical outcome at up to 5 years of follow-up (131). Another study showed that P_{alb} levels were reduced by plasmapheresis in recurrent FSGS, but this did not correlate with either the degree of proteinuria or disease progression (133).

Primary FSGS: Treatment

The goal of therapy for primary FSGS is to induce remission of the nephrotic syndrome and prevent deterioration of kidney function. Glucocorticoids are used as first-line therapy for primary FSGS, based on the assumption of an underlying immunologic basis for the permeability factor. However, only approximately 30% of cases of pediatric FSGS respond to steroids (134), and it is not possible to predict which cases will respond. The standard therapy for children with idiopathic nephrotic syndrome is oral prednisone (60 mg/m² of body surface per day) for 8 to 12 weeks (22). In adults, glucocorticoid therapy may be given as 1 mg/kg of body weight daily or as 2 mg/kg on alternate days. Most cases of pediatric idiopathic nephrotic syndrome that respond to steroids will do so within 4 weeks of starting therapy; therefore, steroid resistance in children is generally defined as persistent proteinuria after 1 month of daily prednisone therapy followed by 1 month of intermittent administration (135). In adults, a response to glucocorticoids may take up to 16 weeks (136), followed by a slow taper over a period of 3 to 6 months; therefore, at least 6 months, therapy is required before declaring steroid resistance. There is little evidence to recommend glucocorticoid therapy in primary FSGS not accompanied by the nephrotic syndrome.

Additional therapies that have been studied in controlled trials include calcineurin inhibitors (68,137,138) and mycophenolate mofetil (68). One study showed that a 6-month course of CsA in steroid-resistant FSGS led to completion of partial remissions in 69% of patients, versus 4% with placebo. However, 44% of these patients relapsed within 6 months of discontinuing CsA therapy, and kidney function continued to deteriorate, possibly due to the nephrotoxicity of CsA, with no improvement in renal survival rate at 4 years (138). Another study showed no difference in remission rates in patients receiving CsA and steroids versus those receiving steroids alone (137). A large NIH-sponsored multicenter trial showed that mycophenolate mofetil with oral dexamethasone pulses was equivalent to cyclosporine in steroid-resistant FSGS (68). In this randomized controlled prospective study of 138 patients, 67% of whom were less than 18 years of age and 57% of whom were black, approximately 10% to 20% of treated patients had a complete remission and 30% to 40% achieved at least a partial remission. However, 33% of the CsA-treated group who had at least partial remission subsequently relapsed after therapy was discontinued, as did 18% of the mycophenolate mofetil and dexamethasone group. For cases of steroid-resistant FSGS, a regimen of methylprednisolone pulse combined with alternate-day prednisone, and for nonresponsive cases (78%), the addition of an alkylating agent (cyclophosphamide or chlorambucil) produced remissions in 66% of children, with few

side effects (135,139). Other studies have shown no benefit from cyclophosphamide (140) or chlorambucil (with steroids, but without methylprednisolone pulse) in steroid-resistant FSGS (141).

In adult patients with potential contraindications to steroid use, such as those with diabetes mellitus, psychiatric disorders, or severe osteoporosis, a calcineurin inhibitor alone may be used as first-line therapy. Cyclosporine is given in divided doses of 3 to 5 mg/kg/d for 4 to 6 months to induce remission and continued for at least 12 months before slowly tapering. In addition to the systemic immunosuppressive properties of glucocorticoids and calcineurin inhibitors, these drugs exert direct effects on the podocyte that enhance prosurvival pathways and stabilize the actin cytoskeleton (142,143). Angiotensin-converting enzyme inhibitors, angiotensin receptor blockers, and lipid-lowering agents (including statins and fibrates) are also widely used in FSGS, both for control of blood pressure and hyperlipidemia as well as to reduce proteinuria and slow progression.

Recurrence of Primary FSGS in the Renal Allograft

FSGS recurs in the renal allograft in approximately 20% to 30% of cases and is an important cause of graft failure. Risk factors for recurrence include young age at diagnosis of FSGS (especially less than 6 years of age), white race, rapid progression to ESRD (i.e., within 3 years of diagnosis), recurrence in a previous allograft, and living related donor kidney. Recurrence usually occurs in the early posttransplantation period (i.e., before 3 months and often within the first 48 hours) and is typically manifested by heavy proteinuria or the nephrotic syndrome (144). Recurrence tends to occur earlier in children than in adults (145). The recurrence of proteinuria in the immediate postoperative period provides strong evidence for a circulating permeability factor in the recipient (see Pathogenesis above).

Serial biopsies in patients with recurrent FSGS show a sequence of pathologic findings. The initial biopsies typically show no pathologic alteration or only foot process effacement, followed by the development of FSGS lesions from 2 to 11 months posttransplantation (100,146). Immunohistochemical stains reveal loss of the normal polarized distribution of actin and integrins in early recurrent FSGS (147). Increased expression of the parietal epithelial cell activation marker CD44 in visceral and parietal anatomic locations is another early finding in recurrent FSGS (148). Several studies have noted a high prevalence of cellular FSGS as the earliest morphologic feature in recurrent FSGS, suggesting that this variant may represent an early stage in the evolution of FSGS (100,146). One study showed general concordance between the collapsing and cellular variants in the native kidney and in recurrent FSGS, that is, three of five cases with collapsing FSGS recurred with a collapsing pattern, as did two of three cases with cellular FSGS (13). There were no transitions between cellular and collapsing variants, supporting their distinct morphogenesis (13). Of note, three of ten cases with NOS in the native kidney developed collapsing FSGS in the allograft, but two of these cases occurred late (i.e., at 108 days and more than 10 years, respectively), suggesting the possibility of de novo, rather than recurrent, FSGS (13).

Overall, recurrent FSGS followed the native FSGS variant directly in most cases (60%) or after an intermediate “minimal change” phase in 20% of cases. In only 20% of cases was there discordance between the FSGS variants in the native and transplanted kidney (13).

On the other hand, two other studies showed greater discordance between FSGS variant findings in the native kidney and the allograft, and the native variant was not predictive of either recurrence or the variant observed posttransplantation (69,149). Such comparisons between FSGS morphologic variants in the native kidney and in the renal allograft are problematic for several reasons. First, NOS variant in the native kidney likely includes some cases of the other variants where the distinguishing morphologic features either were not sampled or had transformed to NOS during disease progression. Second, FSGS variants in the allograft may result from other causes besides recurrent disease, such as NOS or perihilar variants resulting from adaptive responses to reduced nephron number (e.g., due to pediatric donor kidneys or chronic rejection), and drug toxicity or acute vasooclusion giving rise to collapsing variant (150). Third, the underlying pathogenic factors (e.g., circulating permeability factors) may be modified by immunosuppressive therapy. Fourth, sample variability and differences in the time between onset of proteinuria and biopsy may affect the biopsy findings. In summary, the variable clinical-pathologic features observed in recurrent FSGS likely reflect a complex interplay between pathogenetic factors, donor kidney characteristics, and the immunologic and pharmacologic milieu in the posttransplant setting.

The clinical management of recurrent FSGS and a review of other causes of FSGS in the renal allograft are discussed in Chapter 29.

GENETIC CAUSES AND FAMILIAL FORMS OF FSGS

Since identification of nephrin gene (*NPHS1*) mutations in CNS in 1998 (151), the list of genetic causes of the nephrotic syndrome and FSGS has grown (Table 6.5). These include rare monogenic diseases and mitochondrial cytopathies, with or without syndromic features. In addition, common genetic polymorphisms may predispose to FSGS in larger populations. Many of these genes were first identified by positional cloning or homozygosity mapping in families affected by CNS or familial FSGS. These include the genes for nephrin (*NPHS1*), podocin (*NPHS2*), α -actinin 4 (*ACTN4*), phospholipase C epsilon 1 (*PLCE1*), inverted formin-2 (*INF2*), transient receptor potential cation channel (*TRPC6*), myo1E (*MYO1E*), and protein tyrosine phosphatase receptor type O (*PTPRO*). Other gene defects, such as CD2-associated protein (*CD2AP*), were identified serendipitously while studying other disease systems. Others have been identified in animal models of FSGS, but their relevance to human disease remains undetermined. Most of these genetic defects have been validated in animal models using knockouts of the causative gene or overexpression of the mutated gene. Mutations that typically present with CNS (*NPHS1*) or are associated with diffuse mesangial sclerosis (e.g., *WT-1*, *PLCE1*, and *LAMB2*) are reviewed in more detail in Chapter 5.

TABLE 6.5 Genetic causes of FSGS

Human gene product	Gene	Inheritance	Chromosome	Function	Clinical features
Slit Diaphragm Proteins					
Nephrin	<i>NPHS1</i>	AR	19q13.1	Major structural component of slit diaphragm; signaling platform	Finnish-type congenital nephrotic syndrome and some cases of sporadic childhood FSGS
Podocin	<i>NPHS2</i>	AR	1q25-31	Stomatin family member anchoring nephrin, NEPH, and CD2AP to lipid rafts; signaling complex at slit diaphragm	Familial or sporadic steroid-resistant FSGS or DMS in early childhood
CD2-associated protein	<i>CD2AP</i>	AD; rarely AR	6p12	Adaptor protein linked to nephrin and podocin at slit diaphragm. Also expressed by T lymphocytes	Adult onset FSGS; rarely presents in childhood
Cell membrane-associated proteins					
Transient receptor potential cation channel 6	<i>TRPC6</i>	AD	11q21-22	Cation channel with roles in calcium influx, mechanosensation, cell growth; gain-of-function mutation	Familial or sporadic adult onset FSGS
Protein tyrosine phosphatase receptor type O (GLEPP1)	<i>GLEPP-1</i>	AR	12p22	Tyrosine phosphatase expressed on the apical foot process membrane; roles in contact inhibition and signaling	Familial FSGS in mid-childhood
Laminin- β_2	<i>LAMB2</i>	AR	3p21	Anchors the basal podocyte membrane to GBM	Pierson syndrome in infancy (microcoria, neuromuscular junction defects, early onset DMS or FSGS)
β_4 integrin	<i>ITGB4</i>	AR	17q11	Anchors the basal podocyte membrane to GBM	Epidermolysis bullosa; infantile FSGS
Tetraspanin CD151	<i>CD151</i>	AR	11p15	Anchors the basal podocyte membrane to GBM	Epidermolysis bullosa; deafness, infantile FSGS
Cytosolic and cytoskeletal proteins					
α -Actinin 4	<i>ACTN4</i>	AD	19q13	Spectrin family member that cross-links actin filaments; gain-of-function mutation	Familial or sporadic adult onset FSGS with subnephrotic or nephrotic-range proteinuria
Phospholipase C ϵ 1	<i>PLCE1</i>	AR	10q23-24	Located in podocyte cell body; catalyzes hydrolysis of phosphatidylinositol to generate IP3 and DAG; roles in cell growth, differentiation, and motility	Nonsyndromic DMS or early-onset childhood FSGS
Myosin heavy chain 9	<i>MYH9</i>	AD	22q12.3	Nonmuscle myosin IIA heavy chain; role in actin-based cell contraction and motility	Epstein-Fechtner syndrome (FSGS, deafness, cataracts, macrothrombocytopenia, leukocyte inclusions)

(Continued)

TABLE 6.5 Genetic causes of FSGS (Continued)

Human gene product	Gene	Inheritance	Chromosome	Function	Clinical features
Inverted formin 2	<i>INF2</i>	AD	14q32	Formin family member, regulation of actin filament nucleation and polymerization	Familial FSGS with onset in adolescence or adulthood
Myosin 1E	<i>MYH9</i>	AR	15q21-26	Member of class I myosins that interact with the cell membranes via C-terminus and with actin filaments via N-terminus motor domain	Familial FSGS with onset in mid-childhood
Nuclear proteins					
Wilms tumor 1	<i>WT1</i>	AD	11p13	Zinc-finger transcription factor; role in the development of genitourinary tract and maintenance of mature podocyte phenotype	Frasier syndrome (FSGS, male pseudohermaphroditism, gonadoblastoma), isolated DMS or FSGS. Denys-Drash syndrome (DMS, male pseudohermaphroditism, Wilms tumor)
SMARCA-like protein	<i>SMARCA1</i>	AR	2q34-36	Chromatin bundling protein that probably regulates gene transcription	Schimke immuno-osseous dysplasia (immunodeficiency, skeletal dysplasia, childhood FSGS)
Mitochondrial					
tRNA ^{Leu}	mtDNA-A3242G	Maternal	mtDNA	Mitochondrial tRNA required for the synthesis of mitochondrial proteins	MELAS (mitochondrial myopathy, encephalopathy, lactic acidosis, stroke-like episodes) and FSGS
Para-hydroxybenzoate-polyprenyl transferase	<i>COQ2</i>	AR	4q21-22	Mitochondrial respiratory chain electron carrier	Coenzyme Q deficiency; collapsing FSGS and encephalopathy in infancy
Coenzyme Q10 biosynthesis monooxygenase 6	<i>COQ16</i>	AR	14q24.3	Required for synthesis of coenzyme Q10, which is a mitochondrial respiratory chain electron carrier	Familial FSGS or DMS and deafness in early childhood
Lysosomal protein					
Lysosomal integral membrane protein type 2	<i>LIMP2</i>	AR	4q13-21	Integral lysosomal membrane protein; role in membrane recycling	Action myoclonus-renal failure syndrome (ataxia, myoclonus, collapsing FSGS)
Unknown cellular location					
Apolipoprotein L1	<i>APOL1</i>	AR	22q12	Podocyte function unknown; confers resistance to sleeping sickness by lysing trypanosomal organisms	Risk factor for FSGS, HIVAN, and hypertensive nephrosclerosis in individuals of African descent

AD, autosomal dominant; AR, autosomal recessive; DAG, diacylglycerol; DMS, diffuse mesangial sclerosis; GLEPP1, glomerular epithelial protein 1. Adapted from D'Agati VD, Kaskel FJ, Falk RJ. Focal segmental glomerulosclerosis. *N Engl J Med* 2011;365(25):2398–2411.

Clinical Presentation

Genetic forms of FSGS are typically associated with SRNS, progression to ESRD, and a low rate of recurrence following transplantation. However, some variants have a more benign clinical course and some may respond to therapeutic interventions. Diseases with an autosomal recessive inheritance pattern typically present with nephrotic syndrome earlier in life and have a more severe renal phenotype compared to autosomal dominant cases. Accumulation of second hits over years, for example, due to shear stress, stretch tension, oxidative stress, and DNA damage, may act in concert with a genetic predisposition to cause late onset of FSGS in adults with autosomal dominant mutations. Podocyte-specific genetic mutations, particularly for structural proteins and enzymes involved in maintaining the slit diaphragm complex and actin-based cytoskeleton, usually present with SRNS in infancy and early childhood. Mutations in gene products expressed in the nucleus, mitochondria, and lysosomes have broader cellular effects and commonly display extrarenal syndromic manifestations, in addition to FSGS (87). Many of these diseases display incomplete penetrance and genotypic-phenotypic discordance, suggesting a role for other modifying genes or environmental factors.

Genetic testing is most likely to uncover a basis for FSGS in infants, young children, and patients with syndromic disease or a positive family history. Single-gene mutations in one of only four genes, *NPHS1*, *NPHS2*, *LAMB2*, and *WT1*, have been identified in up to two thirds of patients with SRNS in the 1st year of life and 10% to 28% of all childhood cases, underscoring the importance of genetic testing in this age group (152,153). A small but clinically important subset of older children and adults with sporadic steroid-resistant disease may also harbor disease-causing mutations (154).

Pathologic Features

The renal pathologic manifestations in genetic forms of nephrotic syndrome are variable and nonspecific. These include foot process effacement with minimal histologic alterations (resembling MCD), FSGS, diffuse mesangial sclerosis, and mesangial hypercellularity (with or without IgM deposits). There are few detailed descriptions of the pathologic features in genetic forms of FSGS but most appear to be the NOS variant. Some exceptions include mutations for parahydroxybenzoate-polyprenyl transferase (*COQ2*), lysosomal integral membrane protein type 2 (*LIMP2*), and α -actinin 4 (*ACTN4* (88)), which may produce collapsing FSGS, and mitochondrial tRNA^{Leu} mutation, which is associated with perihilar FSGS (see below).

Pathogenesis

Nephrin (*NPHS1* Gene)

Nephrin gene (*NPHS1*) mutations were identified as the first genetic cause of nephrotic syndrome in 1998 (151). Nephrin is a transmembrane protein of the immunoglobulin superfamily. It is the major structural component of the slit diaphragm, where it forms a zipper-like structure via homophilic

interactions with nephrin molecules in adjacent foot processes. Nephrin is complexed to podocin, Neph1, and CD2AP in lipid rafts and is coupled to the actin cytoskeleton via Nck proteins (155). *NPHS1* mutations most commonly present with CNS but occasionally present with childhood SRNS and FSGS. CNS is discussed more fully in Chapter 5. In brief, this is defined as nephrotic syndrome present at birth or developing within the first 3 months after birth. The incidence of CNS is highest in Finnish patients, most of whom have genetic mutations in nephrin (*NPHS1*) (151). Most Finnish patients with CNS have an autosomal recessive disorder caused by one of two truncating mutations in the *NPHS1* gene: Fin-major (L41fsX91) (78% of mutated alleles) and Fin-minor (R1109X) (16% of mutated alleles). Fin-major and Fin-minor mutations are rare in non-Finnish populations, suggesting a founder effect.

Over 140 different *NPHS1* mutations have been identified in patients with CNS, most of which are private mutations in non-Finnish patients. *NPHS1* mutations are identified with variable frequency in CNS in other ethnic groups, ranging from 15% of Japanese patients to 34.3% of Central Europeans and 54.5% of Turkish patients (156). In two large studies comprising non-Finnish European, North American, and North African patients, the rate of *NPHS1* mutations was approximately 60% (157,158). CNS typically does not show features of FSGS until late in the disease course, but rare cases of congenital FSGS are associated with a triallelic inheritance of *NPHS1* and *NPHS2* mutations (159). The *NPHS1* mutations associated with severe CNS include deletions, insertions, splice-site mutations, and nonsense mutations, resulting in frameshifts or stop codons. These mutant gene products are retained in the endoplasmic reticulum, and the slit diaphragms do not form. Other *NPHS1* mutations may have a milder phenotype. The p.R1160X mutation has a milder phenotype in 50% of cases, most of whom are female, suggesting a gender effect (159). This mutation leads to a truncated protein lacking the C-terminal amino acids involved in podocin interactions. Biopsy findings were typical of CNS (i.e., microcystic tubular dilatation), but patients have a benign clinical course, with mild proteinuria or remission between the ages of 5 and 19 years (159). In addition, patients who are compound heterozygous for one mild missense *NPHS1* mutation present with SRNS at a later age (i.e., after 3 months of age) and often have normal renal function at 6 years of age (160). These cases show normal protein trafficking to the plasma membranes and retain the ability to form nephrin homodimers and heterodimers with Neph1. Two Japanese siblings with compound heterozygous missense mutations, one mild and one severe, retained partial plasma membrane trafficking and had self-limited episodes of nephrotic syndrome triggered by upper respiratory infections (161). Most cases of CNS due to *NPHS1* mutations progress rapidly to ESRD and many patients die from infectious complications within the 1st year.

Recurrence of nephrotic syndrome posttransplantation has been described in up to 25% of patients with Fin-major or Fin-minor mutations and may be related to the development of antinephrin antibodies (162). Biopsies performed in these cases showed diffuse foot process effacement, reduced number

of slit diaphragms, and granular podocyte staining for nephrin, but without features of membranous glomerulonephritis (162).

Autosomal Recessive Steroid-Resistant Nephrotic Syndrome

Podocin (*NPHS2* Gene)

Podocin is a transmembrane protein of the stomatin family that localizes to lipid raft microdomains in the slit diaphragm. Podocin recruits nephrin into lipid rafts and enhances nephrin signaling. Podocin knockout mice develop severe albuminuria in utero and die within 1 week, with pathologic findings of mesangiolysis and mesangial sclerosis, but not FSGS (163). These animals show up-regulation of *NPHS1* gene expression and decreased expression of the zona occludens (*ZO*)-1 and *CD2AP* genes. In adult mice, conditional podocyte-specific inactivation of podocin produces nephrotic syndrome and FSGS after 4 weeks, accompanied by perturbation of cell cycle regulation and proliferation pathways (164).

NPHS2 mutations were first identified in autosomal recessive SRNS (165) and have since been identified in up to 20% of pediatric FSGS cases (89), 15% of SRNS in children (87) (26% to 34% of familial and 11% to 19% of sporadic cases (89,166)) and 15% to 34 % of CNS in non-Finnish subjects (152,158). *NPHS2* mutations are rare in cases from Asia (167) and sub-Saharan Africa. More than 90 different pathogenic mutations have been identified, the most common being R138Q, which represents up to 32% of mutant alleles (166,168). Most affected patients have homozygous or compound heterozygous *NPHS2* mutations and present with SRNS around 3 years of age. However, *NPHS2* mutations are also an important cause of CNS, particularly in European patients (152,158), and occasionally present in adolescence or in adulthood. Age at onset is earlier with frameshift or nonsense mutations and homozygous R138Q missense mutations (166). Two mutations, V180M and R238S, have a milder phenotype, with later onset of nephrotic syndrome and ESRD (166).

NPHS2 variants may also predispose to sporadic steroid-resistant FSGS in adults (169,170). The R229Q missense variant, present in 3.6% of the white population (170), demonstrates decreased binding to nephrin in vitro, suggesting that it may be pathogenic (166). The R229Q variant was associated with microalbuminuria in Brazilian patients of mixed European and African ancestries (171). Compound heterozygosity for R229Q with a disease-causing *NPHS2* mutation was detected in 14% of familial and 6% of sporadic cases of SRNS in the second and third decades of life, in a cohort comprising European, Middle Eastern, North African, and South American patients (169). Heterozygosity for R138Q was associated with a fivefold increased risk of sporadic or HIV-associated adult-onset FSGS in African Americans and white Americans (172). However, other studies showed no *NPHS2* mutations or polymorphisms in 18 African American children with SRNS (173) and no differences in long-term outcome in children with a single *NPHS1* or *NPHS2* variant (including R229Q variant) after controlling for response to therapy (174). Two other large studies did not find disease-causing mutations or

an increased risk with R229Q variant in adult-onset sporadic FSGS (175,176).

The pathology of podocin mutations consists of FSGS NOS in most cases. Other findings include minimal histologic abnormalities (which may subsequently progress to FSGS), mesangial proliferation, with or without IgM deposition, and diffuse mesangial sclerosis (89,166,177). This form of FSGS is almost uniformly steroid resistant. Recurrence of proteinuria and FSGS posttransplantation has been described (178) but appears to be uncommon (8%, vs. 35% for those without *NPHS2* mutations (166)). Some of these recurrent cases may be related to other factors (e.g., calcineurin inhibitor toxicity) while others may be associated with a circulating glomerular permeability factor (166,178). Antipodocin antibodies have not been detected in any of these cases (166,179).

Phospholipase C Epsilon (*PCLE1* Gene)

The *PCLE1* gene, located on chromosome 10q, encodes one of a family of phospholipase C enzymes (PLC ϵ 1). This isoform of phospholipase C catalyzes the hydrolysis of membrane phospholipids to generate the second messenger molecules inositol 1,4,5-triphosphate and diacylglycerol, which participate in intracellular pathways of cell growth and differentiation. PLC ϵ 1 is present in the cytoplasm of mature glomeruli and is highly expressed in the capillary loop stage of development. *PCLE1* mutations cause glomerular developmental arrest and reduced nephrin and podocin expression (180). *PCLE1* mutations were first identified in 14 patients from seven families with familial SRNS. Eight of these patients presented in the 1st year of life, and one had CNS (180). Truncating mutations were associated with onset of nephrotic syndrome before 4 years of age, progression to ESRD before 5 years, and biopsy findings of diffuse mesangial sclerosis, whereas a missense mutation presented in later childhood and had biopsy findings of FSGS. Interestingly, some patients with homozygous truncating mutations and nephrotic syndrome may be responsive to steroids or CsA (180,181). *PCLE1* mutations have also been identified in up to 28% of cases of sporadic diffuse mesangial sclerosis (181) and 8% of familial FSGS cases without *NPHS2* mutations (182).

Myosin 1E (*MYO1E* Gene)

MYO1E encodes myosin 1E (a nonmuscle class I myosin) that links actin to the podocyte cell membrane. Homozygous mutations have been described in three families with autosomal recessive FSGS (183,184). Two families displayed missense mutations, and the other had a truncating mutation in *MYO1E*. One of these families also had a potentially pathogenic homozygous mutation in nei endonuclease VIII-like 1 (*NEIL1*), encoding a base-excision DNA repair enzyme (184). *MYO1E* appears to be important for podocyte motility and may stabilize the actin cytoskeleton. Of note, all of these patients had SRNS, but some responded to CsA, perhaps due to stabilization of the actin cytoskeleton by blocking calcineurin-induced synaptopodin dephosphorylation (143).

Protein Tyrosine Phosphatase Receptor Type 0 (PTPRO Gene)

PTPRO encodes GLEPP-1, a tyrosine phosphatase expressed on the apical membrane of podocyte foot processes. It is thought to play a role in contact inhibition and maintenance of foot process architecture. Loss of PTPRO expression has been observed in experimental models and human proteinuric diseases, such as primary FSGS (185) and IgA nephropathy (186). In PAN nephropathy, PTPRO downregulation preceded the onset of proteinuria, and the blockade of PTPRO by specific antibodies increased albumin permeability in isolated rat and rabbit glomeruli, supporting the essential role of this protein in maintaining glomerular permselectivity. Mutations in PTPRO have been identified in autosomal recessive SRNS presenting in childhood or adolescence (91). Biopsies showed either MCD or FSGS. Interestingly, partial response to intensified immunosuppressive treatment was found, consistent with a role for steroids in modulating phosphatase activity (91).

CD2-Associated Protein (CD2AP Gene)

CD2AP is an integral component of the slit diaphragm complex and has multiple roles, including regulation of the actin cytoskeleton, endocytosis, phosphoinositide 3-OH kinase-dependent AKT signaling, and repression of transforming growth factor-beta (TGF β) induced apoptosis (187). CD2AP is a 70-kDa adaptor protein that was initially described as involved in T-cell activation. It contains a coiled coil domain and three Src homology 3 (SH3) domains, which serve as attachment sites for other proteins. CD2AP knockout mice develop CNS and die from renal failure after 6 weeks, whereas haploinsufficient mice develop glomerular lesions at 9 months and are more susceptible to glomerular injury due to nephrotoxic antibodies or immune complexes (188). A homozygous truncating *CD2AP* mutation was reported in a patient with infantile nephrotic syndrome and collapsing FSGS (189), and compound heterozygous *CD2AP* and *NPHS2* mutations were identified in a patient with sporadic childhood SRNS and FSGS (190). Heterozygous mutations have also been identified in a small number of adult patients with sporadic primary FSGS (191,192). These mutations were associated with reduced mRNA and protein expression for CD2AP, nephrin, and podocin, suggesting that haploinsufficiency for CD2AP may be a risk factor for FSGS by interfering with composition of the slit diaphragm (192).

Autosomal Dominant FSGS

α -Actinin 4 (ACTN4 Gene)

α -Actinin 4 is an actin-binding protein that cross-links actin filaments and localizes to the podocyte foot processes. Disease-causing missense mutations cause a rigid cytoskeleton by exposing a buried actin-binding site that is independent of calcium regulation, leading to a gain of function (193). This leads to disordered assembly and disassembly of filamentous actin, interfering with podocyte motility. Mutations may also cause abnormal protein folding and degradation. Cultured podocytes from *Actn-4* null mice show reduced adherence to basement membrane components, suggesting a mechanism for podocyte loss in the development of FSGS (194).

Clinically, *ACTN4* mutations are associated with autosomal dominant FSGS and typically present with nephrotic syndrome in adolescence and slow progression to ESRD by the fifth decade (195). However, there is considerable genotypic-phenotypic heterogeneity, with some carriers of the mutant allele being asymptomatic (i.e., incomplete penetrance), others having only microalbuminuria, and others presenting with severe nephrotic syndrome and rapid progression to ESRD in childhood (88,196). At least five potentially pathogenic *ACTN4* variants have been identified (196). It is estimated that *ACTN4* mutations account for approximately 4% of familial FSGS (196). The pathologic features of *ACTN4*-associated FSGS include NOS, cellular, perihilar, and collapsing variants (88,197). A peculiar ultrastructural finding in *ACTN4*-associated FSGS is the presence of electron-dense aggregates in the podocyte cytoplasm (197).

Inverted Formin 2 (INF2 Gene)

Inverted formin-2 is a member of the formin protein family that has essential roles in regulating the actin and microtubule cytoskeletons. Mutations in *INF2* have been identified in up to 17% of families with autosomal dominant FSGS (198,199). All of the identified mutations were missense variants involving the N-terminal diaphanous inhibitory domain of the protein, a region that interacts with the C-terminal diaphanous autoregulatory domain, thereby competing for actin monomer binding and inhibiting depolymerization. Cell transfection studies show that the mutated gene products have a different subcellular localization from wild-type proteins, and the distribution of the associated F-actin is also abnormal (198). Electron microscopy revealed less prominent actin filament bundles in transfected cells compared to normal cells (198). Affected patients usually present with moderate proteinuria without the full nephrotic syndrome, with onset in childhood, adolescence, or adulthood and slow progression to ESRD. Renal biopsies show FSGS NOS (198). *INF2* mutations have also been described in cases of syndromic FSGS associated with Charcot-Marie-Tooth syndrome (200).

Transient Receptor Potential Cation Channel (TRPC6 Gene)

TRPC6 is a member of a family of cation channels with six membrane-spanning domains. These channels modulate ion homeostasis and phospholipase C-dependent calcium entry. TRPC6 has a wide tissue distribution, including the kidney, placenta, spleen, ovary, small intestine, and lung. In the kidney, TRPC6 is expressed in podocyte cell body and at the slit diaphragm, in addition to being expressed in endothelial cells and tubular epithelial cells. TRPC6 mutations have been identified in several families with autosomal dominant FSGS (201–204). Most of the reported mutations are gain-of-function missense mutations causing increased calcium influx, which may play a role in the regulation of actin polymerization. Penetrance is incomplete. It is estimated the TRPC6 mutations account for approximately 7% of familial FSGS (203). Patients typically present with nephrotic syndrome in the third or fourth decade, with progressive renal failure over the next 10 years. However, *TRPC6* mutations have also been identified in 4 of 33 children with early onset and sporadic SRNS, including one case with collapsing FSGS (205).

Syndromic FSGS

Denys-Drash and Frasier Syndrome (*WT1* Gene)

These conditions typically display pathologic findings of diffuse mesangial sclerosis, as well as FSGS, and are reviewed in detail in Chapter 5.

The product of the Wilms tumor gene (*WT1*), located on chromosome 11p13, is a zinc-finger transcription factor that regulates many genes, including genes regulating normal genitourinary tract and mesothelial development. In the developing kidney, WT-1 is expressed in many nephron progenitor cells but becomes restricted to the podocyte in the mature kidney, where it plays a role in down-regulation of proliferation and maintenance of the mature podocyte phenotype. Loss of WT-1 was first identified in patients with Wilms tumor, aniridia, genitourinary malformations, and mental retardation (WAGR) syndrome, suggesting a tumor suppressor function.

WT1 mutations have been identified in over 90% of patients with Denys-Drash syndrome and Frasier syndrome. Denys-Drash syndrome is comprised of male pseudohermaphroditism (46XY genotype), diffuse mesangial sclerosis, nephrogenic rests, and an increased incidence of Wilms tumor. Patients display either ambiguous external genitalia or normal-appearing female external genitalia. The internal genital organs may be hypoplastic, dysplastic, or normal appearing. Patients present with nephrotic syndrome within the 1st year of life, with rapid progression to ESRD (206). Frasier syndrome is characterized by male pseudohermaphroditism, fully feminized external genitalia, streak gonads, and later onset of a more slowly progressive glomerulopathy with pathologic features of FSGS (207). ESRD develops in adolescence or early adulthood. In Frasier syndrome, there is an increased risk of developing gonadoblastoma, but not Wilms tumor.

More than 60 different *WT1* mutations have been identified, most of which cluster in exons 8 and 9 and encode zinc fingers 2 and 3. In Denys-Drash syndrome, two *WT1* mutations occur, the first of which is a germ-line mutation that leads to the development of dysgenetic gonads, glomerulopathy, and nephrogenic rests. The second, postzygotic mutation occurs in nephrogenic rests, resulting in the loss of heterozygosity and the development of Wilms tumors. In Frasier syndrome, there is a heterozygous mutation in a splicing region (intron) of *WT1*, leading to altered ratios of *WT1* isoforms, rather than a mutant product (207).

WT1 mutations have also been detected in up to 9% of cases of isolated sporadic SRNS, without features of Denys-Drash or Frasier syndromes (152,208,209). These cases may present with isolated congenital or infantile nephrotic syndrome and have normal-appearing external genitalia. Therefore, it is recommended that all female children (and males with genital abnormalities) who present with SRNS be tested for *WT1* mutations to identify those at risk of developing tumors and for genetic counseling. Karyotyping is recommended in all children with diffuse mesangial sclerosis to rule out male pseudohermaphroditism.

In both the syndromic and isolated forms of disease, normal expression of WT-1 is lost in mature podocytes and expression of another transcription factor, PAX-2, which is normally restricted to parietal cells in the mature kidney, is increased. These abnormalities contribute to the synthesis of an abnormal GBM and mesangial matrix during glomerular development, resulting in diffuse mesangial sclerosis. The expanded matrix has a reticulated spongy appearance, which is

best appreciated with silver stains, without increase in cellularity. The GBMs are segmentally thickened, and podocytes are hypertrophied. Shrunken, sclerotic glomeruli surrounded by a corona of hypertrophied podocytes and immature glomeruli are commonly seen. Podocyte hypertrophy and hyperplasia may mimic a cellular crescent. With disease progression, FSGS lesions appear accompanied by progressive tubular atrophy, interstitial fibrosis, and interstitial inflammation. A corticomedullary gradient of involvement is present, with more severe changes in the outer cortex and milder features in the inner cortex. Nephrogenic rests may be seen.

Pierson Syndrome (*LAMB2* Gene)

The *LAMB2* gene located at chromosome 3p21 encodes laminin β_2 , a major glycoprotein component of the GBM. Laminin β_2 is incorporated in heterotrimeric isoforms, the most common consisting of α_5 , β_2 , and γ_1 subunits, and is expressed in the GBMs, intraocular muscles and lens, and neuromuscular synapses. Homozygous or compound heterozygous truncating or missense mutations of *LAMB2* leading to absent or reduced laminin β_2 expression, respectively, were first described in five families with Pierson syndrome (94). This autosomal recessive disorder is characterized by CNS, diffuse mesangial sclerosis, and ocular abnormalities including enlarged corneas and narrow, unreactive pupils (microcoria), and variable neurodevelopmental deficits, including congenital muscular weakness/myasthenia and developmental retardation (94). Subsequently, *LAMB2* mutations were also found in Pierson syndrome patients with a milder phenotype, including CNS and minor or no ocular abnormalities and later onset of symptoms (between 5 and 10 years of age) (210,211). In addition, homozygous or compound heterozygous *LAMB2* mutations have been identified in approximately 3% of patients presenting with isolated congenital or infantile nephrotic syndrome, with renal biopsy findings of diffuse mesangial sclerosis or FSGS (152,210). Missense mutations and small in-frame deletions have a higher mean age at onset of renal disease and absence of neurologic abnormalities, suggesting that at least some of these may represent hypomorphic alleles (210).

Action Myoclonus-Renal Failure Syndrome (*SCARB2* Gene)

Lysosomal integral membrane protein (LIMP) type 2 is a ubiquitously expressed transmembrane protein of the CD36 superfamily, which is necessary for the synthesis and maintenance of lysosomes and late endosomes. LIMP-2 is a trafficking receptor for beta-glucocerebrosidase, which is defective in Gaucher disease. Mutations in the *SCARB2* gene encoding LIMP-2 were identified in patients with action myoclonus-renal failure (AMRF) syndrome, a rare autosomal recessive disorder characterized by progressive myoclonic epilepsy, ataxia, and renal failure (212). These mutations led to undetectable synthesis of LIMP-2. AMRF typically presents in late adolescence or early adulthood with neurologic symptoms and proteinuria and pathologic findings of FSGS, typically with collapsing features (213). Progression to ESRD occurs within 5 years. How abnormal lysosomal function due to lack of LIMP-2 results in proteinuria and FSGS is unclear but may involve altered recycling or degradation of other proteins required for podocyte homeostasis.

Schimke Immuno-Osseous Dysplasia (*SMARCAL1* Gene)

Schimke immuno-osseous dysplasia is an autosomal recessive disease characterized by spondyloepiphyseal dysplasia, T-cell immunodeficiency, FSGS, and progressive renal failure by 5 to 15 years of age. Variable other clinical manifestations are present (214). This disease is caused by mutations in the switch/sucrose nonfermenting (*swi/snf*)-related, matrix-associated, actin-dependent regulator of chromatin, subfamily a-like 1 gene (*SMARCAL1*), located at chromosome 2q35 (215). The gene product is a member of a family of proteins that regulate DNA-nucleosome restructuring. Most mutations are nonsense or frame-shifting mutations that lead to loss of function. Biallelic mutations are present in over 50% of cases and patients with two missense mutations have a milder phenotype (216). It is likely that this chromatin bundling protein causes altered transcription of other vital podocyte genes.

Integrin β_4 (*ITGB4* gene)

Integrins anchor the podocyte to the GBM via its interactions with laminin-5. The major integrin expressed by podocytes is $\alpha_3\beta_1$, but there are also lower levels of other integrin heterodimers, such as $\alpha_6\beta_4$. Mutations of the *ITGB4* gene encoding $\alpha_6\beta_4$ are most commonly associated with epidermolysis bullosa and pyloric atresia (217). There is a single case report of child with epidermolysis bullosa, pyloric atresia, and FSGS who presented with CNS and was found to have a homozygous mutation of *ITGB4*, associated with reduced podocyte expression of β_4 integrin by immunofluorescence staining (95).

Mitochondriopathies Associated with FSGS

FSGS is associated with maternal inheritance of point mutations of leucine transfer RNA (tRNA^{Leu}) and autosomally inherited defects of coenzyme Q10 (CoQ10) biosynthesis. Mitochondrial DNA (mtDNA) encodes 13 subunits of the respiratory chain, 22 transfer RNAs (tRNAs), and two ribosomal RNAs. The remaining mitochondrial proteins are encoded by nuclear DNA. Hereditary defects of mtDNA have a maternal inheritance pattern and heterogeneous clinical phenotypes, including neuromuscular, cardiac, endocrine, gastrointestinal, ocular, and cutaneous manifestations. Renal manifestations include Fanconi syndrome, proteinuria or nephrotic syndrome, tubulointerstitial nephritis, cystic kidney disease, myoglobinuria, and renal failure (218).

Mitochondrial $\text{tRNA}^{\text{Leu}}(\text{URR})$

A point mutation (A3243G) in the mitochondrial gene *MTTL1* encoding $\text{tRNA}^{\text{Leu}}(\text{URR})$ was initially identified in infants and children with MELAS syndrome (mitochondrial myopathy, encephalopathy, lactic acidosis, and stroke) (219). Subsequently, this mutation was identified in patients with FSGS who presented in later childhood or in adulthood with proteinuria, diabetes mellitus, deafness, and cardiomyopathy (220–223). In the series of Guery et al. (220), eight of nine patients had extrarenal manifestations including deafness (eight), diabetes mellitus (three), neuromuscular symptoms (two), hypertrophic cardiomyopathy (one), and macular dystrophy (one). Although the prevalence of renal disease associated with the A3243 mutation is unknown, it may be relatively common because of its association with type 2 diabetes

mellitus. The association of maternally inherited diabetes mellitus and deafness is seen in 0.5% to 2.8% of patients with type 2 diabetes, and Guillausseau et al. (224) reported 45 of these patients with the mtDNA A3243G mutation of whom 28% had kidney disease.

Although tubular dysfunction is the most common manifestation of the A3243G mutation, FSGS has also been reported (220,225) presenting with proteinuria or the nephrotic syndrome (222,223). When neurosensory deafness is present, progressive renal disease in patients with mitochondrial cytopathy is distinguished clinically from Alport syndrome by the absence of hematuria, severity of renal involvement in females, the lack of ultrastructural findings of Alport syndrome, steroid-induced diabetes mellitus, and neurologic findings (226,227). The clinical course is one of progressive renal failure in some but not all affected individuals (220,222,223,226). The glomerular lesion does not respond to steroid treatment (222,223), and successful transplantation for ESRD without recurrence has been reported (220,223).

The renal pathology associated with the A3243G mutation is variable. In nine patients with the mutation and prominent renal manifestations diagnosed as adults (mean age 35 years), Guery et al. (220) reported two cases of FSGS, three cases of tubulointerstitial nephritis, and one case of bilaterally enlarged cystic kidneys. The FSGS lesions begin at the glomerular hilum (i.e., are perihilar) and spread to involve the entire tuft (221,228). In contrast to the perihilar FSGS seen in adaptive forms of FSGS (see below), glomerulomegaly is not a feature (222). Several investigators have noted the presence of a vasculopathy with hyalinosis of small arteries and myocyte necrosis (221,228). Electron microscopy shows podocyte injury manifested by cell body attenuation, pseudocyst formation, and binucleate forms and variable changes in the mitochondria including increased numbers, variations in size, shape, and outline, and disorganization and loss of cristae. Tubular epithelium also displays increased numbers of dysmorphic mitochondria, giving rise to a granular appearance by light microscopy, which may be a clue to the presence of a mitochondrial disease (229).

The clinical and pathologic heterogeneity has been attributed to the proportion of wild-type *MTTL1* present in the mitochondria (heteroplasmy) (221), and affected individuals have as much as 85% mutant *MTTL1* (230). Furthermore, mutations in mtDNA owing to age and oxidative stress accumulate in long-lived cells such as neurons, myocytes, and podocytes, providing a neat explanation for the target organs in the MELAS syndrome. Yamagata et al. (230) demonstrated accumulation of the mutated mtDNA within podocytes but not in tubular epithelium in some cases of apparent idiopathic FSGS and IgA nephropathy, suggesting that free radical-induced oxidative injury to mtDNA may predispose to glomerular scarring in these diseases (230).

Coenzyme Q10 Synthesis Defects

Mutations in the *COQ2*, *COQ6*, and *PDS22* genes leading to coenzyme Q10 deficiency have been associated with FSGS (231,232). The *COQ2* gene encodes para-hydroxybenzoate-polypprenyl transferase, and several cases of FSGS due to compound heterozygous or homozygous *COQ2* mutations have been described. Three siblings presented with childhood SRNS and progressive encephalopathy, with improvement of neurologic signs following oral ubiquinone therapy (233).

One additional case developed SRNS at 12 months of age and progressed to ESRD but neurologic symptoms improved after oral CoQ10 therapy (234). This patient's younger sister received oral CoQ10 immediately after she developed nephrotic syndrome at 12 months of age; she never developed neurologic disease and had normal kidney function (albeit with persistent proteinuria) after 50 months of therapy (234). Both of these siblings had biopsy findings of FSGS NOS (231). Another case presented at 18 months of age with SRNS and collapsing FSGS, without any extrarenal symptoms (231). One other patient presented at 5 days of life with oliguric kidney failure, renal biopsy showed severe extracapillary proliferation and death ensued at the age of 6 months from progressive epileptic encephalopathy (231). Combined complex II + III activity and CoQ10 level were decreased in renal cortex and in skeletal muscle in both of the latter two cases, and ultrastructural examination showed an increased number of dysmorphic mitochondria in glomerular epithelial cells (231). One additional case of COQ2 deficiency presenting with CNS was related to a single base pair frameshift deletion in the *COQ2* gene (235).

Heeringa et al. (232) identified homozygous or compound heterozygous *COQ6* mutations in 13 individuals from seven families by homozygosity mapping (232). These mutations were linked to early-onset SRNS with sensorineural deafness. Renal biopsies showed FSGS (seven cases) or diffuse mesangial sclerosis (one case). In rats, COQ6 was located within cell processes and the Golgi apparatus of renal glomerular podocytes and in stria vascularis cells of the inner ear, consistent with an otorenal disease phenotype. Interestingly, the renal symptoms in patients improved following oral coenzyme Q10 treatment.

Infantile SRNS due to compound heterozygous *PDS22* mutations encoding decaprenyl diphosphate synthase subunit 2 has been reported in a child with Leigh syndrome (236). The podocyte-specific phenotype caused by *PDSS2* mutations leading to primary CoQ10 deficiency was shown in the *Pdss2* knockout mouse (237), in which conditional knockouts targeted to renal tubular epithelium, monocytes, or hepatocytes did not show disease manifestation. The pathogenesis of CoQ10 deficiency remains unclear. Why the podocyte in particular is affected by *PDSS2*-dependent CoQ10 deficiency is uncertain, given that this cell is less energy dependent than tubular epithelium. Possible mechanisms may include increased apoptosis, impaired nucleotide metabolism, loss of antioxidant function, and increased autophagy, all of which have been linked to CoQ10 deficiency. Importantly, renal disease due to CoQ10 deficiency may respond dramatically to CoQ10 therapy.

Risk Alleles in Patients of African Descent

In addition to the monogenic and mitochondrial forms of FSGS, genetic polymorphisms may account for the higher incidence of FSGS and ESRD seen in African Americans of all ages. This genetic predisposition has been linked to allelic variants in human chromosome 22 in a region including coding for myosin heavy chain 9 (*MYH9*) and apolipoprotein L1 (*APOL1*), which are in close linkage disequilibrium (238,239). Myosin heavy chain 9 is a component of the podocyte cytoskeleton, and *MYH9* mutations are known to cause a rare autosomal dominant form of FSGS in patients with Epstein-Fechtner syndromes (renal disease, sensorineural

deafness, and macrothrombocytopenia) (240,241). Genome-wide scans identified three single nucleotide polymorphisms in intron 23 of the *MYH9* gene as conferring risk for primary FSGS and hypertensive ESRD among blacks in an autosomal recessive model (239,242). However, further investigation revealed two independent sequence variants (called G1 and G2) in the last exon of the neighboring *APOL1* gene that had a stronger association with FSGS, with a combined signal that was increased by a factor of 35 over that of *MYH9* (238,243). Thus, *APOL1* was implicated as the actual susceptibility gene. Recent studies confirmed that *APOL1* variants are associated with FSGS, hypertensive kidney disease, HIVAN, and ESRD (244–246), but not with IgA nephropathy (245), in African Americans. Moreover, these variants are also associated with microalbuminuria (247) and younger age at onset of dialysis in nondiabetic African Americans (248) suggesting that these might be a general risk factor for kidney disease beyond FSGS.

Selection tests in Europeans and Africans revealed that the *APOL1* G1 and G2 haplotypes were under strong selective pressure only in Africa (238). Apolipoprotein L1 is a constituent of high-density lipoprotein (HDL) particles in the blood and confers protection against sleeping sickness by lysing *Trypanosoma brucei brucei*. The emergence of subspecies of trypanosoma resistant to lysis by apolipoprotein L1 led to natural selection of human *APOL1* variants that could counteract the resistance. This subspecies, *Trypanosoma brucei rhodesiense*, produces a virulence factor named serum resistance-associated (SRA) factor that neutralizes APOL1 by binding to its C terminus. Both *APOL1* G1 and G2 variants have alterations in the amino acid sequence within the C-terminal SRA-binding site, thereby preserving lytic activity and conferring *T. b. rhodesiense* resistance to heterozygous carriers. Analogous to the sickle cell allele, which confers resistance to malaria, the parasiticidal effect of APOL1 is dominant, whereas the association with host disease is recessive.

How the *APOL1* G1 and G2 variants act mechanistically on the podocyte to cause FSGS has not been delineated. Renal allografts from donors carrying two risk alleles show a higher rate of failure, suggesting that intrinsic expression is important (249). APOL1 is normally expressed in podocytes, proximal tubular epithelial cells, and arterial endothelium, with reduced podocyte expression and de novo arterial medial myocyte expression seen in HIVAN and FSGS (250). Whether this expression reflects endogenous synthesis or uptake from the circulation is uncertain. APOL1 may have a role in lipid metabolism and autophagy (251), functions that are important in maintaining podocyte homeostasis (252).

ADAPTIVE FSGS

Adaptive FSGS results from structural and functional adaptations mediated by intrarenal vasodilatation, increased glomerular capillary pressures, and increased plasma flow rates, producing *glomerular hypertension* (253). These responses may be initially compensatory, in the setting of a reduced number of functioning nephrons, or they may occur in settings that place hemodynamic stress on an initially normal nephron population (see Table 6.1). Adaptive FSGS plays an important role in the progression of many forms of chronic renal disease, in addition to primary glomerular diseases (254).

Clinical Features

Conditions associated with adaptive FSGS include morbid obesity (255), hypertensive arterionephrosclerosis, increased lean muscle mass (e.g., due to bodybuilding) (256), oligomeganephronia, sickle cell disease, reflux nephropathy and chronic pyelonephritis, solitary kidney (257), very low birth weight (258), cyanotic congenital heart disease (259), cholesterol embolization (260), allograft kidney, and any advanced renal disease leading to significant loss of functioning nephrons. Patients with adaptive FSGS have variable proteinuria that is most often subnephrotic. Proteinuria in some patients may reach nephrotic levels but is generally less severe than in primary FSGS. Even those adaptive FSGS patients with nephrotic-range proteinuria usually have normal serum albumin levels and lack full nephrotic syndrome, which is a helpful clinical distinction (255). A history of long-standing systemic hypertension and established renal insufficiency usually precedes the onset of proteinuria in hypertensive arterionephrosclerosis.

Obesity-related glomerulopathy (ORG) occurs with all grades of obesity (body mass index [BMI] > 30.0) (255) but is most commonly reported in those with morbid obesity (BMI > 40.0). In the initial stages, the GFR may be elevated (greater than 120 mL/min). Oligomeganephronia is a rare congenital form of bilateral renal hypoplasia without renal dysplasia or other urinary tract abnormalities. Patients present with polyuria and polydipsia in infancy and develop progressive renal insufficiency and proteinuria during the later stages of disease (261). Most cases of oligomeganephronia are sporadic, but some are associated with ocular abnormalities and *PAX2* mutations (261).

Pathologic Features

Light Microscopy

Segmental sclerosis lesions are typically perihilar, and podocyte hypertrophy and hyperplasia are infrequent in adaptive FSGS. However, cellular and collapsing FSGS lesions may occur in the setting of acute ischemia (e.g., due to cholesterol embolization). Importantly, glomerular hypertrophy (glomerulomegaly) is commonly present (Fig. 6.46). This feature

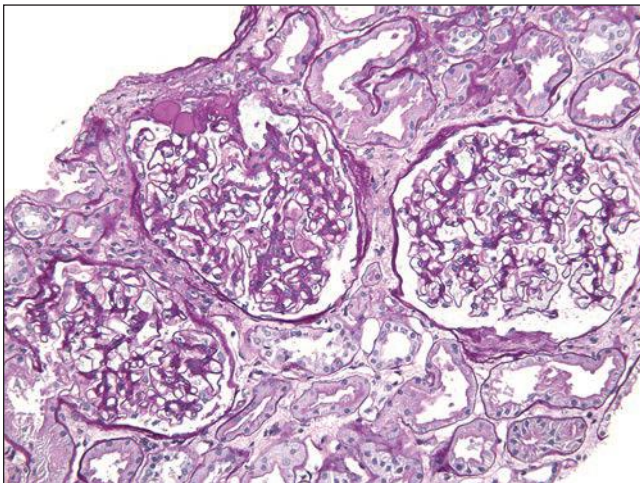


FIGURE 6.46 FSGS, perihilar variant. In this case of obesity-related glomerulopathy, one glomerulus shows segmental perihilar hyalinosis. Glomeruli are moderately enlarged. (PAS, $\times 200$.)

should be assessed in a plane of section that transects the hilus of the glomerulus. The measured glomerular diameter generally exceeds 1.5 times normal (255). Hypertrophied glomeruli can be easily recognized without morphometric analysis if they fill the microscopic visual field when examined with a 40 \times objective lens. In secondary FSGS resulting from loss of renal mass, there is usually extensive global glomerulosclerosis with corresponding tubular atrophy and interstitial fibrosis.

In hypertensive arterionephrosclerosis, prominent arteriolar hyalinosis and arteriosclerosis are common. Glomerulosclerosis predominantly affects the outer cortex and may be accompanied by subcapsular scars. Atubular glomeruli are commonly identified in the subcapsular region. These display cystic dilatation of the Bowman space with a shrunken tuft that may be partially resorbed into the Bowman capsule (Fig. 6.47). Chronic tubulointerstitial disease is invariably present. Ischemic atrophic tubules may resemble endocrine glands (“endocrine tubular atrophy”).

In oligomeganephronia, kidneys are small and normally shaped but display only four or five lobes, compared to the normal 11 to 14. Glomerular number is one fifth normal, and there is marked hypertrophy of glomeruli (two to three times normal size), in addition to enlargement of the juxtaglomerular apparatus and tubules (262).

Immunofluorescence Microscopy

Focal and segmental glomerular staining for IgM and C3 is seen in lesions of segmental sclerosis.

Electron Microscopy

Foot process effacement is usually severe overlying segmental sclerosis lesions. However, careful attention should be directed to patent capillaries, where the degree of foot process effacement is typically relatively mild and focal, involving less than 50% of the total podocyte surface area (see Fig. 6.43). This feature of adaptive FSGS probably relates to the more heterogeneous

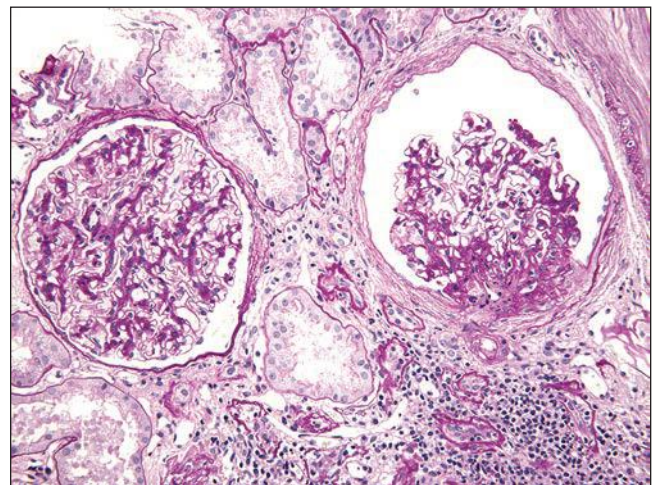


FIGURE 6.47 FSGS, perihilar variant (hypertensive nephrosclerosis). The glomerulus on the right shows perihilar FSGS and shrinkage of the glomerular tuft with wrinkling of the basement membranes. Unlike collapsing variant FSGS, there is no swelling or hyperplasia or glomerular epithelial cells. (PAS, $\times 200$.)

state of adaptation in individual glomeruli. However, because of sample variability and disease variation, this criterion alone does not reliably distinguish adaptive FSGS from primary FSGS. The combination of mild foot process effacement, perihilar segmental sclerosis, and glomerulomegaly in a biopsy should raise strong suspicion of adaptive FSGS, requiring close clinical correlation. In hypertensive arterionephrosclerosis, there may be ischemic-type wrinkling and thickening of the GBMs and subendothelial widening (see Fig. 6.43).

Pathologic Differential Diagnosis

The differential diagnosis includes primary FSGS and other secondary causes of FSGS (see Table 6.1). The absence of full nephrotic syndrome and findings of glomerulomegaly, perihilar FSGS, and focal foot process effacement favor a diagnosis of adaptive FSGS.

Etiology and Pathogenesis of Adaptive FSGS

Adaptive FSGS is mediated by increased glomerular capillary pressures and flow rates as part of an adaptive response to the reduced number of functioning nephrons or other hemodynamic stresses. Increased wall tension causes mechanical strain on the connection between the podocyte foot process and the GBM, leading to local dilatation of capillaries and podocyte stretch. Severe and prolonged tension causes progressive podocyte cell body attenuation, pseudocyst formation, and detachment from the GBM. Podocyte detachment exposes bare patches of the GBM that may form synechial attachment to the Bowman capsule, permitting misdirected flow of filtrate, obliteration of the tubular pole, and microcystic dilatation of the Bowman capsule (263). These synechiae form the nidus for segmental sclerosis lesions to develop.

The sequence of events and the central role of podocyte depletion have been elucidated in several animal models of adaptive FSGS. In the rat remnant kidney model (264), compensatory glomerular hypertrophy and hypertension occur in the remnant glomeruli, due to reflex vasodilatation in both the afferent and efferent arterioles, but which is more pronounced in the afferent arteriole. This leads to glomerular hypertension (increased glomerular capillary pressures and flows) and an elevated single-nephron GFR proportionate to the amount of kidney tissue excised. The resulting increase in glomerular volume and surface area leads to a reduction in podocyte density and podocyte detachment, followed by covering of the exposed stretches of the GBM by cells recruited from the Bowman capsule and synechial attachments between the glomerular tuft and Bowman capsule (265). This leads to misdirected flow of the glomerular ultrafiltrate into the interstitium, instead of the urinary space, which stimulates fibrogenesis and compromises the tubular outlet, leading to dependent tubular atrophy (263). The synechial attachments between the denuded basement membrane and parietal epithelial cells form a nidus for the growth of FSGS lesions, which typically begin in the perihilar region (265).

In hypertensive arterionephrosclerosis, elevated glomerular capillary pressure is associated with systemic hypertension and adaptive response to loss of functioning nephrons. In ORG and increased lean muscle mass (e.g., in bodybuilders), the increased body mass relative to kidney mass is associated with increased GFR and increased renal plasma flow. Hypoxia

related to sleep apnea activates the sympathetic nervous system, thereby stimulating the renin-angiotensin system (RAS) and glomerular hypertension. In addition, obese subjects show increased levels of growth hormone and insulin-like growth factor, which may contribute to renal injury in ORG (266). In the secondary form of FSGS associated with anabolic steroid use, the etiology of FSGS may be multifactorial, including elevated BMI leading to hyperfiltration, exercise-induced systemic hypertension, high-protein diet and other supplements, and possible direct toxic effects of anabolic steroids on podocytes (256).

The loss of a critical number of nephrons promotes the activation of the RAS, exacerbating proteinuria and setting the stage for progressive glomerulosclerosis regardless of the initial cause. Angiotensin II also has direct proapoptotic effects on podocytes (98). Excessive protein uptake by podocytes induces podocyte TGF β (267), which promotes apoptosis and leads to endoplasmic reticulum stress, cytoskeletal reorganization, and dedifferentiation (268).

Animal Models Prove Podocyte Depletion Theory of FSGS

Podocyte depletion is now recognized as a final common pathway to FSGS in primary and secondary forms (3). Genetic engineering in rodents has been exploited to prove the theory that podocyte depletion is sufficient to cause FSGS. These models allow delivery of a toxin specifically and exclusively to podocytes, with determination of cell fate over time. Together, the findings from these important experimental models have provided groundbreaking insight into the role of podocyte loss as a common mechanism underlying all forms of FSGS, regardless of etiology. The hDTR Fischer 344 transgenic rat model expresses human diphtheria toxin receptor under the control of a podocyte-specific promoter, podocin. The human receptor was chosen because the rat homologue does not recognize diphtheria toxin. In this model, a single brief exposure to diphtheria toxin causes podocyte death by the inhibition of protein synthesis (269,270). The degree of podocyte depletion correlates with structural and functional measures of glomerular injury (270). Loss of up to 20% of podocytes causes transient proteinuria with mild mesangial matrix increase and no effect on renal function, whereas 21% to 40% podocyte loss results in synechiae and mild FSGS accompanied by sustained mild proteinuria and normal renal function. Loss of greater than 40% of podocytes leads to well-developed FSGS with high-grade proteinuria and renal insufficiency (270). These findings support the concept that there is a threshold level of podocyte loss above which podocytes can no longer compensate by hypertrophy for their reduced numbers and FSGS lesions develop.

In a model in which podocytes expressed human CD25 (human interleukin 2 light receptor) under control of the nephrin promoter, injection of *Pseudomonas* exotoxin fused to the variable region of anti-CD25 antibody leads to dose-dependent progressive proteinuria and glomerulosclerosis (269). In a subsequent chimeric model in which only some podocytes expressed CD25, Ichikawa et al. (271) showed that dedifferentiation spread to neighboring toxin-resistant podocytes that had escaped the initial insult, suggesting that injury can propagate from injured podocytes to previously

healthy podocytes in a domino-like fashion, leading to progressively more severe injury. This local spread of podocyte injury could explain the segmentality of the lesions seen pathologically (99). Although the mediators are unknown, a secondary wave of podocyte injury hypothetically might decrease podocyte survival factors that signal through nephrin and glutamate receptors (272) or might increase noxious factors, such as shear stress, angiotensin II, or TGF β (273). In the diphtheria toxin model, podocytes are shed into the urine for months after a brief toxin exposure, indicating a secondary, autonomous phase of podocyte loss that likely contributes to progressive sclerosis (274). Progressive podocyte loss and progressive glomerulosclerosis in this model are preventable by angiotensin II blockade (combined enalapril and losartan), indicating that activation of the RAS is important in the progressive stage of FSGS, after the initial injury has abated (275).

Historically, one of the most studied animal models of FSGS is Adriamycin nephropathy, which can be produced in rats and only a few mouse strains. Anthracycline doxorubicin (Adriamycin) causes FSGS in BALB/c mice, whereas most other mouse strains are protected. The cause of this strain susceptibility in BALB/c mice has been identified as an ancestral mutation in *Prkdc* (protein kinase, DNA-activated, catalytic polypeptide), which is part of the repair machinery for double-stranded DNA breaks (276). BALB/c mice exposed to Adriamycin are unable to perform non-homologous end-joining DNA repair after intercalation of doxorubicin into podocyte DNA, leading to mtDNA depletion (276). This murine model illustrates the importance of protective mechanisms against genotoxic stress to enhance podocyte longevity.

Another animal model widely used to study FSGS is the PAN toxin model in rodents (277,278). In this model, puromycin causes podocyte injury by generation of oxygen radicals. Affected animals demonstrate lesions of MCD or FSGS, depending on the cumulative dose used. At lower doses, podocytes show reversible diffuse foot process effacement associated with alterations in the actin cytoskeleton and altered expression of nephrin, podocin, podocalyxin, and actin. With higher doses of PAN, pseudocysts form beneath podocytes, which subsequently undergo apoptosis or necrosis and are shed into the urine, followed by replacement by parietal cells derived from the Bowman capsule (279).

Treatment and Prognosis of Adaptive FSGS

Treatment of adaptive FSGS consists of ameliorating the underlying cause, where possible, such as control of systemic blood pressure, weight loss, and sleep apnea therapy. Steroids and immunosuppressive therapy have no proven benefit in adaptive FSGS and are contraindicated in ORG, as these may exacerbate obesity or unmask latent diabetes mellitus. The mainstay of therapy is drugs that inhibit the RAS (such as angiotensin-converting enzyme [ACE] inhibitors and angiotensin receptor blockers), which lower intraglomerular filtration pressures through the inhibition of angiotensin II-mediated vasoconstriction of the efferent arteriole. ACE inhibition also augments bradykinin, which contributes to efferent arteriolar dilatation. The resulting reduction in proteinuria exerts a protective effect on podocytes and tubular cells.

VIRUS-ASSOCIATED FSGS

Viruses may cause podocyte injury via direct infection of renal epithelial cells or by inducing the release of cytokines that interact with podocyte receptors. HIVAN is the best studied example of FSGS caused by direct viral infection (see Chapter 11). FSGS has also been linked to other infections, including parvovirus B19 (280), simian virus 40 (281), cytomegalovirus (CMV) (282,283), and Epstein-Barr virus; however, the evidence of a role for viral infection in these cases is relatively weak, being derived from retrospective epidemiologic studies and case reports. FSGS has also been described in some patients with HCV infection but is confounded by the presence of other risk factors for FSGS in this population, including black race, hypertension, and intravenous drug use (284).

Clinical Features and Pathogenesis

The clinical characteristics of virus-associated FSGS other than HIVAN have not been described in detail. Parvovirus B19 infection has been linked to one case each of FSGS associated with sickle cell disease (285) and de novo FSGS in a renal allograft (286). Tanawattanacharoen et al. (287) reported a high prevalence of amplifiable parvovirus B19 DNA in renal tissues showing diverse diseases, including 8 of 10 patients with idiopathic FSGS, 9 of 10 patients with collapsing FSGS, 6 of 10 patients with membranous glomerulonephritis, 5 of 10 patients with MCD, and two of four cancer nephrectomy samples. The prevalence of parvovirus B19 DNA was significantly greater among patients with idiopathic FSGS and collapsing FSGS compared to other diagnoses (287). However, parvovirus B19 DNA could not be demonstrated by in situ hybridization in any of these tissues, suggesting that the virus was probably not replicating and might represent latent DNA from past infection. Moudgil et al. (280) also showed a significantly higher prevalence of parvovirus B19 DNA in renal biopsies and peripheral blood from patients with primary collapsing FSGS compared to HIVAN, idiopathic FSGS, and controls but were able to demonstrate parvovirus B19 DNA by in situ hybridization in glomerular parietal and visceral epithelial and tubular cells, suggesting a direct pathogenetic relationship between parvovirus B19 infection and collapsing FSGS (280).

Li et al. (281) showed a higher frequency of SV40 infection by polymerase chain reaction (PCR) in urine cells, peripheral blood monocytes, and renal biopsies of patients with FSGS (including primary FSGS and HIVAN) compared to minimal change disease and membranous glomerulonephritis.

Collapsing FSGS leading to ESRD was reported in a 60-year-old immunocompetent Afro-Caribbean woman with primary CMV infection, in whom CMV DNA was detected by PCR in the renal biopsy (282). Another case report described collapsing FSGS in a 16-year-old black girl with CMV viremia; in that case, renal function improved on corticosteroids and ganciclovir (283).

Pathologic Findings

The pathologic features of virus-associated FSGS are nonspecific. As noted above, parvovirus B19, SV40 infection, and CMV may be associated with collapsing FSGS. Testing for

the presence of parvovirus B19 or CMV infection by *in situ* hybridization or immunohistochemical staining may reveal evidence of viral infection but is not used routinely in most renal pathology practices unless there is other clinical evidence suggesting viral infection.

DRUG-ASSOCIATED FSGS

Several drugs, both illicit and therapeutic, have been linked to the development of FSGS, including heroin and other opiates, pamidronate, interferon, calcineurin inhibitors, sirolimus, lithium, and anabolic steroids. As with other forms of drug-induced renal disease, a causative role is supported by a temporal association with drug use, the absence of any other plausible explanation for renal disease, and clinical improvement in renal abnormalities following discontinuation of the offending agent.

Clinical Features

The association of FSGS with illicit opiates, specifically heroin, was first described in 11 of 13 black intravenous drug users (IVDU) in 1974 (288). Patients presented with nephrotic syndrome and renal insufficiency and progressed rapidly to ESRD. This entity subsequently became known as “heroin-associated nephropathy,” even though the pathologic spectrum of glomerular disease in IVDU (most of whom are opiate abusers) is heterogeneous and includes membranoproliferative glomerulonephritis (MPGN) due to hepatitis C infection, secondary amyloidosis, and postinfectious glomerulonephritis, in addition to FSGS (60,289). FSGS and nephrotic syndrome have also been linked to intravenous use of pentazocine and tripeleonnamine (290). Importantly, heroin-associated FSGS mostly affects African Americans, whereas MPGN predominates in Caucasian IVDU (291–293), consistent with the general increased predisposition to FSGS seen in African Americans.

Interestingly, the incidence of heroin-associated FSGS has diminished dramatically since its peak in the early 1980s, despite the growing prevalence of heroin use and the increasing purity of street heroin (294). This finding suggests the possibility that heroin-associated FSGS might be caused by other factors (e.g., unknown adulterants used prior to the 1980s), rather than heroin itself. An alternative explanation for the decline is that the emergence of HIVAN in the 1980s may have superseded or masked the development of heroin-associated FSGS.

The bisphosphonate pamidronate is an osteoclast inhibitor used for the control of hypercalcemia in patients with multiple myeloma and metastatic carcinoma. The inadvertent use of supratherapeutic doses of pamidronate was associated with the development of nephrotic syndrome, renal failure, and collapsing FSGS (295–298). In all of these cases, baseline renal function was normal before pamidronate therapy, and nephrotic-range proteinuria (8 to 17 g/24 h) developed following drug exposure. Deterioration in renal function occurred on average after 2 to 3 years of therapy with cumulative pamidronate doses of 2 to 3 g. Proteinuria and renal failure typically improved after withdrawal of the drug.

Interferon alfa (used to treat hepatitis C), interferon beta (indicated for multiple sclerosis), and interferon gamma (formerly used in idiopathic pulmonary fibrosis and indicated for chronic granulomatous disease and malignant osteopetrosis)

have all been reported to induce collapsing variant FSGS (71). Renal disease improved following discontinuation of interferon therapy. FSGS was identified in 50% of patients with a history of chronic lithium use undergoing renal biopsy and was associated with proteinuria greater than 1 g/d (299). In the transplanted kidney, collapsing variant FSGS has been linked to the use of calcineurin inhibitors (150,300) and the mammalian target of rapamycin (mTOR) inhibitor, sirolimus (301).

Pathologic Features

Most of the reported cases of heroin-associated FSGS were the NOS variant, although some cases with collapsing features (i.e., collapsing variant) have been noted (60). Lithium is associated with FSGS NOS and disproportionately severe tubulointerstitial scarring and glomerulomegaly, suggesting that some of these cases represent secondary (adaptive) FSGS related to chronic tubulointerstitial nephropathy. However, approximately 37% of lithium-associated FSGS cases show diffuse (greater than 50%) foot process effacement, and lithium has been reported to induce MCD, suggesting a role for direct podocyte toxicity in some cases with nephrotic proteinuria (299). Pamidronate, calcineurin inhibitors, sirolimus, and interferon have all been linked to collapsing FSGS (71,150,295,300,301). Interferon therapy typically induces TRIs in endothelial cells, which is a helpful albeit nonspecific ultrastructural feature, as similar findings are seen in HIVAN and lupus podocytopathy (72).

Pathogenesis

Given the absence of animal models of heroin-induced FSGS and the lack of prospective epidemiologic studies to support the existence of heroin-associated nephropathy, it is possible that the occurrence of FSGS in IVDU might reflect differences in genetic susceptibilities that predispose to the development of nephropathy in African Americans (such as ApoL1 variants) or other genetic variables (e.g., HLA-BW53 (302)), in addition to a direct toxicologic effect of heroin (289).

Pamidronate has direct toxic effects on osteoclasts, including disruption of the actin cytoskeleton, suggesting the possibility of a similar effect on the podocyte cytoskeleton. In some cases, increased numbers of podocyte mitochondria are seen by electron microscopy, suggesting a possible role for mitochondrial toxicity (295,303). The podocyte has receptors for interferon alfa and interferon beta and expresses major histocompatibility complex class II antigen in response to interferon gamma, suggesting potential direct podocyte effects of interferon.

Cases of FSGS associated with calcineurin inhibitors may be mediated by acute vasoocclusive injury, as collapsing FSGS has also been reported with renal atheroembolism (260) and severe renovascular disease (304). Sirolimus may induce FSGS by reducing podocyte expression of critical proteins in the slit diaphragm and cytoskeleton, including nephrin (305).

FSGS IN SYSTEMIC LUPUS ERYTHEMATOSUS (LUPUS PODOCYTOPATHY)

There are several reports of patients with SLE, nephrotic syndrome, and renal biopsy findings of MCD or FSGS (72,306–308). Biopsies typically show severe diffuse foot process effacement in the absence of peripheral capillary wall immune

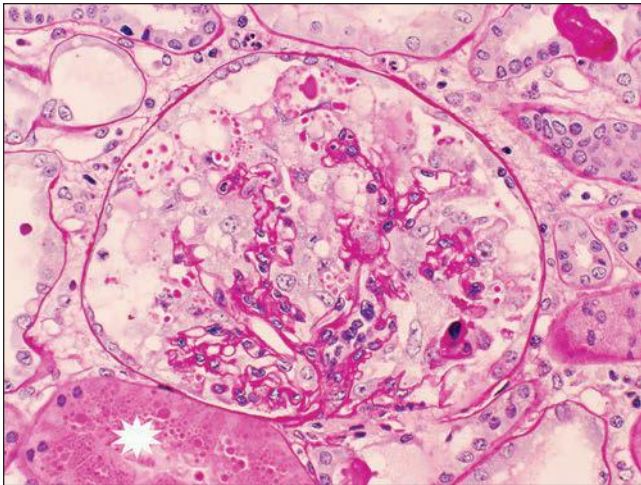


FIGURE 6.48 Collapsing FSGS in a patient with systemic lupus erythematosus and nephrotic syndrome. There is global capillary collapse. Podocytes are hypertrophied and display vacuoles and prominent PAS-positive droplets. Immunofluorescence microscopy revealed “full-house” mesangial staining for IgG, IgM, IgA, C3, and C1q. Electron microscopy showed mesangial electron-dense deposits. The adjacent tubule contains prominent resorption droplets (*asterisk*). (PAS, $\times 330$.)

deposits or endocapillary hypercellularity; however, mesangial immune deposits, with or without mesangial hypercellularity, may be present. In cases with FSGS, collapsing variant and NOS variant have been described (Fig. 6.48) (72). Endothelial TRIs may be seen (72). The higher incidence of podocytopathy in SLE than in the general population and the rapid remission of nephrotic syndrome after steroid therapy in all 11 patients with MCD and three of seven with FSGS support the concept of a “lupus podocytopathy” (306,307). Lupus podocytopathy is usually seen early in the course of SLE (within 1 month of diagnosis in many cases (307)) or after a disease flare. The pathogenesis may involve T-cell dysregulation, altered cytokine milieu, or nonsteroidal anti-inflammatory drug (NSAID) use (in some cases of MCD). Importantly, this entity appears to be a highly steroid-responsive form of FSGS.

C1Q NEPHROPATHY

Definition

C1q nephropathy (C1qN) is an uncommon glomerular disease characterized by dominant or codominant ($\geq 2+$) mesangial staining for C1q, usually with immunoglobulins, in the absence of clinical or laboratory evidence of SLE (309). The etiology and pathogenesis of C1qN are unknown and the clinical and pathologic manifestations are heterogeneous, possibly reflecting the use of variable diagnostic criteria and differences in standard renal biopsy practice among different populations studied. For example, the original case series of Jennette and Hipp excluded cases with histologic features of MPGN and specifically noted the absence of codominant staining for IgA, whereas other studies have included at least some cases with MPGN features and/or codominant IgA staining. Most approaches to diagnosis of C1q nephropathy require exclusion of MPGN and IgA nephropathy.

Cases of C1qN fall into one of two clinical-pathologic categories: (1) a podocytopathy with pathologic features of FSGS or MCD (i.e., with minimal histologic alterations) and variable, often diffuse foot process effacement, or (2) a proliferative glomerulonephritis of unknown etiology. In our experience, most cases fall into the first category. C1qN with MCD/FSGS features usually presents with the nephrotic syndrome, (6) whereas those with features of proliferative glomerulonephritis have more diverse clinical presentations, including asymptomatic urinary abnormalities, heavy proteinuria, gross hematuria, rapidly progressive glomerulonephritis, or chronic renal insufficiency (310,311). There are also case reports of C1qN presenting in children with either rapidly progressive glomerulonephritis (312) or gross hematuria and no proteinuria (313). However, it remains to be determined whether C1qN represents a single disease with diverse clinical and pathologic features (akin to primary IgA nephropathy) or different diseases that share a common immunopathologic finding of C1q predominant deposits.

Clinical Features

The overall biopsy prevalence of C1qN ranges from 0.2% (6) to 9% (314) but has been reported in up to 16.3% of children with treatment-resistant nephrotic syndrome (315). C1qN is most commonly diagnosed in children and young adults but may occur at any age. In the United States, it may be more common in African Americans than Caucasians (60%, 74%, and 82% of cases in three series (6,309,316)). However, one other pediatric study reported a predominance (78%) of Hispanic patients (315). By definition, SLE must be excluded clinically and serologically. Serum complement levels should be normal and if these are decreased, an alternative diagnosis, such as lupus nephritis or primary MPGN, should be considered.

In the first report of C1qN, Jennette and Hipp (309) described 15 patients who presented in the second or third decade of life with nephrotic-range proteinuria in most (93%), mostly normal renal function, and hematuria in less than 50% of cases. Biopsies showed proliferative glomerulonephritis ($n = 8$), mesangial hypercellularity ($n = 3$), or MCD ($n = 2$); light microscopy was not available in two cases. Nine patients received steroids, and only one had a decline in renal function at last follow-up. Subsequently, Iskandar et al. (317) described 15 pediatric patients with C1qN (age 2 to 16 years), nine of whom were fully nephrotic and were steroid resistant or steroid dependent prior to undergoing renal biopsy. Seven biopsies showed FSGS and eight showed MCD. Nine patients received steroids, three underwent remission, and two progressed to ESRD. The Columbia University series consisted of 19 patients whose mean age was 24.2 years (range 3 to 42 years) and clinical presentations included nephrotic-range proteinuria (78.9%), nephrotic syndrome (50%), and renal insufficiency (27.8%) (6). FSGS was seen in 17 cases and MCD in 2. Eleven patients received steroids, with one complete remission and six partial remissions; two patients had declining renal function and two progressed to ESRD at last follow-up.

The largest study of C1qN to date included 28 children and 44 adults from Slovenia, all of whom were white and 68% of whom were male (310). Based on light microscopy, cases were classified as no lesions (37.5%), FSGS (15.2%),

proliferative glomerulonephritis (27.8%), and other findings (19.4%). Renal clinical presentations included nephrotic syndrome or nephrotic-range proteinuria in 47%, renal insufficiency in 46%, and hematuria in 69%. Most patients with no lesions had the nephrotic syndrome (63%) and presumably MCD-like disease, all FSGS cases presented with the nephrotic syndrome, whereas those with proliferative glomerulonephritis presented with asymptomatic urinary abnormalities (20%) or chronic kidney disease (75%). At last follow-up, 77% of those with MCD-like lesions had remission of the nephrotic syndrome following immunosuppressive therapy; progression to ESRD occurred in 33% of FSGS cases (despite treatment in most cases); and renal disease was stable in 57% of those with proliferative glomerulonephritis, only a minority of whom (4 of 14 patients) received immunosuppressive therapy.

In a large Japanese series of 61 patients (age 1 to 67 years), 36 (59%) had asymptomatic urinary abnormalities that were discovered on school screening tests or random urine testing and the remaining 25 (41%) had the nephrotic syndrome (311). Biopsy findings included MCD (75%), FSGS (13%), and proliferative glomerulonephritis (12%). MCD was more common in the nephrotic group, and hematuria was more common in the asymptomatic group. Nine patients in the asymptomatic group received steroids because of biopsy findings of FSGS or proliferative glomerulonephritis, with progression to ESRD in two cases. Twenty-four other patients in the asymptomatic group had persistent urinary abnormalities at last follow-up, while 10 had normal urinalysis. All 25 patients with nephrotic syndrome received steroids, with 8 complete remissions, 3 with persistent proteinuria, 13 with frequent relapses, and 1 with developing ESRD.

C1q nephropathy has also been reported to occur *de novo* in the renal allograft, where it is considered a morphologic finding of unclear significance because most patients lack significant proteinuria (318).

Pathologic Features

Light Microscopy

C1qN may show normal-appearing glomeruli, mesangial proliferation, focal or diffuse endocapillary proliferation, or FSGS. Collapsing, cellular, and NOS variants of FSGS are seen (6). Transition from MCD to FSGS and loss of C1q staining may be observed in repeat biopsies (311). Three recent pediatric studies of C1qN described a predominance of FSGS and MCD. A study on 12 Slovenian children revealed FSGS in 6 patients, MCD in 4, and focal glomerulonephritis in 2 (314). A series of 20 children from Tennessee included 8 cases with FSGS and 6 with MCD (316). The remaining children had either mesangial proliferation or globally sclerotic glomeruli without segmental lesions. A series of 30 children with C1qN in Japan included 22 with MCD, 2 with FSGS, and 6 with mesangial proliferative glomerulonephritis (319).

Immunofluorescence Microscopy

Glomeruli display mesangial staining for C1q, with variable costaining for IgG, IgM, IgA, and C3 in a similar distribution (Fig. 6.49). Most reports require $\geq 2+$ staining intensity of C1q. The pattern of C1q staining is typically comma-shaped because of the tendency for deposits to pool in the paramesangial regions. Most cases have similarly intense staining for IgG. Of note, codominant staining for IgA is

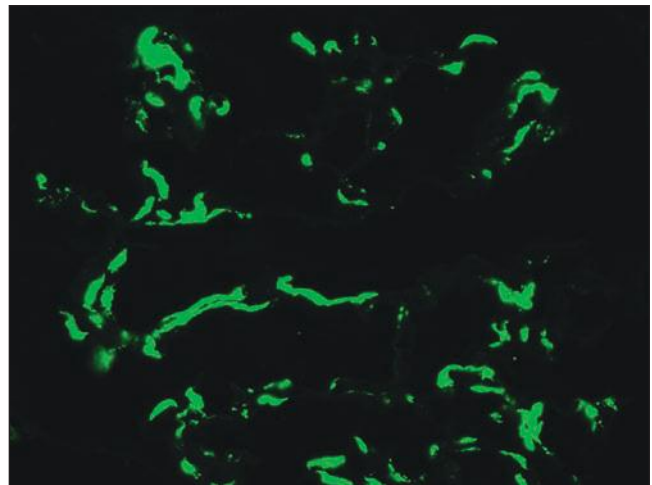


FIGURE 6.49 C1q nephropathy. Mesangial and paramesangial comma-shaped deposits of C1q are seen. (FITC anti-human C1q, $\times 400$.)

diagnostic of IgA nephropathy and excludes the diagnosis of C1qN. Small amounts of peripheral capillary wall staining may also be seen.

Electron Microscopy

Mesangial electron dense deposits are uniformly seen and are typically paramesangial in location (i.e., subjacent to the glomerular basement reflection) (Fig. 6.50). In the majority of cases, particularly those with more severe proteinuria, moderate to marked foot process effacement is noted in the absence of peripheral capillary wall deposits, a finding that supports podocytopathy. Peripheral capillary wall deposits tend to be sparse, and endothelial TRIs are absent. If endothelial TRIs are seen, SLE and HIV infection should be carefully excluded.

Differential Diagnosis

The differential diagnosis of C1qN includes lupus nephritis, HIV-related “lupus-like” glomerulonephritis, and primary MPGN type 1, all of which commonly exhibit some degree of C1q staining. A history of hypocomplementemia should suggest an alternate diagnosis than C1qN (6). Codominant staining for IgA is diagnostic of IgA nephropathy and excludes the diagnosis of C1qN.

Etiology and Pathogenesis

C1q is synthesized constitutively by antigen-presenting cells and is present in the circulation together with C1r and C1s as the C1 complex, the first component of the classical pathway of complement activation. Following binding of immunoglobulin to antigen, C1q binds to the CH2 domain of IgG and the CH3 domain of IgM, leading to cleavage of C4 and C2 by C1s, and generation of the classical C3 convertase (C4b2b). The frequent codeposition of IgG or IgM in C1qN supports the concept of an immune complex-mediated glomerulonephritis, particularly in cases that show features of proliferative glomerulonephritis (309). However, C1q is a highly cationic molecule that also binds to other anionic substrates, ligands,

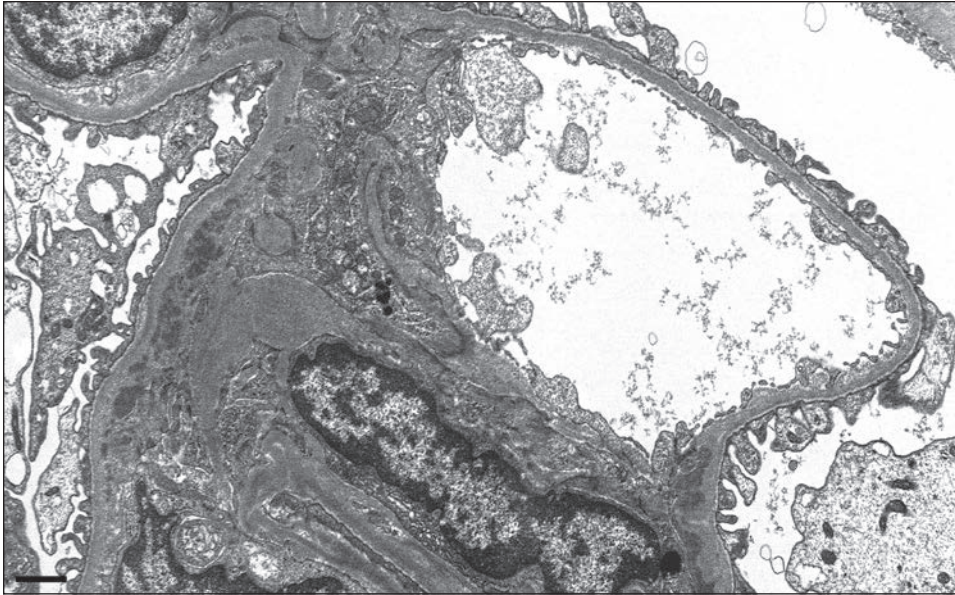


FIGURE 6.50 C1q nephropathy.

The mesangium contains immune-type electron dense deposits. Podocyte foot processes are effaced. The glomerular basement membranes appear normal. No capillary wall deposits are seen. (Electron photomicrograph, original magnification $\times 10,000$.)

and receptors, including DNA, serum amyloid A protein, C-reactive peptide, gram-negative bacteria, and lipopolysaccharide, among others (320). In addition, C1q receptors have been identified on mesangial cells (321). Therefore, mesangial staining for C1q may reflect interactions other than immune complex deposition, such as binding to neopeptides released by apoptotic cells (e.g., DNA) or other proteins trapped in the glomerulus, or binding to cell surface C1q receptors. Because C1qN lacks evidence of hypocomplementemia or other clinical evidence of systemic autoimmune or infectious disease, it has been postulated that C1q may become fixed to immunoglobulin or other anionic molecules that have been trapped nonspecifically in the mesangium in the course of glomerular proteinuria (6). Thus, in the setting of podocytopathy with heavy proteinuria (e.g., MCD or primary FSGS), the presence of C1q staining might simply reflect defective clearing of plasma proteins, rather than complement activation by immune complexes.

There is a single report of C1qN affecting two sisters, both of them presenting before 2 years of age, suggesting a possible role for genetic factors, or shared exposure to a shared environmental trigger (322). The de novo mesangial C1q deposits seen as a transient finding in the renal allograft are of unknown etiology, with no apparent clinical associations or prognostic significance (318).

Treatment and Prognosis

Pediatric C1qN cases with MCD features typically respond well to steroids but may have a higher rate of frequent relapses (315). Most of the reported cases with FSGS were treated with steroids and had generally poor responses (steroid resistance in 60%), not unlike primary FSGS (314,316,319,323). However, many of these cases were steroid dependent or steroid resistant prior to biopsy, thus the true rate of steroid responsiveness in C1qN is unknown. In the initial report of C1qN with proliferative glomerulonephritis features, none of the nine patients with

heavy proteinuria who received steroids achieved remission (309). In contrast, better outcomes were seen in other series that included young adults (6). Twelve of sixteen patients with available follow-up received treatment with corticosteroids (five of whom also received cyclosporine), and over a mean follow-up of 27.1 months, 75% had stable renal function (6). Follow-up evaluation of proteinuria was available in 13 patients, among whom 1 had complete and 6 had partial remission (6). Rituximab has shown clinical benefit in two cases of C1qN, with histologic resolution of C1q deposits in one of these cases (324).

REFERENCES

1. D'Agati VD, Kaskel FJ, Falk RJ. Focal segmental glomerulosclerosis. *N Engl J Med* 2011;365(25):2398–2411.
2. D'Agati VD. The spectrum of focal segmental glomerulosclerosis: new insights. *Curr Opin Nephrol Hypertens* 2008;17(3):271–281.
3. D'Agati VD. Pathobiology of focal segmental glomerulosclerosis: new developments. *Curr Opin Nephrol Hypertens* 2012;21(3):243–250.
4. Wei C, El Hindi S, Li J, et al. Circulating urokinase receptor as a cause of focal segmental glomerulosclerosis. *Nat Med* 2011;17(8):952–960.
5. McCarthy ET, Sharma M, Savin VJ. Circulating permeability factors in idiopathic nephrotic syndrome and focal segmental glomerulosclerosis. *Clin J Am Soc Nephrol* 2010;5(11):2115–2121.
6. Markowitz GS, Schwimmer JA, Stokes MB, et al. C1q nephropathy: a variant of focal segmental glomerulosclerosis. *Kidney Int* 2003;64(4):1232–1240.
7. Fahr T, ed. *Anatomie des morbus brightii*. In: Henke F, Lubarsch O, eds. *Handbuch der speziellen pathologischen Anatomie und Histologie*. Berlin: Springer, 1925.
8. Rich AR. A hitherto undescribed vulnerability of the juxtamedullary glomeruli in lipoid nephrosis. *Bull Johns Hopkins Hosp* 1957;100(4):173–186.
9. Churg J, Habib R, White RH. Pathology of the nephrotic syndrome in children: a report for the International Study of Kidney Disease in Children. *Lancet* 1970;760(1):1299–1302.
10. Kitiyakara C, Kopp JB, Eggers P. Trends in the epidemiology of focal segmental glomerulosclerosis. *Semin Nephrol* 2003;23(2):172–182.
11. U.S. Renal Data System. *USRDS 2011 Annual Data Report: Atlas of Chronic Kidney Disease and End-Stage Renal Disease in the United States*. Bethesda: National Institutes of Health, National Institute of Diabetes and Digestive and Kidney Diseases, 2011.

12. Kitiyakara C, Eggers P, Kopp JB. Twenty-one-year trend in ESRD due to focal segmental glomerulosclerosis in the United States. *Am J Kidney Dis* 2004;44(5):815–825.
13. Ijpeelaar DH, Farris AB, Goemaere N, et al. Fidelity and evolution of recurrent FSGS in renal allografts. *J Am Soc Nephrol* 2008;19(11):2219–2224.
14. Dijkman HB, Wetzels JF, Gemmink JH, et al. Glomerular involution in children with frequently relapsing minimal change nephrotic syndrome: an unrecognized form of glomerulosclerosis? *Kidney Int* 2007;71(1):44–52.
15. Ma J, Rossini M, Yang HC, et al. Effects of podocyte injury on glomerular development. *Pediatr Res* 2007;62(4):417–421.
16. Giannico G, Yang H, Neilson EG, et al. Dystroglycan in the diagnosis of FSGS. *Clin J Am Soc Nephrol* 2009;4(11):1747–1753.
17. Schmid H, Henger A, Cohen CD, et al. Gene expression profiles of podocyte-associated molecules as diagnostic markers in acquired proteinuric diseases. *J Am Soc Nephrol* 2003;14(11):2958–2966.
18. Yoshikawa N, Ito H, Akamatsu R, et al. Focal segmental glomerulosclerosis with and without nephrotic syndrome in children. *J Pediatr* 1986;109(1):65–70.
19. Paik KH, Lee BH, Cho HY, et al. Primary focal segmental glomerular sclerosis in children: clinical course and prognosis. *Pediatr Nephrol* 2007;22(3):389–395.
20. A report of the Southwest Pediatric Nephrology Study Group. Focal segmental glomerulosclerosis in children with idiopathic nephrotic syndrome. *Kidney Int* 1985;27(2):442–449.
21. Hogg R, Middleton J, Vehaskari VM. Focal segmental glomerulosclerosis—epidemiology aspects in children and adults. *Pediatr Nephrol* 2007;22(2):183–186.
22. Hodson EM, Knight JF, Willis NS, et al. Corticosteroid therapy for nephrotic syndrome in children. *Cochrane Database Syst Rev* 2005;(1):CD001533.
23. Filler G, Young E, Geier P, et al. Is there really an increase in non-minimal change nephrotic syndrome in children? *Am J Kidney Dis* 2003;42(6):1107–1113.
24. Srivastava T, Simon SD, Alon US. High incidence of focal segmental glomerulosclerosis in nephrotic syndrome of childhood. *Pediatr Nephrol* 1999;13(1):13–18.
25. Abrantes MM, Cardoso LS, Lima EM, et al. Clinical course of 110 children and adolescents with primary focal segmental glomerulosclerosis. *Pediatr Nephrol* 2006;21(4):482–489.
26. El-Refaey AM, Bakr A, Hammad A, et al. Primary focal segmental glomerulosclerosis in Egyptian children: a 10-year single-centre experience. *Pediatr Nephrol* 2010;25(7):1369–1373.
27. D'Agati V. The many masks of focal segmental glomerulosclerosis. *Kidney Int* 1994;46(4):1223–1241.
28. Davison AM, Johnston PA. Glomerulonephritis in the elderly. *Nephrol Dial Transplant* 1996;11(Suppl 9):34–37.
29. Moutzouris DA, Herlitz L, Appel GB, et al. Renal biopsy in the very elderly. *Clin J Am Soc Nephrol* 2009;4(6):1073–1082.
30. Ingulli E, Tejani A. Racial differences in the incidence and renal outcome of idiopathic focal segmental glomerulosclerosis in children. *Pediatr Nephrol* 1991;5(4):393–397.
31. North American Pediatric Renal Transplant Cooperative Study (NAPRTCS). *Annual Report 2011*. Boston: NAPRTCS Administrative Office, 2011.
32. Haas M, Meehan SM, Karrison TG, et al. Changing etiologies of unexplained adult nephrotic syndrome: a comparison of renal biopsy findings from 1976–1979 and 1995–1997. *Am J Kidney Dis* 1997;30(5):621–631.
33. Korbet SM. Primary focal segmental glomerulosclerosis. *J Am Soc Nephrol* 1998;9(7):1333–1340.
34. Haas M, Spargo BH, Coventry S. Increasing incidence of focal-segmental glomerulosclerosis among adult nephropathies: a 20-year renal biopsy study. *Am J Kidney Dis* 1995;26(5):740–750.
35. Korbet SM, Genchi RM, Borok RZ, et al. The racial prevalence of glomerular lesions in nephrotic adults. *Am J Kidney Dis* 1996;27(5):647–651.
36. Dragovic D, Rosenstock JL, Wahl SJ, et al. Increasing incidence of focal segmental glomerulosclerosis and an examination of demographic patterns. *Clin Nephrol* 2005;63(1):1–7.
37. Gulati S, Sharma AP, Sharma RK, et al. Changing trends of histopathology in childhood nephrotic syndrome. *Am J Kidney Dis* 1999;34(4):646–650.
38. Korbet SM, Schwartz MM, Lewis EJ. The prognosis of focal segmental glomerular sclerosis of adulthood. *Medicine (Baltimore)* 1986;65(5):304–311.
39. Pontier PJ, Patel TG. Racial differences in the prevalence and presentation of glomerular disease in adults. *Clin Nephrol* 1994;42(2):79–84.
40. Remuzzi A, Mazerska M, Gephardt GN, et al. Three-dimensional analysis of glomerular morphology in patients with subtotal nephrectomy. *Kidney Int* 1995;48(1):155–162.
41. Newbold KM, Sandison A, Howie AJ. Comparison of size of juxtamedullary and outer cortical glomeruli in normal adult kidney. *Virchows Arch A Pathol Anat Histopathol* 1992;420(2):127–129.
42. Skov K, Nyengaard JR, Patwardan A, et al. Large juxtamedullary glomeruli and afferent arterioles in healthy primates. *Kidney Int* 1999;55(4):1462–1469.
43. Smeets B, Kuppe C, Sicking EM, et al. Parietal epithelial cells participate in the formation of sclerotic lesions in focal segmental glomerulosclerosis. *J Am Soc Nephrol* 2011;22(7):1262–1274.
44. Suzuki J, Yoshikawa N, Nakamura H. A quantitative analysis of the glomeruli in focal segmental glomerulosclerosis. *Pediatr Nephrol* 1994;8(4):416–419.
45. Nishimoto K, Shiiki H, Nishino T, et al. Reversible glomerular hypertrophy in adult patients with primary focal segmental glomerulosclerosis. *J Am Soc Nephrol* 1997;8(11):1668–1678.
46. Corwin HL, Schwartz MM, Lewis EJ. The importance of sample size in the interpretation of the renal biopsy. *Am J Nephrol* 1988;8(2):85–89.
47. Fogo A, Glick AD, Horn SL, et al. Is focal segmental glomerulosclerosis really focal? Distribution of lesions in adults and children. *Kidney Int* 1995;47(6):1690–1696.
48. Fuiano G, Comi N, Magri P, et al. Serial morphometric analysis of sclerotic lesions in primary "focal" segmental glomerulosclerosis. *J Am Soc Nephrol* 1996;7(1):49–55.
49. Deegens JK, Dijkman HB, Borm GF, et al. Podocyte foot process effacement as a diagnostic tool in focal segmental glomerulosclerosis. *Kidney Int* 2008;74(12):1568–1576.
50. Howie AJ, Brewer DB. The glomerular tip lesion: a previously undescribed type of segmental glomerular abnormality. *J Pathol* 1984;142(3):205–220.
51. Howie AJ, Pankhurst T, Sarioglu S, et al. Evolution of nephrotic-associated focal segmental glomerulosclerosis and relation to the glomerular tip lesion. *Kidney Int* 2005;67(3):987–1001.
52. Schwartz MM, Lewis EJ. Focal segmental glomerular sclerosis: the cellular lesion. *Kidney Int* 1985;28(6):968–974.
53. Schwartz MM, Korbet SM, Rydell J, et al. Primary focal segmental glomerular sclerosis in adults: prognostic value of histologic variants. *Am J Kidney Dis* 1995;25(6):845–852.
54. Weiss M, Daquiao E, Margolin E, et al. Nephrotic syndrome, progressive irreversible renal failure, and glomerular "collapse." A new clinicopathologic entity? *Am J Kidney Dis* 1986;7:20–28.
55. Detwiler RK, Falk RJ, Hogan SL, et al. Collapsing glomerulopathy: a clinically and pathologically distinct variant of focal segmental glomerulosclerosis. *Kidney Int* 1994;45(5):1416–1424.
56. Valeri A, Barisoni L, Appel GB, et al. Idiopathic collapsing focal segmental glomerulosclerosis: a clinicopathologic study. *Kidney Int* 1996;50(5):1734–1746.
57. Laurinavicius A, Hurwitz S, Rennke HG. Collapsing glomerulopathy in HIV and non-HIV patients: a clinicopathological and follow-up study. *Kidney Int* 1999;56(6):2203–2213.
58. Rao TK, Filippone EJ, Nicastrì AD, et al. Associated focal and segmental glomerulosclerosis in the acquired immunodeficiency syndrome. *N Engl J Med* 1984;310(11):669–673.
59. Cohen AH, Nast CC. HIV-associated nephropathy. A unique combined glomerular, tubular, and interstitial lesion. *Mod Pathol* 1988;1(2):87–97.
60. D'Agati V, Suh JJ, Carbone L, et al. Pathology of HIV-associated nephropathy: a detailed morphologic and comparative study. *Kidney Int* 1989;35(6):1358–1370.

61. Chun MJ, Korbet SM, Schwartz MM, et al. Focal segmental glomerulosclerosis in nephrotic adults: presentation, prognosis, and response to therapy of the histologic variants. *J Am Soc Nephrol* 2004;15(8):2169–2177.
62. D'Agati VD, Fogo AB, Bruijn JA, et al. Pathologic classification of focal segmental glomerulosclerosis: a working proposal. *Am J Kidney Dis* 2004;43(2):368–382.
63. Silverstein DM, Craver R. Presenting features and short-term outcome according to pathologic variant in childhood primary focal segmental glomerulosclerosis. *Clin J Am Soc Nephrol* 2007;2(4):700–707.
64. Thomas DB, Franceschini N, Hogan SL, et al. Clinical and pathologic characteristics of focal segmental glomerulosclerosis pathologic variants. *Kidney Int* 2006;69(5):920–926.
65. Deegens JK, Steenbergen EJ, Borm GF, et al. Pathological variants of focal segmental glomerulosclerosis in an adult Dutch population—epidemiology and outcome. *Nephrol Dial Transplant* 2008;23(1):186–192.
66. Nada R, Kharbanda JK, Bharti A, et al. Primary focal segmental glomerulosclerosis in adults: is the Indian cohort different? *Nephrol Dial Transplant* 2009;24(12):3701–3707.
67. Taneda S, Honda K, Uchida K, et al. Histological heterogeneity of glomerular segmental lesions in focal segmental glomerulosclerosis. *Int Urol Nephrol* 2012;44(1):183–196.
68. Gipson DS, Trachtman H, Kaskel FJ, et al. Clinical trial of focal segmental glomerulosclerosis in children and young adults. *Kidney Int* 2011;80(8):868–878.
69. Canaud G, Dion D, Zuber J, et al. Recurrence of nephrotic syndrome after transplantation in a mixed population of children and adults: Course of glomerular lesions and value of the Columbia classification of histological variants of focal and segmental glomerulosclerosis (FSGS). *Nephrol Dial Transplant* 2010;25(4):1321–1328.
70. Stokes MB, Valeri AM, Markowitz GS, et al. Cellular focal segmental glomerulosclerosis: clinical and pathologic features. *Kidney Int* 2006;70(10):1783–1792.
71. Markowitz GS, Nasr SH, Stokes MB, et al. Treatment with IFN- α , β , or γ is associated with collapsing focal segmental glomerulosclerosis. *Clin J Am Soc Nephrol* 2010;5(4):607–615.
72. Salvatore SP, Barisoni LM, Herzenberg AM, et al. Collapsing glomerulopathy in 19 patients with systemic lupus erythematosus or lupus-like disease. *Clin J Am Soc Nephrol* 2012;7(6):914–925.
73. Stokes MB, Markowitz GS, Lin J, et al. Glomerular tip lesion: a distinct entity within the minimal change disease/focal segmental glomerulosclerosis spectrum. *Kidney Int* 2004;65(5):1690–1702.
74. Haas M, Yousefzadeh N. Glomerular tip lesion in minimal change nephropathy: a study of autopsies before 1950. *Am J Kidney Dis* 2002;39(6):1168–1175.
75. Howie AJ, Agarwal A, Sebire NJ, et al. Glomerular tip changes in childhood minimal change nephropathy. *Pediatr Nephrol* 2008;23(8):1281–1286.
76. D'Agati VD, Alster JM, Jennette JC, et al. Association of histologic variants in FSGS clinical trial with presenting features and outcomes. *Clin J Am Soc Nephrol* 2013;8(3):399–406.
77. Howie AJ. Changes at the glomerular tip: a feature of membranous nephropathy and other disorders associated with proteinuria. *J Pathol* 1986;150(1):13–20.
78. Arias LF, Franco-Alzate C, Rojas SL. Tip variant of focal segmental glomerulosclerosis: Outcome and comparison to 'not otherwise specified' variant. *Nephrol Dial Transplant* 2011;26(7):2215–2221.
79. Rydel JJ, Korbet SM, Borok RZ, et al. Focal segmental glomerular sclerosis in adults: presentation, course, and response to treatment. *Am J Kidney Dis* 1995;25(4):534–542.
80. Martinelli R, Okumura AS, Pereira LJ, et al. Primary focal segmental glomerulosclerosis in children: prognostic factors. *Pediatr Nephrol* 2001;16(8):658–661.
81. Troyanov S, Wall CA, Miller JA, et al. Focal and segmental glomerulosclerosis: definition and relevance of a partial remission. *J Am Soc Nephrol* 2005;16(4):1061–1068.
82. Deegens JK, Assmann KJ, Steenbergen EJ, et al. Idiopathic focal segmental glomerulosclerosis: a favourable prognosis in untreated patients? *Neth J Med* 2005;63(10):393–398.
83. Besbas N, Ozaltin F, Emre S, et al. Clinical course of primary focal segmental glomerulosclerosis (FSGS) in Turkish children: a report from the Turkish Pediatric Nephrology FSGS Study Group. *Turk J Pediatr* 2010;52(3):255–261.
84. Wehrmann M, Bohle A, Bogenschutz O, et al. Long-term prognosis of chronic idiopathic membranous glomerulonephritis. An analysis of 334 cases with particular regard to tubulo-interstitial changes. *Clin Nephrol* 1989;31(2):67–76.
85. Benzing T. Signaling at the slit diaphragm. *J Am Soc Nephrol* 2004;15(6):1382–1391.
86. Welsh GI, Saleem MA. The podocyte cytoskeleton—key to a functioning glomerulus in health and disease. *Nat Rev Nephrol* 2012;8(1):14–21.
87. Benoit G, Machuca E, Antignac C. Hereditary nephrotic syndrome: a systematic approach for genetic testing and a review of associated podocyte gene mutations. *Pediatr Nephrol* 2010;25(9):1621–1632.
88. Choi HJ, Lee BH, Cho HY, et al. Familial focal segmental glomerulosclerosis associated with an ACTN4 mutation and paternal germline mosaicism. *Am J Kidney Dis* 2008;51(5):834–838.
89. Ruf RG, Lichtenberger A, Karle SM, et al. Patients with mutations in NPHS2 (podocin) do not respond to standard steroid treatment of nephrotic syndrome. *J Am Soc Nephrol* 2004;15(3):722–732.
90. Galeano B, Klootwijk R, Manoli I, et al. Mutation in the key enzyme of sialic acid biosynthesis causes severe glomerular proteinuria and is rescued by N-acetylmannosamine. *J Clin Invest* 2007;117(6):1585–1594.
91. Ozaltin F, Ibsirlioglu T, Taskiran EZ, et al. Disruption of PTPRO causes childhood-onset nephrotic syndrome. *Am J Hum Genet* 2011;89(1):139–147.
92. Sachs N, Kreft M, van den Bergh Weerman MA, et al. Kidney failure in mice lacking the tetraspanin CD151. *J Cell Biol* 2006;175(1):33–39.
93. Karamatic Crew V, Burton N, Kagan A, et al. CD151, the first member of the tetraspanin (TM4) superfamily detected on erythrocytes, is essential for the correct assembly of human basement membranes in kidney and skin. *Blood* 2004;104(8):2217–2223.
94. Zenker M, Aigner T, Wendler O, et al. Human laminin beta2 deficiency causes congenital nephrosis with mesangial sclerosis and distinct eye abnormalities. *Hum Mol Genet* 2004;13(21):2625–2632.
95. Kambham N, Tanji N, Seigle RL, et al. Congenital focal segmental glomerulosclerosis associated with beta4 integrin mutation and epidermolysis bullosa. *Am J Kidney Dis* 2000;36(1):190–196.
96. Mundel P, Reiser J. Proteinuria: an enzymatic disease of the podocyte? *Kidney Int* 2010;77(7):571–580.
97. Sever S, Altintas MM, Nankoe SR, et al. Proteolytic processing of dynamin by cytoplasmic cathepsin L is a mechanism for proteinuric kidney disease. *J Clin Invest* 2007;117(8):2095–2104.
98. Shankland SJ. The podocyte's response to injury: role in proteinuria and glomerulosclerosis. *Kidney Int* 2006;69(12):2131–2147.
99. D'Agati V. Podocyte injury can be catching. *J Am Soc Nephrol* 2011;22(7):1181–1183.
100. Bariety J, Bruneval P, Hill G, et al. Posttransplantation relapse of FSGS is characterized by glomerular epithelial cell transdifferentiation. *J Am Soc Nephrol* 2001;12(2):261–274.
101. Bariety J, Nochy D, Mandet C, et al. Podocytes undergo phenotypic changes and express macrophagic-associated markers in idiopathic collapsing glomerulopathy. *Kidney Int* 1998;53(4):918–925.
102. Barisoni L, Kriz W, Mundel P, et al. The dysregulated podocyte phenotype: A novel concept in the pathogenesis of collapsing idiopathic focal segmental glomerulosclerosis and HIV-associated nephropathy. *J Am Soc Nephrol* 1999;10(1):51–61.
103. Shankland SJ, Eitner F, Hudkins KL, et al. Differential expression of cyclin-dependent kinase inhibitors in human glomerular disease: Role in podocyte proliferation and maturation. *Kidney Int* 2000;58(2):674–683.
104. Dijkman H, Smeets B, van der Laak J, et al. The parietal epithelial cell is crucially involved in human idiopathic focal segmental glomerulosclerosis. *Kidney Int* 2005;68(4):1562–1572.
105. Appel D, Kershaw DB, Smeets B, et al. Recruitment of podocytes from glomerular parietal epithelial cells. *J Am Soc Nephrol* 2009;20(2):333–343.
106. Smeets B, Uhlig S, Fuss A, et al. Tracing the origin of glomerular extracapillary lesions from parietal epithelial cells. *J Am Soc Nephrol* 2009;20(12):2604–2615.

107. Smeets B, Angelotti ML, Rizzo P, et al. Renal progenitor cells contribute to hyperplastic lesions of podocytopathies and crescentic glomerulonephritis. *J Am Soc Nephrol* 2009;20(12):2593–2603.
108. Suzuki T, Matsusaka T, Nakayama M, et al. Genetic podocyte lineage reveals progressive podocytopenia with parietal cell hyperplasia in a murine model of cellular/collapsing focal segmental glomerulosclerosis. *Am J Pathol* 2009;174(5):1675–1682.
109. Shkreli M, Sarin KY, Pech MF, et al. Reversible cell-cycle entry in adult kidney podocytes through regulated control of telomerase and Wnt signaling. *Nat Med* 2011;18(1):111–119.
110. Ronconi E, Sagrinati C, Angelotti ML, et al. Regeneration of glomerular podocytes by human renal progenitors. *J Am Soc Nephrol* 2009;20(2):322–332.
111. Prodromidi EI, Poulsom R, Jeffery R, et al. Bone marrow-derived cells contribute to podocyte regeneration and amelioration of renal disease in a mouse model of Alport syndrome. *Stem Cells* 2006;24(11):2448–2455.
112. Meyer-Schwesinger C, Lange C, Brocker V, et al. Bone marrow-derived progenitor cells do not contribute to podocyte turnover in the puromycin aminoglycoside and renal ablation models in rats. *Am J Pathol* 2011;178(2):494–499.
113. Hodgins JB, Borczuk AC, Nasr SH, et al. A molecular profile of focal segmental glomerulosclerosis from formalin-fixed, paraffin-embedded tissue. *Am J Pathol* 2010;177(4):1674–1686.
114. Chen CA, Hwang JC, Guh JY, et al. Reduced podocyte expression of alpha3beta1 integrins and podocyte depletion in patients with primary focal segmental glomerulosclerosis and chronic PAN-treated rats. *J Lab Clin Med* 2006;147(2):74–82.
115. Hara M, Yanagihara T, Kihara I. Urinary podocytes in primary focal segmental glomerulosclerosis. *Nephron* 2001;89(3):342–347.
116. Petermann A, Floege J. Podocyte damage resulting in podocyturia: A potential diagnostic marker to assess glomerular disease activity. *Nephron Clin Pract* 2007;106(2):c61–c66.
117. Friedrich C, Endlich N, Kriz W, et al. Podocytes are sensitive to fluid shear stress in vitro. *Am J Physiol Renal Physiol* 2006;291(4):F856–F865.
118. El Karoui K, Hill GS, Karras A, et al. Focal segmental glomerulosclerosis plays a major role in the progression of IgA nephropathy. II. Light microscopic and clinical studies. *Kidney Int* 2011;79(6):643–654.
119. Howie AJ, Kizaki T, Beaman M, et al. Different types of segmental sclerosing glomerular lesions in six experimental models of proteinuria. *J Pathol* 1989;157(2):141–151.
120. Shalhoub RJ. Pathogenesis of lipoid nephrosis: a disorder of T-cell function. *Lancet* 1974;2(7880):556–560.
121. Garcia CD, Bittencourt VB, Tumelero A, et al. Plasmapheresis for recurrent posttransplant focal segmental glomerulosclerosis. *Transplant Proc* 2006;38(6):1904–1905.
122. Savin VJ, Sharma R, Sharma M, et al. Circulating factor associated with increased glomerular permeability to albumin in recurrent focal segmental glomerulosclerosis. *N Engl J Med* 1996;334(14):878–883.
123. McCarthy ET, Sharma M, Sharma R, et al. Sera from patients with collapsing focal segmental glomerulosclerosis increase albumin permeability of isolated glomeruli. *J Lab Clin Med* 2004;143(4):225–229.
124. Gallon L, Leventhal J, Skaro A, et al. Resolution of recurrent focal segmental glomerulosclerosis after retransplantation. *N Engl J Med* 2012;366(17):1648–1649.
125. Savin VJ, McCarthy ET, Sharma R, et al. Galactose binds to focal segmental glomerulosclerosis permeability factor and inhibits its activity. *Transl Res* 2008;151(6):288–292.
126. Wei C, Trachtman H, Li J, et al. Circulating suPAR in two cohorts of primary FSGS. *J Am Soc Nephrol* 2012;23(12):2051–2059.
127. Wei C, Moller CC, Altintas MM, et al. Modification of kidney barrier function by the urokinase receptor. *Nat Med* 2008;14(1):55–63.
128. Coward RJ, Foster RR, Patton D, et al. Nephrotic plasma alters slit diaphragm-dependent signaling and translocates nephrin, Podocin, and CD2 associated protein in cultured human podocytes. *J Am Soc Nephrol* 2005;16(3):629–637.
129. Lennon R, Singh A, Welsh GI, et al. Hemopexin induces nephrin-dependent reorganization of the actin cytoskeleton in podocytes. *J Am Soc Nephrol* 2008;19(11):2140–2149.
130. Carraro M, Caridi G, Bruschi M, et al. Serum glomerular permeability activity in patients with podocin mutations (NPHS2) and steroid-resistant nephrotic syndrome. *J Am Soc Nephrol* 2002;13(7):1946–1952.
131. Trachtman H, Greenbaum LA, McCarthy ET, et al. Glomerular permeability activity: prevalence and prognostic value in pediatric patients with idiopathic nephrotic syndrome. *Am J Kidney Dis* 2004;44(4):604–610.
132. Cattran D, Neogi T, Sharma R, et al. Serial estimates of serum permeability activity and clinical correlates in patients with native kidney focal segmental glomerulosclerosis. *J Am Soc Nephrol* 2003;14(2):448–453.
133. Feld SM, Figueroa P, Savin V, et al. Plasmapheresis in the treatment of steroid-resistant focal segmental glomerulosclerosis in native kidneys. *Am J Kidney Dis* 1998;32(2):230–237.
134. A report of the International Study of Kidney Disease in Children. Nephrotic syndrome in children: Prediction of histopathology from clinical and laboratory characteristics at time of diagnosis. *Kidney Int* 1978;13(2):159–165.
135. Tune BM, Mendoza SA. Treatment of the idiopathic nephrotic syndrome: regimens and outcomes in children and adults. *J Am Soc Nephrol* 1997;8(5):824–832.
136. Banfi G, Moriggi M, Sabadini E, et al. The impact of prolonged immunosuppression on the outcome of idiopathic focal-segmental glomerulosclerosis with nephrotic syndrome in adults. A collaborative retrospective study. *Clin Nephrol* 1991;36(2):53–59.
137. Ponticelli C, Rizzoni G, Edefonti A, et al. A randomized trial of cyclosporine in steroid-resistant idiopathic nephrotic syndrome. *Kidney Int* 1993;43(6):1377–1384.
138. Cattran DC, Greenwood C, Ritchie S, et al. A controlled trial of cyclosporine in patients with progressive membranous nephropathy. Canadian Glomerulonephritis Study Group. *Kidney Int* 1995;47(4):1130–1135.
139. Tune BM, Kirpekar R, Sibley RK, et al. Intravenous methylprednisolone and oral alkylating agent therapy of prednisone-resistant pediatric focal segmental glomerulosclerosis: a long-term follow-up. *Clin Nephrol* 1995;43(2):84–88.
140. Tarshish P, Tobin JN, Bernstein J, et al. Cyclophosphamide does not benefit patients with focal segmental glomerulosclerosis. A report of the International Study of Kidney Disease in Children. *Pediatr Nephrol* 1996;10(5):590–593.
141. Imbasciati E, Cagnoli L, Case N, et al. [Controlled study of treatment of steroids and chlorambucil, in alternate months, for membranous nephropathy and focal glomerulosclerosis. Preliminary evaluation of the results]. *Minerva Nefrol* 1980;27(4):571–575.
142. Schonenberger E, Ehrlich JH, Haller H, et al. The podocyte as a direct target of immunosuppressive agents. *Nephrol Dial Transplant* 2011;26(1):18–24.
143. Faul C, Donnelly M, Merscher-Gomez S, et al. The actin cytoskeleton of kidney podocytes is a direct target of the antiproteinuric effect of cyclosporine A. *Nat Med* 2008;14(9):931–938.
144. Ponticelli C. Recurrence of focal segmental glomerular sclerosis (FSGS) after renal transplantation. *Nephrol Dial Transplant* 2010;25(1):25–31.
145. Hwang JH, Han SS, Huh W, et al. Outcome of kidney allograft in patients with adulthood-onset focal segmental glomerulosclerosis: Comparison with childhood-onset FSGS. *Nephrol Dial Transplant* 2012;27(6):2559–2565.
146. Verani RR, Hawkins EP. Recurrent focal segmental glomerulosclerosis. A pathological study of the early lesion. *Am J Nephrol* 1986;6(4):263–270.
147. Kemeny E, Mihatsch MJ, Durmuller U, et al. Podocytes lose their adhesive phenotype in focal segmental glomerulosclerosis. *Clin Nephrol* 1995;43(2):71–83.
148. Fatima H, Moeller MJ, Smeets B, et al. Parietal epithelial cell activation marker in early recurrence of FSGS in the transplant. *Clin J Am Soc Nephrol* 2012;7(11):1852–1858.
149. Schachter ME, Monahan M, Radhakrishnan J, et al. Recurrent focal segmental glomerulosclerosis in the renal allograft: single center experience in the era of modern immunosuppression. *Clin Nephrol* 2010;74(3):173–181.
150. Stokes MB, Davis CL, Alpers CE. Collapsing glomerulopathy in renal allografts: a morphological pattern with diverse clinicopathologic associations. *Am J Kidney Dis* 1999;33(4):658–666.
151. Kestila M, Lenkkeri U, Mannikko M, et al. Positionally cloned gene for a novel glomerular protein—nephrin—is mutated in congenital nephrotic syndrome. *Mol Cell* 1998;1(4):575–582.

152. Hinkes BG, Mucha B, Vlangos CN, et al. Nephrotic syndrome in the first year of life: Two-thirds of cases are caused by mutations in 4 genes (NPHS1, NPHS2, WT1, and LAMB2). *Pediatrics* 2007;119(4):e907–e919.
153. Karle SM, Uetz B, Ronner V, et al. Novel mutations in NPHS2 detected in both familial and sporadic steroid-resistant nephrotic syndrome. *J Am Soc Nephrol* 2002;13(2):388–393.
154. Santin S, Bullich G, Tazon-Vega B, et al. Clinical utility of genetic testing in children and adults with steroid-resistant nephrotic syndrome. *Clin J Am Soc Nephrol* 2011;6(5):1139–1148.
155. Jones N, New LA, Fortino MA, et al. Nck proteins maintain the adult glomerular filtration barrier. *J Am Soc Nephrol* 2009;20(7):1533–1543.
156. Machuca E, Benoit G, Antignac C. Genetics of nephrotic syndrome: Connecting molecular genetics to podocyte physiology. *Hum Mol Genet* 2009;18(R2):R185–R194.
157. Lenkkeri U, Mannikko M, McCready P, et al. Structure of the gene for congenital nephrotic syndrome of the Finnish type (NPHS1) and characterization of mutations. *Am J Hum Genet* 1999;64(1):51–61.
158. Machuca E, Benoit G, Nevo F, et al. Genotype-phenotype correlations in non-Finnish congenital nephrotic syndrome. *J Am Soc Nephrol* 2010;21(7):1209–1217.
159. Koziell A, Grech V, Hussain S, et al. Genotype/phenotype correlations of NPHS1 and NPHS2 mutations in nephrotic syndrome advocate a functional inter-relationship in glomerular filtration. *Hum Mol Genet* 2002;11(4):379–388.
160. Philippe A, Nevo F, Esquivel EL, et al. Nephtrin mutations can cause childhood-onset steroid-resistant nephrotic syndrome. *J Am Soc Nephrol* 2008;19(10):1871–1878.
161. Kitamura A, Tsukaguchi H, Hiramoto R, et al. A familial childhood-onset relapsing nephrotic syndrome. *Kidney Int* 2007;71(9):946–951.
162. Patrakka J, Ruotsalainen V, Reponen P, et al. Recurrence of nephrotic syndrome in kidney grafts of patients with congenital nephrotic syndrome of the Finnish type: role of nephtrin. *Transplantation* 2002;73(3):394–403.
163. Roselli S, Heidt L, Sich M, et al. Early glomerular filtration defect and severe renal disease in podocin-deficient mice. *Mol Cell Biol* 2004;24(2):550–560.
164. Mollet G, Ratelade J, Boyer O, et al. Podocin inactivation in mature kidneys causes focal segmental glomerulosclerosis and nephrotic syndrome. *J Am Soc Nephrol* 2009;20(10):2181–2189.
165. Boute N, Gribouval O, Roselli S, et al. NPHS2, encoding the glomerular protein podocin, is mutated in autosomal recessive steroid-resistant nephrotic syndrome. *Nat Genet* 2000;24(4):349–354.
166. Weber S, Gribouval O, Esquivel EL, et al. NPHS2 mutation analysis shows genetic heterogeneity of steroid-resistant nephrotic syndrome and low post-transplant recurrence. *Kidney Int* 2004;66(2):571–579.
167. Maruyama K, Iijima K, Ikeda M, et al. NPHS2 mutations in sporadic steroid-resistant nephrotic syndrome in Japanese children. *Pediatr Nephrol* 2003;18(5):412–416.
168. Hinkes B, Vlangos C, Heeringa S, et al. Specific podocin mutations correlate with age of onset in steroid-resistant nephrotic syndrome. *J Am Soc Nephrol* 2008;19(2):365–371.
169. Machuca E, Hummel A, Nevo F, et al. Clinical and epidemiological assessment of steroid-resistant nephrotic syndrome associated with the NPHS2 R229Q variant. *Kidney Int* 2009;75(7):727–735.
170. Tsukaguchi H, Sudhakar A, Le TC, et al. NPHS2 mutations in late-onset focal segmental glomerulosclerosis: R229Q is a common disease-associated allele. *J Clin Invest* 2002;110(11):1659–1666.
171. Pereira AC, Pereira AB, Mota GF, et al. NPHS2 R229Q functional variant is associated with microalbuminuria in the general population. *Kidney Int* 2004;65(3):1026–1030.
172. McKenzie LM, Hendrickson SL, Briggs WA, et al. NPHS2 variation in sporadic focal segmental glomerulosclerosis. *J Am Soc Nephrol* 2007;18(11):2987–2995.
173. Chernin G, Heeringa SF, Gbadegesin R, et al. Low prevalence of NPHS2 mutations in African American children with steroid-resistant nephrotic syndrome. *Pediatr Nephrol* 2008;23(9):1455–1460.
174. Caridi G, Gigante M, Ravani P, et al. Clinical features and long-term outcome of nephrotic syndrome associated with heterozygous NPHS1 and NPHS2 mutations. *Clin J Am Soc Nephrol* 2009;4(6):1065–1072.
175. Tonna SJ, Needham A, Polu K, et al. NPHS2 variation in focal and segmental glomerulosclerosis. *BMC Nephrol* 2008;9:13.
176. He N, Zahirieh A, Mei Y, et al. Recessive NPHS2 (Podocin) mutations are rare in adult-onset idiopathic focal segmental glomerulosclerosis. *Clin J Am Soc Nephrol* 2007;2(1):31–37.
177. Caridi G, Bertelli R, Di Duca M, et al. Broadening the spectrum of diseases related to podocin mutations. *J Am Soc Nephrol* 2003;14(5):1278–1286.
178. Bertelli R, Ginevri F, Caridi G, et al. Recurrence of focal segmental glomerulosclerosis after renal transplantation in patients with mutations of podocin. *Am J Kidney Dis* 2003;41(6):1314–1321.
179. Becker-Cohen R, Bruschi M, Rinat C, et al. Recurrent nephrotic syndrome in homozygous truncating NPHS2 mutation is not due to anti-podocin antibodies. *Am J Transplant* 2007;7(1):256–260.
180. Hinkes B, Wiggins RC, Gbadegesin R, et al. Positional cloning uncovers mutations in PLCE1 responsible for a nephrotic syndrome variant that may be reversible. *Nat Genet* 2006;38(12):1397–1405.
181. Gbadegesin R, Hinkes BG, Hoskins BE, et al. Mutations in PLCE1 are a major cause of isolated diffuse mesangial sclerosis (IDMS). *Nephrol Dial Transplant* 2008;23:1291–1297.
182. Boyer O, Benoit G, Gribouval O, et al. Mutational analysis of the PLCE1 gene in steroid resistant nephrotic syndrome. *J Med Genet* 2010;47(7):445–452.
183. Mele C, Iatropoulos P, Donadelli R, et al. MYO1E mutations and childhood familial focal segmental glomerulosclerosis. *N Engl J Med* 2011;365(4):295–306.
184. Sanna-Cherchi S, Burgess KE, Nees SN, et al. Exome sequencing identified MYO1E and NEIL1 as candidate genes for human autosomal recessive steroid-resistant nephrotic syndrome. *Kidney Int* 2011;80(4):389–396.
185. Sharif K, Goyal M, Kershaw D, et al. Podocyte phenotypes as defined by expression and distribution of GLEPP1 in the developing glomerulus and in nephrotic glomeruli from MCD, CNE, and FSGS. A dedifferentiation hypothesis for the nephrotic syndrome. *Exp Nephrol* 1998;6(3):234–244.
186. Tian J, Wang HP, Mao YY, et al. Reduced glomerular epithelial protein 1 expression and podocyte injury in immunoglobulin A nephropathy. *J Int Med Res* 2007;35(3):338–345.
187. Yaddanapudi S, Altintas MM, Kistler AD, et al. CD2AP in mouse and human podocytes controls a proteolytic program that regulates cytoskeletal structure and cellular survival. *J Clin Invest* 2011;121(10):3965–3980.
188. Shih NY, Li J, Karpitskii V, et al. Congenital nephrotic syndrome in mice lacking CD2-associated protein. *Science* 1999;286(5438):312–315.
189. Lowik MM, Groenen PJ, Pronk I, et al. Focal segmental glomerulosclerosis in a patient homozygous for a CD2AP mutation. *Kidney Int* 2007;72(10):1198–1203.
190. Lowik M, Levchenko E, Westra D, et al. Bigenic heterozygosity and the development of steroid-resistant focal segmental glomerulosclerosis. *Nephrol Dial Transplant* 2008;23(10):3146–3151.
191. Gigante M, Pontrelli P, Montemurno E, et al. CD2AP mutations are associated with sporadic nephrotic syndrome and focal segmental glomerulosclerosis (FSGS). *Nephrol Dial Transplant* 2009;24(6):1858–1864.
192. Kim JM, Wu H, Green G, et al. CD2-associated protein haploinsufficiency is linked to glomerular disease susceptibility. *Science* 2003;300(5623):1298–1300.
193. Weins A, Schlondorff JS, Nakamura F, et al. Disease-associated mutant alpha-actinin-4 reveals a mechanism for regulating its F-actin-binding affinity. *Proc Natl Acad Sci U S A* 2007;104(41):16080–16085.
194. Dandapani SV, Sugimoto H, Matthews BD, et al. Alpha-actinin-4 is required for normal podocyte adhesion. *J Biol Chem* 2007;282(1):467–477.
195. Kaplan JM, Kim SH, North KN, et al. Mutations in ACTN4, encoding alpha-actinin-4, cause familial focal segmental glomerulosclerosis. *Nat Genet* 2000;24(3):251–256.
196. Weins A, Kenlan P, Herbert S, et al. Mutational and biological analysis of alpha-actinin-4 in focal segmental glomerulosclerosis. *J Am Soc Nephrol* 2005;16(12):3694–3701.
197. Henderson JM, Alexander MP, Pollak MR. Patients with ACTN4 mutations demonstrate distinctive features of glomerular injury. *J Am Soc Nephrol* 2009;20(5):961–968.

198. Brown EJ, Schlondorff JS, Becker DJ, et al. Mutations in the formin gene *INF2* cause focal segmental glomerulosclerosis. *Nat Genet* 2010;42(1):72–76.
199. Boyer O, Benoit G, Gribouval O, et al. Mutations in *INF2* are a major cause of autosomal dominant focal segmental glomerulosclerosis. *J Am Soc Nephrol* 2011;22(2):239–245.
200. Boyer O, Nevo F, Plaisier E, et al. *INF2* mutations in Charcot-Marie-Tooth disease with glomerulopathy. *N Engl J Med* 2011;365(25):2377–2388.
201. Winn MP, Conlon PJ, Lynn KL, et al. A mutation in the *TRPC6* cation channel causes familial focal segmental glomerulosclerosis. *Science* 2005;308(5729):1801–1804.
202. Heeringa SF, Moller CC, Du J, et al. A novel *TRPC6* mutation that causes childhood FSGS. *PLoS One* 2009;4(11):e7771.
203. Reiser J, Polu KR, Moller CC, et al. *TRPC6* is a glomerular slit diaphragm-associated channel required for normal renal function. *Nat Genet* 2005;37(7):739–744.
204. Zhu B, Chen N, Wang ZH, et al. Identification and functional analysis of a novel *TRPC6* mutation associated with late onset familial focal segmental glomerulosclerosis in Chinese patients. *Mutat Res* 2009;664(1–2):84–90.
205. Gigante M, Caridi G, Montemurno E, et al. *TRPC6* mutations in children with steroid-resistant nephrotic syndrome and atypical phenotype. *Clin J Am Soc Nephrol* 2011;6(7):1626–1634.
206. Habib R, Loirat C, Gubler MC, et al. The nephropathy associated with male pseudohermaphroditism and Wilms' tumor (Drash syndrome): a distinctive glomerular lesion—report of 10 cases. *Clin Nephrol* 1985;24(6):269–278.
207. Denamur E, Bocquet N, Mougnot B, et al. Mother-to-child transmitted *WT1* splice-site mutation is responsible for distinct glomerular diseases. *J Am Soc Nephrol* 1999;10(10):2219–2223.
208. Ruf RG, Schultheiss M, Lichtenberger A, et al. Prevalence of *WT1* mutations in a large cohort of patients with steroid-resistant and steroid-sensitive nephrotic syndrome. *Kidney Int* 2004;66(2):564–570.
209. Mucha B, Ozaltin F, Hinkes BG, et al. Mutations in the Wilms' tumor 1 gene cause isolated steroid resistant nephrotic syndrome and occur in exons 8 and 9. *Pediatr Res* 2006;59(2):325–331.
210. Matejas V, Hinkes B, Alkandari F, et al. Mutations in the human laminin beta2 (*LAMB2*) gene and the associated phenotypic spectrum. *Hum Mutat* 2010;31(9):992–1002.
211. Matejas V, Al-Gazali L, Amirlak I, et al. A syndrome comprising childhood-onset glomerular kidney disease and ocular abnormalities with progressive loss of vision is caused by mutated *LAMB2*. *Nephrol Dial Transplant* 2006;21(11):3283–3286.
212. Berkovic SF, Dibbens LM, Oshlack A, et al. Array-based gene discovery with three unrelated subjects shows *SCARB2/LIMP-2* deficiency causes myoclonus epilepsy and glomerulosclerosis. *Am J Hum Genet* 2008;82(3):673–684.
213. Badhwar A, Berkovic SF, Dowling JP, et al. Action myoclonus-renal failure syndrome: Characterization of a unique cerebro-renal disorder. *Brain* 2004;127(Pt 10):2173–2182.
214. Schimke RN, Horton WA, King CR, et al. Chondroitin-6-sulfate mucopolysaccharidosis in conjunction with lymphopenia, defective cellular immunity and the nephrotic syndrome. *Birth Defects Orig Artic Ser* 1974;10(12):258–266.
215. Boerkoel CF, Takashima H, John J, et al. Mutant chromatin remodeling protein *SMARCA1* causes Schimke immuno-osseous dysplasia. *Nat Genet* 2002;30(2):215–220.
216. Clewing JM, Fryssira H, Goodman D, et al. Schimke immunoosseous dysplasia: Suggestions of genetic diversity. *Hum Mutat* 2007;28(3):273–283.
217. Pulkkinen L, Rouan F, Bruckner-Tuderman L, et al. Novel *ITGB4* mutations in lethal and nonlethal variants of epidermolysis bullosa with pyloric atresia: Missense versus nonsense. *Am J Hum Genet* 1998;63(5):1376–1387.
218. Emma F, Bertini E, Salviati L, et al. Renal involvement in mitochondrial cytopathies. *Pediatr Nephrol* 2012;27(4):539–550.
219. Goto Y, Nonaka I, Horai S. A mutation in the *tRNA(Leu)(UUR)* gene associated with the MELAS subgroup of mitochondrial encephalomyopathies. *Nature* 1990;348(6302):651–653.
220. Guery B, Choukroun G, Noel LH, et al. The spectrum of systemic involvement in adults presenting with renal lesion and mitochondrial *tRNA(Leu)* gene mutation. *J Am Soc Nephrol* 2003;14(8):2099–2108.
221. Doleris LM, Hill GS, Chedin P, et al. Focal segmental glomerulosclerosis associated with mitochondrial cytopathy. *Kidney Int* 2000;58(5):1851–1858.
222. Hotta O, Inoue CN, Miyabayashi S, et al. Clinical and pathologic features of focal segmental glomerulosclerosis with mitochondrial *tRNA(Leu)(UUR)* gene mutation. *Kidney Int* 2001;59(4):1236–1243.
223. Hameed R, Raafat F, Ramani P, et al. Mitochondrial cytopathy presenting with focal segmental glomerulosclerosis, hypoparathyroidism, sensorineural deafness, and progressive neurological disease. *Postgrad Med J* 2001;77(910):523–526.
224. Guillausseau PJ, Massin P, Dubois-LaFargue D, et al. Maternally inherited diabetes and deafness: a multicenter study. *Ann Intern Med* 2001;134(9 Pt 1):721–728.
225. Emma F, Bertini E, Salviati L, et al. Renal involvement in mitochondrial cytopathies. *Pediatr Nephrol* 2012;27(4):539–550.
226. Jansen JJ, Maassen JA, van der Woude FJ, et al. Mutation in mitochondrial *tRNA(Leu)(UUR)* gene associated with progressive kidney disease. *J Am Soc Nephrol* 1997;8(7):1118–1124.
227. Cheong HI, Chae JH, Kim JS, et al. Hereditary glomerulopathy associated with a mitochondrial *tRNA(Leu)* gene mutation. *Pediatr Nephrol* 1999;13(6):477–480.
228. Lowik MM, Hol FA, Steenbergen EJ, et al. Mitochondrial *tRNA(Leu)(UUR)* mutation in a patient with steroid-resistant nephrotic syndrome and focal segmental glomerulosclerosis. *Nephrol Dial Transplant* 2005;20(2):336–341.
229. Kobayashi A, Goto Y, Nagata M, et al. Granular swollen epithelial cells: a histologic and diagnostic marker for mitochondrial nephropathy. *Am J Surg Pathol* 2010;34(2):262–270.
230. Yamagata K, Muro K, Usui J, et al. Mitochondrial DNA mutations in focal segmental glomerulosclerosis lesions. *J Am Soc Nephrol* 2002;13(7):1816–1823.
231. Diomedi-Camassei F, Di Giandomenico S, Santorelli FM, et al. *COQ2* nephropathy: A newly described inherited mitochondriopathy with primary renal involvement. *J Am Soc Nephrol* 2007;18(10):2773–2780.
232. Heeringa SF, Chernin G, Chaki M, et al. *COQ6* mutations in human patients produce nephrotic syndrome with sensorineural deafness. *J Clin Invest* 2011;121(5):2013–2024.
233. Rotig A, Appelkvist EL, Geromel V, et al. Quinone-responsive multiple respiratory-chain dysfunction due to widespread coenzyme Q10 deficiency. *Lancet* 2000;356(9227):391–395.
234. Montini G, Malaventura C, Salviati L. Early coenzyme Q10 supplementation in primary coenzyme Q10 deficiency. *N Engl J Med* 2008;358(26):2849–2850.
235. Moller J, Giurgea I, Schlemmer D, et al. Prenyldiphosphate synthase, subunit 1 (*PDSS1*) and OH-benzoate polyprenyltransferase (*COQ2*) mutations in ubiquinone deficiency and oxidative phosphorylation disorders. *J Clin Invest* 2007;117(3):765–772.
236. Lopez LC, Schuelke M, Quinzii CM, et al. Leigh syndrome with nephropathy and CoQ10 deficiency due to decaprenyl diphosphate synthase subunit 2 (*PDSS2*) mutations. *Am J Hum Genet* 2006;79(6):1125–1129.
237. Peng M, Falk MJ, Haase VH, et al. Primary coenzyme Q deficiency in *Pdss2* mutant mice causes isolated renal disease. *PLoS Genet* 2008;4(4):e1000061.
238. Genovesi G, Friedman DJ, Ross MD, et al. Association of trypanolytic ApoL1 variants with kidney disease in African Americans. *Science* 2010;329(5993):841–845.
239. Kopp JB, Smith MW, Nelson GW, et al. *MYH9* is a major-effect risk gene for focal segmental glomerulosclerosis. *Nat Genet* 2008;40(10):1175–1184.
240. Ghiggeri GM, Caridi G, Magrini U, et al. Genetics, clinical and pathological features of glomerulonephritis associated with mutations of nonmuscle myosin IIA (Fechtner syndrome). *Am J Kidney Dis* 2003;41(1):95–104.
241. Sekine T, Konno M, Sasaki S, et al. Patients with Epstein-Fechtner syndromes owing to *MYH9* R702 mutations develop progressive proteinuric renal disease. *Kidney Int* 2010;78(2):207–214.

242. Kao WH, Klag MJ, Meoni LA, et al. MYH9 is associated with non-diabetic end-stage renal disease in African Americans. *Nat Genet* 2008;40(10):1185–1192.
243. Tzur S, Rosset S, Shemer R, et al. Missense mutations in the APOL1 gene are highly associated with end stage kidney disease risk previously attributed to the MYH9 gene. *Hum Genet* 2010;128(3):345–350.
244. Kopp JB, Nelson GW, Sampath K, et al. APOL1 genetic variants in focal segmental glomerulosclerosis and HIV-associated nephropathy. *J Am Soc Nephrol* 2011;22(11):2129–2137.
245. Papeta N, Kiryluk K, Patel A, et al. APOL1 variants increase risk for FSGS and HIVAN but not IgA nephropathy. *J Am Soc Nephrol* 2011;22(11):1991–1996.
246. Fine DM, Wasser WG, Estrella MM, et al. APOL1 risk variants predict histopathology and progression to ESRD in HIV-related kidney disease. *J Am Soc Nephrol* 2012;23(2):343–350.
247. Friedman DJ, Kozlitina J, Genovese G, et al. Population-based risk assessment of APOL1 on renal disease. *J Am Soc Nephrol* 2011;22(11):2098–2105.
248. Kanji Z, Powe CE, Wenger JB, et al. Genetic variation in APOL1 associates with younger age at hemodialysis initiation. *J Am Soc Nephrol* 2011;22(11):2091–2097.
249. Reeves-Daniel AM, DePalma JA, Bleyer AJ, et al. The APOL1 gene and allograft survival after kidney transplantation. *Am J Transplant* 2011;11(5):1025–1030.
250. Madhavan SM, O'Toole JF, Konieczkowski M, et al. APOL1 localization in normal kidney and nondiabetic kidney disease. *J Am Soc Nephrol* 2011;22(11):2119–2128.
251. Wan G, Zhaorigetu S, Liu Z, et al. Apolipoprotein L1, a novel Bcl-2 homology domain 3-only lipid-binding protein, induces autophagic cell death. *J Biol Chem* 2008;283(31):21540–21549.
252. Hartleben B, Godel M, Meyer-Schwesinger C, et al. Autophagy influences glomerular disease susceptibility and maintains podocyte homeostasis in aging mice. *J Clin Invest* 2010;120(4):1084–1096.
253. Rennke HG, Klein PS. Pathogenesis and significance of nonprimary focal and segmental glomerulosclerosis. *Am J Kidney Dis* 1989;13(6):443–456.
254. Barisoni L, Schnaper HW, Kopp JB. A proposed taxonomy for the podocytopathies: A reassessment of the primary nephrotic diseases. *Clin J Am Soc Nephrol* 2007;2(3):529–542.
255. Kambham N, Markowitz GS, Valeri AM, et al. Obesity-related glomerulopathy: an emerging epidemic. *Kidney Int* 2001;59(4):1498–1509.
256. Herlitz LC, Markowitz GS, Farris AB, et al. Development of focal segmental glomerulosclerosis after anabolic steroid abuse. *J Am Soc Nephrol* 2010;21(1):163–172.
257. Bhatena DB, Julian BA, McMorro RG, et al. Focal sclerosis of hypertrophied glomeruli in solitary functioning kidneys of humans. *Am J Kidney Dis* 1985;5(5):226–232.
258. Hodgin JB, Rasoulpour M, Markowitz GS, et al. Very low birth weight is a risk factor for secondary focal segmental glomerulosclerosis. *Clin J Am Soc Nephrol* 2009;4(1):71–76.
259. Hida K, Wada J, Yamasaki H, et al. Cyanotic congenital heart disease associated with glomerulomegaly and focal segmental glomerulosclerosis: Remission of nephrotic syndrome with angiotensin converting enzyme inhibitor. *Nephrol Dial Transplant* 2002;17(1):144–147.
260. Greenberg A, Bastacky SI, Iqbal A, et al. Focal segmental glomerulosclerosis associated with nephrotic syndrome in cholesterol atheroembolism: Clinicopathological correlations. *Am J Kidney Dis* 1997;29(3):334–344.
261. Salomon R, Tellier AL, Attie-Bitach T, et al. PAX2 mutations in oligomeganephronia. *Kidney Int* 2001;59(2):457–462.
262. Habib R, Courteuisse V, Mathieu H, et al. [A peculiar anatomo-clinical type of chronic renal insufficiency in the child: bilateral congenital oligonephronic hypoplasia]. *J Urol Nephrol (Paris)* 1962;68:139–143.
263. Kriz W, Hosser H, Hahnel B, et al. From segmental glomerulosclerosis to total nephron degeneration and interstitial fibrosis: a histopathological study in rat models and human glomerulopathies. *Nephrol Dial Transplant* 1998;13(11):2781–2798.
264. Brenner BM, Meyer TW, Hostetter TH. Dietary protein intake and the progressive nature of kidney disease: the role of hemodynamically mediated glomerular injury in the pathogenesis of progressive glomerular sclerosis in aging, renal ablation, and intrinsic renal disease. *N Engl J Med* 1982;307(11):652–659.
265. Nagata M, Kriz W. Glomerular damage after uninephrectomy in young rats. II. Mechanical stress on podocytes as a pathway to sclerosis. *Kidney Int* 1992;42(1):148–160.
266. Frystyk J, Skjaerbaek C, Vestbo E, et al. Circulating levels of free insulin-like growth factors in obese subjects: the impact of type 2 diabetes. *Diabetes Metab Res Rev* 1999;15(5):314–322.
267. Abbate M, Zoja C, Morigi M, et al. Transforming growth factor-beta1 is up-regulated by podocytes in response to excess intraglomerular passage of proteins: a central pathway in progressive glomerulosclerosis. *Am J Pathol* 2002;161(6):2179–2193.
268. Inagi R, Nangaku M, Onogi H, et al. Involvement of endoplasmic reticulum (ER) stress in podocyte injury induced by excessive protein accumulation. *Kidney Int* 2005;68(6):2639–2650.
269. Matsusaka T, Xin J, Niwa S, et al. Genetic engineering of glomerular sclerosis in the mouse via control of onset and severity of podocyte-specific injury. *J Am Soc Nephrol* 2005;16(4):1013–1023.
270. Wharram BL, Goyal M, Wiggins JE, et al. Podocyte depletion causes glomerulosclerosis: Diphtheria toxin-induced podocyte depletion in rats expressing human diphtheria toxin receptor transgene. *J Am Soc Nephrol* 2005;16(10):2941–2952.
271. Ichikawa I, Ma J, Motojima M, et al. Podocyte damage damages podocytes: autonomous vicious cycle that drives local spread of glomerular sclerosis. *Curr Opin Nephrol Hypertens* 2005;14(3):205–210.
272. Pultiti A, Rossi PI, Caridi G, et al. Albuminuria and glomerular damage in mice lacking the metabotropic glutamate receptor 1. *Am J Pathol* 2011;178(3):1257–1269.
273. Matsusaka T, Sandgren E, Shintani A, et al. Podocyte damage damages other podocytes: study of genetically engineered chimeric glomeruli. *J Am Soc Nephrol* 2011;22(7):1275–1285.
274. Sato Y, Wharram BL, Lee SK, et al. Urine podocyte mRNAs mark progression of renal disease. *J Am Soc Nephrol* 2009;20(5):1041–1052.
275. Fukuda A, Wickman LT, Venkatreddy MP, et al. Angiotensin II-dependent persistent podocyte loss from destabilized glomeruli causes progression of end stage kidney disease. *Kidney Int* 2012;81(1):40–55.
276. Papeta N, Zheng Z, Schon EA, et al. Prkdc participates in mitochondrial genome maintenance and prevents Adriamycin-induced nephropathy in mice. *J Clin Invest* 2010;120(11):4055–4064.
277. Pippin JW, Brinkkoetter PT, Cormack-Aboud FC, et al. Inducible rodent models of acquired podocyte diseases. *Am J Physiol Renal Physiol* 2009;296(2):F213–F229.
278. Caulfield JP, Reid JJ, Farquhar MG. Alterations of the glomerular epithelium in acute aminonucleoside nephrosis. Evidence for formation of occluding junctions and epithelial cell detachment. *Lab Invest* 1976;34(1):43–59.
279. Peti-Peterdi J, Sipos A. A high-powered view of the filtration barrier. *J Am Soc Nephrol* 2010;21(11):1835–1841.
280. Moudgil A, Nast CC, Bagga A, et al. Association of parvovirus B19 infection with idiopathic collapsing glomerulopathy. *Kidney Int* 2001;59(6):2126–2133.
281. Li RM, Branton MH, Tanawattanacharoen S, et al. Molecular identification of SV40 infection in human subjects and possible association with kidney disease. *J Am Soc Nephrol* 2002;13(9):2320–2330.
282. Tomlinson L, Boriskin Y, McPhee I, et al. Acute cytomegalovirus infection complicated by collapsing glomerulopathy. *Nephrol Dial Transplant* 2003;18(1):187–189.
283. Presne C, Cordonnier C, Makdassi R, et al. [Collapsing glomerulopathy and cytomegalovirus, what are the links?]. *Presse Med* 2000;29(33):1815–1817.
284. Stehman-Breen C, Alpers CE, Fleet WP, et al. Focal segmental glomerular sclerosis among patients infected with hepatitis C virus. *Nephron* 1999;81(1):37–40.
285. Wierenga KJ, Pattison JR, Brink N, et al. Glomerulonephritis after human parvovirus infection in homozygous sickle-cell disease. *Lancet* 1995;346(8973):475–476.
286. Moudgil A, Shidban H, Nast CC, et al. Parvovirus B19 infection-related complications in renal transplant recipients: Treatment with intravenous immunoglobulin. *Transplantation* 1997;64(12):1847–1850.
287. Tanawattanacharoen S, Falk RJ, Jennette JC, et al. Parvovirus B19 DNA in kidney tissue of patients with focal segmental glomerulosclerosis. *Am J Kidney Dis* 2000;35(6):1166–1174.

288. Rao TK, Nicastrì AD, Friedman EA. Natural history of heroin-associated nephropathy. *N Engl J Med* 1974;290(1):19–23.
289. Jaffe JA, Kimmel PL. Chronic nephropathies of cocaine and heroin abuse: A critical review. *Clin J Am Soc Nephrol* 2006;1(4):655–667.
290. May DC, Helderman JH, Eigenbrodt EH, et al. Chronic sclerosing glomerulopathy (heroin-associated nephropathy) in intravenous T's and Blues abusers. *Am J Kidney Dis* 1986;8(6):404–409.
291. do Sameiro Faria M, Sampaio S, Faria V, et al. Nephropathy associated with heroin abuse in Caucasian patients. *Nephrol Dial Transplant* 2003;18(11):2308–2313.
292. Dettmeyer R, Wessling B, Madea B. Heroin associated nephropathy—a post-mortem study. *Forensic Sci Int* 1998;95(2):109–116.
293. Cunningham EE, Brentjens JR, Zielezny MA, et al. Heroin nephropathy. A clinicopathologic and epidemiologic study. *Am J Med* 1980;68(1):47–53.
294. Friedman EA, Tao TK. Disappearance of uremia due to heroin-associated nephropathy. *Am J Kidney Dis* 1995;25(5):689–693.
295. Markowitz GS, Appel GB, Fine PL, et al. Collapsing focal segmental glomerulosclerosis following treatment with high-dose pamidronate. *J Am Soc Nephrol* 2001;12(6):1164–1172.
296. Barri YM, Munshi NC, Sukumalchandra S, et al. Podocyte injury associated glomerulopathies induced by pamidronate. *Kidney Int* 2004;65(2):634–641.
297. Desikan R, Veksler Y, Raza S, et al. Nephrotic proteinuria associated with high-dose pamidronate in multiple myeloma. *Br J Haematol* 2002;119(2):496–499.
298. Nagahama M, Sica DA. Pamidronate-induced kidney injury in a patient with metastatic breast cancer. *Am J Med Sci* 2009;338(3):225–228.
299. Markowitz GS, Radhakrishnan J, Kambham N, et al. Lithium nephrotoxicity: A progressive combined glomerular and tubulointerstitial nephropathy. *J Am Soc Nephrol* 2000;11(8):1439–1448.
300. Nadasdy T, Allen C, Zand MS. Zonal distribution of glomerular collapse in renal allografts: Possible role of vascular changes. *Hum Pathol* 2002;33(4):437–441.
301. Izzedine H, Brocheriou I, Frances C. Post-transplantation proteinuria and sirolimus. *N Engl J Med* 2005;353(19):2088–2089.
302. Haskell LP, Glicklich D, Senitzer D. HLA associations in heroin-associated nephropathy. *Am J Kidney Dis* 1988;12(1):45–50.
303. Sauter M, Julg B, Porubsky S, et al. Nephrotic-range proteinuria following pamidronate therapy in a patient with metastatic breast cancer: Mitochondrial toxicity as a pathogenetic concept? *Am J Kidney Dis* 2006;47(6):1075–1080.
304. Thadhani R, Pascual M, Nickleit V, et al. Preliminary description of focal segmental glomerulosclerosis in patients with renovascular disease. *Lancet* 1996;347(8996):231–233.
305. Vollenbroeker B, George B, Wolfgart M, et al. mTOR regulates expression of slit diaphragm proteins and cytoskeleton structure in podocytes. *Am J Physiol Renal Physiol* 2009;296(2):F418–F426.
306. Hertig A, Droz D, Lesavre P, et al. SLE and idiopathic nephrotic syndrome: Coincidence or not? *Am J Kidney Dis* 2002;40(6):1179–1184.
307. Kraft SW, Schwartz MM, Korbet SM, et al. Glomerular podocytopathy in patients with systemic lupus erythematosus. *J Am Soc Nephrol* 2005;16(1):175–179.
308. Dube GK, Markowitz GS, Radhakrishnan J, et al. Minimal change disease in systemic lupus erythematosus. *Clin Nephrol* 2002;57(2):120–126.
309. Jennette JC, Hipp CG. C1q nephropathy: a distinct pathologic entity usually causing nephrotic syndrome. *Am J Kidney Dis* 1985;6(2):103–110.
310. Vizjak A, Ferluga D, Rozic M, et al. Pathology, clinical presentations, and outcomes of C1q nephropathy. *J Am Soc Nephrol* 2008;19(11):2237–2244.
311. Hisano S, Fukuma Y, Segawa Y, et al. Clinicopathologic correlation and outcome of C1q nephropathy. *Clin J Am Soc Nephrol* 2008;3(6):1637–1643.
312. Srivastava T, Chadha V, Taboada EM, et al. C1q nephropathy presenting as rapidly progressive crescentic glomerulonephritis. *Pediatr Nephrol* 2000;14(10–11):976–979.
313. Taggart L, Harris A, El-Dahr S, et al. C1q nephropathy in a child presenting with recurrent gross hematuria. *Pediatr Nephrol* 2010;25(1):165–168.
314. Kersnik Levart T, Kenda RB, Avgustin Cavic M, et al. C1Q nephropathy in children. *Pediatr Nephrol* 2005;20(12):1756–1761.
315. Wong CS, Fink CA, Baechle J, et al. C1q nephropathy and minimal change nephrotic syndrome. *Pediatr Nephrol* 2009;24(4):761–767.
316. Lau KK, Gaber LW, Delos Santos NM, et al. C1q nephropathy: features at presentation and outcome. *Pediatr Nephrol* 2005;20(6):744–749.
317. Iskandar SS, Browning MC, Lorentz WB. C1q nephropathy: a pediatric clinicopathologic study. *Am J Kidney Dis* 1991;18(4):459–465.
318. Said SM, Cornell LD, Valeri AM, et al. C1q deposition in the renal allograft: a report of 24 cases. *Mod Pathol* 2010;23(8):1080–1088.
319. Fukuma Y, Hisano S, Segawa Y, et al. Clinicopathologic correlation of C1q nephropathy in children. *Am J Kidney Dis* 2006;47(3):412–418.
320. Mii A, Shimizu A, Masuda Y, et al. Current status and issues of C1q nephropathy. *Clin Exp Nephrol* 2009;13(4):263–274.
321. van den Dobbelen ME, van der Woude FJ, Schroeijers WE, et al. Both IgG- and C1q-receptors play a role in the enhanced binding of IgG complexes to human mesangial cells. *J Am Soc Nephrol* 1996;7(4):573–581.
322. Kari JA, Jalalah SM. C1q nephropathy in two young sisters. *Pediatr Nephrol* 2008;23(3):487–490.
323. Wenderfer SE, Swinford RD, Braun MC. C1q nephropathy in the pediatric population: pathology and pathogenesis. *Pediatr Nephrol* 2010;25(8):1385–1396.
324. Sinha A, Nast CC, Hristea I, et al. Resolution of clinical and pathologic features of C1q nephropathy after rituximab therapy. *Clin Exp Nephrol* 2011;15(1):164–170.